PASCAL DUBÉ

GEOSTATISTICAL ANALYSIS OF THE TROILUS DEPOSIT

UNCERTAINTY AND RISK ASSESSMENT OF THE MINE PLANNING STRATEGY

Mémoire présenté
à la Faculté des études supérieures de l'Université Laval
dans le cadre du programme de maîtrise en génie des mines
pour l'obtention du grade de Maître ès sciences (M.Sc.)

DÉPARTEMENT DE GÉNIE DES MINES,
DE LA MÉTALLURGIE ET DES MATÉRIAUX
FACULTÉ DES SCIENCES ET DE GÉNIE
UNIVERSITÉ LAVAL
QUÉBEC

2006

© Pascal Dubé, 2006

Résumé

Ce mémoire étudie l'effet de l'incertitude locale et spatiale sur les réserves du gisement d'or Troilus. Deux méthodes géostatistiques ont été utilisées, soit le krigeage des indicatrices et la simulation séquentielle des indicatrices.

En premier lieu, une nouvelle interprétation géologique du gisement a été faite basée sur les trous de forage d'exploration. Pour chaque zone définie, une série de variogrames ont été calculés et un modèle de bloc a été interpolé par krigeage des indicatrices. La calibration de ce modèle a été faite en le comparant au modèle basé sur les trous de forage de production et aux données actuelles de production.

L'incertitude reliée à la variabilité de la minéralization a été quantifiée par l'entremise de 25 simulations séquentielles. Une série de fosses optimales basées sur chaque simulation ont été réalisées afin d'analyser l'impact sur la valeur présente nette, le tonnage de minerai et le nombre d'onces d'or contenues.

Abstract

This thesis examines the effect of local and spatial uncertainty of the mineral reserves estimates for the Troilus gold deposit. Two geostatistical methods have been used: indicator kriging and sequential indicator simulation.

A new set of geological envelope has been defined based on the grade distribution of the exploration hole samples. For each zone, composites, statistics and variograms have been calculated based on gold assays coming from exploration holes (DDH) and production blastholes (BH). A recoverable reserve block model based on indicator kriging was created from the exploration holes and a grade control block model was produced from the production blastholes. The recoverable reserve model was calibrated based on the grade control model and the data from the mined out part of the orebody.

Uncertainty related to the variability of the mineralization was assessed through 25 conditionally simulated block models. Open pit optimization Whittle software was used as a transfer function to compare each model. Elements such as ore tonnage, grade, ounces contained and discounted value (NPV) have been used to analyse the risk inherent to each model. Finally, reserve estimates within an already established pit design were used as a second method of comparison.

Acknowledgements

First and foremost, I would like to express my gratitude to Dan Redmond, for his input, advice, guidance and for always answering my numerous questions during the preparation of this thesis.

I gratefully acknowledge the support of Inmet Mining to pursue this study and the support of my colleague David Warren and Bruno Perron at Troilus Mine.

I would also like to thank Alain Mainville, Manager of Mining Resources & Methods at Cameco Corporation and Professor Kostas Fytas from Université Laval for their comments and time spent reviewing this thesis.

And finally, I would like to thank Mélanie, for her kindness, patience and understanding during my studies.

Table of Contents

CHAPTER 1 Introduction....10
1.1 General introduction....10
1.2 Description of geostatistics....2
1.2.1 Introduction....2
1.2.2 Geostatistics and mining....2
1.2.3 History of geostatistics....4
1.3 Computer software....5
1.4 Troilus Mine....7
1.4.1 Location....7
1.4.2 Historic of Troilus....8
1.5 Problematic and objectives....10

CHAPTER 2 Geology....12
2.1 Introduction....12
2.2 Regional and local geology....12
2.3 Troilus deposit....13
2.3.1 Geology and alteration....13
2.3.2 Mineralization....15
2.3.3 Structure and foliation....17
2.3.4 In-situ density....18
2.4 Conclusion....18

CHAPTER 3 Geological Modelling....19
3.1 Introduction....19
3.2 Database....19
3.2.1 Diamond drill hole (DDH)....19
3.2.2 Blasthole (BH)....20
3.2.3 Review....20
3.3 Geological interpretation....21
3.3.1 Definition....21
3.3.2 Problematic and avenue....21
3.4 Contact profile analysis....25
3.4.1 Definition....25
3.4.2 Application....25
3.5 Conclusion....27

CHAPTER 4 Compositing....28
4.1 Introduction....28
4.2 Diamond drill holes (DDH)....28
4.2.1 Sample data and composite statistics....28
4.2.2 Compositing variance....29
4.3.1 Sample data statistics....30
4.4 Data set comparison....31
4.5 Distribution analysis for the DDH 3m assay composites and BH assay....31

4.6 Conclusion 34

CHAPTER 5 Spatial Continuity Analysis 35
5.1 Introduction 35
5.2 Contour map 35
5.3 Variography 36
5.3.1 Description 36
5.3.2 Data transformation 38
5.3.3 Indicator transformation 38
5.3.4 Indicator cut-off 42
5.3.5 Indicator variogram 43
5.4 Conclusion 47

CHAPTER 6 Reserve Estimation 48
6.1 Introduction 48
6.2 Interpolation method 48
6.2.1 Selection method 48
6.2.2 Method selected 49
6.3 Indicator kriging 49
6.3.1 Pros 49
6.3.2 Cons 50
6.3.3 Implementation 50
6.4 Block size 52
6.5 Block model 52
6.6 Reconciliation 53
6.6.1 Data provided 53
6.6.2 Mineable packet 53
6.6.4 Discussion and analysis 58
6.7 Cross validation 59
6.7.1 Introduction 59
6.7.2 Limitation 59
6.7.3 Misclassification 60
6.8 Conclusion 64

CHAPTER 7 Conditional Simulation 65
7.1 Introduction 65
7.2 Concept 67
7.2.1 Interpolation vs simulation 67
7.2.2 Theory 68
7.2.3 Implementation 69
7.2.4 Reproduction of sample data characteristics 74
7.3 Transfer function 77
7.3.1 Concept 77
7.4 Open pit optimization 78
7.4.1 Parameters 78
7.4.2 Pit shells generation 79
7.4.3 Pushbacks selection 86

7.4.4 Life of mine schedule 88
7.5 Pit design 89
7.6 Conclusion 91

CHAPTER 8 Conclusions and Recommendations 92
8.1 Conclusions 92
8.2 Recommendations 94

REFERENCES 92

APPENDIX A Mathematical Explanation 100
A.1. Variogram 100
A.2. Inverse distance weighting method 103
A.3. Change of support 104
A.4. One point estimation 107
A.5. Two points estimation 111
A.6. Three points estimation 117
A.7. Ordinary kriging 125
A.8. Ordinary kriging estimation of 3 points 127
A.9. One point estimation indicator kriging estimation 130

APPENDIX B Indicator Variogram DDH 134

APPENDIX C Indicator Variogram BH 201

List of Tables

Table 4.1 DDH 1m assay statistics 28
Table 4.2 DDH 3m composite statistics..... 29
Table 4.3 BH assay statistics..... 30
Table 5.1 Parameters used in the calculation of the DDH variogram..... 38
Table 5.2 Parameters used in the calculation of the BH variogram..... 38
Table 5.3 Percentile at different cut-off for 42
the DDH data 42
Table 5.4 Percentile at different cut-off for the BH data 42
Table 5.5 Variogram modelization by zone for the DDH..... 44
Table 5.6 Variogram modelization by zone for the BH..... 44
Table 6.1 Reserve by zone for mined packet - recoverable reserve - grade control model. 56
Table 6.2 Reserve above 0.5 g/t by bench for mined packet –
recoverable reserve - grade control model..... 57
Table 6.3 Cross validation statistics for DDH data set 60
Table 6.4 Cross validation statistics for BH data set 60
Table 6.5 Classification for DDH data..... 61
Table 6.6 Classification for BH data..... 61
Table 7.1 Estimated vs actual grade of gold mining project
in Australia (Warren, M.J. 1991) 66
Table 7.2 Parameters used for the Whittle 4X optimization..... 78
Table 7.3 Output of Whittle optimization for the pit shell 29..... 83
Table 7.4 Incremental pit shell characteristics based on pushback sequence 13-21-29 87
Table 7.5 Cumulative pit shell characteristics based on pushback sequence 13-21-29..... 87
Table 7.6 Whittle life of mine scheduling based on mining sequence #13, #21, #29 88
Table 7.7 Total material mined at the end of the final pit..... 90

List of Figures

Figure 1.1 Flowchart: From exploration to mining....3
Figure 1.2 Location of Chibougamau....7
Figure 1.3 Location of Troilus Mine....8
Figure 1.4 Mineralized boulder leading to the discovery of the 87 zone....9
Figure 2.1 Geology of Troilus - Plan view....13
Figure 2.2 Geology of Troilus – Section 13600N....14
Figure 2.3 Gold mineralization of Troilus....16
Figure 3.1 Diamond dill holes (DDH) selected....20
Figure 3.2 Plan View 5360 - 0.2 g/t Au envelopes....23
Figure 3.3 Section 13400N - 0.2 g/t Au envelopes....23
Figure 3.4 Plan View 5360 - New set of envelopes developed....24
Figure 3.5 Section 13400N – New set of envelopes developed....24
Figure 3.6 Contact profile analysis of the new set of envelope developed based on DDH..26
Figure 4.1 1m assay for hole KN-88....30
Figure 4.2 3m composite for hole KN 88....30
Figure 4.3 DDH 3m assay composites historgram for ALL zone....32
Figure 4.4 BH assay histogram for ALL zone....32
Figure 4.5 DDH 3m assay composites histogram for HW zone....32
Figure 4.6 BH assay histogram for HW zone....32
Figure 4.7 DDH 3m assay composites histogram for CORE zone....33
Figure 4.8 BH assay histogram for CORE zone....33
Figure 4.9 DDH 3m assay composites histogram for FW zone....33
Figure 4.10 BH assay histogram for FW zone....33
Figure 4.11 DDH 3m assay composites histogram for 87S zone....33
Figure 4.12 BH assay histogram for 87S zone....33
Figure 5.1 Grade Contour Map – Bench 5290....36
Figure 5.2 Parameters used in the calculation of the variogram....37
Figure 5.3 Cumulative distribution function of DDH assay for ALL zone....39
Figure 5.4 Cumulative distribution function of BH assay for ALL zone....39
Figure 5.5 Cumulative distribution function of DDH assay for HW zone....40
Figure 5.6 Cumulative distribution function of BH assay for HW zone....40
Figure 5.7 Cumulative distribution function of DDH assay for CORE zone....40
Figure 5.8 Cumulative distribution function of BH assay for CORE zone....40
Figure 5.9 Cumulative distribution function of DDH assay for FW zone....41
Figure 5.10 Cumulative distribution function of BH assay for FW zone....41
Figure 5.11 Cumulative distribution function of DDH assay for 87S zone....41
Figure 5.12 Cumulative distribution function of BH assay for 87S zone....41
Figure 5.13 Parameters of a variogram....43
Figure 5.14 Along strike variogram at 0.5 g/t cut-off for DDH Core zone....45
Figure 5.15 Along strike variogram at 0.5 g/t cut-off for BH Core zone....41
Figure 5.16 Across strike variogram at 0.5 g/t cut-off for DDH CORE zone....46
Figure 5.17 Across strike variogram at 0.5 g/t cut-off for BH CORE zone....46
Figure 5.18 Downhole variogram at 0.5 g/t cut-off for DDH CORE zone....46
Figure 5.19 Downhole variogram at 0.5 g/t cut-off for BH CORE zone....46

Figure 5.20 Omnidirectional variogram at 0.5 g/t cut-off for DDH CORE zone 47
Figure 5.21 Omnidirectional variogram at 0.5 g/t cut-off for BH CORE zone 47
Figure 6.1 Calculation of the estimated grade based on indicator kriging 51
Figure 6.2 Bench 5290 - Mined packet 54
Figure 6.3 Bench 5290 – Recoverable reserve 54
Figure 6.4 Bench 5290 – Grade control 54
Figure 6.5 Cross validation of the HW zone for the DDH data 62
Figure 6.5 Cross validation of the HW zone for the DDH data 62
Figure 6.6 Cross validation of the CORE zone for the DDH data 62
Figure 6.7 Cross validation of the FW zone for the DDH data 63
Figure 6.8 Cross validation of the 87S zone for the DDH data 63
Figure 7.1 Difference between kriging and simulation 68
Figure 7.2 Example of the determination of a node grade 71
Figure 7.3 Section 13400N – Recoverable Reserve Model 72
Figure 7.4 Section 13400N – Simulation #5 72
Figure 7.5 Section 13400N – Simulation #11 72
Figure 7.6 Section 13400N – Simulation #18 72
Figure 7.7 Bench 5290 – Recoverable Reserve Model 73
Figure 7.8 Bench 5290 – Simulation #5 73
Figure 7.9 Bench 5290 – Simulation #11 73
Figure 7.10 Bench 5290 – Simulation #18 73
Figure 7.11 DDH 3m assay composites histogram for HW zone 75
Figure 7.12 Simulation #18 histogram for HW zone 75
Figure 7.13 DDH 3m assay composites histogram for CORE zone 75
Figure 7.14 Simulation #18 histogram for CORE zone 75
Figure 7.15 DDH 3m assay composites histogram for FW zone 75
Figure 7.16 Simulation #18 histogram for FW zone 75
Figure 7.17 DDH 3m assay composites histogram for 87S zone 76
Figure 7.18 Simulation #18 histogram for 87S zone 76
Figure 7.19 Q-Q plot between DDH and simulation #18 for the HW zone 76
Figure 7.20 Q-Q plot between DDH and simulation #18 for the CORE zone 76
Figure 7.21 Q-Q plot between DDH and simulation #18 for the FW zone 77
Figure 7.22 Q-Q plot between DDH and simulation #18 for the 87S zone 77
Figure 7.23 Exported Pit Shell for Pit #29 (340$US/oz) 79
Figure 7.24 Ultimate pit design as of July 2001 79
Figure 7.25 Discounted open pit value for best case mining schedule 81
Figure 7.26 Discounted open pit value for worst case mining schedule 81
Figure 7.27 Standardized probability distribution of discounted open pit value for best case 84
Figure 7.28 Standardized probability distribution of discounted open pit value forworst case 84
Figure 7.29 Standardized probability distribution of Au produced 85
Figure 7.30 Whittle pit by pit graph for Recoverable Reserve model 86
Figure 7.31 Possible mill feed tonnage 90
Figure 7.32 Possible mill feed head grade 91

Chapter 1

Introduction

1.1 General introduction

With most commodity prices near all time low in the last several years and exploration expenditures kept to a minimum, mining companies had to rely on breakthroughs in technology to lower their operating costs and find new deposits. Amongst new technology developed, we can mention the global positioning system (GPS), the haul truck dispatch system, the drill navigation system, heap leaching, bio-leaching and a series of geophysical methods such as induced polarisation (IP), magnetic resistivity and so on. Also included in this group are techniques used to model and estimate mineral deposits. Recently developed techniques comprise indicator-based algorithms for kriging and conditional simulation. During the last 20 years, mining companies realized that in order to stay competitive and maintain their profit margin, they not only had to embrace those new technologies, but also to invest in research and development. People at Inmet Mining, understood this and decided to fund the present project. The objective of this project was to estimate mineral reserves of the Troilus gold deposit with a non-linear interpolation method and to assess the uncertainty of the mineralization through conditional simulation.

The first chapter presents a general introduction of the project. History and description of geostatistics and the Troilus mine are presented. The second chapter describes the geological context in which the Troilus deposit has been created. The third chapter gives details about how the assay data have been used to develop a geological interpretation of the grade distribution. The fourth chapter deals with the compositing of the diamond drill holes and the blasthole data set. Analysis of the spatial continuity is the subject of chapter five. Reserve estimation and the selection of the interpolation method are discussed in chapter six. Chapter seven treats conditional simulation and the different approach used to analyse the risk. Finally, chapter eight summarizes the results and gives some recommendations for future work.

1.2 Description of geostatistics

1.2.1 Introduction

Because mining investments are generally large, the economic consequences of making investment decisions are very important. Therefore, it is crucial that we evaluate the global and local resources very carefully (Clark, I and Frempong, P.K. 1996). The science used for this is called geostatistics. Geostatistics is the use of classical statistical methods adapted to the mining and geological context. Geostatistics distinguish itself from the classical statistical method by the use of spatial information of the variable under study. Examples of such variables are:

- ore grades in a mineral deposit
- depth and thickness of a geological layer
- porosity and thickness of a geological unit
- density of trees of a certain species in a forest
- soil properties in a region
- pressure, temperature and wind velocity in the atmosphere
- concentration of pollutants in a contaminated site

In addition to that, the science of geostatistics is based on regionalized variables and not on random variables. The grade of a gold sample cannot be categorized as a random variable, since its constitution (grade, location) has been influenced by its position and its relationship with its neighbours. Consequently, the general objectives of geostatistics are to characterize and interpret the behaviour of the existing sample data and to use that interpretation to predict likely values at locations that have not been sampled yet.

1.2.2 Geostatistics and mining

In the mining industry, people usually refer to the word geostatistics to describe the amalgamation of the diverse estimation studies realized between the completion of the drilling campaign and the design of the excavation. In most cases, geostatistics is used to

quantify a mineral resource. Estimates of the tonnage and grade are first carried out to give the company and the investor community an idea of the resource potential.

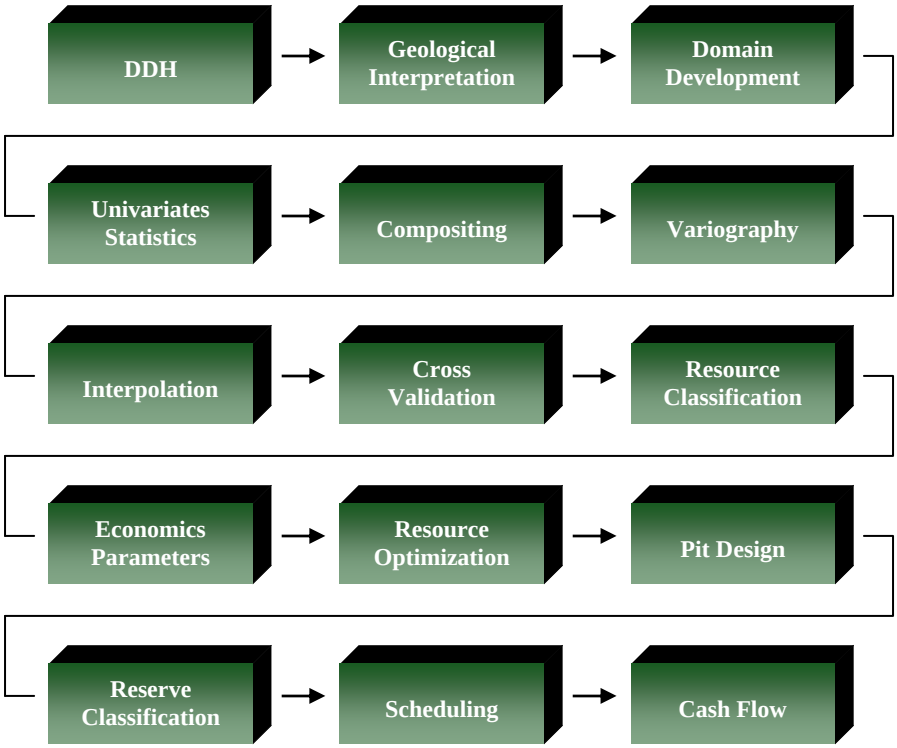

Figure 1.1 Flowchart: From exploration to mining

This estimate is then subdivided into classes based on the level of confidence. Mineral reserve estimates require the contribution of different people with different sets of skills. The flowchart of figure 1.1 shows the different components involved in the development of a mineral reserve base. First, preliminary exploration works such as geology mapping, soil sediment analysis, geochemistry and geophysics are carried out to understand and assess the geological potential of the exploration property. Depending on the results, a drilling campaign could be launched for the purpose of finding enough mineralization of interest to carry the project forward. Up to this stage, exploration geologists are usually in charge of the project. Their focus is mainly to relate the mineralization with geological features such as alteration, lithology and structure. They are also in charge of the geological interpretation of the orebody and its subdivision into different zones. The geostatistician involvement in the project begins when information collected from the exploration campaign results in

enough data to allow a resource estimate concerning the size and potential of the project. Geostatistical analysis of the deposit will provide valuable information, for instance:

- mean, variance and other statistical parameters through univariates statistics
- a measure of continuity of the mineralization through variography
- possible tonnage and grade of the deposit through interpolation method

From this information, a resource estimate will be generated by the geostatistician. This will represent the overall potentially valuable material that is contained within the deposit. Based on the level of geological knowledge and confidence, this resource estimate will be divided into inferred, indicated and measured categories (Anderson, M.J. 1999). Armed with this resource estimate, the exploration geologist will try to add material into each category with more drilling and by proving geological and grade continuity. The mine planning engineer will start to get involved in the project when the measured and indicated resources have sufficient potential material to warrant a preliminary economic assessment. At this stage, the aim is to determine if the current resource has the potential to be mined. This will be evaluated by incorporating mining, processing, financial, environmental, social and legal factors into the resources. If the resources prove to be economical, material previously categorized as measured and indicated will be moved into the reserve categories of proven and probable. In some cases, measured resources will become probable reserves. They will be followed by more detailed work such as excavation design (open pit or underground), process design, environmental impact study and so on, which might ultimately lead to a decision to proceed with the development of a future mine.

1.2.3 History of geostatistics

The application of geostatistics to problems in geology and mining dates back to the early 40's, when Herbert S. Sichel worked on some South African gold mines on the development of a method to predict the grade of an area to be mined from sparsely gold samples. Sichel's work involved the creation of a lognormal distribution table that enabled the calculation of the average of a lognormal variable such as gold. In the 50's, Daniel G. Krige collected an exhaustive set of gold assay data from South African mines. Following that, Krige developed a technique called "Weighted Moving Average" which is a linear

regression used to estimate the value of mining blocks. In 1960 in Sweden, Bertil Matern applied the concept of spatial statistics of forestry industry data.

Among those who have contributed to advance the science of geostatistics, George Matheron is surely the one who moved the geostatistical science to the level known today. During the 1954-1963 period, Matheron rediscovered the pioneering work carried out on the gold deposit of the Witwatersrand by Sichel, Krige and de Wijs, and built the major concepts of the theory for estimating resources, which he named Geostatistics. Between 1962 and 1965, Matheron published two books: "Treatise of Applied Geostatistics" (1963) and "The Regionalized Variables and their Estimation" (1965). The former lays down the fundamental tools of linear geostatistics: variography, variances of estimation and kriging. The latter is his PhD thesis and explains in a more theoretical way the concept of geostatistics. In 1968, the Paris School of Mines created the "Centre de Géostatistique et Morphologie Mathématique" of which Matheron became the director. From 1968 to his retirement in 1996, collaborators such as André Journel, Alain Maréchal and Pierre Delfinerl helped to create the concept of non-linear and non-stationary geostatistics. The period 1980-2000 will see the creation of geostatistical methods for specific applications. The non-parametric geostatistics was developed during the 80's by André Journel to counteract the smearing effect of ordinary kriging on erratic mineralization. With the technological revolution of the 80's, computers became available to a broader range of people, making geostatistics more accessible. Today, conditional simulation algorithms are used in the mining industry to assess the variability of the mineralization and to analyse the sensitivity of ore reserve estimation. The science of geostatistics is not only used in mining, but in a broader range of industries such as: petroleum, forestry, agronomy, oceanography, meteorology, fishery, environmental science, etc…

1.3 Computer software

Due to the large amount of data treated and the numerous geostatistical interpolations and iterations required for the project, the utilization of a powerful pc and the most advanced geostatistical software were a necessity. The principal software used was Gemcom. It is a general mining package capable of treating information coming from geological exploration

up to the design of an open pit mine. In this case, Gemcom was specifically used for geological modelling, compositing and reserve estimation. The analysis of the spatial continuity was carried out with Supervisor, a geological software provided free of charge by Snowden Mining Industry Consultants Pty Ltd of Australia. Supervisor is the grouping of two different softwares: Analysor and Visor. Snowden Analysor was used to generate the univariates statistics for the DDH and BH data and Snowden Visor was used to generate the multiple variograms for the DDH and BH. The conditional simulations were carried out with WinGSLIB, the Windows version of GSLIB. And finally, conditionally simulated models were assessed through a series of pit optimization algorithms using Whittle 4X.

1.4 Troilus Mine

1.4.1 Location

The town of Chibougamau is located 510 kilometres north of Québec, Canada (figure 1.2). The Chibougamau area has been a major gold camp during the 1960' and 1970'.

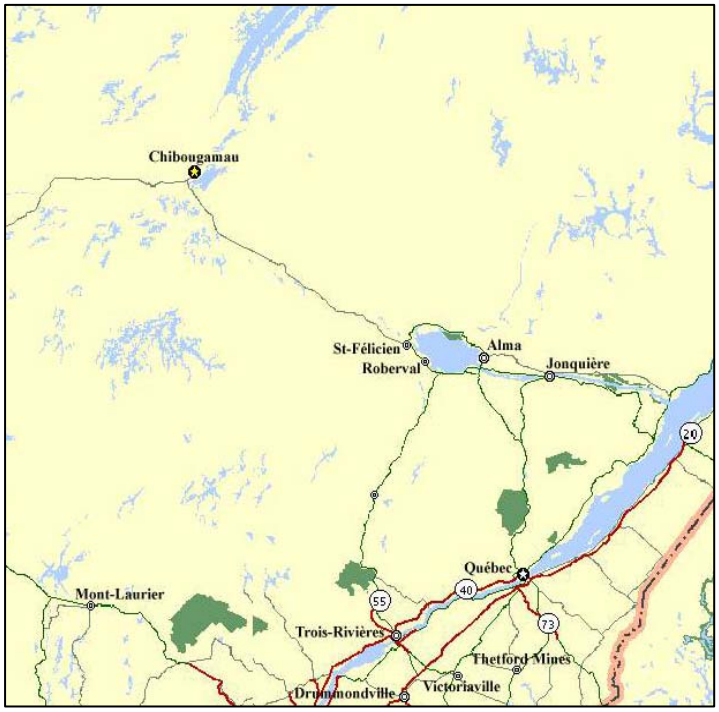

Figure 1.2 Location of Chibougamau

Today, however, only three mines are in operation: Joe Mann and Copper Rand, both underground mines owned and operated by Campbell Resources and Troilus, an open pit mine owned and operated by Inmet Mining. The Troilus Mine is located 174 kilometres north of Chibougamau (figure 1.3). It is accessible by the "Route du Nord" up to 44 kilometres from the site, where a gravel road accesses the property.

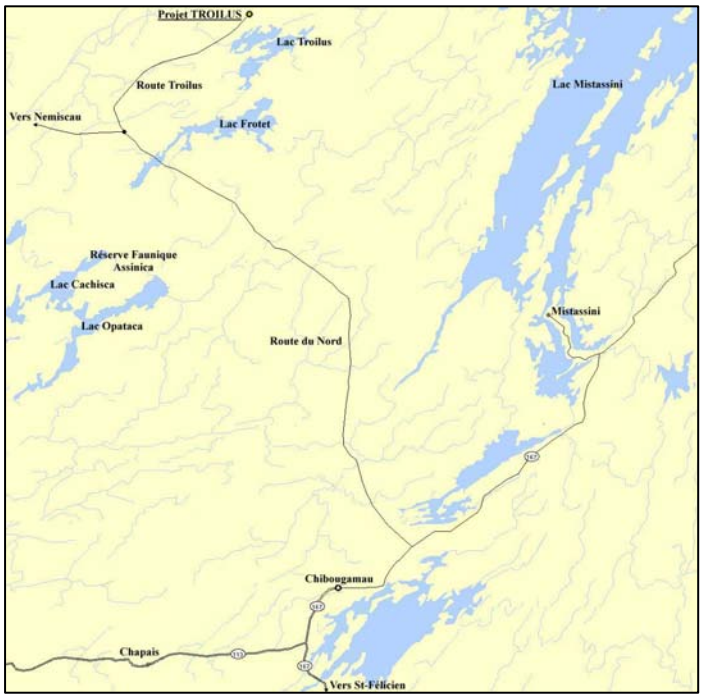

Figure 1.3 Location of Troilus Mine

1.4.2 Historic of Troilus

In 1958, after the discovery of mineralized boulders in the region of the Frotet Lake and Troilus Lake, initial exploration work began. Between 1958 and 1967, some copper and zinc anomalies were identified, including the Baie Moléon massive sulphide deposit discovered in 1961 by Falcondbridge Limited. This small deposit contains mineral resources of 200 000 tonnes at 2.0% Cu, 4.25% Zn, 39.7 g/t Ag and 1.0 g/t Au. In 1971, the Lessard deposit (1.46 Mt at 1.73% Cu, 2.96% Zn, 38.0 g/t Ag and 0.70 g/t Au) was discovered around the Domerque Lake by Selco Mining Corporation. Following this discovery, a geophysical survey of the Frotet Lake and Troilus Lake area was carried out, unfortunately without significant results.

In 1983, the Quebec government released the results of a new geophysical survey. Following the release, some groundwork was carried out again without any major results. In 1985, the Ministry of Energy and Natural Resource of Quebec published a study from a field mapping survey, which indicated some potential for the region to host gold and base metal deposits. Kerr Addison Inc immediately staked an important group of claims in the

area and kicked off an exploration program consisting of field mapping, geophysical survey, geochemistry and core drilling. Finally, the 87 zone was discovered in 1987 following the recovery of a mineralized boulder (figure 1.4).

Figure 1.4 Mineralized boulder leading to the discovery of the 87 zone

In October 1988, a joint venture agreement between Kerr Addison Inc and Minnova Inc was reached. During 1991, a 50-man capacity exploration camp was built between the 87 and J4 zone. During that year, exploration drilling was carried out and a 200 tonnes bulk sample averaging 2.3 g/t Au was taken from the middle of the 87 zone. Of the 200 tonnes bulk sample, 100 tonnes was processed in the facilities of the Centre de Recherches minérales du Québec for a pre-feasibility study; and in 1993, the remaining 100 tonnes were processed at Lakefield pilot plant for a feasibility study. Between December 1992 and March 1993, infill drilling was completed to improve the definition of the 87 and J4 zones and to test some anomalies from the latest geophysical survey. Over the period 1988 to 1993, 565 DDH holes were drilled from surface for a total of 84,600 meters. In February 1993, Metall Mining Corporation took control of Minnova Inc from Kerr Addison Inc and in May 1993, Metall Mining Corporation bought out Kerr Addison's interest in the property. In September 1993, after a due diligence by Coopers and Lybrand of Toronto, the feasibility concluded in the viability of the project. In 1994, Metallgesellscaft AG from Germany sold is 50.1% part in Metall Mining Corporation. Shortly after, Metall Mining Corporation changed its name for Inmet Mining Corporation, which come from the words International and Metals. Finally, in June 1995, financing of the project was completed with a consortium of international banks.

Construction of the Troilus mine began at the end of 1994 and was completed during 1996. The mine being located on land owned by a Cris native band, Inmet agreed to locally employ at least 25% of the mine workforce. Initially, the project had a price tag of 160 million $CDN, but due to problems related to supplies, construction management and a change in the mine plan during the construction phase, the final price came in at 200 million $CDN. The original ore reserve of the Troilus deposit, based on a gold price of 375$US were 49.6Mt at a grade of 1.4 g/t. The mine started commercial production in October 1996 and has run continuously since.

1.5 Problematic and objectives

Many resource/reserve estimates have been carried out on the Troilus deposit over the years. In the majority of the cases, the estimates have been produced by people with limited amount of knowledge and familiarity with the orebody. Although not in their mandate, most of them did not have the chance to question or challenge the underlying hypothesis on which their estimates were based. Moreover, due to time constraints and budget limitations, none of them had the opportunity to take into consideration the effect of local and global uncertainty on their estimates. In view of that, the overall objective of this project is to reconsider the assumptions on which previous resource estimates were based and to assess the significance of uncertainty on the estimates.

First, this thesis will investigate a different approach to the geological interpretation of the Troilus orebody. The modelling of geological features imperative to the grade interpolation is one of the most important steps of a resource/reserve estimate. This phase of the project will serve as the basis from which compositing, variography and interpolation will be derived from. Erroneous or misguided geological interpretation can artificially inflate the ore tonnage of a zone or can include more waste material than it should be.

Secondly, the effect of uncertainty on local estimates will be explored. Instead of only using the distance to assign the grade of a block, this project will include another component that will improve the local estimates. This element is the local distribution of the gold assay surrounding the block to be estimated and it will be incorporated during the interpolation process.

Finally, global uncertainty of the estimates will be assessed through conditional simulation. Through the generation of multiple equi-probable scenarios of mineralization, an analysis of the risk inherent to the orebody will be realized.

CHAPTER 2

Geology

2.1 Introduction

The presentation that follows of the geology of the Troilus deposit was mostly based on an internal report written by Inmet exploration geologist Bernard Boily entitled " Porphyry-type mineralization in the Frotet-Evans greenstone belt – The Troilus Au-Cu deposit". First, the regional and local geology contiguous of the Troilus deposit will be described. Thereafter, characteristics pertaining to the Troilus deposit, such as alteration, mineralization, structure, foliation and in-situ density will be presented.

2.2 Regional and local geology

The Troilus deposit lies within the Frotet-Evans Archean greenstone belt. The greenstones consist of submarine mafic volcanics and cogenetic mafic intrusions. Felsic volcanics and pyroclastic rocks are also present along with epiclastic sedimentary units and ultramafic horizons (figure 2.1, 2.2). Late granitoid plutons and dykes intrude the greenstones. The intrusive rocks range from pre to post tectonic in age. Regional deformation has taken place and produced strong regional foliation. Sub-horizontal mega to mesoscopic folding has affected both the primary layering and regional foliation. Metamorphic grade in the Troilus area ranges from greenschist to lower amphibolite facies. The higher grade metamorphism occurs around the borders of certain intrusions and towards the margins of the greenstone belt. The Frotet-Evans belt is known for its numerous volcanogenic massive sulphide (VMS)deposits. Troilus is the only disseminated Au-Cu volcanic porphyry type deposit located in the belt so far.

2.3 Troilus deposit

2.3.1 Geology and alteration

Two main zones, 87 and J4 have been outlined as well as two sub-economic zones, 86 and J5. The 87 and J4 zones are presently being mined and the amount of information on those zones are much greater than the others. The 87 and J4 zones are hosted in an intermediate porphyritic volcanic unit within which are found elongated zones of hydrothermal breccia and coeval feldspar quartz porphyry dyke/sill swarms (figure 2.1).

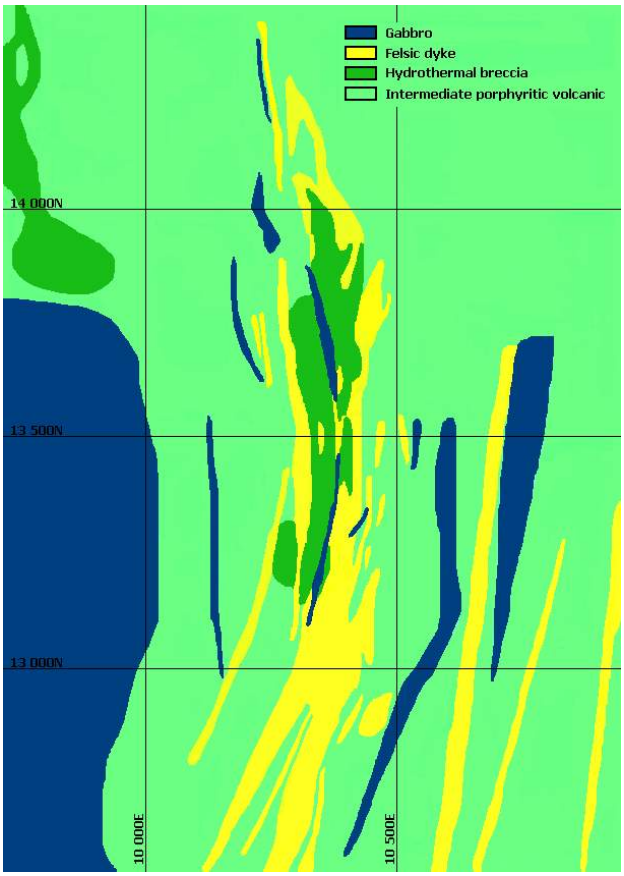

Figure 2.1 Geology of Troilus - Plan view

These rocks dip moderately (60°-70°) to the northwest (figure 2.2). The 87 zone has a wide continuous core of ore (up to 100 m) over some 300 m of strike length. The north and south continuations are bifractated and form narrowing branches of ore amongst weakly mineralized rock.

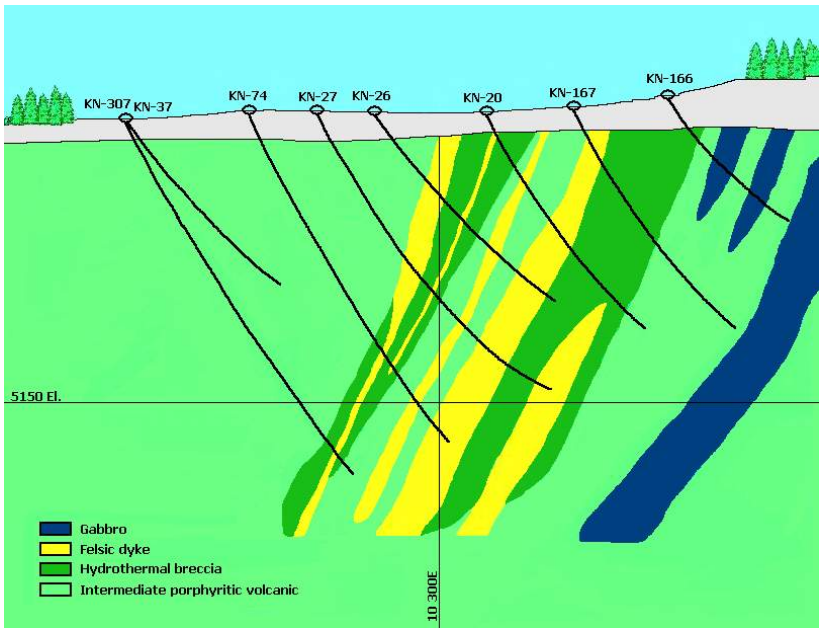

Figure 2.2 Geology of Troilus – Section 13600N

Two branches are well defined in the north. Three branches are less well displayed to the south. The mineralization seems to rake moderately to the north at about 35°. The J4 zone appears to consist of pipe shaped zones. Continuity between sections is not as well established as in the 87 zone. The central part of the mineralized zone coincides with an in situ hydrothermal breccia, which exhibits pseudo-fragments of porphyritic intermediate volcanic rocks in a strongly foliated and altered (biotite-amphibole) matrix. The brecciated texture of the rock comes from the development of polygonal fracturing which channeled hydrothermal solutions. The white colored albitized pseudo-fragments in the breccia represent the less altered portion of the rock.

The breccia is transected by porphyritic felsic dyke swarms, a few mafic dykes and by several deformed small chalcopyrite-bearing quartz veins. Polygonal fractures are abundant in the felsic dykes and are interpreted to have formed during the cooling process of the dykes (columnar jointing). These fractures are also mineralized and Au-bearing thus suggesting that the dykes and the mineralization are contemporaneous. One of the felsic dykes has yielded a radiometric age of 2,786 Ma ± 6 Ma, based on U-Pb dating of zircon.

All these observations suggest that the formation of the Troilus orebody is pre-metamorphic. The main alteration facies defined during the course of core-logging and geological observations made in the pit include, from earliest to latest:

1. Hornfels (very fine biotite)
2. Potassic (biotite – actinolite – K-feldspar)
3. Inner Propylitic (actinolite - albite - epidote)
4. Outer Propylitic (albite - epidote - calcite)
5. Phyllic (sericite - quartz)

The formation of the hydrothermal breccias and the intrusion of the dyke swarms are contemporaneous. Both are deformed and it is interpreted that the effects of tectonism must have ceased during the formation of the potassic assemblage. Potassic, propylitic and phyllic alteration facies are spatially associated with ore. The geological nature of the orebody does not significantly impact the operation. Perhaps the main influence noted to date is that the dykes fragment and comminute differently than the breccia and other volcanic rocks. To what degree these breakage functions affect the operation is not known. Another factor that has no impact but does provide some visual indication of better zones is the amount of biotite. Zones with more biotite correspond closely with better grades.

2.3.2 Mineralization

Chalcopyrite and pyrhotite, with subordinate pyrite, are the main sulphides encountered in the central part of the deposit. The sulphides are most abundant in the breccia matrix along with biotite enrichment. The breccia fragments or protoliths are less enriched. In general, it is thought that the original metalliferous fluids percolated through the rock along openings around the fragments of the volcanic breccia. Ongoing alteration and metamorphic re-mobilization caused further digestion of the protoliths and infiltration of metal rich fluids into the fragments. Hence in the more altered core of the deposit, the fragments are less evident (almost entirely altered) and metal enrichment is ubiquitous. Towards the margins, the fragments are better preserved and metals are restricted more within the matrix infilling.

Hence the mineralization can be characterized as essentially "disseminated" in the core and stringer or sheared towards the margins (figure 2.3).

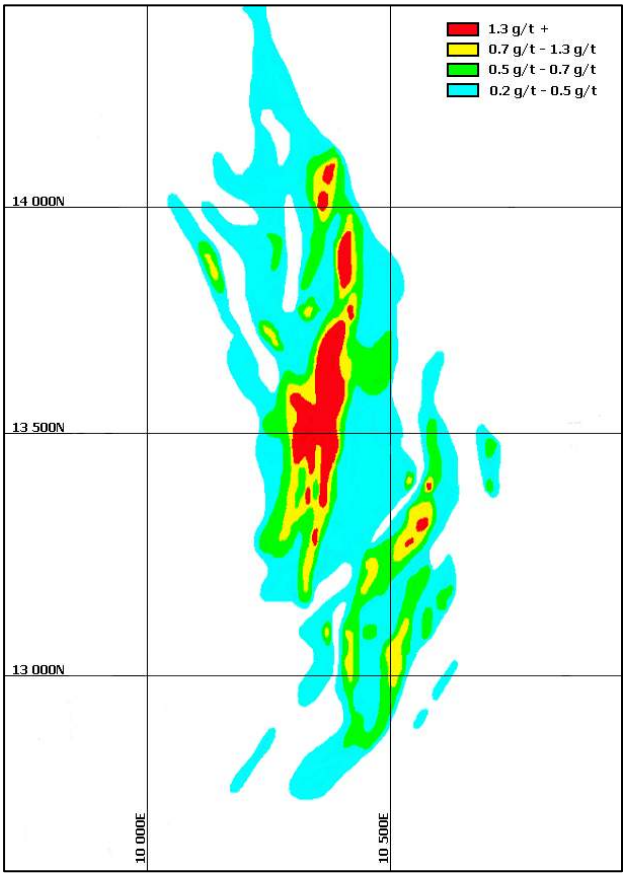

Figure 2.3 Gold mineralization of Troilus

The felsic dykes intruding the breccia contains almost exclusively pyrite. They usually form ore but are poor in copper. There appears to have been at least two phases of mineralization. The first was copper rich and the second gold rich. The two do not exactly overlay. The copper envelope is offset towards the east with respect to the gold envelope. A typical cross section from west to east would have a gold rich, copper poor, hanging wall partition; a wide gold rich and copper rich mid region; and a copper rich gold poor footwall region. Within the central part (more or less the center of the copper envelope) there is a ±15 m wide zone of strong copper enrichment (>0.2% Cu). The copper envelope bulges to the east in the north regions and there are some additional copper rich lenses further into the footwall (outside of the pit walls).

About 25% of the gold reports to dore bars through a gravimetric circuit. The origin of this free gold mineralization has not been accurately located. However if it follows regions of erratic high grade assays, then it would be found closer to the less altered margins and within narrower stringer zones particularly towards the north.

The nature of the mineralization has important implications on the methods used in sampling (lengths of cores, blasthole sampling tools), assaying (size of fire assay, metallic screening) and in interpolating grades within the block model (continuity, top cutting, variogram nugget effect). Also the mineralization affects the mill circuit and recoveries (copper flotation particularly). Although the knowledge of the mineralization has increased, no clear procedures have been established to deal with the differences in mineralogy since the various zones are not easy to localize (not large or discrete enough) and in any case, the selectivity of the mining equipment and short ore supply precludes the use of detailed selection and blending of ore zones to the degree necessary to follow the changes in mineralization. Outwards from this copper/gold-rich zone, chalcopyrite becomes subordinate and pyrite, with lesser pyrhotite, predominates and is particularly abundant over the northern portion of the 87 Zone. This zone overlaps the transition between the potassic and the inner propylitic alteration facies. This area is often characterized by sodic, rather than potassic, alteration.

2.3.3 Structure and foliation

Three main fracture orientations were observed. The first set, oriented at 215° (true north) and dipping at 63°, is sub-parallel to the regional foliation and represents the major fracture system in the pit area. The other two sets (035°/39° and 320°/85°) cut the regional foliation almost at right angles. The combined effect of these fractures has induced local instability in the pit and is directly responsible for the blocky nature of the walls. Faulting is observed in several areas of the pit. A normal dexter fault (315°/55° dip NE mine grid) cuts through and changes the orientation of the mineralization. A second fault in the SE pit region (220°/40° NW) is associated with chalcopyrite enrichment. Regional deformation has strongly flattened and stretched the geological assemblages and alteration pattern.

In the pit area, the effects of this deformation can be observed as follows: strongly elongated felsic dykes (all parallel to the regional foliation); and stretching of the hydrothermal breccia.

2.3.4 In-situ density

The bulk density of in-situ rock is taken as 2.77 t/m^3. For broken muck and stockpiled material, 1.90 t/m^3 is used while overburden weight is 2.20 t/m^3. The value for rock was derived from measurements on drill cores samples and in-pit samples.

2.4 Conclusion

The Troilus deposit lies within the Frotet-Evans Archean greenstone belt. It is the only disseminated Au-Cu volcanic porphyry type deposit located in the belt so far. The deposit consist of two zones, 87 and J4. These zones are hosted in an intermediate porphyritic volcanic unit within which are found elongated zones of hydrothermal breccia. The mineralization can be characterized as disseminated in the core and stringer or sheared towards the margins. There appears to have been at least two phases of mineralization. The first was copper rich and the second gold rich. The mineralization has an azimuth of 35° and dip 60° to 70° to the northwest. Approximately 25% of the gold is free and is recovered by a gravimetric circuit.

CHAPTER 3

Geological Modelling

3.1 Introduction

The geological modelling of an ore deposit entails the separation of mineralization population into homogeneous groups (Coombes, J. 1997). This is done by grouping the mineralization according to geological features such as alteration, foliation, structural unit, and grade homogeneity. At Troilus, the nature of its volcanic porphyry type deposit and its simple geometric configuration makes it somewhat less of a challenge on the modelling side. However, the disseminated feature of the deposit means that more time will have to be spent on modelling the "high grade" core of the deposit to limit its influence on lower grade area. First, a review of the data (DDH, BH) on which the modelling will be based will be carried out to ensure its integrity. Modeling of the grade distribution into subset of homogeneous population will then take place. Finally, assessment of the modelling through a contact profile analysis will be done to confirm the validity of the modelling.

3.2 Database

3.2.1 Diamond drill hole (DDH)

The diamond drill hole (DDH) database on which the recoverable reserve block model and the conditional simulation were based contains information of the exploration and definition drilling campaigns from 1988 to 1999. The database contains a total of 625 holes covering the 87 zone, 87S zone, J4 zone and other exploration targets. Drilling was carried out on parallel fence lines spaced nominally 25 m apart for the upper 25% of the deposit and on every second section (50 m apart) for the deeper holes. Of those 625 holes, only 314 were used for the current grade interpolation. The selected holes cover the area of the 87 and 87S zones (figure 3.1). The database contains assay results for gold in grams per tonne (Au g/t), silver in grams per tonne (Ag g/t) and percent (Cu %). For the purpose of the current study, only gold assay were used for the grade interpolation. This can be related to

the fact that at Troilus, 85% of their revenue is derived from gold and also that main ore reserve problem associated with grade interpolation is related to the gold mineralization.

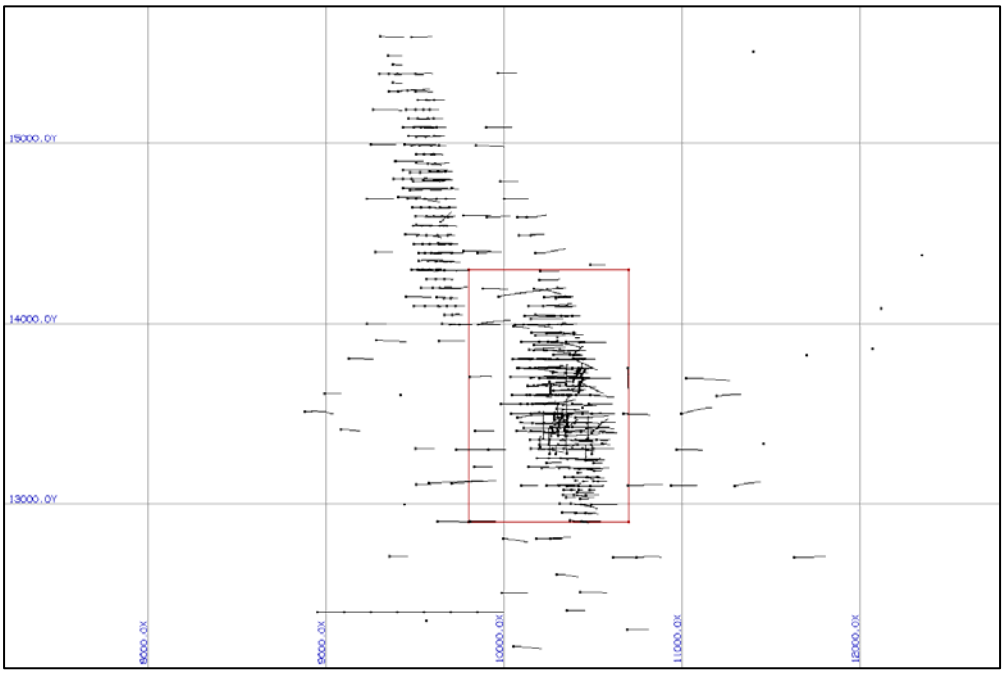

Figure 3.1 Diamond dill holes (DDH) selected

3.2.2 Blasthole (BH)

The blasthole (BH) database used to create the grade control block model contains data from all the blastholes drilled from the beginning of the operation in 1996 until the end of February 2002. The database contains a total of 171,396 blastholes covering the 87 and 87S zones. The average distance between holes, based on the production drilling pattern, which is 5.1 metres by 5.9 meters. The database contains assays for gold in grams per tonne (Au g/t), copper in percent (Cu %) and the NSR (net smelter revenue) value in Canadian dollar per metric tonne (NSR $CAN/t). Again, only gold assay were used for the grade interpolation.

3.2.3 Review

A thorough verification of the DDH and BH database has also been conducted to make sure that the data used for grade interpolation do not contain any data entry errors and that no

data are missing. Since many people have used the current databases, either the mine personnel or external consultants, most of the errors have been sorted out.

3.3 Geological interpretation

3.3.1 Definition

The geological interpretation of an orebody is the most crucial step in resource/reserve estimation. It involves the analysis and interpretation of the following elements:

- type of deposit (porphyry, massive sulphide)
- types of mineralization in the deposit (laterite, oxide, sulphide)
- continuity of mineralization (metres, kilometres)
- structural element of the deposit (fault, vein, dyke)
- spatial distribution of the grade (Au, Cu, Zn)

Most of the time, the geological interpretation used is a computerized simplification of a system far more complex in nature. This comes from the fact that it is almost impossible to model every aspect of a deposit. Despite the fact that we end up with a geological interpretation that is quite simple compared to reality, it is accurate enough for the purpose of grade interpolation. The main reason of creating geological domains or envelopes is to separate data into populations. By combining data that are deemed homogeneous over a domain, the stationary concept can usually be adopted (Goovaerts, P. 1997). Conversely, the availability of enough data to the infer semi-variograms as well as the ability to differentiate different populations will render the subdivision of the data into different domains feasible or not. If possible, it will have a positive effect on kriging by reducing the nugget effect (variability) and by increasing the range of mineralization (continuity).

3.3.2 Problematic and avenue

Previous resource/reserve estimates at Troilus were realized on a set of envelopes based on a cut-off grade of 0.2 g/t Au (Geostat Systems International Inc. 1995). The corresponding set of envelopes was developed on the idea that the mineralization seems to transcend most

lithologic contacts, alteration assemblages and structural domain (Sim, R. 1998). This assumption leads toward the use of "soft" boundaries, which may be diffuse or gradational and result in an over-smoothing of the estimates. In fact, only 2 sets of envelopes had a real impact on the outcome of the grade interpolation; the envelope "Zone #1" for the 87 zone and the envelope "Zone #4" for the 87S zone (figure 3.2, 3.3). Since the current set of envelopes has no boundaries between the high grade and low grade material, the Troilus engineering/geology group reported problems related to the smearing of the grade estimates. One possible avenue to overcome this problem was to change the way the envelopes have been developed. This had previously been carried out by Geostat and the geology group of Troilus (Geostat Systems International Inc. April 1997). By looking at a typical section of the 87/87S zone (figure 3.5), intuitively it can be seen that a core of high grade material exists for both zones. The newly set of envelopes developed are only based on the spatial distribution of the 3m composited gold grade. This comes from the fact that no correlation has been measured so far between the gold distribution and any geological features such as rock type, structure or alteration. In this situation, it is still better to use some sort of local control over the mineralization with an envelope based on grade (Blackney, P.C.J. and Glacken, I.M. 1998). Based on those facts, the "zone #1" has been split into 3 different zone named HW (hangingwall), FW (footwall) and CORE. For the "zone #4", it has been tightened up and renamed 87S (figure 3.4, 3.5). Instead of having one set of variograms for 3 different grade domains as before, the new set of envelopes will have 3 sets of variograms. This should increase the range of continuity of the main zone (CORE) and reduce it for the transitional low grade envelope (HW, FW). The smearing, which took place with the old set of envelopes, should therefore be reduced.

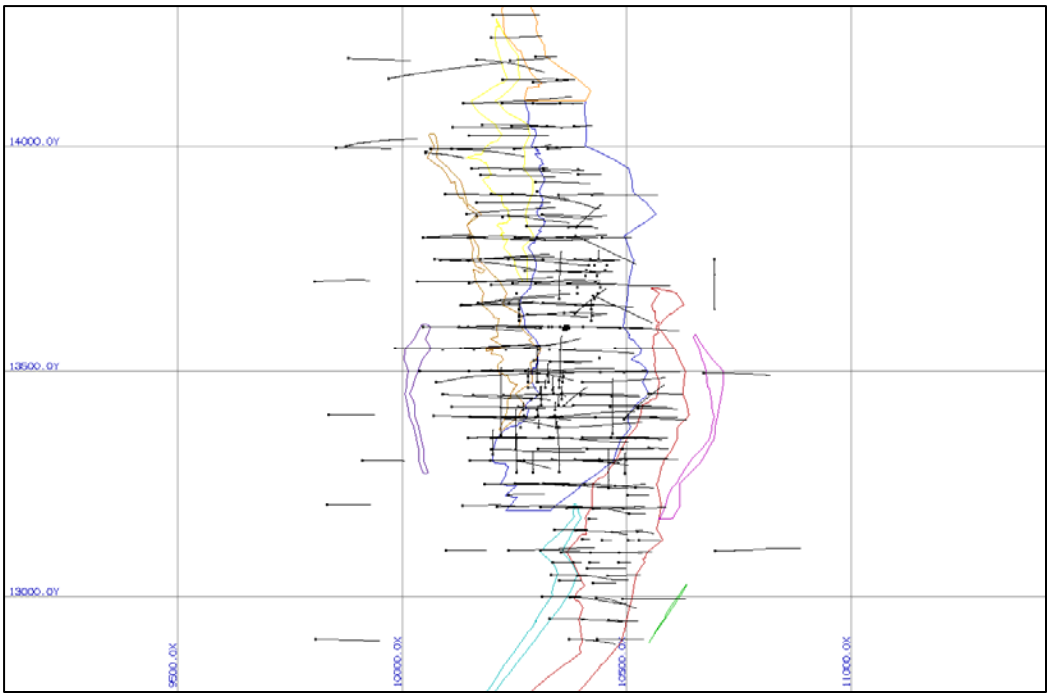

Figure 3.2 Plan View 5360 - 0.2 g/t Au envelopes

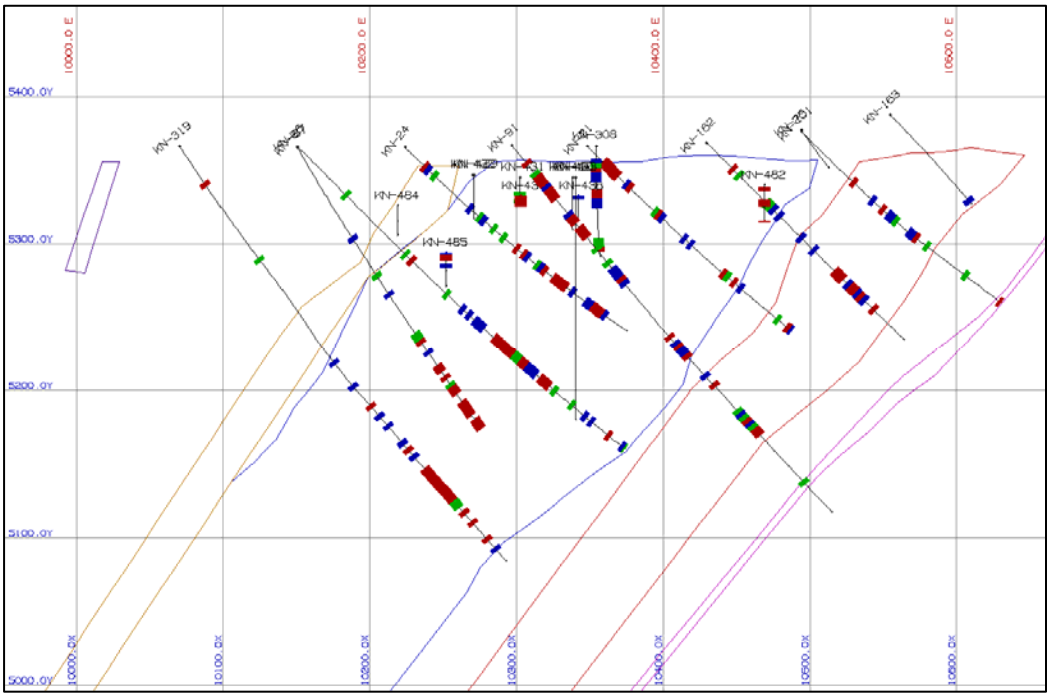

Figure 3.3 Section 13400N - 0.2 g/t Au envelopes

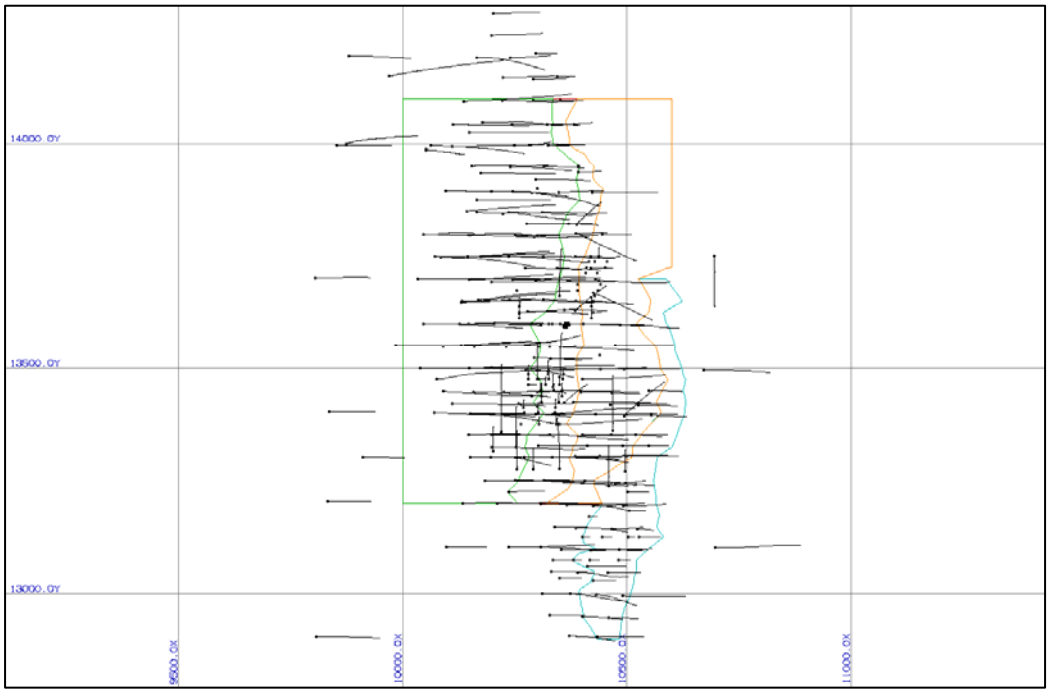

Figure 3.4 Plan View 5360 - New set of envelopes developed

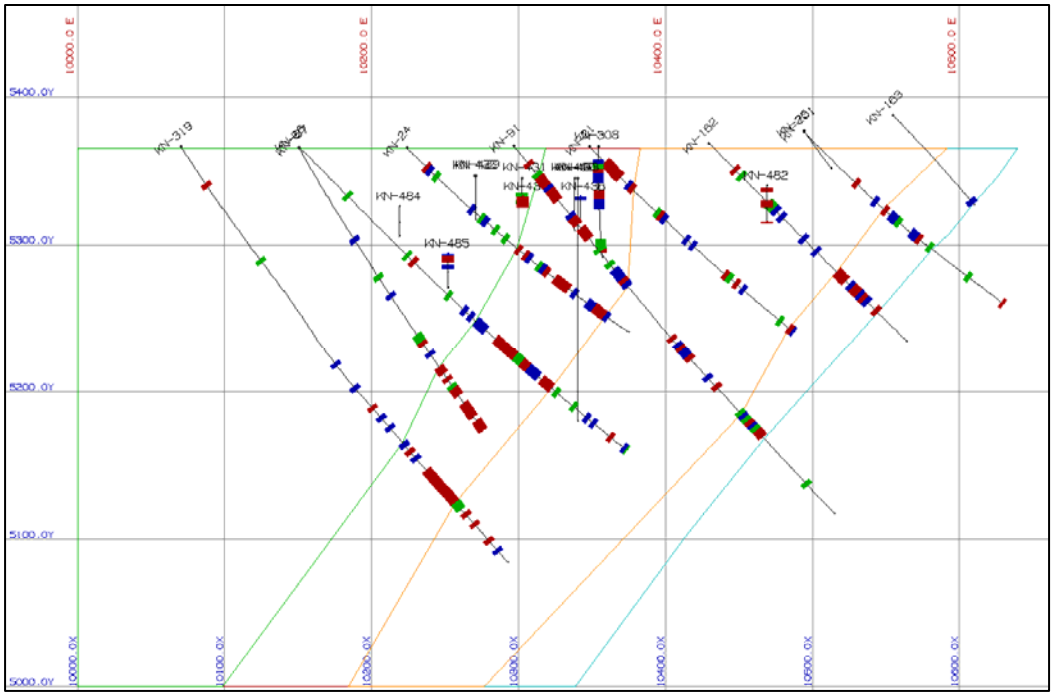

Figure 3.5 Section 13400N – New set of envelopes developed

3.4 Contact profile analysis

3.4.1 Definition

A useful tool to evaluate the validity of an envelope is the use of a contact profile analysis. A series of average grades are calculated for different distances inside an envelope and a graph is produced showing the grade change from an envelope to another. If there is a distinct difference in the average grades across a boundary, then there is evidence that the boundary may be important in constraining the grade estimation. On the other hand, if a "hard" boundary is imposed where grades tend to change gradually, grade may be overestimated on one side of the boundary and underestimated on the other side.

3.4.2 Application

Contact profile analysis has been carried out on the new set of envelopes developed for the DDH data between the HW-CORE zone, CORE-FW zone and FW-87S zone. It can be clearly seen from the following graphics (figure 3.6) that a net difference exits between the low grade envelope (HW, FW) and the high grade envelope (CORE, 87S). The HW envelope has an average of 0.31 g/t Au over the 45 meters analysed compared to 1.08 g/t Au for the CORE zone. For the CORE-FW profile, the CORE envelope has an average of 1.08 g/t Au and the FW zone has an average of 0.35 g/t Au. The same trend exists between the FW (0.23 g/t Au) and the 87S zone (0.98 g/t Au).

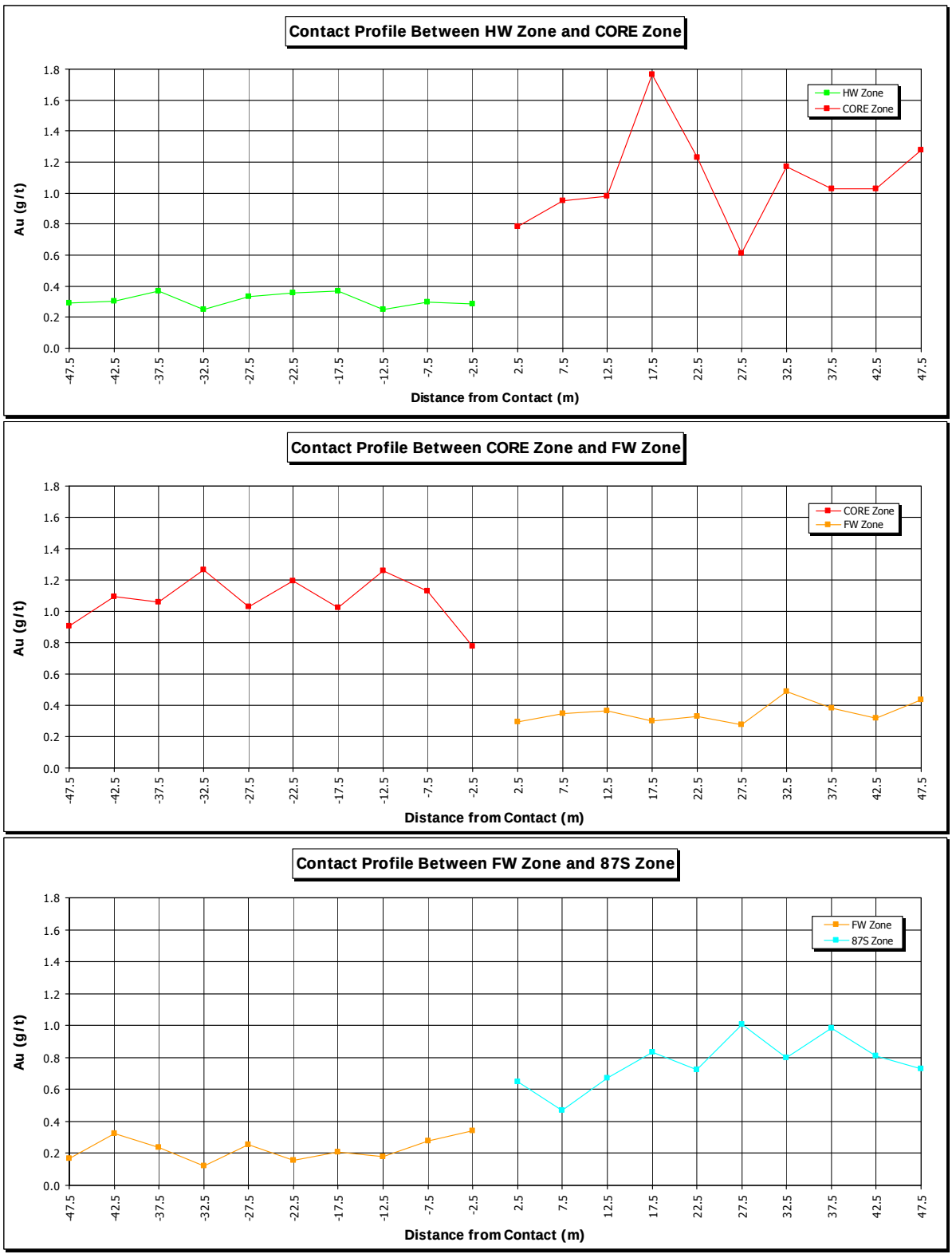

Figure 3.6 Contact profile analysis of the new set of envelope developed based on the DDH

3.5 Conclusion

Modelling of the Troilus deposit has been greatly lightened by the nature of the orebody. In addition, in light of new information and actual mining experience, the original geological interpretation has been reviewed and updated. As a result, focus has been put not so much on associating gold grade to geological features such as alteration and structure but more on domaining the different grade population to minimize the smearing of high grade into the low grade area. Homogeneity of gold grade in each geological envelop has been obtain by subdiving the original Zone#1 and Zone #4 into four new zones named HW, CORE, FW and 87S. A contact profile analysis has been done on the new set of geological envelope and confirmed the merit of tighter envelope in order to achieve stationarity.

CHAPTER 4

Compositing

4.1 Introduction

The compositing of assay interval, also know as regularization, involved the grouping of assay of different interval into a standard length. Composites are in fact a 3D points with its centroid at the middle of the composite interval. Compositing has the benefit to standardize the weight attributed to each assay and to adjust the variability of the composites to be consistent with the scale at which the deposit will be mine. It has also the benefit of lowering the overall variability, which in turns help in modeling the experimental variograms. In the case of Troilus, composites are calculated within each geological envelope.

4.2 Diamond drill holes (DDH)

4.2.1 Sample data and composite statistics

The 314 holes of interest from the DDH database contain a total of 30,060 gold assays. These samples were composited into 3 metres down-the-hole intervals starting from the collar. This composite distance was chosen after taking into account the overall dip of the orebody. With a composite interval of 3 metres and an orebody dip of 60°, this gives a vertical distance of approximately 2.5 metres between each sample. Tables 4.1 and 4.2 give statistics for the 1m assays and 3m composites for each zone.

Zone	Number samples	Maximum	Minimum	Mean	Median	Standard deviation	Variance	Coefficient variation	Number samples > 0.5	Mean > 0.5
ALL	30,060	108.15	0.00	0.62	0.19	2.15	4.63	3.50	8,314	1.85
HW	9,182	42.99	0.00	0.27	0.10	0.84	0.71	3.14	1,160	1.30
CORE	7,767	103.01	0.00	1.22	0.62	2.76	7.63	2.26	4,413	1.98
FW	8,923	108.15	0.00	0.41	0.12	2.02	4.08	4.88	1,509	1.83
87S	4,188	100.08	0.00	0.69	0.23	2.80	7.84	4.07	1,232	1.93

Table 4.1 DDH 1m assay statistics

Zone	Number samples	Maximum	Minimum	Mean	Median	Standard deviation	Variance	Coefficient variation	Number samples > 0.5	Mean > 0.5
ALL	13,378	100.08	0.00	0.54	0.19	1.78	3.17	3.31	3,696	1.58
HW	4,740	31.05	0.00	0.21	0.07	0.64	0.41	3.07	494	1.09
CORE	3,221	40.81	0.00	1.09	0.73	1.63	2.65	1.49	2,002	1.63
FW	3,777	53.89	0.00	0.36	0.14	1.25	1.56	3.44	634	1.45
87S	1,640	100.08	0.00	0.80	0.32	3.85	14.80	4.79	566	1.94

Table 4.2 DDH 3m composite statistics

4.2.2 Compositing variance

When compositing, the mean of the composited data should always be equal to the mean of the assay sample. No matter what the length of the composites we decide to use, the mean has always to be the same. In the present case, when the mean of the 1m assay sample is compared to the mean of the 3m down-the-hole composite samples, it can be see that the mean grade from the 3m composites data is lower. This aberration comes from the way the composites are calculated. In Gemcom, a down-the-hole composite is calculated from the collar of the hole. For example, if there is no 1m assay sample to calculate a composite, a grade of 0 g/t is going to be assigned to this composite. This has the effect of lowering the average grade of the composite sample. On figure 4.1 below, drill hole KN-88 has only one 1m assay sample for the first 48 meters of the hole. Once composited into 3m section, we can see that 15 composites have been added at a grade of 0 g/t (figure 4.2).

When the 87S zone is examined, we can find that the mean for the 3m composites is actually higher than the mean of the assay sample. This can be explained by the fact that in the DDH database, some holes drilled on the 87S zone in 1999 have been sampled at 3 meter intervals. So in this case, the 1m assay sample statistics are in fact a mixed of 2 assay sample population: 1m assay samples and 3m assay samples. This results in a lower mean grade for the 1m assay statistics, since the 3m assays are only counted once instead of being counted 3 times. Looking at the mean grade of the 1m assay sample versus the 3m composite assay at a 0.5 g/t Au cut-off, it can be see that a dilution effect is introduced when the drill holes are composited. In this case, three 1m assays are combined to create one 3m composite. Since there is more lower grade assay than high grade, the result of the compositing is an increase in the tonnage and reduction in the grade at a given cut-off.

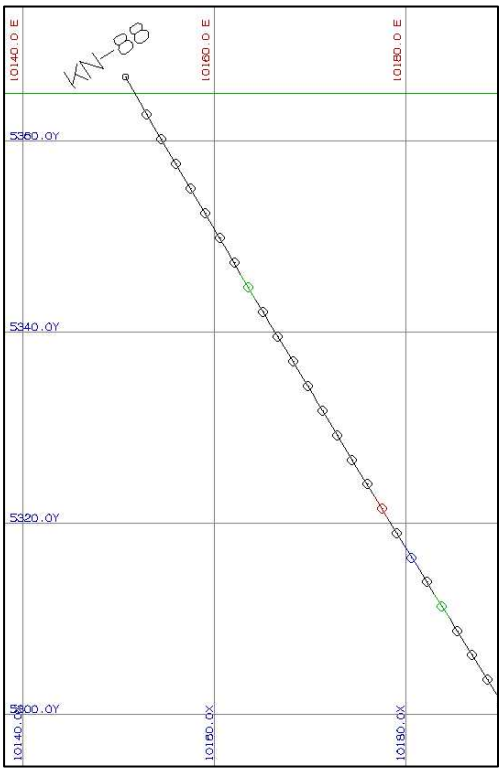

Figure 4.1 1m assay for hole KN-88

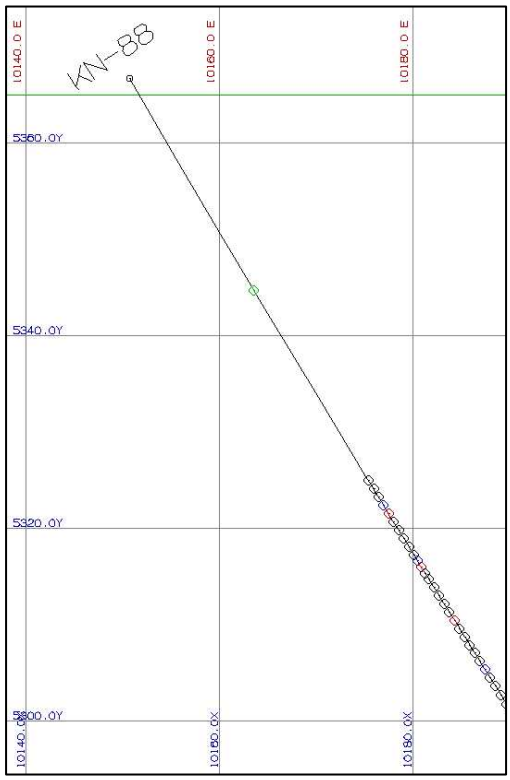

Figure 4.2 3m composite for hole KN-88

4.3.1 Sample data statistics

For the BH assay database, no composites have been calculated. Since most of the database contains samples taken every 5 metres and, only lately, that 10 metre sample intervals have been introduced.

Zone	Number samples	Maximum	Minimum	Mean	Median	Standard deviation	Variance	Coefficient variation	Number samples > 0.5	Mean > 0.5
ALL	189,415	73.54	0.00	0.65	0.34	1.02	1.04	1.57	73,991	1.36
HW	69,163	73.54	0.00	0.34	0.19	0.61	0.37	1.79	13,039	1.07
CORE	65,828	63.02	0.00	1.13	0.80	1.29	1.66	1.15	45,392	1.51
FW	48,925	69.03	0.00	0.46	0.24	0.84	0.71	1.83	13,605	1.19
87S	5,499	22.93	0.00	0.53	0.34	0.70	0.50	1.33	1,955	1.08

Table 4.3 BH assay statistics

On a size of support point of view, having a sample every 5 meters is more than enough and to composite those assays to a smaller support size would not add any benefits to the grade interpolation. Furthermore, when 10 meter samples are used, it is in an area where the level of confidence of the mineralization is high and where one or two samples will not make a difference on the outcome of the average grade when assigning the material type (Ore/Waste) for this hole.

4.4 Data set comparison

When we weigh the BH assay statistics (table 4.3) against the DDH 1m assay (table 4.1) and 3m composites statistics (table 4.2), we can notice the mean of the BH assay is very close to the mean of the 1m assay of the DDH. But when the means above the 0.5 g/t cut-off are compared, the correlation is now better between the BH assay and the DDH 3m composites. This indicates that the portion of the BH assay below the 0.5 g/t cut-off is at a higher grade than the same portion for the DDH 3m composites. Therefore, we can expect a higher overall grade and slightly higher tonnage above the 0.5 g/t cut-off for the Grade Control block model.

4.5 Distribution analysis for the DDH 3m assay composites and BH assay

The shape of the histograms for both data sets clearly shows that the gold samples follow a lognormal distribution (figure 4.3 to 4.12). The lognormality of the distribution has been confirmed by taking the logarithms of the data thus creating a a normal distribution (bell shaped curve). This is also an insight to log transform the original data in order to ease the modeling of the variograms. In this case, a possible transformation could be either logarithmic or indicator. In addition, the shapes of the distribution suggest a highly positively skew set of data. This is also indicated by the fact that the standard deviation is more than three times the mean value. (Clark, I and Harper, W.V. 2000). The shape of the two data sets can be compared by looking at their respective quantiles for each geological zone. Comparison between the DDH 3m composite/BH data for the quantiles of the CORE zone and 87S zone shows a good correlation. The quantiles 25%, 50%, 75% for the

DDH/BH of the CORE zone is 0.29/0.41, 0.73/0.80 and 1.37/1.43 respectively. For the 87S zone, the correlation is 0.14/0.17, 0.32/0.34, 0.67/0.67 for the quantiles 25%, 50% and 75% respectively. On the other hand, the HW and FW zones show a poor correlation between the two data sets. For the HW zone, the correlation is 0.01/0.08, 0.07/0.19, 0.23/0.40 and for the FW zone, the correlation is 0.04/0.10, 0.14/0.24, 0.36/0.55. This can somewhat be explained by the lower amount of information (information effect) from the DDH, where the number of samples is more than 10 times less than that of the BH.

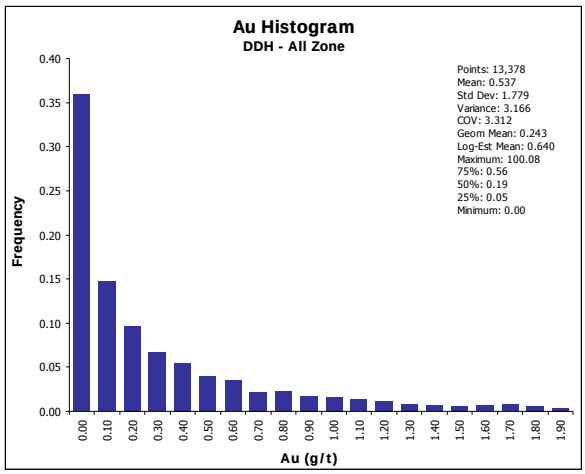

Figure 4.3 DDH 3m assay composites histogram for ALL zone

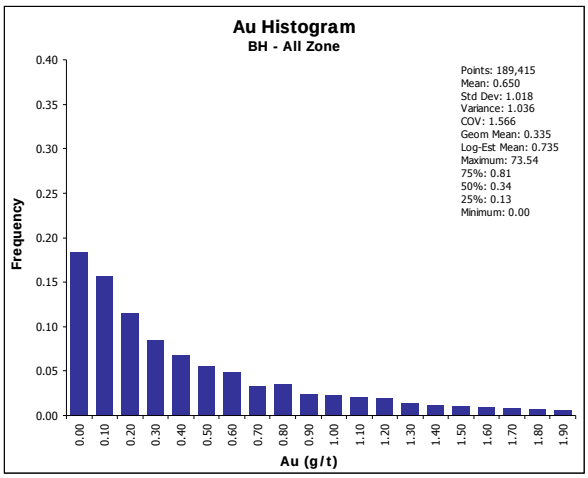

Figure 4.4 BH assay histogram for ALL zone

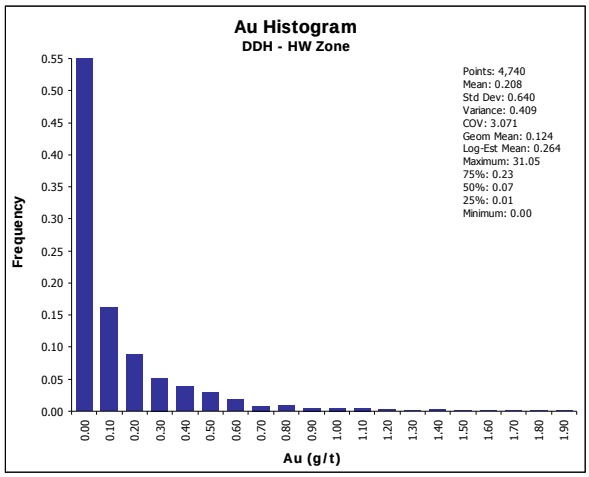

Figure 4.5 DDH 3m assay composites histogram for HW zone

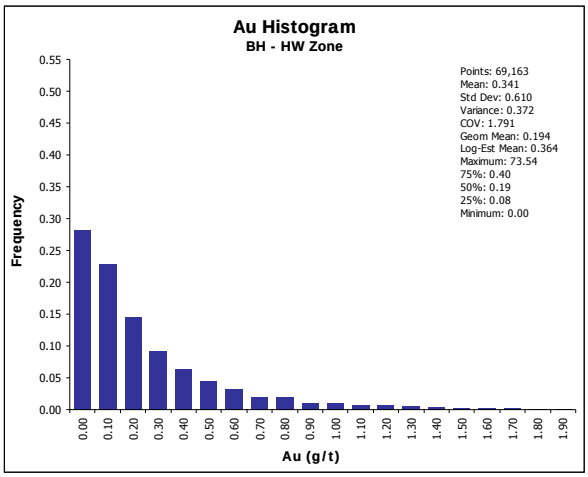

Figure 4.6 BH assay histogram for HW zone

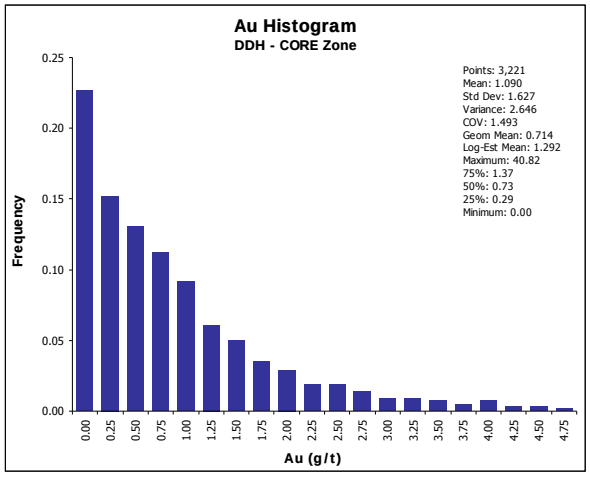

Figure 4.7 DDH 3m assay composites histogram for CORE zone

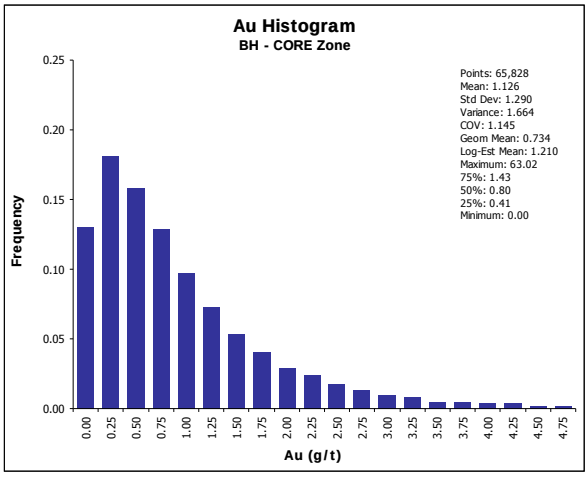

Figure 4.8 BH assay histogram for CORE zone

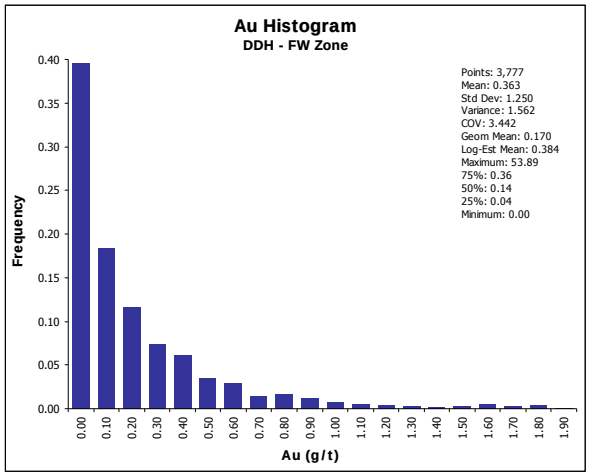

Figure 4.9 DDH 3m assay composites histogram for FW zone

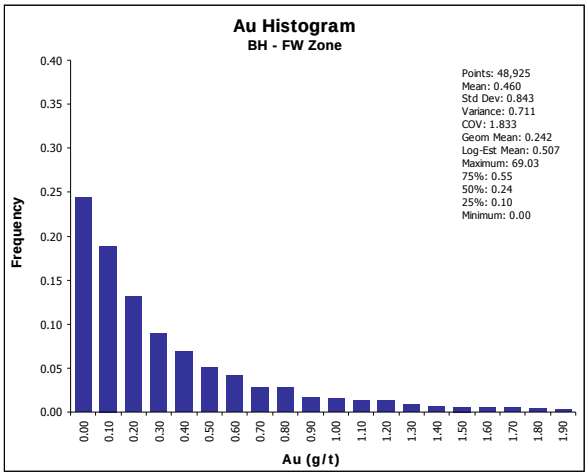

Figure 4.10 BH assay histogram for FW zone

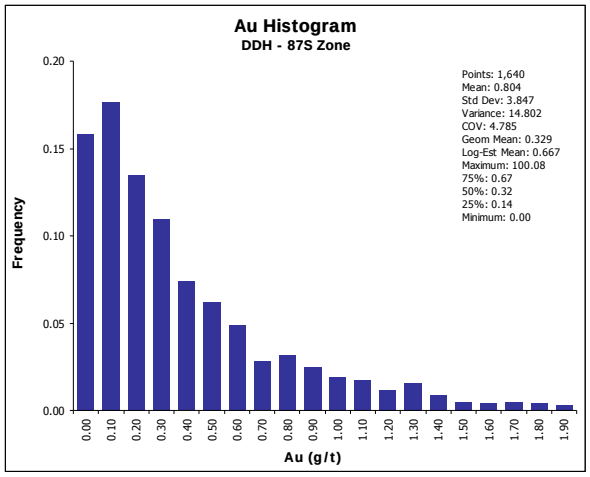

Figure 4.11 DDH 3m assay composites histogram for 87S zone

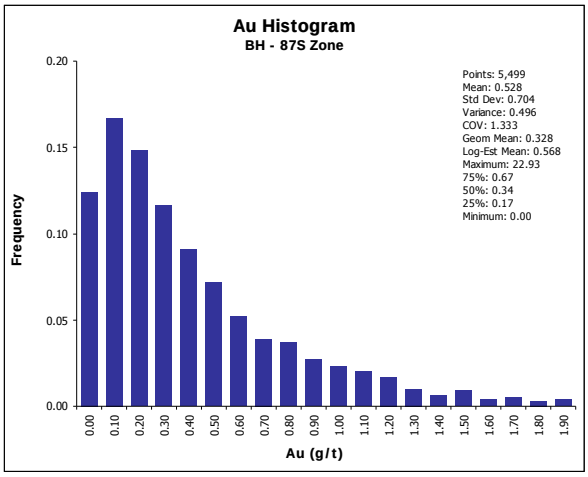

Figure 4.12 BH assay histogram for 87S zone

4.6 Conclusion

Assay samples from diamond drill hole database were composited 3m down-the-hole. In the case of Troilus, the composite length was based on the geometry of the orebody. The 3m length is equal to about 2.5m of true vertical length. The current mining operation uses a bench height of 10m, which translates into 4 composites per hole used vertically during the interpolation. However, this does not concord with the actual sampling practice used during blasthole drilling, which is to take one sample every 5 meter or 2 composites for each 10m bench. This discrepancy can be explained by the fact that there are almost 15 times as many BH composites as there are DDH composites. For this reason, using 4 DDH composites per 10m bench instead of 2 as in the case of BH, should introduce more local variability in the estimated DDH grade. The underlying statistics of BH and DDH composites above a cut-off of 0.5g/t shows a good correlation that supports the composite length adopted for the DDH assays interval.

CHAPTER 5

Spatial Continuity Analysis

5.1 Introduction

Continuity analysis, which can be defined as the methodology of investigating the spatial continuity of variables distributed in space, is the foundation of a geostatistical study. Time spent at this stage to explore, understand and describe the data, will lead the geostatistician to use better assumptions in the variography analysis and will have a major impact on the error associated with the estimation. Furthermore, this crucial step will confirm or reject the previous assumptions made about the mineralization at the early stage of exploration. For example, one might have thought that the mineralization is associated with a geological unit such as an oxide layer, whereas in fact it is structurally controlled by a fault. Having explored the assay data in the previous section with basic summary statistics, we can now spend more time trying to understand and correlate those statistics to the spatial distribution of the gold grade.

5.2 Contour map

One good approach is to use graphical tools such as graphics and maps to describe and grasp the spatial correlation. In the present case, a mix of location maps and grade contour maps was utilized. At first, maps were generated for different bench and for different geological zones. However, due to the small amount of data available for each bench to generate consistent maps, it was decided to group the data altogether. Based on those contour maps, preliminary information related to the orientation of the orebody can be drawn. Overall, the grade distribution seems to have a preferential orientation of about 10 to 30 degrees North Northeast. No apparent plunge can be seen from one bench to another. However, shifting of the orebody from East to West can be picked up from upper benches to lower benches, which indicates that the mineralization is dipping towards West. An example of a contour map for the 5290 bench can be seen on the figure below.

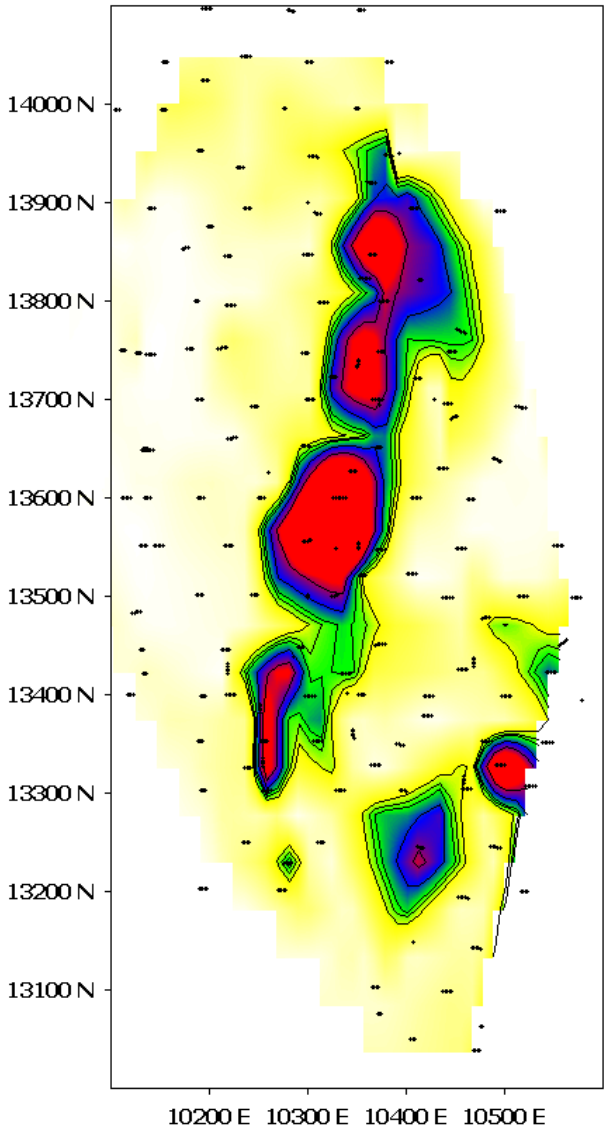

Figure 5.1 Grade Contour Map – Bench 5290

5.3 Variography

5.3.1 Description

The analysis of the spatial continuity is realized with a variogram. Developed by George Matheron, the variogram measures the variability of samples as a function of the distance. Variograms are calculated at different distance intervals (lag distance), for different

orientations (azimuth, dip) and for different conical search dimensions (tolerance angle). Figure 5.2 shows those parameters.

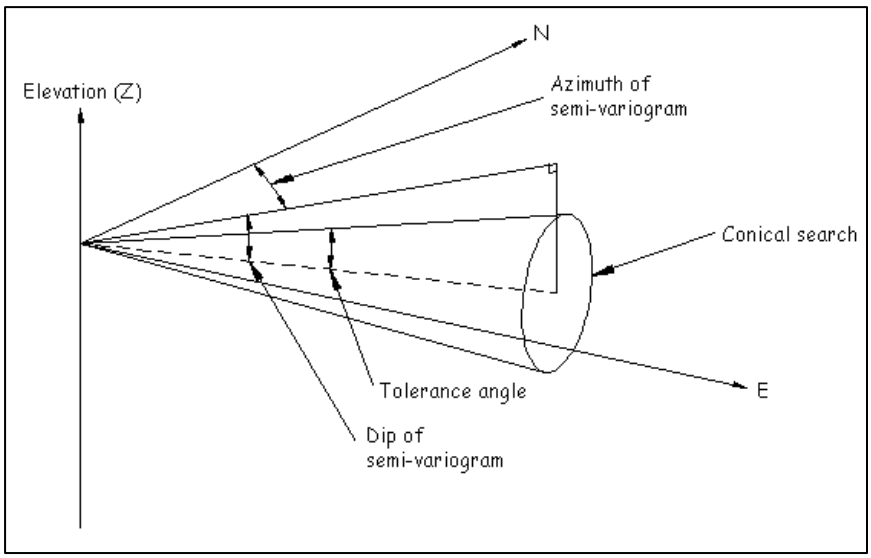

Figure 5.2 Parameters used in the calculation of the variogram

The interval or bin at which the variogram will be calculated (lag distance) should be chosen based on the configuration of the drilling pattern and should be at least equal to the drilling spacing (Coombes, J. 1997). In the case of a regular drilling pattern, the lag distance should be the drilling spacing. If the drilling spacing is irregular, the lag distance can be set to the average distance between drillholes (Goovaerts, P. 1997). The azimuth and dip of the variogram will be assessed for a variety of directions in order to find the anisotropy axis. The tolerance angle is selected in a way to have enough points to calculate the variogram. A small angle will limit the number of samples coming from another direction, but will create an erratic variogram that will be very difficult to modelize. On the other hand, a large tolerance angle will introduce a lot of samples from other directions but will produce a variogram easy to model. A good rule of thumb is to start with a small tolerance angle that will minimize the influence of other directions and to increase it until =there is enough data to create a good variogram. Parameters used in the case of Troilus are summarized in table 5.1 and 5.2. From now on, the designation DDH will refer to assays coming from 3m composite.

Parameter	Downhole	Across Strike	Along Strike	Omnidirectional
Lag distance (m)	12	30	30	30
Maximum distance (m)	200	200	200	200
Tolerance angle (°)	20	30	30	90

Table 5.1 Parameters used in the calculation of the DDH variogram

Parameter	Downhole	Across Strike	Along Strike	Omnidirectional
Lag distance (m)	10	10	10	10
Maximum distance (m)	100	100	100	100
Tolerance angle (°)	15	15	15	90

Table 5.2 Parameters used in the calculation of the BH variogram

5.3.2 Data transformation

Data used in the calculation of the variogram can be transformed to better serve skewed and extreme values. The types of transformation that can be applied to a data set are logarithmic, normal score and indicator (Deutsch, C.V. and Gringarten, E. 2001). The variogram is then calculated on the transformed data. This transformation can help to get a clear and well-defined variogram and would enhance its modelling. Different types of variograms can be created based on original or transformed data. Those types include: traditional, pairwise relative, general relative, madogram, covariance, and correlogram. Each of them has their pros and cons and shares the same goal: to produce a clear picture of the spatial continuity.

5.3.3 Indicator transformation

For Troilus, traditional variograms on indicator-transformed composited assays data for the DDH and on assays data for the BH was the method chosen to evaluate the spatial continuity of the deposit. The choice has been dictated by the method of interpolation used, in this case indicator kriging. The indicator transformation has the advantage of splitting the cumulative distribution function (CDF) into interval. Those intervals, once combined, will give a better definition of the estimated cumulative distribution function. The indicator transformation has also the advantage of removing the extra step of finding the outliers (data with abnormal high values) and treating them accordingly. Instead, all the outliers are kept as they are. This comes from the fact that indicator variograms are calculated based on

the discretization of the grade value into 0 and 1. If the grade value is above the selected cut-off, then the indicator takes the value of 0, otherwise the indicator takes the value of 1. This eliminates the adverse effect of the higher grade assay on the estimation. From the set of cumulative distribution function graphics presented below (figure 5.3 to 5.12), we can observe a steeping up of the curve as the grade increases for both data sets. This indicates an increase in the variability of the samples as the grade increases (Hester, B.W. 1991), which is typical of a disseminated gold deposit like Troilus. On the other hand, the CDF graphics do not show any inflexion point, which signifies that only one population is present in both data sets.

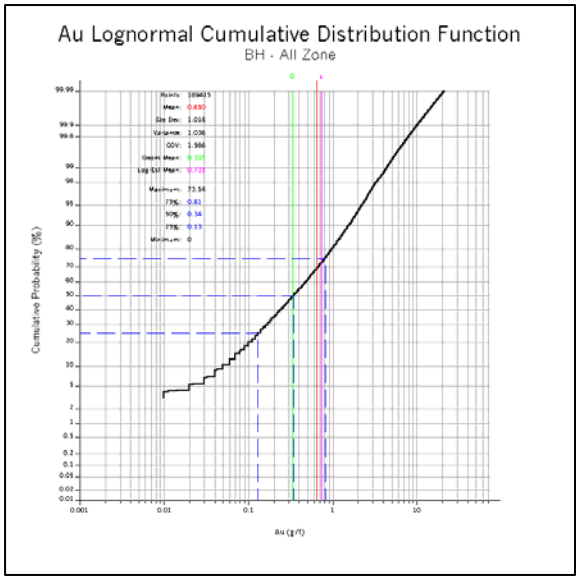

Figure 5.3 Cumulative distribution function of DDH assay for ALL zone

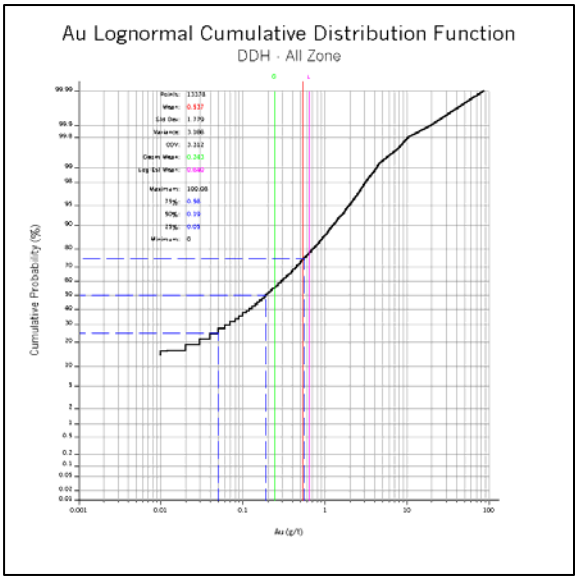

Figure 5.4 Cumulative distribution function of BH assay for ALL zone

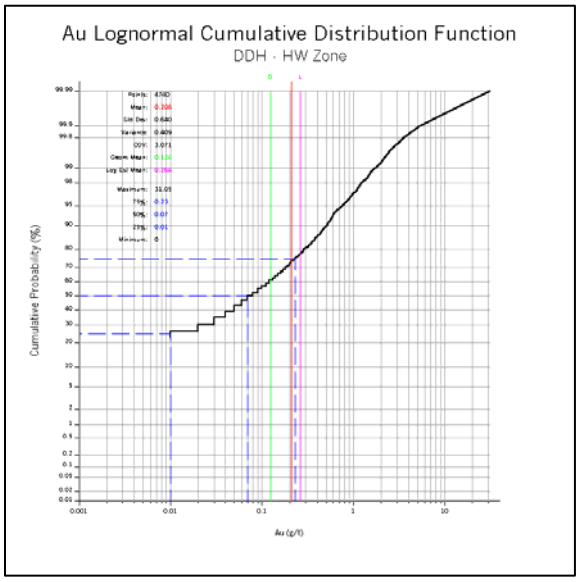

Figure 5.5 Cumulative distribution function of DDH assay for HW zone

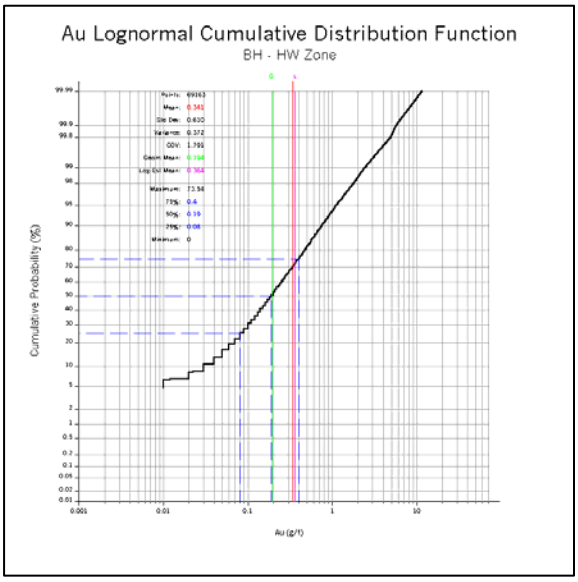

Figure 5.6 Cumulative distribution function of BH assay for HW zone

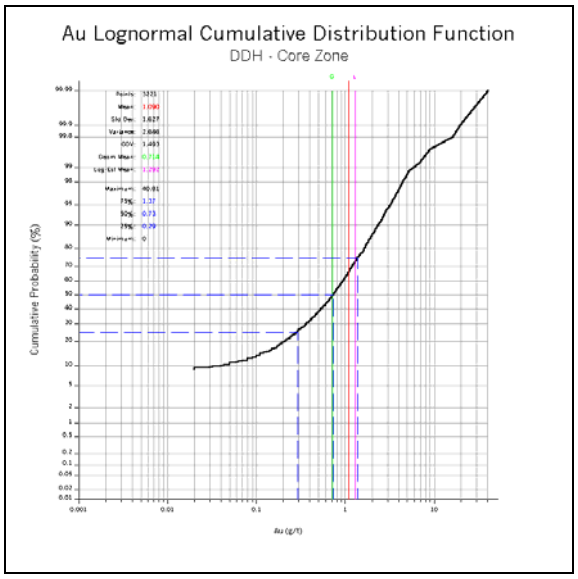

Figure 5.7 Cumulative distribution function of DDH assay for CORE zone

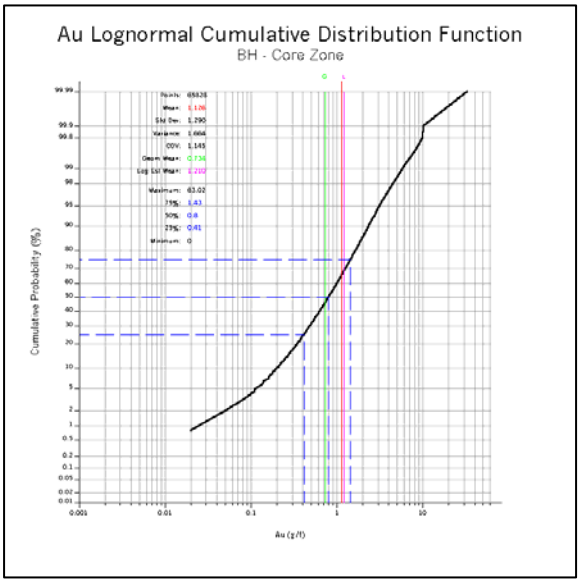

Figure 5.8 Cumulative distribution function of BH assay for CORE zone

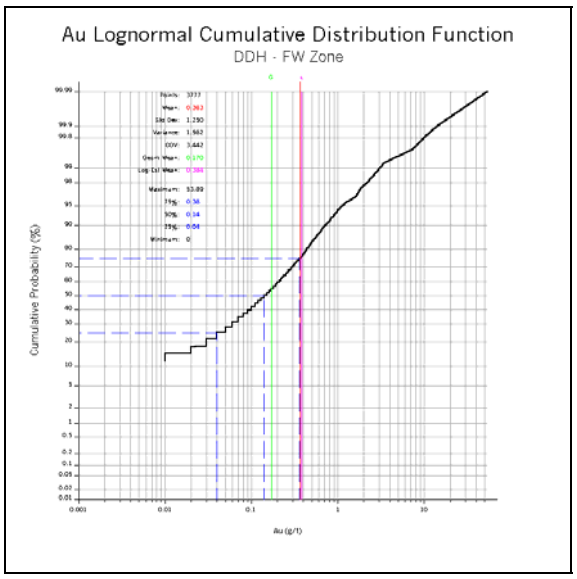

Figure 5.9 Cumulative distribution function of DDH assay for FW zone

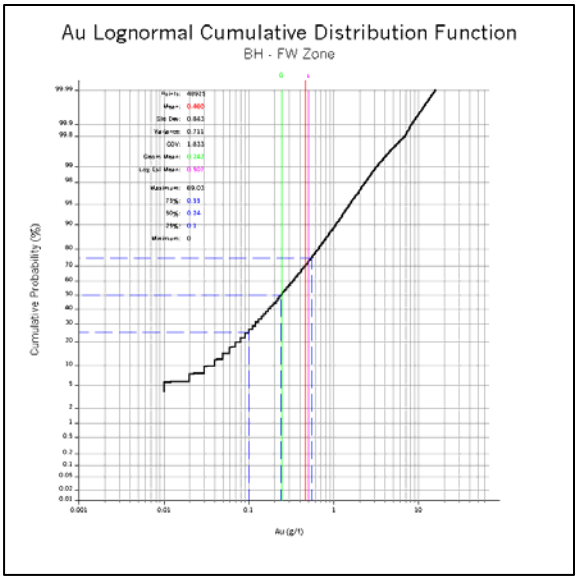

Figure 5.10 Cumulative distribution function of BH assay for FW zone

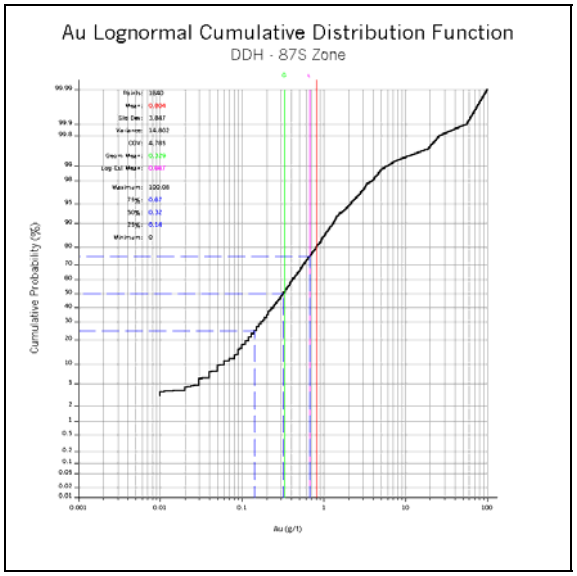

Figure 5.11 Cumulative distribution function of DDH assay for 87S zone

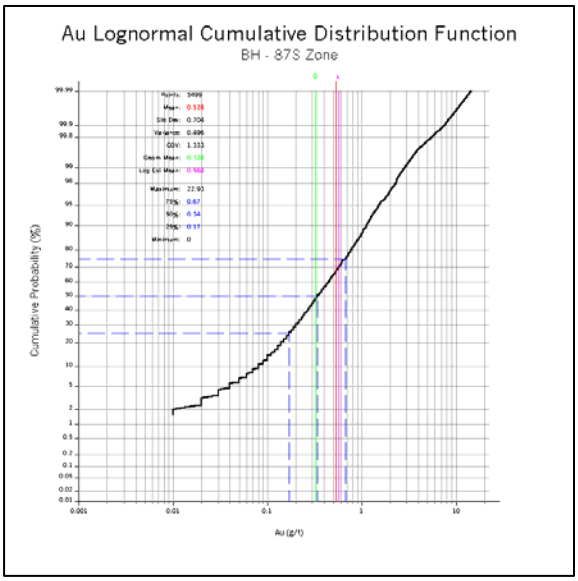

Figure 5.12 Cumulative distribution function of BH assay for 87S zone

5.3.4 Indicator cut-off

Indicator cut-offs can be selected at inflexion points of the CDF graph, at diverse percentile of the CDF distribution or at certain cut-off grades of interest. When considering the number and location of the indicator, we must ensure that enough points are within each of the intervals. Not enough points will limit the definition of the variogram and also limit the effectiveness of the estimated CDF. Since no sudden bend can be seen from the CDF above, indicators have been placed at cut-off grades of interest. The 0.5 g/t cut-off corresponds to the actual economical cut-off grade used. The 0.65 g/t cut-off corresponds to the boundary between LG3 and LG2 material category and the 0.80 g/t cut-off is the boundary between LG2 and ORE material category. Cut-off at 1.10, 1.30, 1.40, 1.50, 2.40 and 3.10 has been also used to have an accurate estimation of the higher segment of the mineralization where an important portion of the metal is contained. The following table shows the percentile at different cut-off for the DDH and BH data.

Cut-off (g/t)	HW Zone	CORE Zone	FW Zone	87S Zone
0.30	80.90	26.47	70.55	48.14
0.50	89.82	38.36	83.78	66.01
0.65	-----	45.81	88.52	74.42
0.80	-----	54.25	-----	79.97
1.30	-----	-----	-----	89.79
1.40	-----	75.71	-----	-----
2.40	-----	90.17	-----	-----

Table 5.3 Percentile at different cut-off for the DDH data

Cut-off (g/t)	HW Zone	CORE Zone	FW Zone	87S Zone
0.30	66.73	-----	57.52	45.00
0.40	-----	24.44	-----	-----
0.50	81.68	31.78	72.82	65.26
0.65	87.51	41.53	79.76	74.71
0.80	-----	50.29	-----	81.11
1.10	94.93	-----	-----	-----
1.40	-----	74.35	-----	-----
1.50	-----	-----	94.77	94.83
3.10	-----	95.01	-----	-----

Table 5.4 Percentile at different cut-off for the BH data

Depending on the cut-off, the percentile value will vary between 5 and 15 percent. For example, the percentile difference between a cut-off of 0.65 g/t and 0.80 g/t for the Core Zone of the DDH data is 8.44 (54.25-45.81), which is enough to notice a variation in the variogram. As the percentile difference between two cut-off decreases, the distinction in the variograms becomes meaningless and no advantage of carrying the extra cut-off is added.

5.3.5 Indicator variogram

Variograms have been developed for each data set and for each different cut-off. An omnidirectional variogram was first computed to establish the nugget effect in all directions. The nugget effect can be defined as the lack of continuity at small distances from a drillhole that cannot be associated to any geological variation (Deutsch, C.V. and Gringarten, E. 2001).

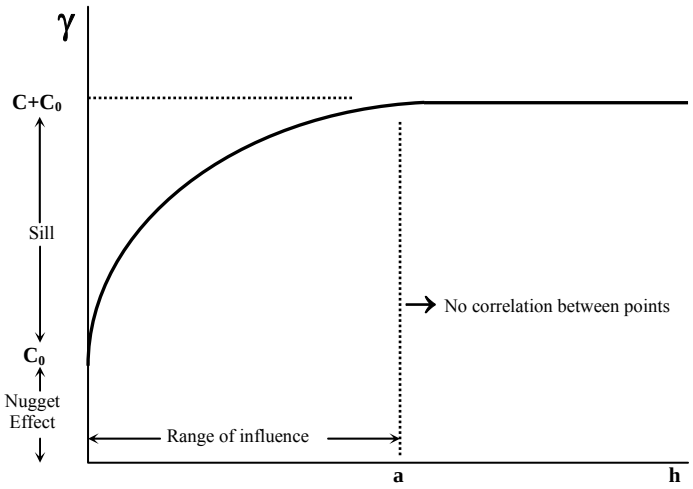

Figure 5.13 Parameters of a variogram

Variograms for major directions such as downhole, along strike and across strike have been calculated and modelled. When the output of the 3 majors direction variograms were analysed, the sill component of the three directions were different. This can be associated to a type of anisotropy called "zonal anisotropy". Two types of anisotropy exist, zonal and geometric. Zonal anisotropy can be defined as for different direction; the sill changes with direction while the range of influence remain constant (figure 5.13). This is the type of anisotropy encountered at Troilus. A geometric anisotropy will have a constant sill while the range of influence changes with directions. To work out this problem, the sill for the first and second structure has been normalized to 1 in respect to the nugget effect. Subsequent of this, averages of the normalized sill for the first and second structure were taken. The complete set of parameters obtained from the variography analysis of the DDH and BH data is included in tables 5.5 and 5.6.

Zone	Cut-off	Anisotropy (az., dip, plunge)	Nugget Effect	1st Structure			2nd Structure		
				Component	Sill	Anisotropy (X, Y, Z)	Component	Sill	Anisotropy (X, Y, Z)
HW	0.30	-10, -60, 0	0.628	Spherical	0.290	77, 11, 16	Spherical	0.082	129, 94, 39
HW	0.50	-15, -60, 0	0.729	Spherical	0.153	12, 11, 9	Spherical	0.117	118, 0, 25
CORE	0.30	-20, -65, 0	0.497	Spherical	0.301	20, 22, 23	Spherical	0.202	87, 78, 71
CORE	0.50	-10, -65, 0	0.223	Spherical	0.431	9, 11, 7	Exponential	0.347	18, 34, 17
CORE	0.65	-10, -60, 0	0.212	Spherical	0.531	11, 11, 10	Exponential	0.257	25, 38, 16
CORE	0.80	-10, -60, 0	0.147	Spherical	0.668	11, 12, 11	Exponential	0.185	42, 39, 41
CORE	1.40	-15, -60, 0	0.648	Spherical	0.207	14, 11, 14	Spherical	0.145	98, 127, 0
CORE	2.40	-10, -70, 0	0.812	Spherical	0.114	63, 47, 16	Spherical	0.074	0, 94, 28
FW	0.30	-10, -65, 0	0.680	Spherical	0.165	64, 39, 15	Spherical	0.155	114, 107, 55
FW	0.50	-10, -60, 0	0.725	Spherical	0.203	10, 35, 14	Spherical	0.072	122, 0, 51
FW	0.65	-10, -65, 0	0.721	Spherical	0.167	70, 35, 15	Spherical	0.111	94, 67, 49
87S	0.30	-20, -65, 0	0.722	Spherical	0.111	47, 36, 18	Exponential	0.167	95, 151, 28
87S	0.50	-20, -65, 0	0.734	Spherical	0.164	65, 38, 39	Spherical	0.102	100, 102, 0
87S	0.65	-20, -65, 0	0.747	Spherical	0.253	80, 37, 18	-----	-----	-----
87S	0.80	-20, -65, 0	0.766	Spherical	0.234	67, 35, 23	-----	-----	-----
87S	1.30	90, 90, 90	0.735	Spherical	0.265	41, 41, 41	-----	-----	-----

Table 5.5 Variogram modelization by zone for the DDH

Zone	Cut-off	Anisotropy (az., dip, plunge)	Nugget Effect	1st Structure			2nd Structure		
				Component	Sill	Anisotropy (X, Y, Z)	Component	Sill	Anisotropy (X, Y, Z)
HW	0.30	-20, -60, 0	0.635	Spherical	0.089	28, 30, 12	Exponential	0.276	82, 81, 81
HW	0.50	-20, -60, 0	0.824	Exponential	0.176	46, 45, 6	-----	-----	-----
HW	0.65	-20, -60, 0	0.876	Exponential	0.124	25, 44, 9	-----	-----	-----
HW	1.10	90, 90, 90	0.965	Spherical	0.035	21, 21, 21	-----	-----	-----
CORE	0.40	-10, -60, 0	0.708	Exponential	0.252	34, 31, 9	Exponential	0.040	0, 0, 58
CORE	0.50	-10, -60, 0	0.695	Exponential	0.305	39, 35, 10	-----	-----	-----
CORE	0.65	-10, -60, 0	0.672	Exponential	0.328	39, 35, 8	-----	-----	-----
CORE	0.80	-10, -60, 0	0.655	Exponential	0.345	34, 37, 7	-----	-----	-----
CORE	1.40	-20, -60, 0	0.740	Exponential	0.260	77, 37, 7	-----	-----	-----
CORE	3.10	-20, -60, 0	0.949	Spherical	0.051	0, 48, 11	-----	-----	-----
FW	0.30	-10, -60, 0	0.645	Exponential	0.355	56, 42, 8	-----	-----	-----
FW	0.50	-10, -60, 0	0.681	Exponential	0.319	72, 59, 8	-----	-----	-----
FW	0.65	-10, -60, 0	0.690	Exponential	0.310	74, 48, 9	-----	-----	-----
FW	1.50	-10, -60, 0	0.773	Exponential	0.227	40, 54, 15	-----	-----	-----
87S	0.30	-20, -60, 0	0.742	Spherical	0.105	30, 50, 19	Spherical	0.153	0, 80, 33
87S	0.50	-20, -60, 0	0.693	Spherical	0.307	30, 65, 30	-----	-----	-----
87S	0.65	-20, -60, 0	0.735	Spherical	0.265	30, 61, 24	-----	-----	-----
87S	0.80	-20, -60, 0	0.754	Spherical	0.246	30, 61, 25	-----	-----	-----
87S	1.50	-20, -60, 0	0.704	Spherical	0.296	30, 55, 25	-----	-----	-----

Table 5.6 Variogram modelization by zone for the BH

From the two tables above, we can analyse the variability of the samples by looking at the percentage of the nugget effect. The percentage of nugget effect related to the sill value will give a good indication of the variability in the results. For the DDH data, the nugget effect of the main zone (CORE) is about 40% of the sill value and about 70% in the three other zones (FW, HW, 87S). On the other hand, the variability of the BH data shows no major difference in the nugget effect amongst the zones and is generally around 70% of the sill value. It can also be noted from the table that only a spherical model is used to model the first structure of the DDH variogram, where in the case of the BH data either a spherical or an exponential model has been used. Figure 5.14 to 5.21 present variograms for the CORE zone for the DDH and BH data. As it can be seen, both sets of data show well-defined semi-

variograms at 0.5 g/t cut-off. Often a concern when dealing with exploration data, the number of pairs used in each lag seems to be enough to generate variograms suitable for modelling. This somehow indicates that the lag distance has been consciously chosen. In general, no major anomalies in the shape of the variograms are present for both sets of data. The only glimpse could be the variograms for the direction along strike of the FW zone (DDH) where proportional effect seems to take place. This seems to be an odd behaviour, since proportional effects are associated with preferential sampling of high values. For those cases, the variograms have been modelled in such a way that the more representatives lag of the variogram would be seized. The complete set of variograms for each data set and for each geological zone can be seen in appendices B and C.

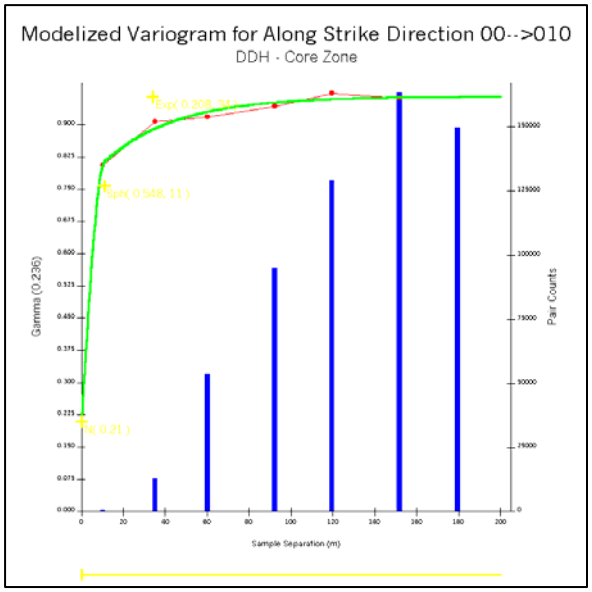

Figure 5.14 Along strike variogram at 0.5 g/t cut-off for DDH CORE zone

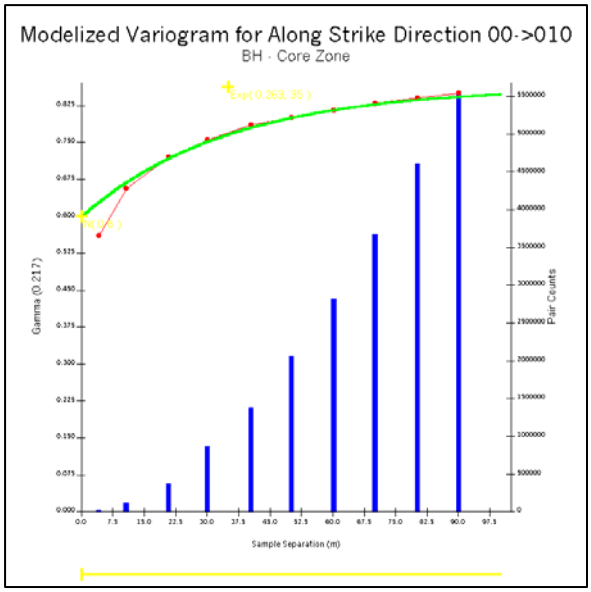

Figure 5.15 Along strike variogram at 0.5 g/t cut-off for BH CORE zone

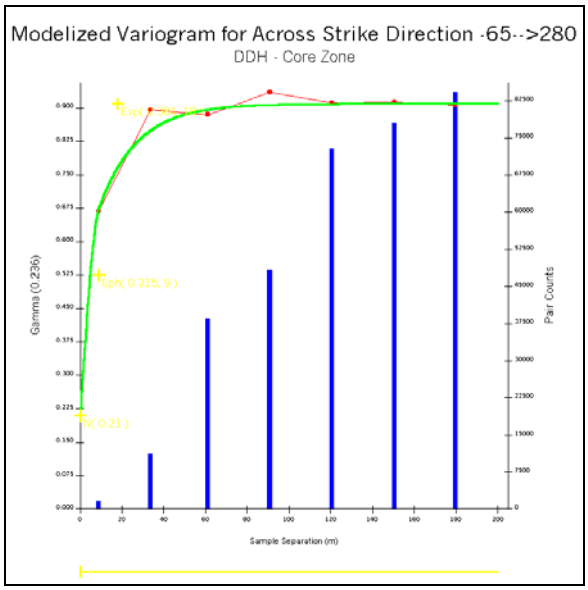

Figure 5.16 Across strike variogram at 0.5 g/t cut-off for DDH CORE zone

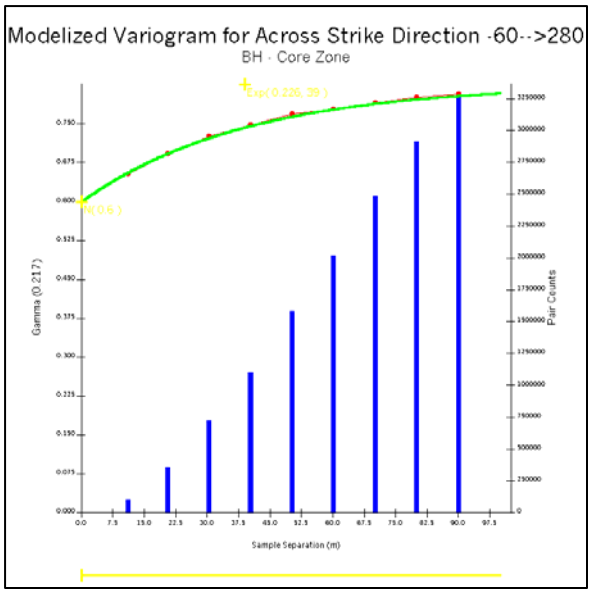

Figure 5.17 Across strike variogram at 0.5 g/t cut-off for BH CORE zone

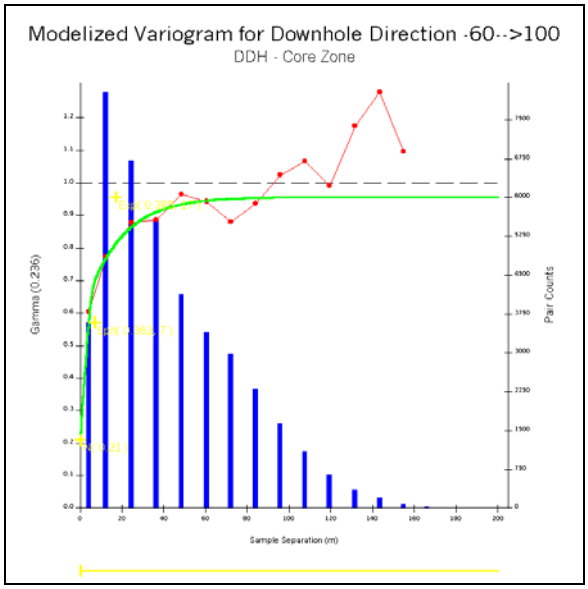

Figure 5.18 Downhole variogram at 0.5 g/t cut-off for DDH CORE zone

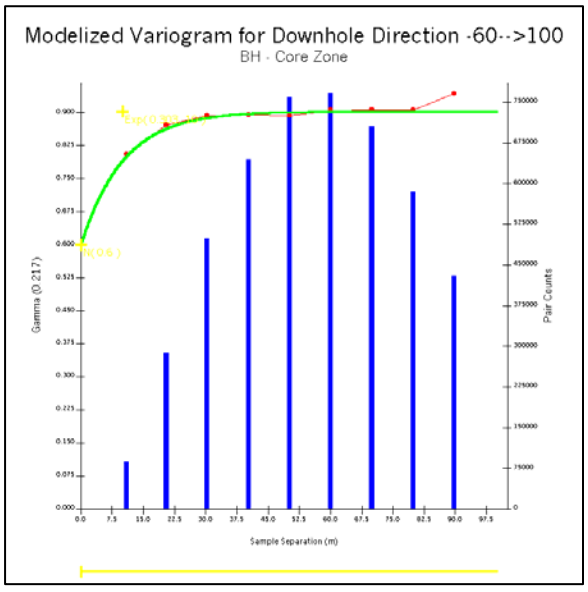

Figure 5.19 Downhole variogram at 0.5 g/t cut-off for BH CORE zone

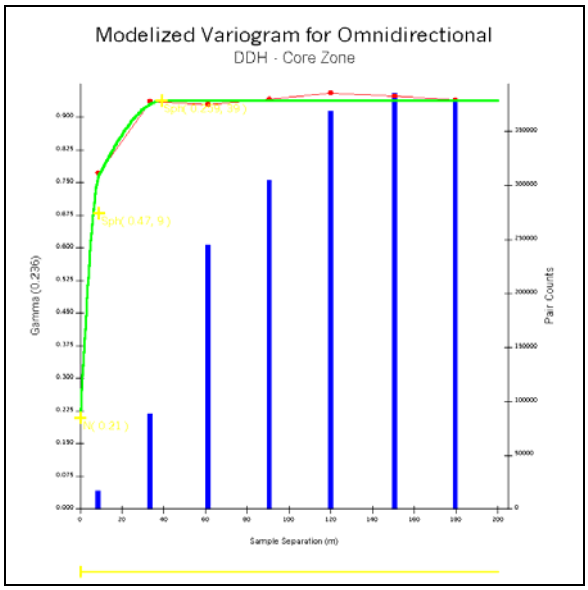

Figure 5.20 Omnidirectional variogram at 0.5 g/t cut-off for DDH CORE zone

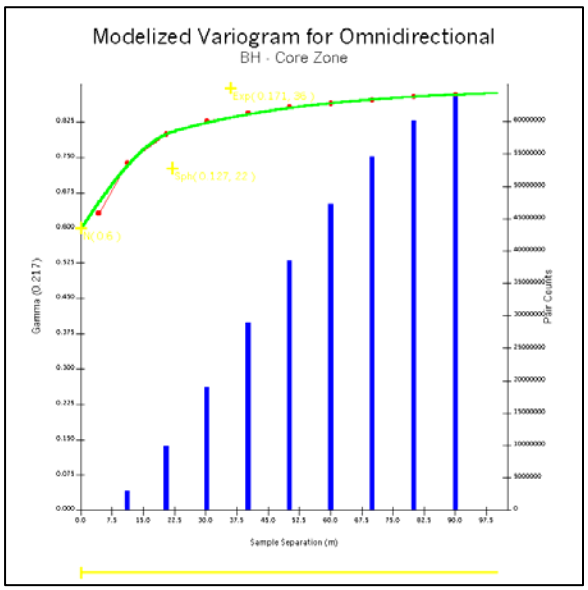

Figure 5.21 Omnidirectional variogram at 0.5 g/t cut-off for BH CORE zone

5.4 Conclusion

Variograms have been generated on indicator transformed assay composites of the DDH dataset and on assays of the BH dataset. Indicator cut-offs have been placed at different gold cut-off grades in order to capture different patterns of continuity and also to generate practical variograms, which was not the case when using untransformed data. Indicator variograms have been generated in the majors directions i.e. along strike, across strike and downhole. An omnidirectional variogram was used to derive the variability at a short scale (nugget effect). The DDH assays composites have 40% to 70% of their variability associated to nugget effect compared to 70% for the BH dataset. In the case of the DDH dataset, indicator variograms have been modelized using a spherical model for the first structure and a spherical or exponential model for the second structure. As for the BH dataset, indicator variograms have been modelized using either a spherical or an exponential model for both structures.

CHAPTER 6

Reserve Estimation

6.1 Introduction

Having established the spatial continuity of the mineralization through variography, the next step is to estimate the grade of the deposit at unsampled locations. This can be achieved by using interpolation method such as inverse distance, simple kriging, ordinary kriging, indicator kriging, logarithmic kriging, cokriging, probability kriging and so on. Those methods can be divided into two different groups, linear and non-linear interpolator (Guibal, D. and Vann, J. 1998). Linear method such as ordinary kriging gives an estimate of the grade that is based solely on the location of the data. On the other hand, non-linear methods such as indicator kriging give not only an estimate of the grade, but also the local uncertainty associated with the estimates. In addition, the non-linear method produces estimates that are a function of the location of the data as well as a function of the grade distribution.

6.2 Interpolation method

6.2.1 Selection method

When considering the choice of an interpolation method, some basic criteria need to be looked at to determine if the method is appropriate or not. Those criteria include: type of deposit (porphyry, massive sulphide, epithermal)

- variability of the mineralization (nugget effect, outliers)
- continuity of mineralization (metres, kilometres)
- type of contact (hard, soft)
- number of sample for interpolation (enough data within each zone)
- advancement of the project (early exploration stage, infill drilling)
- scope of the project (scoping study, feasibility study)
- timeframe for the study (week, month)

6.2.2 Method selected

Indicator kriging interpolation method was chosen based on the previous selection criteria and also on the general aim of the study. In addition, other interpolation methods such as inverse distance, ordinary kriging and logarithmic kriging have been used in the past at Troilus with mitigated success.

6.3 Indicator kriging

6.3.1 Pros

Key advantages of using kriging based algorithm over traditional methods such as inverse distance and polygonal are as follows:

- data declustering through the kriging matrix
- variogram used to weight sample influence
- unbiasedness of the estimator (error mean is zero)
- error variance minimized

In the present study, ordinary kriging was chosen. The major benefit of using ordinary kriging over simple kriging lays in the way each method deals with the concept of stationarity. In the case of simple kriging, the mean has to be known and constant over the whole area under study. On the other hand, ordinary kriging allows local fluctuation of the mean by restricting the domain of stationarity to the dimension of the search ellipsoid. Practically, this means that estimates produced by using ordinary kriging will better follow the fluctuation of the data.

Indicator kriging has the advantage of generating different patterns of continuity for different directions at different cut-offs, enhancing the definition of the variogram to be used into the interpolation. It also has the benefit of assessing the local uncertainty of the estimates, which can be used for risk analysis and decision-making. With methods such as ordinary and simple kriging, uncertainty comes from the error variance. Using the kriging error variance can be misleading, since the variance does not depend on the data value, but on the data location and on the variogram used (Atkinson, P.M. and Lloyd, C.D. 1999).

Therefore, for an identical set of data using the same variogram, the kriging error variance generated would be the same even if the location of each data set were different (Goovaerts, P. 1997).

One other advantage comes from the way indicator kriging handles data. By dividing the data set into cut-off bins, more information is generated, resulting in an increase of the cumulative distribution function resolution. In addition, indicator kriging gives a grade tonnage-curve on a block-by-block basis and a probability of realization associated to each cut-off. The resulting block model, often referred as "recoverable reserve model", is a model which increases the accuracy of predicting the tonnage and grade above a cut-off and has also more flexibility built-in it that helps the mine planner in his planning process.

6.3.2 Cons

On the downside, indicator kriging is a tedious and time consuming method that involves the modelling of a large number of variograms depending on the number of cut-offs considered. It is also known to have problems of order relation deviation related to the probabilities of the cumulative distribution function (Goovaerts, P. 1997). Although, most geostatistical software have a routine to correct this problem; a good practice would be to make sure that enough data are contained within each cut-off bin and that no negative weight is permitted.

6.3.3 Implementation

Indicator kriging discretizes the gold grade into 0 and 1, depending on the cut-off threshold. If the grade value is above the selected cut-off, then the indicator takes the value of 0, otherwise the indicator takes the value of 1. After the discretization of the grade, coded values are interpolated using ordinary kriging. From figure 6.1 below, it can be observed that different probabilities of occurring are associated to each of the bin (cut-off). Each bin will be given a different probability based on the location of their sample relative to the block and based on the respective variogram of the samples. This probability is in fact the weight coming from solving the weighting matrix of the kriging process. The bin average

grade is calculated by discretizing the sample falling in each of the different classes of grade and by taking their average.

This practice is appropriate when dealing with classes that have a distribution of grades nearly linear (Blackney, P.C.J. and Glacken, I.M. 1998). But when dealing with the upper grade classes of a positively skewed data set, taking the average of the class will result in an overestimation. In this particular case, it is recommended to use the median of the class. Multiplying the bin average or median grade by the bin probability will give the grade contribution of that bin to the overall block grade. By adding all the grade contributions of every bin, we finally get the block grade. Besides having the probability and average grade for each of the bins, we can develop a "Cumulative Distribution Function" graph. This graph can also be modified into a "Grade Tonnage Curve" by multiplying the probability by the overall tonnage of the block. For the purpose of the current project, a recoverable reserve model based on DDH data and a grade control model based on BH data were created.

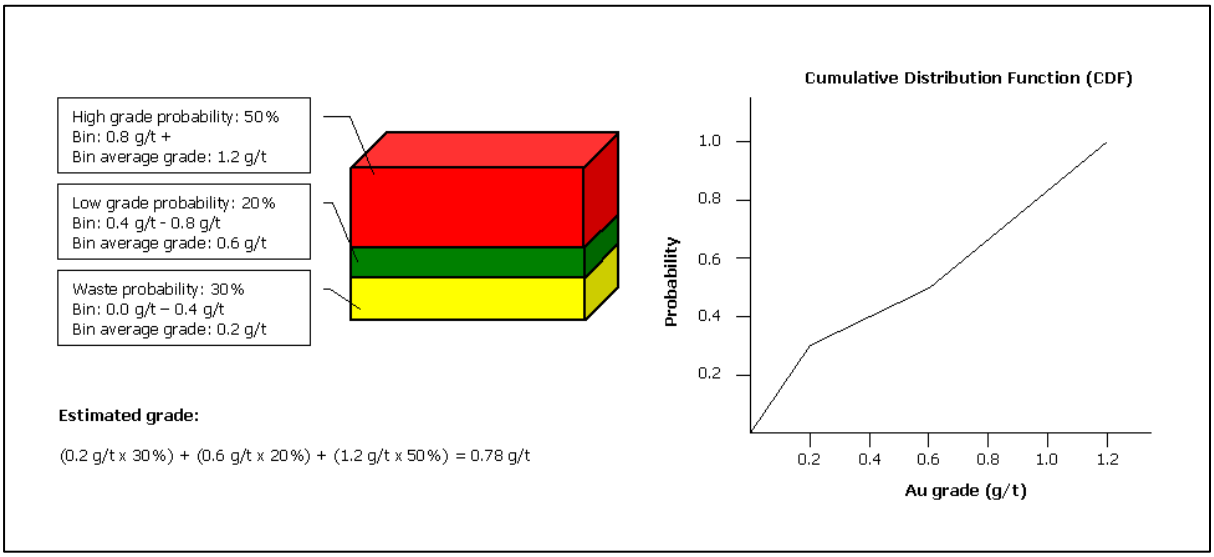

Figure 6.1 Calculation of the estimated grade based on indicator kriging

6.4 Block size

The block size used was set at 10m x 10m x 10m for both models. Block size depends on operational constraints such as (Zhang, S. 1998):

- bench height
- size of loading equipment
- minimum size of mineable packets
- spacing of the exploration holes and of production holes

6.5 Block model

The recoverable reserve model was produced based on 13,378 composited samples of NQ size (47.6 mm) at an average grid spacing of 25m x 25m, whereas the grade control model was based on 189,415 samples of 171 mm size at an average grid spacing of 5.1m x 5.9m. The aim of creating the grade control model was to compare its estimates to the estimates of the recoverable reserve model and to minimize the discrepancy between the two models. Discrepancy can be related to the difference in the number of samples available for the grade interpolation and to the different size of support of the DDH and BH data. The information generated from those two block models were the probabilities, grades, variances and anisotropic distances to the closest point for every zone and every block in the model. Also, a script was run in order to sum all the different block models of every zone into three centralized block model for grades, variances and anisotropic distance to closest point. Once a kriging run was finished, a reconciliation of the recoverable reserve and grade control models was carried out against data from the mine production and correction of different kriging parameters was made to improve the estimates.

6.6 Reconciliation

6.6.1 Data provided

Data provided by Troilus was in the form of month end production reconciliation reports and in Gemcom 3D polygons representing mined packet. The month end production reconciliation covered the period of January 1997 to December 2000 with missing data for the period of June 1998 to August 1999 and for the period of January 2001 to February 2002. The mined packet polygon covered the whole production period from January 1997 to February 2002. The option of comparing the block model estimates to the month end production reconciliation was dropped due to the lack of information and it was decided to only use the mined packet for the purpose of reconciliation.

6.6.2 Mineable packet

The practice of creating mineable packet was under the responsibility of the grade control geologist (figure 6.2). Mineable packets are created based on the following constraints:

- geometry of the orebody
- selective mining unit (SMU) of 10 m in E-W and 15 m in N-S
- displacement due to blast movement
- blasting along strike (north-south)
- mucking direction from west to east
- dilution from surrounding packet

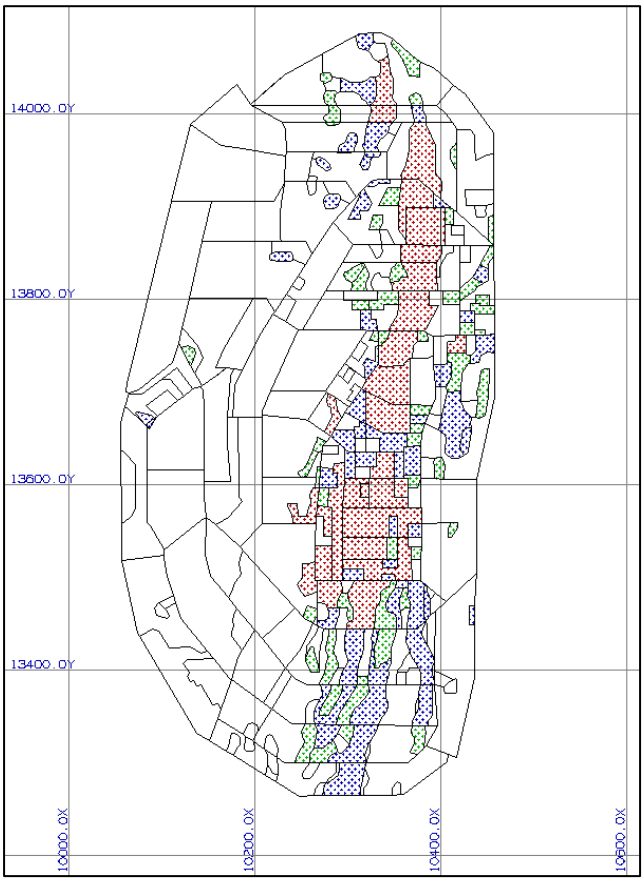

Figure 6.2 Bench 5290 - Mined packet

One problem arising from the use of the mined packet to compare the estimates was the grade. In fact, no grades were attached to the mined packet and only the material type was available to identify the packet. However, the small difference in the grade of each material category used at Troilus made their utilization possible. Following is the material category used at Troilus:

- 1.00 + High Grade (HG)
- 0.80 - 1.00 Ore (ORE)
- 0.64 - 0.80 Low Grade 2 (LG2)
- 0.58 - 0.64 Low Grade 3 (LG3)
- 0.50 - 0.58 Low Grade 1 (LG1)
- 0.00 - 0.50 Waste (WST)
- 6.6.3 Methodology and results

The new set of envelopes created before was used to report reserves. Within the packet, materials for every grade category were divided for each zone. For example, all the mined packets for the bench 5290 belonging to the LG1 grade category were selected and reserves were calculated for each of the zone. As for the grade control model, the new set of envelopes based on DDH was also used, even if they were not as well defined as if based on BH data. Given the large amount of BH falling within the DDH envelope, the difference did not warrant the creation of a second set of envelopes based solely on BH. Material from the grade control model was reported for every zone. Reserves were also reported by zone for the recoverable reserve model.

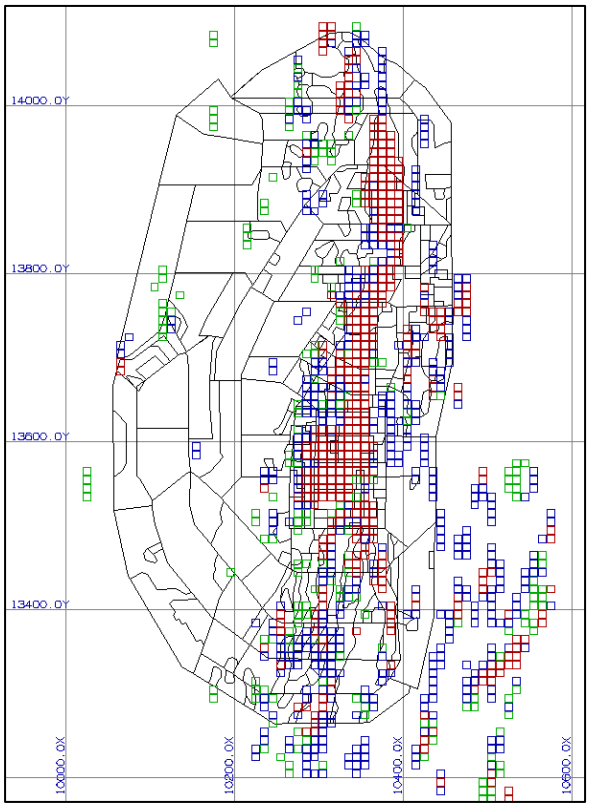

Figure 6.3 Bench 5290 – Recoverable reserve

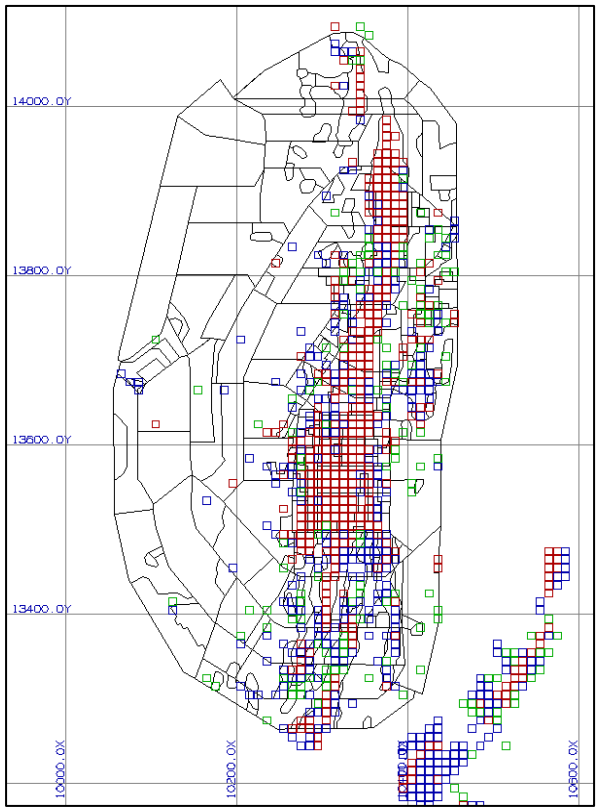

Figure 6.4 Bench 5290 – Grade control

Reconciliation of the two block models against the mined packet have been realized on a bench by bench basis to avoid any problems related to the size of support (figure 6.3, 6.4).

This is especially important for the estimates coming from the recoverable reserve model, which are based on sparse DDH data. As the level of support increase, the accuracy of the recoverable reserve estimates would increase as well. Again, the aim of a resource block model is not to represent the exact location of an ore block with respect to reality, but to give a good approximation of the tonnes and grade of a particular bench. In order for the tonnage estimates of the recoverable reserve and grade control to represent as much as possible the mined packet tonnage for every grade category, kriging parameters such as the range of influence of high grade assay had to be fine tuned. For grade reconciliation, the gold grade of the grade control model was used and was a point of reference for the recoverable reserve model. This can be explained by the fact that the grade control model has been interpolated with the same BH data used to create the mineable packet.

Zone	Grade Category	Grade Range	Mined Packet (t)	Grade Control (t)	Recoverable Reserve (t)	Grade Control (g/t)	Recoverable Reserve (g/t)	Grade Control (oz)	Recoverable Reserve (oz)
ALL	HG	1.00+	12,046,066	11,998,945	11,658,061	1.61	1.54	620,178	577,006
ALL	ORE	0.80-1.00	3,816,839	5,377,433	4,482,894	0.90	0.88	155,624	127,351
ALL	LG2	0.64-0.80	3,194,697	4,560,108	5,673,478	0.71	0.72	103,907	131,165
ALL	LG1-LG3	0.50-0.64	5,382,220	4,776,340	4,224,592	0.56	0.55	86,387	75,309
ALL	TOTAL	0.50+	24,439,822	26,712,826	26,039,025	1.12	1.09	966,097	910,832
HW	HG	1.00+	417,605	913,235	368,929	1.34	1.09	39,205	12,929
HW	ORE	0.80-1.00	468,241	1,655,942	484,922	0.88	0.85	46,713	13,315
HW	LG2	0.64-0.80	525,967	455,664	906,482	0.69	0.75	10,108	21,776
HW	LG1-LG3	0.50-0.64	1,453,919	949,071	2,123,378	0.59	0.54	17,948	37,008
HW	TOTAL	0.50+	2,865,732	3,973,912	3,883,711	0.89	0.68	113,975	85,028
CORE	HG	1.00+	9,731,342	9,332,820	9,586,450	1.67	1.59	500,454	489,666
CORE	ORE	0.80-1.00	2,350,733	2,618,167	2,897,938	0.90	0.89	75,602	83,118
CORE	LG2	0.64-0.80	1,586,212	2,491,266	1,928,959	0.72	0.72	57,372	44,855
CORE	LG1-LG3	0.50-0.64	2,086,583	1,968,948	1,713,587	0.57	0.57	35,904	31,366
CORE	TOTAL	0.50+	15,754,870	16,411,201	16,126,934	1.27	1.25	669,332	649,004
FW	HG	1.00+	1,680,726	1,529,732	1,426,375	1.45	1.36	71,172	62,573
FW	ORE	0.80-1.00	869,337	928,641	936,778	0.95	0.87	28,364	26,142
FW	LG2	0.64-0.80	885,847	1,422,395	2,697,806	0.70	0.71	32,039	61,293
FW	LG1-LG3	0.50-0.64	1,468,433	1,645,724	161,526	0.54	0.56	28,610	2,930
FW	TOTAL	0.50+	4,904,343	5,526,492	5,222,485	0.90	0.91	160,185	152,938
87S	HG	1.00+	216,393	223,158	276,307	1.30	1.33	9,347	11,838
87S	ORE	0.80-1.00	128,528	174,683	163,256	0.88	0.91	4,945	4,777
87S	LG2	0.64-0.80	196,671	190,783	140,231	0.72	0.72	4,388	3,242
87S	LG1-LG3	0.50-0.64	373,285	212,597	226,101	0.57	0.55	3,925	4,005
87S	TOTAL	0.50+	914,877	801,221	805,895	0.88	0.92	22,605	23,862

Table 6.1 Reserve by zone for mined packet - recoverable reserve - grade control model

The material category LG1 and LG3 have been merged together. This decision was based on the fact that it was very difficult for both block models to properly estimate the tonnage for those two material categories due to the very small difference between them (0.08 g/t). Results of the reconciliation by zone and by bench can be consulted in tables 6.1 and 6.2. When total tonnage for both are compared to the mined packet, a slight overestimation in

the order of 9.3% (+2.27Mt) and 6.5% (+1.60Mt) takes place for the grade control and recoverable reserves respectively. The bulk of the discrepancy comes mainly from the HW zone where the tonnage is overestimated by 38.7% (+1.11Mt) for the grade control model and by 35.5% (+1.02Mt) for the recoverable reserve model. This overestimation of the tonnage is also reflected in the reserves by bench above 0.5 g/t, where the first four benches (5350-5340-5330-5320) are overestimated by 19.7% (+1.64Mt) for the grade control model and by 12.7% (+1.06Mt) for the recoverable reserve model.

Bench	Mined Packet (t)	Grade Control (t)	Recoverable Reserve (t)	Grade Control (g/t)	Recoverable Reserve (g/t)	Grade Control (oz)	Recoverable Reserve (oz)
5350	2,357,049	2,527,625	2,043,566	1.10	1.05	89,559	69,052
5340	2,082,042	2,664,913	2,479,324	1.13	1.04	96,945	82,979
5330	1,838,616	2,512,734	2,465,298	1.07	1.07	86,151	85,074
5320	2,055,784	2,271,919	2,403,147	1.11	1.06	81,365	82,052
5310	1,913,072	2,167,004	2,081,999	1.10	1.07	76,596	71,945
5300	1,841,940	1,984,531	2,055,339	1.09	1.08	69,591	71,417
5290	1,841,163	1,859,361	1,884,812	1.13	1.09	67,654	66,166
5260	1,792,522	1,732,634	1,672,214	1.17	1.03	64,929	55,593
5250	1,688,370	1,677,927	1,686,758	1.09	1.04	59,052	56,334
5240	709,896	692,672	731,107	1.02	0.99	22,739	23,310
5230	809,061	1,289,260	1,161,841	1.18	1.11	48,778	41,581
5220	906,788	909,252	952,186	1.05	1.11	30,595	33,924
5210	1,154,537	1,108,866	1,115,790	1.22	1.20	43,418	43,028
5200	1,065,009	1,039,094	1,061,429	1.18	1.20	39,468	40,996
5190	890,500	899,212	888,304	1.18	1.16	34,041	33,231
5180	832,550	819,400	754,130	1.24	1.21	32,713	29,307
5170	660,923	556,422	601,781	1.26	1.28	22,504	24,846
TOTAL	24,439,822	26,712,826	26,039,025	1.12	1.09	966,097	910,832

Table 6.2 Reserve above 0.5 g/t by bench for mined packet – recoverable reserve - grade control model

Grade comparison is carried out directly between the recoverable reserve model and the grade control model. As mentioned previously, this can be explained by the fact that the grade control model has been interpolated with the same BH data used to create the mineable packet. Overall, the contained ounces are underestimated by 5.7% (-55,265oz). The bulk of the discrepancy comes from the HW zone where the recoverable reserve model underestimates the ounces by 25.4% (-28,947oz). The relative discrepancies from the other zones are 20,328oz (-3.0%) for the CORE, 7,247oz (-4.5%) for the FW and 1,257oz (+5.6%) for the 87S zone.

However, attention should be paid towards the weight of each zone on the global figures. The CORE zone holds the vast majority of the ore tonnage and contained ounces with 61.9% and 71.3% respectively. On the other hand, the problematic HW zone represents

only about 14.9% and 9.3% of the ore tonnes and gold ounces. Finally, the FW zone with 20.1% and 16.8% and the 87S zone with 5.6% and 3.1% hold the remaining ore tonnage and contained ounces.

6.6.4 Discussion and analysis

One of the reasons that might explain the cause of this trend is the aggressive grade control strategy exercised by the geology department during the first 3 years of operation. The grade assigned to the mineable packet during that period was derived from the lowest grade value of three different methods of interpolation. The first and second methods were straight averages of the gold assays over two 5m bench and three 5m bench intervals respectively. The third method involved kriging of gold assays over four 5m benches. This methodology has the adverse impact of sometimes misclassifying ore as waste. A low grade zone with a high degree of variability, such as the HW zone with a coefficient of variation of 1.79, will result in a higher degree of variability in the results of the three grade interpolation methods. Therefore, material categorized as LG1 with one of the methods, could actually be categorized as WST by taking the lowest grade value of the three methods. Dilution is another factor that could have contributed to the discrepancy between the packet and the estimates. Once blast movement, grade continuity and mineability of the packet have been analysed, it is possible that a low grade packet would have to be downgraded to a waste packet due to the uncertainty of the recovered grade of the packet. An additional cause of discrepancy between estimates could be the fact that no dilution has been built into the estimates. One particular case where dilution would have made a difference in the estimates is in the case of a single ore block surrounded by waste block. In reality, the grade of this ore block would be diluted to the same grade as the surrounding waste block and categorized as waste, whereas in the present estimates this block is still considered an ore block. When the recoverable reserve model is compared to the grade control model, it can be seen that in general the prediction of the tonnage and the grade are very close. Overall, the recoverable reserve underestimates the tonnage by 2.5% (-673,801 t) and the in-situ once by 5.7% (-55,265 oz). Discrepancy of the in-situ ounces can be attributed to the HW zone, where half (-28,947 oz) of the shortfall comes from. The

average grade of this zone above 0.5 g/t cut-off is 0.89 g/t for the grade control model, compared to 0.68 g/t for the recoverable reserve model. On the other hand, the reserves by bench show a good correlation between the two models, which implies that the overall goal of the resource model has been honoured.

6.7 Cross validation

6.7.1 Introduction

The cross validation method is another tool to calibrate the estimated values versus the true values. Unlike block estimation, cross validation is carried out on a sample support size. By definition, a cross validation study tests the semi-variogram model used by the interpolation method by removing a sample from the sample data set and by estimating its value with the remaining data. It involves the same procedure as a regular resource estimate study, weights of the surrounding samples are based on indicator variograms and the estimated value is calculated by indicator kriging. This is done for every sample contained within each zone for the DDH and BH data set. The estimated results can be compared to the original sample value and different variogram types and weighting techniques can be assessed to minimize the discrepancy.

6.7.2 Limitation

The limitation associated to a cross validation study comes from the representativeness of the estimation, which is concentrated at sample locations. In such circumstances, the results do not reflect the actual performance of the estimates at unsampled locations. Table 6.3 and 6.4 present the results of the cross validation study for the DDH and BH data set. Looking at the results, we can notice the influence of kriging on the distribution of estimates. The spread of the estimate distribution is reduced compared to the sample distribution, which can be attributed to the smoothing effect of kriging. This smoothing effect has also an impact on the ability of properly estimating the number of samples above a certain cut-off. When sample and estimates are compared, we can clearly see an overestimation of the number of samples above the 0.5 g/t cut-off by the estimated distribution. This can, in part, be related to the high nugget effect of the mineralization encountered in the Troilus orebody

and again, to the smoothing of the higher grade sample toward the lower grade sample. On the other hand, the grade of the estimates above the 0.5 g/t cut-off is always lower than the one from the sample distribution, which in the end should almost produce the same number of ounces.

	HW		CORE		FW		87S	
Statistics	Sample	Estimate	Sample	Estimate	Sample	Estimate	Sample	Estimate
Number of samples	4,739	4,739	3,221	3,221	3,777	3,777	1,640	1,640
Maximum (g/t)	31.05	12.69	40.81	20.17	53.89	20.37	100.08	52.16
Minimum (g/t)	0.00	0.00	0.00	0.00	0.00	0.00	0.00	0.00
Mean	0.21	0.21	1.09	1.09	0.36	0.36	0.80	0.82
Quartile 1 (25%)	0.01	0.03	0.29	0.48	0.04	0.09	0.14	0.23
Median	0.07	0.11	0.73	0.90	0.14	0.21	0.32	0.41
Quartile 3 (75%)	0.23	0.26	1.37	1.40	0.36	0.40	0.67	0.74
Standard deviation	0.64	0.41	1.63	1.05	1.25	0.76	3.85	2.63
Variance	0.41	0.17	2.65	1.10	1.56	0.58	14.80	6.92
Coefficient of variation	3.07	2.00	1.49	0.96	3.44	2.09	4.79	3.21
Number of samples > 0.5 g/t	494	467	2,002	2,400	634	697	566	669
Mean > 0.5 g/t	1.09	0.91	1.63	1.38	1.45	1.18	1.94	1.63

Table 6.3 Cross validation statistics for DDH data set

	HW		CORE		FW		87S	
Statistics	Sample	Estimate	Sample	Estimate	Sample	Estimate	Sample	Estimate
Number of samples	68,451	68,451	65,129	65,129	48,136	48,136	5,499	5,499
Maximum (g/t)	73.54	38.58	63.02	20.45	69.03	34.43	22.93	6.68
Minimum (g/t)	0.00	0.00	0.00	0.00	0.00	0.00	0.00	0.01
Mean	0.34	0.34	1.13	1.13	0.46	0.46	0.53	0.53
Quartile 1 (25%)	0.08	0.11	0.41	0.56	0.10	0.13	0.17	0.27
Median	0.19	0.22	0.80	0.93	0.24	0.29	0.34	0.43
Quartile 3 (75%)	0.40	0.42	1.43	1.46	0.55	0.58	0.67	0.67
Standard deviation	0.61	0.49	1.29	0.85	0.85	0.64	0.70	0.43
Variance	0.37	0.24	1.67	0.72	0.72	0.41	0.50	0.18
Coefficient of variation	1.80	1.44	1.14	0.75	1.84	1.40	1.33	0.81
Number of samples > 0.5 g/t	12,888	13,353	44,956	52,069	13,426	14,598	1,955	2,299
Mean > 0.5 g/t	1.07	0.95	1.51	1.33	1.19	1.05	1.08	0.87

Table 6.4 Cross validation statistics for BH data set

6.7.3 Misclassification

Another comparison can be made by assessing the problem of misclassification. This can be done by applying a cut-off to the estimated and sample value and by measuring the extent of misclassification. The following table compares the classification of the estimates and samples for the DDH and BH data set. Scatterplots for each zone of the DDH data are shown on figure 6.5, 6.6, 6.7 and 6.8.

	HW		CORE		FW		87S	
Classification	Sample	Percentage	Sample	Percentage	Sample	Percentage	Sample	Percentage
Ore as Ore	163	3.4%	1,816	56.4%	258	6.8%	349	21.3%
Ore as Waste	331	7.0%	186	5.8%	376	10.0%	217	13.2%
Waste as Ore	293	6.2%	571	17.7%	433	11.5%	313	19.1%
Waste as Waste	3,952	83.4%	648	20.1%	2,710	71.8%	761	46.4%

Table 6.5 Classification for DDH data

	HW		CORE		FW		87S	
Classification	Sample	Percentage	Sample	Percentage	Sample	Percentage	Sample	Percentage
Ore as Ore	6,214	9.1%	41,498	63.7%	8,088	16.8%	1,320	24.0%
Ore as Waste	6,674	9.8%	3,458	5.3%	5,338	11.1%	635	11.5%
Waste as Ore	6,930	10.1%	10,361	15.9%	6,353	13.2%	944	17.2%
Waste as Waste	48,633	71.0%	9,812	15.1%	28,357	58.9%	2,600	47.3%

Table 6.6 Classification for BH data.

From table 6.5 and 6.6, we can see that four types of classifications have been used based on a 0.5 g/t cut-off:

- Ore as Ore: An ore sample has been estimated as ore
- Ore as Waste: An ore sample has been estimated as waste (misclassification)
- Waste as Ore: A waste sample has been estimated as ore (misclassification)
- Waste as Waste: A waste sample has been estimated as waste

Attention must be paid toward two types of misclassification: underestimation (Ore as Waste) and overestimation (Waste as Ore). Analysing those two types, we can notice that their respective percentages are very close for the HW and FW zone of the DDH and BH data. This can be explained by the low grade and high nugget effect characteristics of those two zones, which tend to create estimates that either, over or underestimate the original sample value. This problem may be irrelevant in the present case, where the underestimation and overestimation percentage cancel each other out. In the case of the CORE and 87S zone, an overestimation of the Ore (Waste as Ore) takes place for both sets of data. Since those two zones contain the majority of the ore, it becomes difficult to estimate waste samples accurately. This can also be related to the type of mineralization being estimated. In the case of Troilus, an ore block will, most of the time, have some internal waste sample due to the disseminated characteristics of the Troilus mineralization.

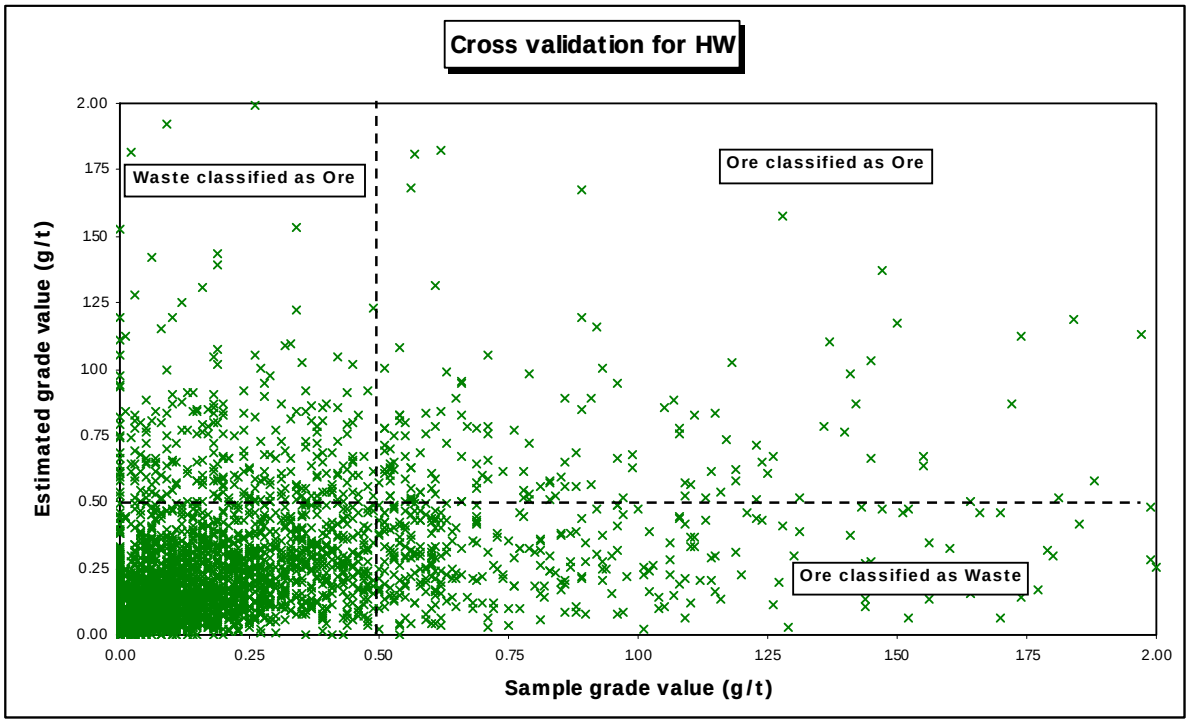

Figure 6.5 Cross validation of the HW zone for the DDH data

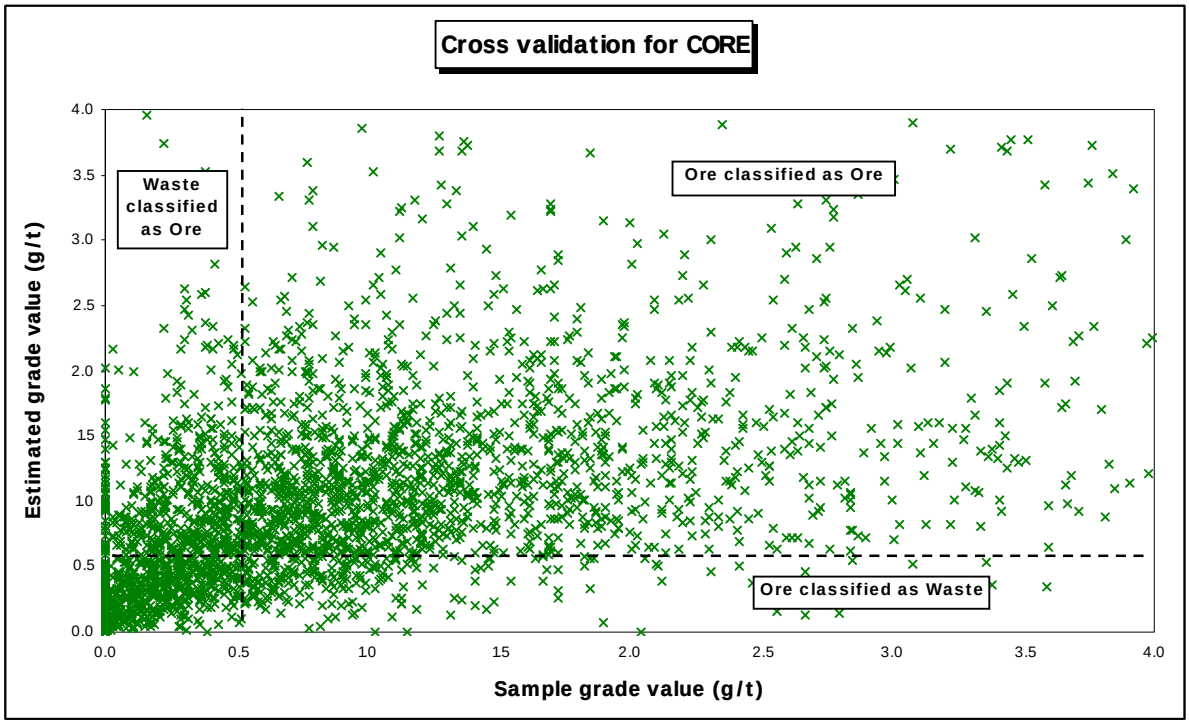

Figure 6.6 Cross validation of the CORE zone for the DDH data

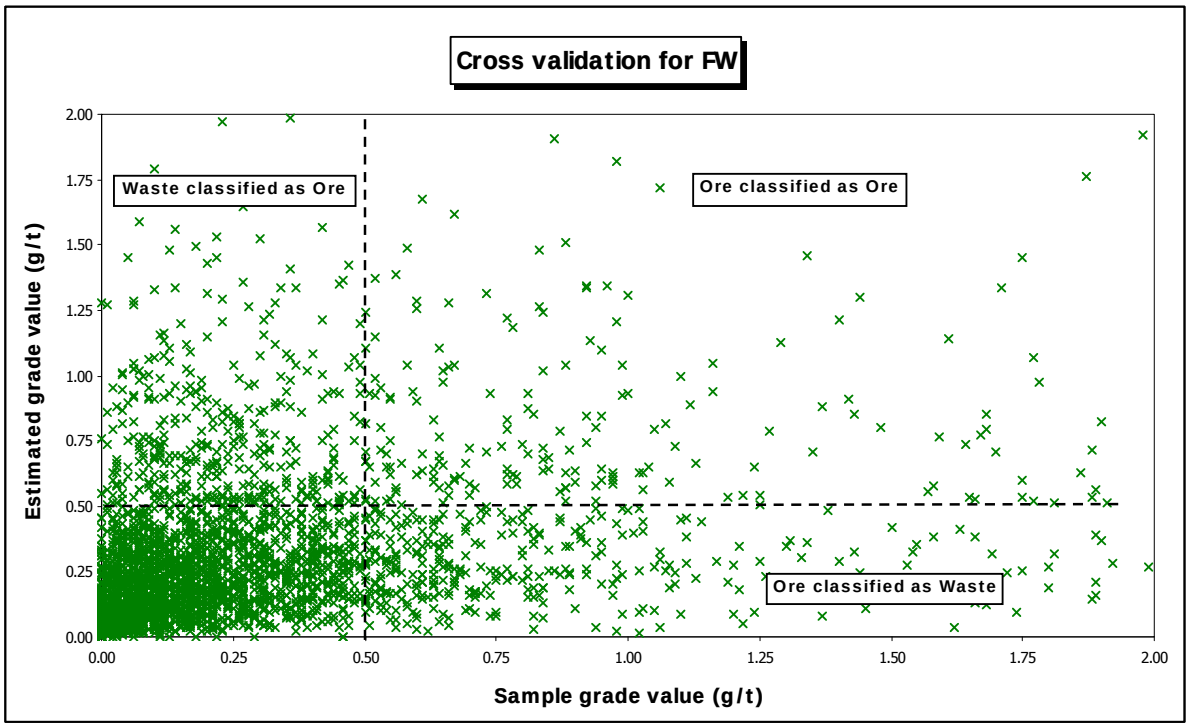

Figure 6.7 Cross validation of the FW zone for the DDH data

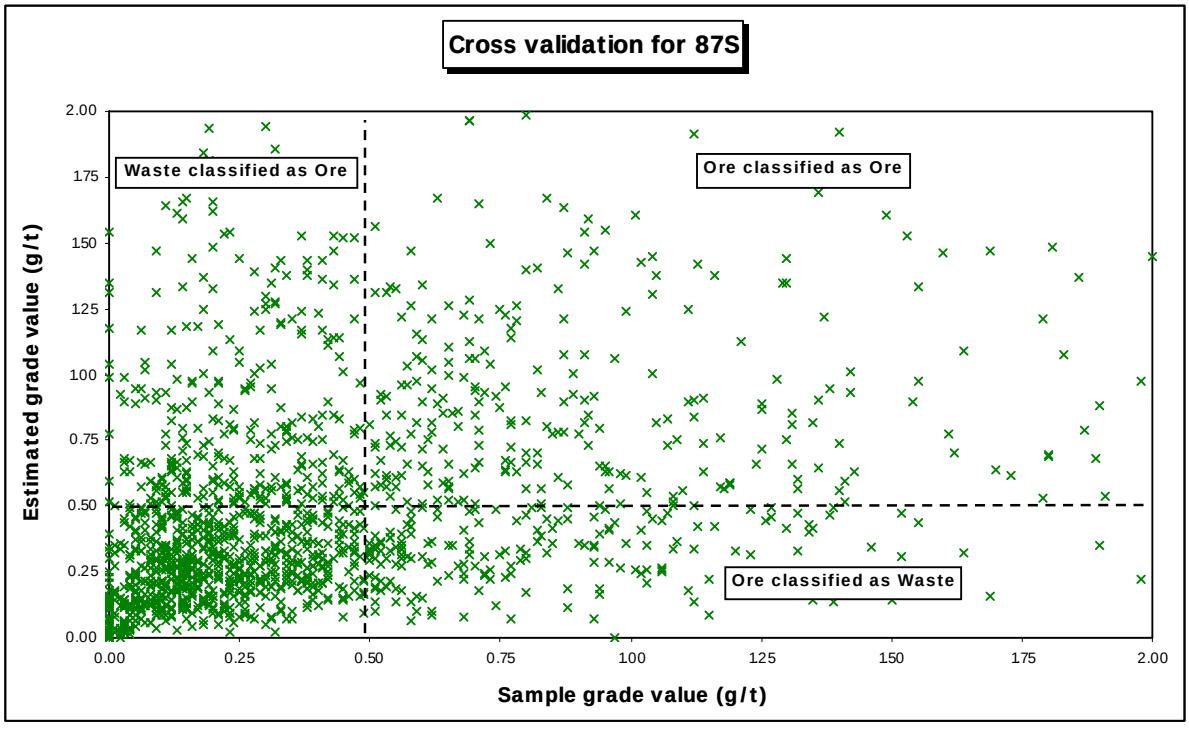

Figure 6.8 Cross validation of the 87S zone for the DDH data

6.8 Conclusion

The estimation of Troilus reserves was carried out using the indicator kriging interpolation method. The major benefit of using this method is its ability to estimate recoverable reserves by taking into account the different patterns of continuity of the mineralization. Two block models were built. A recoverable reserve model based on the DDH composite data was created and a grade control model based on the BH data was used for grade reconciliation purposes. The ore tonnages for both models were reconciled with the actual mined packet. Overall, the recoverable reserve model overestimates the ore tonnage by 6.5% and underestimates the contained ounces by 5.7%. Missclassification was assessed with cross validation. In the main zone of the deposit where over 70% of the ounces are contained (CORE), the recoverable reserve model missclassified ore to waste or waste to ore 23.5% of the time, compared to 21.2% of the time in the case of the grade control.

CHAPTER 7

Conditional Simulation

7.1 Introduction

For a long time, the person in charge of the reserve/resource evaluation had nothing to compare his estimate to. Once the resource block model was created, the only time the estimates could be compared to reality was during a bulk sample campaign at the early exploration stage of the project or when the mine was in production. Methodology to analyse the variability and the sensitivity of the grade estimates of a deposit was nonexistent, leading most of the time to an overestimation of the grade of the estimates. A study in the late 80's by Warren (Warren, M.J. 1991) in the first 12 months of production on 32 mining projects in Australia concluded that only a minority of the projects achieved or exceeded the feasibility grade estimate (table 7.1).

Up until recently, the spatial variability of the grade estimates of a project was, most of the time, assessed by a simple risk/sensitivity analysis based on a percentage increase or decrease of the estimated grade or of the in-situ ounces. This simple method can appropriately be used to analyse the sensitivity of factors such as: mining cost, milling cost, commodity price, discount rate and exchange rate. But when the factor to analyse is non-linear, as for instance the grade of a deposit, this method can unfortunately mislead the decision-maker about the real impact of a 10% decrease in the estimated grade. One way of assessing the variability of the mineralization and to analyse the sensitivity of a deposit is through a conditional simulation study. George Matheron developed the first conditional simulation algorithm during the 70's at the Centre de Géostatistique de Fontainebleau. Due to the limitation of computer speed at that time, only university researchers used conditional simulation. But with the progress made in computer technology during the 90's, conditional simulation is now frequently used by geologists and mining engineers at different stages of a mining project.

Mining Project	Estimate (g/t)	Actual (g/t)	Change (%)
Kidston	1.84	1.80	-1.9
Reedy	4.00	3.77	-5.7
Great Victoria	3.60	2.19	-39.2
Nevoria	5.46	5.00	-8.7
Mt. Percy	3.53	2.45	-30.6
Paddington	3.20	2.88	-9.8
Sons of Gwalia	3.11	3.62	16.5
Porphyry	4.67	3.65	-21.7
The Granites	6.64	6.31	-5.0
Bluebird	4.15	2.70	-34.9
Harbour Lights	5.16	3.12	-39.5
Horseshoe Lights	4.75	3.34	-29.8
Bamboo Creek	9.33	8.10	-13.2
Wiluna Tailings	0.54	0.54	0.0
Lawlers Tailings	1.23	1.16	-5.9
King of the Hills	4.96	4.80	-3.2
Pine Creek	1.65	1.95	18.7
Canbelego	2.20	1.79	-18.6
Westonia	3.13	2.69	-14.2
Golden Crown	23.93	21.14	-11.7
Galtee More	6.22	3.93	-36.8
Cracow Tailings	1.00	0.83	-16.7
Cork Tree Well	2.64	2.35	-11.1
Great Eastern (Lawlers)	4.28	4.00	-6.4
Croydon	2.28	0.95	-58.1
Lady Bountiful	3.81	2.92	-23.4
Brilliant-Tindals	3.08	2.54	-17.6
Broad Arrow	3.39	2.24	-33.9
Mt. Martin	6.91	4.92	-28.8
Gwalia Tailings	0.65	0.53	-18.0
Howley Alluvials	0.47	0.29	-37.4
Hawkins Find	1.24	1.03	-17.6
Average	4.16	3.42	-17.6

Table 7.1 Estimated vs actual grade of gold mining project in Australia (Warren, M.J. 1991)

In the mining industry, conditional simulation is used to assess:

- variability of the spatial distribution of the mineralization
- risk/sensitivity analysis in the mine planning process
- additional drilling depending on uncertainty of the grade
- effect of block size on ore variability

The Troilus deposit is almost a textbook case to carry a conditional simulation. The gold mineralization is disseminated; it has a high nugget effect and the coefficient of variation of the DDH data is always above 1. Therefore, a conditional simulation study should give us a

wide range of equi-probable scenarios to which the recoverable reserve model would be compared.

7.2 Concept

7.2.1 Interpolation vs simulation

To explain the difference between ordinary kriging and conditional simulation, a small illustration on figure 7.1 is used (Chiles, J-P and Definer, P. 1999). The top sketches represent a boat sounding the bottom of the seafloor, which can be associated in mining by the drilling of an orebody. Depth levels of the sea are taken every 100 meters by sonar. Once the data has been collected and analysed, a kriged seafloor was created. The kriged profile gives a good approximation of the shape of the seafloor. The same data was also used to generate a conditionally simulated profile, which gives another idea of how the seafloor is shaped. When we compare the kriged profile to the simulated profile, we can see that the shape of the simulated profile presents more fluctuation and variability. The kriged estimates will give a profile that will be smoothed, where in the case of the simulation, the profile will be more erratic. This distinction comes from the fact that each estimation method aims at different goals. The kriging estimates aim to minimize the estimation error and the variance, which in turn gives a smoothed profile. On the other hand of conditional simulation, variability is intentionally introduced in the estimation, which gives a profile that has more resolution (variability) into it. When both profiles are compared to the true profile, we can notice that each of the estimates gives a profile similar to the true profile.

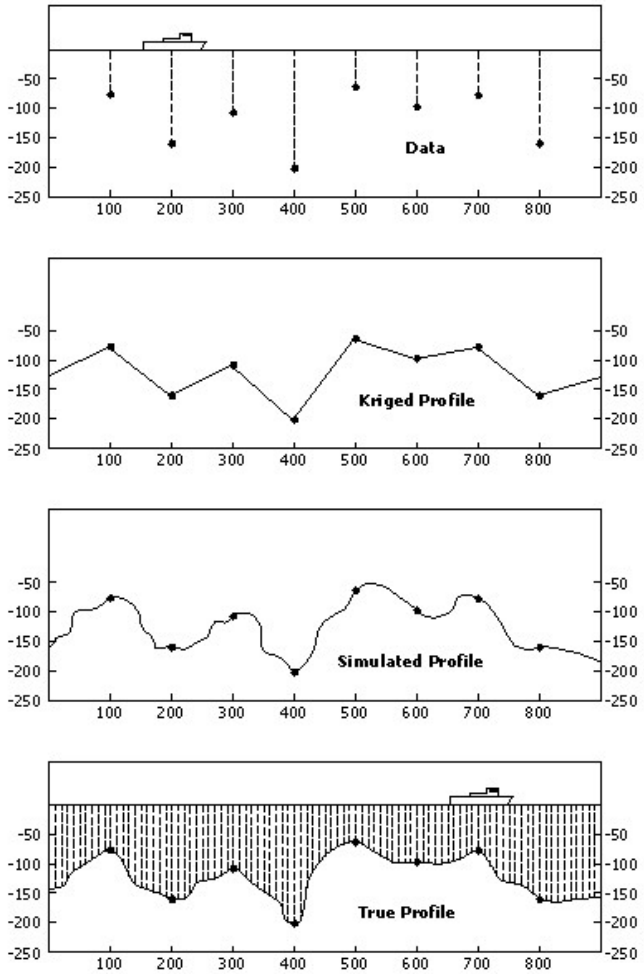

Figure 7.1 Difference between kriging and simulation
(Chiles, J-P and Definer, P. 1999)

7.2.2 Theory

Often misunderstood, a conditional simulation study is simply a regular ordinary kriging exercise that involves the same elements such as: geological modeling, univariates statistics, compositing, variography and interpolation. The difference lies in the fact that a simulation has a random component into it and that the sample value at their respective location are honoured, making the simulation conditional. A single simulation is a poor estimate, but the average of a large number of realizations will give a good estimate and will theoretically be the equivalent of a kriged estimate. Simulations will also give an idea of the worst and best case scenario of a given problem. Unlike an interpolation algorithm,

conditional simulation doesn't smooth out the estimates. For instance, ordinary kriging will not produce value outside the minimum and maximum of the sample data. This, in the end, results in a reduction of the variability of the estimates when compared to the actual grade value (Dimitrakopoulos, R. 2001).

When compared to reality, ordinary kriging estimates will overestimate the low grade material and underestimate the high grade material. This smoothing effect will be more pronounced if the block to estimate is far away from the data than if the block is close to the data location. This shortcoming comes from one of the principles of kriging that is to minimize the error variance. The variation component of the simulation is introduced by the Monte Carlo algorithm which draw random uniformly distributed numbers between 0 and 1. A number of conditional simulation algorithms are available. Amongst the most widely used, we can list the sequential gaussian simulation and the sequential indicator simulation. In the case of Troilus, the Sequential Indicator Simulation (SIS) algorithm was used (Deutsch, C.V. and Journel, A.G. 1992). The WinGSLIB software that was initially developed at Stanford University was used. The reason behind the choice of the SIS algorithm is related to the fact that the SIS method uses indicator kriging as interpolation method. Consequently, all variograms for the different cut-off grade that have already been modelled for the creation of the recoverable reserve block model could be used to generate the SIS simulation. Like indicator kriging, the sequential indicator algorithm allows one to account for different patterns of continuity at different cut off grades.

7.2.3 Implementation

After selecting the simulation algorithm, the number of times that the deposit will be simulated needs to be chosen. There is no clear answer to this question and no rules of thumb can be used to select the appropriate number of simulations for a given deposit. The current limitation has more to do with the considerable amount of time required to post process the simulations than with the actual time to simulate a deposit. Due to the intrinsic variability of the Troilus deposit, 25 simulations were thought to be enough to generate a wide range of possible scenarios. The subsequent step in the implementation process is to design a grid that will cover the area of interest. In the case of Troilus, four different grids

have been defined to cover each of the zones. A grid is defined by a series of nodes. The distance between nodes is important, in that it reflects the size of support of the variable. For example, a node spacing of 5.1m x 5.9m x 10m can reproduce blasthole sampling at Troilus. The present simulations have been done on a support size of 5m x 5m x 5m. With the current block size of the recoverable reserve model being 10x10x10 metres, this gives approx. 27 simulated points to be averaged into a single block. The choice of the 5x5x5 meter nodes size was also based on the total number of nodes to be simulated in a single simulation. Since WinGSLIB doesn't allow rock coding for each zone, each of the four zones had to be simulated over their extended limit in the x and y direction. That is four times 1,200,000 nodes to be simulated and merged together for a single simulation. Given that 25 simulations were carried out, this represents a considerable amount of time to simulate and merge together every simulation. Since the aim of the simulation is to compare with the recoverable reserve model, it was decided that a size of support smaller than 5x5x5 metres would be excessive given that the comparison would be based on the recoverable reserve model, which is based on a block size of 10x10x10 meters.

The general procedure of a conditional simulation study is explained in this section. From the surrounding sample data values and simulated values contained within the search ellipsoid, cumulative probabilities are calculated based on the respective variogram of each of the value. A conditional cumulative distribution function (CCDF) is then created and a random number between 0 and 1 is chosen (0.78) by the Monte Carlo algorithm (figure 7.2). The associated grade (0.91) of this random number becomes the grade of the node. This procedure is repeated to all nodes along the random path.

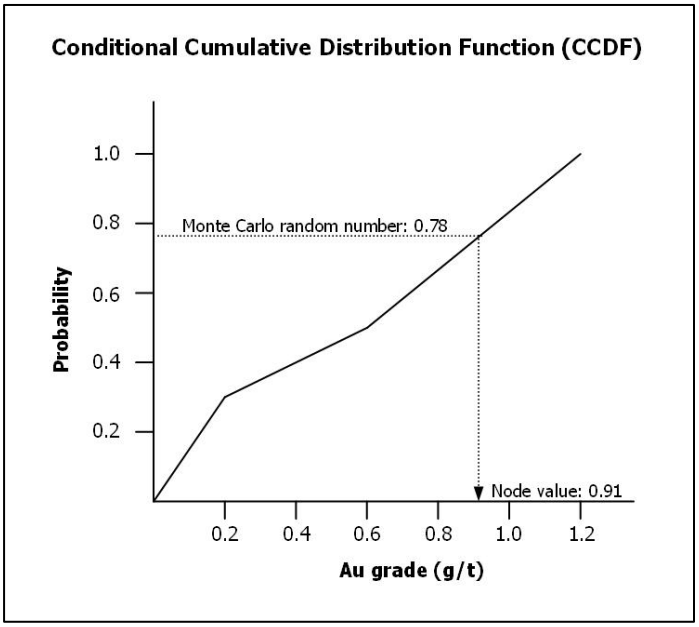

Figure 7.2 Example of the determination of a node grade

The sequential based algorithms involve the CCDF modelling of each point visited along the random sequence. In order to reproduce the semi-variogram model, each CCDF point is not only made conditional to the sample data set, but also to simulated values. As the simulation progresses, more simulated data are used in the kriging system up to a point were the maximum data allowed in the estimation of a single node is reached. For this study, 10 original data and 10 previously simulated values are permitted in the search ellipsoid, allowing a good mix of information in the kriging process. In order to reproduce the long range structure of the semi-variogram model, multiple grid refinement searches have been employed. First, data is simulated for the long range structure on a coarse grid. Once completed, the simulation moves on to a finer grid to reproduce the short range structure of the variogram. It should be noted that the data simulated on the coarse grid are used in the finer grid simulation. It should be noted that if a planned sequence is retained during simulation, it is possible to create an artificial continuity. As a result, a random sequence to simulate data would not only guarantee that no artificial structures are introduced, but would also guarantee that each simulation is significantly different.

Following, figure 7.3 to 7.10 compares results from indicator kriging (recoverable reserve model) and results from simulations for section 13400N and for bench 5290.

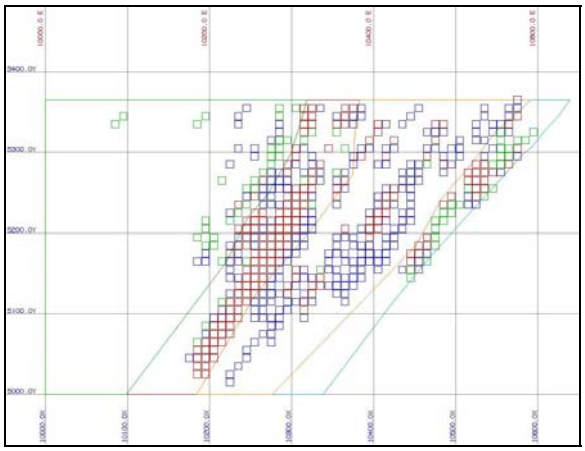

Figure 7.3 Section 13400N – Recoverable Reserve model

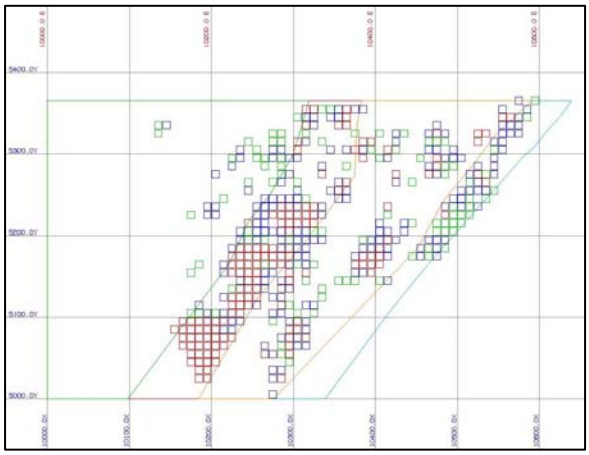

Figure 7.4 Section 13400N – Simulation #5

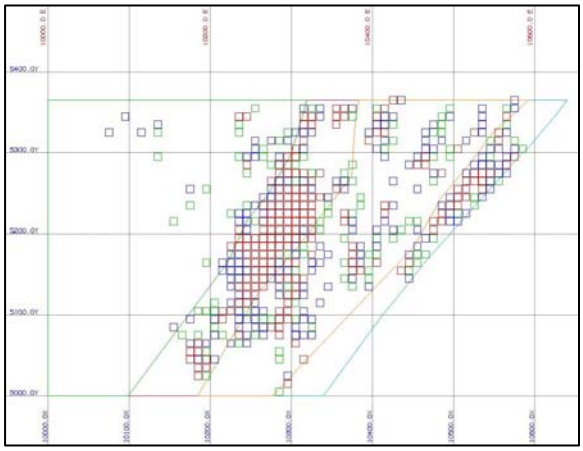

Figure 7.5 Section 13400N – Simulation #11

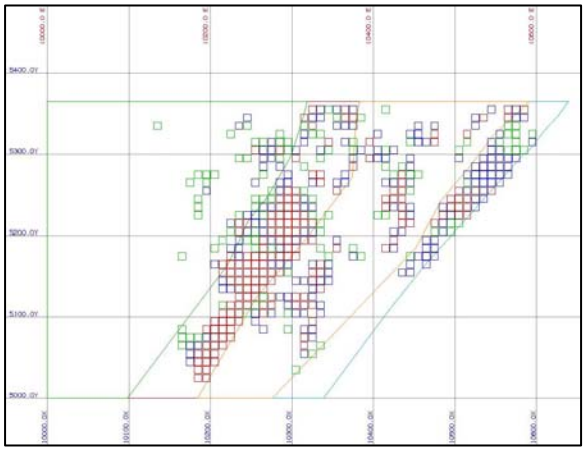

Figure 7.6 Section 13400N – Simulation #18

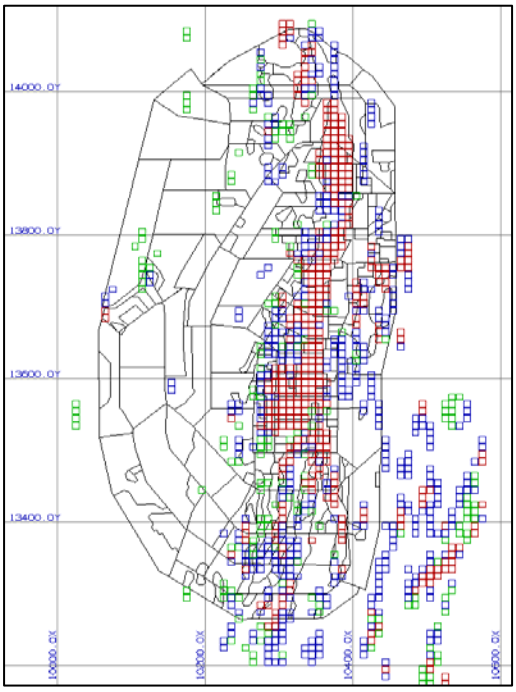

Figure 7.7 Bench 5290 – Recoverable Reserve model

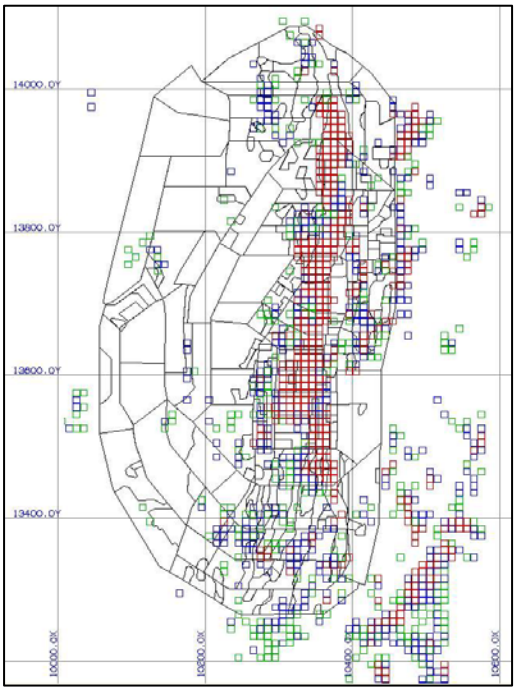

Figure 7.8 Bench 5290 – Simulation #5

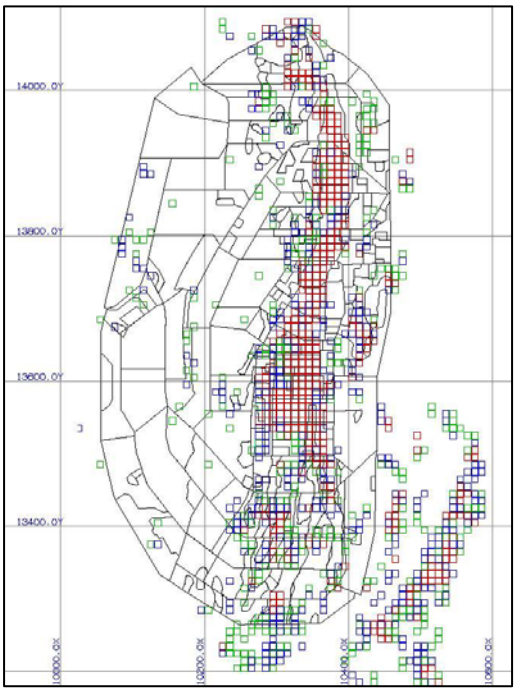

Figure 7.9 Bench 5290 – Simulation #11

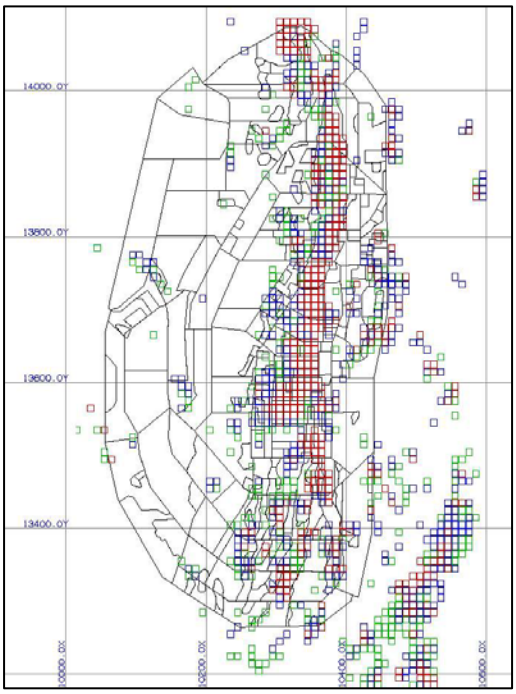

Figure 7.10 Bench 5290 – Simulation #18

7.2.4 Reproduction of sample data characteristics

Discrepancy between kriged and simulated estimates can be seen at the north end and south end of the orebody. This can be related to the sparse density of drilling in those two areas, which is reflected in the simulation by an increase in the variability of the estimates. For example, if a series of high grade values are present on most of the simulations, they will most likely be encountered during mining. Differences can also be found in the duplication of the model statistics by the conditional simulation. As it can be seen from the following histograms (figure 7.11 to 7.18), simulation #18 does not reproduce exactly the 3m gold assay composite statistics. This can be explained by the algorithm used to simulate and by the set of underlying assumptions drawn on by the algorithm. The first source of discrepancy comes from the indicator algorithm. Unlike sequential Gaussian simulation, the indicator based algorithm guarantees only the reproduction of the semi-variogram and CCDF for the class of cut-offs under study; it does not assure the reproduction of the continuous set of values (Goovaerts, P. 1997). However, if averaged over a large number of repetitions, indicator simulations should be very close to the statistics of the original data. The fewer the number of cut-off classes used in the simulation, the greater the impact of the interpolation and extrapolation model on the CCDF. As seen in chapter 5, the number of cut-off classes has been optimized to have enough data in each class to generate reliable statistics and clear semi-variogram and also to have cut-offs located at values of economical interest. Because no CCDF model can be generated beyond the lowest and the highest cut-off, specific models to interpolate and extrapolate are utilized. Linear, power and hyperbolic are amongst the functions used to model the lower tail, the middle classes and the upper tail. Based on the CDF shapes of the original data from the HW, CORE, FW and 87S zone, combinations of linear and power model with coefficients varying from 1.0 to 2.0 were chosen. As it can be seen on the following Q-Q plots (figures 7.19 to 7.22), the simulation matches closely the original data distribution between the lowest and highest cut-off. However, discrepancy appears as the interpolation/extrapolation method is used.

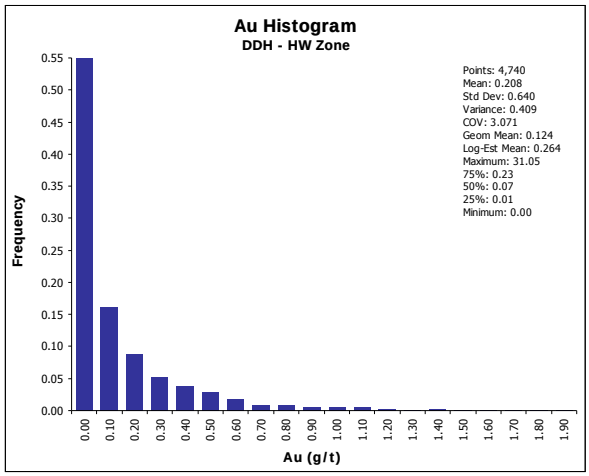

Figure 7.11 DDH 3m assay composites histogram for HW zone

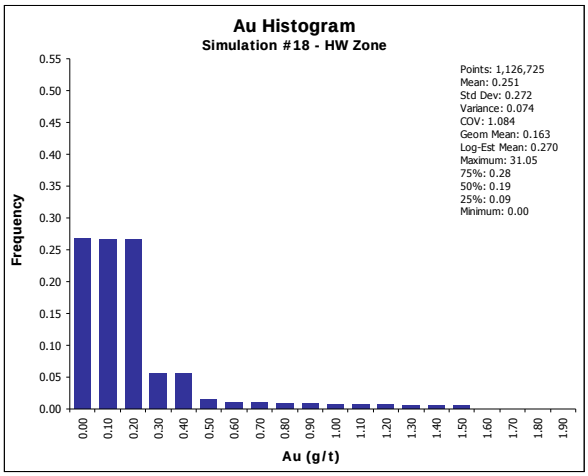

Figure 7.12 Simulation #18 histogram for HW zone

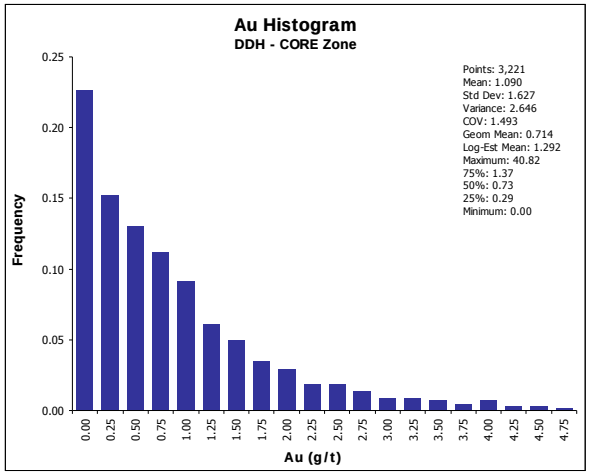

Figure 7.13 DDH 3m assay composites histogram for CORE zone

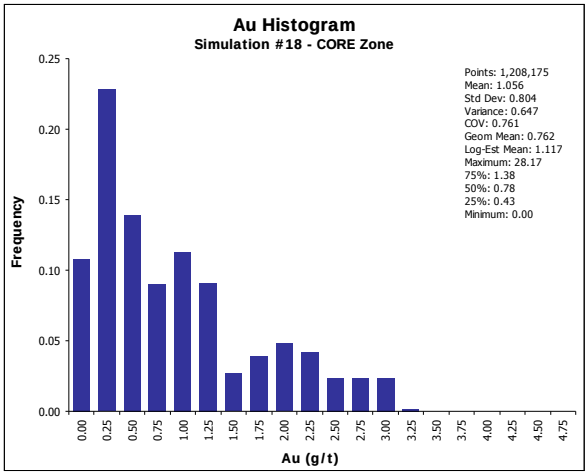

Figure 7.14 Simulation #18 histogram for CORE zone

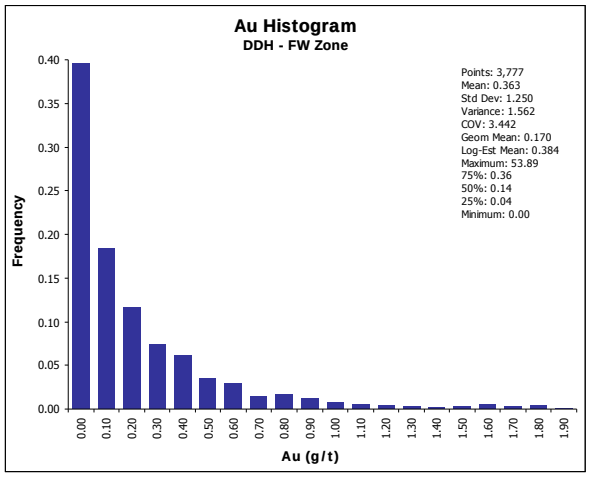

Figure 7.15 DDH 3m assay composites histogram for FW zone

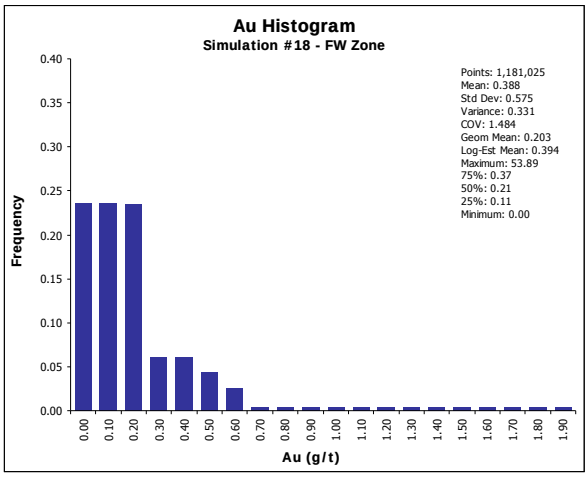

Figure 7.16 Simulation #18 histogram for FW zone

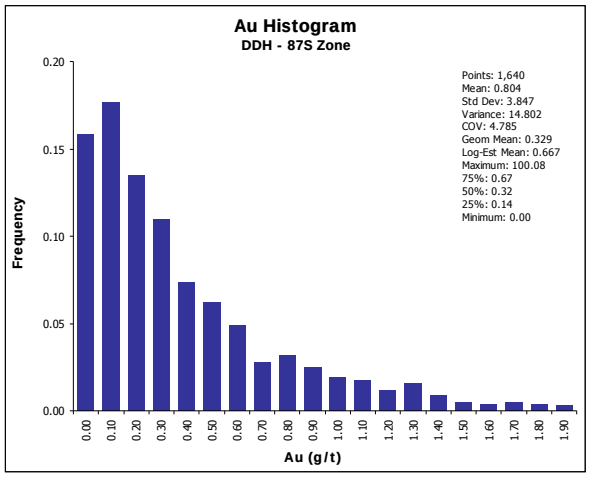

Figure 7.17 DDH 3m assay composites histogram for 87S zone

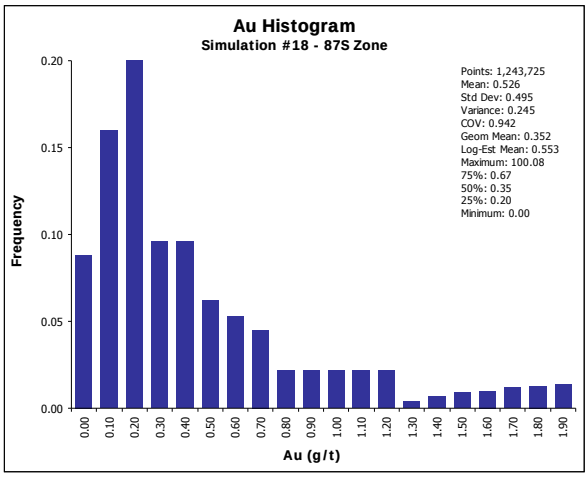

Figure 7.18 Simulation #18 histogram for 87S zone

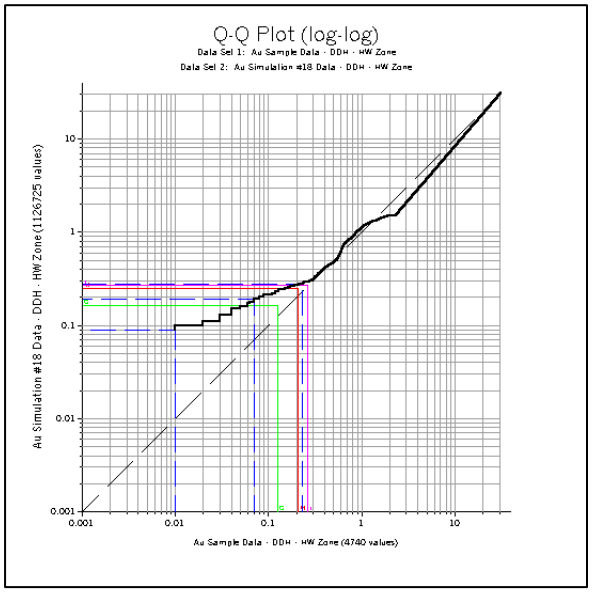

Figure 7.19 Q-Q plot between DDH and simulation #18 for the HW zone

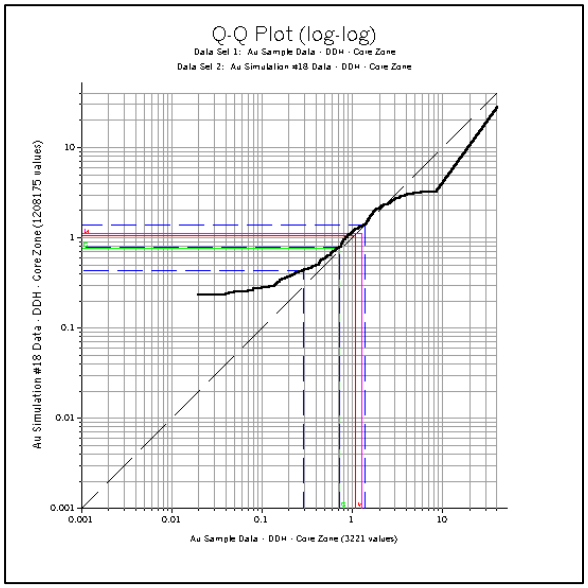

Figure 7.20 Q-Q plot between DDH and simulation #18 for the CORE zone

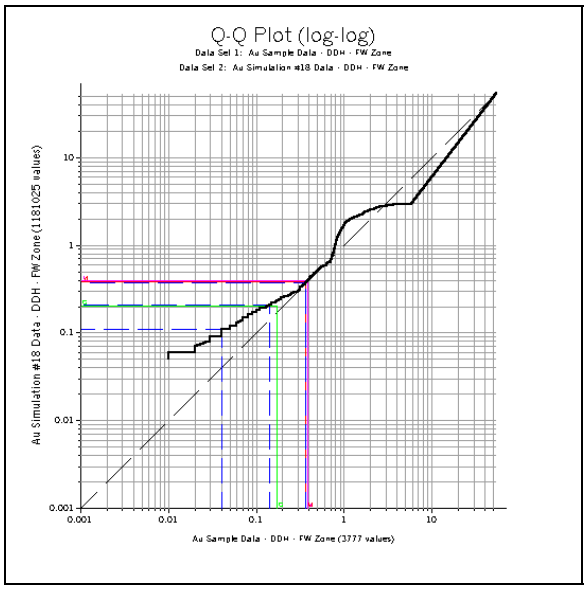

Figure 7.21 Q-Q plot between DDH and simulation #18 for the FW zone

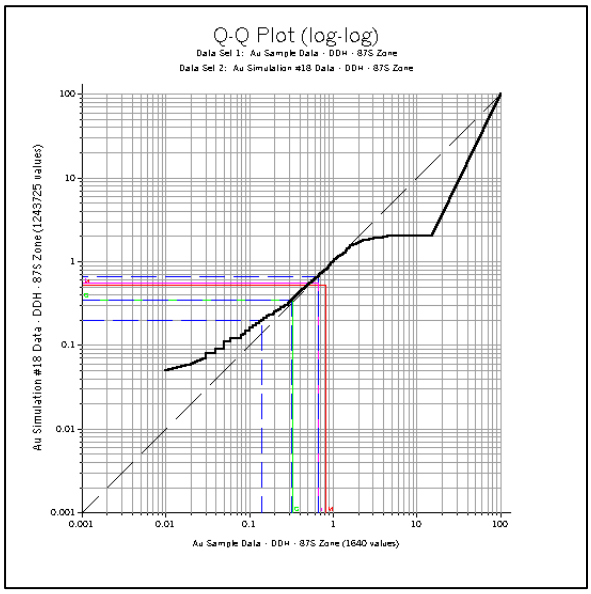

Figure 7.22 Q-Q plot between DDH and simulation #18 for the 87S zone

7.3 Transfer function

7.3.1 Concept

In generating multiple equi-probable realizations of the recoverable reserve model, we need a transfer function to assess the response of each model. The type of transfer function used depends on the problematic of the project (Dimitrakopoulos, R. 1998). Uncertainty resulting from the response of each of the models to the transfer function can then be used in risk analysis and decision-making. In the case of Troilus, two distinct transfer functions will be used to assess the spatial uncertainty of the mineralization.

At the conceptual stage of a mining project, uncertainty of the mineralization can be assessed by generating different schedule scenarios based on common sets of economical parameters (Rossi, M.E., H. Van Brunt, B. 1997). This can be done through pit optimization software. In our case, the Whittle 4X software was chosen. This software uses the Lerch-Grossman algorithm to analyse and forecast the optimal pit for long term projects. Using the block model as input, Whittle 4X can generate up to 100 optimal pit outlines, each within a range of possible economic projections. It also gives detailed analyses of

quantities, grades, stripping ratios, cash flows and discounted cash flows for each optimal pit. By applying different factors to the revenue and re-optimizing for each factor, Whittle 4X produces a set of nested pits which are used to guide the mining sequence during simulation of the operation of the mine. The mining sequence is then translated into a long-term production schedule, with cash flows and discounted cash flows. This software is helpful in the case of project scoping, feasibility studies, sensitivity work, risk analysis, scheduling and for deciding where to drill.

7.4 Open pit optimization

7.4.1 Parameters

To begin an open pit optimization, parameters such as mining cost, processing cost, slope angle, commodity prices and capital expenditures must be defined (table 7.2). It can be noted that this set of parameters has been used in previous pit optimization at Troilus during the fall of 2000. However, parameters such as the initial capital cost and replacement capital cost for each year had to be estimated.

Mining		**Price**	
Rock Mining Cost ($US/t)	1.22	Au Selling Price ($US/oz)	300
Overburden Mining Cost ($US/t)	0.58	Au Refining Price ($US/oz)	11.20
Mining Recovery Fraction (%)	95		
Mining Dilution Fraction (%)	95	**Financial**	
Mining Limit (t/year)	20,000,000	Initial Capital Cost ($US)	137,500,000
		Replacement Capital Cost - Year 1 ($US)	7,500,000
Slope Angle		Replacement Capital Cost - Year 2 ($US)	7,500,000
Azimuth 0 to 40 degrees	53	Replacement Capital Cost - Year 3 ($US)	7,500,000
Azimuth 40 to 150 degrees	47	Replacement Capital Cost - Year 4 ($US)	5,000,000
Azimuth 150 to 330 degrees	51	Replacement Capital Cost - Year 5 ($US)	5,000,000
Azimuth 330 to 0 degrees	49	Replacement Capital Cost - Year 6 ($US)	5,000,000
		Replacement Capital Cost - Year 7 ($US)	5,000,000
Processing		Replacement Capital Cost - Year 8 ($US)	5,000,000
Processing Cost ($US/t)	3.75	Discount Rate per Year (%)	5
Au Recovery (%)	84		
Au Cut-Off (g/t)	0.50		
Processing Limit (t/year)	5,475,000		

Table 7.2 Parameters used for the Whittle 4X optimization

These parameters were used to generate a series of optimum shells for the recoverable reserve model as well as for every simulation. A pit shell can be described as a 3D

representation of an open pit (figure 7.23). It is not well defined as a true open pit design in a sense that no ramp and no safety berm are defined (figure 7.24). But it is precise enough to be used by the mine planning engineer as a guideline to create his detailed design. If the appropriate slope angles have been entered, the difference in tonnage between the pit shell and the actual detailed design should be no greater than 5-10%.

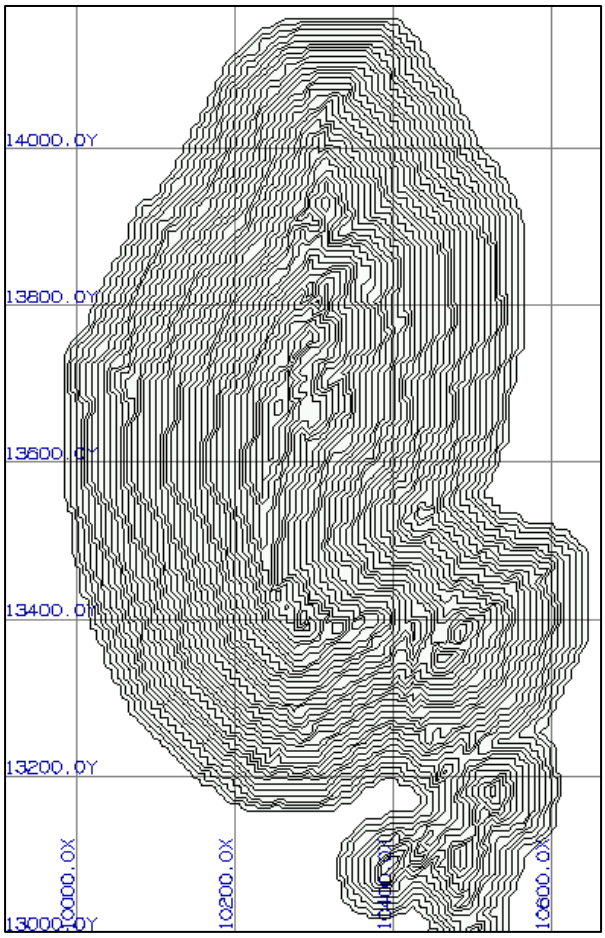

Figure 7.23 Exported Pit Shell for Pit #29 (340$US/oz)

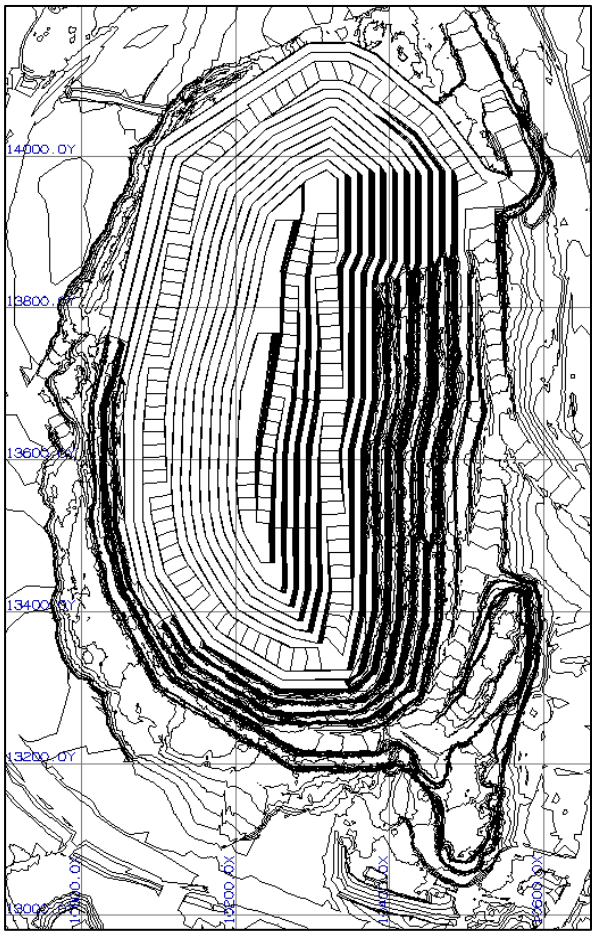

Figure 7.24 Ultimate pit design as of July 2001

7.4.2 Pit shells generation

The current standard practice in the mining industry is to use the kriged block model for pit optimizations. The output consists of a series of values ranging from NPV to ounces contained that can be used in mine planning. However, any deviation from the output of this pit optimization can have serious consequences on the future viability of the mine. One

way to address this is to run a pit optimization on all 25 simulations and on the kriged model (recoverable reserve model). This would give management different scenarios that could be factored into the corporate risk matrix.

Optimized pit shells have been generated by keeping the different parameters outlined in table 7.2 constant and by varying the revenue (gold price). For the current project, the price of gold has been varied from a low of 220 $US/oz to a high of 380 $US/oz. A low gold price will produce a pit shell that will have a high head grade, a low unit cost ($US/oz), a low stripping ratio, a short mine life and a low discounted value (NPV). On the other hand, a high gold price will produce a pit shell that will have a low head grade, a high unit cost, a high stripping ratio, long mine life and a high discounted value (NPV).

Following are two graphics showing the discounted open pit value for the best case and worst case scenario for the recoverable reserve model, the 25 conditional simulations model as well as for the average of the 25 simulations (figure 7.25, 7.26). To understand those two graphics, explanations need to be given about the two possible mining schedules. The best case schedule consists of mining out pit 1, the smallest pit, and then mining out each subsequent pit shell from the top down, before starting the next pit shell. In other words, there are as many intermediate mining pushbacks as there are pit outlines within the one we are mining. This schedule is rarely feasible because the pushbacks are usually too narrow. Its utility lies in setting an upper limit of the achievable discounted open pit value (NPV). The worst case mining schedule consists of mining each bench completely before starting on the next bench. This mining schedule is usually feasible. It also sets a lower limit of the discounted open pit value (NPV). In reality, the NPV that will be achieved will be somewhere between the worst case and best case schedule.

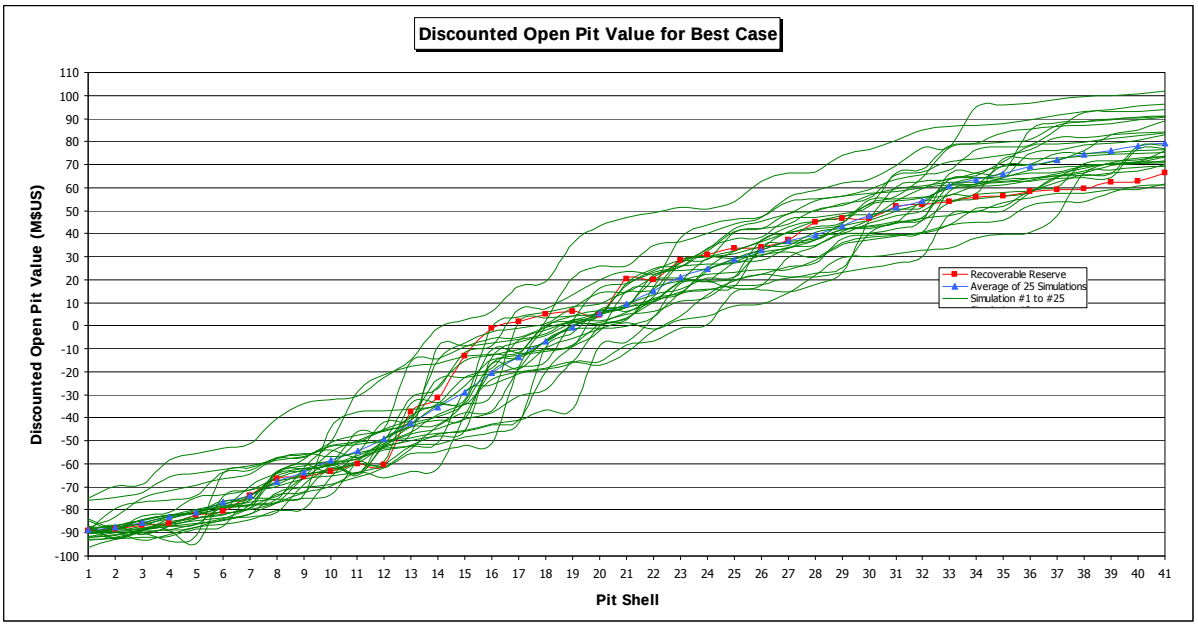

Figure 7.25 Discounted open pit value for best case mining schedule

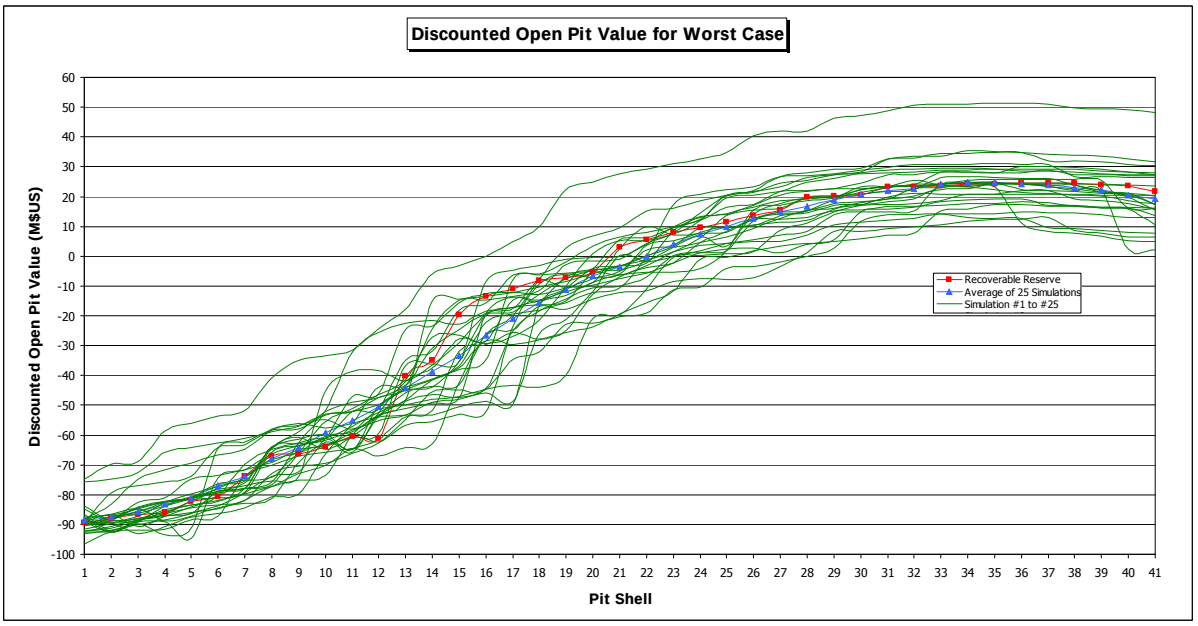

Figure 7.26 Discounted open pit value for worst case mining schedule

From those two graphics (figure 7.25, 7.26), we can see that in most of the pit shells, the recoverable reserve model seems to follow very closely the average of the 25 simulations. This is especially the case for the worst case mining schedule, where very few pit shells show an overestimation in the order of 10%. Overestimations by more than 10% of the recoverable reserve model are limited to pit shells 15 to 18. On the other hand, underestimation by more than 10% by the recoverable reserve model is restricted to pit shells 12, 40, and 41. The best case mining schedule presents a different situation. Discrepancy occurs to a greater number of pit shells, which indicate that the recoverable reserve model reacts differently when mined by the best case schedule. Overestimations by more than 10% take place for pit shells 15 to 18, 21 to 25 and underestimation take place for pit shells 33 to 41. Under normal circumstances, if the resource model (recoverable reserve) has been estimated properly, the kriging estimates should be equal to the average of all conditional simulations. These two graphics (figure 7.25, 7.26) also show the extent to which variability of the grade estimates might affect the expected discounted value of a project. In order to show the variability effects on others parameters, more detail on pit shell 29 is presented in the following table. The reason why this particular pit shell has been chosen will be discussed in larger detail later.

From the following table (7.3), we can analyse the impact of the variability of the grade estimates on other variables. Looking first at the "Discounted Open Pit Value" for best case, we can see that the recoverable reserve model overestimates the average of 25 simulations by 7.1% (+3.11M$US), which seems quite acceptable knowing that the maximum and minimum values around the average show variability in the region of +70% and –47%. When we look at the worst case scenario, the recoverable reserve model again overestimates the average of the 25 simulations by 7.9% (+1.48M$US). With variation above and below the average of 146% and –86%, an overestimation of 7.9% is more than respectable.

When the performance of the recoverable reserve model is analysed for the "Tonnage Input to Processing", it is pretty obvious that the variation has been considerably reduced for this variable. This is reflected in the spread around the average of +14.9% and -3.3% as well as in the performance of the recoverable reserve, which underestimates the tonnage by 2.8% (-

1.23Mt). The "Tonnage of Waste Rock" variable is overestimated by about 1.5% (+1.57Mt). The overall variability of the 25 simulations for this variable comes in at +19.4% and –17.5%. The most interesting variable to compare is the "Quantity of Au Output". The recoverable reserve model predicted the number of ounces produced with an accuracy of 99.9% when compared to the average.

Model	Discounted Open Pit Value for Best Case	Discounted Open Pit Value for Worst Case	Tonnage Input to Processing	Tonnage of Waste Rock	Tonnage Total	Grade of Au Mined Input to Processing	Quantity of Au Output
Recoverable Reserve	46,571,062	20,285,094	42,531,223	103,921,997	146,453,220	1.18	1,358,119
Average of 25 Simulations	43,459,533	18,799,574	43,766,986	102,347,890	146,114,876	1.15	1,358,638
Maximum of 25 Simulations	73,908,802	46,283,224	50,283,490	122,269,610	172,553,100	1.20	1,553,584
Minimum of 25 Simulations	23,178,510	2,610,744	37,918,861	84,427,829	122,346,690	1.12	1,177,007
Simulation #1	44,500,312	18,809,616	45,101,146	106,997,484	152,098,630	1.14	1,392,699
Simulation #2	52,215,872	25,972,630	46,451,105	106,193,585	152,644,690	1.14	1,428,740
Simulation #3	43,508,010	19,999,957	43,953,680	103,823,630	147,777,310	1.15	1,367,161
Simulation #4	40,980,998	14,877,184	45,463,635	110,389,145	155,852,780	1.14	1,393,838
Simulation #5	35,165,672	10,408,367	42,193,733	101,023,307	143,217,040	1.15	1,311,173
Simulation #6	23,192,415	2,610,744	39,253,821	96,479,209	135,733,030	1.16	1,226,143
Simulation #7	56,469,629	27,334,240	46,221,112	115,116,778	161,337,890	1.17	1,465,620
Simulation #8	41,772,608	15,275,945	43,928,681	103,421,599	147,350,280	1.14	1,355,725
Simulation #9	25,092,573	5,489,245	39,056,327	87,574,493	126,630,820	1.14	1,203,095
Simulation #10	46,913,341	20,258,411	45,718,627	107,800,583	153,519,210	1.14	1,409,163
Simulation #11	48,444,562	22,595,528	43,458,695	100,543,455	144,002,150	1.16	1,363,629
Simulation #12	44,905,682	19,665,977	45,283,640	104,723,030	150,006,670	1.13	1,386,516
Simulation #13	73,908,802	46,283,224	47,396,077	109,279,983	156,676,060	1.18	1,512,418
Simulation #14	61,832,927	29,152,650	50,283,490	122,269,610	172,553,100	1.14	1,553,584
Simulation #15	40,164,347	16,093,142	41,006,269	94,664,831	135,671,100	1.16	1,289,911
Simulation #16	36,113,156	15,741,623	38,721,337	94,333,183	133,054,520	1.20	1,255,216
Simulation #17	42,028,019	20,253,909	42,343,729	96,177,061	138,520,790	1.16	1,323,842
Simulation #18	39,741,295	16,989,388	40,873,773	94,581,727	135,455,500	1.17	1,291,591
Simulation #19	53,031,117	27,284,555	46,773,596	106,245,234	153,018,830	1.13	1,431,409
Simulation #20	56,262,358	27,592,628	48,733,537	111,369,233	160,102,770	1.13	1,482,639
Simulation #21	37,877,137	14,047,885	44,371,168	105,569,442	149,940,610	1.14	1,364,412
Simulation #22	41,860,337	17,634,881	43,968,680	99,514,210	143,482,890	1.13	1,341,826
Simulation #23	29,610,377	8,185,630	41,358,758	91,820,282	133,179,040	1.12	1,251,940
Simulation #24	47,718,275	22,566,053	44,341,169	104,358,321	148,699,490	1.16	1,386,644
Simulation #25	23,178,510	4,865,942	37,918,861	84,427,829	122,346,690	1.15	1,177,007

Table 7.3 Output of Whittle optimization for the pit shell 29

The spread above and below the average is limited to +14.3 and –13.4%. Histograms have been attached (figure 7.27, 7.28, 7.29) for the "Discounted Open Pit Value" for the best and worst case and for the "Quantity of Au Output". For each histogram, values have been normalized to reflect the position of each model relative to each other.

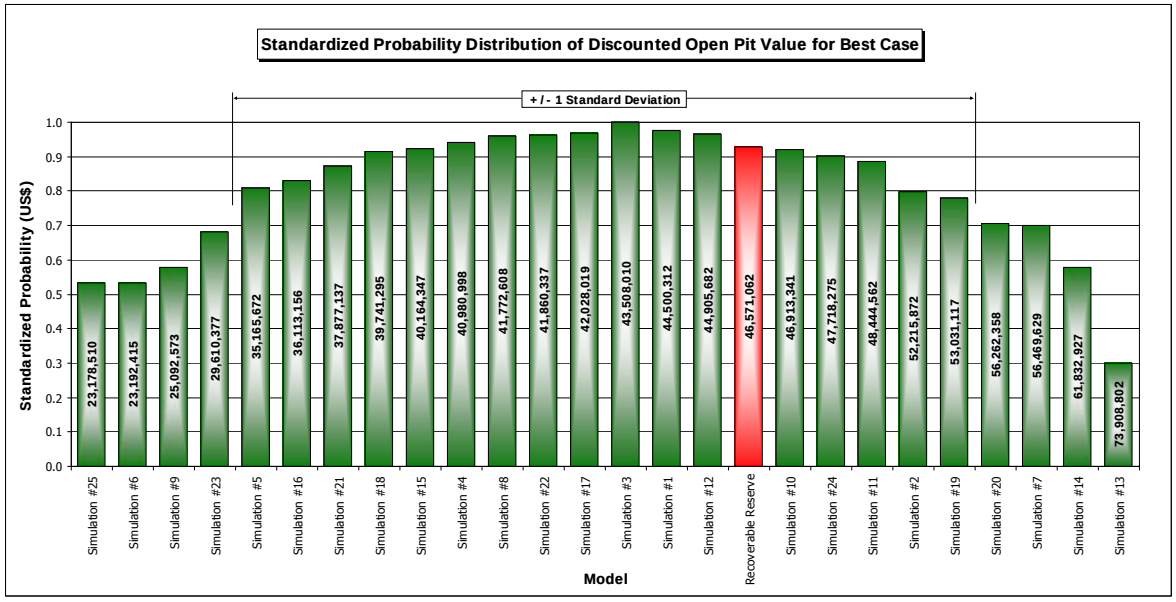

Figure 7.27 Standardized probability distribution of discounted open pit value for best case

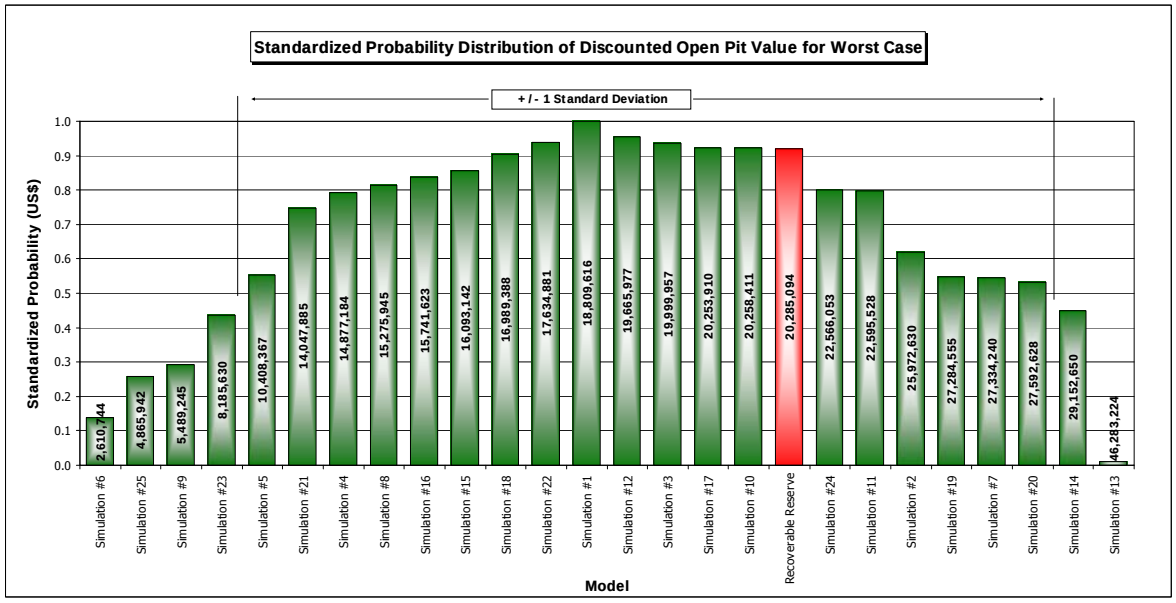

Figure 7.28 Standardized probability distribution of discounted open pit value for worst case

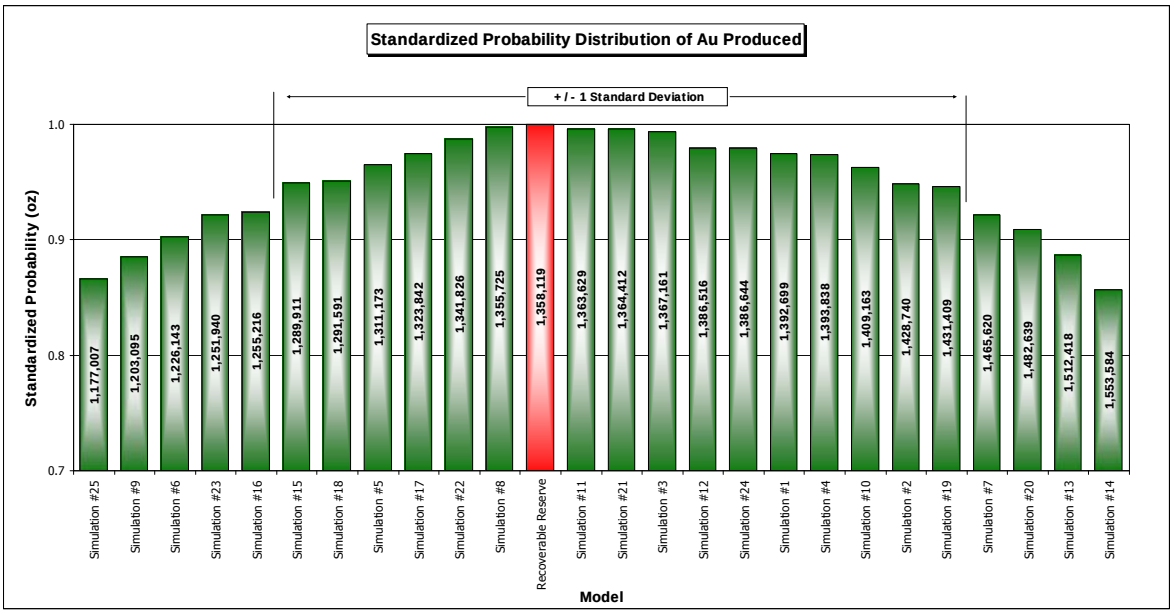

Figure 7.29 Standardized probability distribution of Au produced

Having analysed some variables that give a good indication of how the recoverable reserves performs overall when compared to the average of 25 simulations and it's relative performance in regard to the variability of the 25 simulations, we can conclude that the model is quite robust. The only downfall is on the effectiveness of the model to precisely estimate the NPV of the best and worst case schedule. Since the amounts of ounces produced are almost equal, we should expect the NPV of the model to be closer to the average of 25 simulations than it actually is. This can only be explained by the location of the ore and its grade in the pit in regard to the time that this ore generates revenue (processed). The ore sent to the mill at the early stage of the mine life from the recoverable reserves is probably of higher grade than the average of the 25 simulations, resulting in an increase of the NPV for both schedules. Knowing all these intricacies about the base case kriged model would certainly help in making sound decisions, in understanding and relating the risk to key assumptions. Moreover, the management would be able to change assumptions on linear parameters such as mining cost, mill recoveries and get a true picture of the positive or negative effects of these changes. In this case, if management relied only on the kriged model, as it is too often the case, when starting mining the result would be an

overestimation of the NPV in 64% of the time and an overestimation of the recovered ounces in 44% of the time.

7.4.3 Pushbacks selection

The following figure (7.30) is a graphic exported from Whittle 4X entitled "Pit by Pit Graph". It shows a series of pit shells with their respective discounted open pit values (NPV) for worst and best case mining schedules and tonnages for ore and waste material. In this case, the recoverable reserve model has been chosen as the base case scenario. The reason being that the long term mine planning is carried out based on this model. The "Pit by Pit Graph" is used to get a general understanding of how the deposit reacts to different prices and is also used to select the mining sequence in which the deposit is going to be mined.

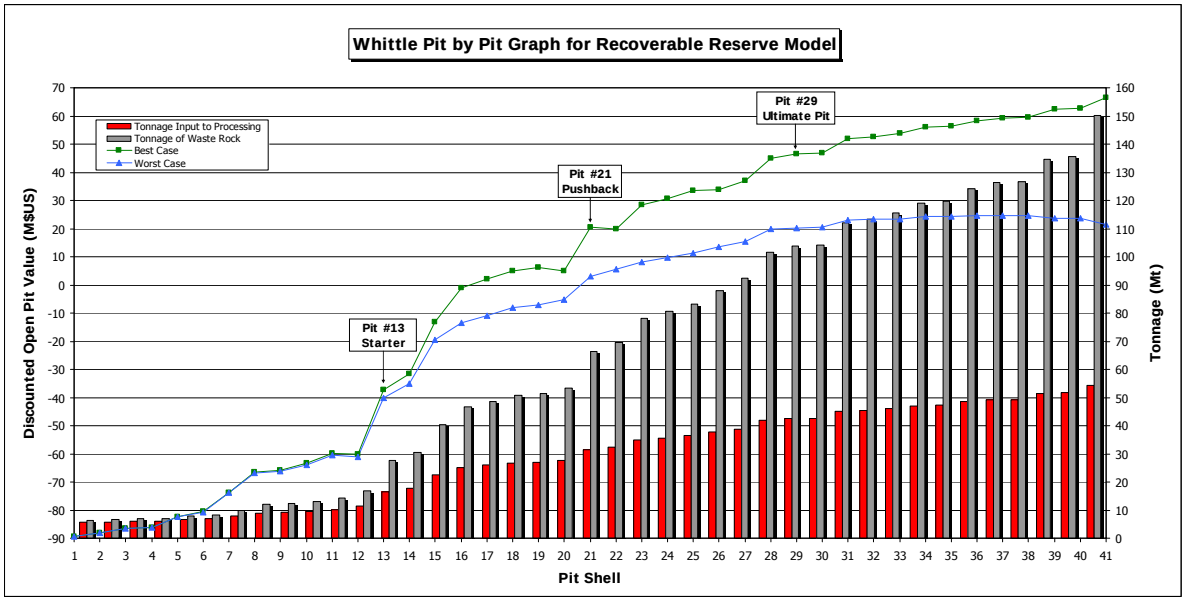

Figure 7.30 Whittle pit by pit graph for Recoverable Reserve model

Analysing this graphic, we can see the worst and best case schedule vary only for a couple of percent for the pit shells 1 to 12. This indicates that for those pit shells, the mining sequence is unimportant from an economic point of view. When a mining company establishes the strategy by which the resource will be mined, they will stage the development of their open pit in a way to increase the net present value (NPV) of the

resource and to minimize the payback period. First, a starter pit (low gold price) will be established to take advantage of the high grade material at the beginning of the operation. By doing this, the mine will generate higher revenues upfront that will be used to repay the capital invested. Then, as mining progresses, pushbacks are introduced in such way that mining operations will have enough room to manoeuvre, stripping of waste material will be minimized and that enough ore will be exposed to feed the mill (table 7.4, 7.5).

Pit Shell	Discounted Open Pit Value for Best Case	Discounted Open Pit Value for Worst Case	Tonnage Input to Processing	Tonnage of Waste Rock	Tonnage Total	Grade of Au Mined Input to Processing	Quantity of Au Output
13 - Starter Pit	-37,351,730	-40,127,644	16,504,504	27,688,526	44,193,030	1.28	570,397
21 - Pushback	57,679,228	43,208,650	15,057,048	38,736,772	53,793,820	1.12	456,975
29 - Ultimate Pit	26,243,564	17,204,088	10,969,671	37,496,699	48,466,370	1.12	330,748

Table 7.4 Incremental pit shell characteristics based on pushback sequence 13-21-29

Pit Shell	Discounted Open Pit Value for Best Case	Discounted Open Pit Value for Worst Case	Tonnage Input to Processing	Tonnage of Waste Rock	Tonnage Total	Grade of Au Mined Input to Processing	Quantity of Au Output
13 - Starter Pit	-37,351,730	-40,127,644	16,504,504	27,688,526	44,193,030	1.28	570,397
21 - Pushback	20,327,498	3,081,006	31,561,552	66,425,298	97,986,850	1.21	1,027,371
29 - Ultimate Pit	46,571,062	20,285,094	42,531,223	103,921,997	146,453,220	1.18	1,358,119

Table 7.5 Cumulative pit shell characteristics based on pushback sequence 13-21-29

In the present mining scenario, pit shell 13, which is based on a gold price of 260$US has been chosen has the initial starter pit. This pit shell contains 16.5Mt of ore, sufficient for 3 years of mill feed based on a processing rate of 5.475Mtpa. Pit shell 21 will be the only pushback needed before getting to the ultimate pit. This shell was based on a gold price of 300$US and contains 15Mt of ore which is sufficient to support milling for 2.8 years. The ultimate pit (pit shell 29) was based on a price of 340$US and sets the ultimate size that the open pit will have. This mining phase has enough ore (11Mt) to feed the mill for 2 years. To suit the processing requirement, the mining rate will vary depending on the waste material that needs to be mined to expose the ore. In the case of the starter pit, the mining rate will need to be around 14.6Mtpa for 3 years. As the mining of the pushback starts, mining rates will need to be increased to 19.6Mtpa for 2.8 years to allow for the increase in waste material. Finally, as mining progresses to the ultimate phase, production will need to be further increased to 24.2Mtpa for the last 2 years of the operation.

7.4.4 Life of mine schedule

From those 3 pit shells, mining schedule can be derived. Based on criteria such as mining rate and processing rate, the Whittle software mines this series of pushback in such a way that the net present value will be maximized and that the operating criteria is respected.

Model	Year	Tonnage Input to Processing	Tonnage of Waste Rock	Tonnage Total	Grade of Au Mined Input to Processing	Quantity of Au Ouput	Discounted Open Pit Value	Cumulative Open Pit Value
Recoverable Reserve	1	4,449,679	15,550,321	20,000,000	1.20	144,748	20,061,948	-117,438,052
Average of 25 Simulations		4,943,948	14,903,098	19,847,046	1.20	160,627	24,596,808	-112,903,192
Maximum of 25 Simulations		5,475,000	16,316,319	20,000,000	1.27	187,443	32,708,656	-104,791,344
Minimum of 25 Simulations		3,683,681	12,867,894	18,342,894	1.14	116,086	11,725,005	-125,774,995
Recoverable Reserve	2	5,474,901	14,525,099	20,000,000	1.28	189,638	30,526,275	-86,911,776
Average of 25 Simulations		5,474,802	13,619,549	19,094,351	1.26	186,150	30,266,280	-82,636,912
Maximum of 25 Simulations		5,475,000	14,526,427	20,000,001	1.34	198,770	34,419,238	-70,372,106
Minimum of 25 Simulations		5,473,573	10,518,907	15,993,907	1.20	177,843	27,260,014	-97,986,330
Recoverable Reserve	3	5,474,997	14,525,003	20,000,000	1.12	165,831	18,659,150	-68,252,627
Average of 25 Simulations		5,384,203	13,244,751	18,628,953	1.10	160,389	18,628,630	-64,008,282
Maximum of 25 Simulations		5,475,000	16,322,804	20,000,000	1.17	171,115	23,540,422	-49,946,665
Minimum of 25 Simulations		3,677,196	8,325,348	13,800,348	1.02	102,265	1,335,843	-80,213,184
Recoverable Reserve	4	5,475,000	13,968,566	19,443,566	1.18	174,365	24,032,456	-44,220,171
Average of 25 Simulations		5,333,560	14,563,844	19,897,404	1.07	154,955	17,464,033	-46,544,250
Maximum of 25 Simulations		5,475,000	15,920,560	20,000,001	1.17	173,481	24,981,115	-35,278,055
Minimum of 25 Simulations		4,079,440	12,296,344	17,771,344	0.89	99,156	834,599	-71,867,392
Recoverable Reserve	5	5,474,723	14,525,277	20,000,000	1.05	155,118	14,872,507	-29,347,663
Average of 25 Simulations		5,456,236	14,543,756	19,999,992	1.08	159,175	16,729,602	-29,814,647
Maximum of 25 Simulations		5,475,000	14,701,270	20,000,000	1.25	184,378	24,000,690	-16,928,047
Minimum of 25 Simulations		5,298,730	14,524,791	19,999,791	0.99	146,935	12,846,223	-55,369,977
Recoverable Reserve	6	5,475,000	14,523,407	19,998,407	1.09	160,756	15,832,339	-13,515,325
Average of 25 Simulations		5,255,849	14,409,341	19,665,190	1.04	148,018	12,958,020	-16,856,627
Maximum of 25 Simulations		5,475,000	15,927,032	20,000,000	1.21	178,541	26,031,212	-2,926,510
Minimum of 25 Simulations		4,072,968	7,971,315	13,446,315	0.93	105,089	2,105,465	-37,268,559
Recoverable Reserve	7	5,475,000	12,023,037	17,498,037	1.21	178,849	21,655,768	8,140,444
Average of 25 Simulations		5,340,816	11,035,408	16,376,224	1.11	159,551	17,557,666	701,039
Maximum of 25 Simulations		5,475,000	16,071,048	20,000,000	1.29	187,728	27,563,186	24,636,676
Minimum of 25 Simulations		3,928,952	3,677,641	8,316,090	0.97	103,683	2,104,811	-25,037,313
Recoverable Reserve	8	5,090,948	4,259,821	9,350,769	1.33	183,425	28,489,290	36,629,734
Average of 25 Simulations		4,659,632	4,963,264	9,622,895	1.27	155,828	21,932,067	22,633,107
Maximum of 25 Simulations		5,475,000	11,760,988	17,235,988	1.69	199,243	31,019,831	38,368,445
Minimum of 25 Simulations		488,030	96,464	584,494	1.01	16,913	-281,899	-6,472,751
Recoverable Reserve	9	140,975	21,466	162,441	1.42	5,389	1,035,159	37,664,893
Average of 25 Simulations		1,718,689	940,694	2,659,382	1.17	66,478	11,955,358	30,267,521
Maximum of 25 Simulations		5,475,000	6,748,253	12,223,252	1.77	194,093	34,484,275	63,311,801
Minimum of 25 Simulations		0	0	0	0.00	0	0	0

Table 7.6 Whittle life of mine scheduling based on mining sequence #13, #21, #29

From table 7.6 above, we can see that overall the schedule respects the upper limit of 20Mt of material mined in a year and that the mill is generally fed at his nominal rate of 5.475Mt per year. The only exception is in the first year where only 4.4Mt is processed for all models. This can be related to the amount of pre-stripping needed in year 1 to expose enough ore. One way of working around this problem would have been to allow some capital expenditure for the pre-stripping of the deposit before production starts. The first 3

years of operation show the recoverable reserve model being very close to the average of the 25 simulations for the "Grade of Au Mined" and for the "Quantity of Au Output". This is also reflected in the "Cumulative Open Pit Value" where both models show almost the same value. Both achieved payback of the capital invested in year 7 and the ultimate "Cumulative Open Pit Value" come in at 37.66M$US for the recoverable reserve model versus 30.26M$US for the average of the 25 simulations. It is interesting to put the final value of the current mining schedule in respect to the best and worst case mining scenarios. As previously discussed, we can expect the present schedule to be somewhere in between the best case and worst case scenario. This is exactly what happens with the current mining schedule of pit 13-21-29. Its final "Cumulative Open Pit Value" lies between 46.57M$US (Best Case) and 20.28M$US (Worst Case).

7.5 Pit design

One other avenue to compare the recoverable reserve model against the simulation is to generate reserve reports using the same pit design. The current ultimate pit design used at Troilus was based on the same parameters as those used for the current pit optimization; therefore it is logical to use it for comparison purposes. Table 7.7 below shows the reserves contained within the final pit for the recoverable reserve and for the 25 simulations. When the recoverable reserve model is compared against the averaged simulation, we can observe that, in general, its estimates came very close. The tonnage of all material is overestimated by 1.1% (+485,346t) and the contained ounces are overestimated by 2.7% (+41,758oz). Once again, most of the difference comes from the low grade HW and FW zones. The ore tonnage difference for the HW zone is 848,817t (+16.2%) and 505,988t (7.2%) for the FW zone. As for the contained ounces, the discrepancies are 22,660oz (+20.3%) and 15,561oz (+7.6%) for the HW and FW zones respectively. On the other hand, the CORE zone and 87S zone shows a different pattern. The ore tonnage is underestimated for both zones by 2.2% (-657,145t) for the CORE zone and by 22.4% (-212,315t) for the 87S zone.

	ALL			HW			CORE			FW			87S		
Model	Tonnage	Au (g/t)	Au (oz)	Tonnage	Au (g/t)	Au (oz)	Tonnage	Au (g/t)	Au (oz)	Tonnage	Au (g/t)	Au (oz)	Tonnage	Au (g/t)	Au (oz)
Recoverable Reserve	44,046,768	1.14	1,609,100	6,077,504	0.69	134,428	29,708,009	1.29	1,232,960	7,526,284	0.91	219,540	734,971	0.94	22,171
Average of 25 Simulations	43,561,422	1.12	1,567,343	5,228,687	0.66	111,769	30,365,154	1.26	1,227,020	7,020,296	0.90	203,979	947,286	0.81	24,575
Maximum of 25 Simulations	44,613,673	1.16	1,623,044	5,861,185	0.67	124,655	31,084,606	1.30	1,285,539	8,453,380	0.93	252,690	1,109,895	0.86	29,371
Minimum of 25 Simulations	41,770,997	1.09	1,503,997	4,593,688	0.66	97,308	29,645,026	1.22	1,178,624	5,706,648	0.88	160,796	775,310	0.74	19,563
Simulation #1	43,639,247	1.10	1,546,288	5,424,913	0.67	116,413	30,004,301	1.24	1,199,832	7,428,478	0.88	209,591	781,555	0.81	20,452
Simulation #2	44,574,105	1.11	1,584,603	5,309,266	0.66	113,158	29,791,790	1.25	1,194,506	8,453,380	0.93	252,690	1,019,669	0.74	24,249
Simulation #3	43,322,463	1.12	1,561,451	5,120,710	0.67	110,168	30,785,238	1.25	1,240,815	6,495,344	0.90	187,143	921,171	0.79	23,325
Simulation #4	43,451,435	1.11	1,553,553	5,861,185	0.66	124,655	30,013,368	1.26	1,212,339	6,650,910	0.90	192,117	925,972	0.82	24,443
Simulation #5	42,638,518	1.12	1,536,862	4,593,688	0.66	97,308	29,790,146	1.25	1,198,597	7,381,726	0.91	216,865	872,958	0.86	24,093
Simulation #6	41,770,997	1.12	1,503,997	5,139,164	0.67	111,056	29,874,061	1.25	1,204,382	5,706,648	0.88	160,796	1,051,124	0.82	27,762
Simulation #7	42,877,098	1.16	1,595,439	5,028,003	0.67	108,149	30,762,178	1.30	1,285,539	6,034,069	0.89	173,297	1,052,848	0.84	28,455
Simulation #8	43,045,220	1.12	1,556,898	5,254,609	0.66	112,147	30,262,381	1.26	1,225,987	6,625,352	0.92	195,323	902,878	0.81	23,442
Simulation #9	43,281,669	1.10	1,535,384	5,287,281	0.67	113,732	29,793,762	1.23	1,178,624	7,176,828	0.93	215,532	1,023,798	0.84	27,496
Simulation #10	44,140,494	1.12	1,590,814	5,439,288	0.67	116,330	31,024,984	1.26	1,256,132	6,660,048	0.90	191,842	1,016,174	0.81	26,510
Simulation #11	43,508,770	1.14	1,594,125	5,352,410	0.67	114,468	31,084,606	1.28	1,278,816	6,089,247	0.89	174,306	982,507	0.84	26,536
Simulation #12	43,172,160	1.11	1,540,972	5,219,504	0.66	111,445	30,315,672	1.25	1,215,393	6,740,970	0.88	191,734	896,014	0.78	22,400
Simulation #13	44,113,790	1.14	1,623,044	4,921,585	0.66	103,819	30,642,157	1.29	1,267,333	7,440,153	0.93	222,521	1,109,895	0.82	29,371
Simulation #14	44,183,034	1.12	1,588,910	4,868,305	0.66	102,661	30,785,063	1.25	1,237,271	7,678,785	0.92	227,811	850,881	0.77	21,167
Simulation #15	43,441,793	1.14	1,587,086	5,246,305	0.67	112,703	30,774,963	1.28	1,263,532	6,448,229	0.89	185,303	972,296	0.82	25,549
Simulation #16	42,981,949	1.15	1,582,552	4,838,059	0.66	102,550	30,644,722	1.29	1,269,336	6,723,858	0.88	191,103	775,310	0.78	19,563
Simulation #17	44,340,741	1.12	1,593,282	5,243,048	0.67	112,143	30,719,007	1.25	1,237,955	7,566,556	0.92	222,880	812,130	0.78	20,305
Simulation #18	43,992,477	1.13	1,600,569	4,885,283	0.66	104,272	30,703,654	1.27	1,257,327	7,311,912	0.90	211,478	1,091,628	0.78	27,492
Simulation #19	44,613,673	1.10	1,584,621	5,468,558	0.67	117,553	30,144,794	1.24	1,201,506	8,040,652	0.93	240,968	959,669	0.80	24,595
Simulation #20	44,374,237	1.10	1,570,900	5,376,113	0.66	113,931	30,350,008	1.24	1,210,224	7,821,063	0.89	224,374	827,053	0.84	22,371
Simulation #21	42,821,872	1.11	1,535,009	5,046,622	0.67	107,916	29,645,026	1.25	1,194,399	7,158,201	0.90	207,364	972,023	0.81	25,331
Simulation #22	43,850,286	1.11	1,560,280	5,136,071	0.66	109,703	30,594,534	1.24	1,222,507	7,121,653	0.88	202,306	998,028	0.80	25,763
Simulation #23	43,736,286	1.09	1,527,312	5,681,140	0.66	121,375	30,146,652	1.22	1,178,726	6,907,681	0.91	202,267	1,000,813	0.78	24,944
Simulation #24	43,999,643	1.12	1,587,512	5,472,179	0.67	117,869	30,390,171	1.27	1,236,996	7,243,661	0.90	209,736	893,632	0.80	22,911
Simulation #25	43,163,600	1.11	1,542,099	5,503,880	0.67	118,691	30,085,600	1.25	1,207,429	6,601,995	0.90	190,123	972,125	0.83	25,857

Table 7.7 Total material mined at the end of the final pit

As far as the contained ounces are concerned, an overestimation of 5,940oz (+0.5%) and an underestimation of 2,404oz (-9.8%) occur for the CORE and 87S zone respectively. Figures 7.31 and 7.32 show graphically the potential variation in the material feeding the mill (tonnage and head grade).

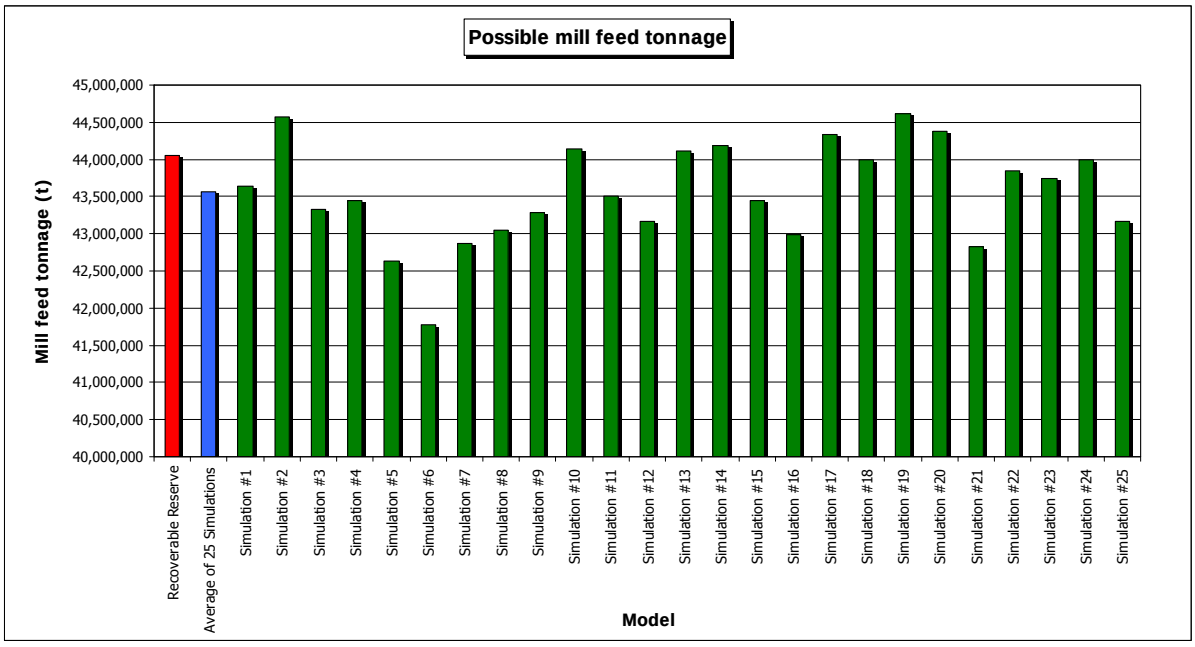

Figure 7.31 Possible mill feed tonnage

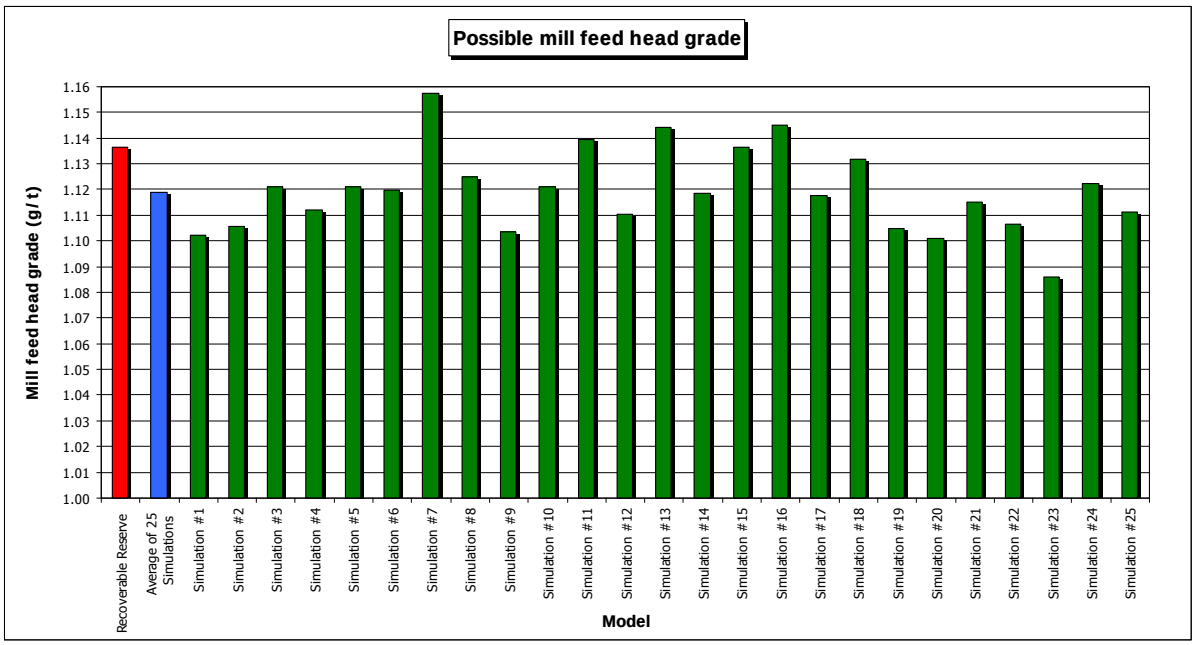

Figure 7.32 Possible mill feed head grade

7.6 Conclusion

Sequential indicator conditional simulation was used to simulate the Troilus orebody. The overall statistics of simulated data are representative of the underlying composite data, which indicate that no bias was introduced during the simulation. As a means to compare simulations, an open pit optimization program was used as a transfer function. Outputs from the optimization reveal the effect of the high variability in the Troilus orebody. The net present values show a spread of –47% to +70% around the average of the 25 simulations, whereas a spread of –13% to +14% is observed for the ounces recovered. The recoverable reserve model overestimates the net present value in 64% of the time and overestimates recovered ounces in 44% of the time. A comparison was also carried out on a certain volume of material within the designed open pit currently used at Troilus. In this case, the recoverable reserve model overestimates ore tonnage in 72% of the time and overestimates recovered ounces in 96% of the time.

CHAPTER 8

Conclusions and Recommendations

8.1 Conclusions

The use of geostatistics to quantify the tonnage and the grade of a mineralized deposit is a common practice widely acknowledged in the mining industry. However, people should not forget that the end product of a resource/reserve estimation is just that, an estimation. Underlying this estimation are assumptions made by the geologist and geostatistician that will have a great influence on the outcome. To start, geological modelling will be synthesized into something that will be, most of time, far less complicated than it is in reality. This can be explained by the lack of information and by the limitation of today's mining software to handle complex geological deposits. Once the geological modelling is finished, another set of assumptions will be introduced regarding the compositing of assays, the continuity of the deposit and the interpolation method. They will be based on previous experiences of the geostatistician on this type of deposits, on the time and budget allowed to conduct the study and to a certain extent, to the technical understanding of the person in charge of the estimation. Mixed altogether, those series of assumptions can generate a wide range of estimation results. The objective of this thesis was to revisit the early assumptions used in order to improve the resource/reserve estimation of the Troilus orebody.

The first thing to be looked at was the geological interpretation of the orebody. Previous geological domains were derived from DDH at a mineralization threshold value of 0.2 g/t, which resulted in using one set of variograms to estimate the majority of the block of the 87 zone. From discussions with the senior geologist of the mine and by analysing the spatial distribution of the gold assays, it became obvious that a core of high grade material was present in the central portion of the 87 and 87S zones. As a result of this, a new set of geological envelopes were created named HW, CORE, FW and 87S. As demonstrated by the contact profile analysis, the average grades of the 87 and 87S zones are significantly higher than those of the zone sitting on the outside (HW and FW), confirming the presence of 4 distinct populations. This change had for effect to improve variogram modelling and to

enhance the resolution of the model by allowing each individual zone to be modified and adjusted to better reconcile with past production. Another benefit was the reconciliation problem encountered with the HW zone, which otherwise would be unidentified if the old 0.2 g/t envelop had been used. Finally, those new domains will be helpful to decide where to focus time and effort in order to develop a better representative model for every geological domain.

The use of indicator kriging interpolation methods for the project was another distinctive element from previous estimates. Non-linear techniques have the advantage of factoring the grades distribution into the interpolation process and to assess the local uncertainty of the estimates. They also have the benefit of improving the resolution of the cumulative distribution function by subdividing the data into multiple subsets. The application of this method has resulted in a model capable of estimating the tonnage and grade within reasonable limits. The overall tonnage was overestimated by 6.5%. Putting aside the problematic HW zone, where the bulk of the discrepancy is contained; the overestimation would have been 2.4%. As for the contained ounces, the model underestimates it by 5.7%. Again, if the HW zone was not considered, the underestimation would have been lowered to 2.7%. Fluctuations over a large area have been kept minimal, which led to conclude that the general goals of the recoverable reserve model have been fulfilled. As a result, the operating plan should be achieved without any surprises.

Finally, the variability of the mineralization was assessed through an extensive conditional simulation study. This was something that has never been done before at Troilus and proved to be successful in determining the risk associated with the model. As expected, with the type of mineralization encountered at Troilus, the spread among the simulations was quite significant, indicating that risk is inherent to the mineralization and that cautious attention should be given to the resource estimation. As for the model itself, the number of ounces and the tonnage of ore are almost identical to the averaged simulation when a pit optimization is used as transfer function. Substantial discrepancy and fluctuation among the different models occurs when the actual time of mining and processing an ore block is taken into consideration. The recoverable reserve model overestimates the NPV by 7.1% and by 7.9% for the best case and worst case mining scenario. This should, however, be put

into perspective with the overall spread among the estimates, which comes in at +70% and -47%. The robustness of the model is clearly demonstrated when it is compared to the average simulation for the pit design transfer function. The model overestimates the tonnage of ore and the contained ounces by 1.1% and 2.7% respectively. Overall, comparison against the averaged simulation shows that the model presents minimum risk and is representative of the mineralization.

8.2 Recommendations

The new set of methods applied on the Troilus deposit to estimate the resource and to analyse the risk could be extended to other areas not covered in this thesis. One avenue would be to use the probabilities from the indicator kriged model to manage the sampling strategy in the area of high grade material where the chances of occurrence are low. In the same line of thought, the planning engineer could use the probability from the model to correlate production to the uncertainty levels.

Another possibility could be to introduce the risk related to mineralization into the budgeting process, which would give management a heads up about possible fluctuations of ore tonnage and grade mined. Simulation could be also be used to assess the potential of different mineralized zones around the 87 zone. The J4 zone and possibly the extension of the 87S zone could be assessed through conditional simulation to generate better drilling targets, hence possibly expanding the resources base. On the operation side, the level of selectivity could be balanced through a bench height study. Due to its small size relative to the 87 zone, the J4 zone might require a higher degree of selection. And finally, at the corporate level, risk analysis through simulation could be introduced to rank different grassroots and advanced projects based on their risk prior to joint venturing or acquisition.

REFERENCES

Anderson, M.J., *Open pit mine planning using simulated gold grades*, M.Sc. Thesis, Queen's University, 1999.

Armstrong, M. and Matheron, G., *Geostatistical Case Studies*, Boston, Kluwer Academic Publishers, 1987. 248p.

Atkinson, P.M. and Lloyd, C.D., *Designing optimal sampling configurations with ordinary and indicator kriging*, Proceedings of the 4th International Conference on GeoComputation, Mary Washington College, Fredericksburg, Virginia, USA, 1999.

Blackney, P.C.J. and Glacken, I.M., *A practitioners implementation of indicator kriging*, The Geostatistical Association of Australasia. "Beyond Ordinary Kriging" Seminar, Perth, Western Australia, 1998.

Blackwell, G.H., *Open pit mine planning with simulated gold grades,* CIM Bulletin, Vol. 93, No 1039, 2000.

Boily, B., *Porphyry-type mineralization in the Frotet-Evans greenstone belt – The Troilus Au-Cu deposit*, Internal report from Inmet Mining Corporation, 1997.

Cater, D., Perron, B, Savard, C. and Warren, D., *Inmet Mining Corporation – Troilus Project – 1997 Mine Reconciliation Report*, Internal report from Inmet Mining Corporation, 1997.

Chiles, J-P and Definer, P., *Geostatistics : Modeling Spatial Uncertainty*, New York, John Wiley & Sons, Inc. Scientific, Technical and Medical Division., 1999. 672 p.

Clark, I., *Block by block reserve estimation – a case study*, 2nd International Surface Mining and Quarrying Symposium, Bristol, England, 1983.

Clark, I., *The art of cross validation in geostatistical applications.* 19th International Application of Computers and Operations Research in the Mineral Industry Symposium, Pennsylvania State University, USA, 1986. pp.211-220.

Clark, I., *Practical reserve estimation in a shear-hosted gold deposit*, International Mining Geology Conference, Kalgoorlie-Boulder, Western Australia, Australia, 1993. pp.157- 160.

Clark, I and Frempong, P.K., *Geostatistical studies and assessment of geological and mining reserves of Palabora Phosphate and Vermiculite deposits,* International Conference on Surface Mining, Johannesburg, Symposium Series S 15, 1996.

Clark, I and Harper, W.V., *Practical Geostatistics 2000,* Ecosse North America Llc. Columbus, 2000. 442 p.

Clark, I. and Vieler, J.D.S., *Hole effects in diamond cores from Palabora Mine*, Quantitative Geology and Geostatistics Volume 5, Geostatistics Troia 92, Vol. 2, 1992. pp.1001- 1012.

Clark, I. And White, B., *Geostatistical modelling of an ore body as an aid to mine planning*, 14th International Application of Computers and Operations Research in the Mineral Industry Symposium, Pennsylvania State University, USA, 1976. pp.1004-1012.

Coombes, J., *Handy hints for variography*, Proceedings of AusIMM Ironmaking Resources and Reserves Conference, 1997. pp. 127-130.

Coombes, J., Gifford, M., Jepsen, L. and Thomas, G.S., *Assessing the risk of incorrect prediction – A nickel/cobalt case study*, Proceedings of the Mine to Mill Conference, Brisbane, Australia, 1998.

Coombes J., Glacken I., Snowden V and Thomas G., *Conditional simulation - which method for mining?*, Geostatistics Conference 2000, Cape Town, South Africa, 2000.

Coombes, J., Richards, W.L. and Thomas, G.S., *Practical conditional simulation for geologists and mining engineers,* Proceedings of the 3rd Regional Application of Computers and Operations Research in the Mineral Industry Symposium, Kalgoorlie, Western Australia, Australia, 1998. pp.19-26.

Coombes, J. and Snowden, V., *Applied Mining Geostatistics – Short Course Notes*, Toronto, 1998.

Costa, J.F.C.L., Koppe, J.C. and Zingano, A.C., *Conditional simulation for oil grade estimation and mine planning*, Mine Planning and Equipment Selection. Balkema, Rotterdam, 1996.

Costa, J.F., Koppe, J.C. and Zingano, A.C., *Simulation - an approach to risk analysis in coal mining*, Exploration and Mining Geology Journal. Vol.9, No. 1, 2000. pp.43-49.

David, M., *Handbook of applied advanced geostatistical ore reserve estimation*, New York, Elsevier Science Publishing Company, 1988. 216 p.

Deutsch, C.V. and Gringarten, E., *Teacher's aide variogram interpretation and modeling. Mathematical Geology*, Vol. 33, No. 4, 2001. pp. 507-534.

Deutsch, C.V. and Journel, A.G., *GSLIB Geostatistical Software Library and User's Guide* New York, Oxford University Press. Oxford, 1992. 340 p.

Dimitrakopoulos, R., *Conditional simulations: Tools for modelling uncertainty in open pit optimisation,* Optimizing with Whittle 1997 Proceedings, Perth, 1997. pp. 31-42.

Dimitrakopoulos, R,. *Conditional simulation algorithms for modelling orebody uncertainty in open pit optimisation*, International Journal of Surface Mining, Reclamation and Environment 12, 1998. pp.173-179.

Dimitrakopoulos, R., *Geostatistical simulation for the mining industry: Orebody uncertainty, risk assessment and profitability in ore reserves, grade control and mine planning – Short Course Notes,* WH Bryan Mining Geology Research Centre, University of Queensland, Australia. 2001.

Dimitrakopoulos, R., Farrelly, C.T. and Godoy, M., *I'd rather be approximately right than precisely wrong: Grade uncertainty, risks effects and decision making in open pit desig,* Optimizing with Whittle 2001 Proceedings, Perth, 2001. pp. 35-42.

Farrelly, C.T. and Dimitrakopoulos, R., *Support effects when optimising with Whittle Four-D, Wirralie gold deposit, North Queensland*, Optimizing with Whittle 1999 Proceedings, Perth, 1999. pp. 51-59.

Fytas, K., *Estimation des réserves*. Courses notes, Université Laval. 1995.

Geostat Systems International Inc., *Grade interpolation parameters for small blocks in zones/lenses of the Troilus-Frotet Au-Cu deposit*, Internal report from Inmet Mining Corporation, 1993.

Geostat Systems International Inc., *Update of resource/reserve model for 87/87S deposit of the Troilus deposit*, Internal report from Inmet Mining Corporation, 1995.

Geostat Systems International Inc., *Geostatistical analysis of Troilus BH data,* Internal report from Inmet Mining Corporation, April 1997.

Geostat Systems International Inc., *Geostatistical analysis of Troilus BH data*, Internal report from Inmet Mining Corporation, December 1997.

Geostat Systems International Inc., *Update of Troilus long term resource model*, Internal report from Inmet Mining Corporation, 1998.

Gervais, R., *Évaluation des réserves géologiques du gisement Goldex des mines Agnico-Eagle*, Maîtrise, École des gradués, Université Laval, 2000.

Glacken, I.M., *Change of support and use of economic parameters for block selection*, Proceedings Geostatistics Wollongong '96, Vol 2, 1997. pp. 811-821.

Goovaerts, P., *Geostatistics for natural resources evaluation,* Oxford New York, Oxford University Press, 1997. 483 p.

Guibal, D. and Vann, J., *Beyond ordinary kriging : An overview of non-linear estimation*, The Geostatistical Association of Australasia, "Beyond Ordinary Kriging" Seminar, Perth, Western Australia, 1998.

Gypton, Chris., *How have we done? Feasibility performance since 1980*, E&MJ, Engineering and Mining Journal, January 2002.

Hester, B.W., *What else can gold assays tell us?,* E&MJ, Engineering and Mining Journal, June 1991, 1991. pp. 1611-1620.

Isaaks, E.H. and Srivastava, R.M., *Applied Geostatistics,* Oxford New York, Oxford University Press, 1989. 561 p.

Khosrowshahi, S. and Shaw, W.J. 1997. *Conditional simulation for resource characterisation and grade control - principles and practice*. World Gold 1997 Conference Proceedings, Singapore, pp.275-282.

Khosrowshahi, S., Gaze, R.L. and Shaw, W.J., *Change of support for recoverable resource estimation*, Society for mining, metallurgy and exploration. For presentation at the SME Annual Meeting Denver, Colorado - March 1 - March 3, 1999, 1999.

Marcotte, D., *Géostatistique et géologie minières,* Courses notes, École Polytechnique, 2001.

Maunula, T., *Review of the Troilus J4 zone*, MRDI Canada, 2001.

Parrish, I.S., *Geologist's Gordian Knot: To cut or not to cut,* Mining Engineering. April 1997, 1997.

Redmond, D. and Soever, A., *Do the assumptions utilised in many geostatistical resource estimations reflect reality or wishful thinking,* Prospectors & Developers Association of Canada, Convention 2000, 2000.

Rendu, J.M., *Practical geostatistics at Newmont Gold: A story of adaptation*, Mining Engineering. February 1998, 1998.

Rossi, M.E., H. Van Brunt, B., *Optimizing conditionally simulated orebodies with Whittle Four-D*, Optimizing with Whittle 1997 Proceedings, Perth, 1997. pp. 119-124.

Rossi, M.E., *Improving the estimates of recoverable reserves*, Mining Engineering, January 1999, 1999.

Schofield, N., *Recoverable resource model and optimization*, Optimizing with Whittle 1995 Proceedings, Perth, 1995. pp. 125-134.

Sim, R., *Resource estimates for the 87/87S and J4 zones of the Troilus mine, Quebec*, Internal report from Inmet Mining Corporation, 1998.

Sim, R., *Resource/Reserve estimates for the 87 zones of the Troilus mine, Quebec*, Internal report from Inmet Mining Corporation, 1999.

Sim, R., *Update of Troilus block model*, Internal report from Inmet Mining Corporation, 2000.

Sim, R., *87 zone models with blasthole database*, Internal report from Inmet Mining Corporation, 2001.

Thomas, G.S., *Interactive analysis and modelling of semi-variograms,* Proceedings of 1st International Conference on Information Technologies in the Minerals Industry, Paper GT67, 1997.

Van Brunt, B.H., *Analyzing project risk due to deposit grade variation*, Whittle North American Strategic Mine Planning Conference, Colorado, 2000. pp. 1-14.

Warren, M.J., *Pre-feasibility and feasibility studies: A case for improvements*, Mining Industry Optimization Conference, AusIMM, June 1991, 1991.

Whittle 4X., *Reference manual*, 1998.

Wingle, W.L., *Evaluating subsurface uncertainty using modified geostatistical techniques*, Ph.D Thesis, Colorado School of Mines, Chapter 2, 1997. pp. 3-25.

Zhang, S., *Multimetal recoverable reserve estimation and its impact on the Cove ultimate pit design*, Mining Engineering, July 1998, 1998.

APPENDIX A – Mathematical Explanation

A.1 Variogram

The proofs, formulas and examples are paraphrased from the book Practical Geostatistics 2000 (Clark, I and Harper, W.V. 2000). For more detail of the theory, refer to this book.

The general equation of variogram is:

$$\gamma(h) = \frac{1}{2N_h} \sum_{h} (g_i - g_j)^2$$

Where: $\gamma(h)$ = sample variance at distance "h"

g_i = grade at location i
g_j = grade at location j
N = number of sample used
h = distance between sample used

The following shows a sample grid with gold sample values that will be used for explanation.

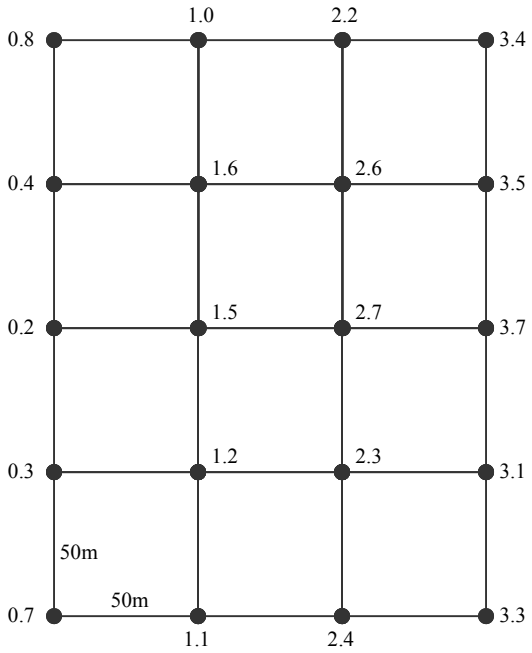

Let's pretend that we want to estimate the variogram in the direction North-South at a distance "h" of 50m. The sample variance would be calculated as follows:

$$\gamma(h) = \frac{1}{2 \times 20} \begin{Bmatrix} (0.7-0.3)^2 + (0.3-0.2)^2 + (0.2-0.4)^2 + (0.4-0.8)^2 \\ (1.1-1.2)^2 + (1.2-1.5)^2 + (1.5-1.6)^2 + (1.6-1.0)^2 \\ (2.4-2.3)^2 + (2.3-2.7)^2 + (2.7-2.6)^2 + (2.6-2.2)^2 \\ (3.3-3.1)^2 + (3.1-3.7)^2 + (3.7-3.5)^2 + (3.5-3.4)^2 \end{Bmatrix} = 0.041$$

If we change the distance "h" to 100m, the sample variance $\gamma(h)$ becomes:

$$\gamma(h) = \frac{1}{2 \times 12} \begin{Bmatrix} (0.7-0.2)^2 + (0.2-0.8)^2 \\ (1.1-1.5)^2 + (1.5-1.0)^2 \\ (2.4-2.7)^2 + (2.7-2.2)^2 \\ (3.3-3.7)^2 + (3.7-3.4)^2 \end{Bmatrix} = 0.067$$

After having calculated the variance $\gamma(h)$ for different distance (lag distance), we can plot those values. On the variogram graphic, the nugget effect corresponds to the variability of the sample at a very short distance, while the sill represents the variability of the sample from the nugget effect to the maximum variability of the sample. The range of influence indicates the distance from which the sample does not show any correlation between them.

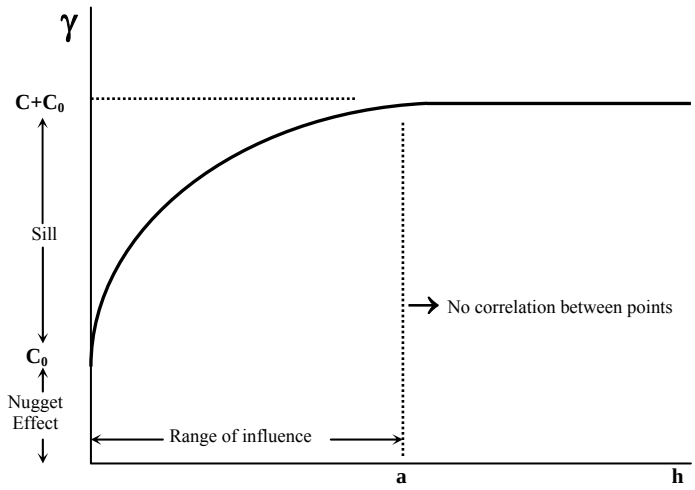

In order for kriging to proceed, the variogram curve needs to be modelized with a positive define function. The mathematical equation and the graphical representation of the most common model used is presented below:

Spherical model:

$$\gamma(h) = C_0 + C\left[\frac{3h}{2a} - \frac{h^3}{2a^3}\right]$$

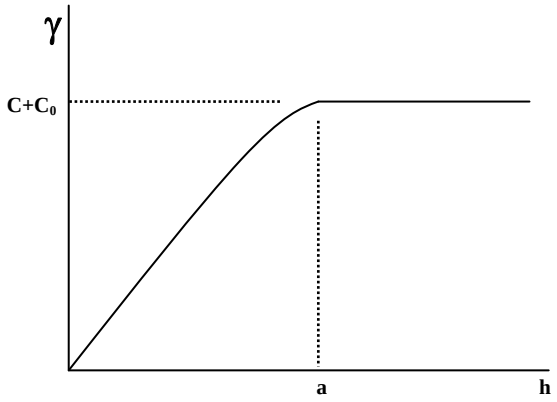

Exponential model:

$$\gamma(h) = C_0 + C\left[1 - \exp\left(-\frac{h}{a}\right)\right]$$

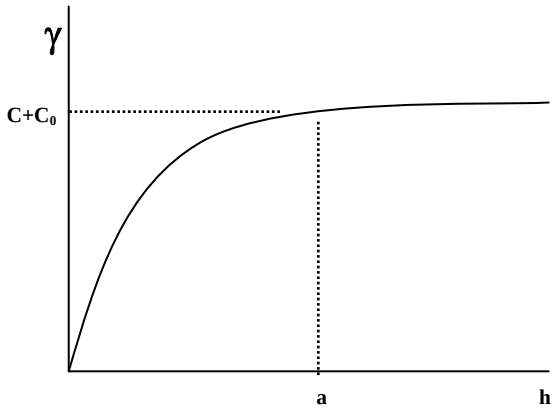

Gaussian model:

$$\gamma(h) = C_0 + C\left[1 - \exp\left(-\frac{h^2}{a^2}\right)\right]$$

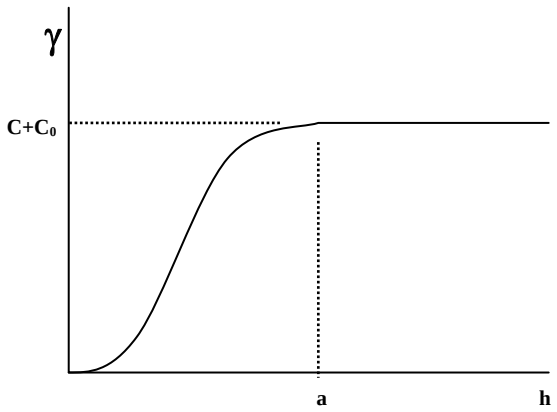

A.2 Inverse distance weighting method

The proofs, formulas and example are paraphrased from the book Practical Geostatistics 2000 (Clark, I and Harper, W.V. 2000). For more detail of the theory, referred to this book.

The general equation of the inverse distance estimation method is:

$$T^* = \sum_{i=1}^{m} w_i g_i$$ where: T^* = estimated value for T

w_i = weight of sample "i" where $\sum_{i=1}^{m} w_i = 1$

g_i = grade of sample "i"

The weight of the sample w_i are coming from an inverse function based on the distance of the sample from the unsample point to be estimated. This function is:

$\frac{1}{d^n}$ where "n" is the power of the function.

The following shows a sample grid with values. As an example, let's pretend that we want to estimate the unsampled point "**T**". Detail of how the point "**T**" is calculated is presented in the following table.

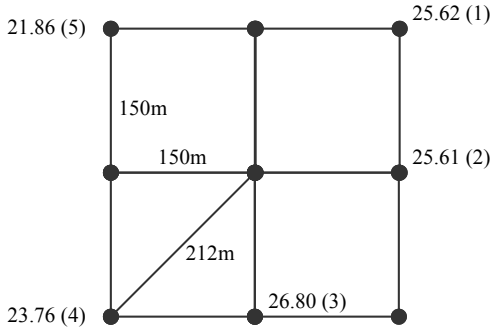

Sample i	d_i	$1/(d_i)^2$	$W_i=[1/(d_i)^2]/[\sum 1/(d_i)^2]$	G_i	$T^*=W_iG_i$
1	212	0.000022249	0.000022249/0.000155638 = 0.1430	25.62	3.6637
2	150	0.000044444	0.000044444/0.000155638 = 0.2855	25.61	7.3117
3	150	0.000044444	0.000044444/0.000155638 = 0.2855	26.80	7.6514
4	212	0.000022249	0.000022249/0.000155638 = 0.1430	23.76	3.3977
5	212	0.000022249	0.000022249/0.000155638 = 0.1430	21.86	3.1260
$\sum$		0.000155638	1.0000		25.1505

After calculation, the estimation of the grade at the unsample point "**T**" is equal to 25.1505.

A.3 Change of support

The best way to handle the change of support is to do our estimation on the same block size as our sample data, which is, unfortunately, impracticable. The principal concept behind the change of support, is to assess the problematic associated with the block size at which the deposit is going to be mined. In order to do so, some mathematical methods have been developed such as the affine correction and the indirect lognornal correction. Those two methods are based on two features: they leave the mean of the original sample data distribution unchanged and they adjust the variance of the transformed distribution by a factor called the "variance adjustment factor (f)" (Isaaks, E.H. and Srivastava, R.M. 1989). Following is an example describing the different steps involved to determine the impact on the distribution for a different size of support. Let's assume the following:

Variogram model: Spherical

Nugget effect: 0 $(g/t)^2$

Sill: 0.75 $(g/t)^2$

Range of influence: 50m

Block size: 15m x 15m x 15m

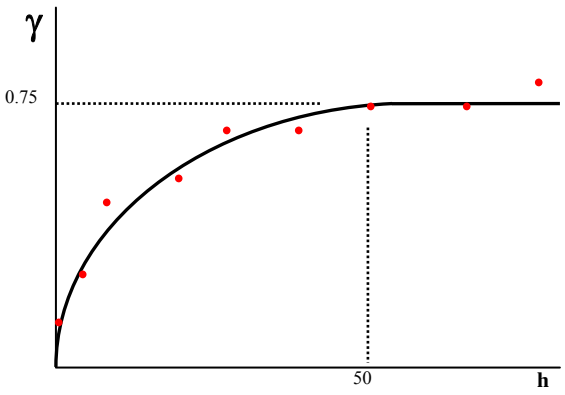

The variance adjustment factor "f" is determined by the function F(L,L,b)

where: $L = \frac{l}{a} = \frac{15m}{50m} = 0.30$ $B = \frac{b}{a} = \frac{15m}{50m} = 0.30$

From a table which lists value for the function F(L,L,B), we can find that for F(0.3,0.3,0.3), the variance adjustment factor "f" is equal to 0.291.

The affine correction method consists of reducing the distribution variance without changing its mean by squashing all of the values closer to the mean. The general equation of this method is as follow:

$q' = \sqrt{f} \times (q - m) + m$ where: q'= quantile of the new distribution

q= quantile of one distribution

f= variance adjustment factor

m= mean of both distribution

Let's suppose that the following histogram and univariate statistics represent the sample distribution of a gold deposit:

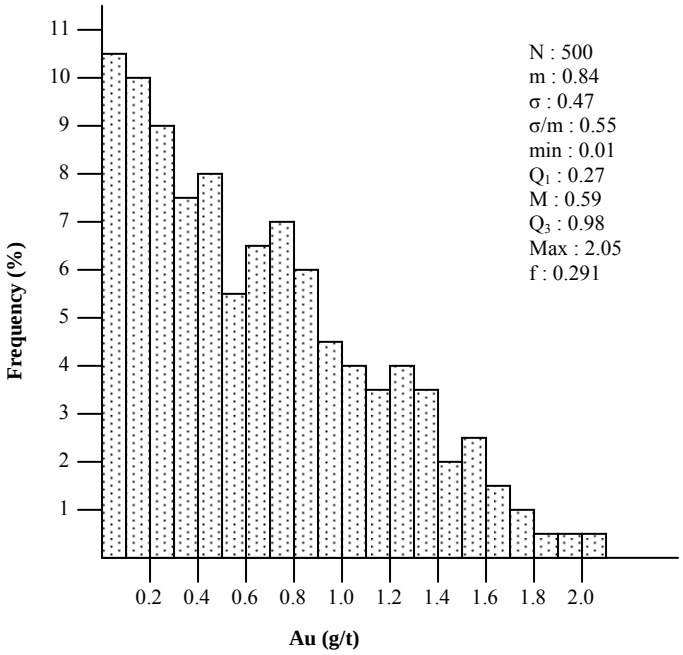

From the histogram's statistics, we can calculate the quartile "Q_1" of the new distribution:

$$q_1^{'} = \sqrt{f} \times (q_1 - m) + m \quad \Rightarrow \quad \sqrt{0.291} \times (0.27 - 0.47) + 0.47 = 0.3621$$

We can also do the same exercise for each decile, which will give us more points to make a histogram graph of the transformed distribution.

The other method is the indirect lognormal correction and consists of transforming a lognormal distribution to fit another lognormal distribution. To use this method, we have to make the assumption that both distributions are lognormal. The general equation of this method is as follows:

$q' = aq^b$ where: q'= quantile of the new distribution

q= quantile of one distribution

$$a = \frac{m}{\sqrt{f \times CV^2 + 1}} \left[\frac{\sqrt{CV^2 + 1}}{m} \right]^b \qquad b = \sqrt{\frac{\ln\left(f \times CV^2 + 1\right)}{\ln\left(CV^2 + 1\right)}}$$

From the histogram's statistics, we can calculate the quartile "Q_1" of the new distribution:

$$b = \sqrt{\frac{\ln\left(f \times CV^2 + 1\right)}{\ln\left(CV^2 + 1\right)}} \Rightarrow \sqrt{\frac{\ln\left(0.291 \times 0.55^2 + 1\right)}{\ln\left(0.55^2 + 1\right)}} = 0.5650$$

$$a = \frac{m}{\sqrt{f \times CV^2 + 1}} \left[\frac{\sqrt{CV^2 + 1}}{m} \right]^b \Rightarrow \frac{0.84}{\sqrt{0.291 \times 0.55^2 + 1}} \left[\frac{\sqrt{0.55^2 + 1}}{0.84} \right]^{0.5650} = 0.9575$$

$$q_1^{'} = aq_1^b \Rightarrow 0.9575 \times 0.27^{0.5650} = 0.4569$$

To summarize, the relation between block size and variance can be expressed with a probability plot as follows. It can be seen that as the block size increase, the variance around the mean decrease.

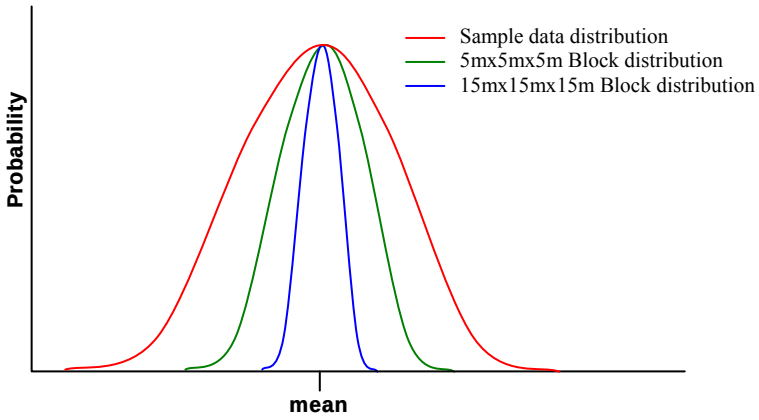

A.4 One point estimation

The proofs, formulas and examples are paraphrased from the book Practical Geostatistics 2000 (Clark, I and Harper, W.V. 2000). For more detail of the theory, refer to this book.

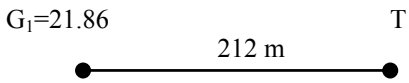

Estimation of T is given by the following equation:

$$T^* = w_1 g_1 + w_2 g_2 + w_3 g_3 + \ldots + w_n g_n$$

Where: T^* = estimated value for T

w_n = weight of sample "n" where $\sum_{i=1}^{n} w_i = 1$

g_n = grade of sample "n"

The error of the estimation is: $\varepsilon = T^* - T$

Where: ε = estimation error

T^* = estimated value for T

T = true value for T

In this example, the g_n values are coming from a normal distribution. Hence, the value of "T" will follow a normal distribution, as well as the estimated value of T (T^*) and it's error (ε). The mean of the estimator error "ε" will also come from a normal distribution. Hence the mean value is:

$$\mu_\varepsilon = E(\varepsilon)$$

Where: μ_ε = mean of the estimation error "ε"

$E(\varepsilon)$ = average for the population "ε"

With $\varepsilon = T^* - T$ then $\mu_\varepsilon = E(T^* - T)$

In our case, because we are only estimating 1 point, T^* takes the value of the only point considered in the estimation, hence: $T^* = g_1$, so

$$\mu_\varepsilon = E(w_1 g_1 - T) \Rightarrow E(w_1 g_1) - E(T) \Rightarrow w_1 E(g_1) - E(T) \Rightarrow w_1 \mu - \mu$$

This relationship can be understood with the following example:

n	g_n	T_n	G_n-T_n
1	25.61	26.60	-0.99
2	26.60	26.11	0.49
3	29.30	28.98	0.32
4	30.46	28.75	1.71
5	28.75	25.39	3.36
6	25.39	25.24	0.15
∑:	166.11	161.07	5.04
Average:	27.685	26.845	0.84
	μ_ε=E(g_n)-E(T) → 27.685 - 26.845 = 0.84		μ_ε=E(g_n-T) = 0.84

Assuming there is no trend or population change between the sample location and the unsampled location: $\mu_\varepsilon = w_1 E(g_1) - E(T) \Rightarrow w_1\mu - \mu = 0$

This implies that the average of the error distribution (ε) is zero. In other words, our estimator is unbiased in the absence of a trend or other "non-stationary". The variance of the estimation error "ε" will also come from a normal distribution. Hence, the variance value is:

$$\sigma_\varepsilon^2 = E(\varepsilon - \mu_\varepsilon)^2$$

Where: σ_ε^2 = variance of the estimation error (ε)

E = average of the $(\varepsilon - \mu_\varepsilon)^2$

ε = estimation error

μ_ε = mean of the estimation error "ε"

Since $\mu_\varepsilon = E(g_1) - E(T) = 0$, then $\sigma_\varepsilon^2 = E\left[(\varepsilon)^2\right]$

With $\varepsilon = T^* - T$ then $\sigma_\varepsilon^2 = E\left[(T^* - T)^2\right]$

In our case, because we are only estimating 1 point, T^* takes the value of the only point considered in the estimation, hence: $T^* = g_1$, so:

$$\sigma_\varepsilon^2 = E\left[(g_1 - T)^2\right]$$

Since the semi-variogram general equation:

$$\gamma(h) = \frac{1}{2N_h}\sum_h (g_i - g_j)^2$$

is very similar to: $\sigma_\varepsilon^2 = E\left[(g_1 - T)^2\right]$, we can give it the same look by re-arranging the semi-variogram equation:

$$\gamma(h) = \frac{1}{2N_h}\sum_h (g_i - g_j)^2$$

Because of only 1 point estimation: $(g_i - g_j)^2 = (g_1 - T)^2$

Because of only 1 point estimation, we don't need the term $\sum_h$

Can be replace by E

$$\gamma(h) = \frac{1}{2}E\left[(g_1 - T)^2\right] \Rightarrow 2\gamma(h) = E\left[(g_1 - T)^2\right] \Rightarrow 2\gamma(h) = \sigma_\varepsilon^2 = E\left[(g_1 - T)^2\right]$$

In this example, the semi-variogram model is linear having the following form:

$$\gamma(h) = C_0 + ph^\alpha$$

Where: $C_0 = 0$

$p = 0.0016$

$h = 212$

$\alpha = 1.25$

$$\gamma(212) = 0 + 0.0016 \times 212^{1.25} = 1.2953$$

In this case, the estimation error has a variance of:

$$2\gamma(h) = \sigma_\varepsilon^2 = E\left[(g_1 - T)^2\right] = 2\gamma(212) = 2 \times 1.2953 = 2.5906$$

and the standard deviation is:

$$\sigma_\varepsilon = \sqrt{\sigma_\varepsilon^{\,2}} = \sqrt{2.5906} = 1.61$$

The grade at the unsampled location T is:

$$T^* = w_1 g_1 = 1 \times 21.86 = 21.86$$

A.5 Two points estimation

The proofs, formulas and examples are paraphrased from the book Practical Geostatistics 2000 (Clark, I and Harper, W.V. 2000). For more detail of the theory, refer to this book.

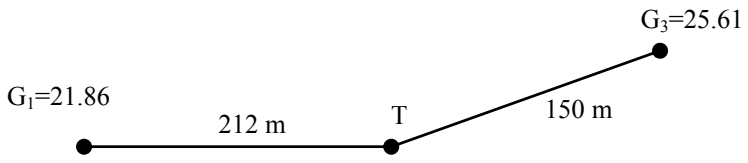

Estimation of T is given by the following equation:

$$T^* = w_1 g_1 + w_2 g_2 + w_3 g_3 + \ldots + w_n g_n$$

Where: T^* = estimated value for T

w_n = weight of sample "n" where $\sum_{i=1}^{n} w_i = 1$

g_n = grade of sample "n"

The error of the estimation is: $\varepsilon = T^* - T$

Where: ε = estimation error

T^* = estimated value for T

T = true value for T

In this example, the value of g_1 and g_3 are coming from a normal distribution. Hence, the value of "T" will follow a normal distribution, as well as the estimated value of T (T^*) and it's error (ε). The mean of the estimator error "ε" will also come from a normal distribution. Hence the mean value is:

$$\mu_\varepsilon = E(\varepsilon)$$

Where: μ_ε = mean of the estimation error "ε"

$E(\varepsilon)$ = average for the population "ε"

With $\varepsilon = T^* - T$ then $\mu_\varepsilon = E(T^* - T)$

In our case, because we are estimating only 2 points, T^* takes the value of the 2 points considered with their respective weight.

$$\mu_\varepsilon = E(w_1 g_1 + w_3 g_3 - T) \Rightarrow w_1 E(g_1) - w_3 E(g_3) - E(T) \Rightarrow w_1 \mu - w_3 \mu - \mu = 0$$

This implies that the average of the error distribution (ε) is zero. In other words our estimator is unbiased in the absence of a trend or other "non-stationary". The variance of the estimation error "ε" will also come from a normal distribution. Hence, the variance value is:

$$\sigma_\varepsilon^2 = E(\varepsilon - \mu_\varepsilon)^2$$

Where: $\sigma_\varepsilon^2 =$ variance of the estimation error (ε)

$E =$ average of the $(\varepsilon - \mu_\varepsilon)^2$

$\varepsilon =$ estimation error

$\mu_\varepsilon =$ mean of the estimation error "ε"

Since $\mu_\varepsilon = E(g_1) - E(T) = 0$, then $\sigma_\varepsilon^2 = E\left[(\varepsilon)^2\right]$

With $\varepsilon = T^* - T$ then $\sigma_\varepsilon^2 = E\left[(T^* - T)^2\right]$

Again, because we are estimating only 2 points, T^* takes the value of the 2 points considered with their respective weight:

$$\sigma_\varepsilon^2 = E\left[(w_1 g_1 - w_3 g_3 - T)^2\right]$$

At this step, we want to make a relation between the variance equation σ_ε^2 and the semi-variogram equation γ(h). For this, we have to play with the σ_ε^2 equation in order to make it down into terms which involve the square of difference between 2 samples $\left[(g_i - g_j)^2\right]$.

In order to do that, we add the weight w_1 and w_3 to the "T" term:

$$\sigma_\varepsilon^2 = E\left[(w_1 g_1 - w_3 g_3 - T)^2\right]$$

$$\sigma_\varepsilon^2 = E\left[(w_1 g_1 - w_3 g_3 - w_1 T - w_3 T)^2\right]$$

$$\sigma_\varepsilon^2 = E\left[\left[w_1(g_1 - T) + w_3(g_3 - T)\right]^2\right]$$

$$\sigma_\varepsilon^2 = E\left[\left[w_1(g_1 - T) + w_3(g_3 - T)\right] \times \left[w_1(g_1 - T) + w_3(g_3 - T)\right]\right]$$

$$\sigma_\varepsilon^2 = E\left[\left[w_1(g_1 - T)\right]^2 + \left[w_3(g_3 - T)\right]^2 + 2 \times \left[w_1(g_1 - T)\right] \times \left[w_3(g_3 - T)\right]\right]$$

If we modify the equation of the semi-variogram like as follows:

$$\gamma(h) = \frac{1}{2N_h}\sum_h (g_i - g_j)^2 = \frac{1}{2}E\left[(g_i - g_j)^2\right] \Rightarrow 2\gamma(h) = E\left[(g_i - g_j)^2\right]$$

We can than associate the first term $\sigma_\varepsilon^2 = E\left[\left[w_1(g_1 - T)\right]^2\right]$ to the modified semi-variogram equation:

$$\sigma_\varepsilon^2 = E\left[\left[w_1(g_1 - T)\right]^2\right] = w_1^2 E\left[(g_1 - T)^2\right], \qquad 2\gamma(h) = E\left[(g_i - g_j)^2\right] = E\left[(g_1 - T)^2\right]$$

$\sigma_\varepsilon^2 = w_1^2\, 2\gamma(h)$ where "h" is the distance between "g_1" et "T",

hence: $\sigma_\varepsilon^2 = w_1^2\, 2\gamma(g_1, T) = w_1^2\, 2\gamma(212)$

We can do the same for the second term:

$$\sigma_\varepsilon^2 = E\left[\left[w_3(g_3 - T)\right]^2\right] = w_3^2 E\left[(g_3 - T)^2\right], \qquad 2\gamma(h) = E\left[(g_i - g_j)^2\right] = E\left[(g_3 - T)^2\right]$$

$\sigma_\varepsilon^2 = w_3^2\, 2\gamma(h)$ where "h" is the distance between "g_3" et "T",

hence: $\sigma_\varepsilon^2 = w_3^2\, 2\gamma(g_3, T) = w_3^2\, 2\gamma(150)$

For the third term, a little bit more algebraic is going to be needed.

$$\sigma_\varepsilon^2 = E\left[\,2 \times \left[w_1(g_1 - T)\right] \times \left[w_3(g_3 - T)\right]\,\right] = 2\underbrace{w_1 w_3 E}\left[\,(g_1 - T) \times (g_3 - T)\,\right]$$

Constant that can be removed to simplify the following calculation

$$\sigma_\varepsilon^2 = 2 \times (g_1 - T) \times (g_3 - T) = 2g_1g_3 - 2g_1T - 2g_3T + 2T^2 = 2g_1g_3 - 2g_1T - 2g_3T + T^2 + T^2$$

$$\sigma_\varepsilon^2 = 2g_1g_3 - 2g_1T - 2g_3T + T^2 + T^2 = 2g_1g_3 - \underbrace{2g_1T + T^2} - \underbrace{2g_3T + T^2}$$

$(g_3 - T)^2 = g_3 - 2g_3T + T^2$

$(g_1 - T)^2 = g_1 - 2g_1T + T^2$

Hence:

$$\sigma_\varepsilon^2 = 2g_1g_3 - 2g_1T - 2g_3T + T^2 + T^2 = (g_1 - T)^2 + (g_3 - T)^2 + (g_1 - g_3)^2$$

$$\sigma_\varepsilon^2 = (g_1 - T)^2 + (g_3 - T)^2 + (g_1 - g_3)^2 = w_1 w_3 E\left[(g_1 - T)^2 + (g_3 - T)^2 + (g_1 - g_3)^2\right]$$

From equation: $2\gamma(h) = E\left[(g_i - g_j)^2\right]$, then

$$\sigma_\varepsilon^2 = w_1 w_3 \left[2\gamma(g_1, T) + 2\gamma(g_3, T) - 2\gamma(g_1, g_3) \right]$$

If we re-arrange the general equation:

$$\sigma_\varepsilon^2 = E\left[[w_1(g_1 - T)]^2 + [w_3(g_3 - T)]^2 + 2 \times [w_1(g_1 - T)] \times [w_3(g_3 - T)] \right]$$

$$\sigma_\varepsilon^2 = w_1^2 E\left[(g_1 - T)^2\right] + w_3^2 E\left[(g_3 - T)^2\right] + 2w_1 w_3 E\left[(g_1 - T)^2 + (g_3 - T)^2 - (g_1 - g_3)^2\right]$$

$$\sigma_\varepsilon^2 = w_1^2\, 2\gamma(g_1, T) + w_3^2\, 2\gamma(g_3, T) + w_1 w_3 \left[2\gamma(g_1, T) + 2\gamma(g_3, T) - 2\gamma(g_1, g_3) \right]$$

$$\sigma_\varepsilon^2 = w_1^2\, 2\gamma(g_1, T) + w_3^2\, 2\gamma(g_3, T) + w_1 w_3 2\gamma(g_1, T) + w_1 w_3 2\gamma(g_3, T) - w_1 w_3 2\gamma(g_1, g_3)$$

By re-organizing the terms:

$$\sigma_\varepsilon^2 = w_1(w_1 + w_3) 2\gamma(g_1, T) + w_3(w_1 + w_3) 2\gamma(g_3, T) - w_1 w_3 2\gamma(g_1, g_3)$$

Since the sum of all the weight (w_1,w_3) must equal to 1, then:

$$\sigma_\varepsilon^2 = w_1 2\gamma(g_1, T) + w_3 2\gamma(g_3, T) - w_1 w_3 2\gamma(g_1, g_3)$$

If: $w_1 = 0.45$

$w_3 = 0.55$

$\gamma(g_1, T) = \gamma(212) = 1.2953$

$\gamma(g_3, T) = \gamma(150) = 0.8399$

$\gamma(g_1, g_3) = \gamma(335) = 2.2966$

Then:

$$T^* = w_1 g_1 + w_3 g_3 = 0.45 \times 21.86 + 0.55 \times 25.61 = 23.92$$

$$\sigma_\varepsilon^2 = w_1 2\gamma(g_1, T) + w_3 2\gamma(g_3, T) - w_1 w_3 2\gamma(g_1, g_3)$$

$$\sigma_\varepsilon^2 = 0.45 \times 2 \times 1.2953 + 0.55 \times 2 \times 0.8399 - 0.45 \times 0.55 \times 2.2966 = 0.9528$$

$$\sigma_\varepsilon = \sqrt{\sigma_\varepsilon^2} = \sqrt{0.9528} = 0.976$$

A.6 Three points estimation

The proofs, formulas and examples are paraphrased from the book Practical Geostatistics 2000 (Clark, I and Harper, W.V. 2000). For more detail of the theory, refer to this book.

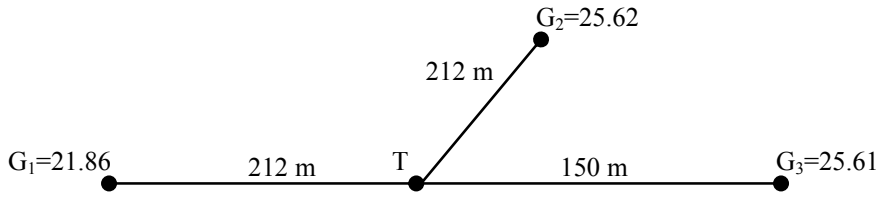

Estimation of T is given by the following equation:

$$T^* = w_1 g_1 + w_2 g_2 + w_3 g_3 \quad \text{where} \quad \sum_{i=1}^{3} w_i = 1$$

As before, our estimation error will follow a normal distribution with a mean of:

$$\mu_\varepsilon = E(\varepsilon) \text{ with } \varepsilon = T^* - T \text{ then } \mu_\varepsilon = E(T^* - T)$$

$$\mu_\varepsilon = E(w_1 g_1 + w_2 g_2 + w_3 g_3 - T) \Rightarrow w_1 E(g_1) - w_2 E(g_2) - w_3 E(g_3) - E(T)$$

$$\mu_\varepsilon = w_1\mu - w_2\mu - w_3\mu - \mu = 0$$

The variance of the estimation error "ε" will also come from a normal distribution. Hence, the variance value is:

$$\sigma_\varepsilon^2 = E(\varepsilon - \mu_\varepsilon)^2$$

Since $\mu_\varepsilon = E(g_1) - E(T) = 0$, then $\sigma_\varepsilon^2 = E\left[(\varepsilon)^2\right]$

With $\varepsilon = T^* - T$ then $\sigma_\varepsilon^2 = E\left[(T^* - T)^2\right]$

$$\sigma_\varepsilon^2 = E\left[(w_1 g_1 - w_2 g_2 - w_3 g_3 - T)^2\right]$$

From the 2 samples example above, we can find the equation for a 3 samples case. From the 2 samples cases:

$$\sigma_\varepsilon^2 = w_1 2\gamma(g_1, T) + w_3 2\gamma(g_3, T) - w_1 w_3 2\gamma(g_1, g_3)$$

We can add a 3rd sample to the 2 samples equation:

$$\sigma_\varepsilon^2 = w_1 2\gamma(g_1, T) + w_2 2\gamma(g_2, T) + w_3 2\gamma(g_3, T) - w_1 w_2 2\gamma(g_1, g_2) - w_1 w_3 2\gamma(g_1, g_3) - w_2 w_3 2\gamma(g_2, g_3)$$

We can transform this equation into another form such as:

$$\sigma_{\varepsilon}^{2} = w_1 2\gamma(g_1, T) + w_2 2\gamma(g_2, T) + w_3 2\gamma(g_3, T) -$$

$$\begin{bmatrix} w_1^2\gamma(g_1,g_1) & + w_1w_2\gamma(g_1,g_2) & + w_1w_3\gamma(g_1,g_3) \\ w_2w_1\gamma(g_2,g_1) & + w_2^2\gamma(g_2,g_2) & + w_2w_3\gamma(g_2,g_3) \\ w_1w_3\gamma(g_1,g_3) & + w_2w_3\gamma(g_2,g_3) & + w_3^2\gamma(g_3,g_3) \end{bmatrix} \underbrace{-\gamma(T,T)}_{\text{Nugget effect}}$$

If: $w_1 = 0.3$

$w_2 = 0.3$

$w_3 = 0.4$

$\gamma(g_1, T) = \gamma(212) = 1.2953$

$\gamma(g_2, T) = \gamma(212) = 1.2953$

$\gamma(g_3, T) = \gamma(150) = 0.8399$

$\gamma(g_1, g_1) = \gamma(0) = 0$

$\gamma(g_2, g_2) = \gamma(0) = 0$

$\gamma(g_3, g_3) = \gamma(0) = 0$

$\gamma(g_1, g_2) = \gamma(g_2, g_1) = \gamma(300) = 1.997$

$\gamma(g_1, g_3) = \gamma(g_3, g_1) = \gamma(335) = 2.2966$

$\gamma(g_2, g_3) = \gamma(g_3, g_2) = \gamma(150) = 0.8399$

$$T^{*} = w_1 g_1 + w_2 g_2 + w_3 g_3 = 0.3 \times 21.86 + 0.3 \times 25.62 + 0.4 \times 25.61 = 24.69$$

$$\sigma_\varepsilon^2 = 0.3 \times 2\gamma\ (212) + 0.3 \times 2\gamma\ (212) + 0.4 \times 2\gamma\ (150) -$$

$$\begin{bmatrix} 0.3^2\gamma(0) & + 0.3 \times 0.3 \times \gamma(300) & + 0.3 \times 0.4 \times \gamma(335) \\ 0.3 \times 0.3 \times \gamma(300) & + 0.3^2\gamma(0) & + 0.3 \times 0.4 \times \gamma(150) \\ 0.3 \times 0.4 \times \gamma(335) & + 0.3 \times 0.4 \times \gamma(150) & + 0.4^2\gamma(0) \end{bmatrix} - \gamma(0)$$

$$\sigma_\varepsilon^2 = 1.11393 \Rightarrow \sigma_\varepsilon = \sqrt{\sigma_\varepsilon^{\ 2}} = \sqrt{1.11393} = 1.055$$

From the example above, let's suppose that we don't know the weight for w_1,w_2,w_3.

$$\sigma_\varepsilon^2 = w_1 2\gamma\ (212) + w_2 2\gamma\ (212) + w_3 2\gamma\ (150) -$$

$$\begin{bmatrix} w_1^2\gamma(0) & + w_1 w_2 \gamma(300) & + w_1 w_3 \gamma(335) \\ w_2 w_1 \gamma(300) & + w_2^2\gamma(0) & + w_2 w_3 \gamma(150) \\ w_1 w_3 \gamma(150) & + w_2 w_3 \gamma(150) & + w_3^2\gamma(0) \end{bmatrix} - \gamma(0)$$

By using the appropriate value for each term:

$$\sigma_\varepsilon^2 = w_1 \times 2 \times 1.2953 + w_2 \times 2 \times 1.2953 + w_3 \times 2 \times 0.8399 -$$

$$\begin{bmatrix} w_1^2 \times 0 & + w_1 w_2 \times 1.9977 & + w_1 w_3 \times 2.2966 \\ w_2 w_1 \times 1.9977 & + w_2^2 \times 0 & + w_2 w_3 \times 0.8399 \\ w_1 w_3 \times 2.2966 & + w_2 w_3 \times 0.8399 & + w_3^2 \times 0 \end{bmatrix} - 0$$

$$\sigma_\varepsilon^2 = 2.5906 w_1 + 2.5906 w_2 + 1.6798 w_3 - 2 \times 1.9977 w_2 w_1 - 2 \times 2.2966 w_3 w_1 - 2 \times 0.8399 w_2 w_3$$

$$\sigma_\varepsilon^2 = 2.5906 w_1 + 2.5906 w_2 + 1.6798 w_3 - 3.9954 w_2 w_1 - 4.5932 w_3 w_1 - 1.6798 w_2 w_3$$

If we want the weight w_1,w_2,w_3 that is going to give the minimum value of the estimation variance σ_ε^2, we have to differentiate σ_ε^2 for every weight:

$$\frac{\partial \sigma_\varepsilon^2}{\partial w_1} = 2.5906 - 3.9954w_2 - 4.5932w_3 = 0$$

$$\frac{\partial \sigma_\varepsilon^2}{\partial w_2} = 2.5906 - 3.9954w_1 - 1.6798w_3 = 0$$

$$\frac{\partial \sigma_\varepsilon^2}{\partial w_3} = 1.6798 - 4.5932w_1 - 1.6798w_2 = 0$$

Hence:
$$3.9954w_2 + 4.5932w_3 = 2.5906$$
$$3.9954w_1 + 1.6798w_3 = 2.5906$$
$$4.5932w_1 + 1.6798w_2 = 1.6798$$

By solving these 3 equations, we found:

$$w_1 = 0.3885,\ w_2 = -0.0623,\ w_3 = 0.6182$$

Since $\sum_{i=1}^{3} w_i = 1 \Rightarrow 0.3885 - 0.0623 + 0.6182 = 0.9444 \neq 1$,

this would mean that the expected value of our estimation error would be:

$$\mu_\varepsilon = w_1\mu - w_2\mu - w_3\mu - \mu = 0 \Rightarrow 0.3885\mu - 0.0623\mu - 0.6182\mu - \mu = -0.0556\mu$$

So, we would need to adjust our estimator by $+0.0556\mu$ to make it unbiased. That is, our estimator would have to be:

$$T^* = w_1 g_1 + w_2 g_2 + w_3 g_3 + 0.0556\mu$$

$$T^* = 0.3885 \times 21.86 - 0.0623 \times 25.62 + 0.6182 \times 25.61 + 0.0556\mu$$

$$T^* = 22.73 + 0.0556\mu$$

The minimum estimation variance based on the optimal weight of w_1, w_2, w_3 is:

$$\sigma_\varepsilon^2 = 2.5906w_1 + 2.5906w_2 + 1.6798w_3 - 3.9954w_2w_1 - 4.5932w_3w_1 - 1.6798w_2w_3$$

with $w_1 = 0.3885,\ w_2 = -0.0623,\ w_3 = 0.6182$

$$\sigma_\varepsilon^2 = 0.9177 \Rightarrow \sigma_\varepsilon = \sqrt{\sigma_\varepsilon^{\,2}} = \sqrt{0.9177} = 0.9579$$

The general form of the optimal estimator equation is:

$$T^* = w_1 g_1 + w_2 g_2 + w_3 g_3 \pm w_i \mu$$

$$T^* = \sum_{i=1}^{m} w_i g_i + \left(1 - \sum_{i=1}^{m} w_i\right)\mu$$

$$\sigma_\varepsilon^2 = w_1 2\gamma\,(g_1, T) + w_2 2\gamma\,(g_2, T) + w_3 2\gamma\,(g_3, T) -$$

$$\begin{bmatrix} w_1^2\gamma(g_1,g_1) & + w_1w_2\gamma(g_1,g_2) & + w_1w_3\gamma(g_1,g_3) \\ w_2w_1\gamma(g_2,g_1) & + w_2^2\gamma(g_2,g_2) & + w_2w_3\gamma(g_2,g_3) \\ w_1w_3\gamma(g_1,g_3) & + w_2w_3\gamma(g_2,g_3) & + w_3^2\gamma(g_3,g_3) \end{bmatrix} - \gamma(T,T)$$

$$\sigma_\varepsilon^2 = 2\sum_{i=1}^{m} w_i\gamma(g_i, T) - \sum_{i=1}^{m}\sum_{j=1}^{m} w_i w_j \gamma(g_i, g_j) - \gamma(T,T)$$

$$\sigma_\varepsilon^2 = 2.5906w_1 + 2.5906w_2 + 1.6798w_3 - 3.9954w_2w_1 - 4.5932w_3w_1 - 1.6798w_2w_3$$

$$\frac{\partial\sigma_\varepsilon^2}{\partial w_1} = 2.5906 - 3.9954w_2 - 4.5932w_3 = 0$$

$$\frac{\partial\sigma_\varepsilon^2}{\partial w_2} = 2.5906 - 3.9954w_1 - 1.6798w_3 = 0$$

$$\frac{\partial\sigma_\varepsilon^2}{\partial w_3} = 1.6798 - 4.5932w_1 - 1.6798w_2 = 0$$

$$\sum_{j=1}^{m} w_i\gamma(g_i, g_j) = \gamma(g_i, T)$$

From the equation above, let's pretend that i=1 and that j=1,2,3

$$w_1\gamma(g_1,g_1) + w_2\gamma(g_1,g_2) + w_3\gamma(g_1,g_3) = \gamma(g_1,T)$$

$$w_1\gamma(0) + w_2\gamma(300) + w_3\gamma(335) = \gamma(212)$$

$$0 + 1.9977w_2 + 2.2966w_3 = 1.2953$$

if we multiply these equations by 2

$$0 \quad + 3.9954w_2 \quad + 4.5932w_3 \quad = 2.5906$$

From the equation above, let's pretend that i=2 and that j=1,2,3

$$w_1\gamma(g_2,g_1) + w_2\gamma(g_2,g_2) + w_3\gamma(g_2,g_3) = \gamma(g_2,T)$$
$$w_1\gamma(300) \quad + w_2\gamma(0) \quad + w_3\gamma(150) \quad = \gamma(212)$$
$$1.9977w_1 \quad + 0 \quad + 0.8399w_3 \quad = 1.2953$$

if we multiply these equations by 2

$$3.9954w_1 \quad + 0 \quad + 1.6798w_3 \quad = 2.5906$$

From the equation above, let's pretend that i=3 and that j=1,2,3

$$w_1\gamma(g_3,g_1) + w_2\gamma(g_3,g_2) + w_3\gamma(g_3,g_3) = \gamma(g_3,T)$$
$$w_1\gamma(335) \quad + w_2\gamma(150) \quad + w_3\gamma(0) \quad = \gamma(150)$$
$$2.2966w_1 \quad + 0.8399w_2 \quad + 0 \quad = 0.8399$$

if we multiply these equations by 2

$$4.5932w_1 \quad + 1.6798w_2 \quad + 0 \quad = 1.6798$$

A.7 Ordinary kriging

The proofs, formulas and examples are paraphrased from the book Practical Geostatistics 2000 (Clark, I and Harper, W.V. 2000). For more detail of the theory, refer to this book.

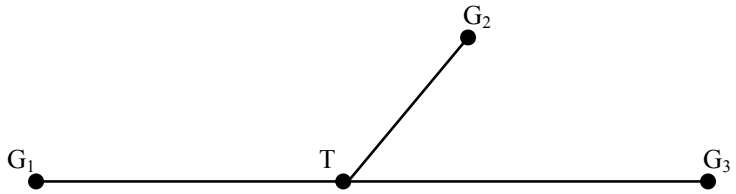

We know from previous theory and worked example that:

$$T^* = w_1 g_1 + w_2 g_2 + w_3 g_3$$

$$\sigma_\varepsilon^2 = w_1 2\gamma(g_1, T) + w_2 2\gamma(g_2, T) + w_3 2\gamma(g_3, T) - w_1 w_2 2\gamma(g_1, g_2) - w_1 w_3 2\gamma(g_1, g_3) - w_2 w_3 2\gamma(g_2, g_3)$$

or

$$\sigma_\varepsilon^2 = w_1 2\gamma(g_1, T) + w_2 2\gamma(g_2, T) + w_3 2\gamma(g_3, T) -$$

$$\begin{bmatrix} w_1^2\gamma(g_1, g_1) & + w_1 w_2 \gamma(g_1, g_2) & + w_1 w_3 \gamma(g_1, g_3) \\ w_2 w_1 \gamma(g_2, g_1) & + w_2^2 \gamma(g_2, g_2) & + w_2 w_3 \gamma(g_2, g_3) \\ w_1 w_3 \gamma(g_1, g_3) & + w_2 w_3 \gamma(g_2, g_3) & + w_3^2 \gamma(g_3, g_3) \end{bmatrix} - \gamma(T, T)$$

or

$$\sigma_\varepsilon^2 = 2\sum_{i=1}^{m} w_i \gamma(g_i, T) - \sum_{i=1}^{m}\sum_{j=1}^{m} w_i w_j \gamma(g_i, g_j) - \gamma(T, T)$$

To solve this system, we have "m" equations with "m" weight. But, by introducing the term $\sum_{i=1}^{m} w_i = 1$, we have now "m+1" equations with "m" weight. In order to work around that, we introduce the "Lagrangian Multiplier (λ)" that we multiply to our condition $\sum_{i=1}^{m} w_i = 1$. We end up with $\lambda \sum_{i=1}^{m} w_i = 1$, that we insert in the estimation variance equation:

$$\sigma_\varepsilon^2 = w_1 2\gamma(g_1, T) + w_2 2\gamma(g_2, T) + w_3 2\gamma(g_3, T) - w_1 w_2 2\gamma(g_1, g_2) - w_1 w_3 2\gamma(g_1, g_3) - w_2 w_3 2\gamma(g_2, g_3) - 2\lambda(\sum w_i - 1) = \gamma(T, T)$$

If we differentiate the previous equation:

$$\frac{\partial \sigma_\varepsilon^2}{\partial w_1} = 2\gamma(g_1, T) - 2\left[w_1\gamma(g_1, g_2) - w_2\gamma(g_2, g_3) - w_3\gamma(g_1, g_3) \right] - 2\gamma = 0$$

$$\gamma(g_1, T) = w_1\gamma(g_1, g_2) + w_2\gamma(g_2, g_3) + w_3\gamma(g_1, g_3) + \gamma$$

or on a general mathematical form:

$$\gamma(g_i, T) = w_1\gamma(g_i, g_1) + w_2\gamma(g_i, g_2) + w_3\gamma(g_i, g_3) + \ldots + w_m\gamma(g_i, g_m) + \gamma$$

We can generalize the previous equation and build an ordinary kriging system:

$$\begin{aligned}
&w_1\gamma(g_1, g_1) + w_2\gamma(g_1, g_2) + w_3\gamma(g_1, g_3) + \ldots + w_m\gamma(g_1, g_m) + \lambda = \gamma(g_1, T)\\
&w_1\gamma(g_2, g_1) + w_2\gamma(g_2, g_2) + w_3\gamma(g_2, g_3) + \ldots + w_m\gamma(g_2, g_m) + \lambda = \gamma(g_2, T)\\
&w_1\gamma(g_3, g_1) + w_2\gamma(g_3, g_2) + w_3\gamma(g_3, g_3) + \ldots + w_m\gamma(g_3, g_m) + \lambda = \gamma(g_3, T)\\
&\ldots\ldots\ldots\ldots\ldots\ldots\ldots\ldots\ldots\ldots\ldots\ldots\ldots\ldots = \ldots\ldots\ldots\\
&w_1\gamma(g_m, g_1) + w_2\gamma(g_m, g_2) + w_3\gamma(g_m, g_3) + \ldots + w_m\gamma(g_m, g_m) + \lambda = \gamma(g_m, T)
\end{aligned}$$

Also we can put those equations in a matrix system as follow:

$$A = \begin{bmatrix} \gamma(g_1,g_1) & \gamma(g_1,g_2) & \gamma(g_1,g_3) & +\ldots+ & \gamma(g_1,g_m) & 1 \\ \gamma(g_2,g_1) & \gamma(g_2,g_2) & \gamma(g_2,g_3) & +\ldots+ & \gamma(g_2,g_m) & 1 \\ \gamma(g_3,g_1) & \gamma(g_3,g_2) & \gamma(g_3,g_3) & +\ldots+ & \gamma(g_3,g_m) & 1 \\ \ldots\ldots & \ldots\ldots & \ldots\ldots & \ldots & \ldots\ldots & . \\ \gamma(g_m,g_1) & \gamma(g_m,g_2) & \gamma(g_m,g_3) & +\ldots+ & \gamma(g_m,g_m) & 1 \\ 1 & 1 & 1 & 1 & 1 & 1 \end{bmatrix} \quad B' = \begin{bmatrix} w_1 \\ w_2 \\ w_3 \\ .. \\ w_m \\ \lambda \end{bmatrix} \quad C = \begin{bmatrix} \gamma(g_1,T) \\ \gamma(g_2,T) \\ \gamma(g_3,T) \\ \ldots\ldots \\ \gamma(g_m,T) \\ 1 \end{bmatrix}$$

Where:

- Ordinary Kriging system become AB'=C
- Weight is $B'=A^{-1}C$
- Grade estimation is given by $T^*=Bg$ where "g" are the grade value
- Estimation variance $\sigma^2_{o.k.}$ is given by BC-$\gamma(T,T)$
- Matrix A is used to decluster the data
- The Lagrangian Multiplier λ is used to make sure that the sum of all the weight equal to 1.

A.8 Ordinary kriging estimation of 3 points

The proofs, formulas and examples are paraphrased from the book Practical Geostatistics 2000 (Clark, I and Harper, W.V. 2000). For more detail of the theory, refer to this book.

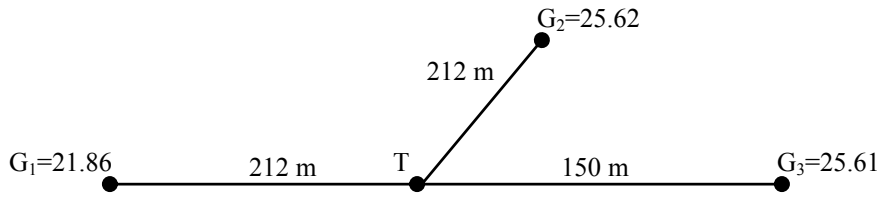

The ordinary kriging equation system is:

$$w_1\gamma(g_1,g_1)+w_2\gamma(g_1,g_2)+w_3\gamma(g_1,g_3)+\ldots+w_m\gamma(g_1,g_m)+\lambda=\gamma(g_1,T)$$
$$w_1\gamma(g_2,g_1)+w_2\gamma(g_2,g_2)+w_3\gamma(g_2,g_3)+\ldots+w_m\gamma(g_2,g_m)+\lambda=\gamma(g_2,T)$$
$$w_1\gamma(g_3,g_1)+w_2\gamma(g_3,g_2)+w_3\gamma(g_3,g_3)+\ldots+w_m\gamma(g_3,g_m)+\lambda=\gamma(g_3,T)$$
$$w_1+w_2+w_3=1$$

$$w_1\gamma(0)+w_2\gamma(300)+w_3\gamma(335)+\lambda=\gamma(212)$$
$$w_1\gamma(300)+w_2\gamma(0)+w_3\gamma(150)+\lambda=\gamma(212)$$
$$w_1\gamma(335)+w_2\gamma(150)+w_3\gamma(0)+\lambda=\gamma(150)$$
$$w_1+w_2+w_3=1$$

$$0w_1+1.9977w_2+2.2966w_3+\lambda=1.2953$$
$$1.9977w_1+0w_2+0.8399w_3+\lambda=1.2953$$
$$2.2966w_1+0.8399w_2+0w_3+\lambda=0.8399$$
$$w_1+w_2+w_3=1$$

By solving those equation, we get:

$$w_1=0.4136,\ w_2=-0.0515,\ w_3=0.6379,\ \lambda=-0.0668$$

$$T^*=w_1g_1+w_2g_2+w_3g_3$$

$$T^*=0.4136\times21.86-0.0515\times25.62+0.6379\times25.61=24.06$$

$$\sigma^2_{o.k.}=BC-\gamma(T,T)=w_1\gamma(g_1,T)+w_2\gamma(g_2,T)+w_3\gamma(g_3,T)+\lambda-\gamma(T,T)$$

$$\sigma^2_{o.k.}=0.4136\times1.2953-0.0515\times1.2953+0.6379\times0.8399-0.0668-0=0.9380$$

We can solve this same problem with the matrix system:

$$A = \begin{bmatrix} \gamma(g_1,g_1) & \gamma(g_1,g_2) & \gamma(g_1,g_3) & 1 \\ \gamma(g_2,g_1) & \gamma(g_2,g_2) & \gamma(g_2,g_3) & 1 \\ \gamma(g_3,g_1) & \gamma(g_3,g_2) & \gamma(g_3,g_3) & 1 \\ 1 & 1 & 1 & 1 \end{bmatrix} \quad B' = \begin{bmatrix} w_1 \\ w_2 \\ w_3 \\ \lambda \end{bmatrix} \quad C = \begin{bmatrix} \gamma(g_1,T) \\ \gamma(g_2,T) \\ \gamma(g_3,T) \\ 1 \end{bmatrix}$$

$$A = \begin{bmatrix} \gamma(0) & \gamma(300) & \gamma(335) & 1 \\ \gamma(300) & \gamma(0) & \gamma(150) & 1 \\ \gamma(335) & \gamma(150) & \gamma(0) & 1 \\ 1 & 1 & 1 & 1 \end{bmatrix} \quad B' = \begin{bmatrix} w_1 \\ w_2 \\ w_3 \\ \lambda \end{bmatrix} \quad C = \begin{bmatrix} \gamma(212) \\ \gamma(212) \\ \gamma(150) \\ 1 \end{bmatrix}$$

$$A = \begin{bmatrix} 0 & 1.997 & 2.2966 & 1 \\ 1.9977 & 0 & 0.8399 & 1 \\ 2.2966 & 0.8399 & 0 & 1 \\ 1 & 1 & 1 & 1 \end{bmatrix} \quad B' = \begin{bmatrix} w_1 \\ w_2 \\ w_3 \\ \lambda \end{bmatrix} \quad C = \begin{bmatrix} 1.2953 \\ 1.2953 \\ 0.8399 \\ 1 \end{bmatrix}$$

The weight are by solving the system $B'=A^{-1}C$

$$A^{-1} = \begin{bmatrix} 0 & 1.997 & 2.2966 & 1 \\ 1.9977 & 0 & 0.8399 & 1 \\ 2.2966 & 0.8399 & 0 & 1 \\ 1 & 1 & 1 & 1 \end{bmatrix}^{-1} = \begin{bmatrix} -0.262 & 0.177 & 0.084 & 0.452 \\ 0.177 & -0.716 & 0.538 & 0.194 \\ 0.084 & 0.538 & -0.622 & 0.354 \\ 0.452 & 0.194 & 0.354 & -1.201 \end{bmatrix}$$

$$\begin{bmatrix} w_1 \\ w_2 \\ w_3 \\ \lambda \end{bmatrix} = \begin{bmatrix} -0.262 & 0.177 & 0.084 & 0.452 \\ 0.177 & -0.716 & 0.538 & 0.194 \\ 0.084 & 0.538 & -0.622 & 0.354 \\ 0.452 & 0.194 & 0.354 & -1.201 \end{bmatrix} \times \begin{bmatrix} 1.2953 \\ 1.2953 \\ 0.8399 \\ 1 \end{bmatrix}$$

$$w_1 = -0.262 \times 1.2953 + 0.177 \times 1.2953 + 0.084 \times 0.8399 + 0.452 \times 1 = 0.4124$$
$$w_2 = 0.177 \times 1.2953 - 0.716 \times 1.2953 + 0.538 \times 0.8399 + 0.194 \times 1 = -0.0523$$
$$w_3 = 0.084 \times 1.2953 + 0.538 \times 1.2953 - 0.622 \times 0.8399 + 0.354 \times 1 = 0.6373$$
$$\lambda = 0.452 \times 1.2953 + 0.194 \times 1.2953 + 0.354 \times 0.8399 - 1.201 \times 1 = -0.0669$$

The grade estimation is found with $T^* = w_1 g_1 + w_2 g_2 + w_3 g_3 = Bg$

$$B = \left[w_1, w_2, w_3, \lambda\right] \quad g = \begin{bmatrix} g_1 \\ g_2 \\ g_3 \\ 0 \end{bmatrix} \Rightarrow \quad T^* = \left[0.4124, -0.0523, 0.6373, -0.0669\right] \times \begin{bmatrix} 21.86 \\ 25.62 \\ 25.61 \\ 0 \end{bmatrix}$$

$$T^* = 0.4124 \times 21.86 - 0.0523 \times 25.62 + 0.6373 \times 25.61 - 0.0669 \times 0 = 23.996$$

The estimation variance $\sigma^2_{o.k.}$ is given by BC-$\gamma(T,T)$ where $\gamma(T,T)$ is equal to 0, because in this example, there nugget effect is equal to zero.

$$B = \left[w_1, w_2, w_3, \lambda\right] \; C = \begin{bmatrix} \gamma(g_1, T) \\ \gamma(g_2, T) \\ \gamma(g_3, T) \\ 1 \end{bmatrix} \Rightarrow \sigma^2_{o.k.} = \left[0.4124, -0.0523, 0.6373, -0.0669\right] \times \begin{bmatrix} 1.2953 \\ 1.2953 \\ 0.8399 \\ 1 \end{bmatrix}$$

$$\sigma^2_{o.k.} = 0.4124 \times 1.2933 - 0.0523 \times 1.2953 + 0.6373 \times 0.8399 - 0.0669 \times 1 - 0 = 0.9348$$

A.9 One point estimation indicator kriging estimation

The indicator kriging estimation method is based on the same mathematics as the ordinary kriging method, except the indicator method works with the discretization of the grade value into 0 and 1. If the grade value is above the selected cut-off, then the indicator takes the value of 0, otherwise the indicator takes the value of 1. For example, let's say that we

want to estimate the gold grade of the following 150m x 200m block. The gold grade distribution is coming from the same exploration grid data that was used in section A.1. The kriging weights associated to each sample grid node should have been calculated by solving the kriging matrix, as thoroughly described in section A6, A7 and A.8. Since the objective of this example is to show how the indicator kriging estimated grade is derived, the kriging weights are fictitious. For the purpose of this example, we are interested to look around the economic cut-off grade of 1.5 g/t Au.

Sample grade distribution

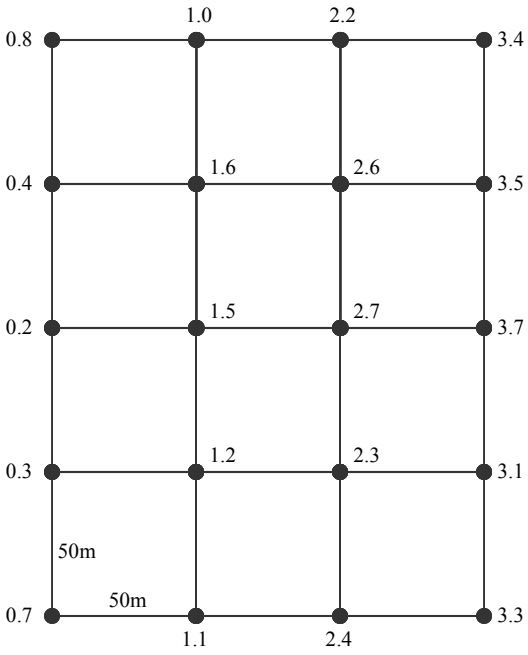

Kriging weight distribution

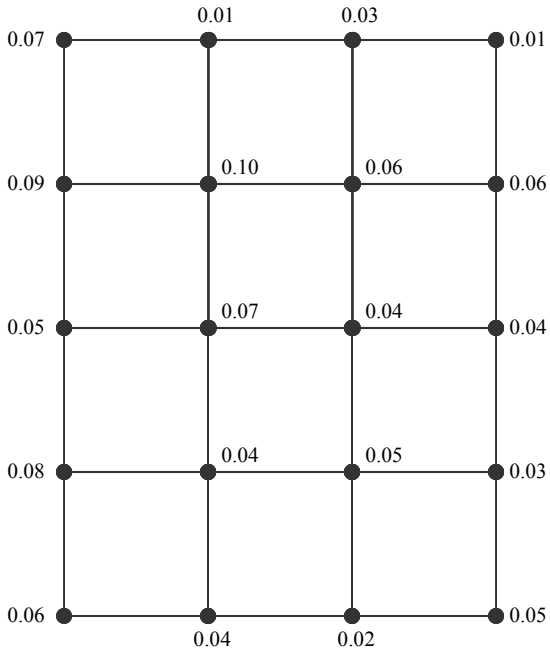

Following is the indicator distribution based on a cut-off grade of 1.5 g/t. In the case of indicator kriging, the weights of the samples are used as probability. Since all the weight needs to equal to 1, this respects the definition of a probability plot in which the sum of all the probability needs to be also equal to 1.

Indicator distribution

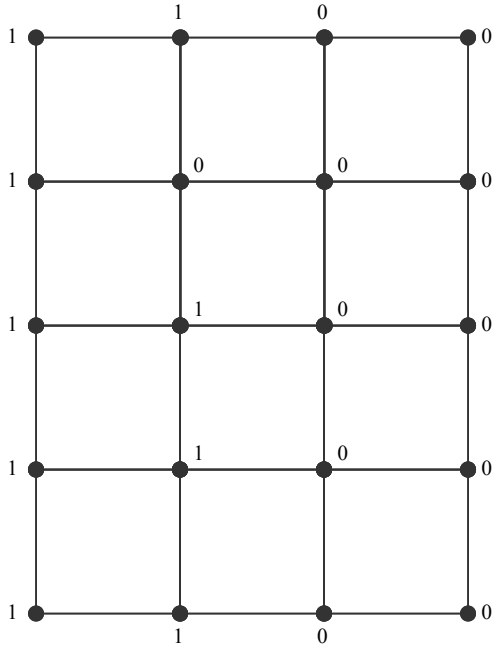

Kriging weight distribution

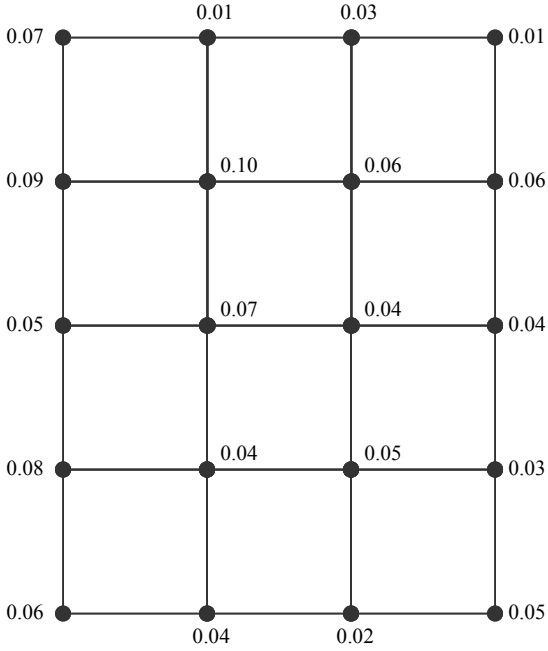

To calculate the probability of the block of being between the bin grade interval 0.0-1.5 g/t, we need to multiply the indicator value by the probability for each node.

$$\text{Prob. block} < 1.5 \text{ g/t} = \begin{Bmatrix} (1 \times 0.07) + (1 \times 0.09) + (1 \times 0.05) + (1 \times 0.08) + (1 \times 0.06) \\ (1 \times 0.01) + (0 \times 0.10) + (1 \times 0.07) + (1 \times 0.04) + (1 \times 0.04) \\ (0 \times 0.03) + (0 \times 0.06) + (0 \times 0.04) + (0 \times 0.05) + (0 \times 0.02) \\ (0 \times 0.01) + (0 \times 0.06) + (0 \times 0.04) + (0 \times 0.03) + (0 \times 0.05) \end{Bmatrix} = 0.51$$

The probability for the block of being in the interval 0.0-1.5 g/t is 0.51. Since the sum of the probability must equal to 1, we can get the probability of the block of being in the interval 1.5-∞ g/t.

$$\text{Prob. block} > 1.5 \text{ g/t} = (1 - 0.51) = 0.49$$

The only element missing to get the grade of the block is the mean grade of each bin considered. In this case, the mean grade for the bin 0.0-1.5 g/t is equal to 0.80 g/t, whereas the mean grade for the bin 1.5-∞ g/t is equal to 2.80 g/t.

Finally the grade of the block is obtained by multiplying the probability by the mean grade for each bin.

$$\text{Block grade } = (0.51 \times 0.80) + (0.49 \times 2.80) = 1.78 \text{ g/t}$$

APPENDIX B – Indicator Variogram DDH

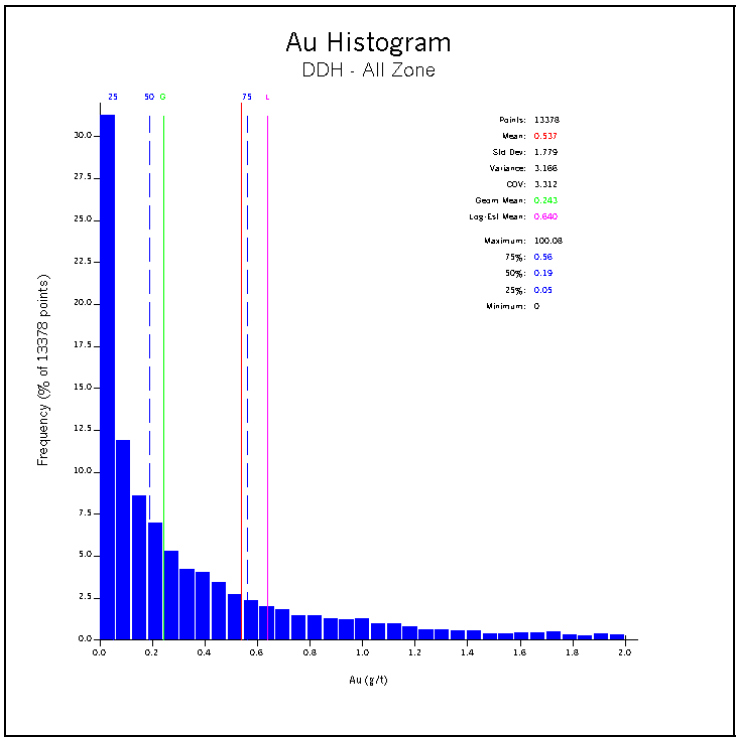

Figure B.1 Au Normal Histogram – All Zone

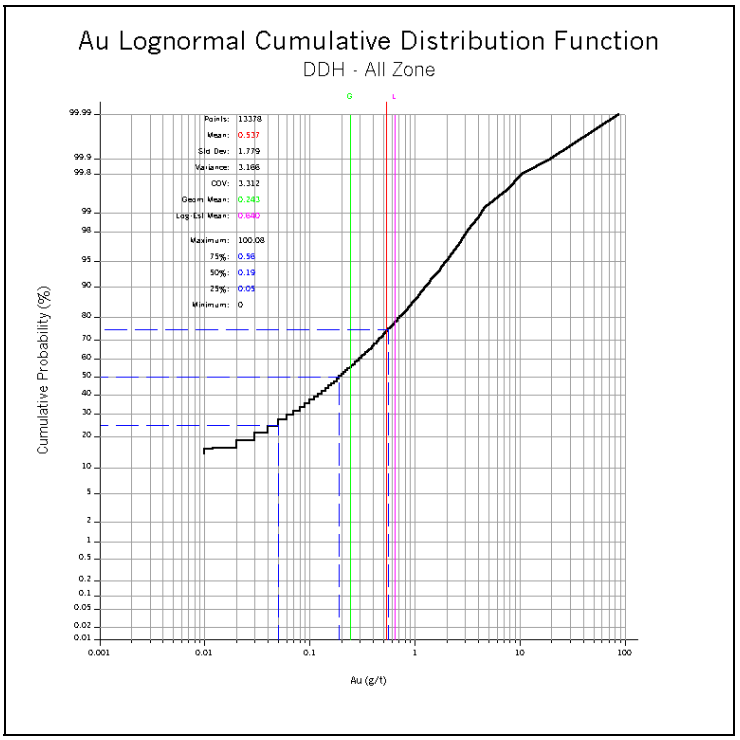

Figure B.2 Au Lognormal Cumulative Distribution Function – All Zone

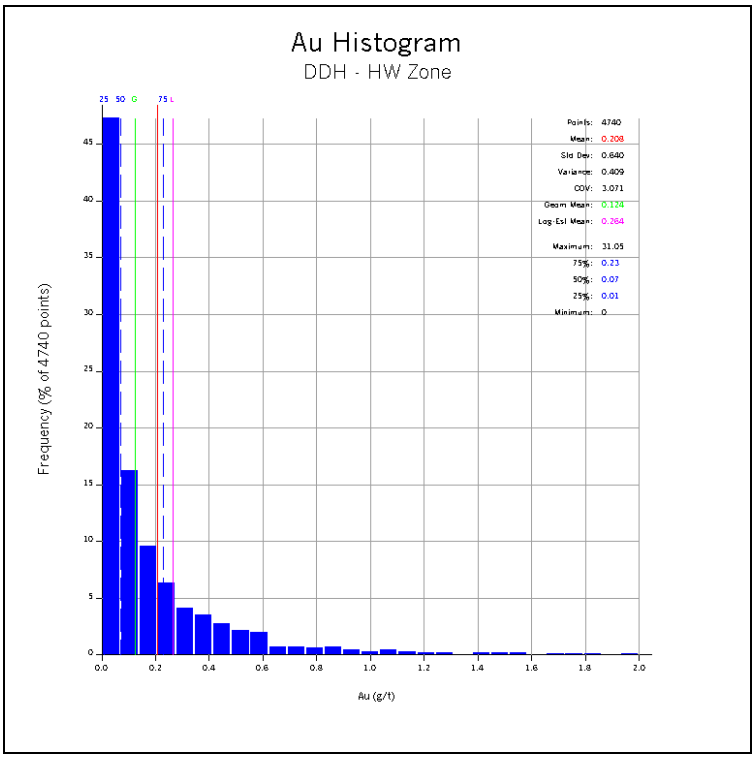

Figure B.3 Au Normal Histogram – HW Zone

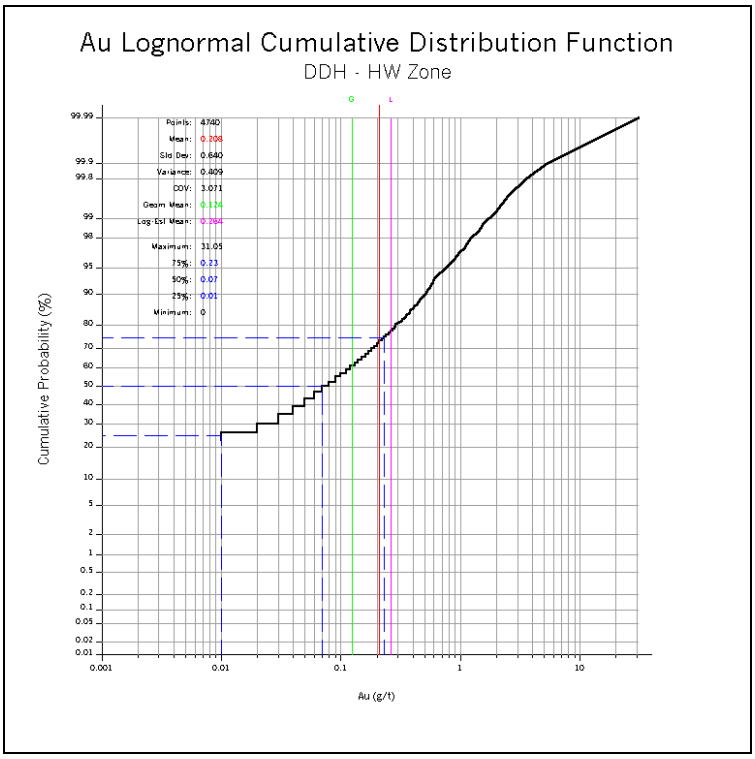

Figure B.4 Au Lognormal Cumulative Distribution Function – HW Zone

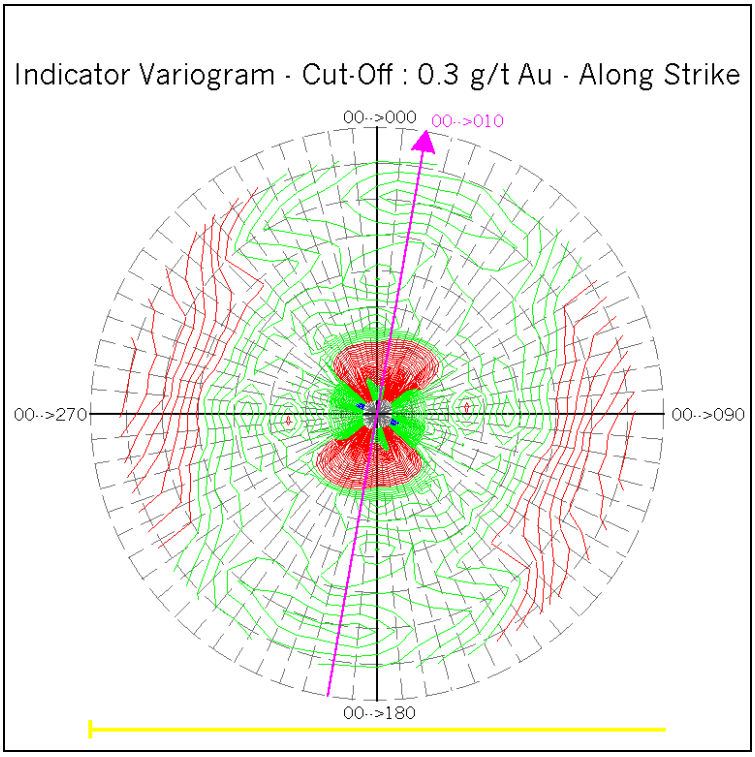

Figure B.5 Fan of Indicator Variograms – HW Zone Cut-Off at 0.3 g/t Au – Along Strike

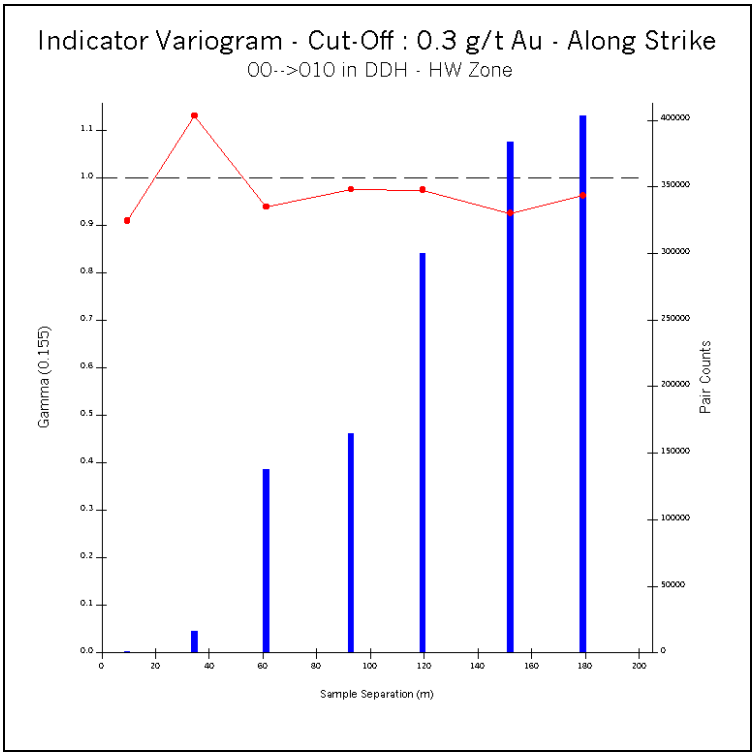

Figure B.6 Indicator Variogram – HW Zone Cut-Off at 0.3 g/t Au – Along Strike

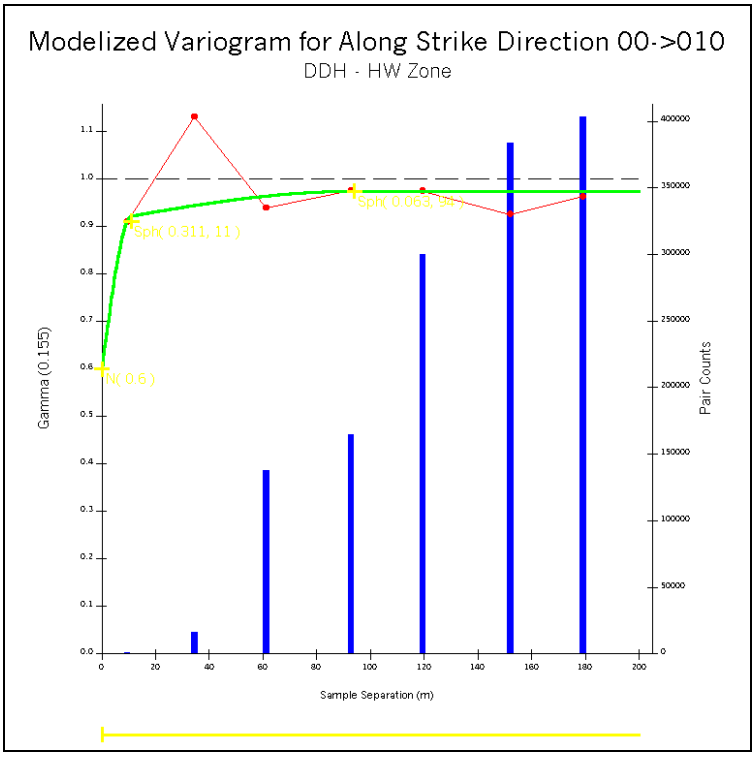

Figure B.7 Modelized Indicator Variogram – HW Zone Cut-Off at 0.3 g/t Au – Along Strike

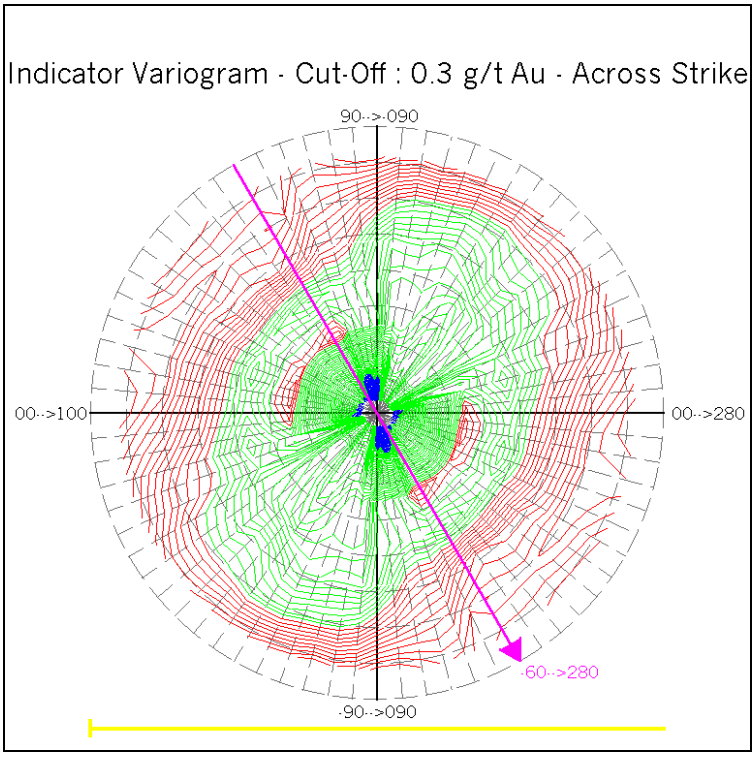

Figure B.7 Modelized Indicator Variogram – HW Zone Cut-Off at 0.3 g/t Au – Along Strike

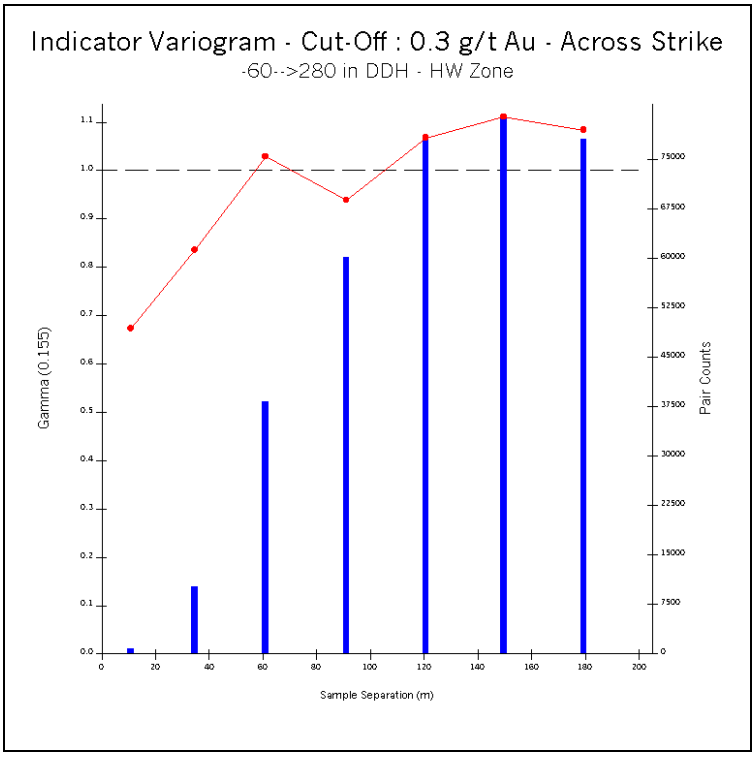

Figure B.9 Indicator Variogram – HW Zone Cut-Off at 0.3 g/t Au – Across Strike

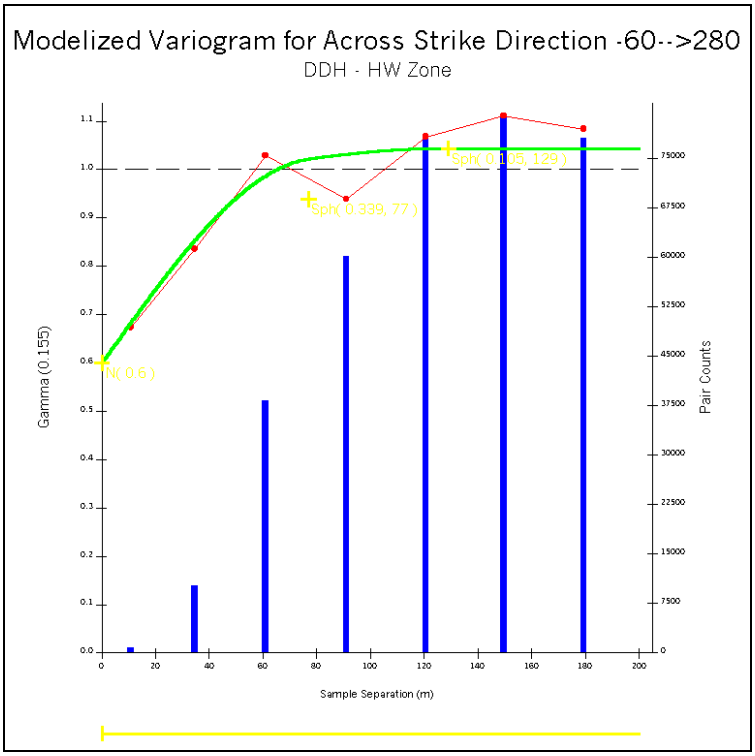

Figure B.10 Modelized Indicator Variogram – HW Zone Cut-Off at 0.3 g/t Au – Across Strike

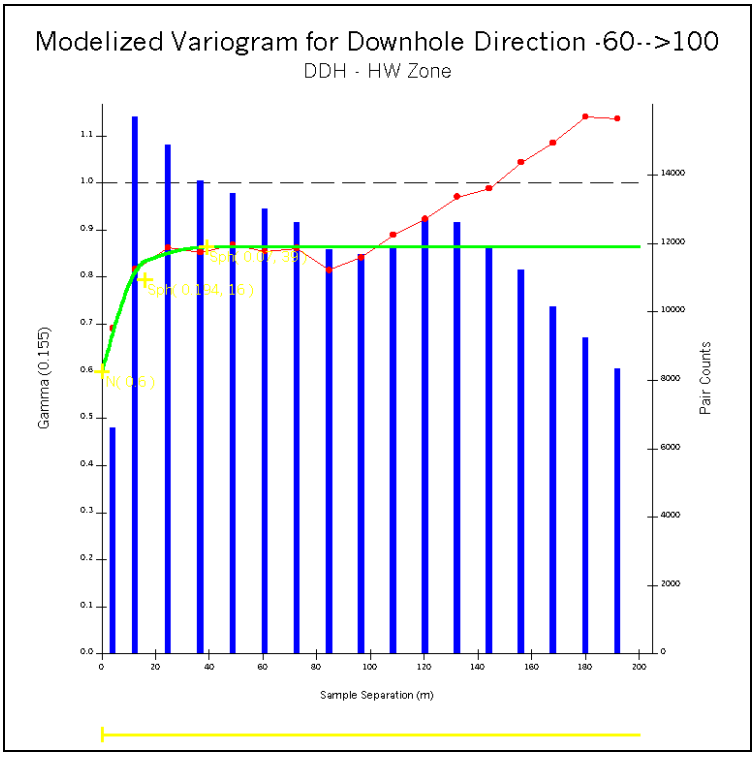

Figure B.11 Modelized Indicator Variogram – HW Zone Cut-Off at 0.3 g/t Au – Downhole

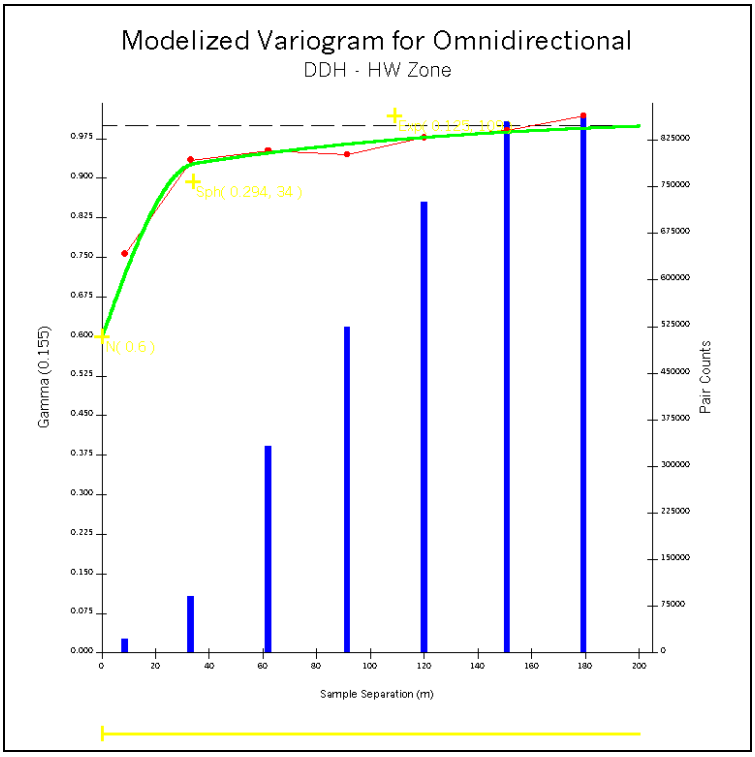

Figure B.12 Modelized Indicator Variogram – HW Zone Cut-Off at 0.3 g/t Au – Omnidirectional

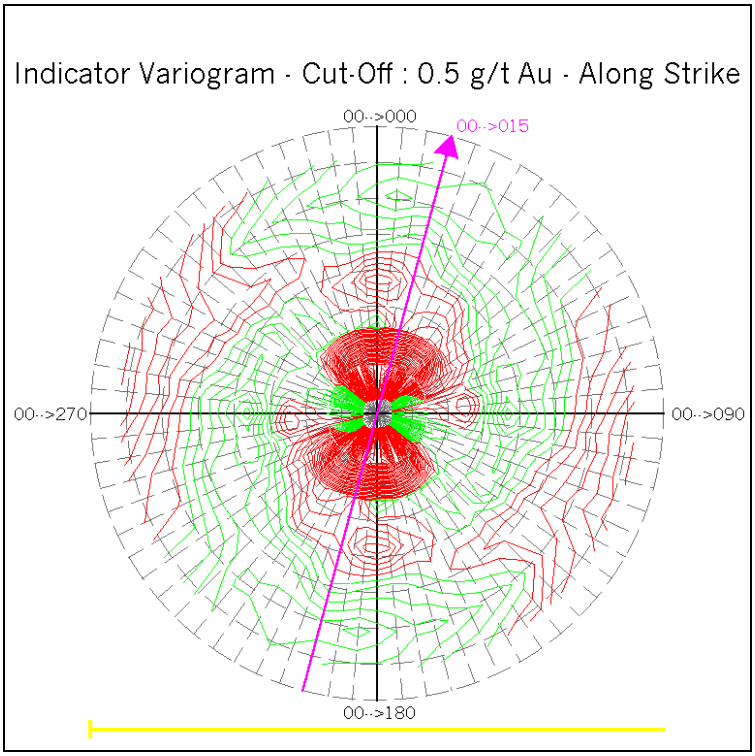

Figure B.13 Fan of Indicator Variograms – HW Zone Cut-Off at 0.5 g/t Au – Along Strike

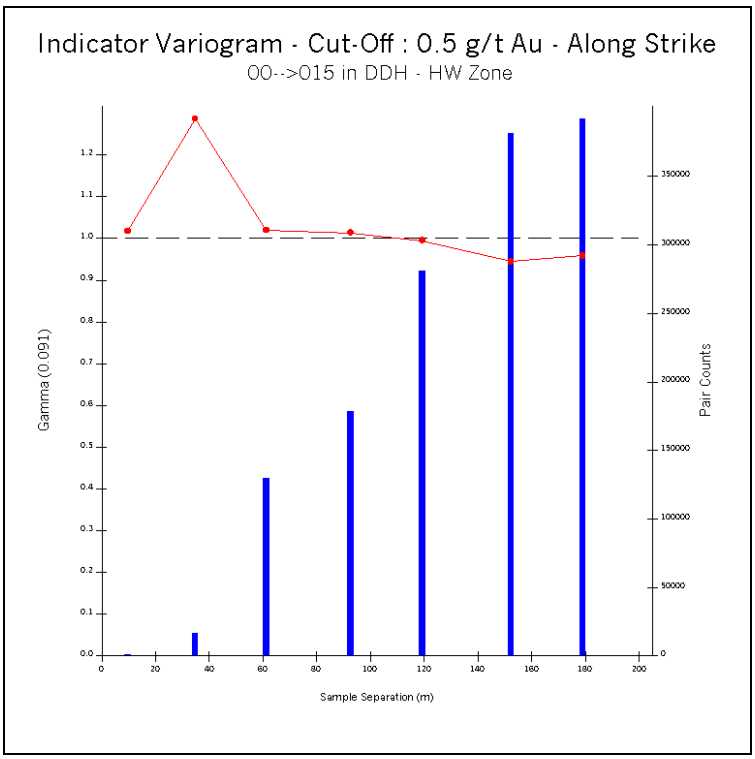

Figure B.14 Indicator Variogram – HW Zone Cut-Off at 0.5 g/t Au – Along Strike

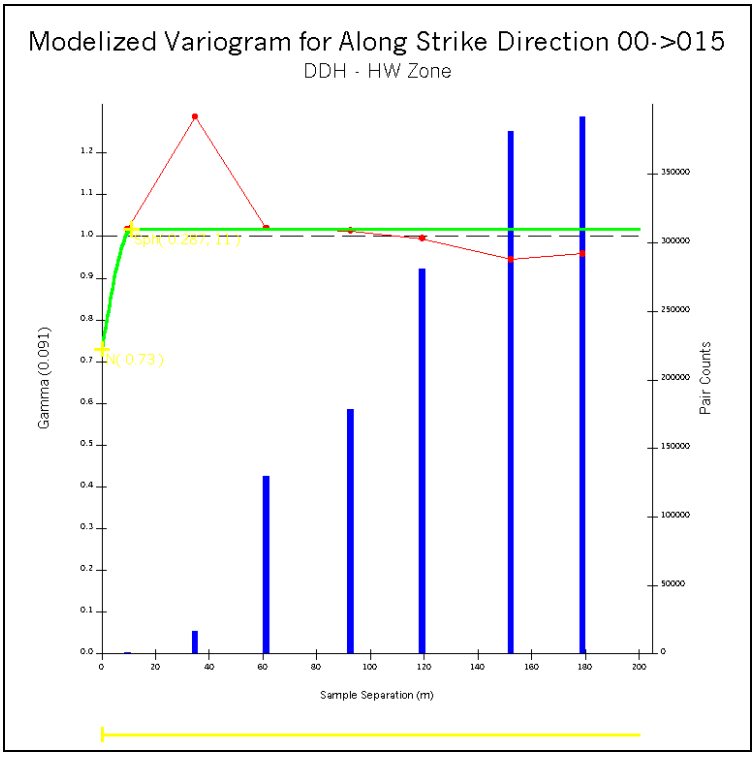

Figure B.15 Modelized Indicator Variogram – HW Zone Cut-Off at 0.5 g/t Au – Along Strike

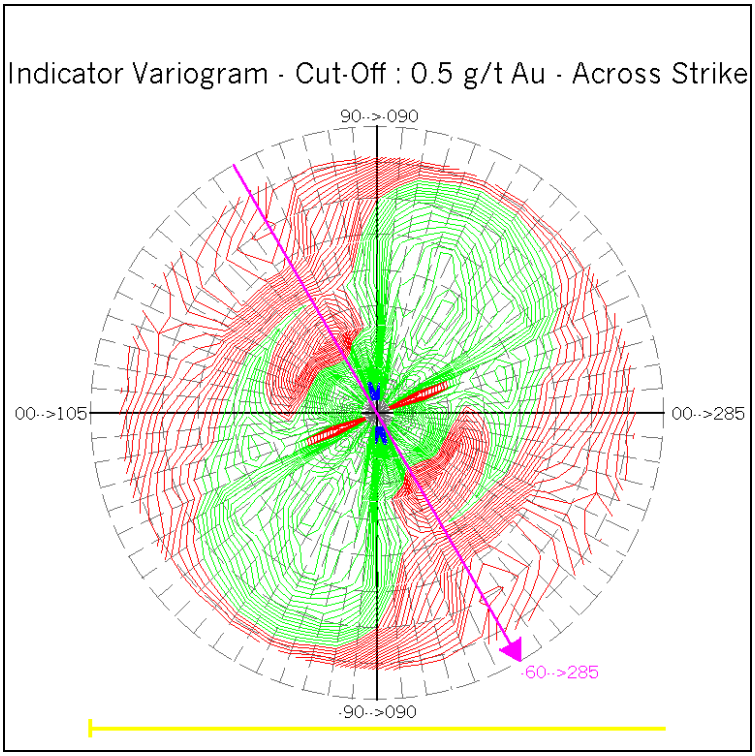

Figure B.16 Fan of Indicator Variograms – HW Zone Cut-Off at 0.5 g/t Au – Across Strike

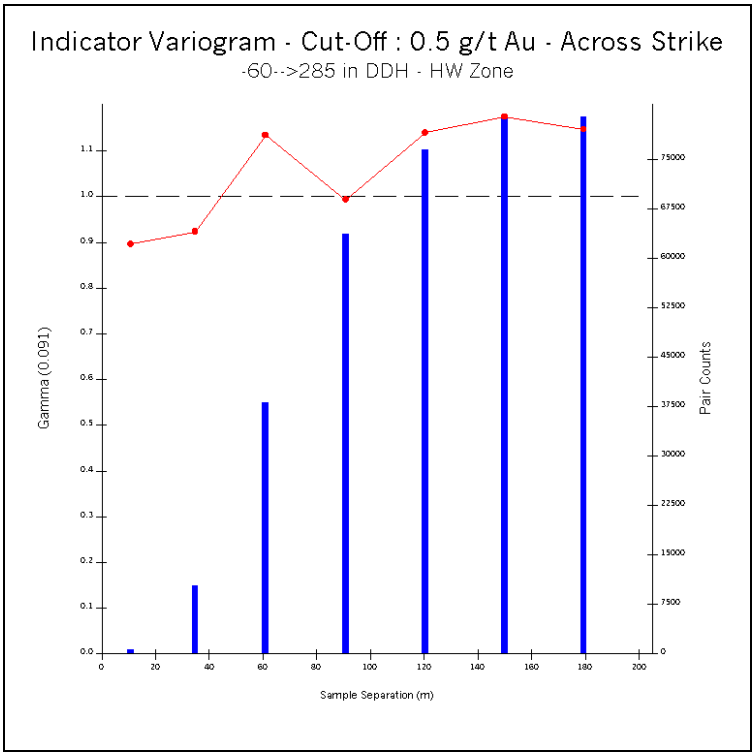

Figure B.17 Indicator Variogram – HW Zone Cut-Off at 0.5 g/t Au – Across Strike

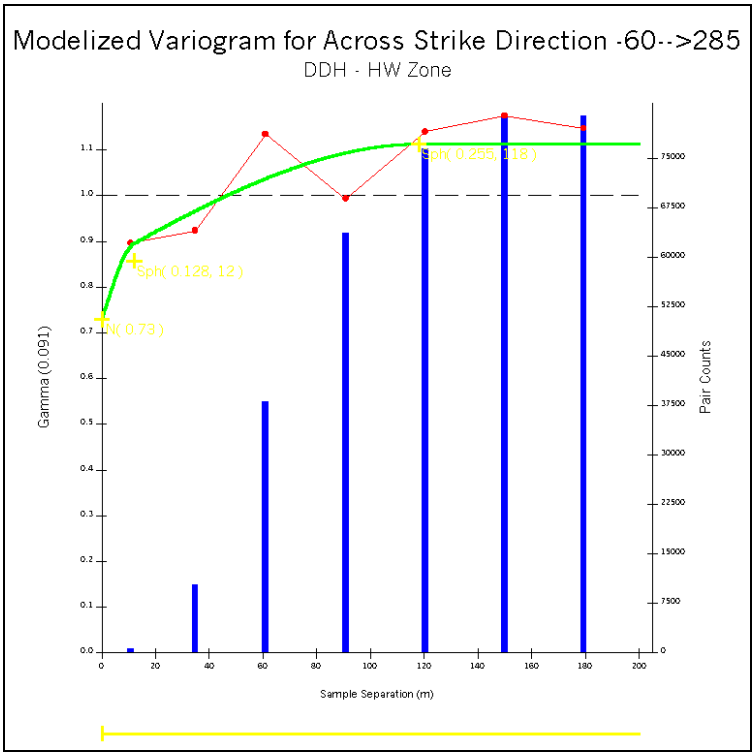

Figure B.18 Modelized Indicator Variogram – HW Zone Cut-Off at 0.5 g/t Au – Across Strike

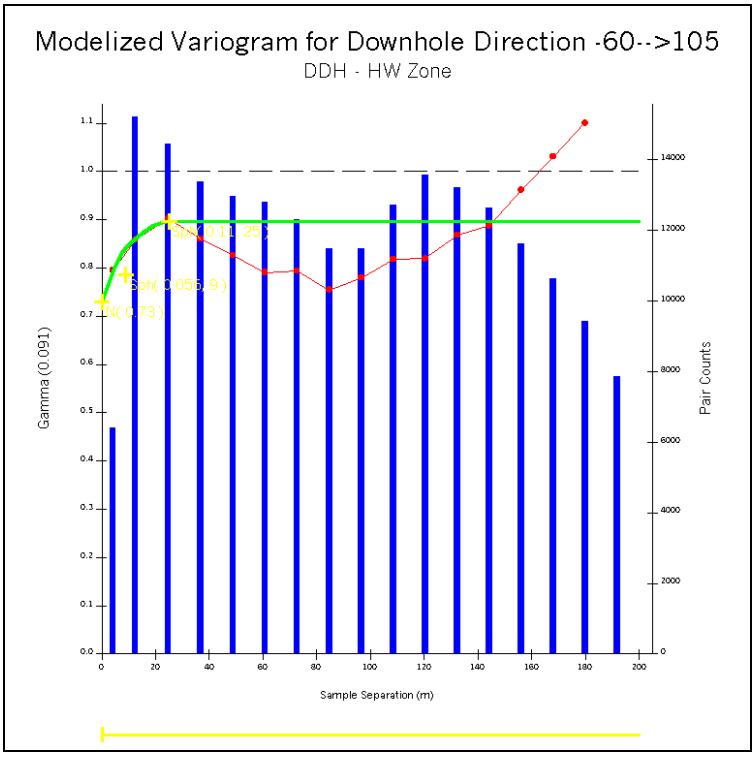

Figure B.19 Modelized Indicator Variogram – HW Zone Cut-Off at 0.5 g/t Au – Downhole

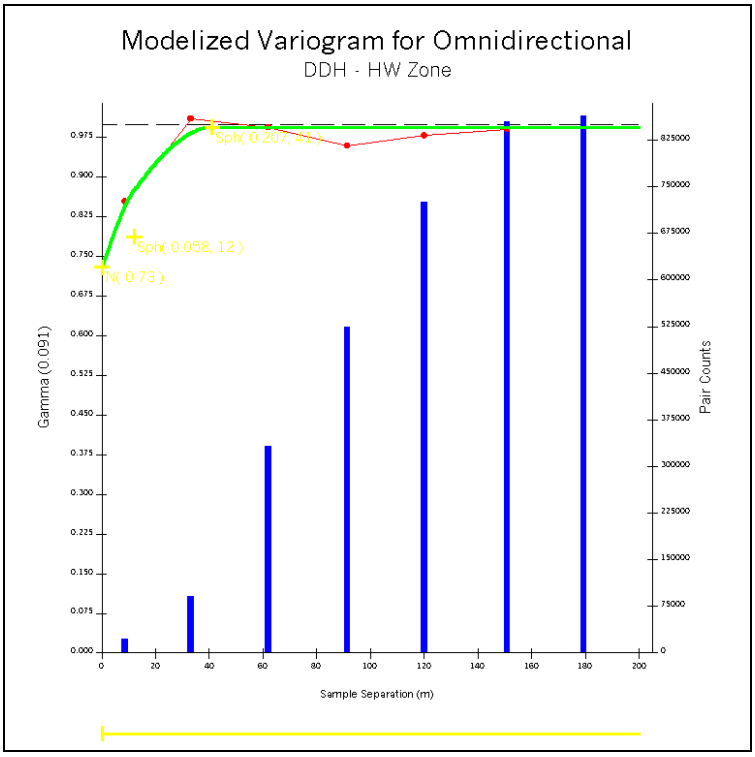

Figure B.20 Modelized Indicator Variogram – HW Zone Cut-Off at 0.5 g/t Au – Omnidirectional

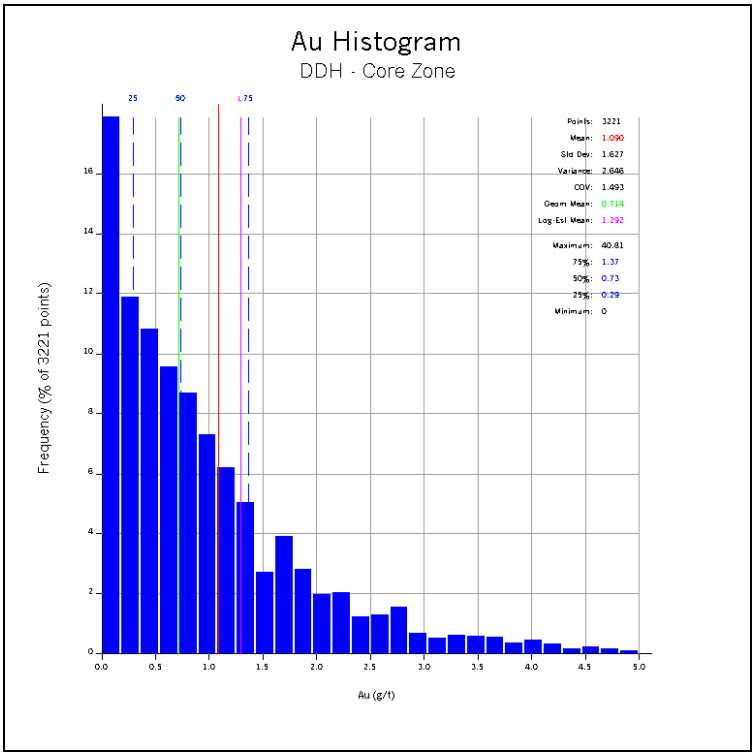

Figure B.21 Au Normal Histogram – CORE Zone

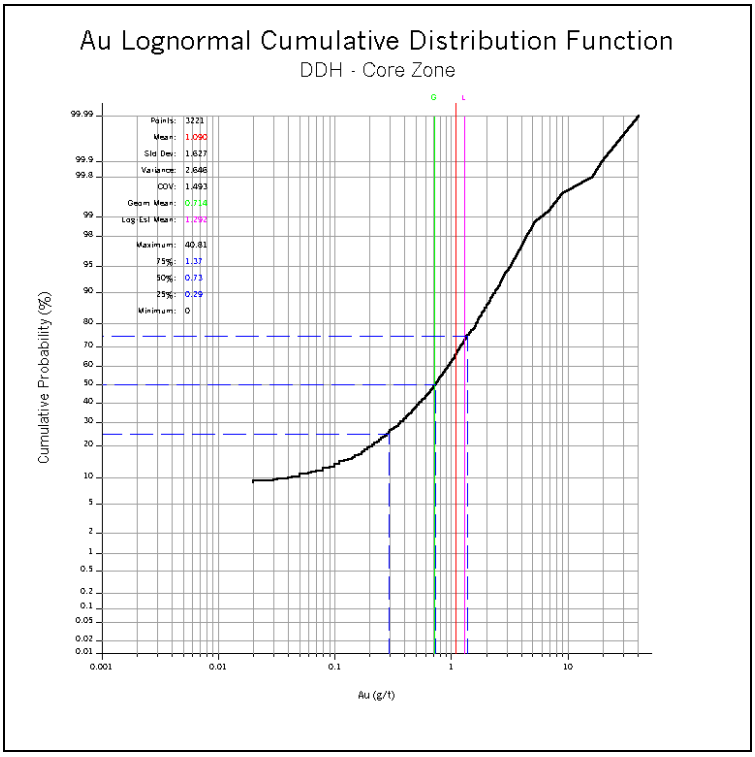

Figure B.22 Au Lognormal Cumulative Distribution Function – CORE Zone

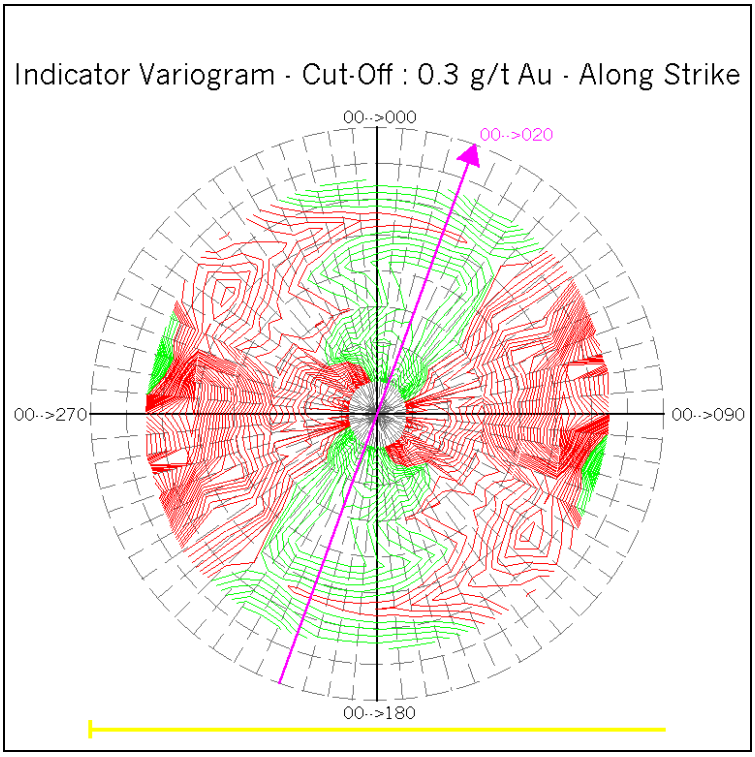

Figure B.23 Fan of Indicator Variograms – CORE Zone Cut-Off at 0.3 g/t Au – Along Strike

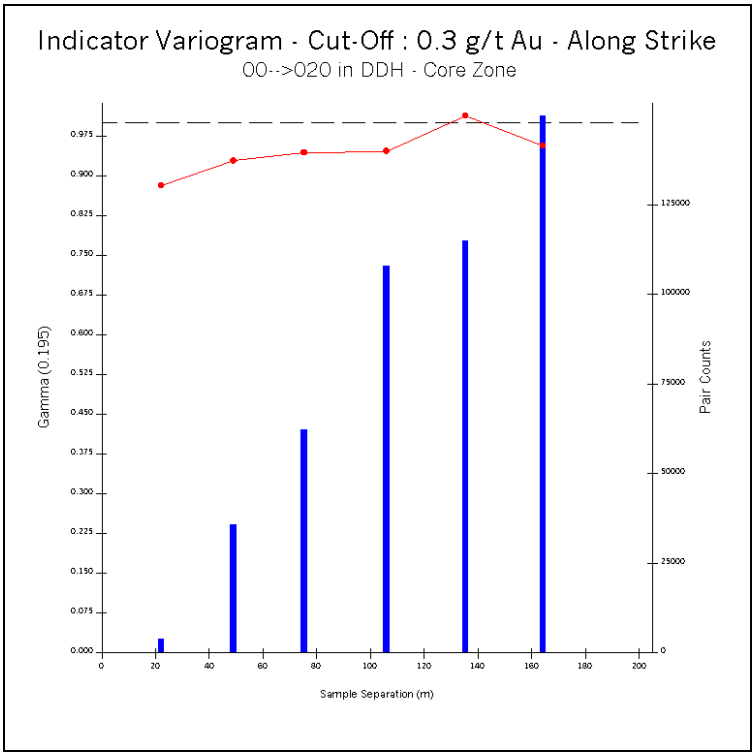

Figure B.24 Indicator Variogram – CORE Zone Cut-Off at 0.3 g/t Au – Along Strike

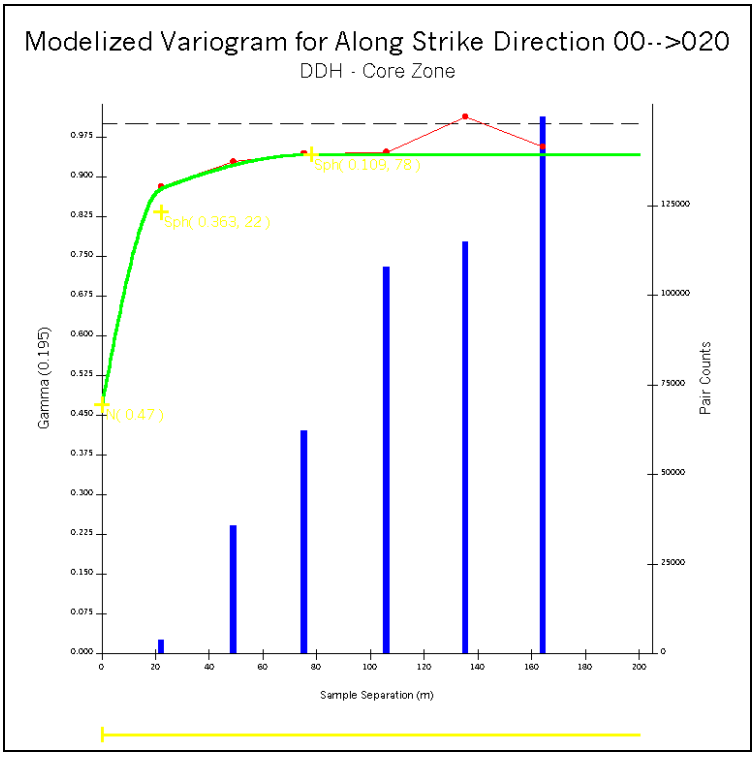

Figure B.25 Modelized Indicator Variogram – CORE Zone Cut-Off at 0.3 g/t Au – Along Strike

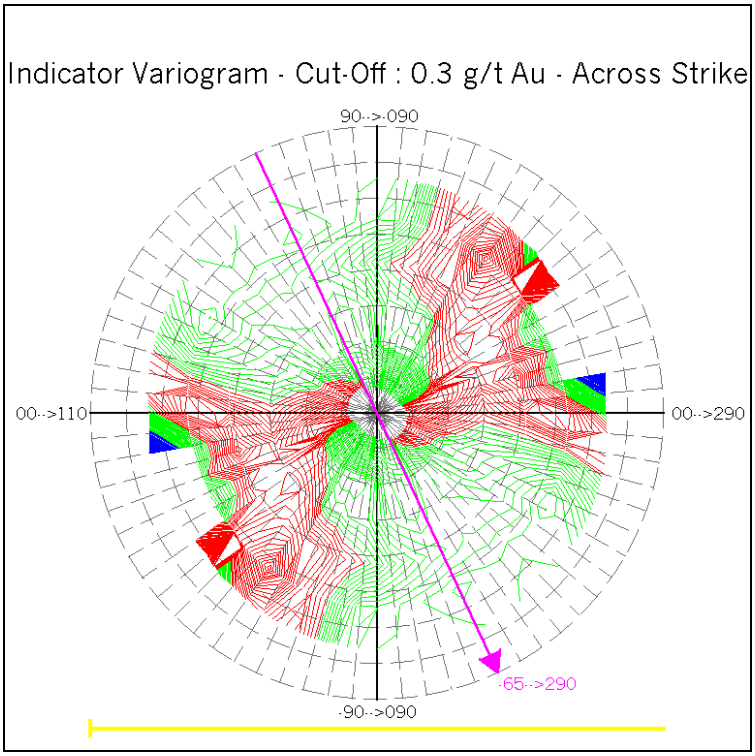

Figure B.26 Fan of Indicator Variograms – CORE Zone Cut-Off at 0.3 g/t Au – Across Strike

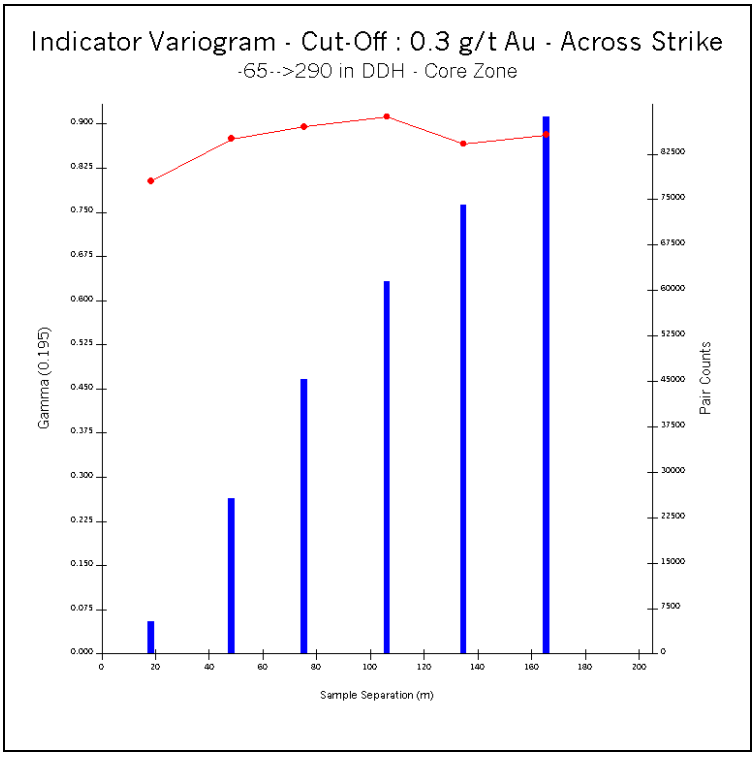

Figure B.27 Indicator Variogram – CORE Zone Cut-Off at 0.3 g/t Au – Across Strike

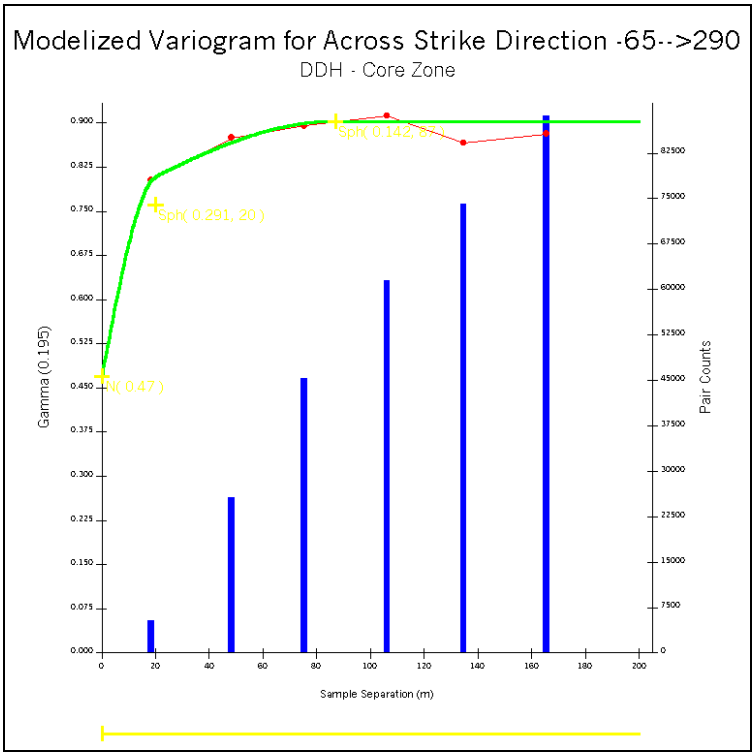

Figure B.28 Modelized Indicator Variogram – CORE Zone Cut-Off at 0.3 g/t Au – Across Strike

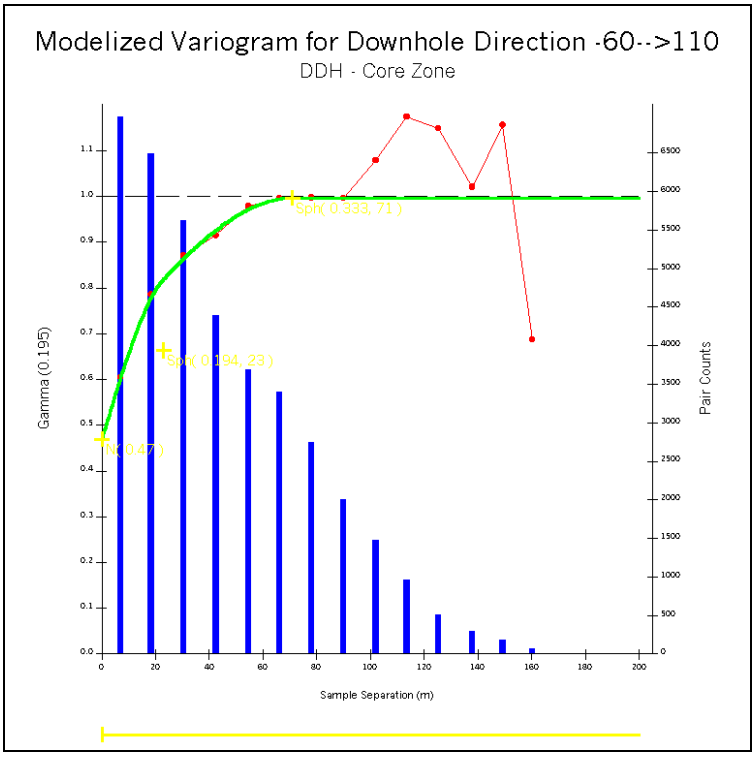

Figure B.29 Modelized Indicator Variogram – CORE Zone Cut-Off at 0.3 g/t Au – Downhole

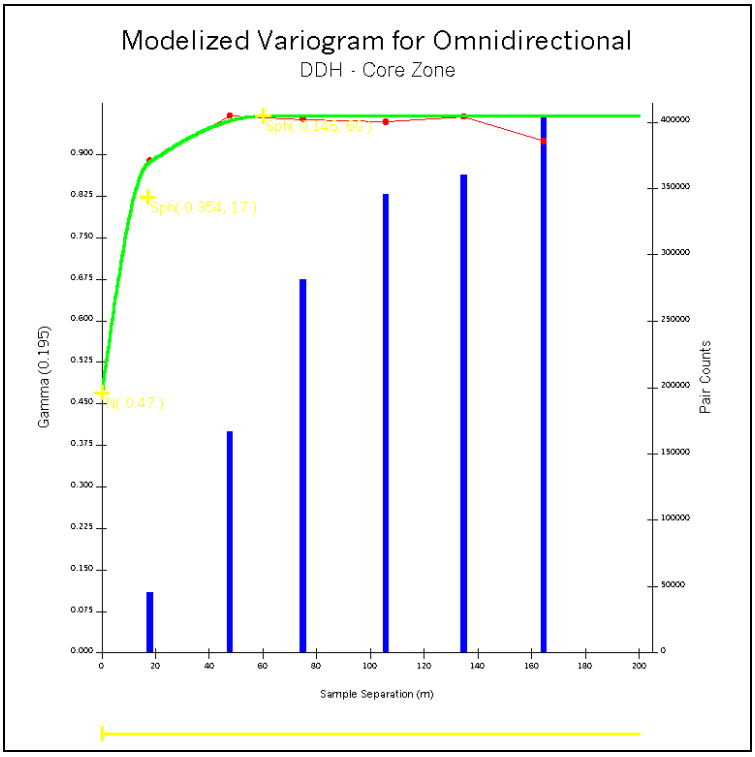

Figure B.30 Modelized Indicator Variogram – CORE Zone Cut-Off at 0.3 g/t Au – Omnidirectional

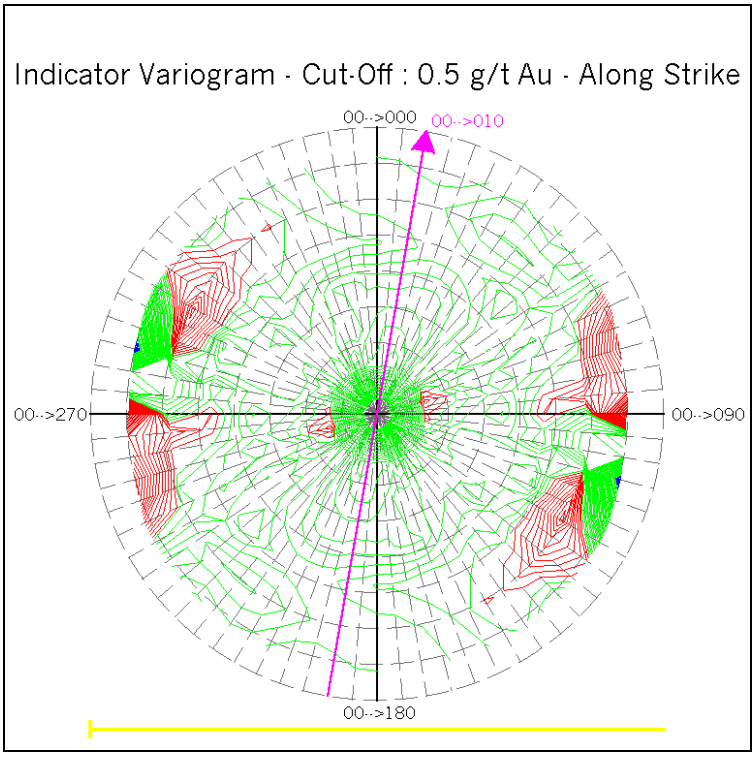

Figure B.31 Fan of Indicator Variograms – CORE Zone Cut-Off at 0.5 g/t Au – Along Strike

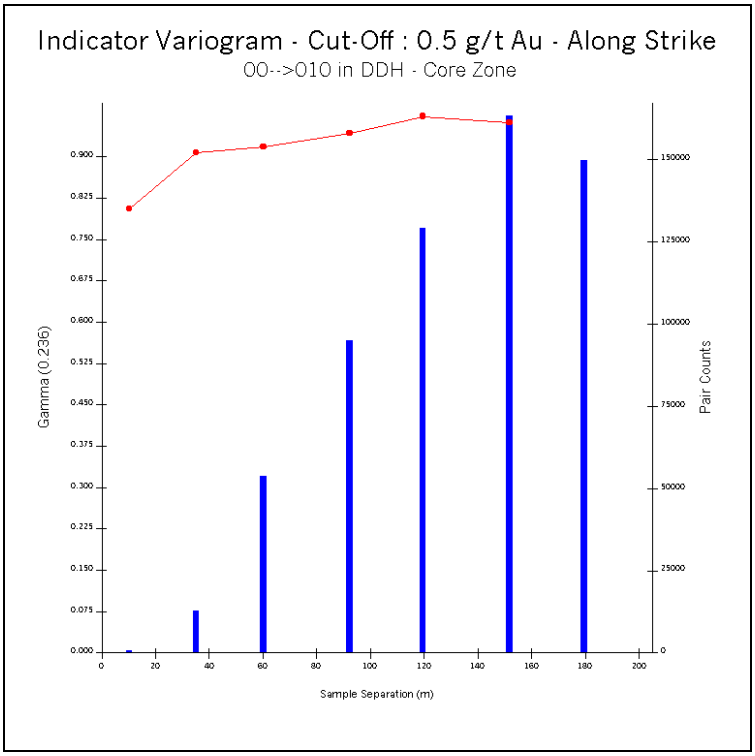

Figure B.32 Indicator Variogram – CORE Zone Cut-Off at 0.5 g/t Au – Along Strike

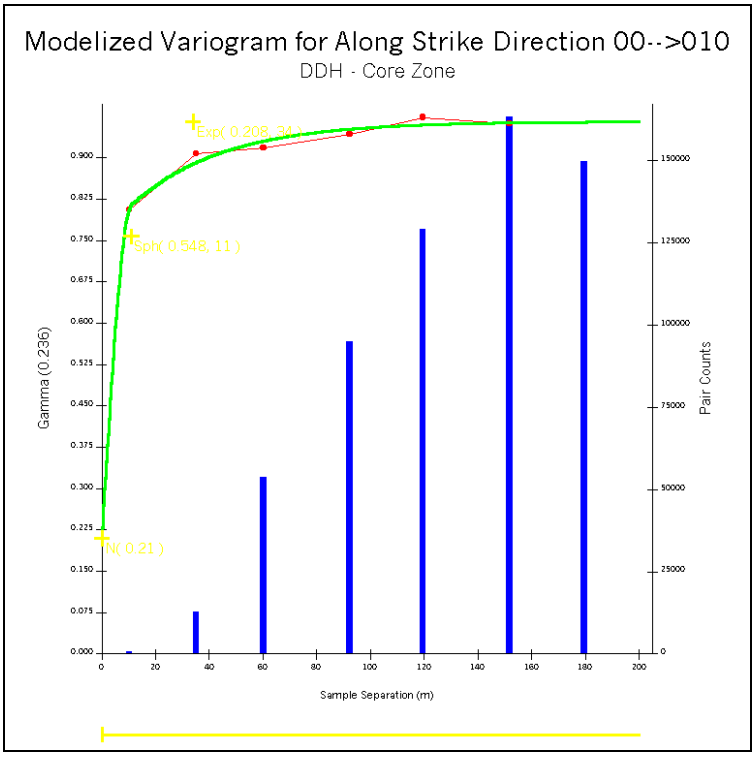

Figure B.33 Modelized Indicator Variogram – CORE Zone Cut-Off at 0.5 g/t Au – Along Strike

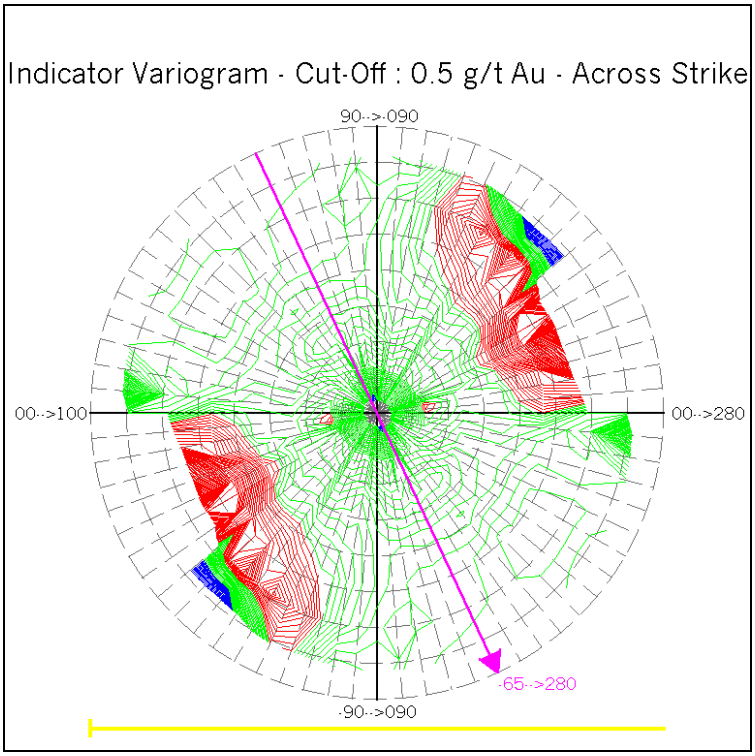

Figure B.34 Fan of Indicator Variograms – CORE Zone Cut-Off at 0.5 g/t Au – Across Strike

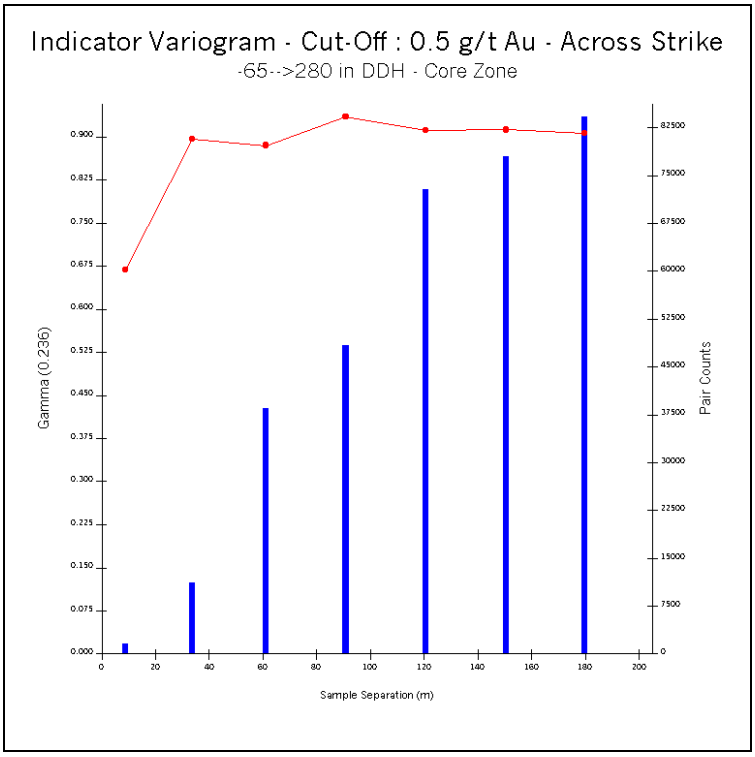

Figure B.35 Indicator Variogram – CORE Zone Cut-Off at 0.5 g/t Au – Across Strike

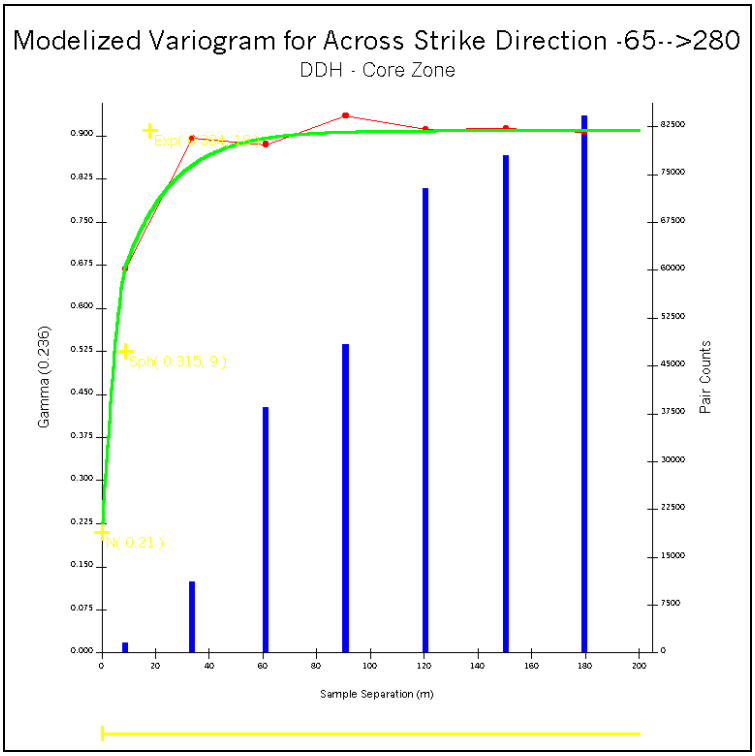

Figure B.36 Modelized Indicator Variogram – CORE Zone Cut-Off at 0.5 g/t Au – Across Strike

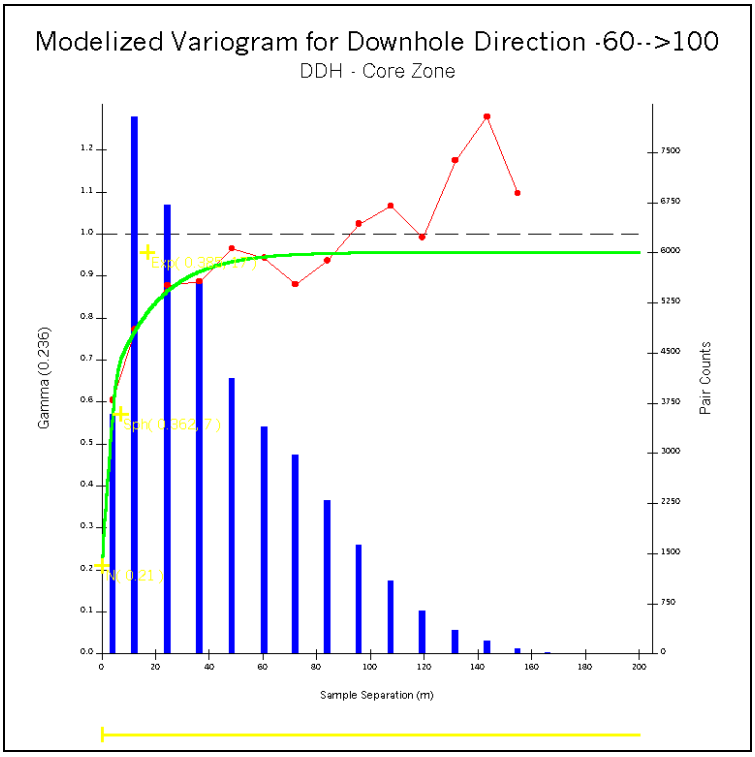

Figure B.37 Modelized Indicator Variogram – CORE Zone Cut-Off at 0.5 g/t Au – Downhole

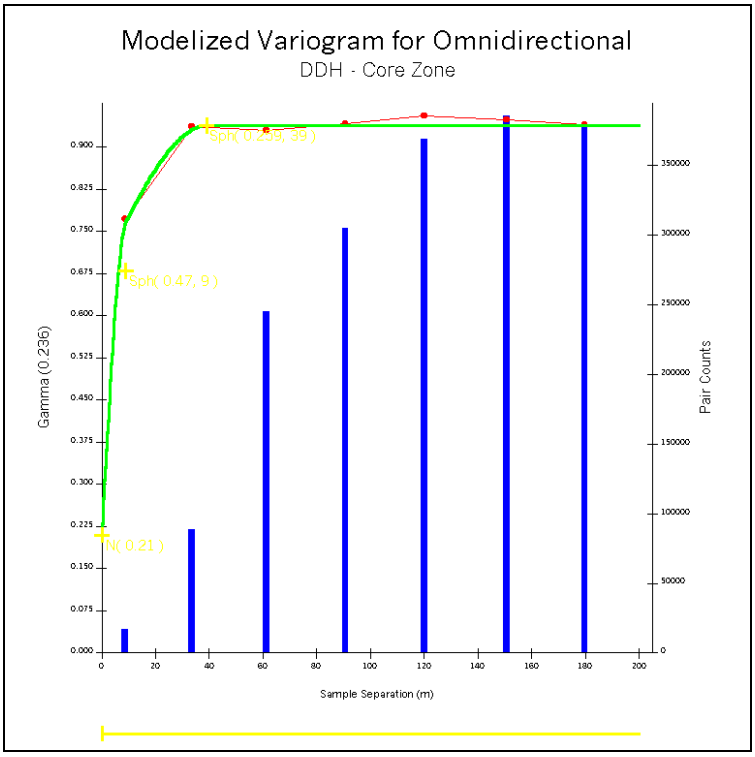

Figure B.38 Modelized Indicator Variogram – CORE Zone Cut-Off at 0.5 g/t Au – Omnidirectional

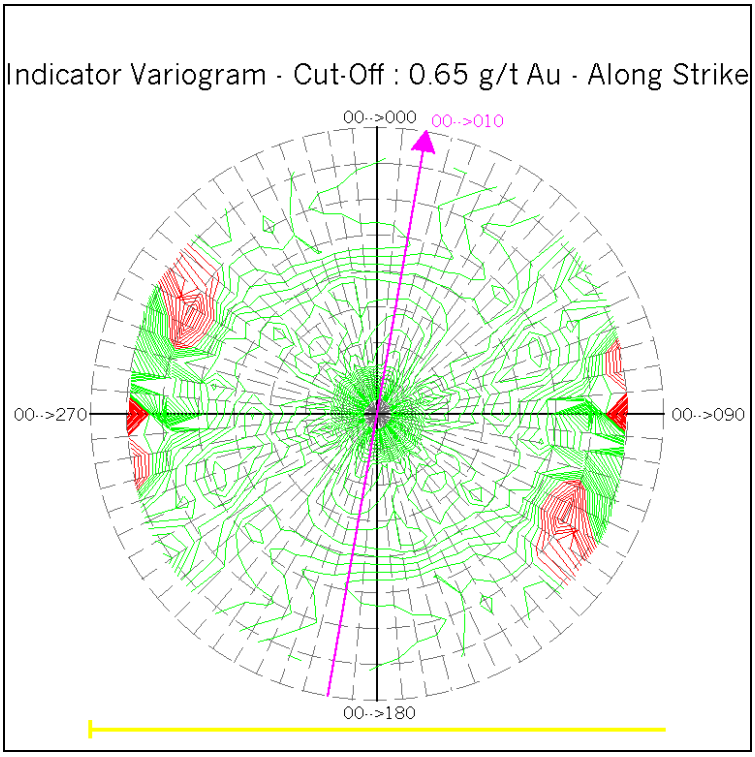

Figure B.39 Fan of Indicator Variograms – CORE Zone Cut-Off at 0.65 g/t Au – Along Strike

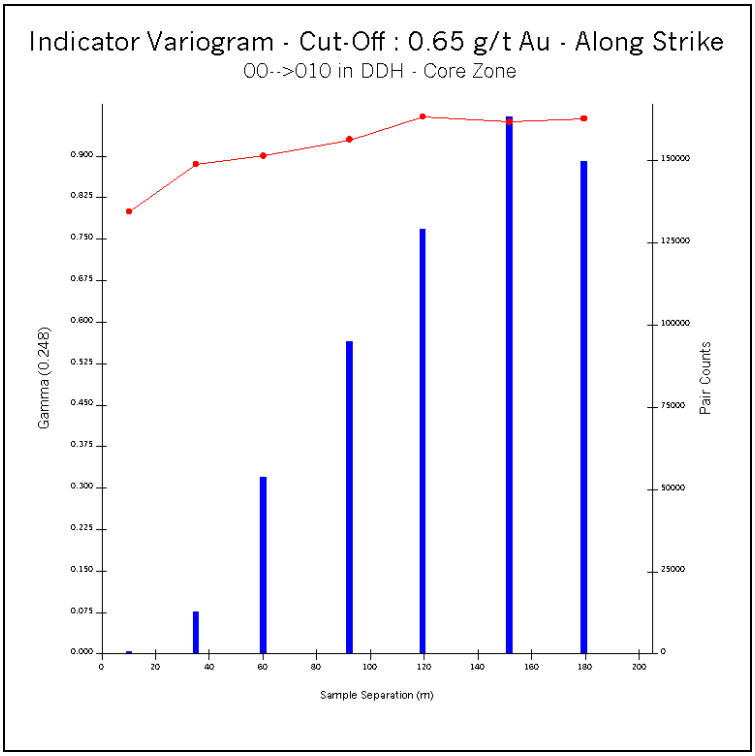

Figure B.40 Indicator Variogram – CORE Zone Cut-Off at 0.65 g/t Au – Along Strike

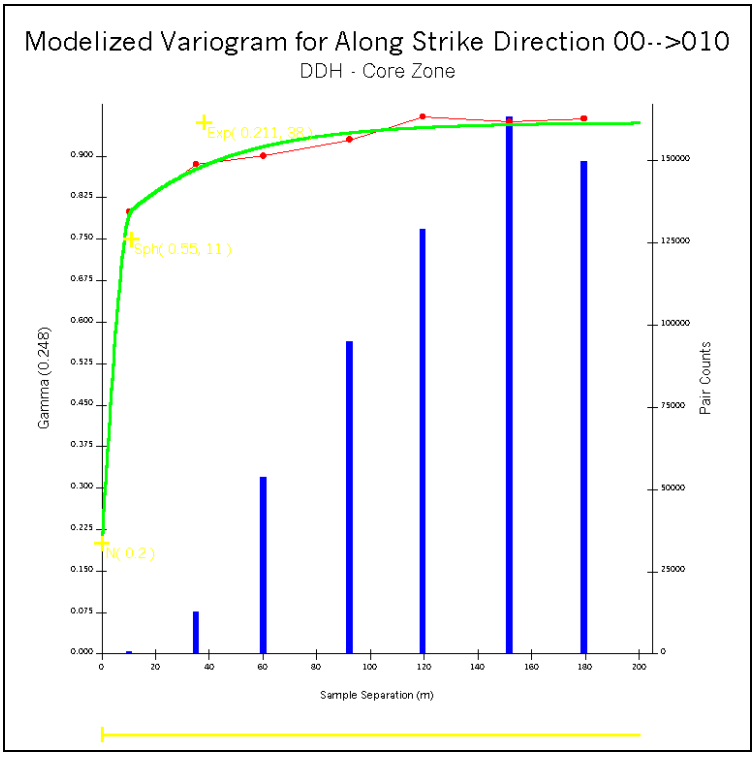

Figure B.41 Modelized Indicator Variogram – CORE Zone Cut-Off at 0.65 g/t Au – Along Strike

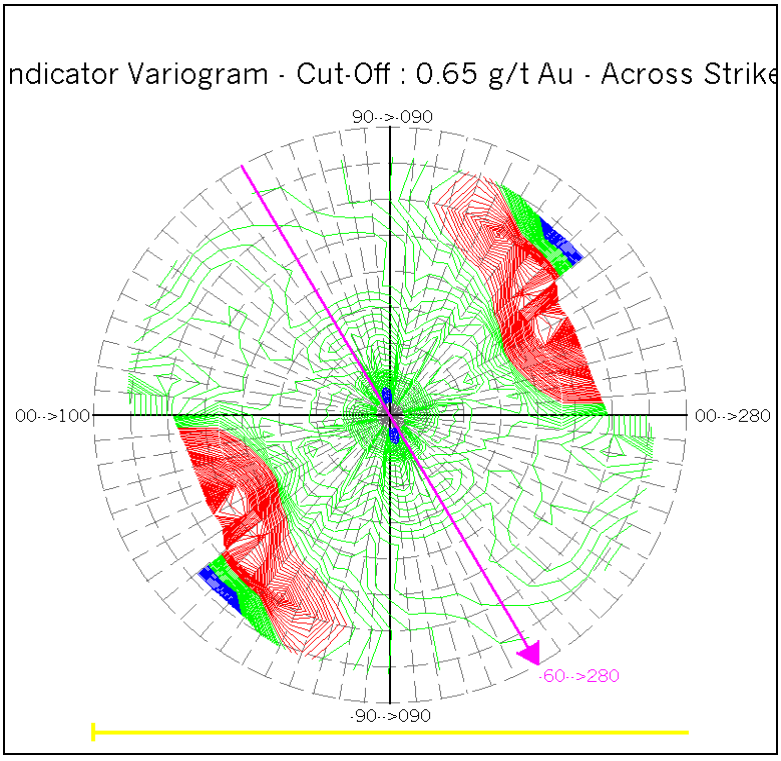

Figure B.42 Fan of Indicator Variograms – CORE Zone Cut-Off at 0.65 g/t Au – Across Strike

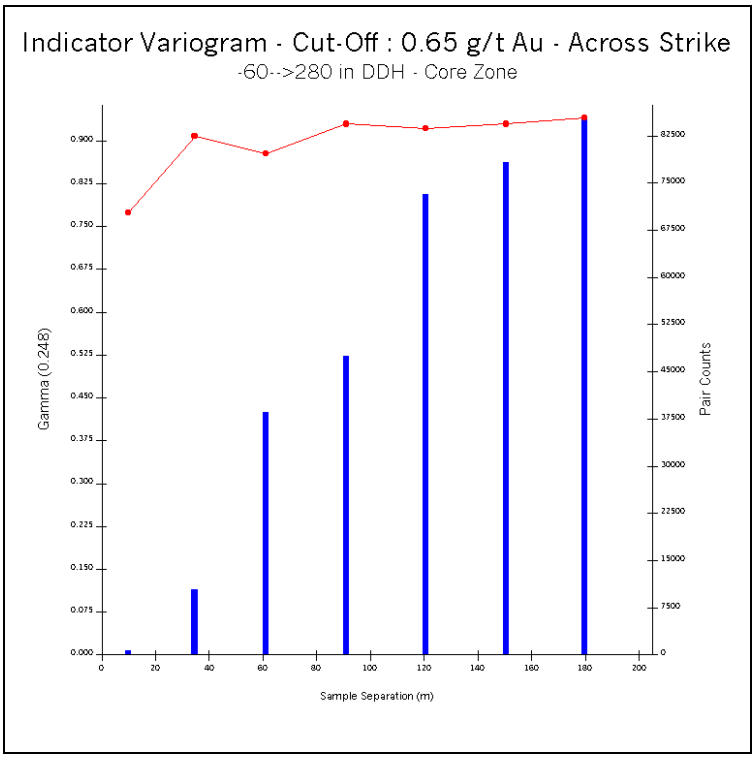

Figure B.43 Indicator Variogram – CORE Zone Cut-Off at 0.65 g/t Au – Across Strike

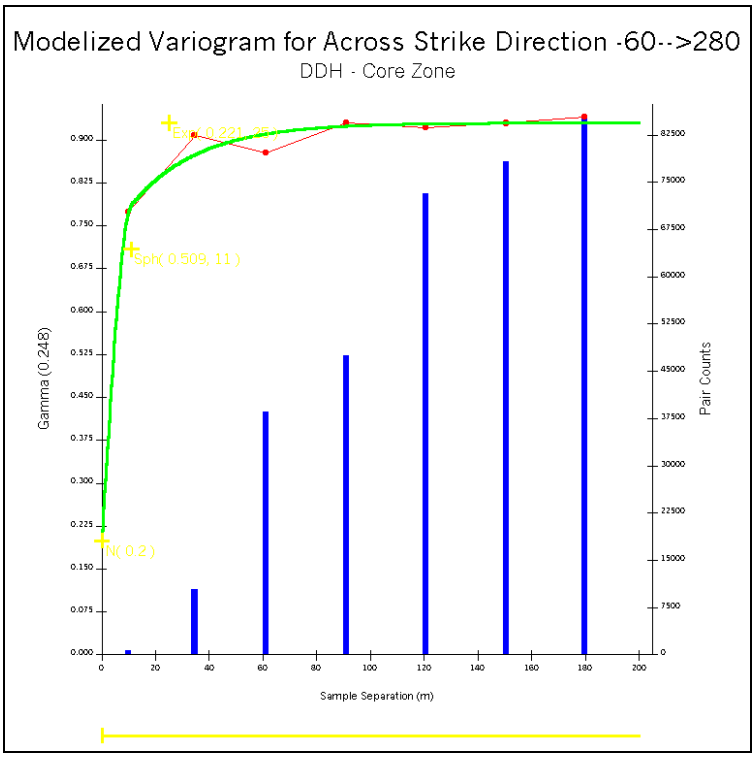

Figure B.44 Modelized Indicator Variogram – CORE Zone Cut-Off at 0.65 g/t Au – Across Strike

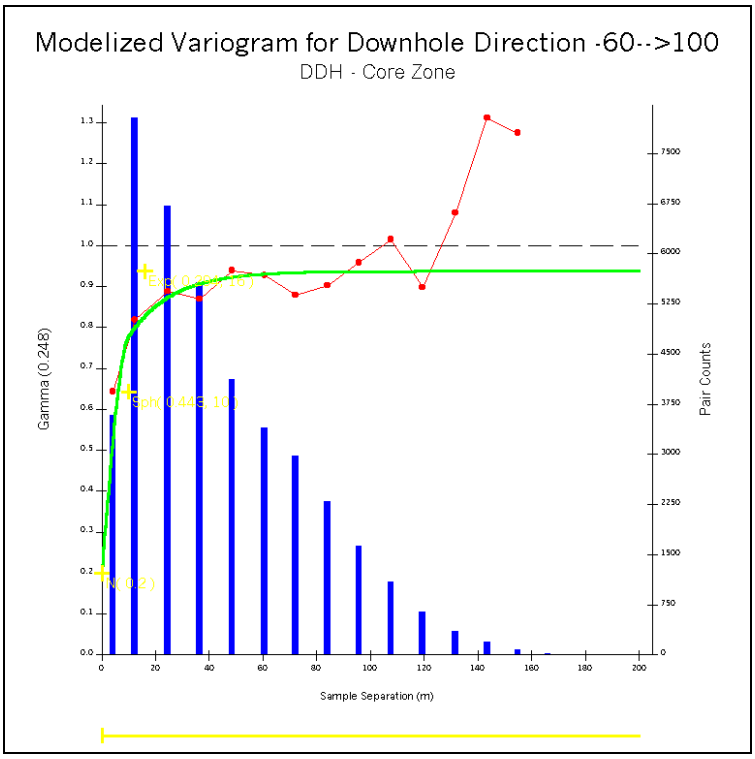

Figure B.45 Modelized Indicator Variogram – CORE Zone Cut-Off at 0.65 g/t Au – Downhole

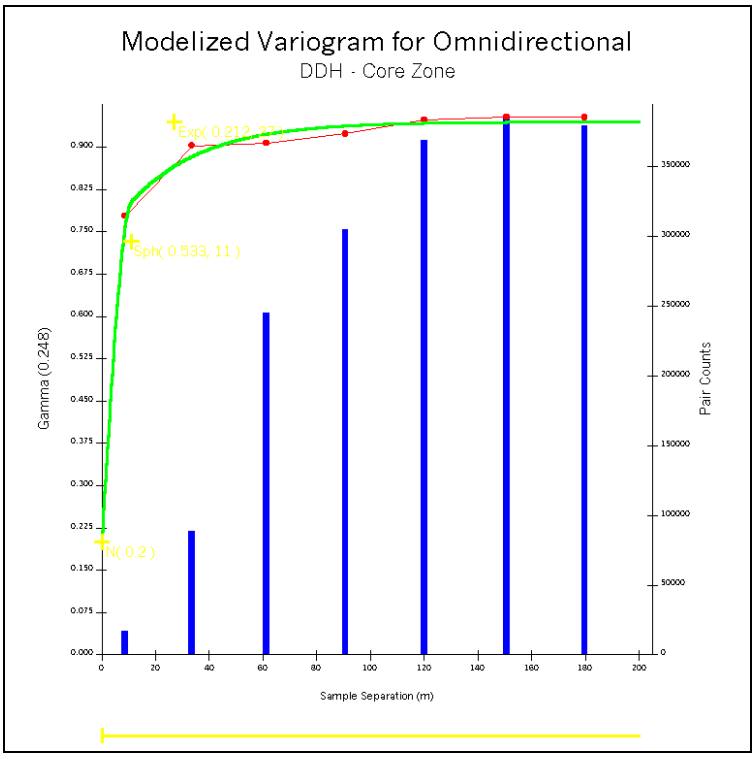

Figure B.46 Modelized Indicator Variogram – CORE Zone Cut-Off at 0.65 g/t Au – Omnidirectional

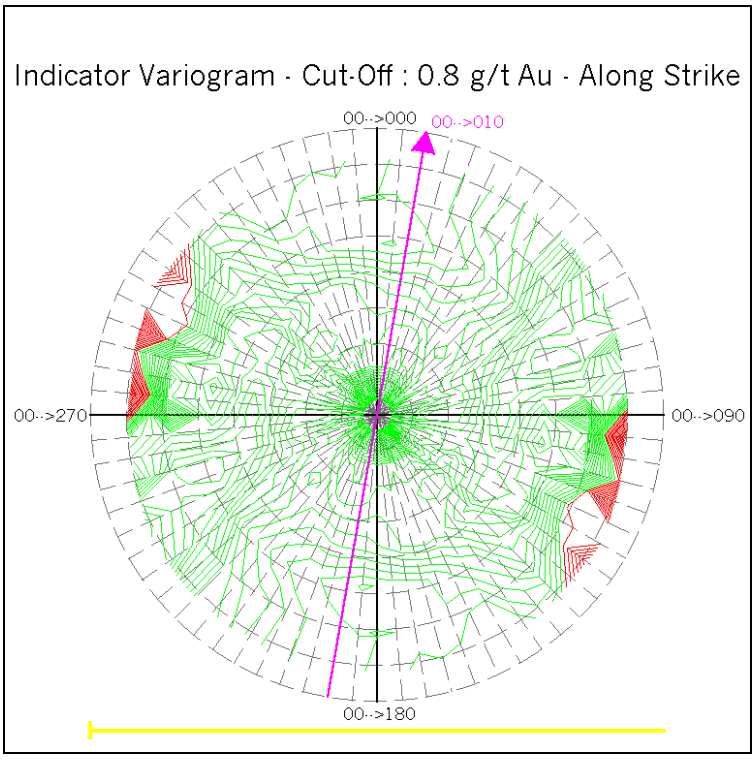

Figure B.47 Fan of Indicator Variograms – CORE Zone Cut-Off at 0.8 g/t Au – Along Strike

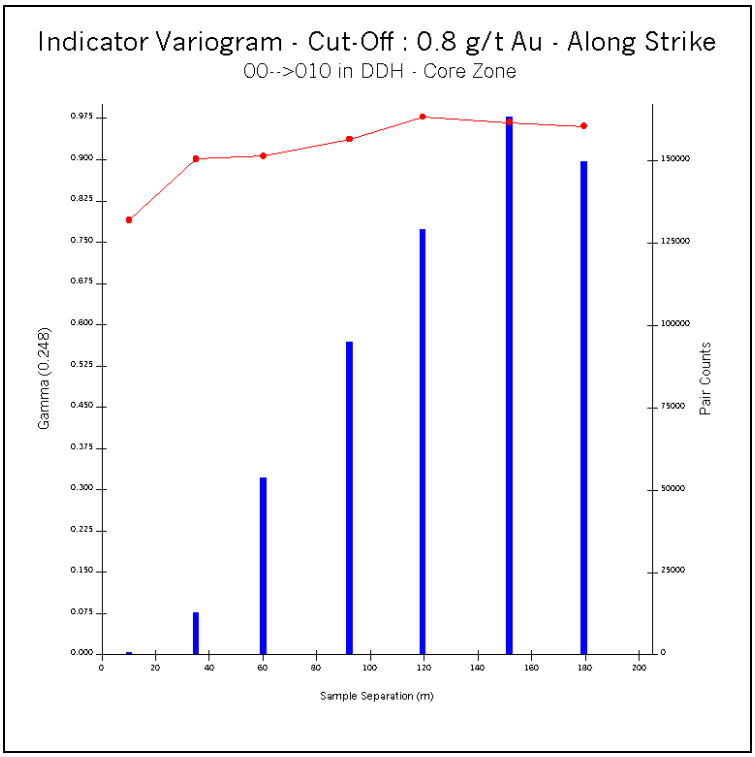

Figure B.48 Indicator Variogram – CORE Zone Cut-Off at 0.8 g/t Au – Along Strike

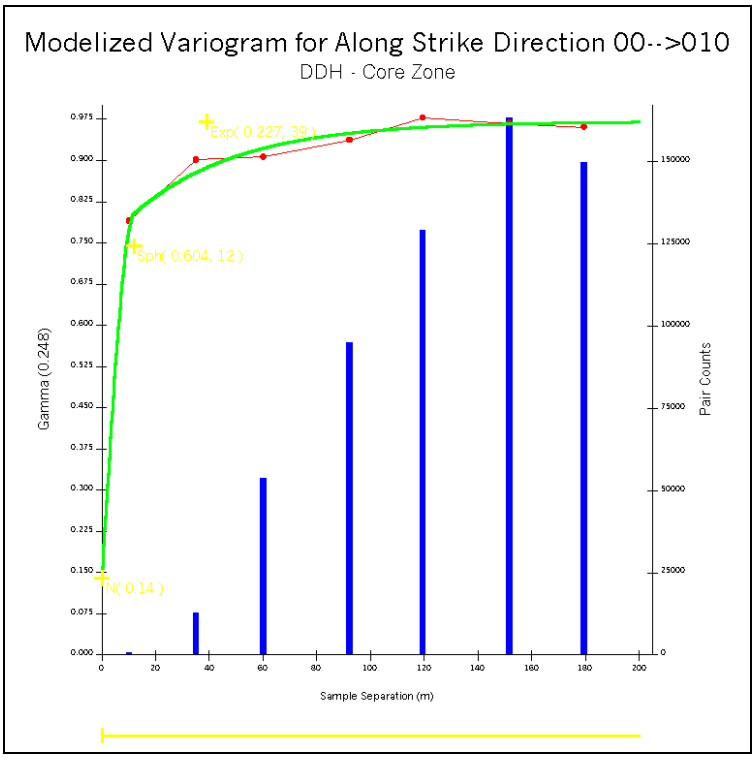

Figure B.49 Modelized Indicator Variogram – CORE Zone Cut-Off at 0.8 g/t Au – Along Strike

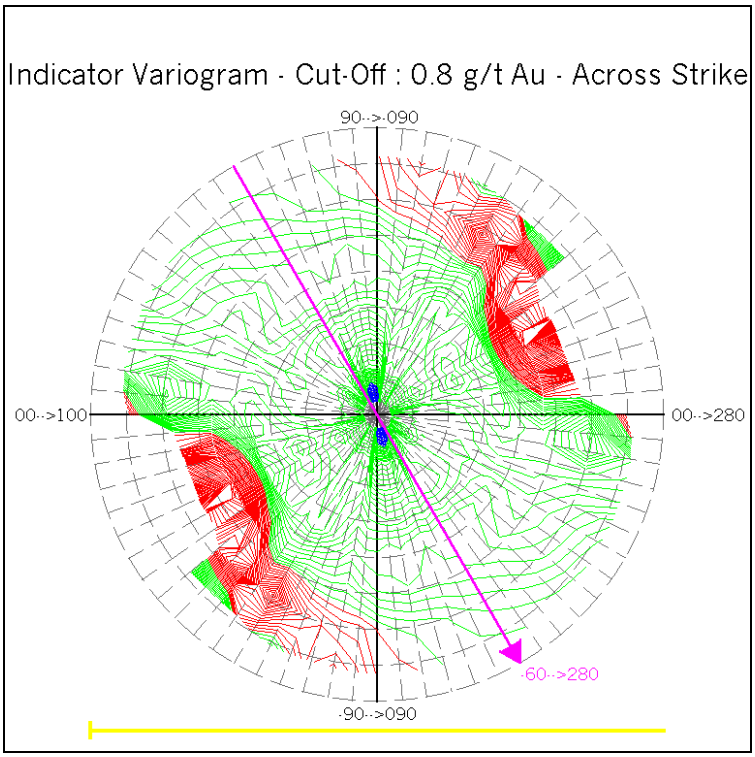

Figure B.50 Fan of Indicator Variograms – CORE Zone Cut-Off at 0.8 g/t Au – Across Strike

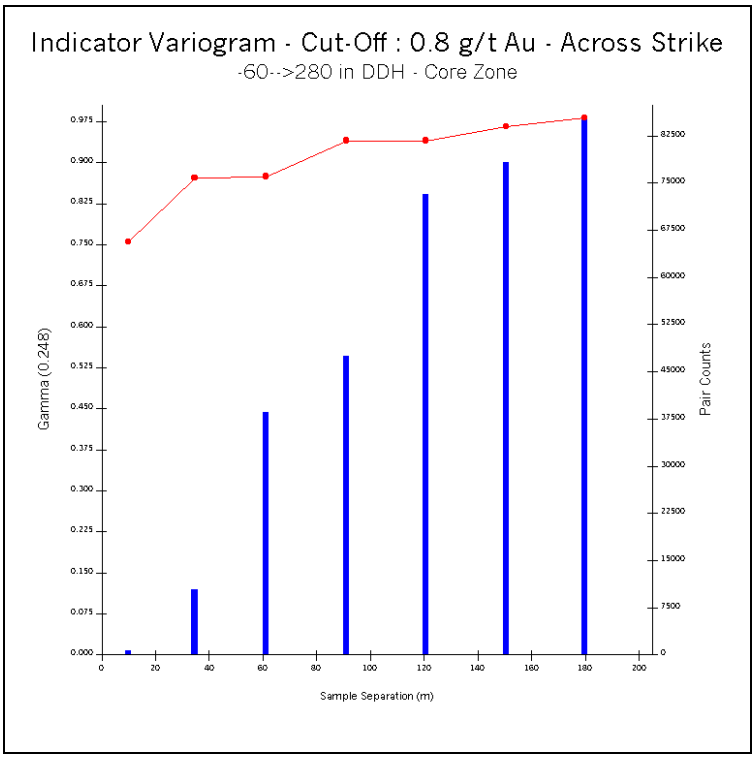

Figure B.51 Indicator Variogram – CORE Zone Cut-Off at 0.8 g/t Au – Across Strike

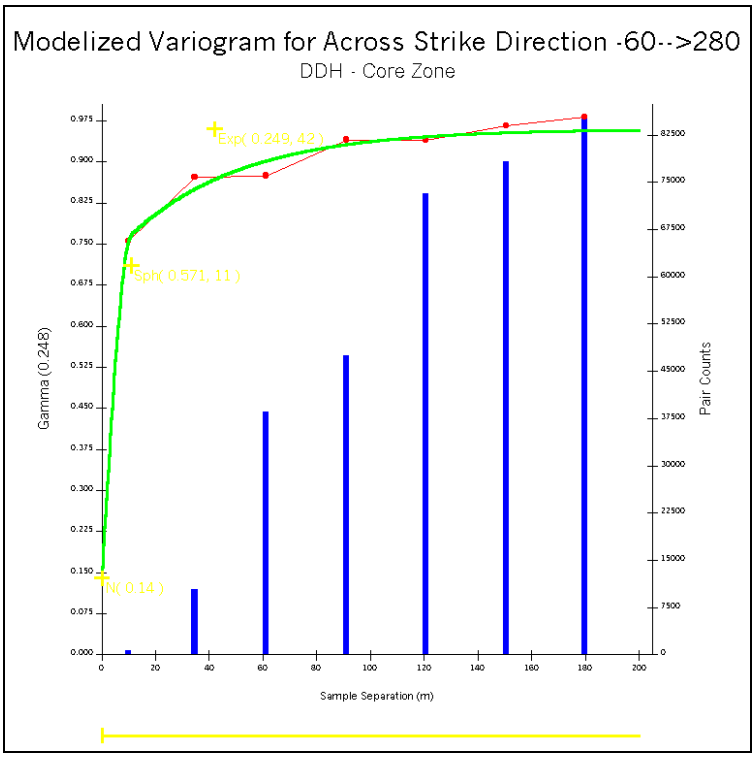

Figure B.52 Modelized Indicator Variogram – CORE Zone Cut-Off at 0.8 g/t Au – Across Strike

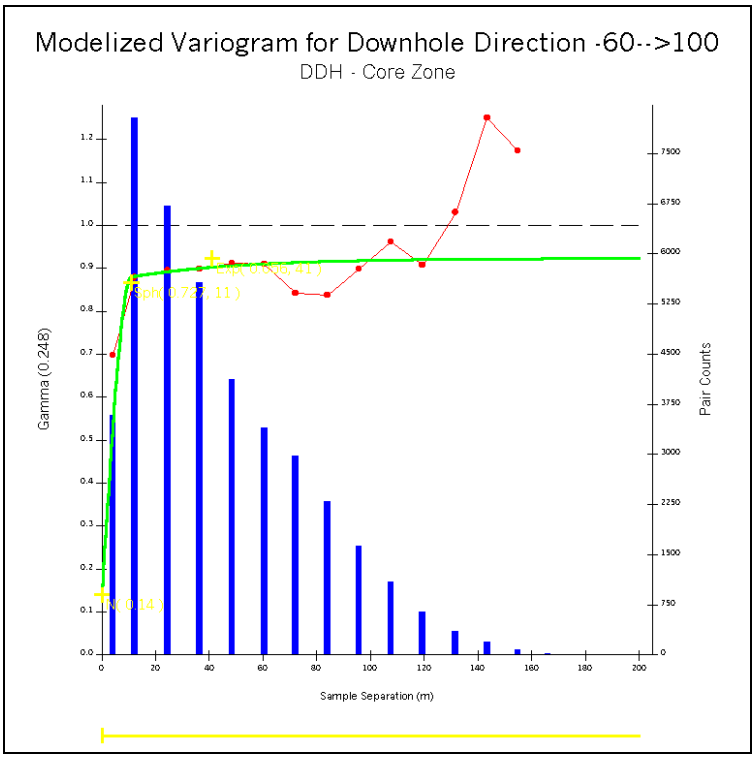

Figure B.53 Modelized Indicator Variogram – CORE Zone Cut-Off at 0.8 g/t Au – Downhole

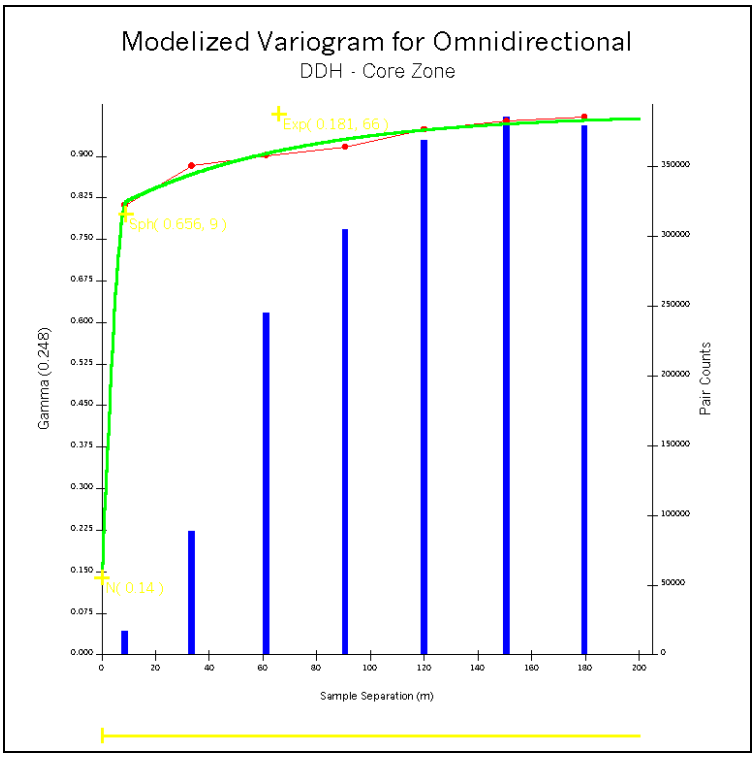

Figure B.54 Modelized Indicator Variogram – CORE Zone Cut-Off at 0.8 g/t Au – Omnidirectional

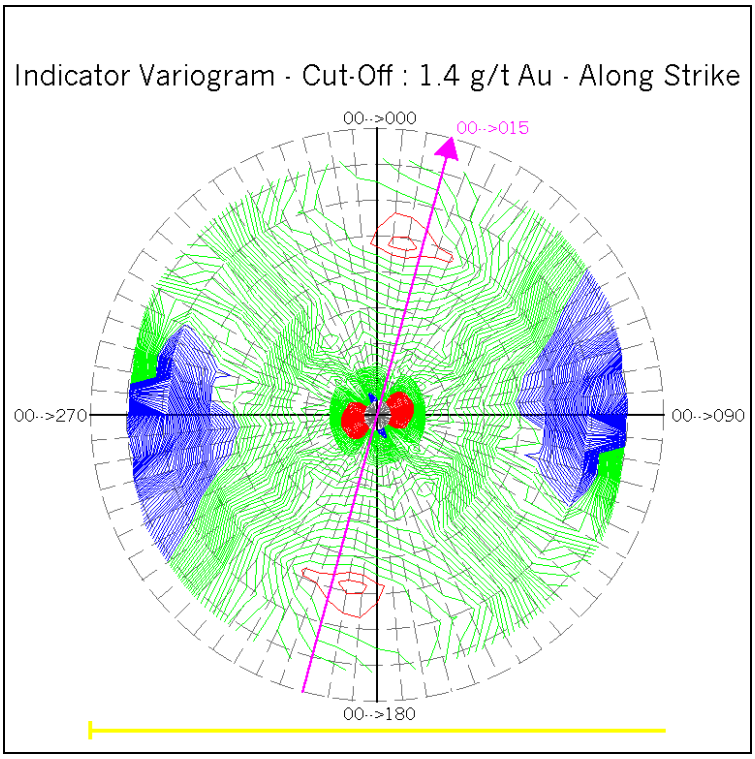

Figure B.55 Fan of Indicator Variograms – CORE Zone Cut-Off at 1.4 g/t Au – Along Strike

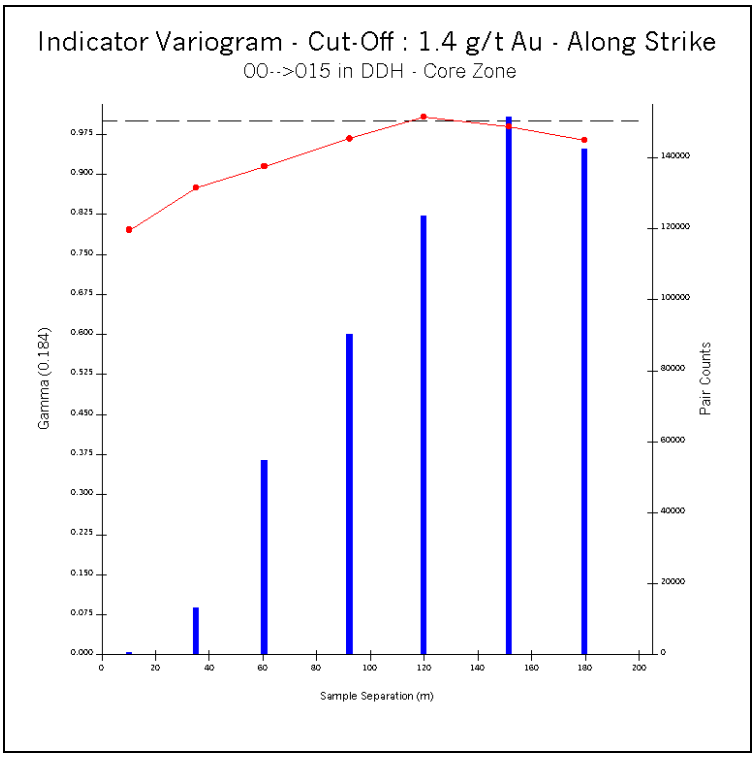

Figure B.56 Indicator Variogram – CORE Zone Cut-Off at 1.4 g/t Au – Along Strike

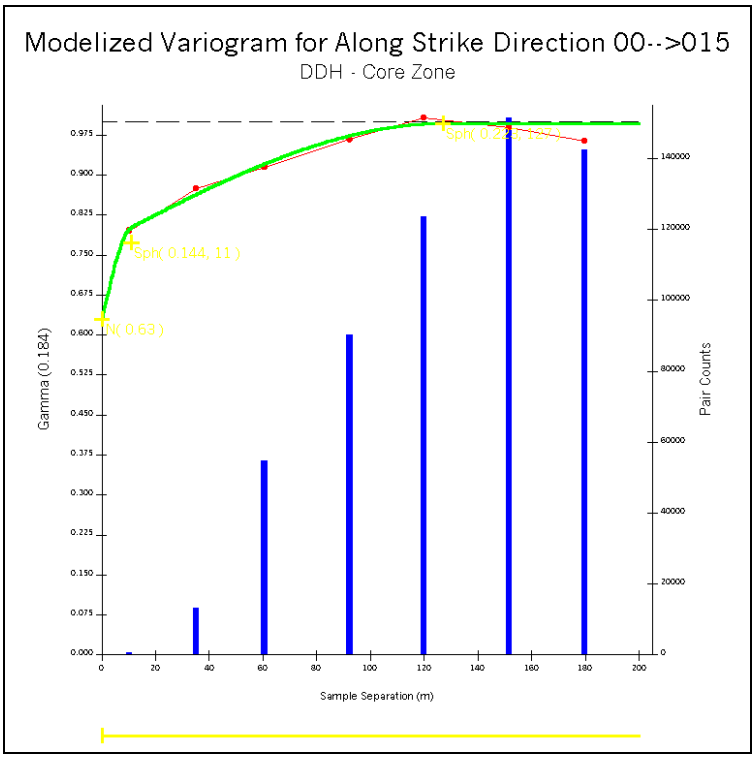

Figure B.57 Modelized Indicator Variogram – CORE Zone Cut-Off at 1.4 g/t Au – Along Strike

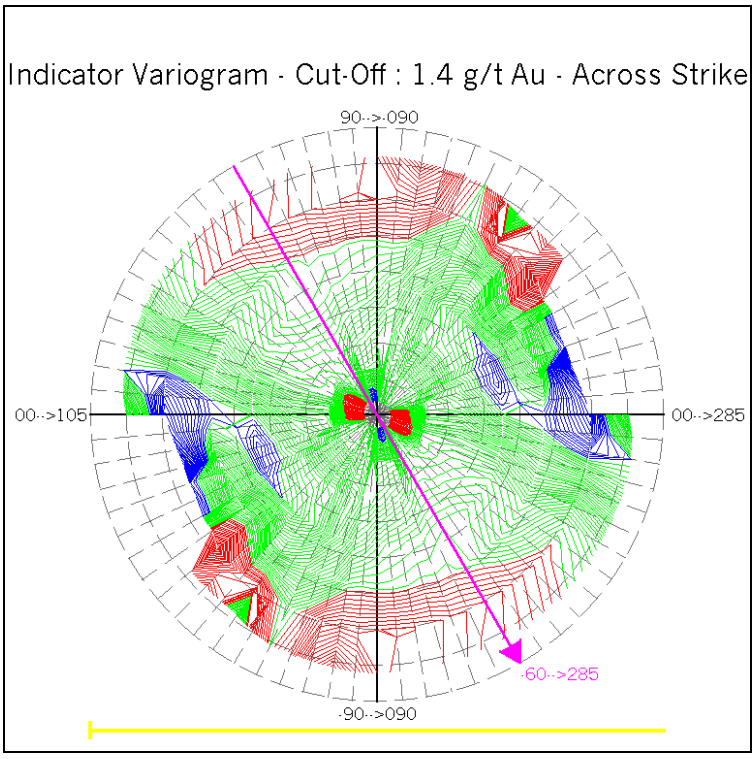

Figure B.58 Fan of Indicator Variograms – CORE Zone Cut-Off at 1.4 g/t Au – Across Strike

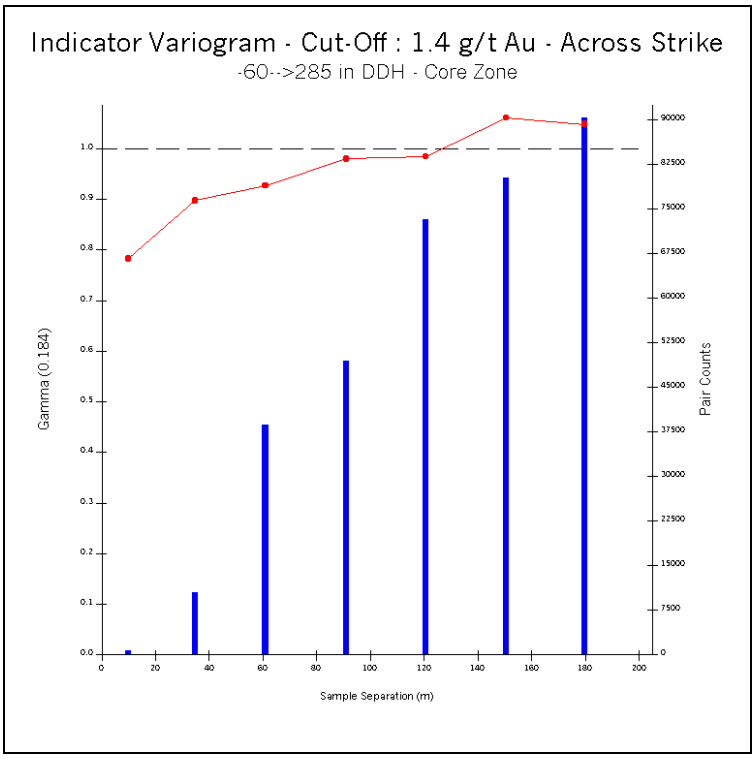

Figure B.59 Indicator Variogram – CORE Zone Cut-Off at 1.4 g/t Au – Across Strike

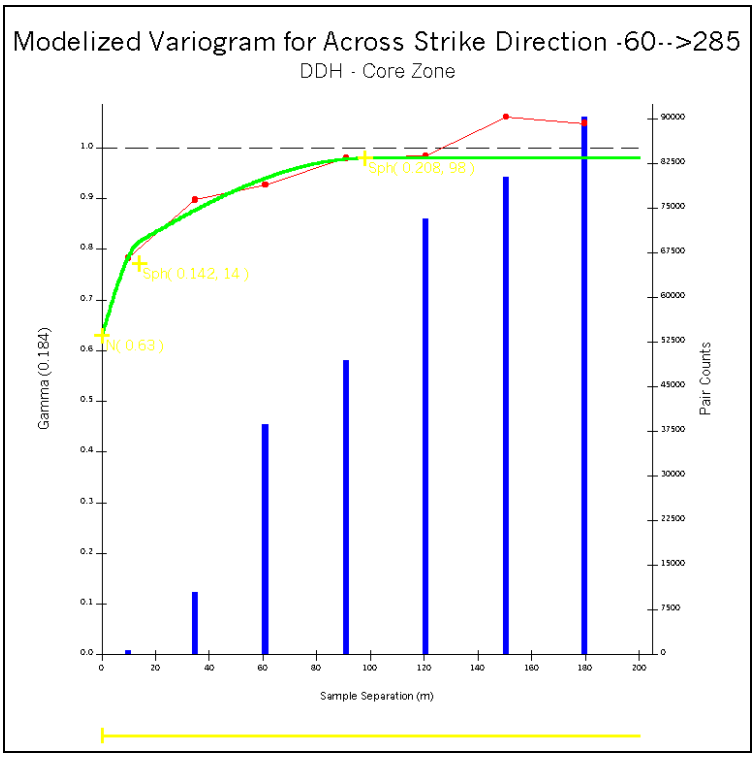

Figure B.60 Modelized Indicator Variogram – CORE Zone Cut-Off at 1.4 g/t Au – Across Strike

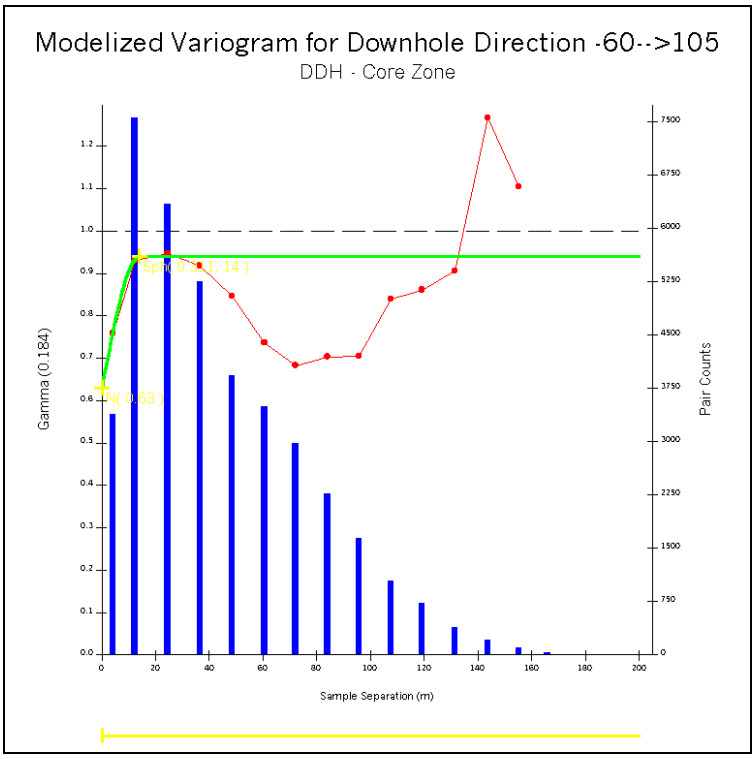

Figure B.61 Modelized Indicator Variogram – CORE Zone Cut-Off at 1.4 g/t Au – Downhole

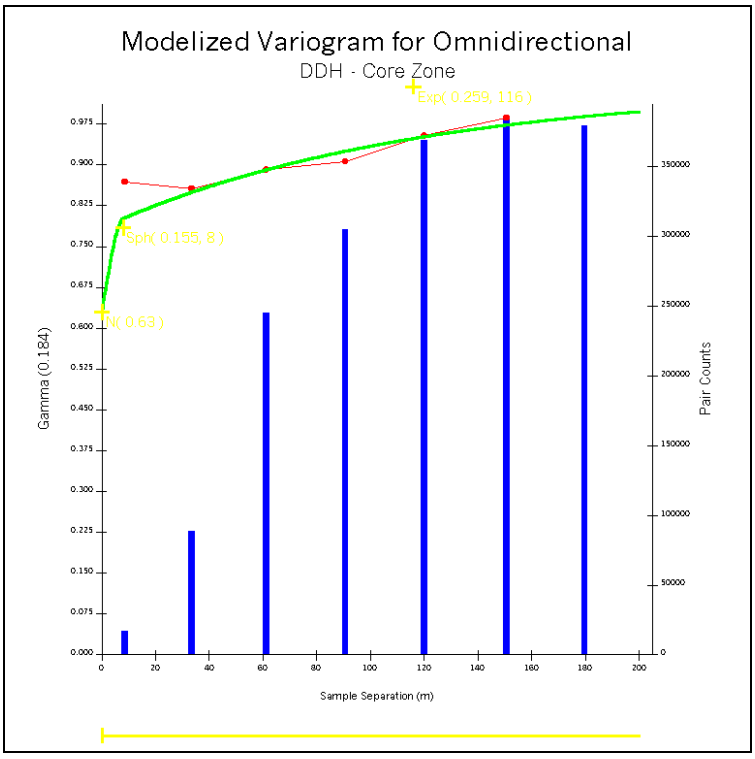

Figure B.62 Modelized Indicator Variogram – CORE Zone Cut-Off at 1.4 g/t Au – Omnidirectional

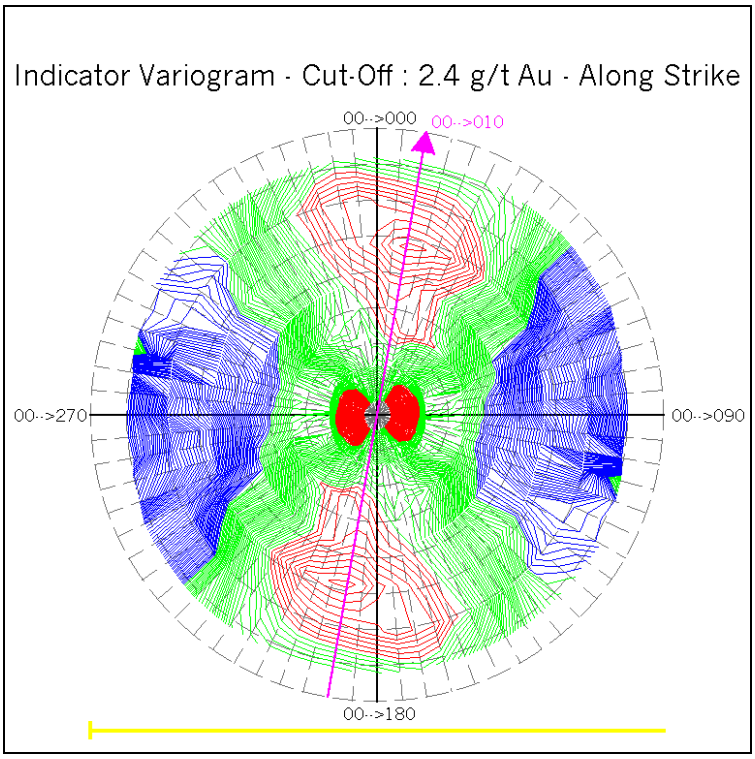

Figure B.63 Fan of Indicator Variograms – CORE Zone Cut-Off at 2.4 g/t Au – Along Strike

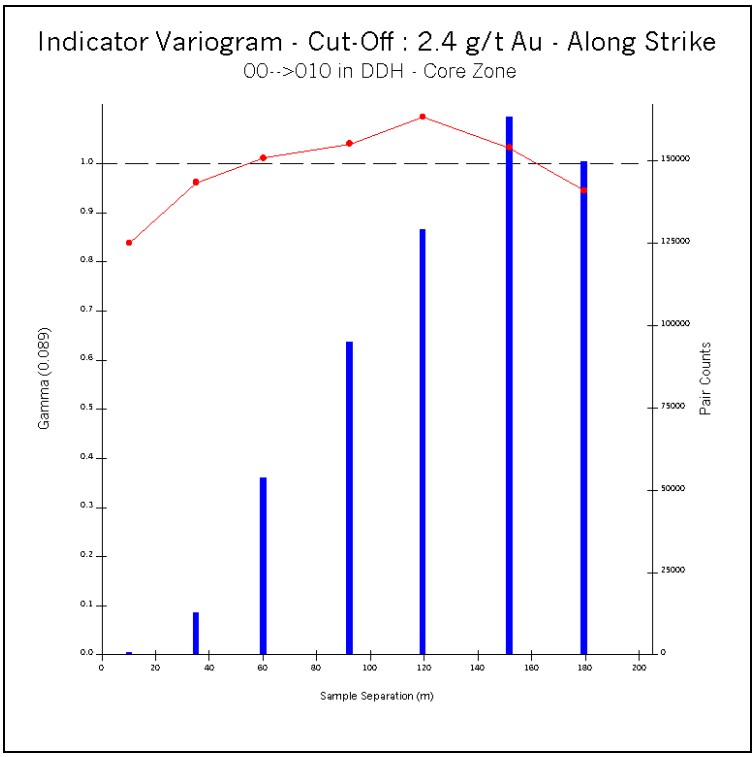

Figure B.64 Indicator Variogram – CORE Zone Cut-Off at 2.4 g/t Au – Along Strike

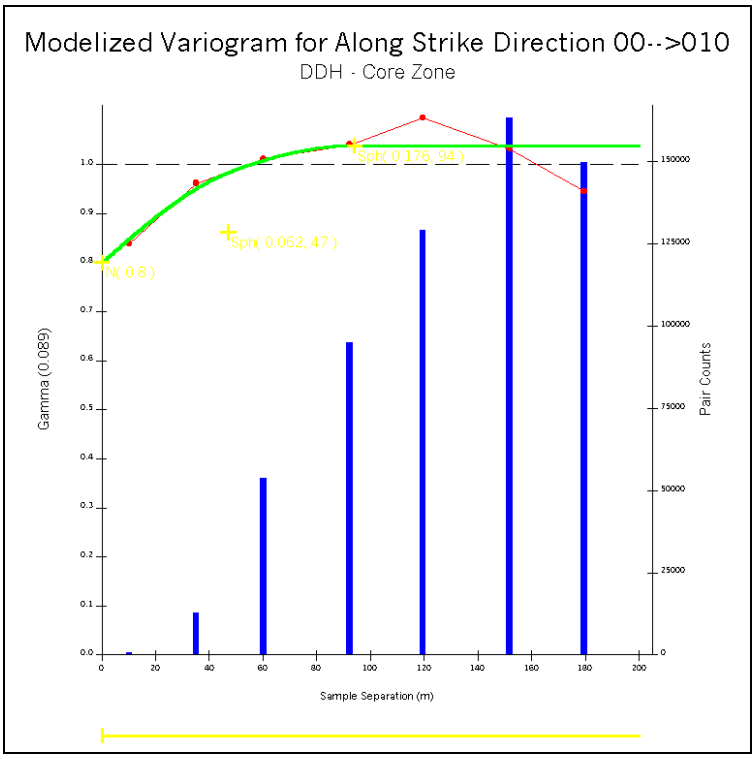

Figure B.65 Modelized Indicator Variogram – CORE Zone Cut-Off at 2.4 g/t Au – Along Strike

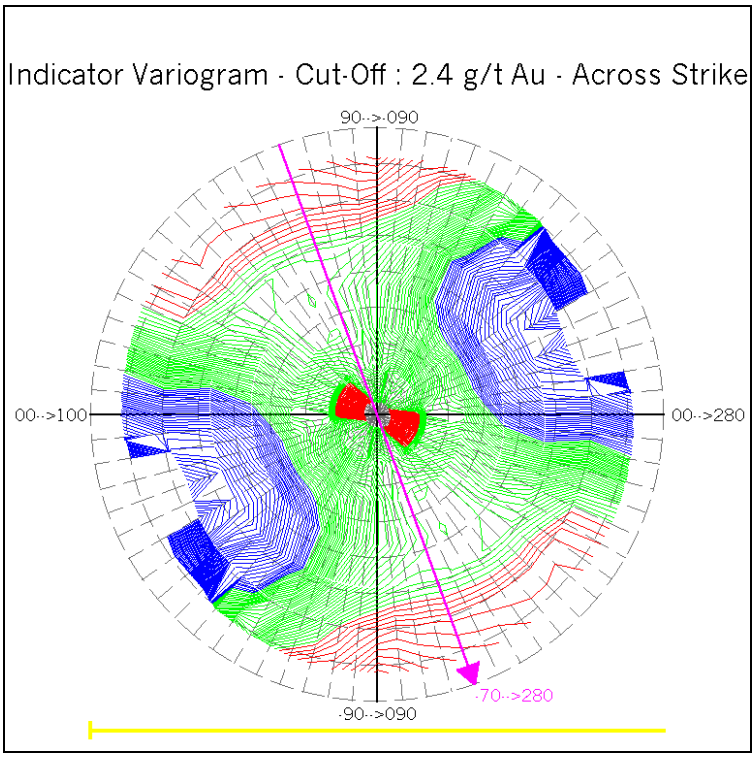

Figure B.66 Fan of Indicator Variograms – CORE Zone Cut-Off at 2.4 g/t Au – Across Strike

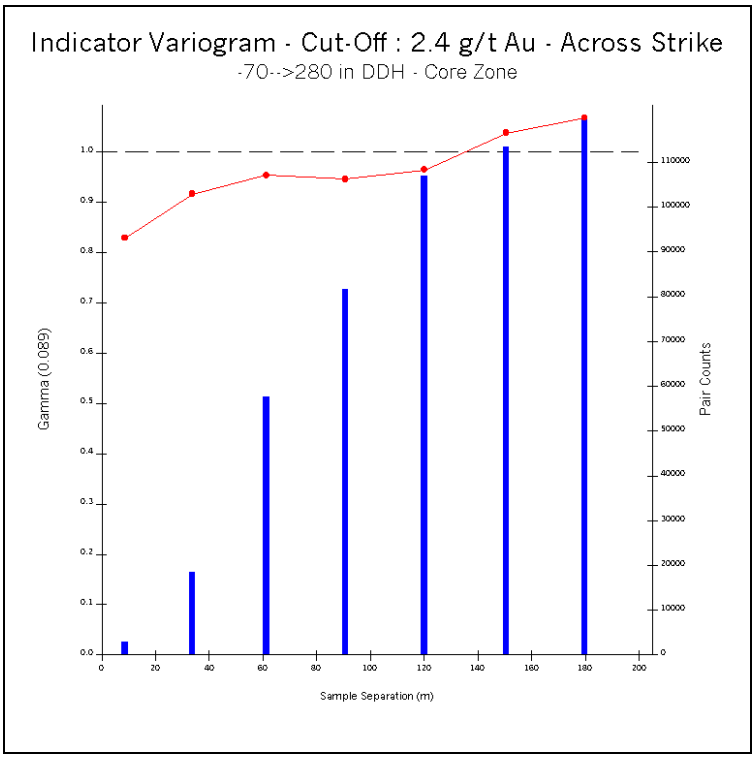

Figure B.67 Indicator Variogram – CORE Zone Cut-Off at 2.4 g/t Au – Across Strike

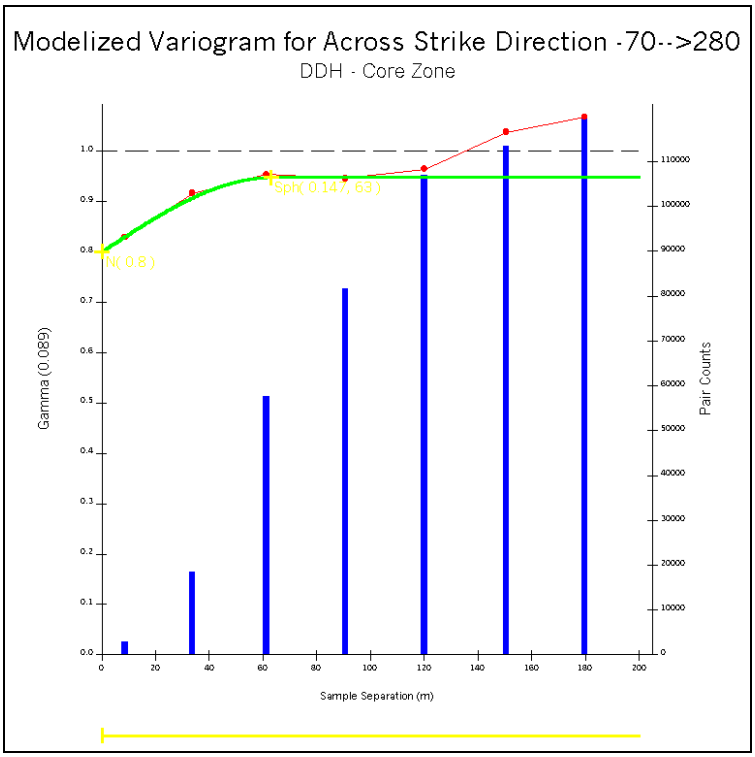

Figure B.68 Modelized Indicator Variogram – CORE Zone Cut-Off at 2.4 g/t Au – Across Strike

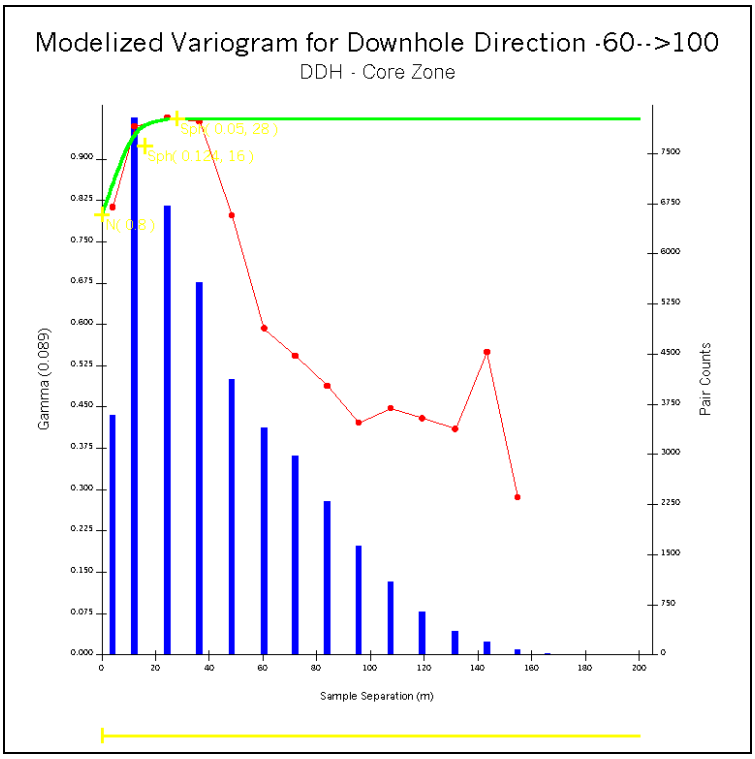

Figure B.69 Modelized Indicator Variogram – CORE Zone Cut-Off at 2.4 g/t Au – Downhole

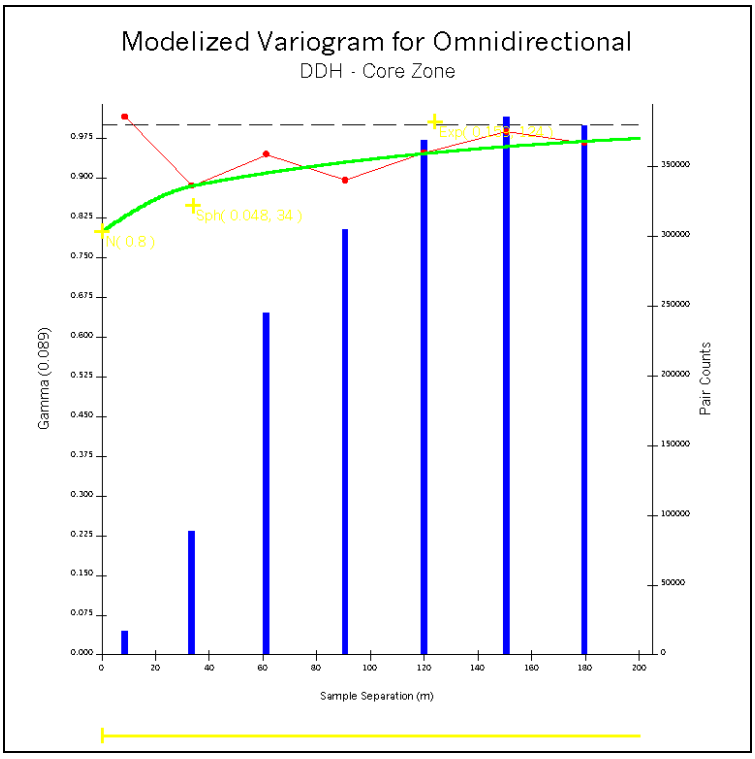

Figure B.70 Modelized Indicator Variogram – CORE Zone Cut-Off at 2.4 g/t Au – Omnidirectional

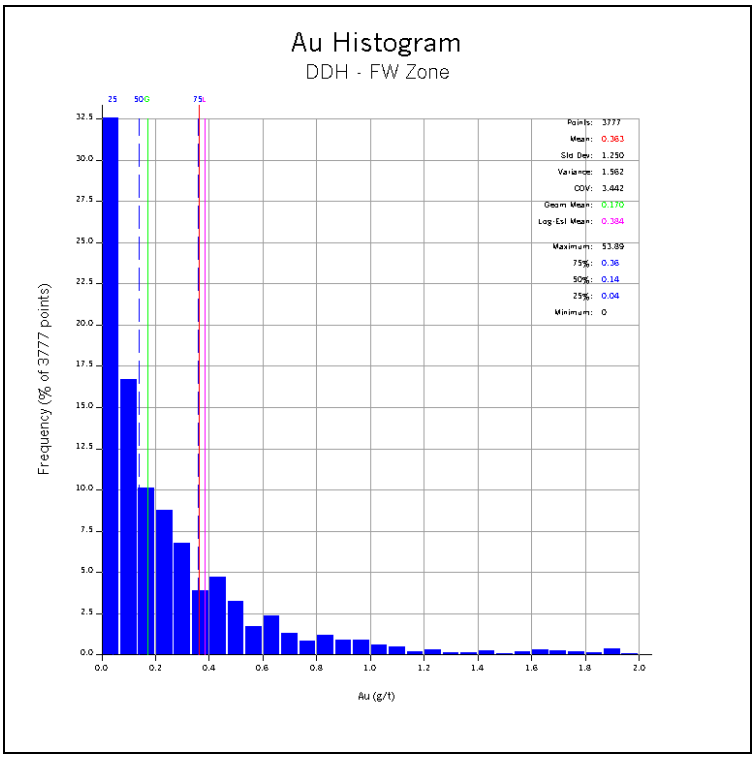

Figure B.71 Au Normal Histogram – FW Zone

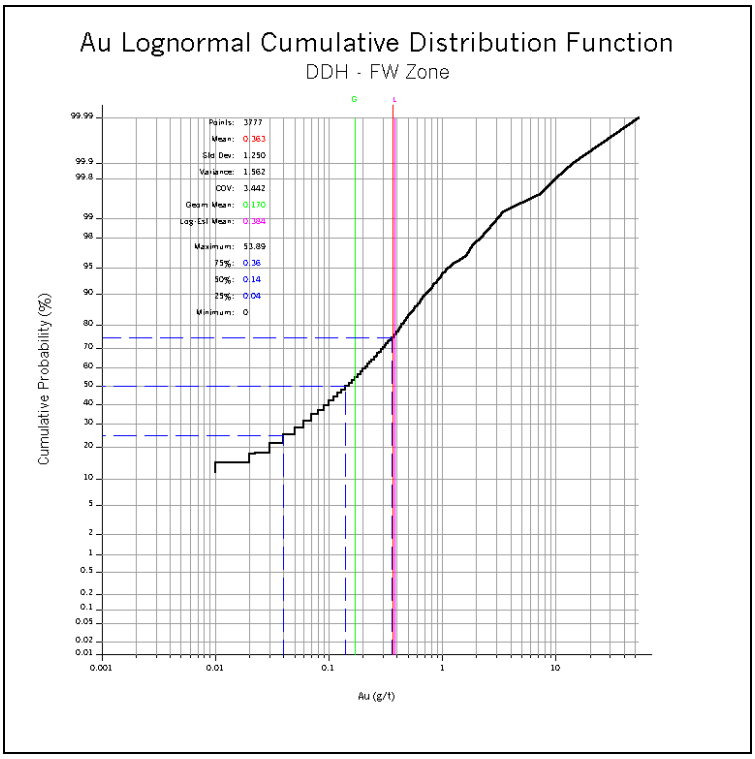

Figure B.72 Au Lognormal Cumulative Distribution Function – FW Zone

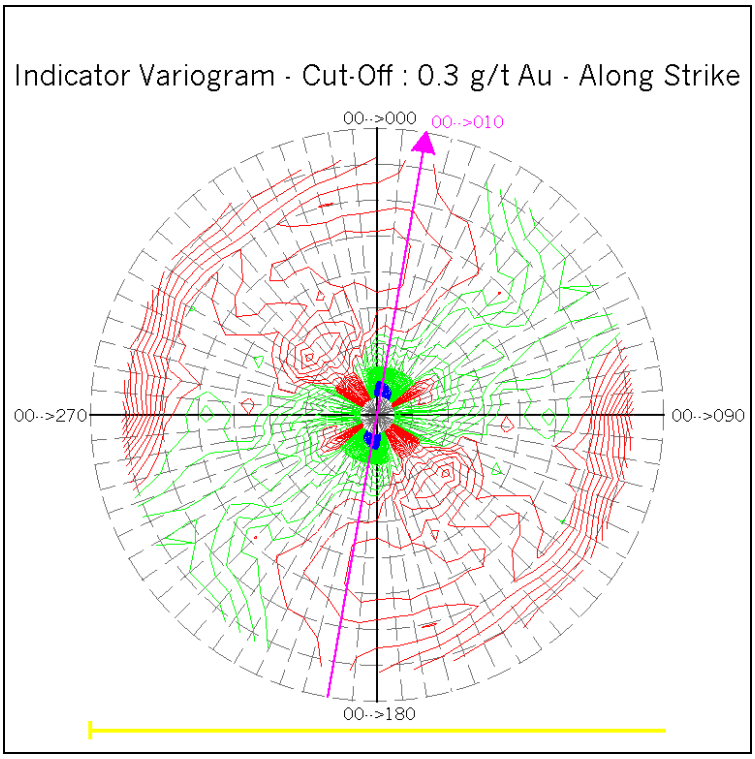

Figure B.73 Fan of Indicator Variograms – FW Zone Cut-Off at 0.3 g/t Au – Along Strike

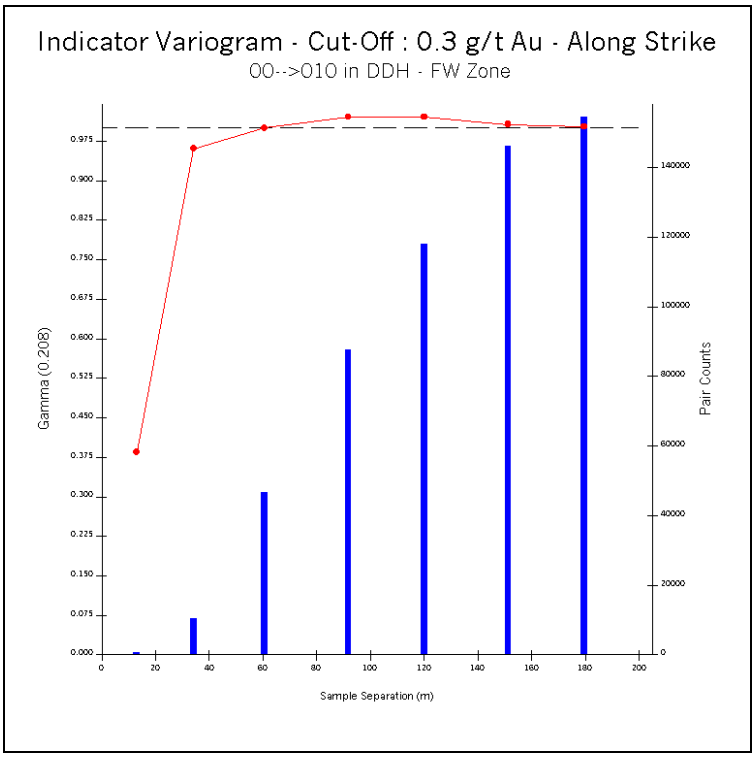

Figure B.74 Indicator Variogram – FW Zone Cut-Off at 0.3 g/t Au – Along Strike

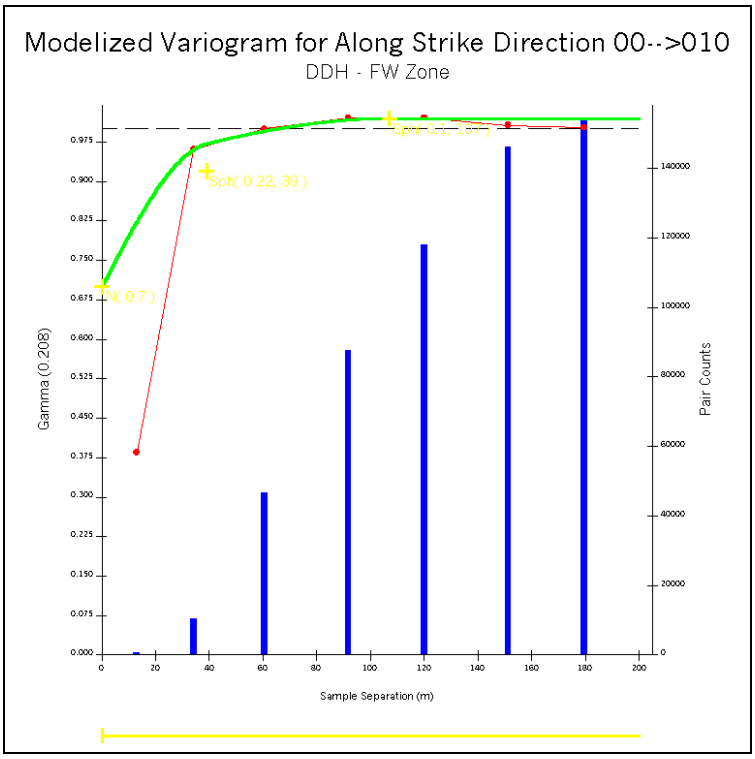

Figure B.75 Modelized Indicator Variogram – FW Zone Cut-Off at 0.3 g/t Au – Along Strike

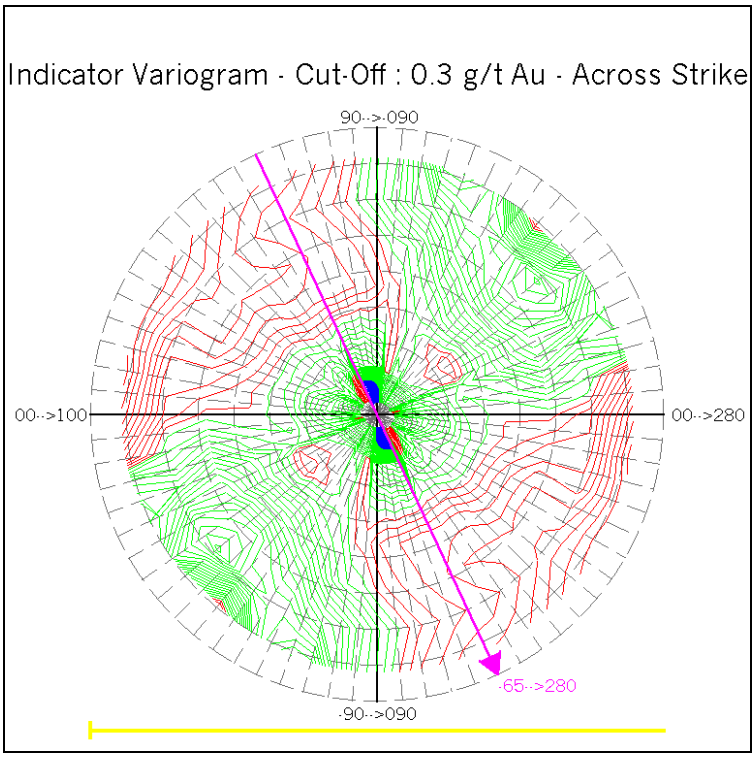

Figure B.76 Fan of Indicator Variograms – FW Zone Cut-Off at 0.3 g/t Au – Across Strike

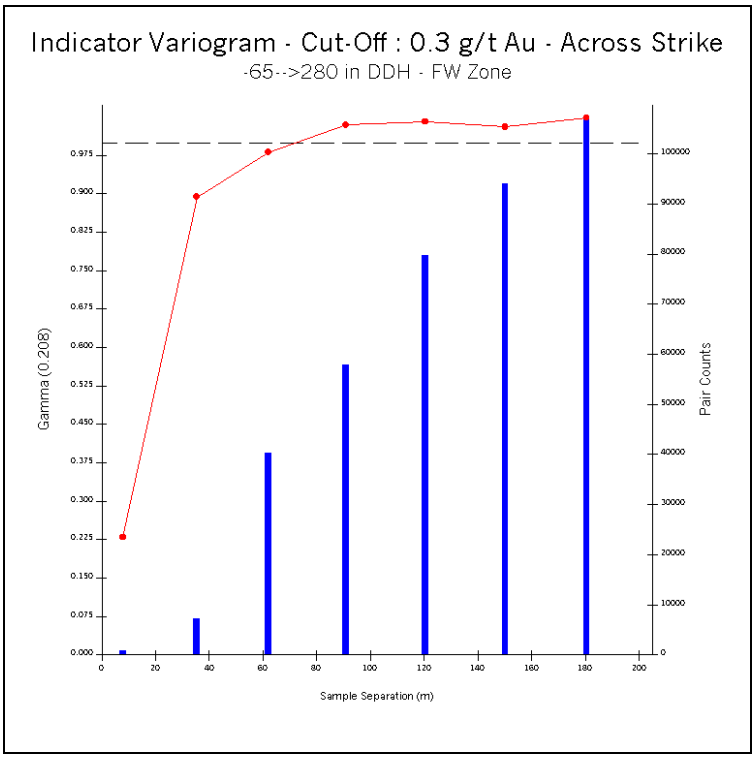

Figure B.77 Indicator Variogram – FW Zone Cut-Off at 0.3 g/t Au – Across Strike

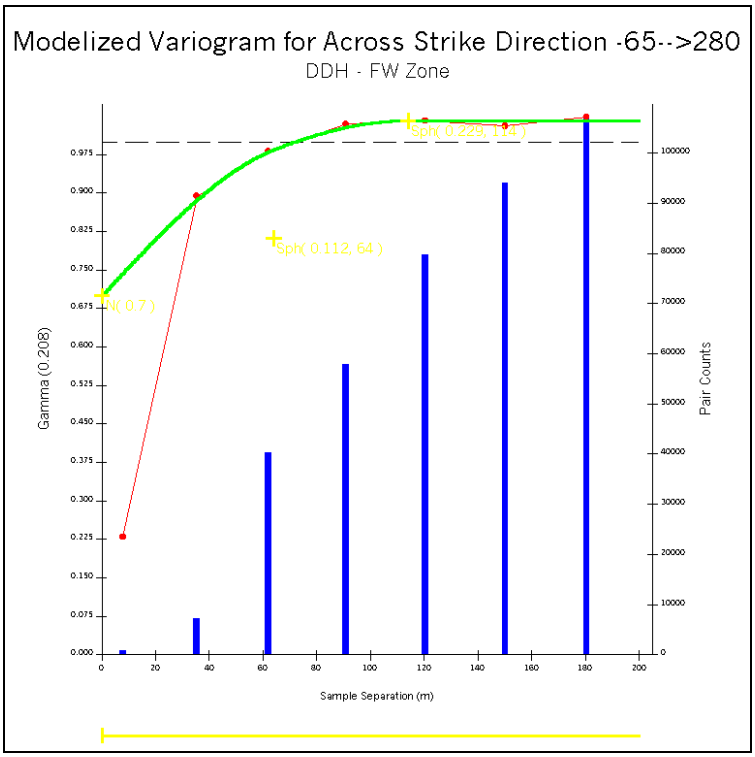

Figure B.78 Modelized Indicator Variogram – FW Zone Cut-Off at 0.3 g/t Au – Across Strike

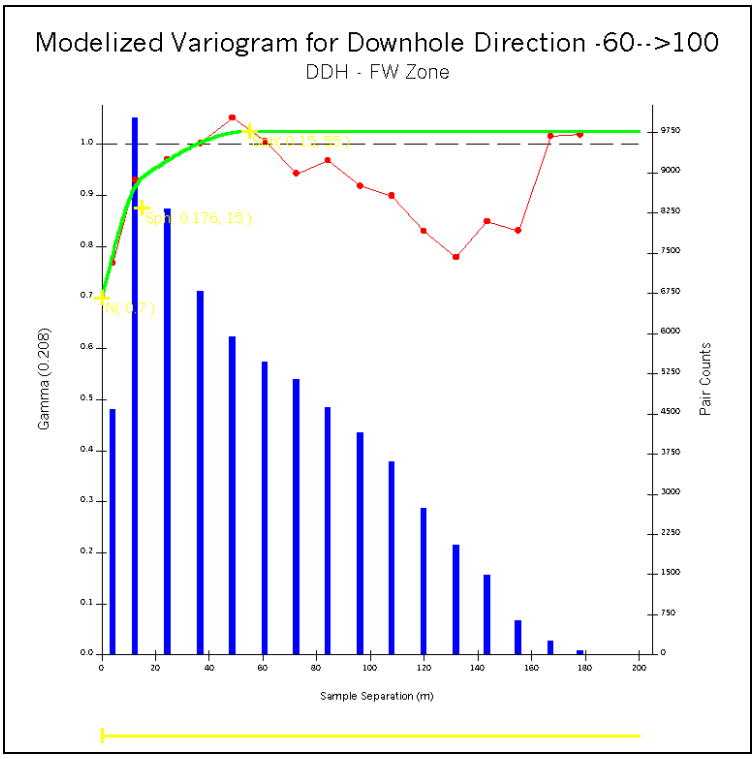

Figure B.79 Modelized Indicator Variogram – FW Zone Cut-Off at 0.3 g/t Au – Downhole

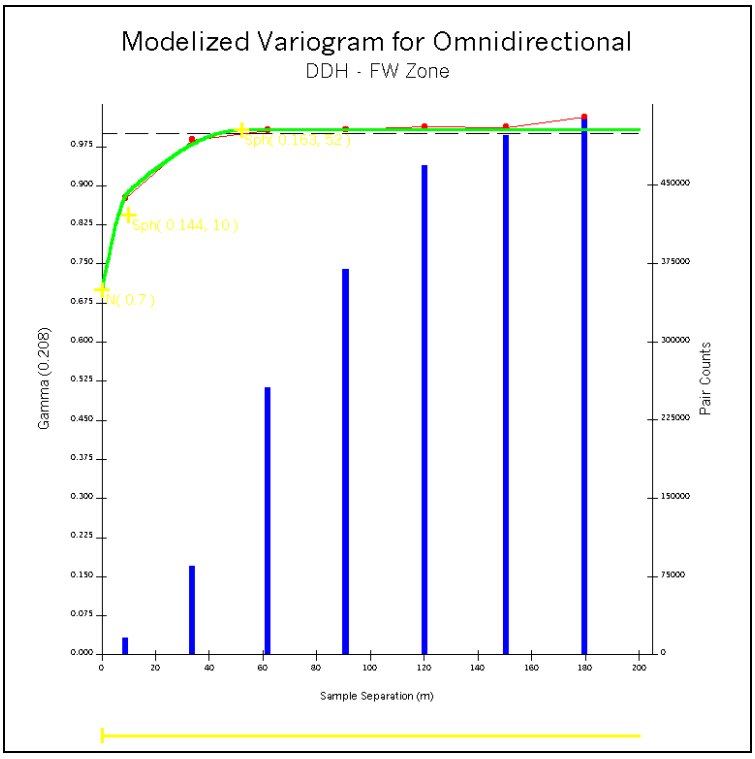

Figure B.80 Modelized Indicator Variogram – FW Zone Cut-Off at 0.3 g/t Au – Omnidirectional

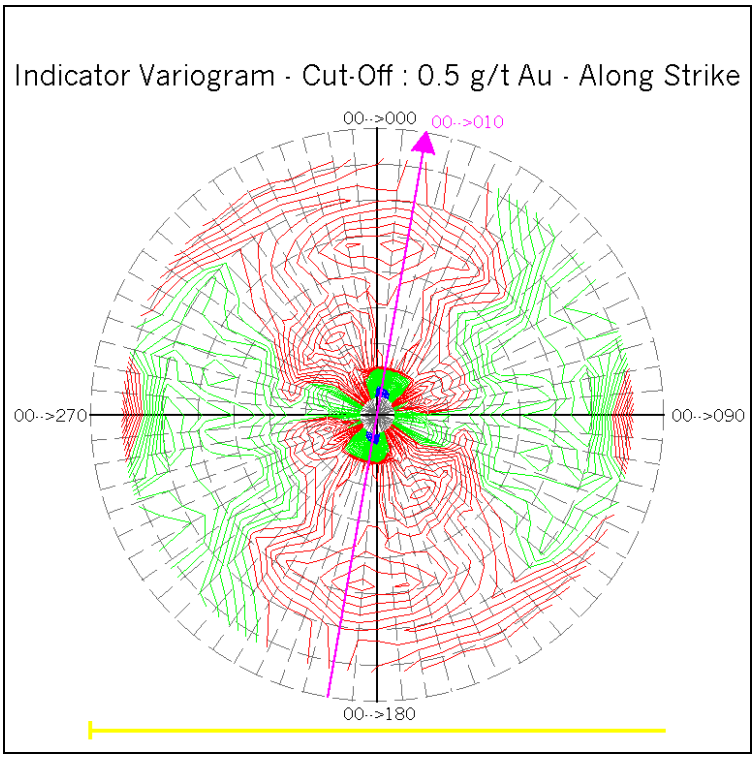

Figure B.81 Fan of Indicator Variograms – FW Zone Cut-Off at 0.5 g/t Au – Along Strike

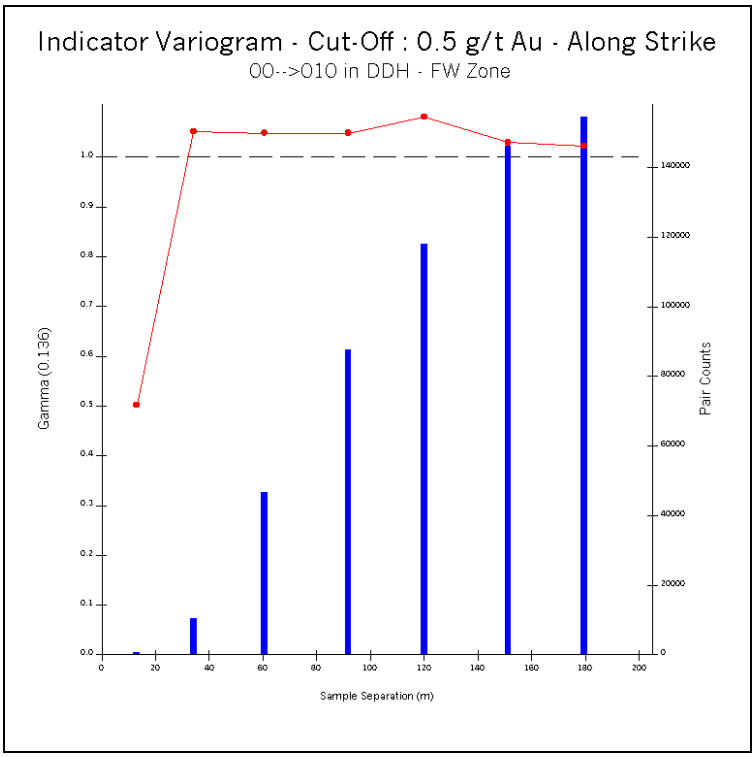

Figure B.82 Indicator Variogram – FW Zone Cut-Off at 0.5 g/t Au – Along Strike

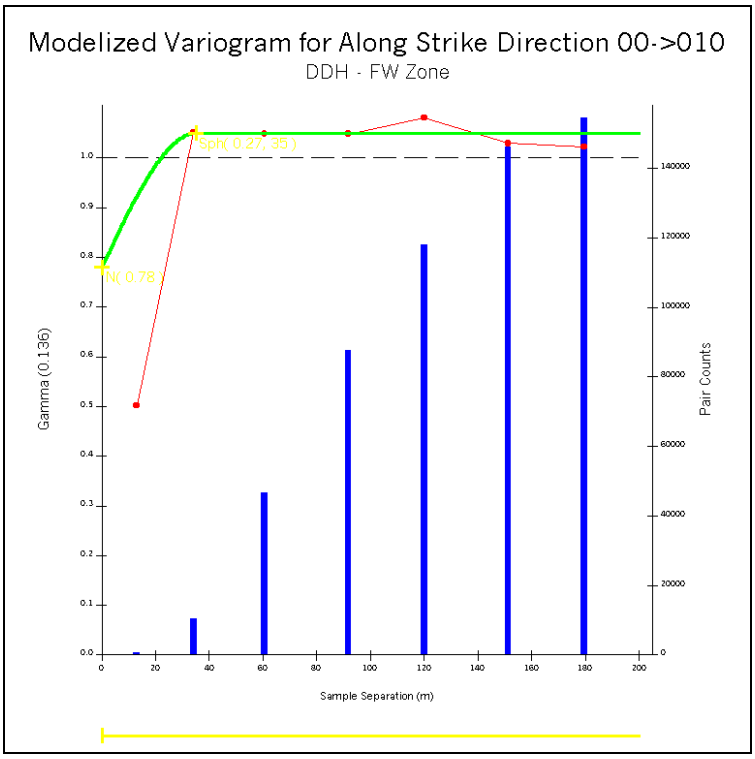

Figure B.83 Modelized Indicator Variogram – FW Zone Cut-Off at 0.5 g/t Au – Along Strike

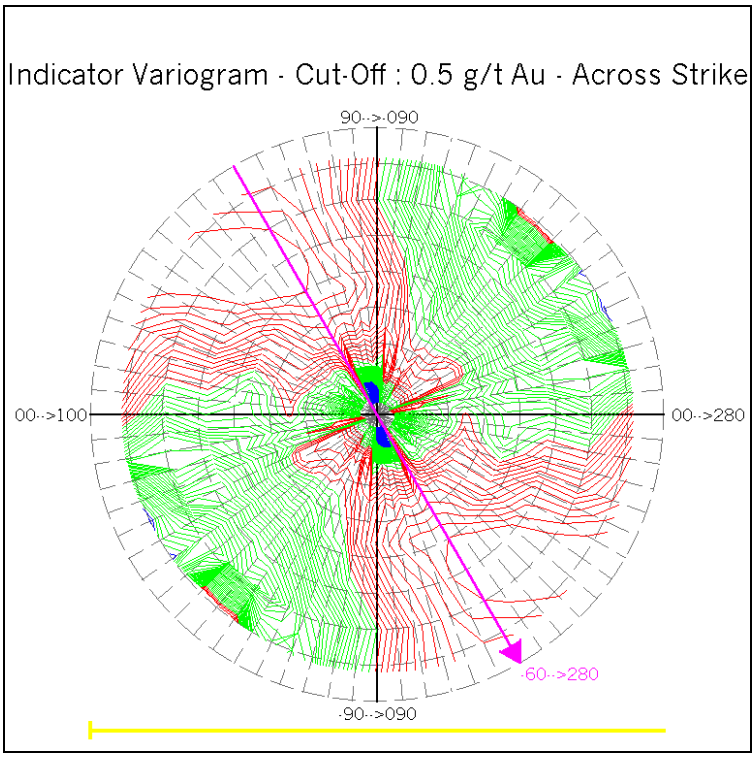

Figure B.84 Fan of Indicator Variograms – FW Zone Cut-Off at 0.5 g/t Au – Across Strike

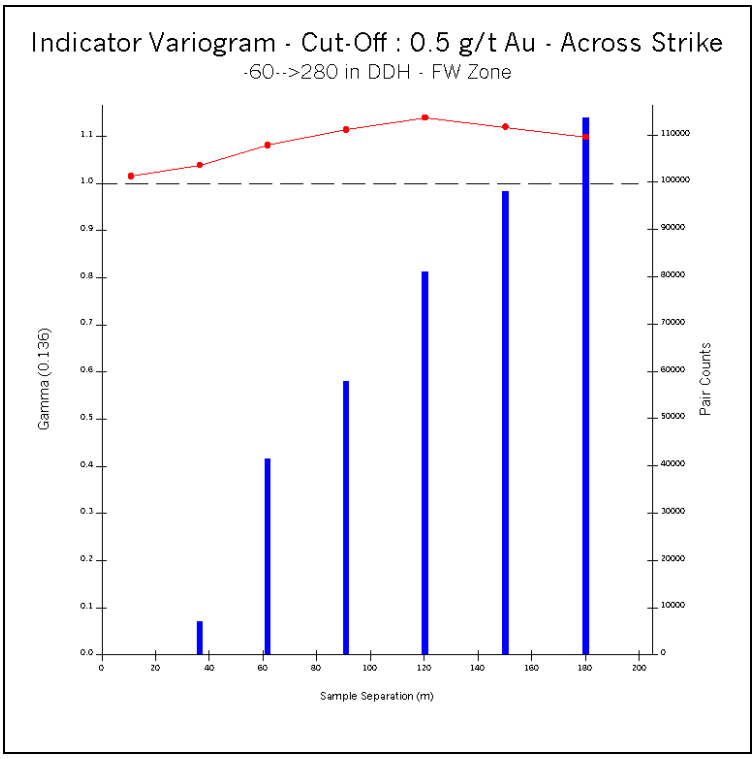

Figure B.85 Indicator Variogram – FW Zone Cut-Off at 0.5 g/t Au – Across Strike

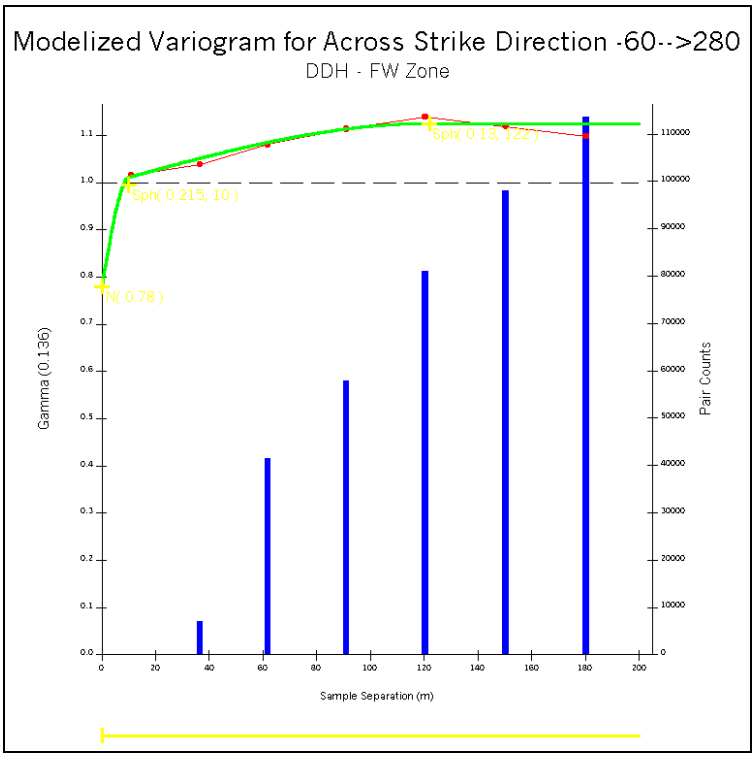

Figure B.86 Modelized Indicator Variogram – FW Zone Cut-Off at 0.5 g/t Au – Across Strike

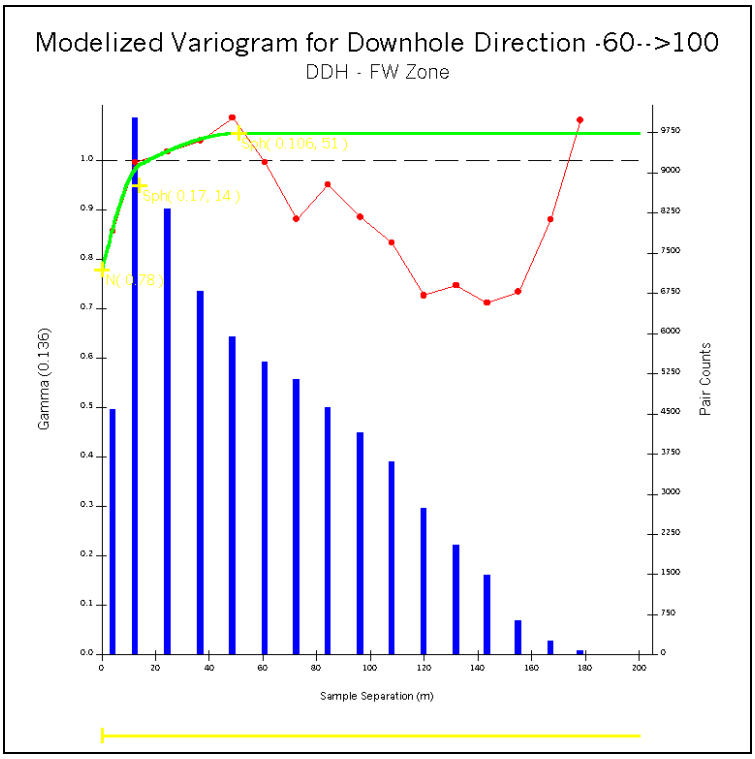

Figure B.87 Modelized Indicator Variogram – FW Zone Cut-Off at 0.5 g/t Au – Downhole

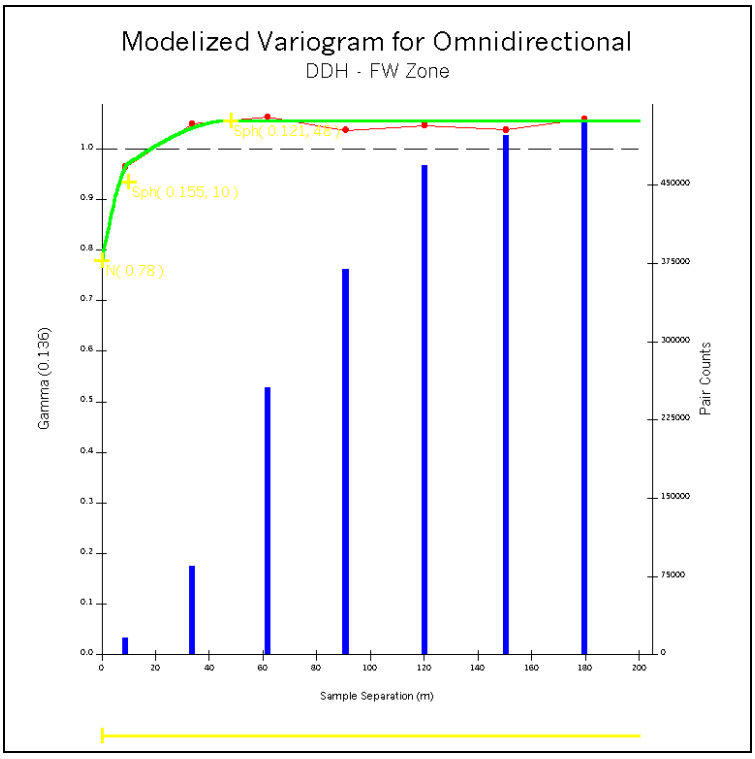

Figure B.88 Modelized Indicator Variogram – FW Zone Cut-Off at 0.5 g/t Au – Omnidirectional

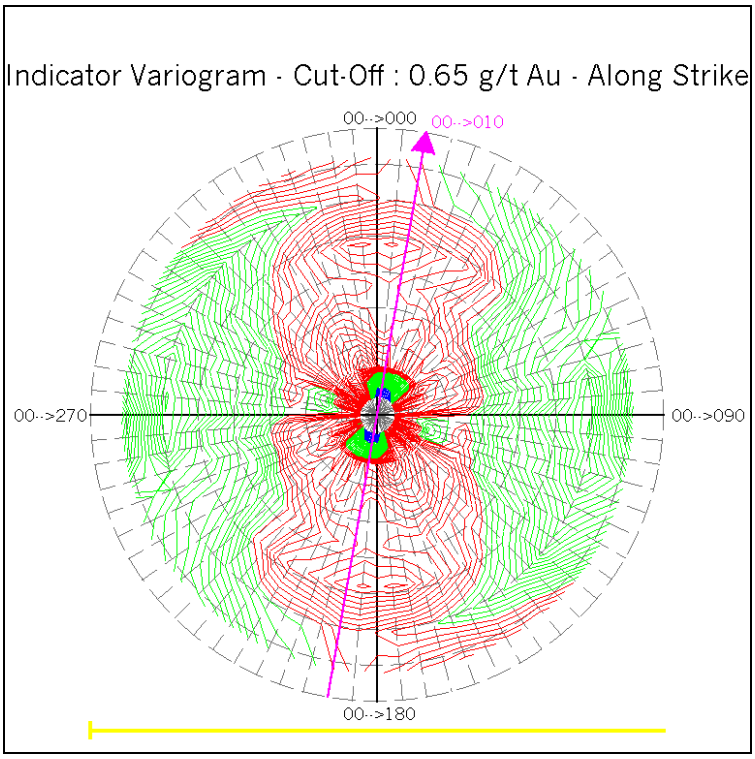

Figure B.89 Fan of Indicator Variograms – FW Zone Cut-Off at 0.65 g/t Au – Along Strike

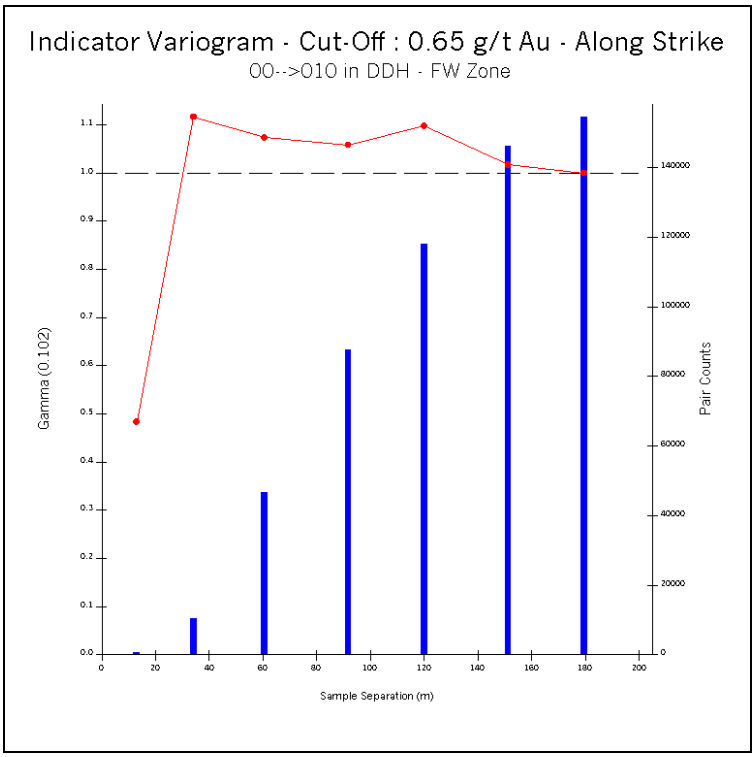

Figure B.90 Indicator Variogram – FW Zone Cut-Off at 0.65 g/t Au – Along Strike

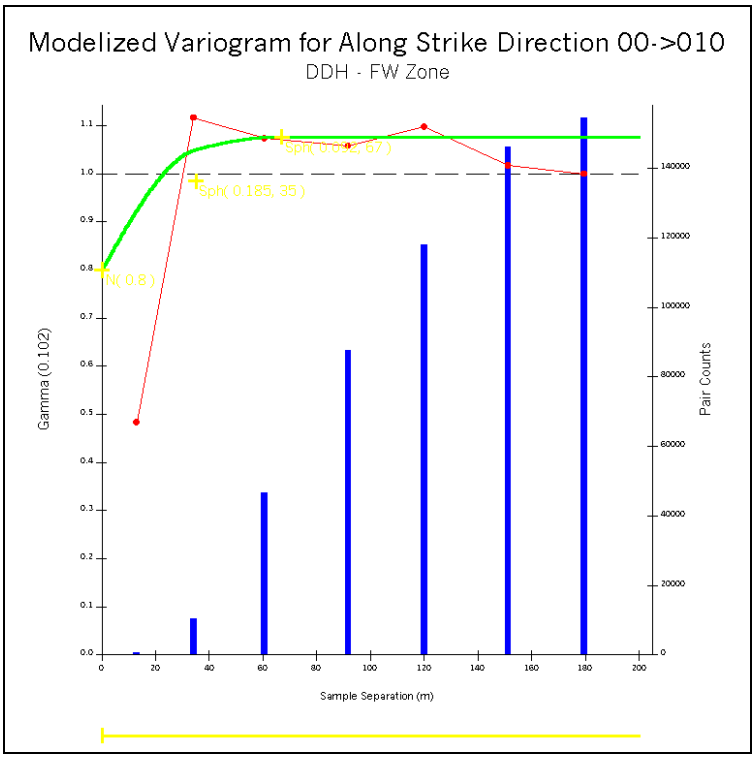

Figure B.91 Modelized Indicator Variogram – FW Zone Cut-Off at 0.65 g/t Au – Along Strike

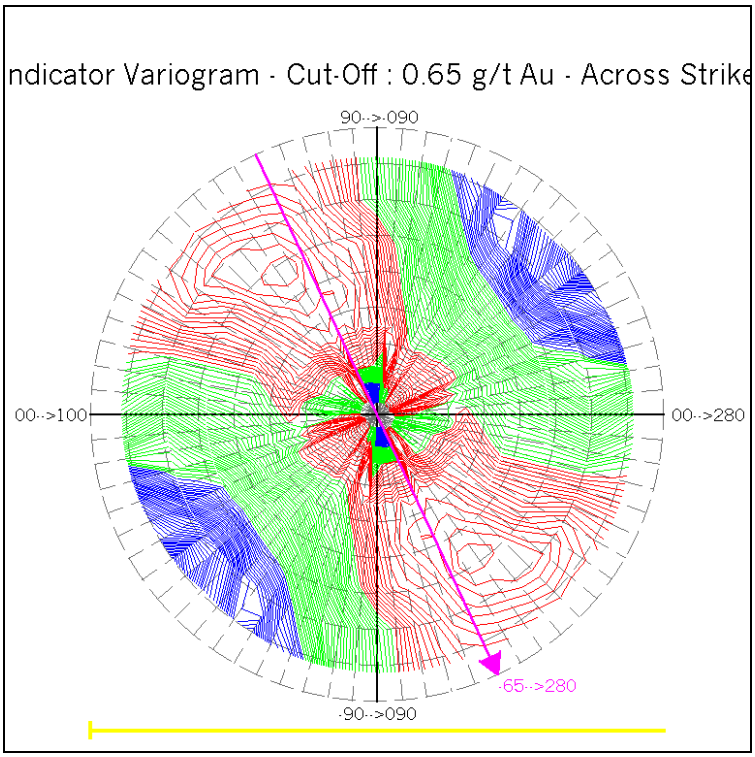

Figure B.92 Fan of Indicator Variograms – FW Zone Cut-Off at 0.65 g/t Au – Across Strike

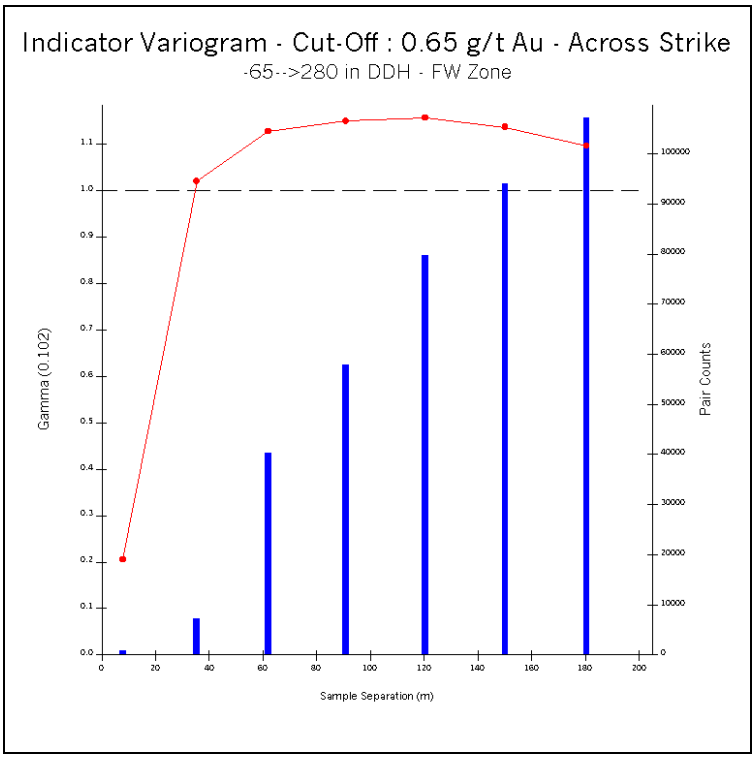

Figure B.93 Indicator Variogram – FW Zone Cut-Off at 0.65 g/t Au – Across Strike

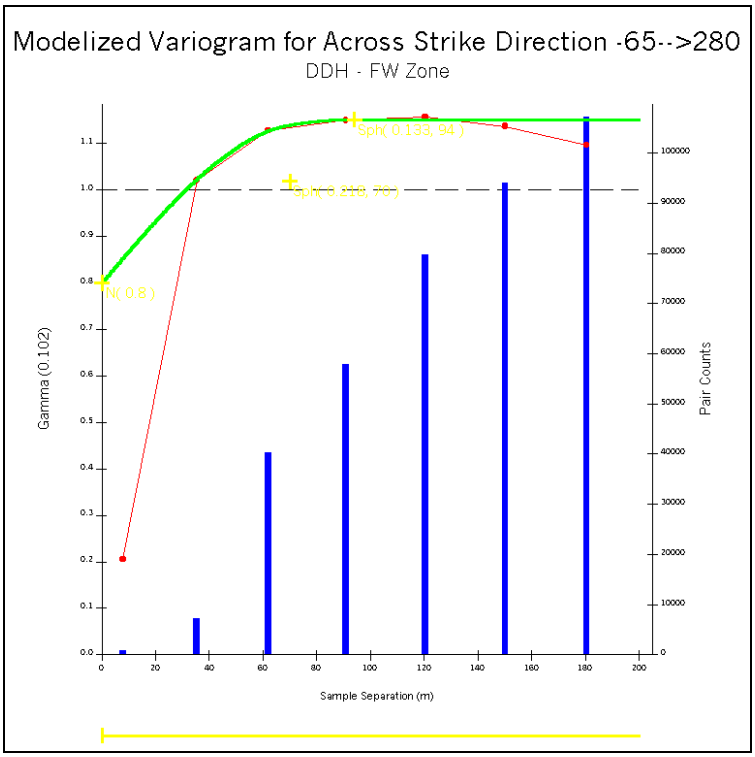

Figure B.94 Modelized Indicator Variogram – FW Zone Cut-Off at 0.65 g/t Au – Across Strike

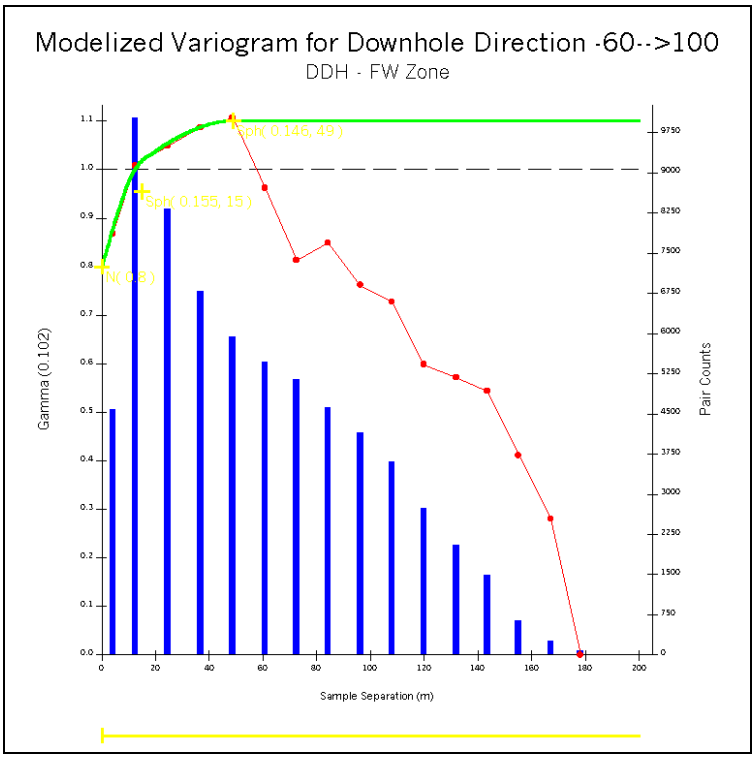

Figure B.95 Modelized Indicator Variogram – FW Zone Cut-Off at 0.65 g/t Au – Downhole

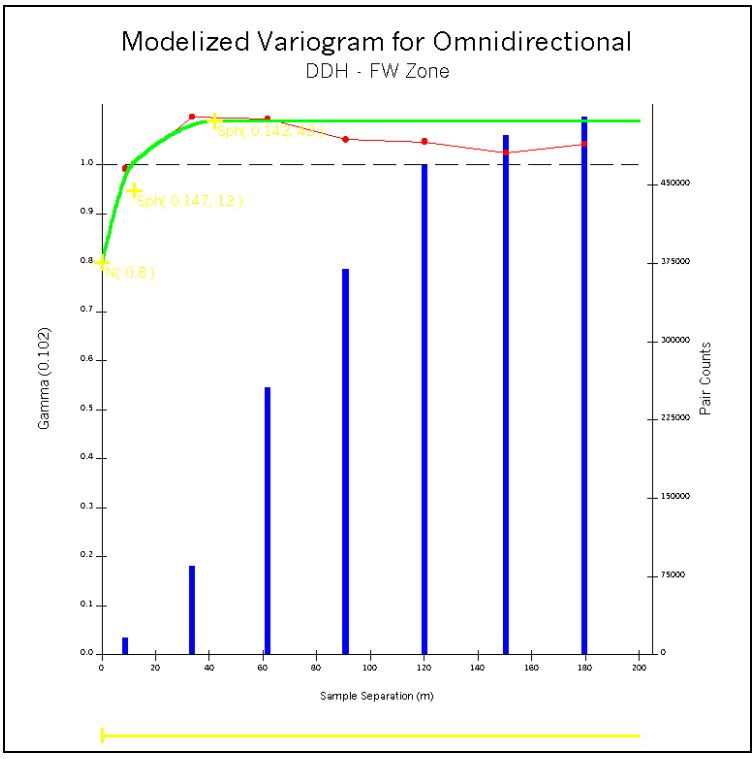

Figure B.96 Modelized Indicator Variogram – FW Zone Cut-Off at 0.65 g/t Au – Omnidirectional

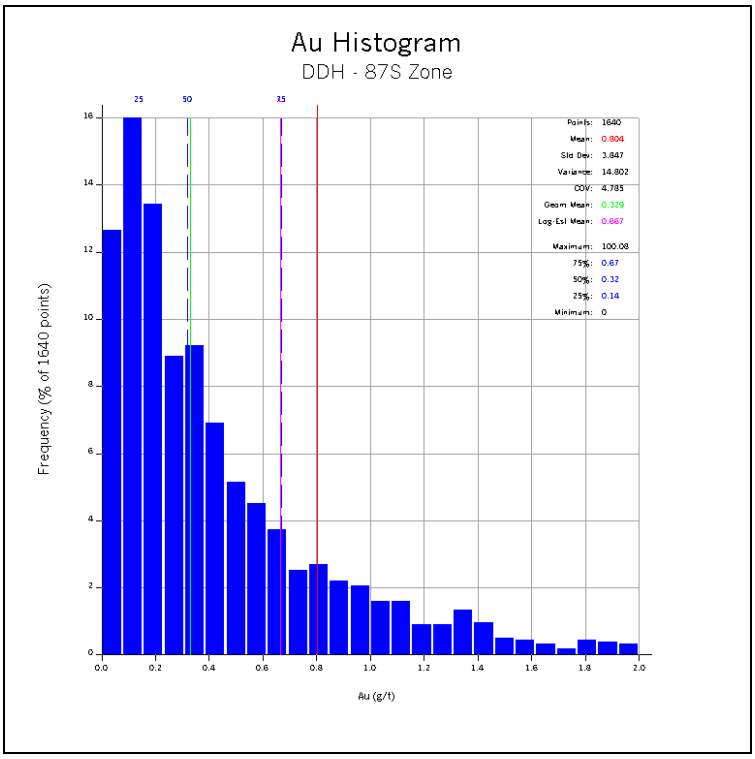

Figure B.97 Au Normal Histogram – 87S Zone

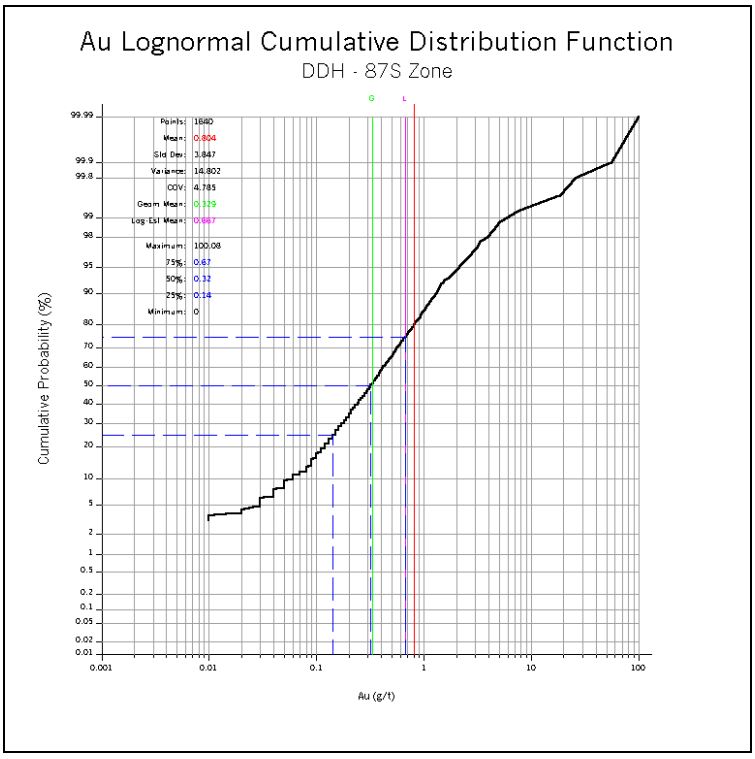

Figure B.98 Au Lognormal Cumulative Distribution Function – 87S Zone

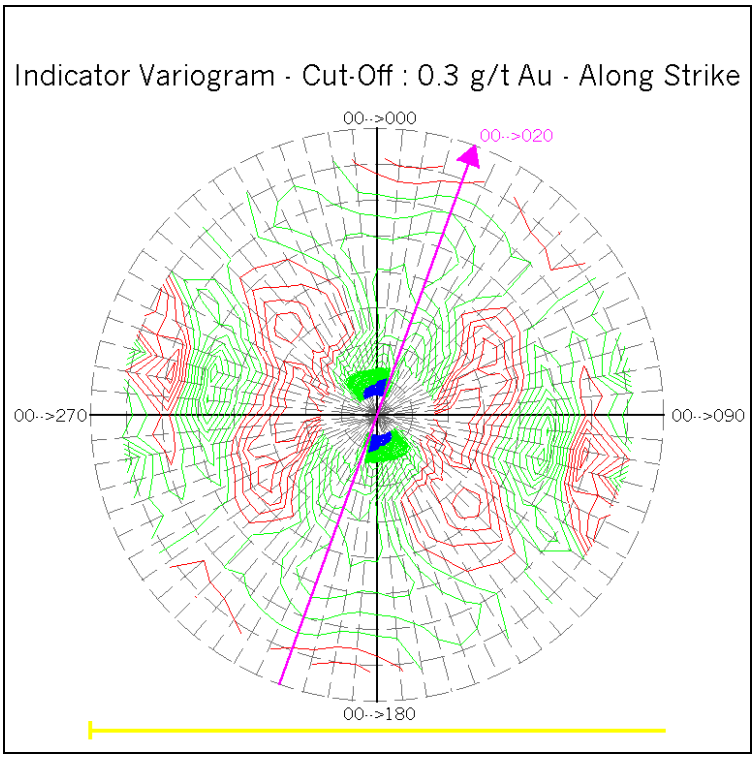

Figure B.99 Fan of Indicator Variograms – 87S Zone Cut-Off at 0.3 g/t Au – Along Strike

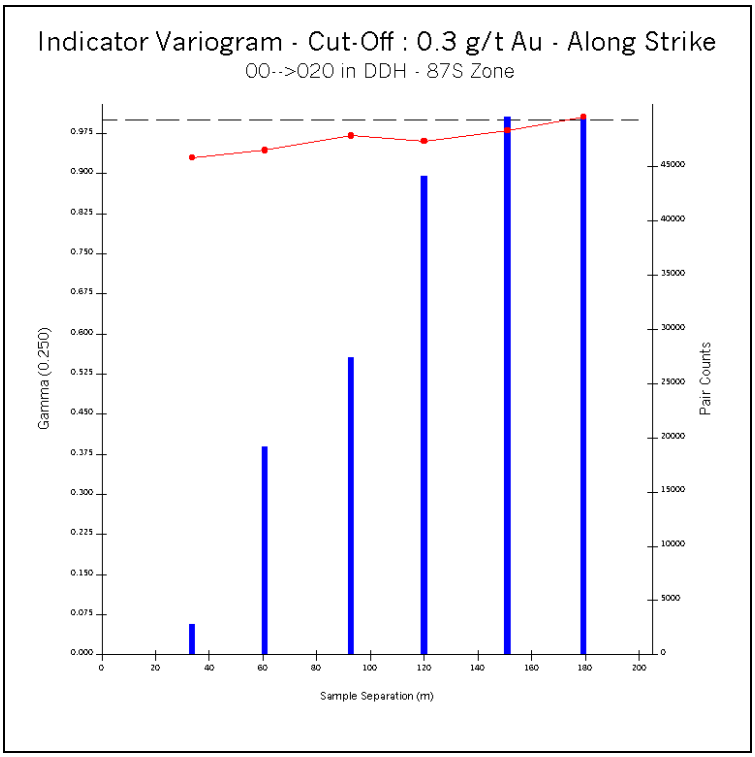

Figure B.100 Indicator Variogram – 87S Zone Cut-Off at 0.3 g/t Au – Along Strike

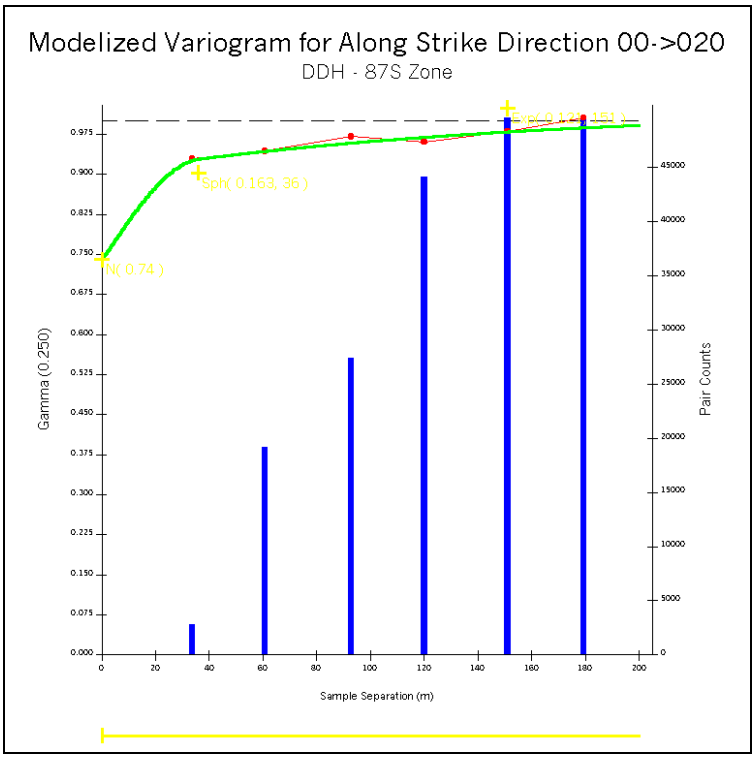

Figure B.101 Modelized Indicator Variogram – 87S Zone Cut-Off at 0.3 g/t Au – Along Strike

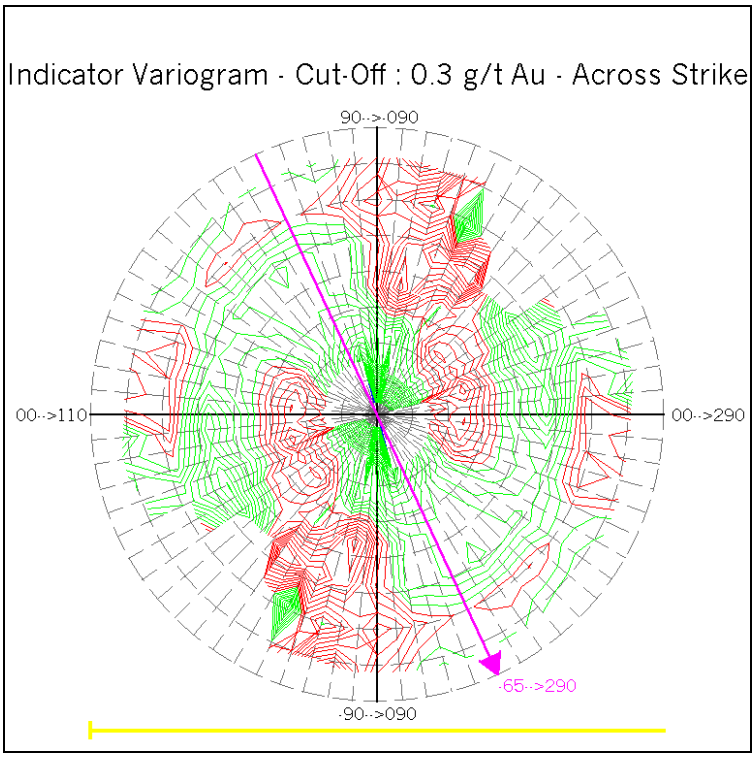

Figure B.102 Fan of Indicator Variograms – 87S Zone Cut-Off at 0.3 g/t Au – Across Strike

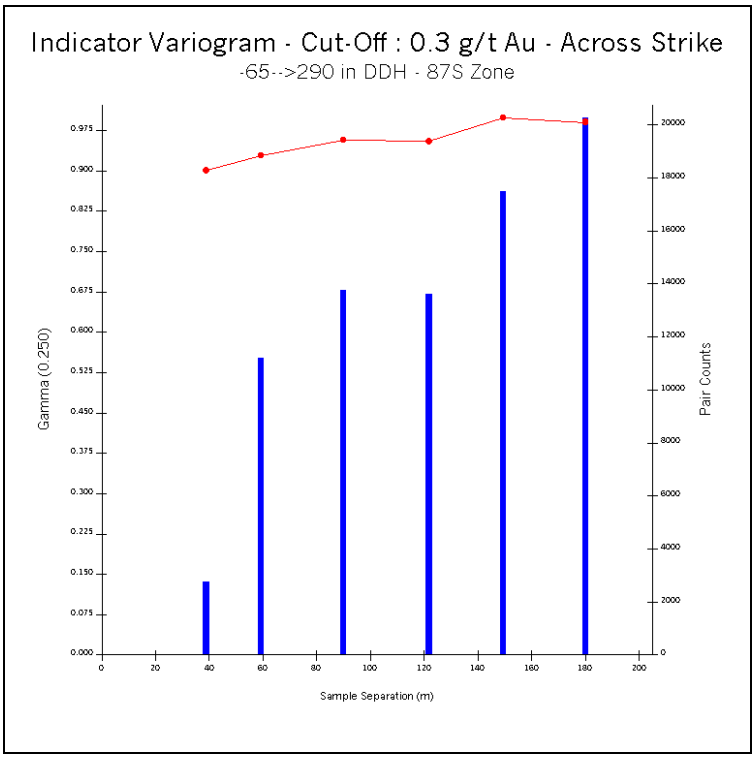

Figure B.103 Indicator Variogram – 87S Zone Cut-Off at 0.3 g/t Au – Across Strike

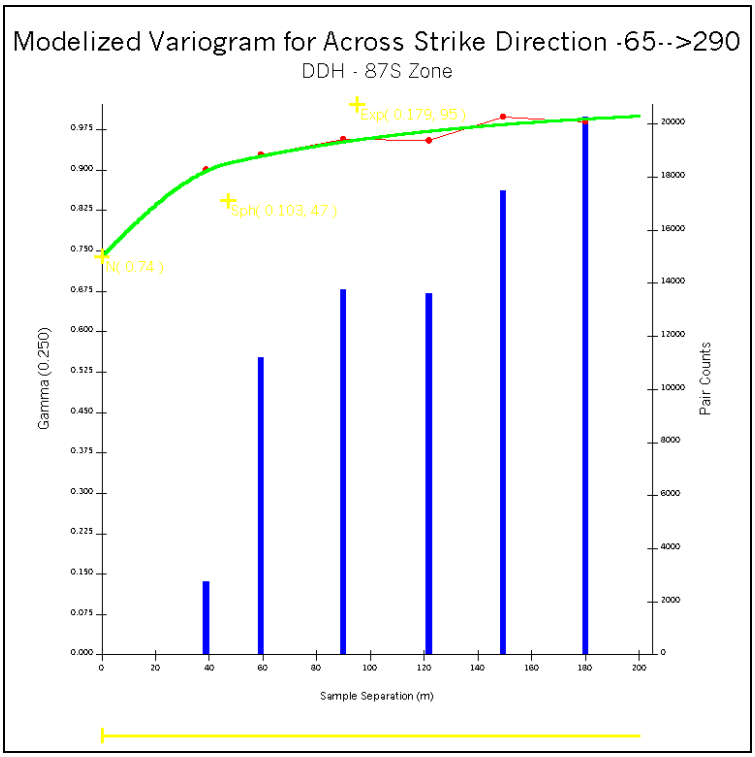

Figure B.104 Modelized Indicator Variogram – 87S Zone Cut-Off at 0.3 g/t Au – Across Strike

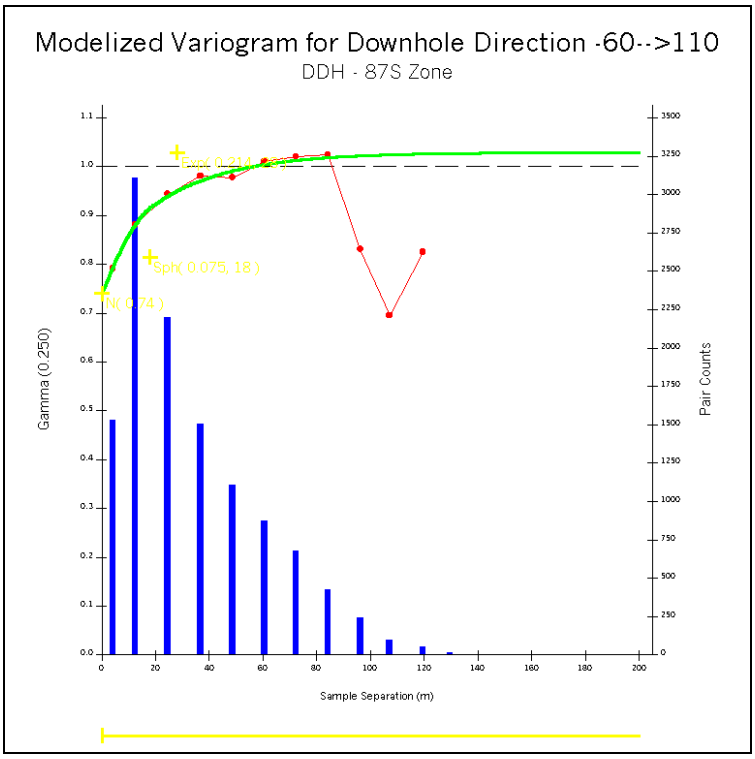

Figure B.105 Modelized Indicator Variogram – 87S Zone Cut-Off at 0.3 g/t Au – Downhole

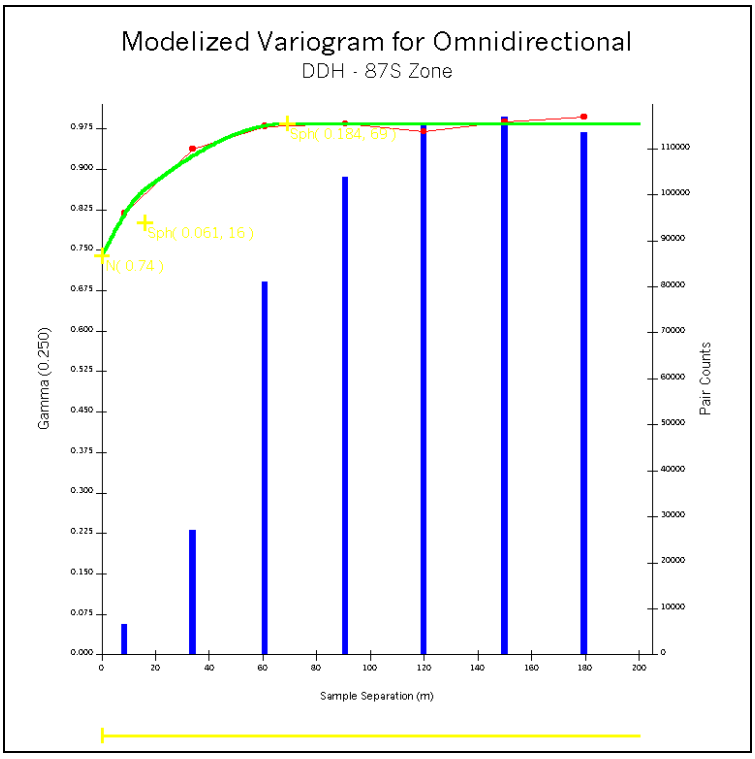

Figure B.106 Modelized Indicator Variogram – 87S Zone Cut-Off at 0.3 g/t Au – Omnidirectional

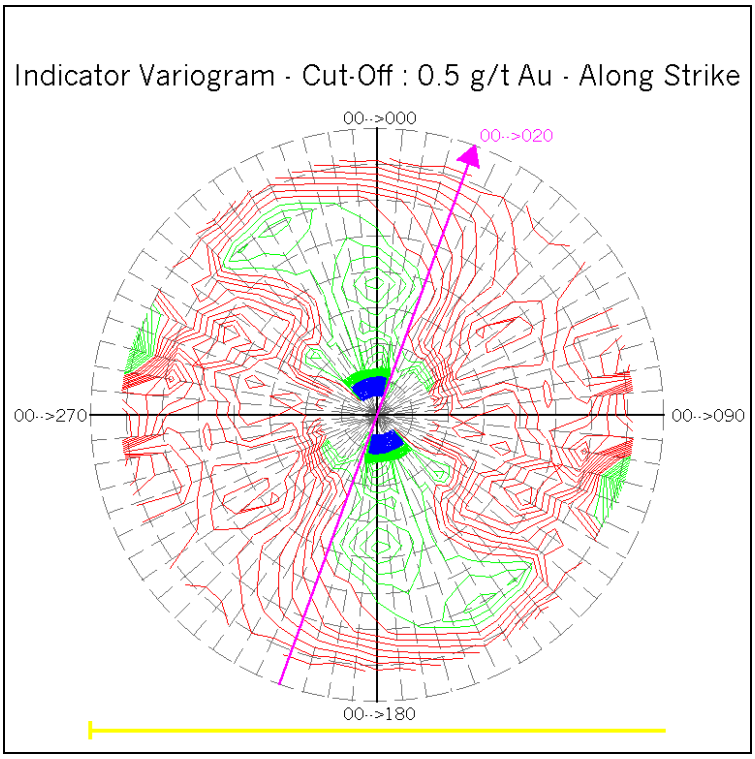

Figure B.107 Fan of Indicator Variograms – 87S Zone Cut-Off at 0.5 g/t Au – Along Strike

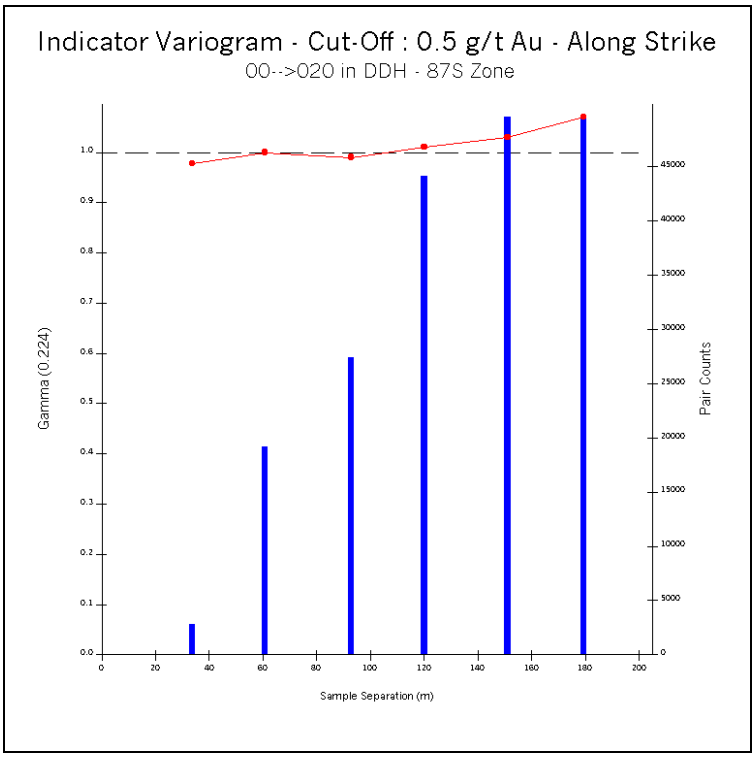

Figure B.108 Indicator Variogram – 87S Zone Cut-Off at 0.5 g/t Au – Along Strike

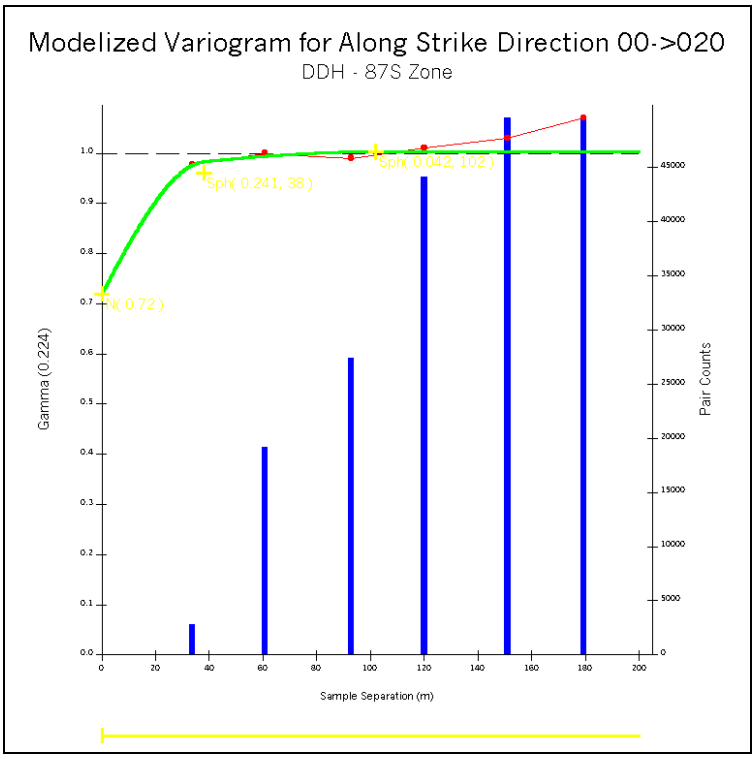

Figure B.109 Modelized Indicator Variogram – 87S Zone Cut-Off at 0.5 g/t Au – Along Strike

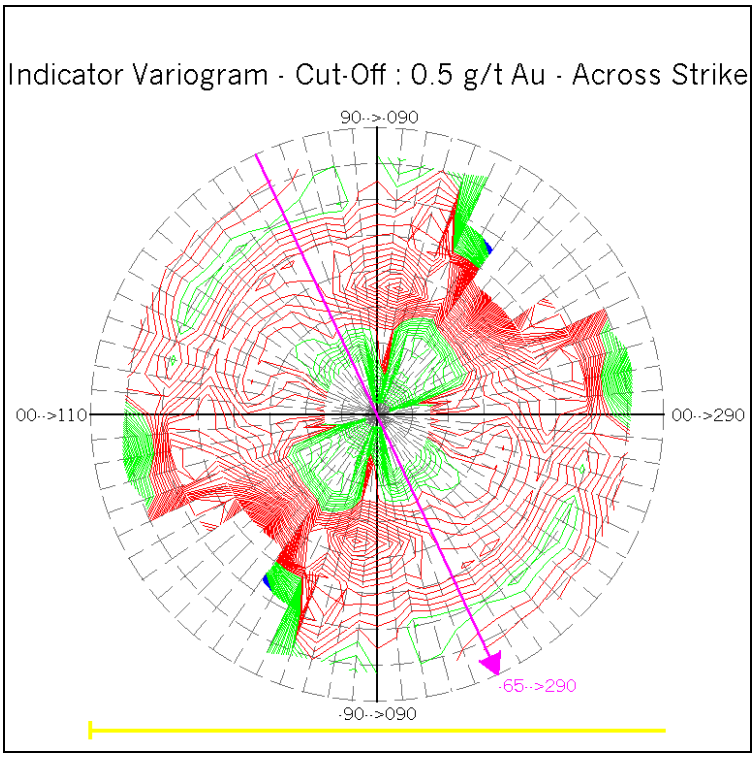

Figure B.110 Fan of Indicator Variograms – 87S Zone Cut-Off at 0.5 g/t Au – Across Strike

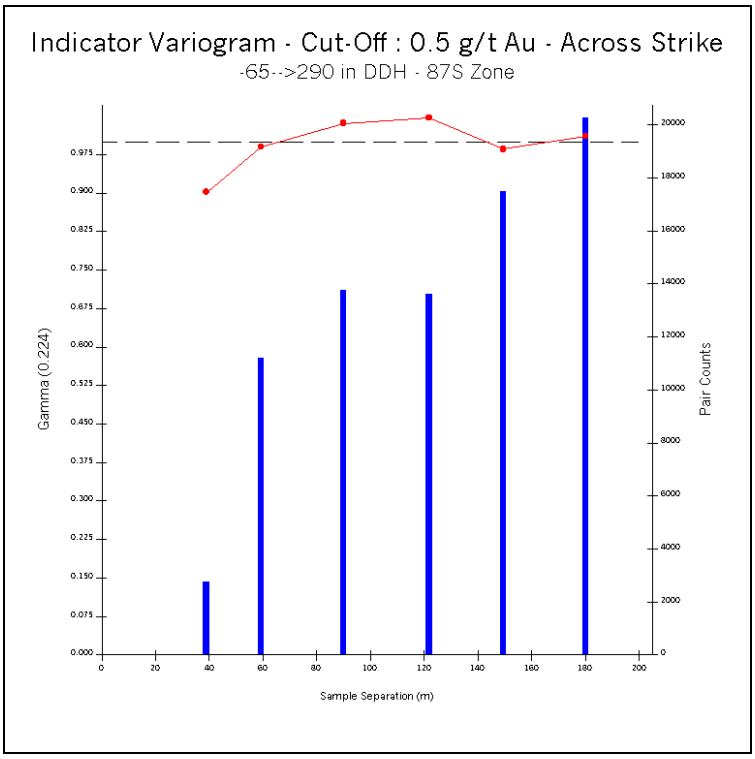

Figure B.111 Indicator Variogram – 87S Zone Cut-Off at 0.5 g/t Au – Across Strike

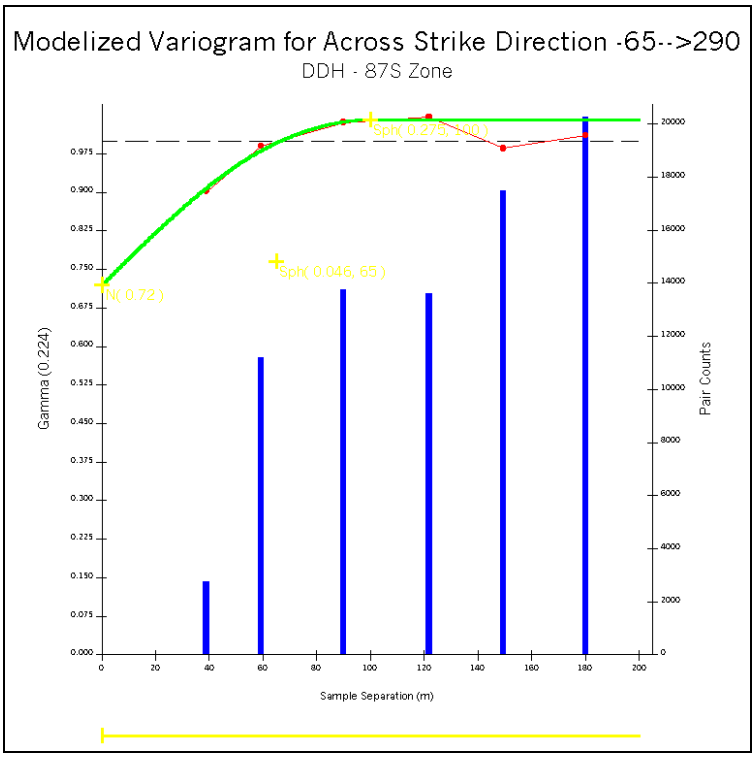

Figure B.112 Modelized Indicator Variogram – 87S Zone Cut-Off at 0.5 g/t Au – Across Strike

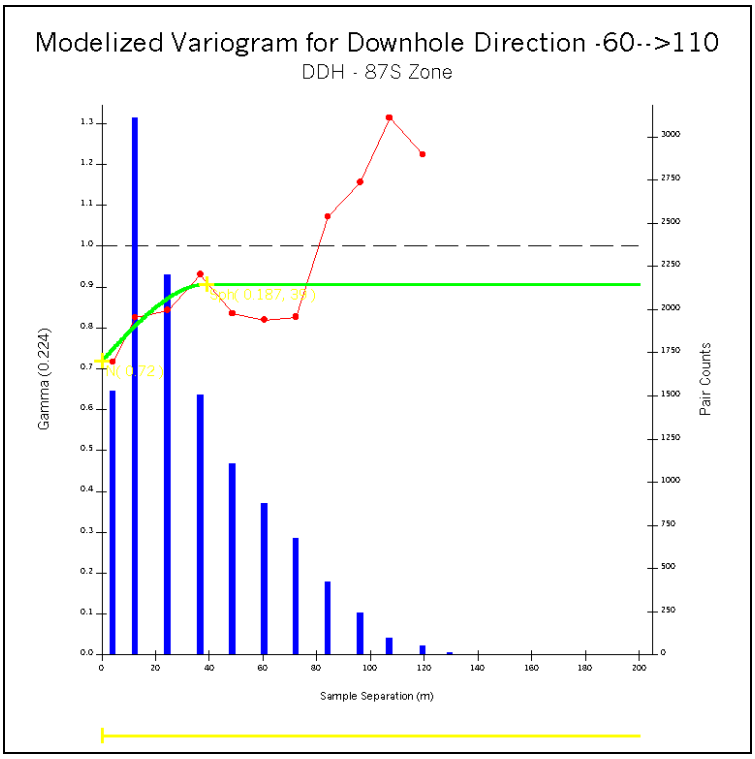

Figure B.113 Modelized Indicator Variogram – 87S Zone Cut-Off at 0.5 g/t Au – Downhole

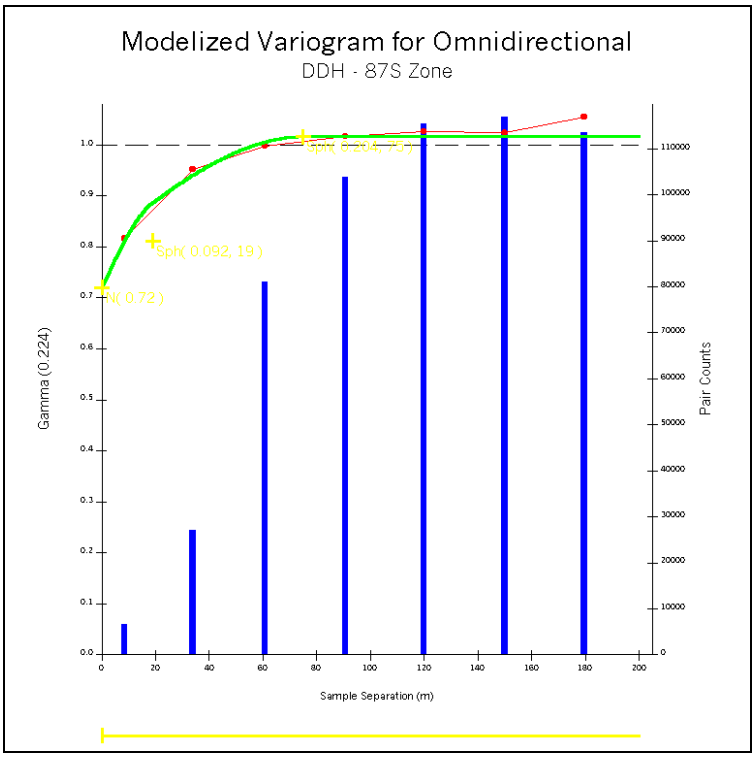

Figure B.114 Modelized Indicator Variogram – 87S Zone Cut-Off at 0.5 g/t Au – Omnidirectional

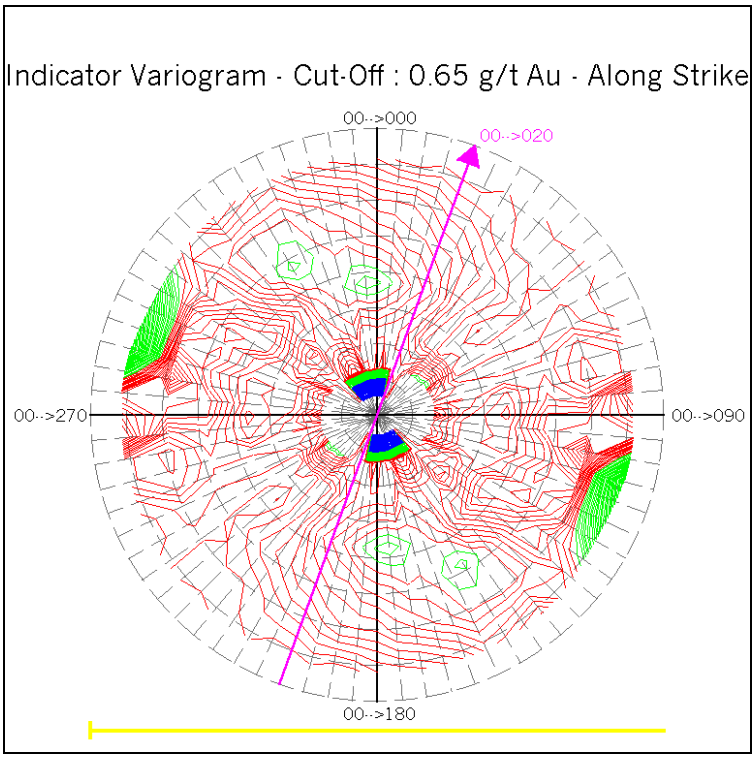

Figure B.115 Fan of Indicator Variograms – 87S Zone Cut-Off at 0.65 g/t Au – Along Strike

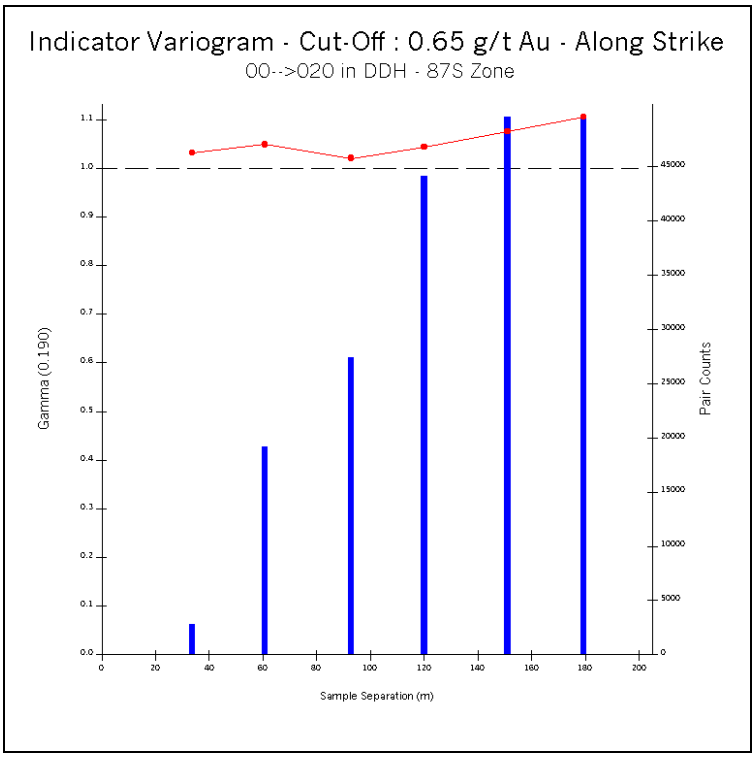

Figure B.116 Indicator Variogram – 87S Zone Cut-Off at 0.65 g/t Au – Along Strike

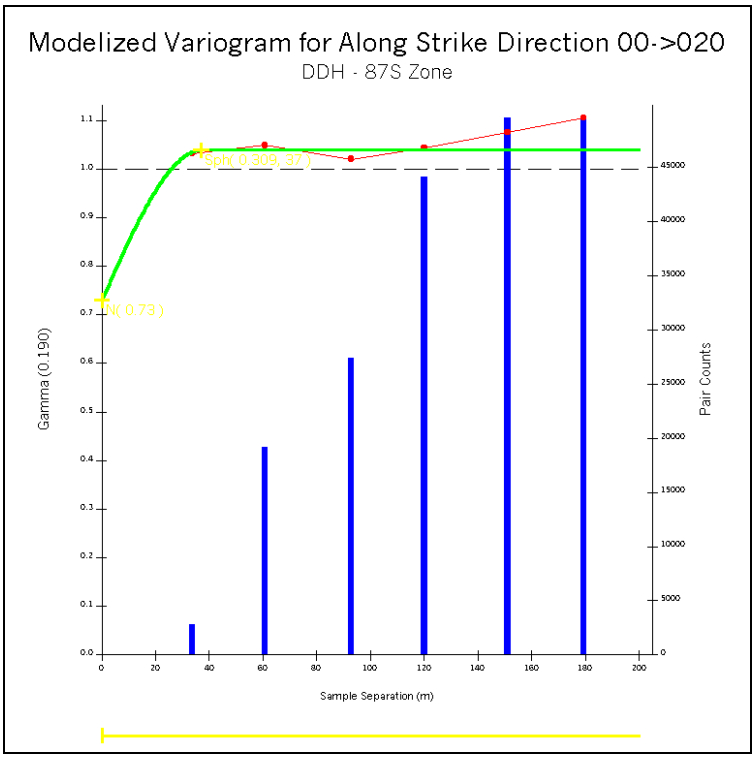

Figure B.117 Modelized Indicator Variogram – 87S Zone Cut-Off at 0.65 g/t Au – Along Strike

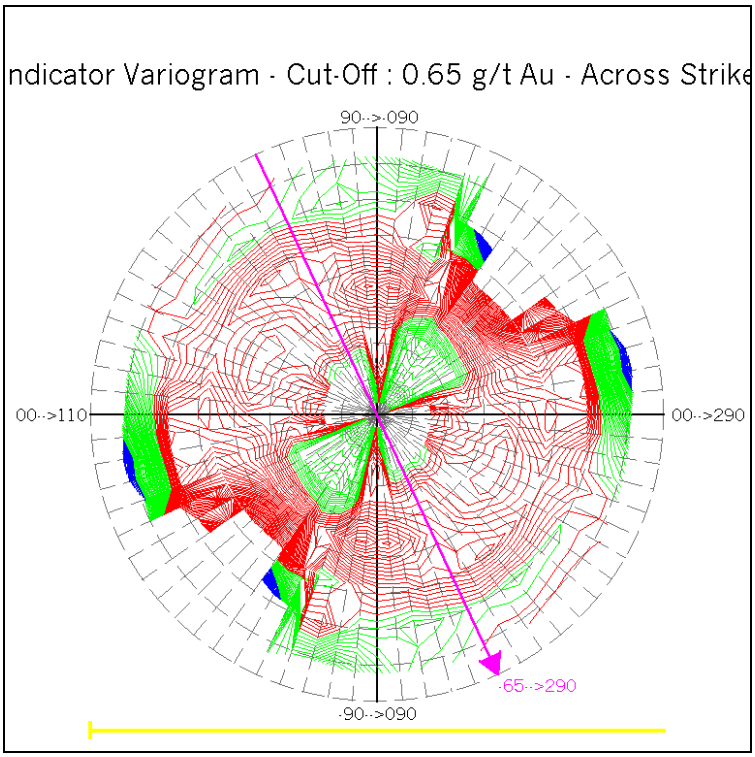

Figure B.118 Fan of Indicator Variograms – 87S Zone Cut-Off at 0.65 g/t Au – Across Strike

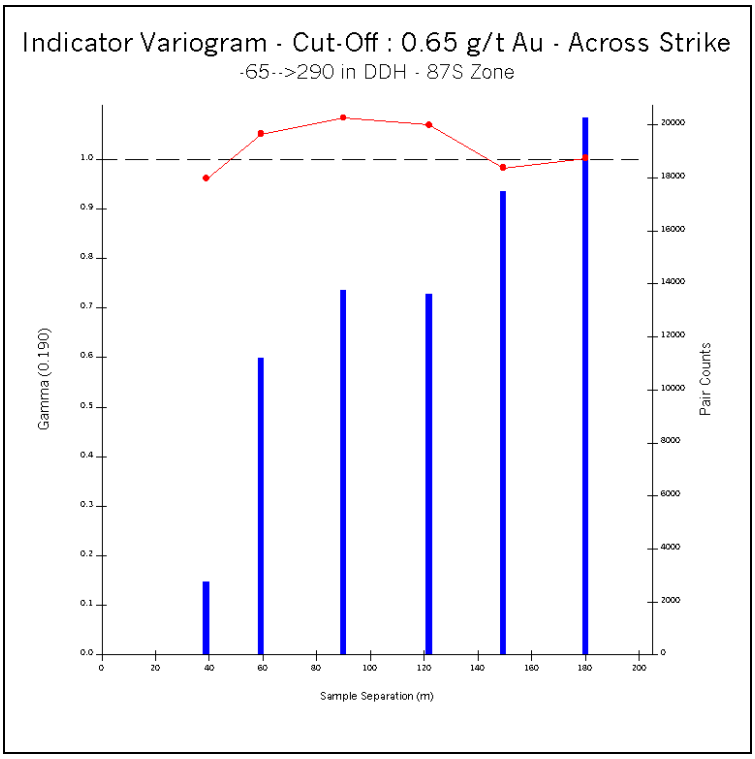

Figure B.119 Indicator Variogram – 87S Zone Cut-Off at 0.65 g/t Au – Across Strike

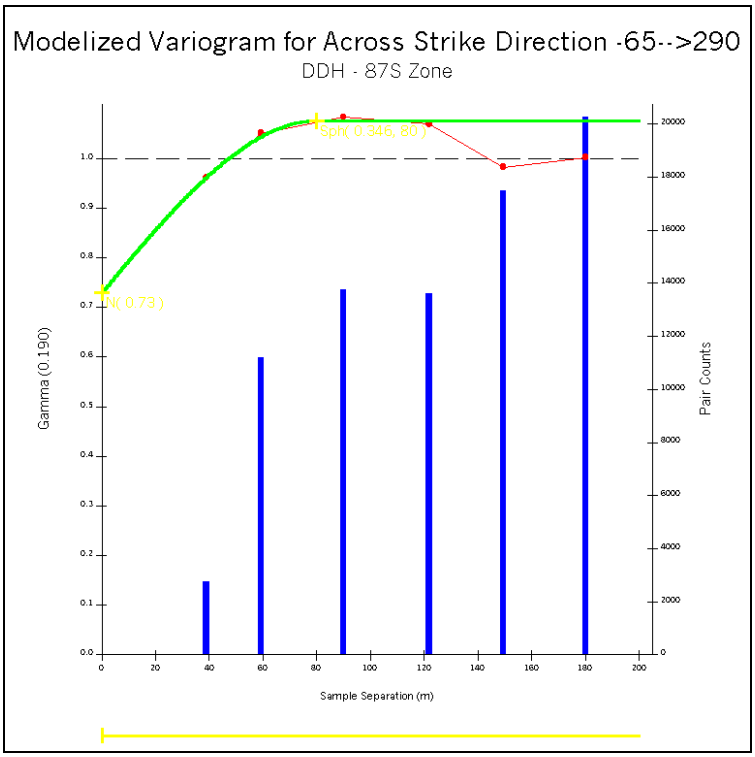

Figure B.120 Modelized Indicator Variogram – 87S Zone Cut-Off at 0.65 g/t Au – Across Strike

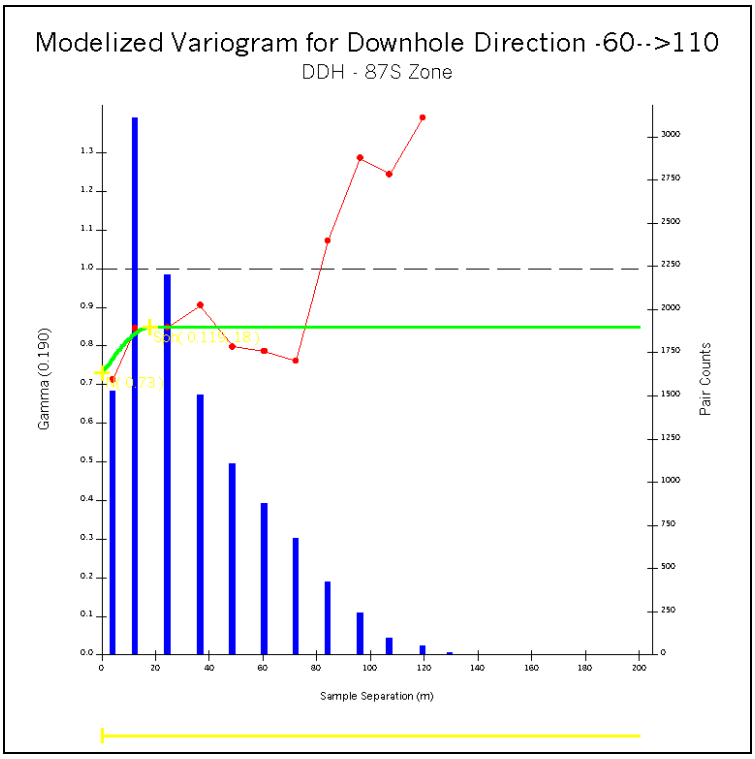

Figure B.121 Modelized Indicator Variogram – 87S Zone Cut-Off at 0.65 g/t Au – Downhole

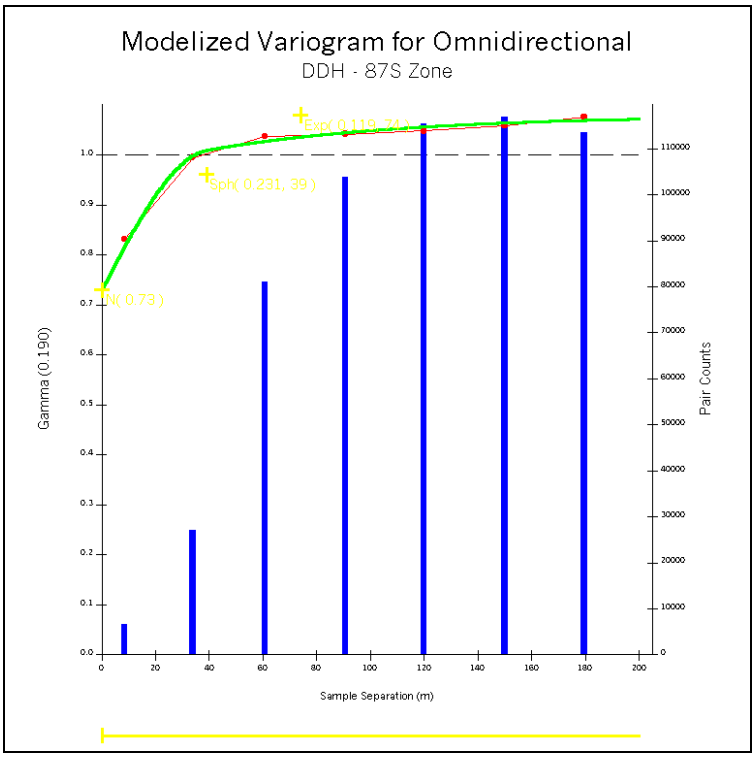

Figure B.122 Modelized Indicator Variogram – 87S Zone Cut-Off at 0.65 g/t Au – Omnidirectional

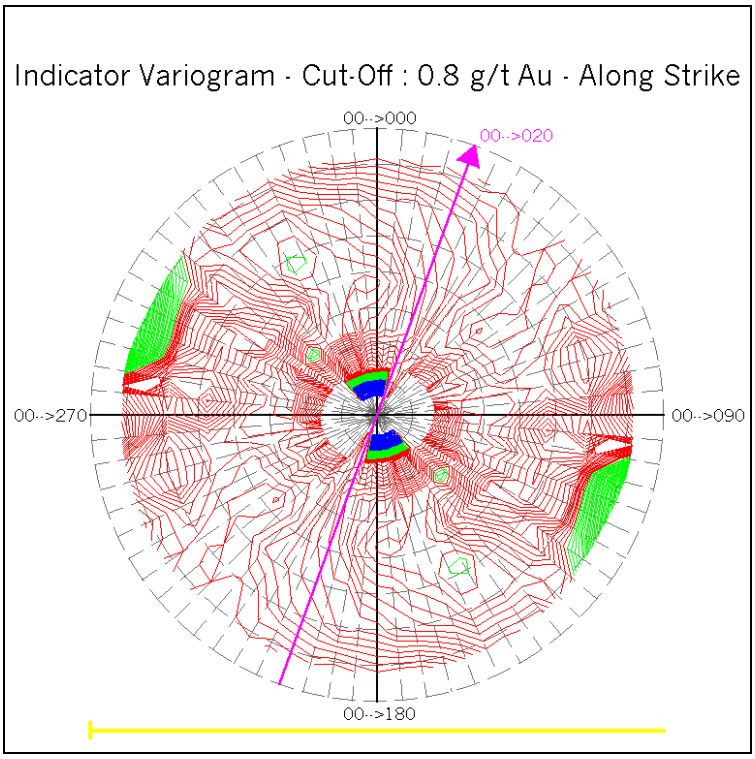

Figure B.123 Fan of Indicator Variograms – 87S Zone Cut-Off at 0.8 g/t Au – Along Strike

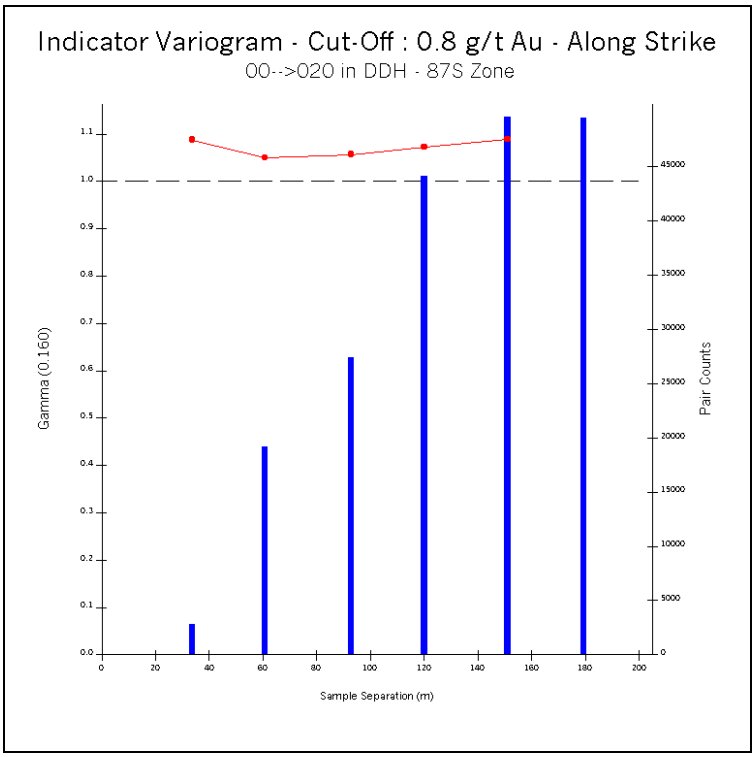

Figure B.124 Indicator Variogram – 87S Zone Cut-Off at 0.8 g/t Au – Along Strike

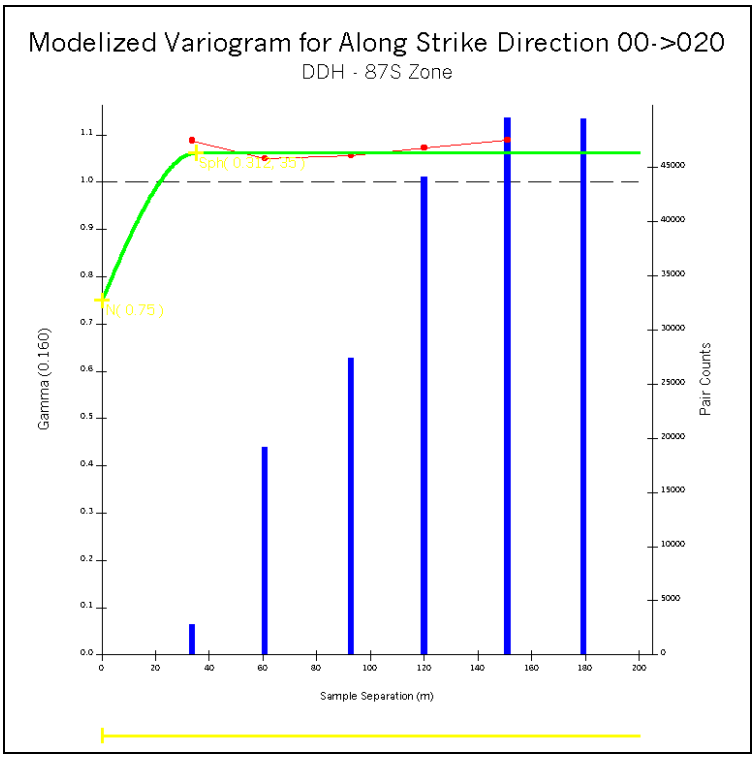

Figure B.125 Modelized Indicator Variogram – 87S Zone Cut-Off at 0.8 g/t Au – Along Strike

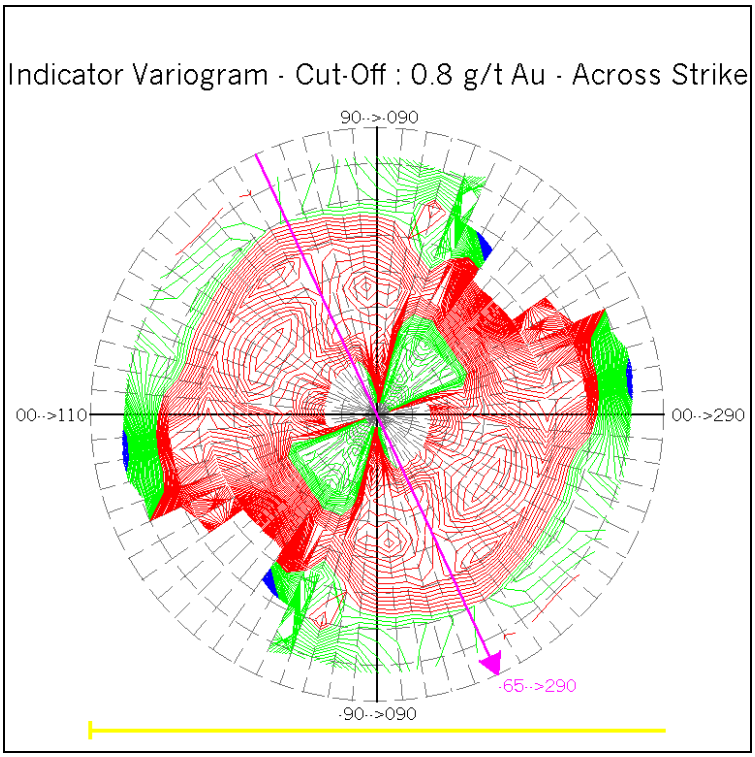

Figure B.126 Fan of Indicator Variograms – 87S Zone Cut-Off at 0.8 g/t Au – Across Strike

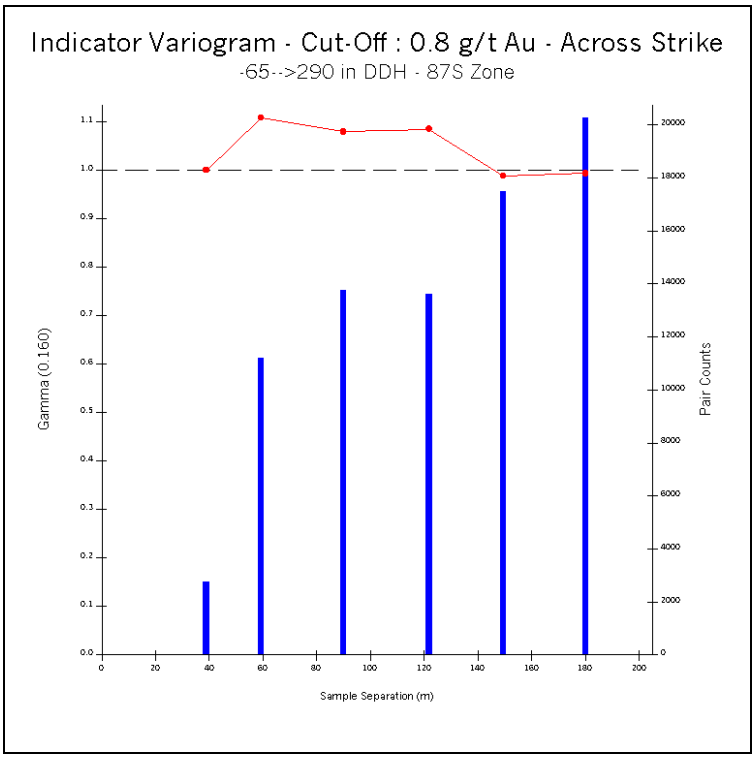

Figure B.127 Indicator Variogram – 87S Zone Cut-Off at 0.8 g/t Au – Across Strike

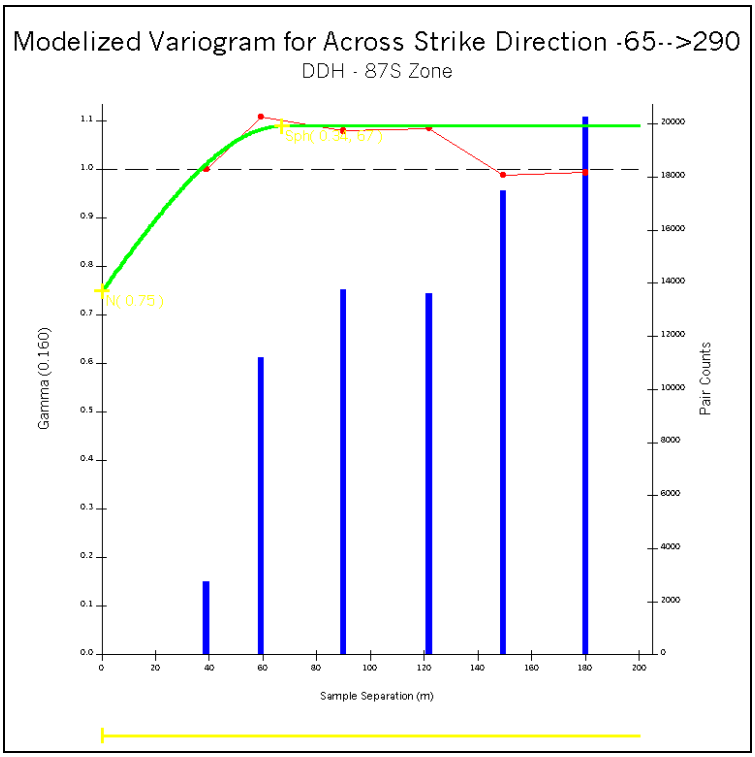

Figure B.128 Modelized Indicator Variogram – 87S Zone Cut-Off at 0.8 g/t Au – Across Strike

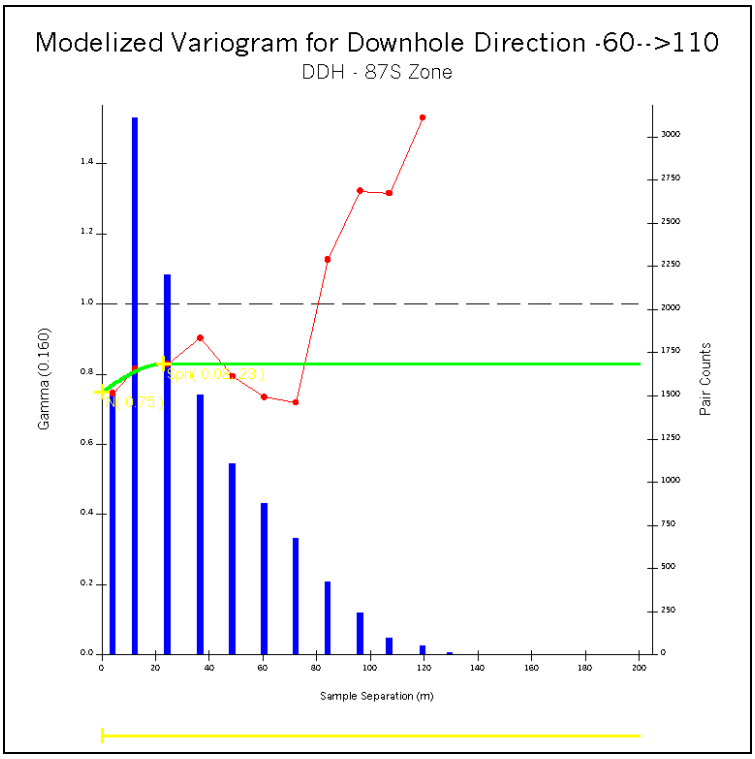

Figure B.129 Modelized Indicator Variogram – 87S Zone Cut-Off at 0.8 g/t Au – Downhole

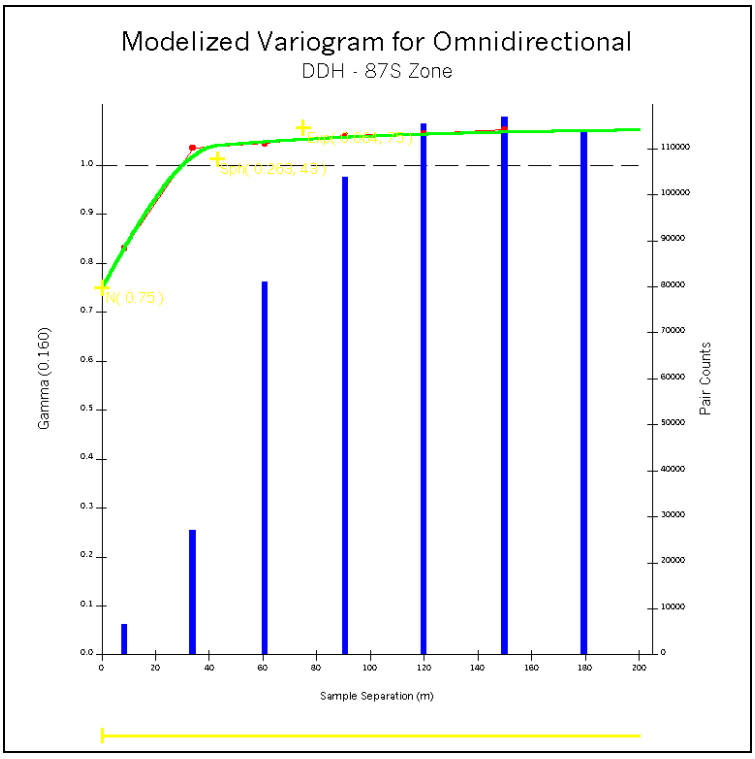

Figure B.130 Modelized Indicator Variogram – 87S Zone Cut-Off at 0.8 g/t Au – Omnidirectional

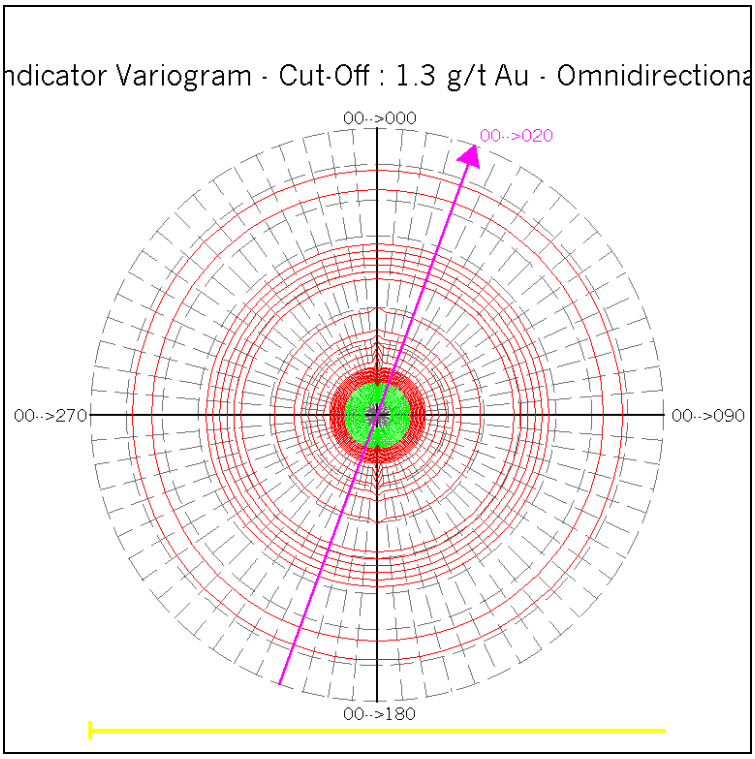

Figure B.131 Fan of Indicator Variograms – 87S Zone Cut-Off at 1.3 g/t Au – Omnidirectional

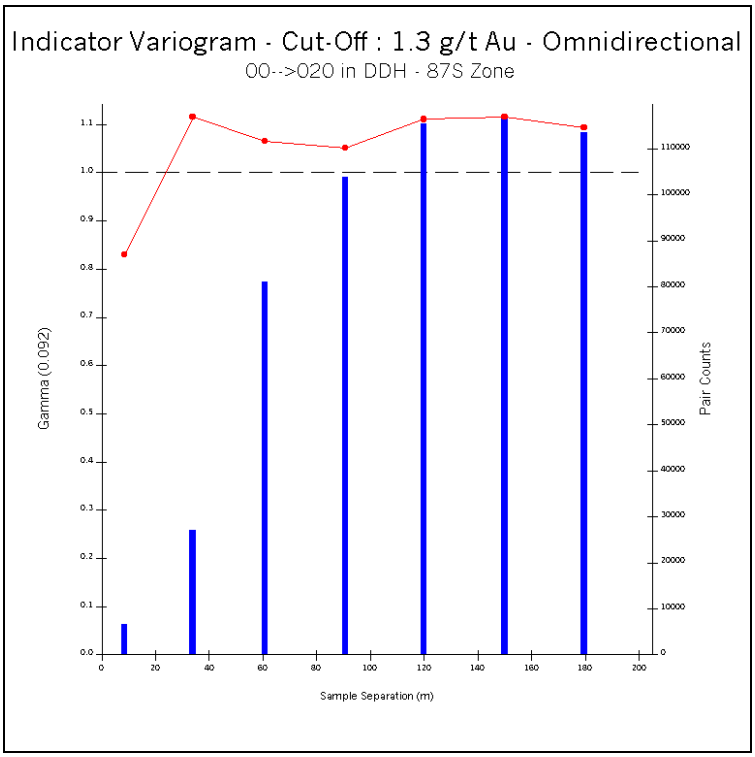

Figure B.132 Indicator Variogram – 87S Zone Cut-Off at 1.3 g/t Au – Omnidirectional

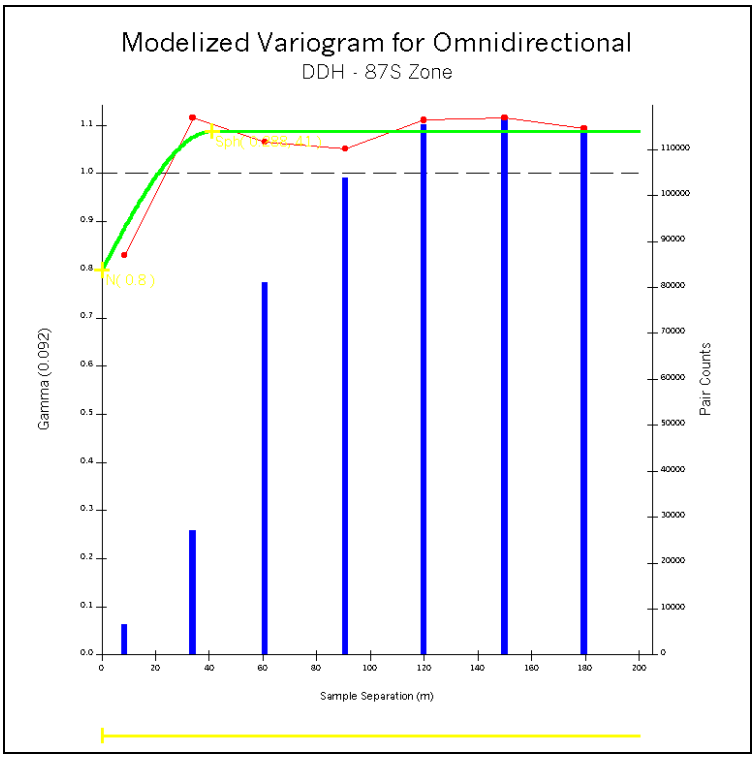

Figure B.133 Modelized Indicator Variogram – 87S Zone Cut-Off at 1.3 g/t Au – Omnidirectional

APPENDIX C – Indicator Variogram BH

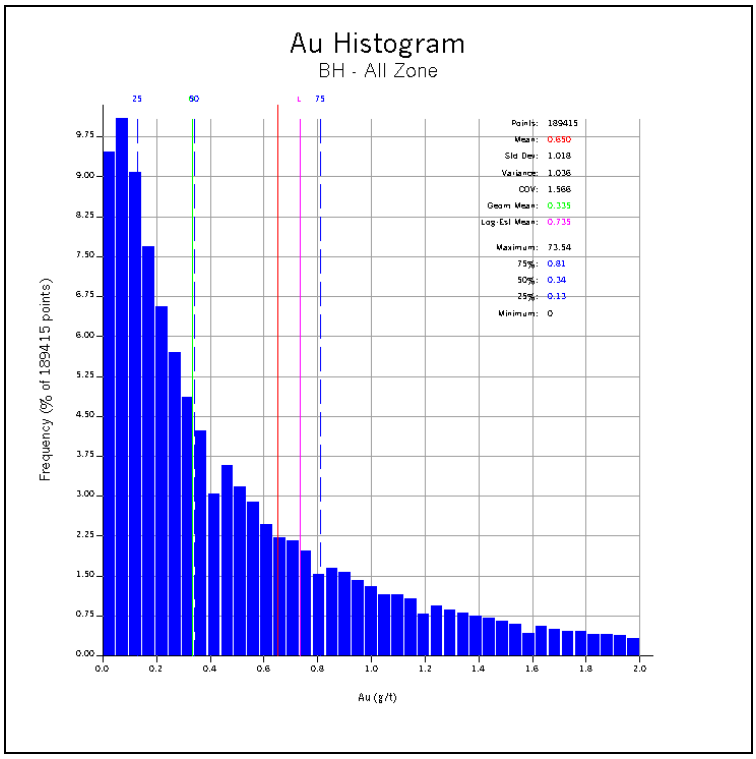

Figure C.1 Au Normal Histogram – All Zone

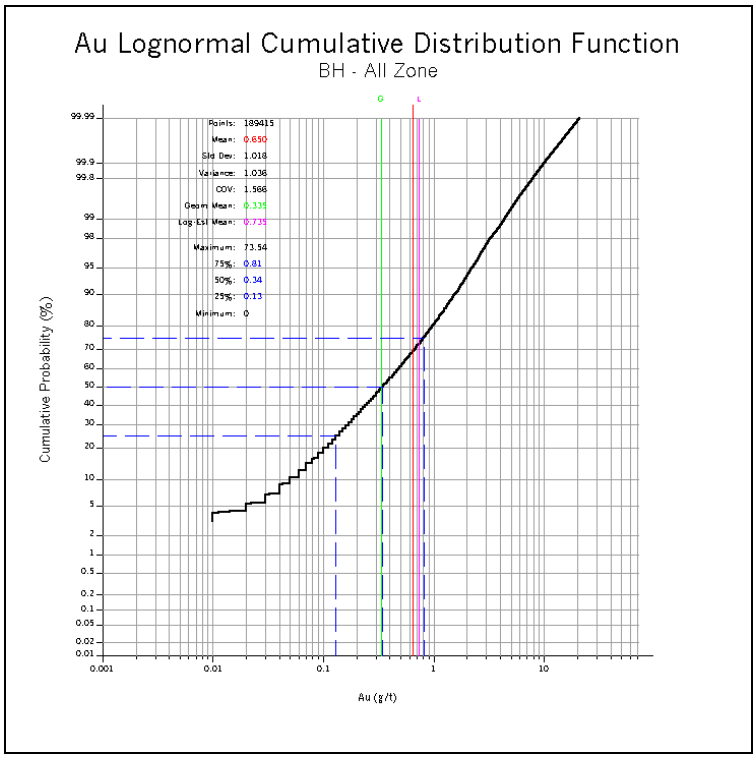

Figure C.2 Au Lognormal Cumulative Distribution Function – All Zone

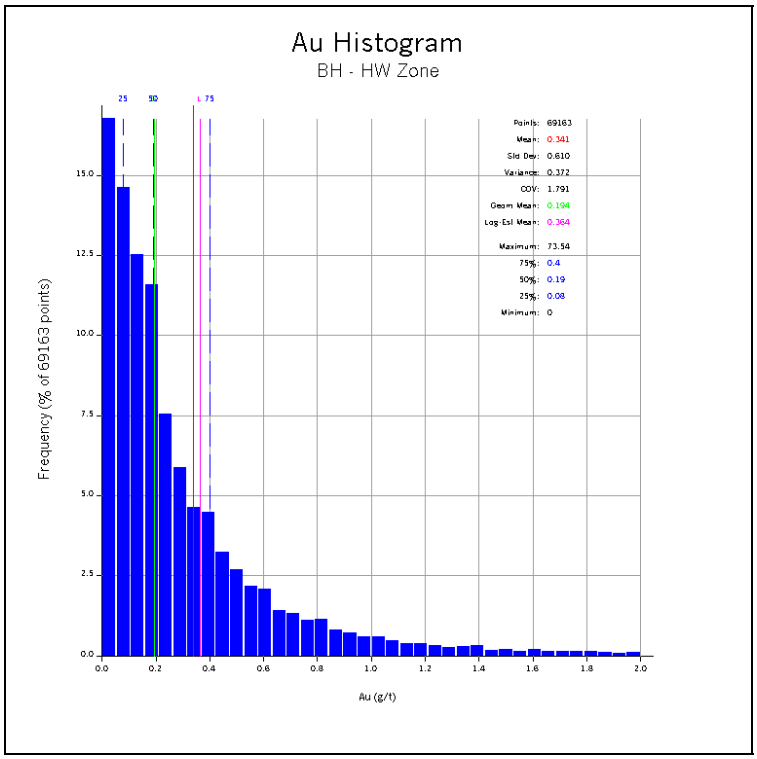

Figure C.3 Au Normal Histogram – HW Zone

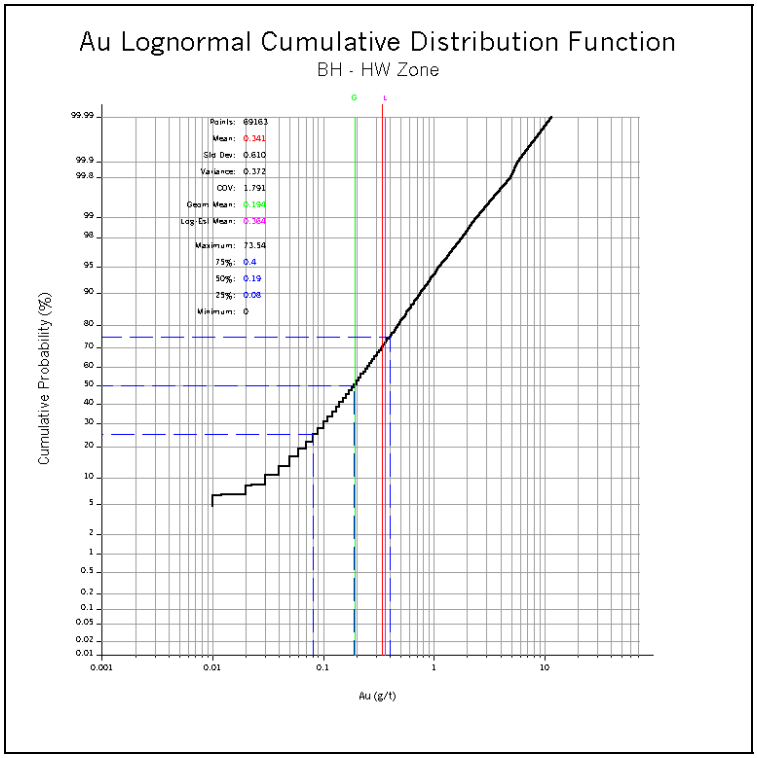

Figure C.4 Au Lognormal Cumulative Distribution Function – HW Zone

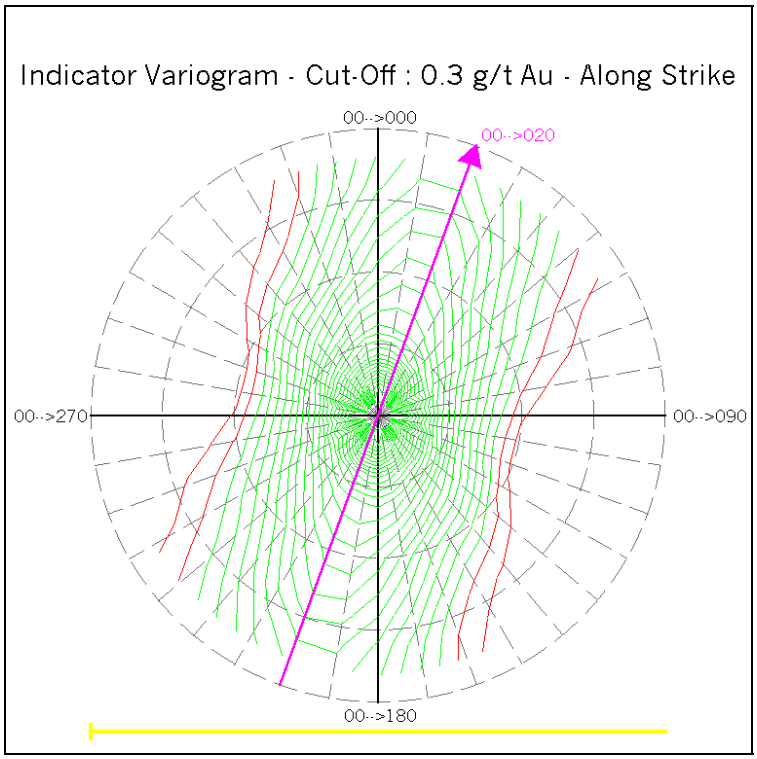

Figure C.5 Fan of Indicator Variograms – HW Zone Cut-Off at 0.3 g/t Au – Along Strike

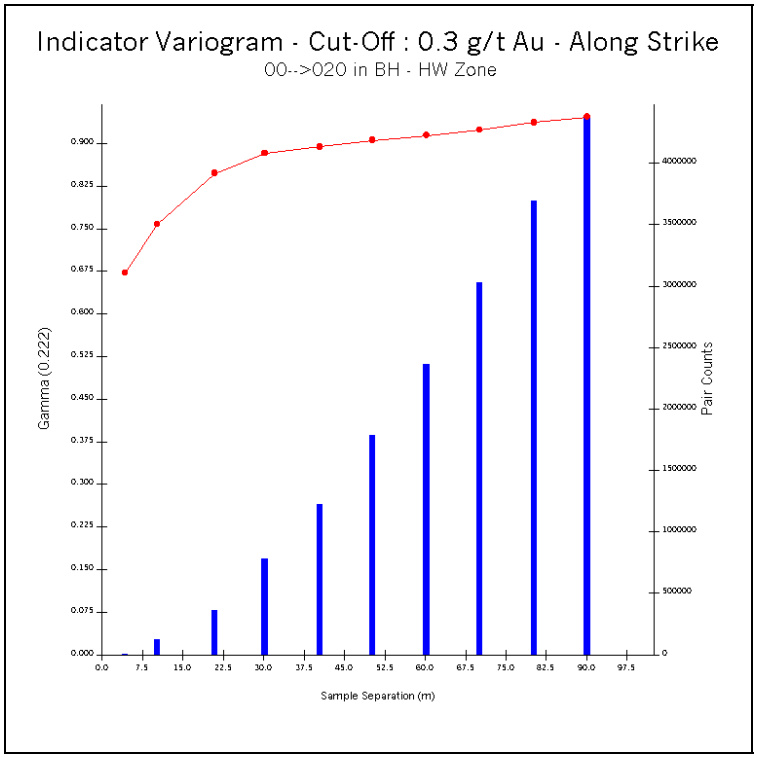

Figure C.6 Indicator Variogram – HW Zone Cut-Off at 0.3 g/t Au – Along Strike

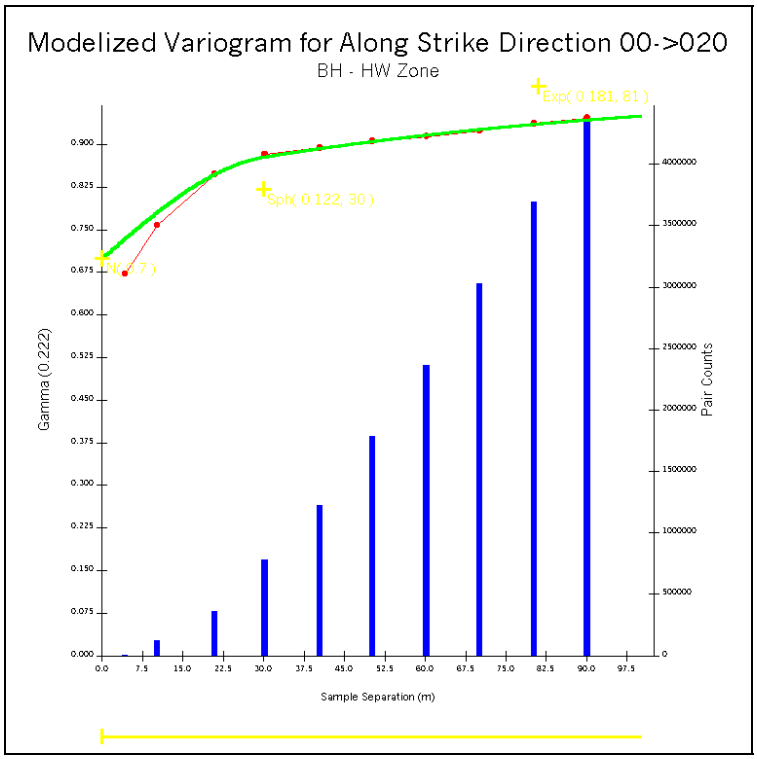

Figure C.7 Modelized Indicator Variogram – HW Zone Cut-Off at 0.3 g/t Au – Along Strike

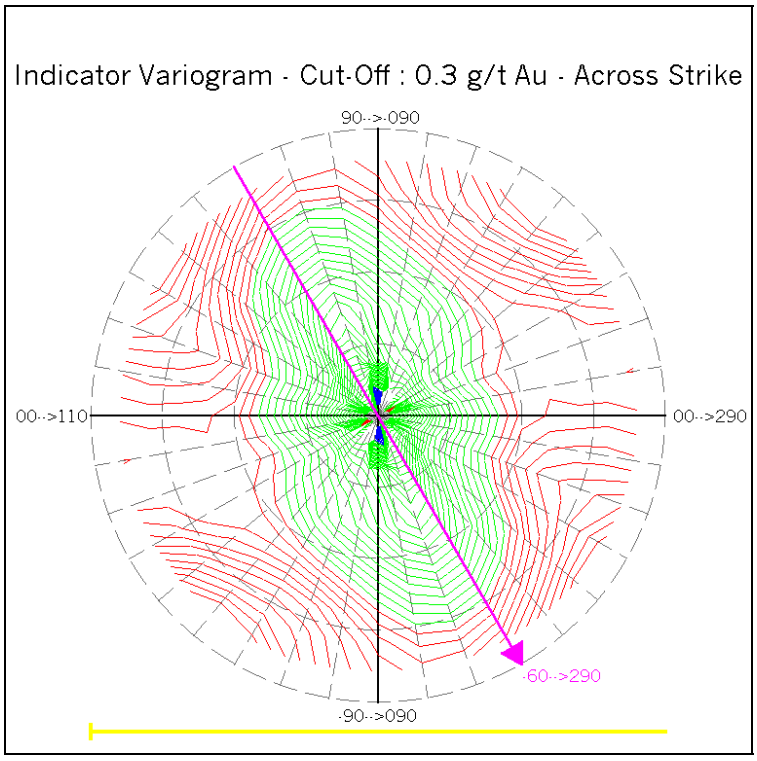

Figure C.8 Fan of Indicator Variograms – HW Zone Cut-Off at 0.3 g/t Au – Across Strike

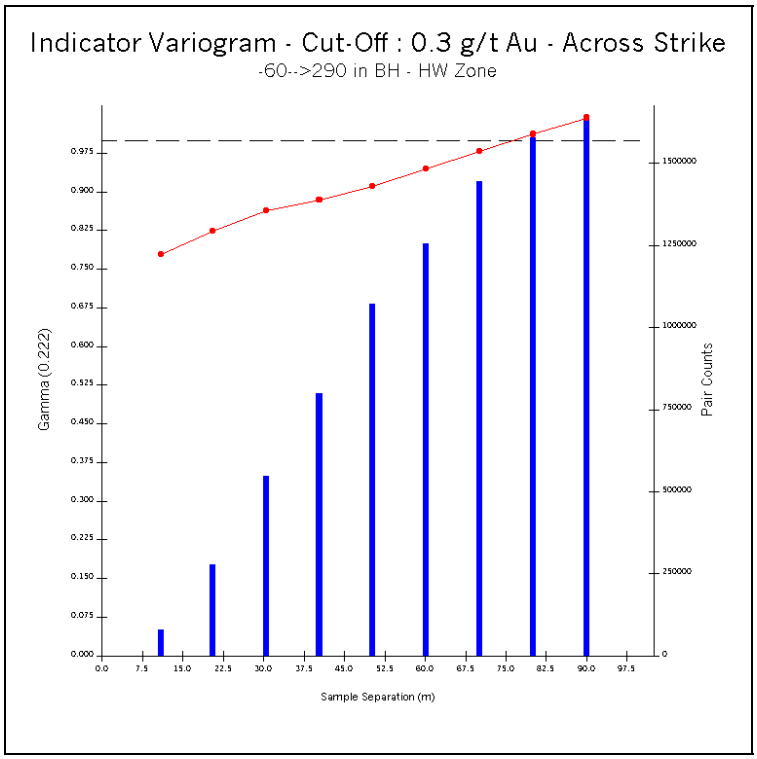

Figure C.9 Indicator Variogram – HW Zone Cut-Off at 0.3 g/t Au – Across Strike

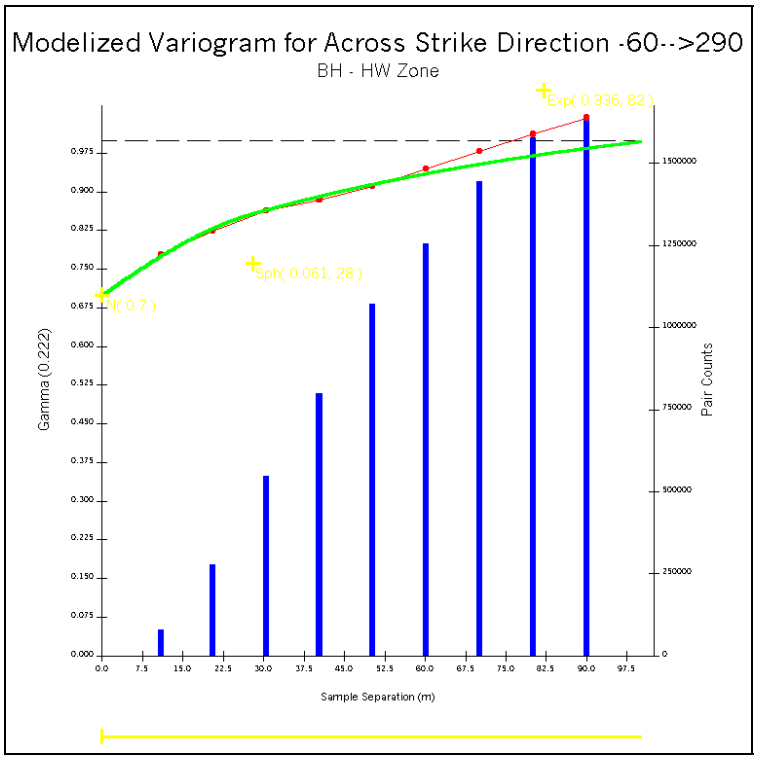

Figure C.10 Modelized Indicator Variogram – HW Zone Cut-Off at 0.3 g/t Au – Across Strike

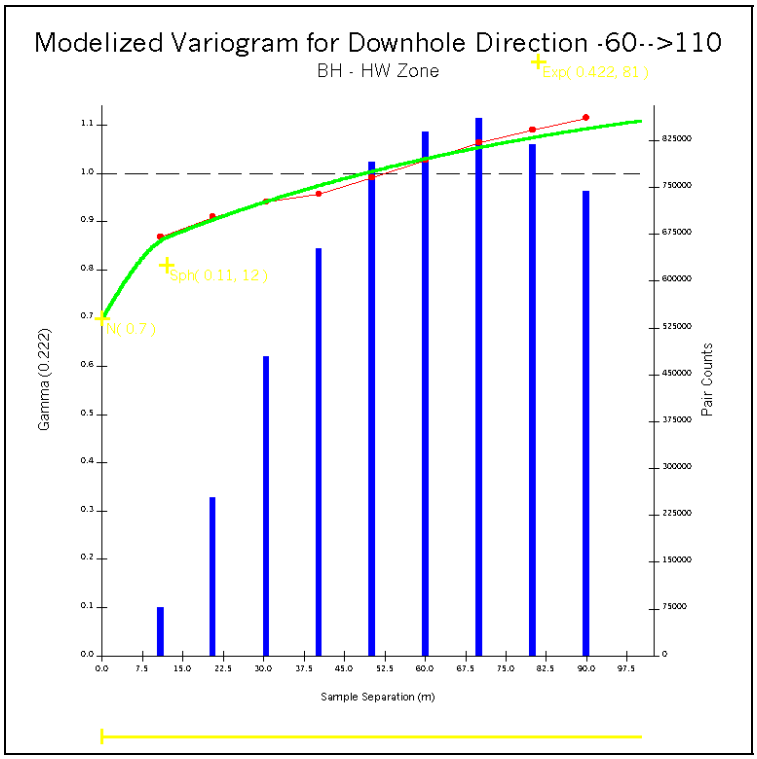

Figure C.11 Modelized Indicator Variogram – HW Zone Cut-Off at 0.3 g/t Au – Downhole

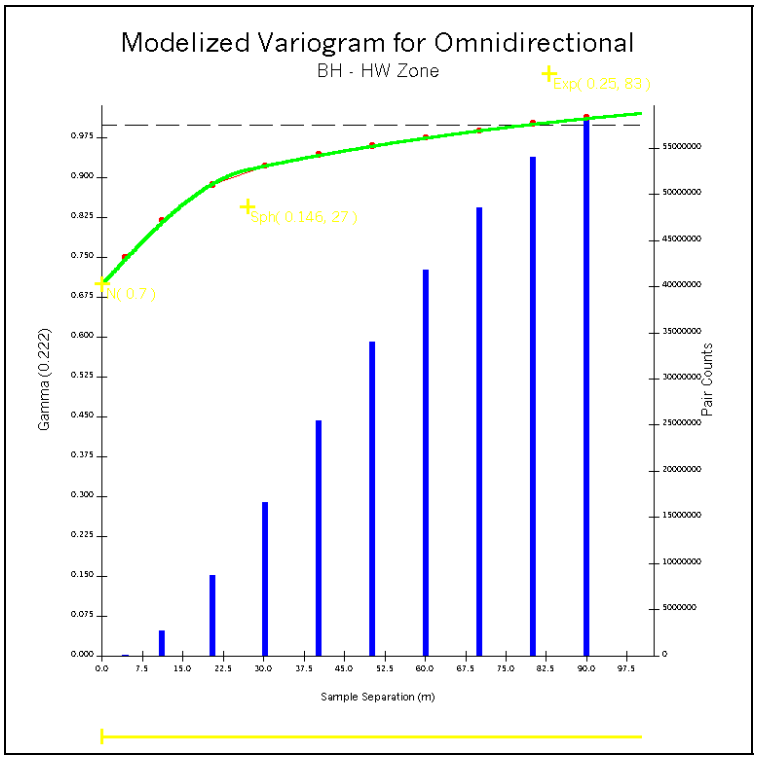

Figure C.12 Modelized Indicator Variogram – HW Zone Cut-Off at 0.3 g/t Au – Omnidirectional

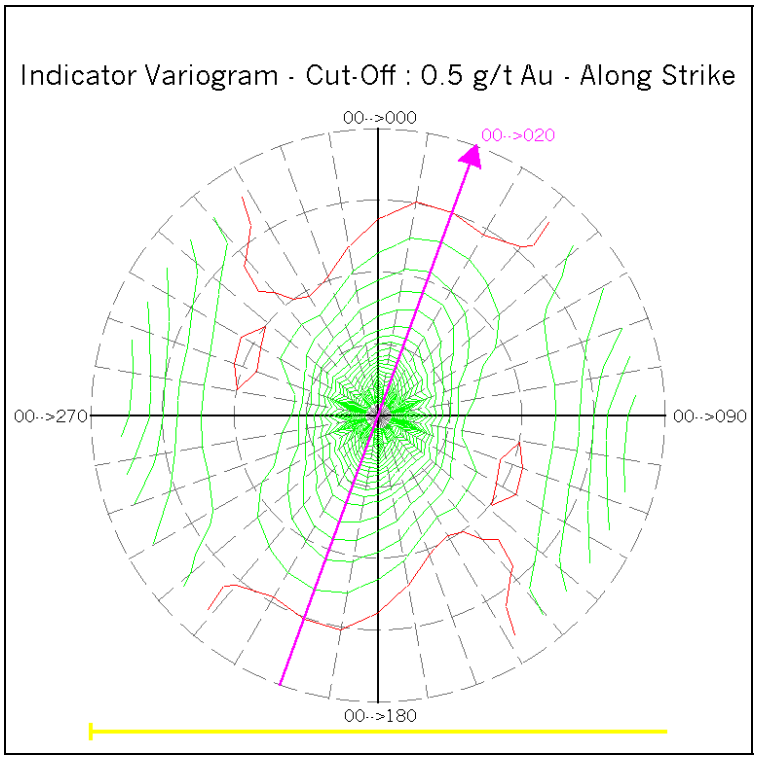

Figure C.13 Fan of Indicator Variograms – HW Zone Cut-Off at 0.5 g/t Au – Along Strike

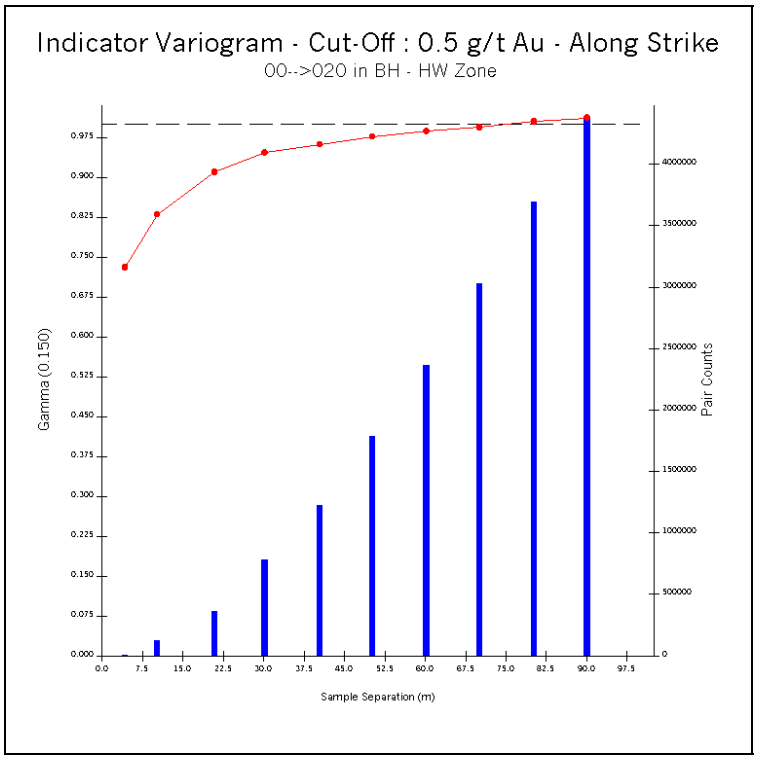

Figure C.14 Indicator Variogram – HW Zone Cut-Off at 0.5 g/t Au – Along Strike

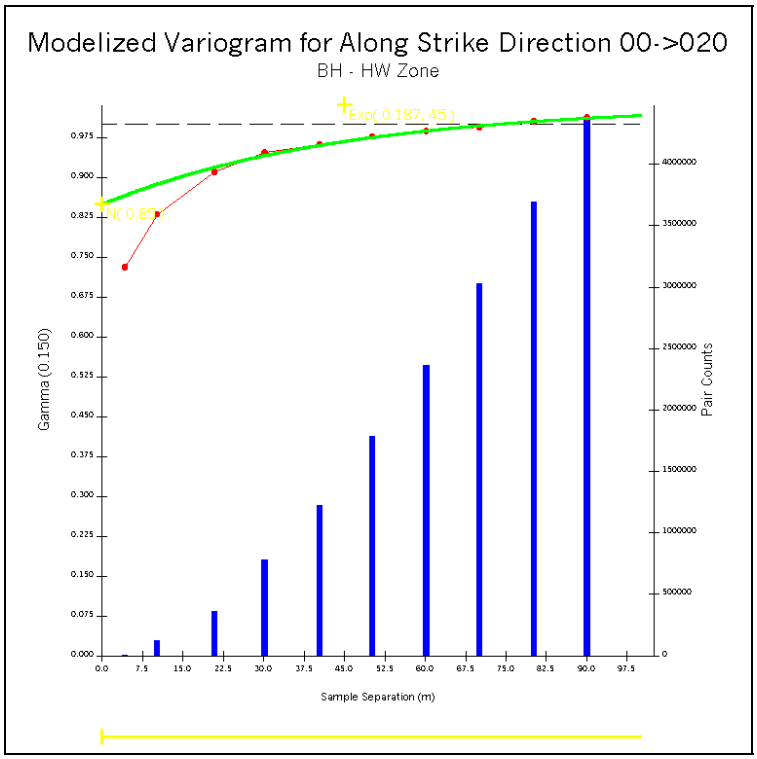

Figure C.15 Modelized Indicator Variogram – HW Zone Cut-Off at 0.5 g/t Au – Along Strike

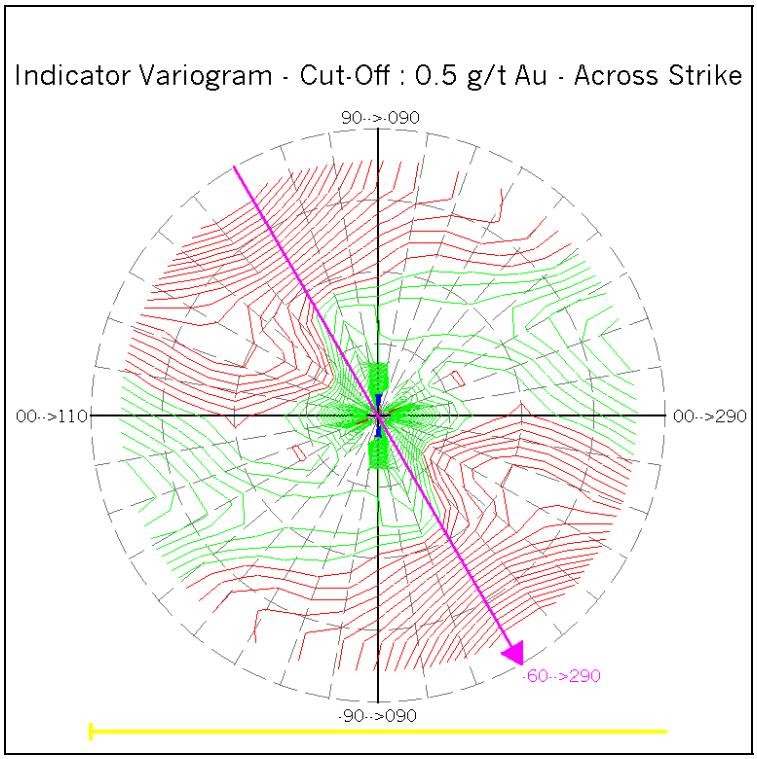

Figure C.16 Fan of Indicator Variograms – HW Zone Cut-Off at 0.5 g/t Au – Across Strike

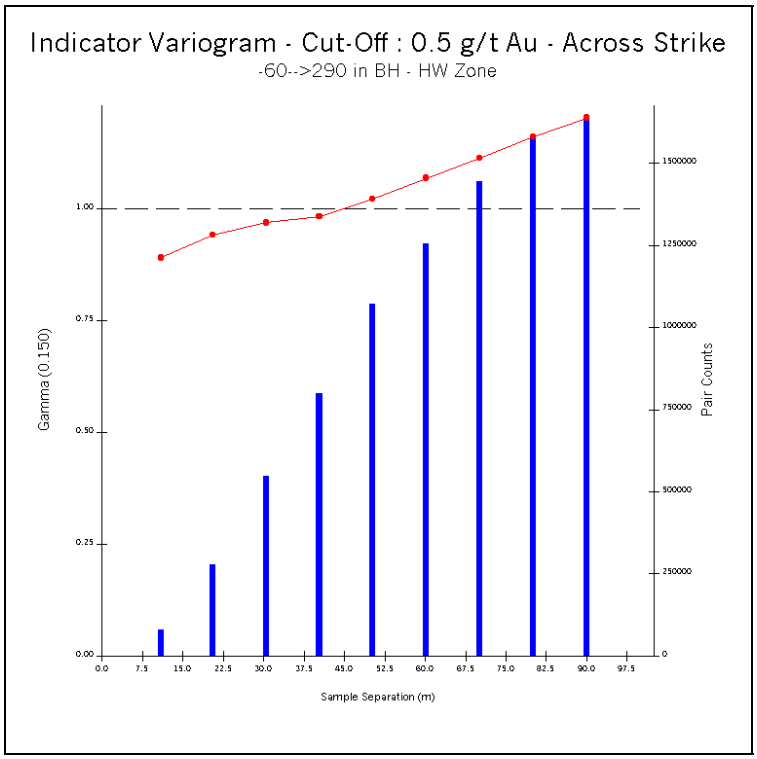

Figure C.17 Indicator Variogram – HW Zone Cut-Off at 0.5 g/t Au – Across Strike

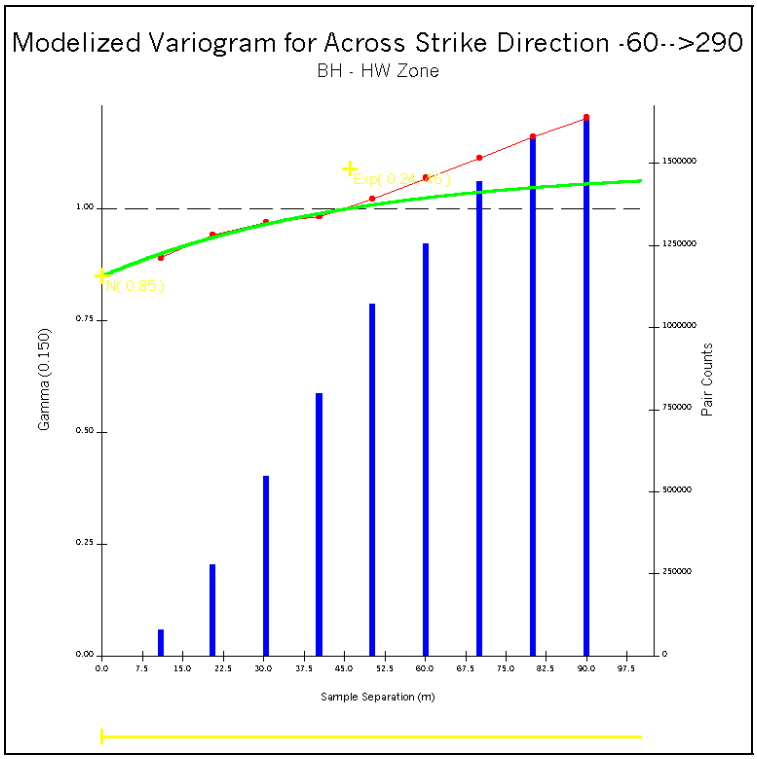

Figure C.18 Modelized Indicator Variogram – HW Zone Cut-Off at 0.5 g/t Au – Across Strike

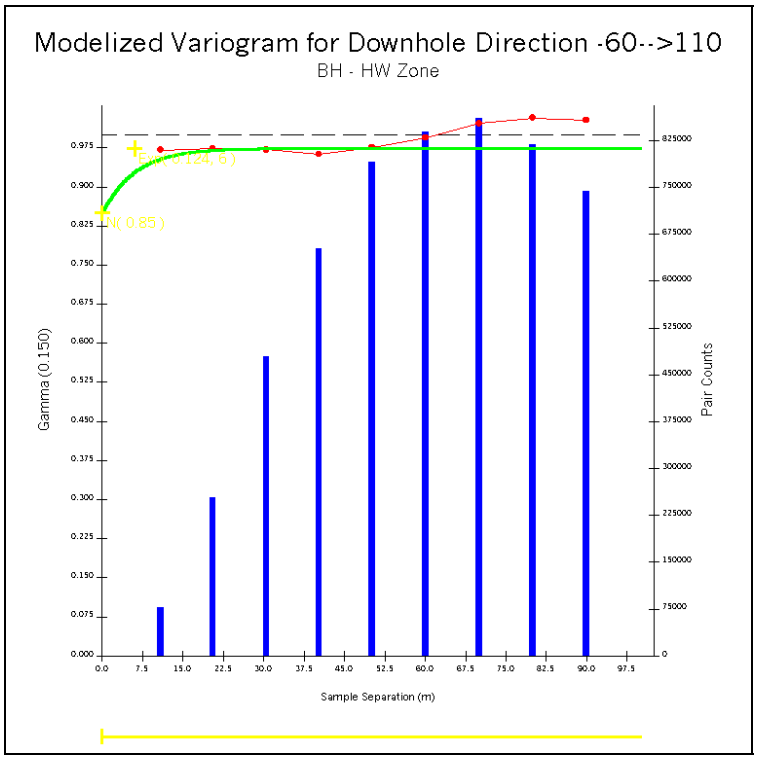

Figure C.19 Modelized Indicator Variogram – HW Zone Cut-Off at 0.5 g/t Au – Downhole

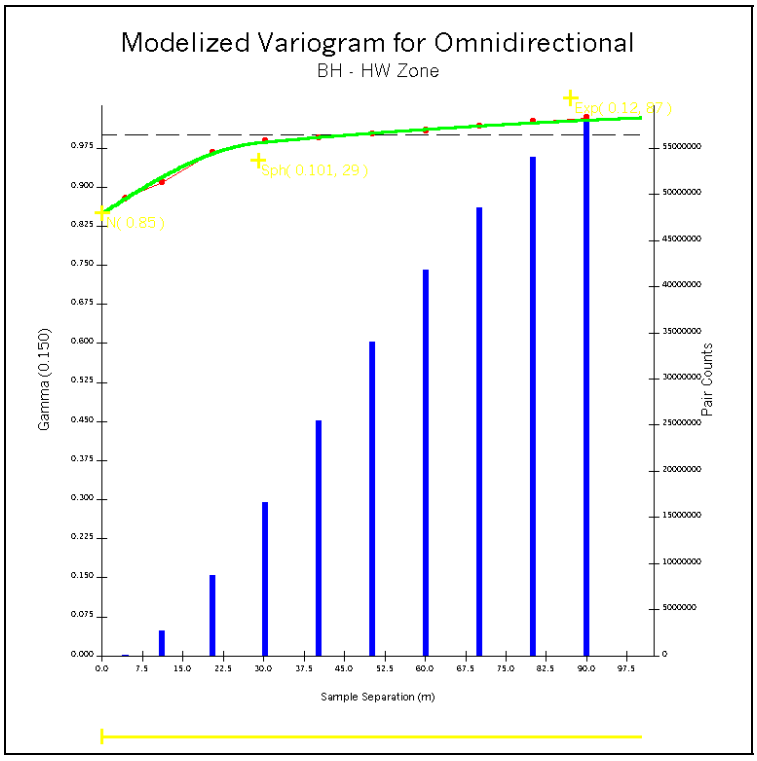

Figure C.20 Modelized Indicator Variogram – HW Zone Cut-Off at 0.5 g/t Au – Omnidirectional

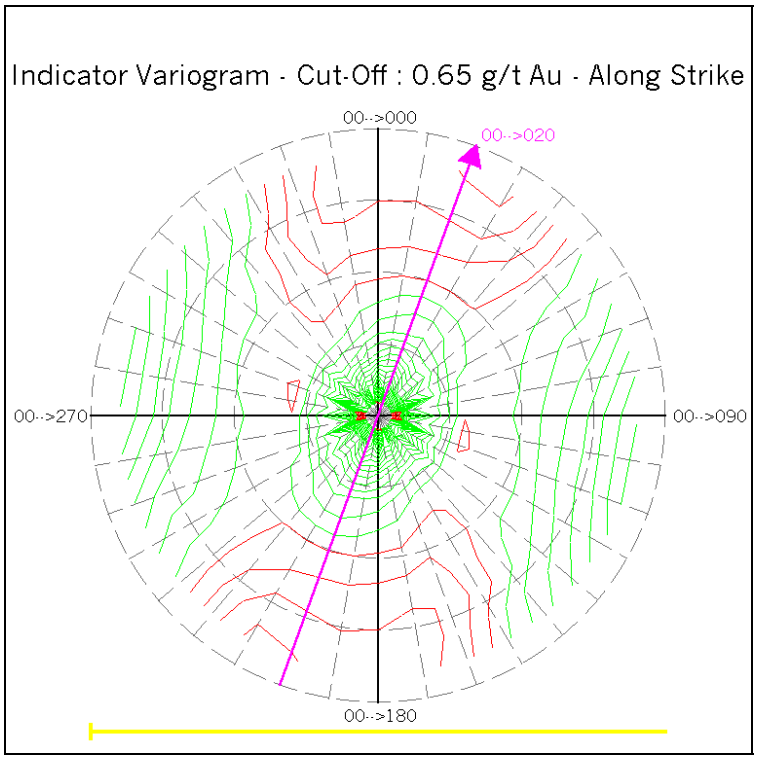

Figure C.21 Fan of Indicator Variograms – HW Zone Cut-Off at 0.65 g/t Au – Along Strike

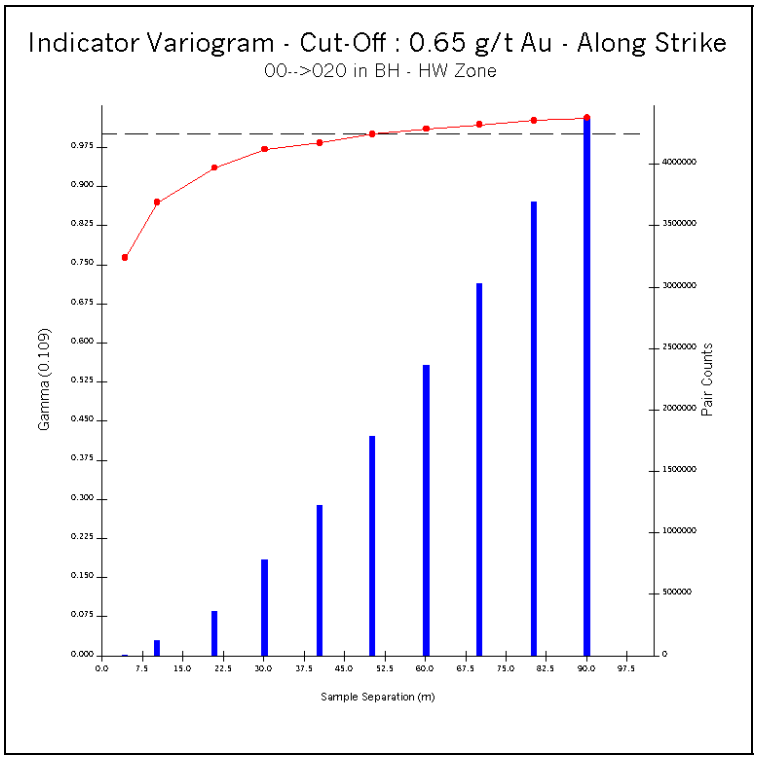

Figure C.22 Indicator Variogram – HW Zone Cut-Off at 0.65 g/t Au – Along Strike

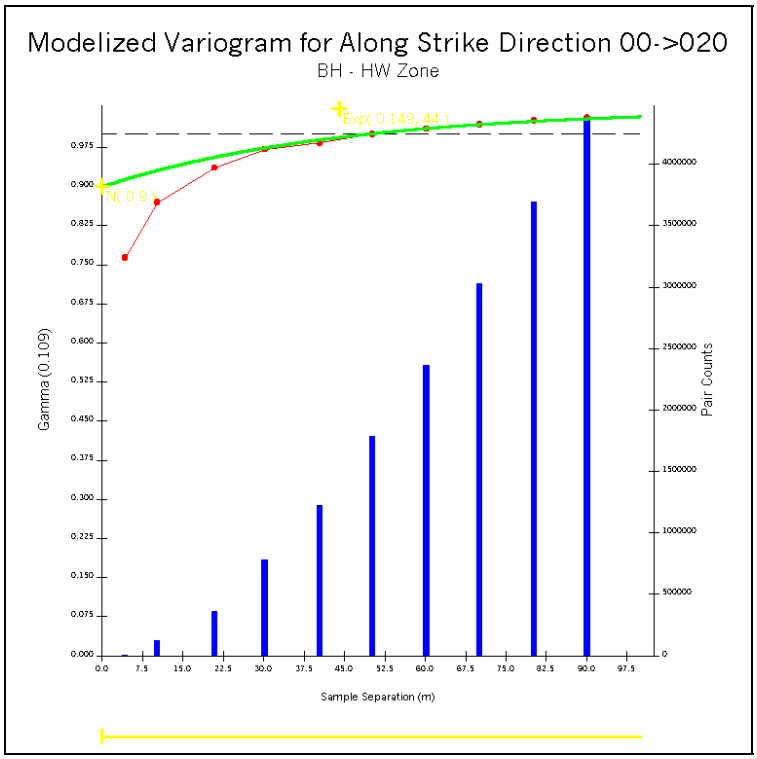

Figure C.23 Modelized Indicator Variogram – HW Zone Cut-Off at 0.65 g/t Au – Along Strike

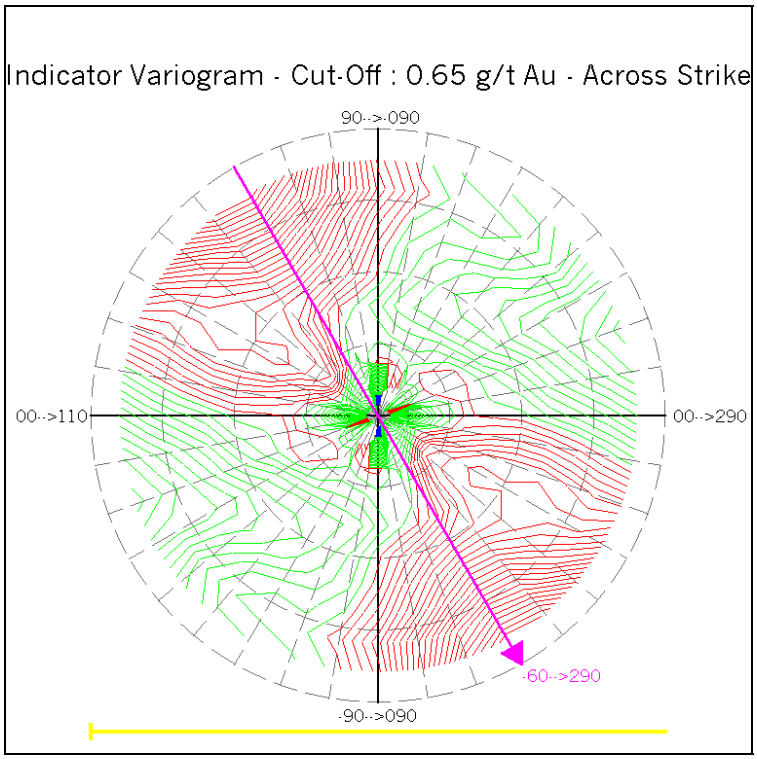

Figure C.24 Fan of Indicator Variograms – HW Zone Cut-Off at 0.65 g/t Au – Across Strike

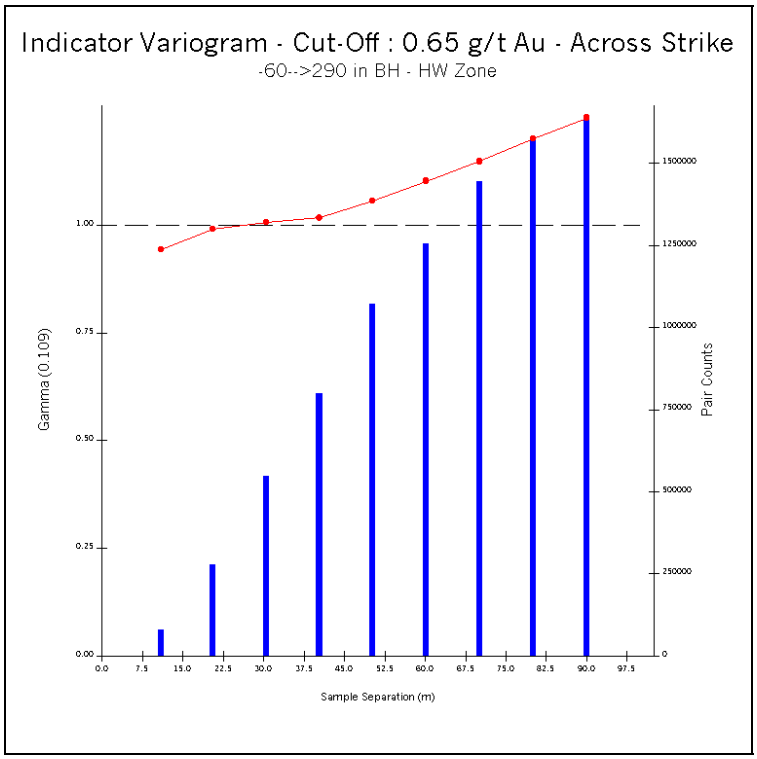

Figure C.25 Indicator Variogram – HW Zone Cut-Off at 0.65 g/t Au – Across Strike

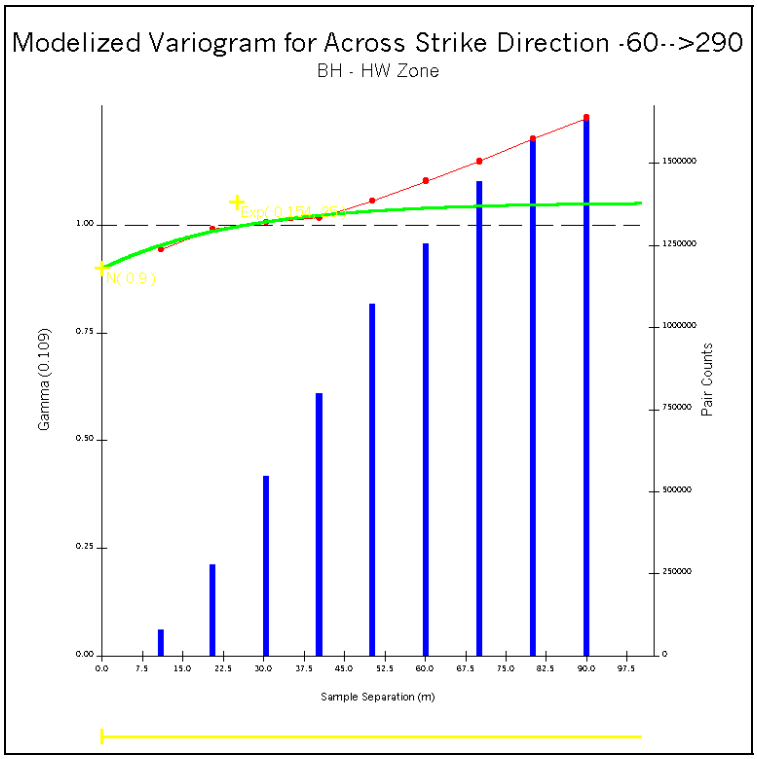

Figure C.26 Modelized Indicator Variogram – HW Zone Cut-Off at 0.65 g/t Au – Across Strike

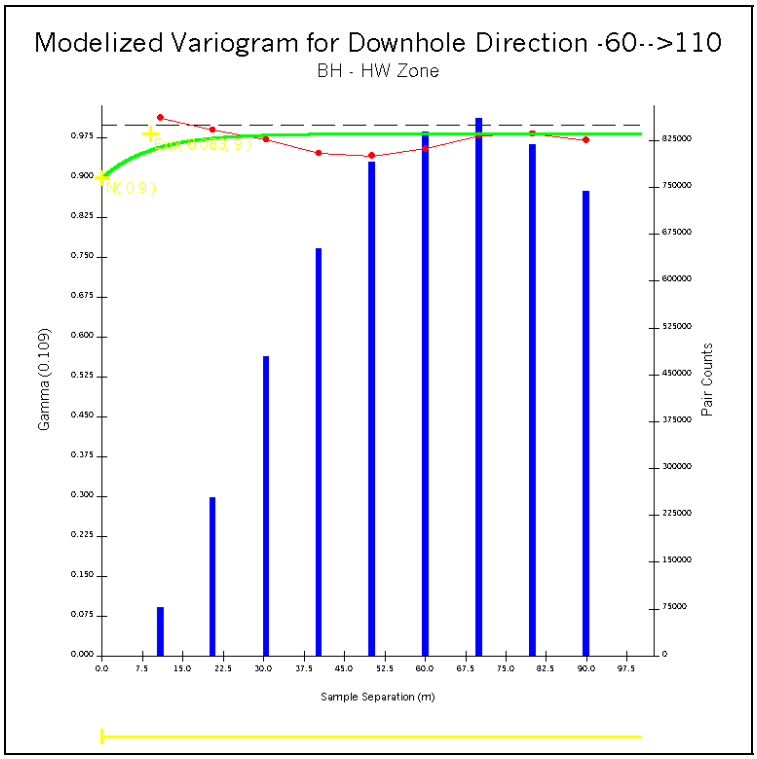

Figure C.27 Modelized Indicator Variogram – HW Zone Cut-Off at 0.65 g/t Au – Downhole

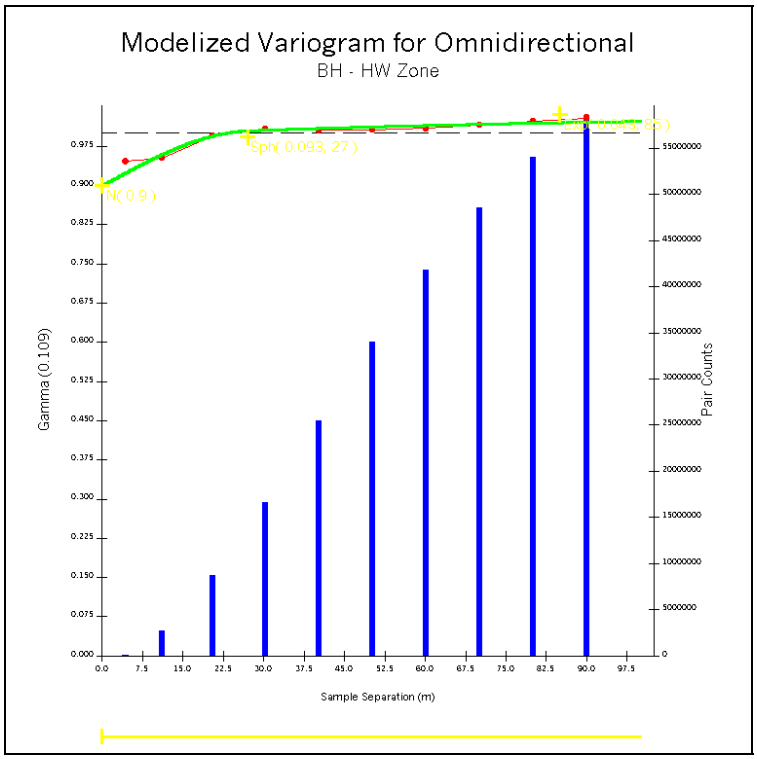

Figure C.28 Modelized Indicator Variogram – HW Zone Cut-Off at 0.65 g/t Au – Omnidirectional

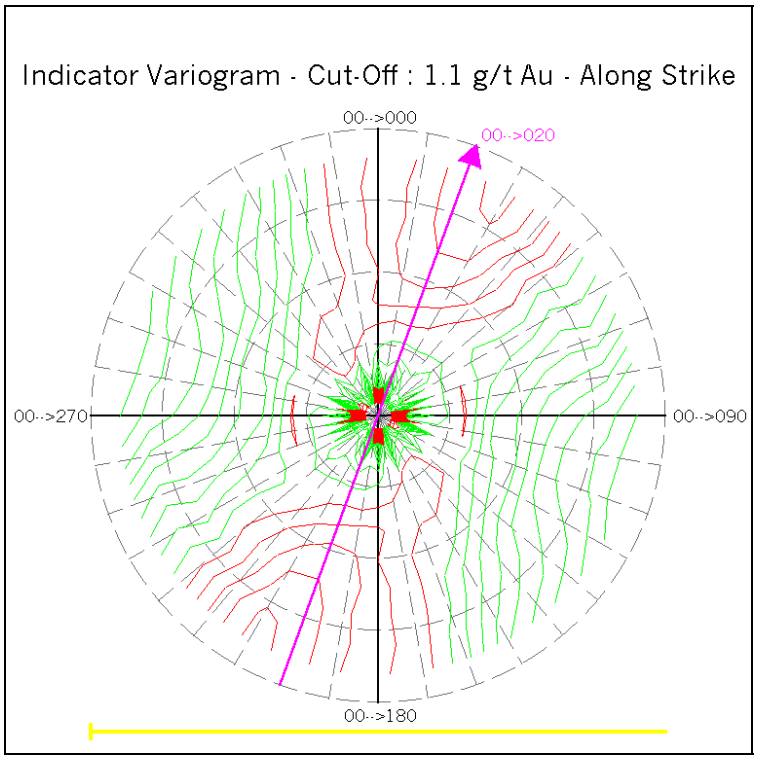

Figure C.29 Fan of Indicator Variograms – HW Zone Cut-Off at 1.1 g/t Au – Along Strike

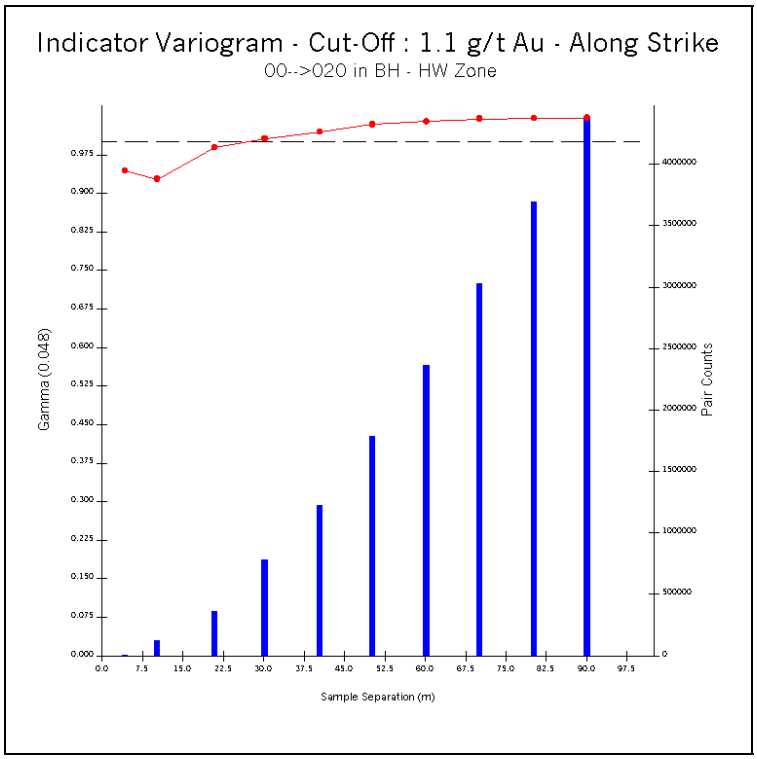

Figure C.30 Indicator Variogram – HW Zone Cut-Off at 1.1 g/t Au – Along Strike

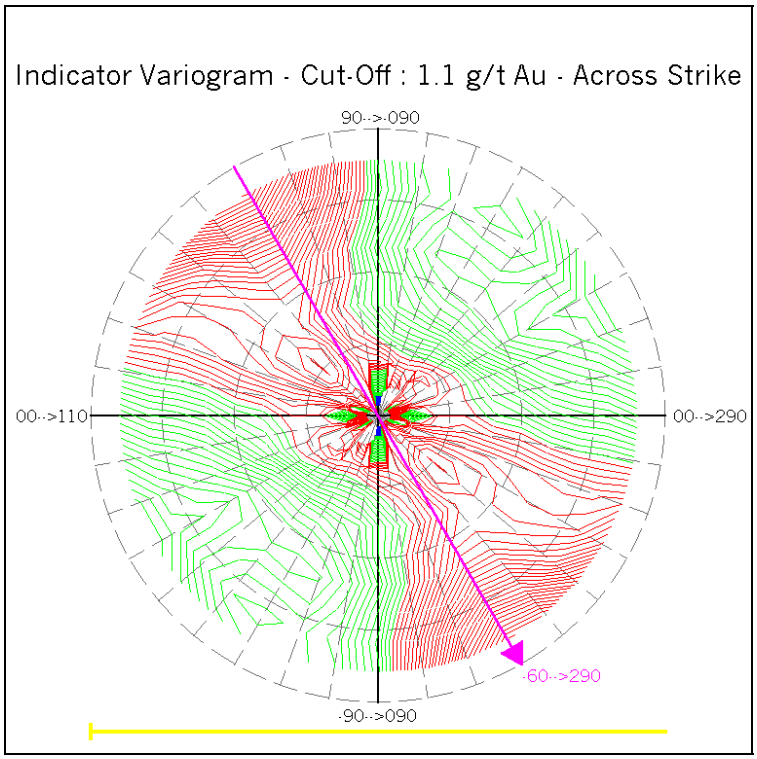

Figure C.31 Fan of Indicator Variograms – HW Zone Cut-Off at 1.1 g/t Au – Across Strike

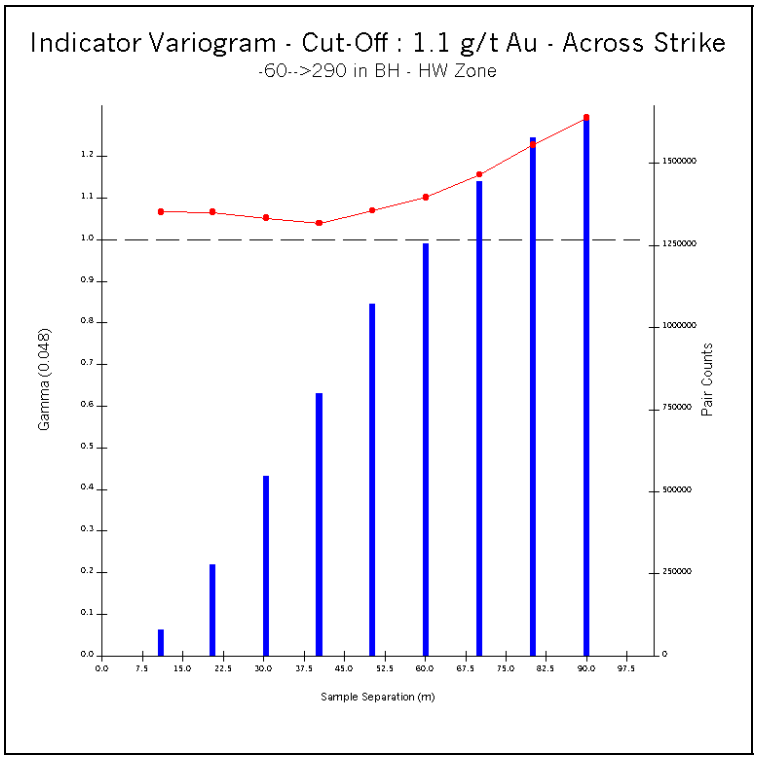

Figure C.32 Indicator Variogram – HW Zone Cut-Off at 1.1 g/t Au – Across Strike

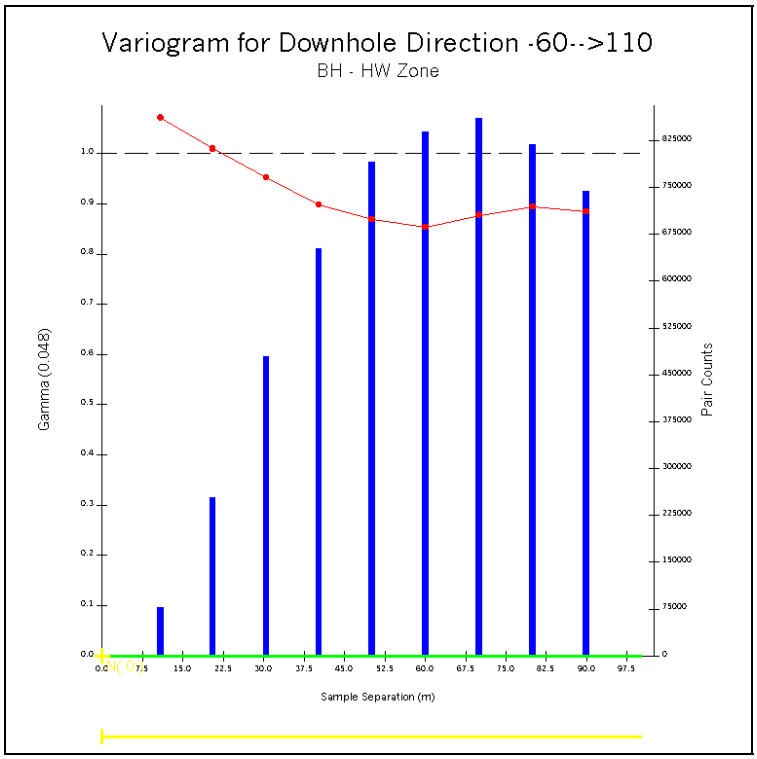

Figure C.33 Indicator Variogram – HW Zone Cut-Off at 1.1 g/t Au – Downhole

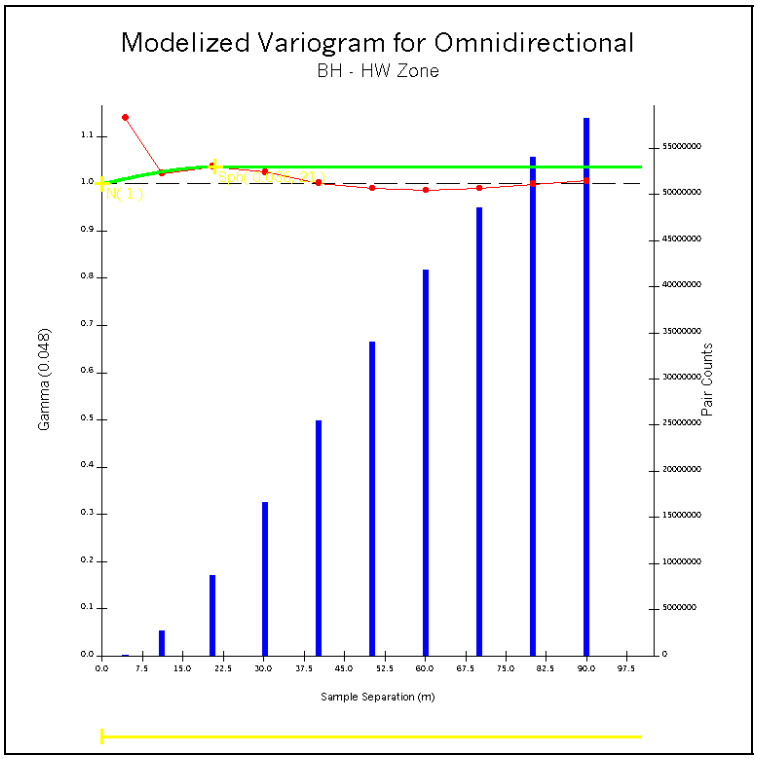

Figure C.34 Indicator Variogram – HW Zone Cut-Off at 1.1 g/t Au – Omnidirectional

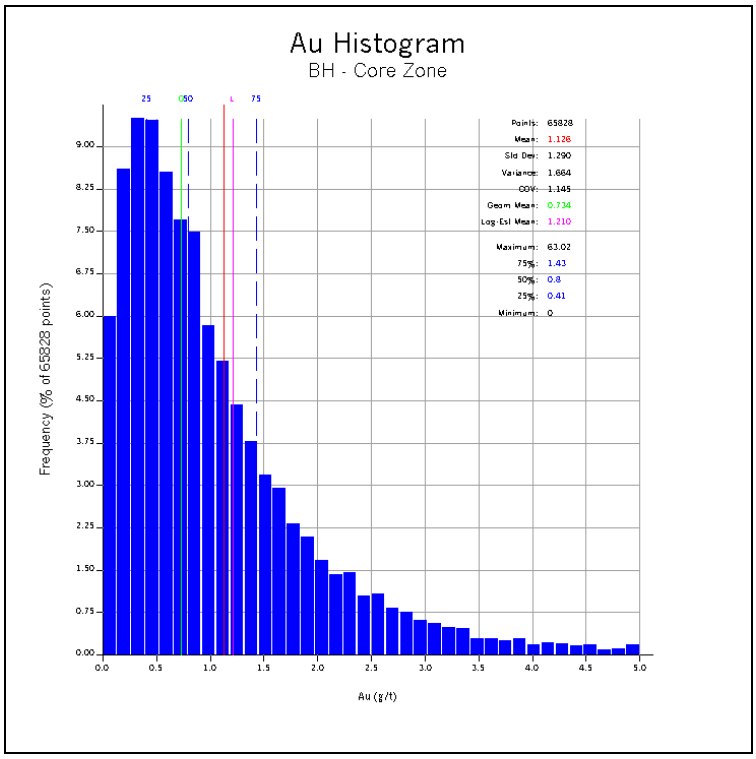

Figure C.35 Au Normal Histogram – CORE Zone

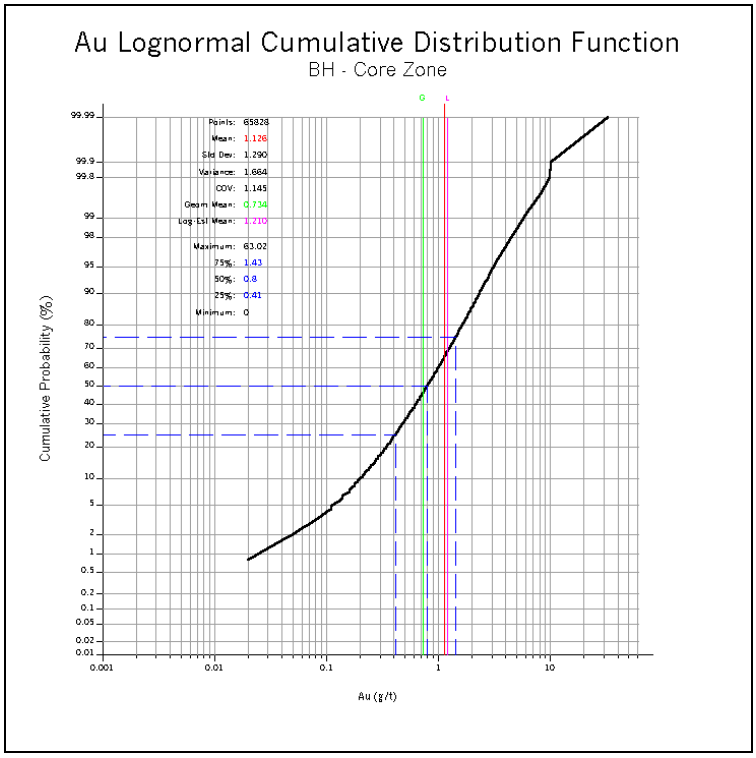

Figure C.36 Au Lognormal Cumulative Distribution Function – CORE Zone

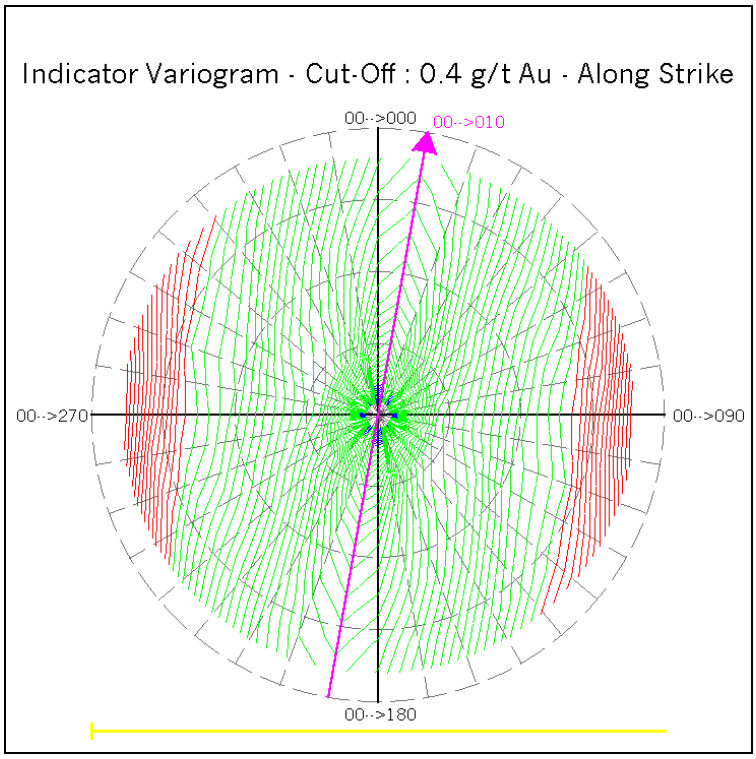

Figure C.37 Fan of Indicator Variograms – CORE Zone Cut-Off at 0.4 g/t Au – Along Strike

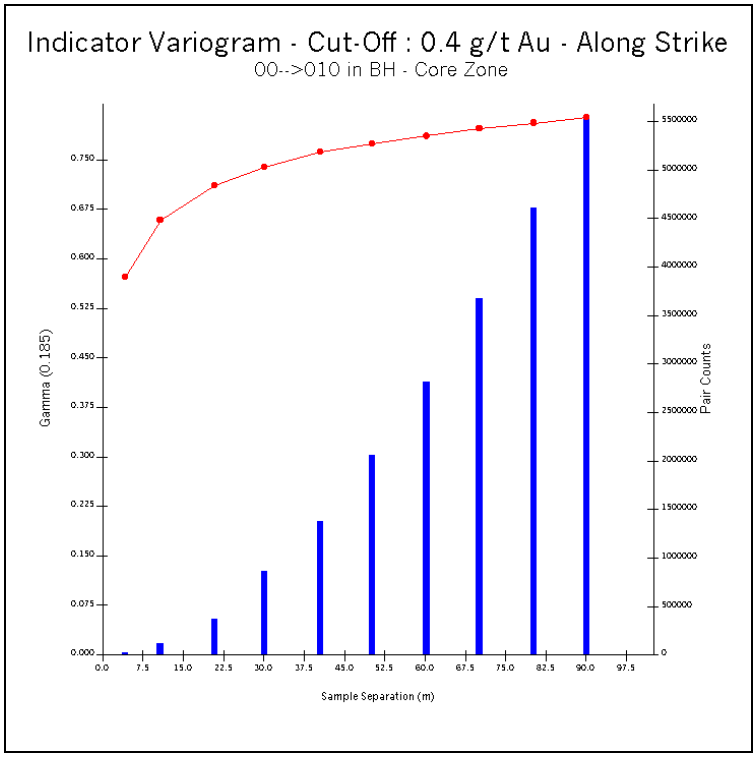

Figure C.38 Indicator Variogram – CORE Zone Cut-Off at 0.4 g/t Au – Along Strike

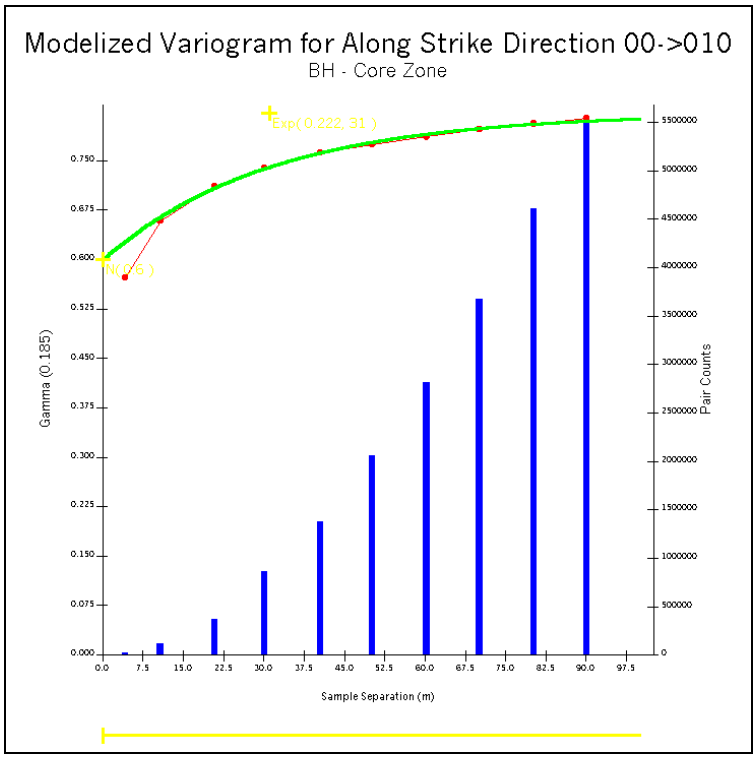

Figure C.39 Modelized Indicator Variogram – CORE Zone Cut-Off at 0.4 g/t Au – Along Strike

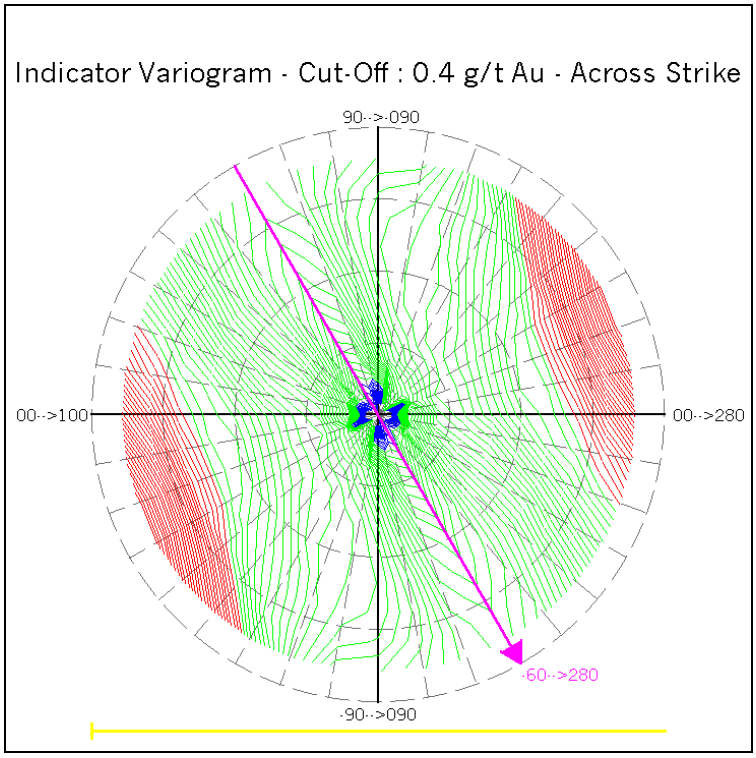

Figure C.40 Fan of Indicator Variograms – CORE Zone Cut-Off at 0.4 g/t Au – Across Strike

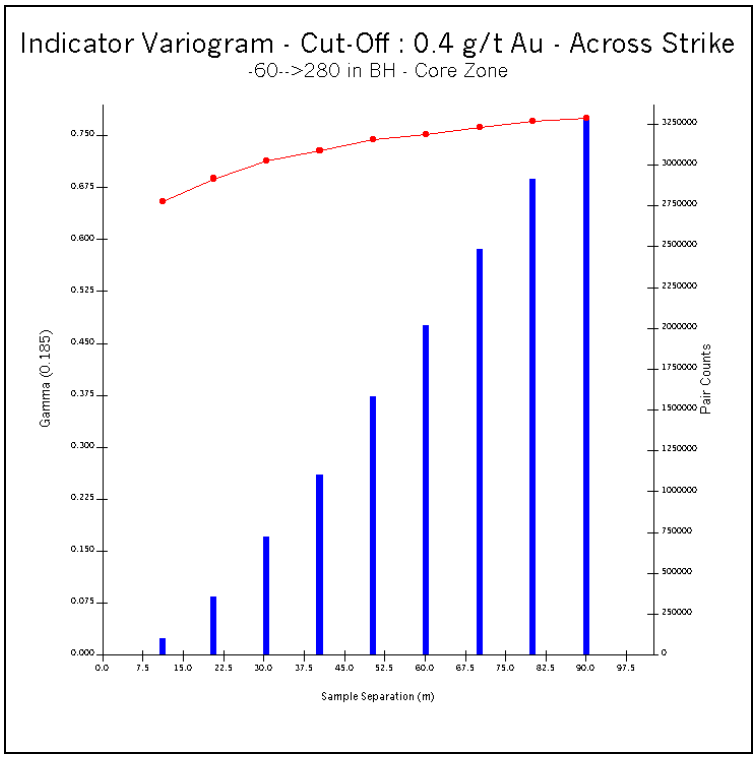

Figure C.41 Indicator Variogram – CORE Zone Cut-Off at 0.4 g/t Au – Across Strike

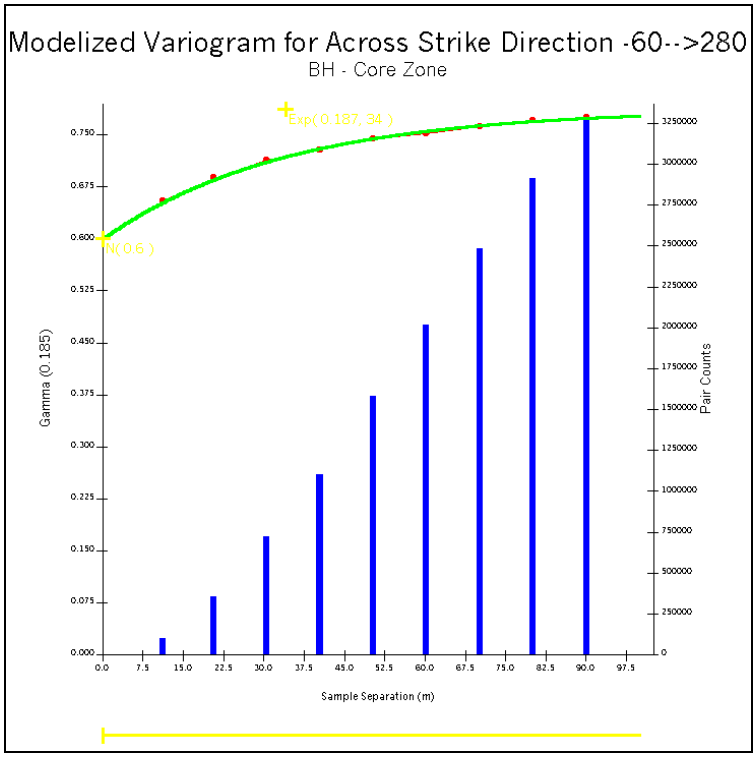

Figure C.42 Modelized Indicator Variogram – CORE Zone Cut-Off at 0.4 g/t Au – Across Strike

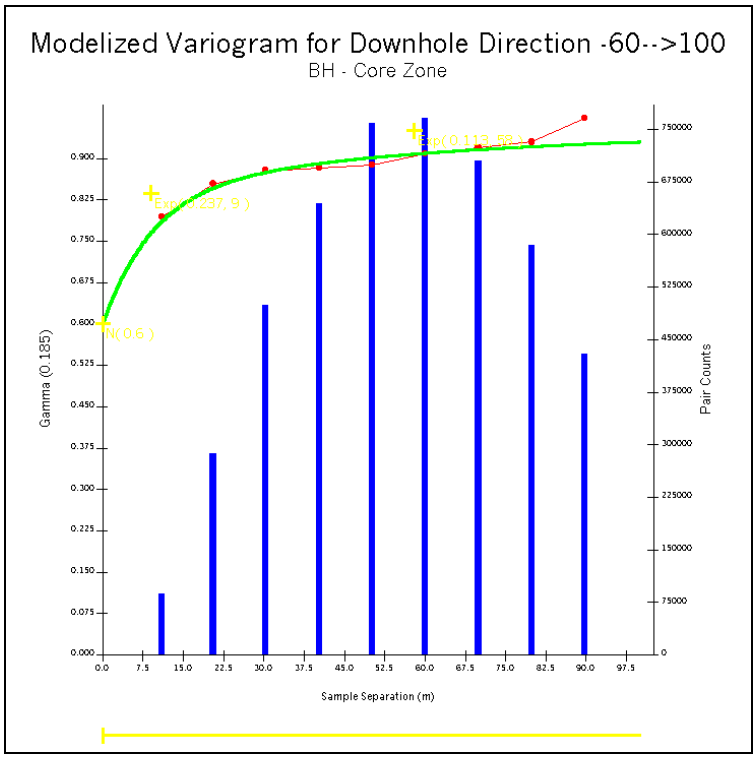

Figure C.43 Modelized Indicator Variogram – CORE Zone Cut-Off at 0.4 g/t Au – Downhole

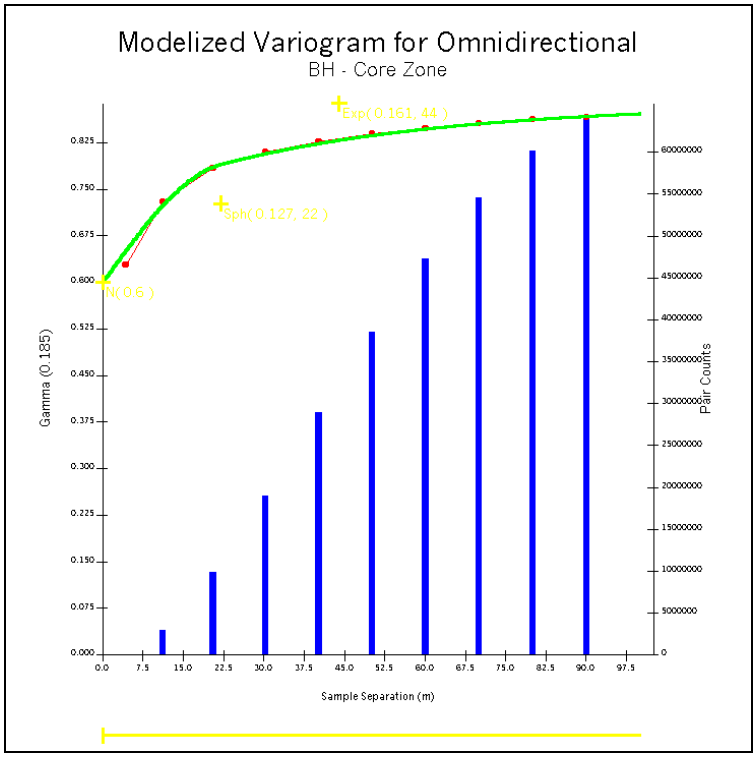

Figure C.44 Modelized Indicator Variogram – CORE Zone Cut-Off at 0.4 g/t Au – Omnidirectional

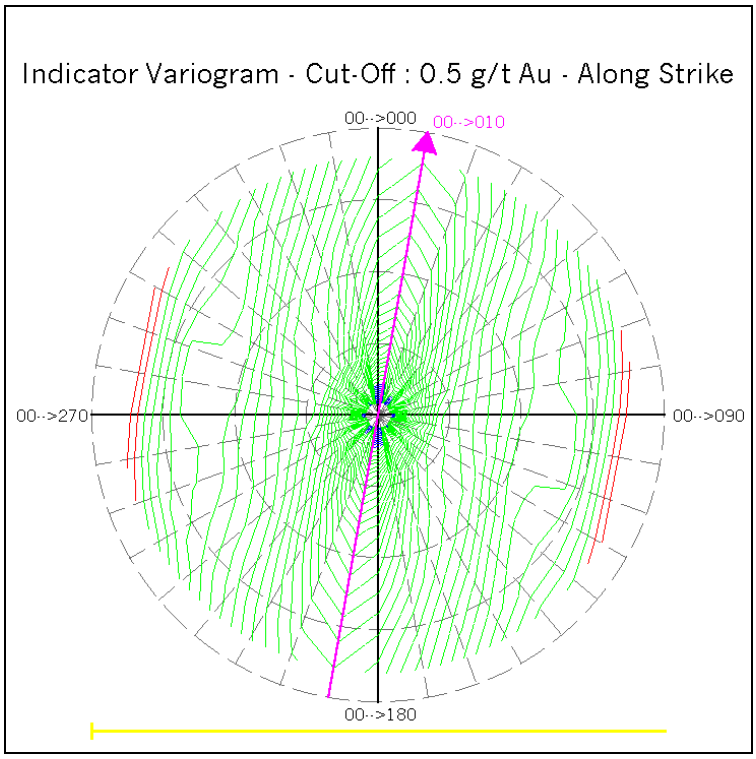

Figure C.45 Fan of Indicator Variograms – CORE Zone Cut-Off at 0.5 g/t Au – Along Strike

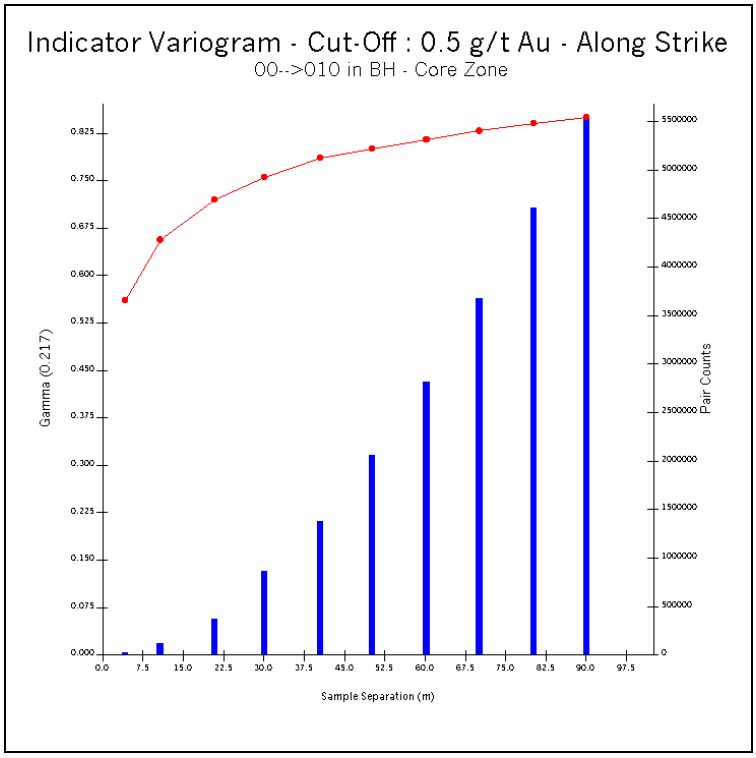

Figure C.46 Indicator Variogram – CORE Zone Cut-Off at 0.5 g/t Au – Along Strike

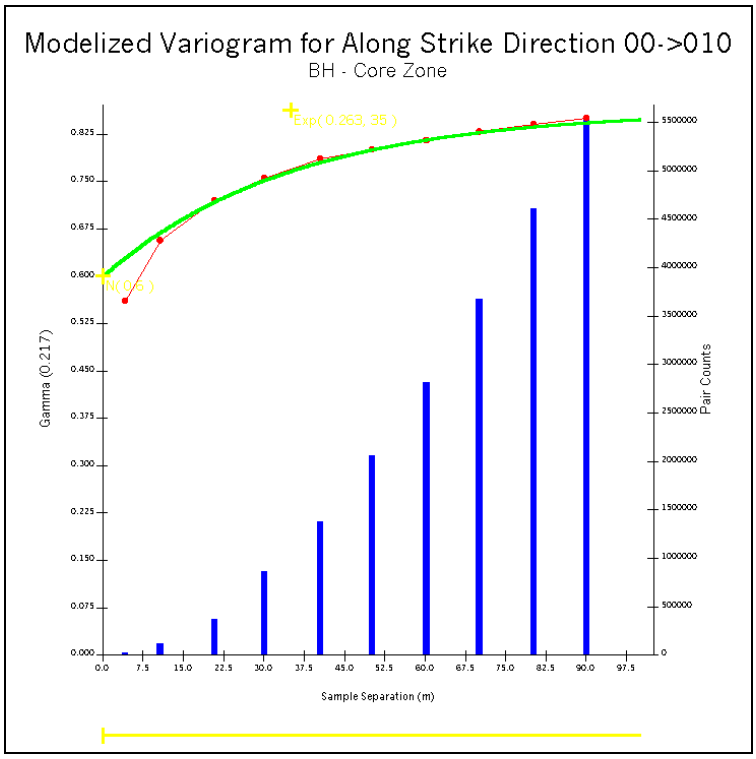

Figure C.47 Modelized Indicator Variogram – CORE Zone Cut-Off at 0.5 g/t Au – Along Strike

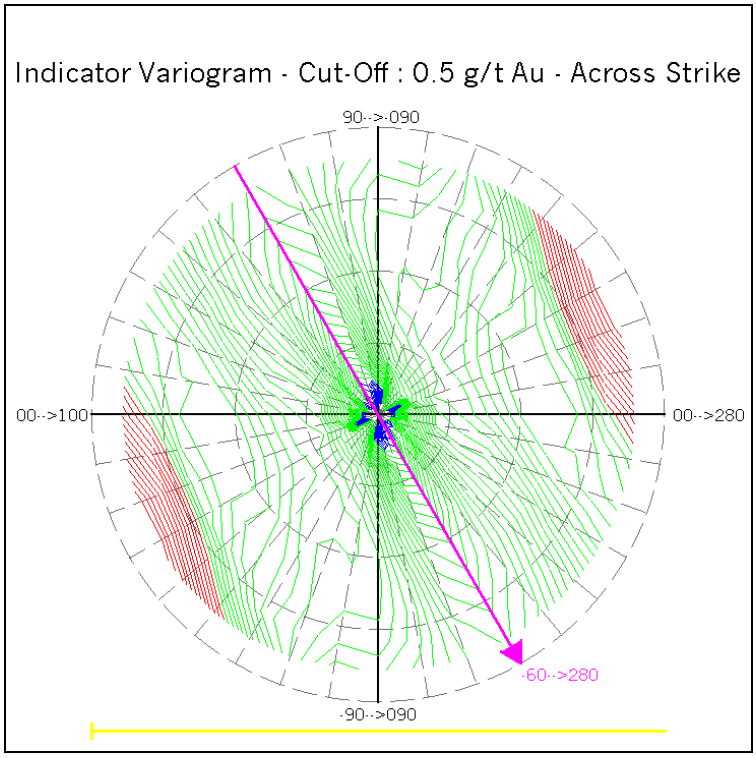

Figure C.48 Fan of Indicator Variograms – CORE Zone Cut-Off at 0.5 g/t Au – Across Strike

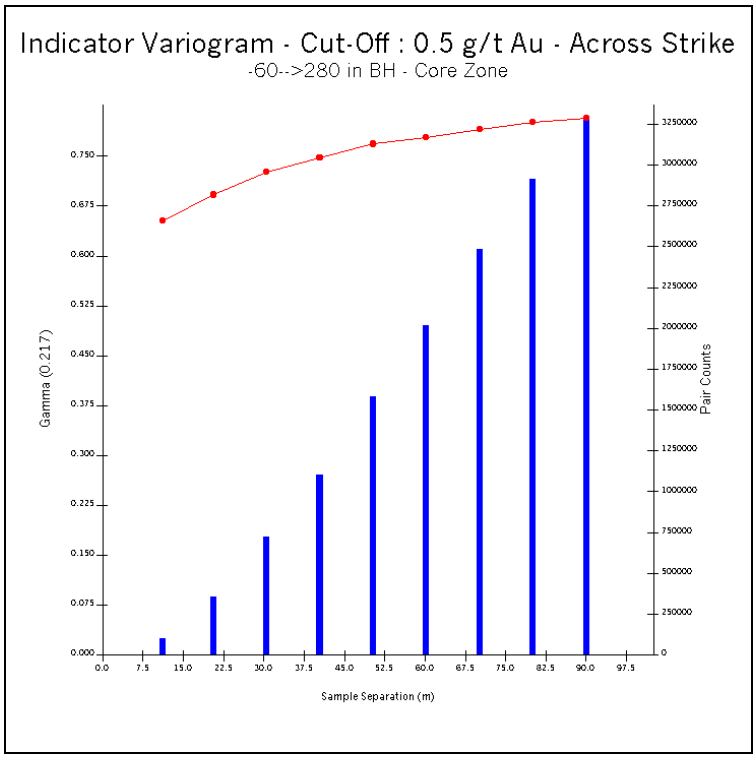

Figure C.49 Indicator Variogram – CORE Zone Cut-Off at 0.5 g/t Au – Across Strike

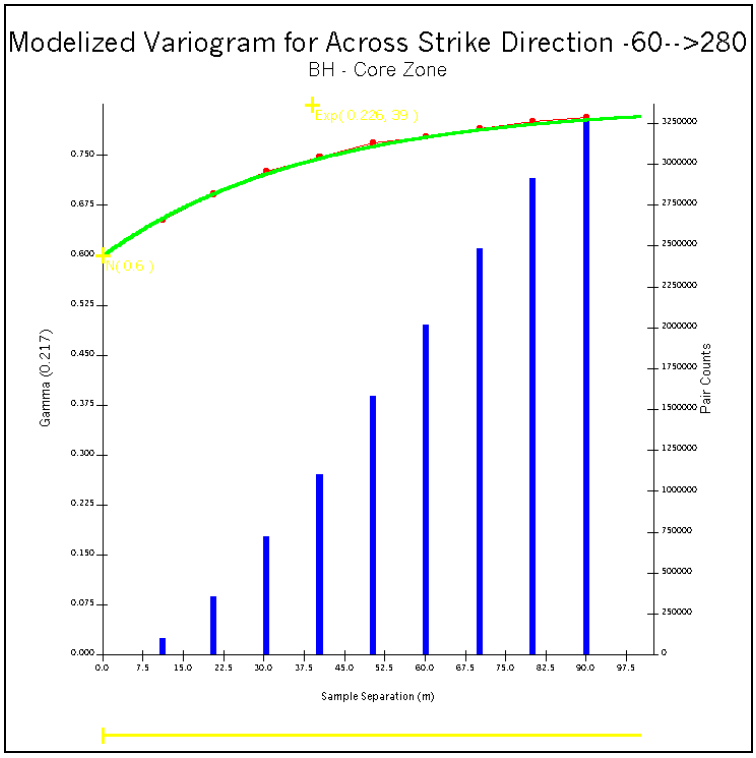

Figure C.50 Modelized Indicator Variogram – CORE Zone Cut-Off at 0.5 g/t Au – Across Strike

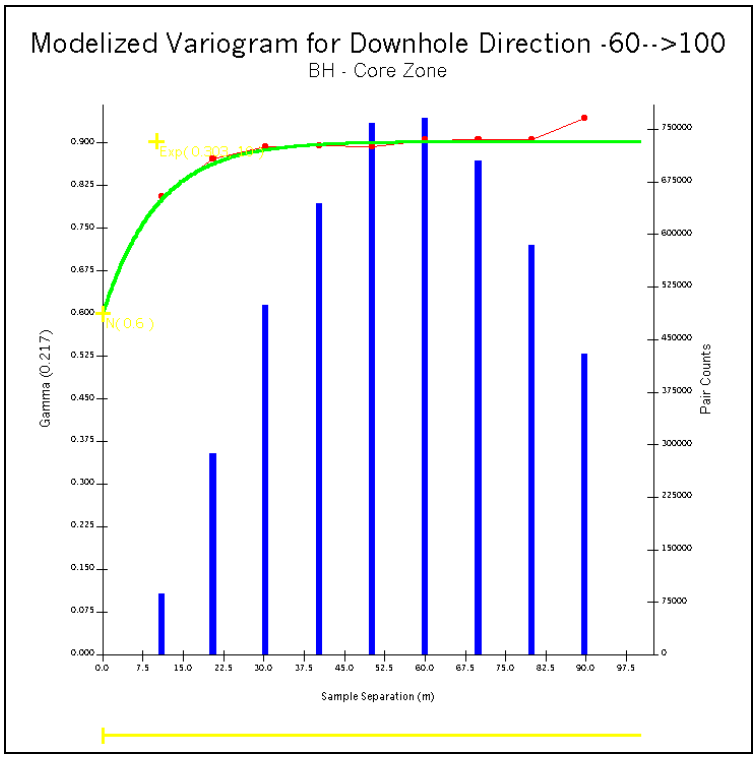

Figure C.51 Modelized Indicator Variogram – CORE Zone Cut-Off at 0.5 g/t Au – Downhole

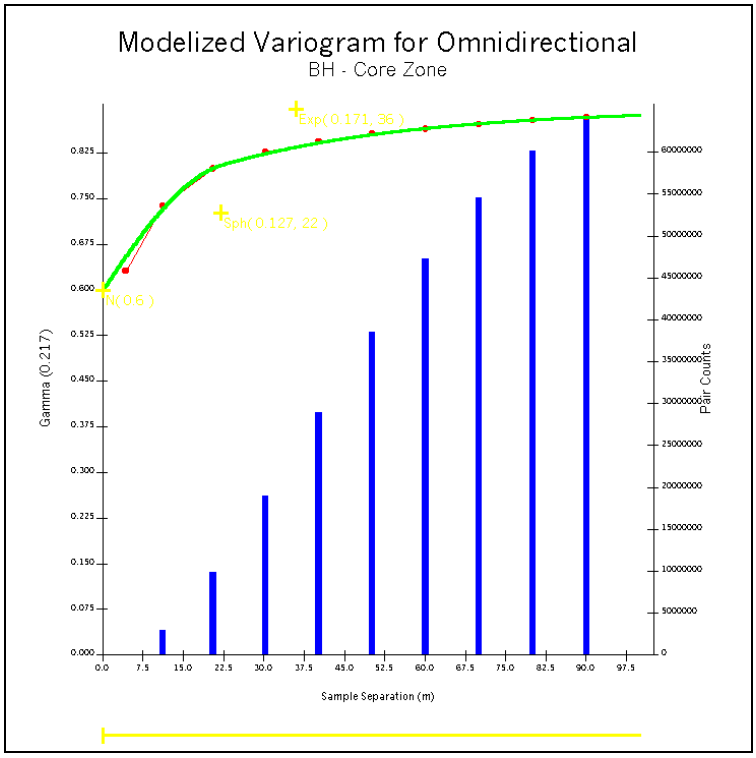

Figure C.52 Modelized Indicator Variogram – CORE Zone Cut-Off at 0.5 g/t Au – Omnidirectional

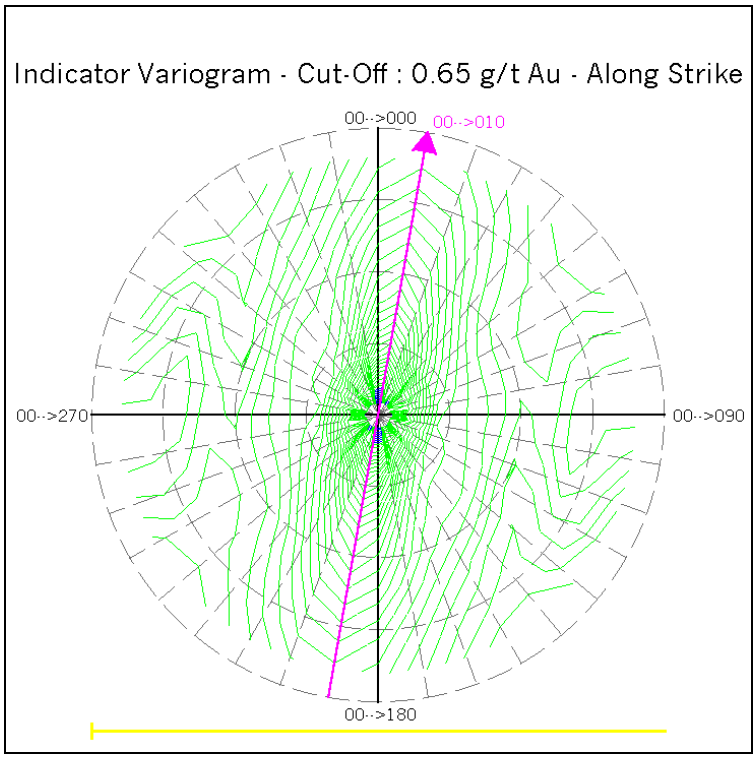

Figure C.53 Fan of Indicator Variograms – CORE Zone Cut-Off at 0.65 g/t Au – Along Strike

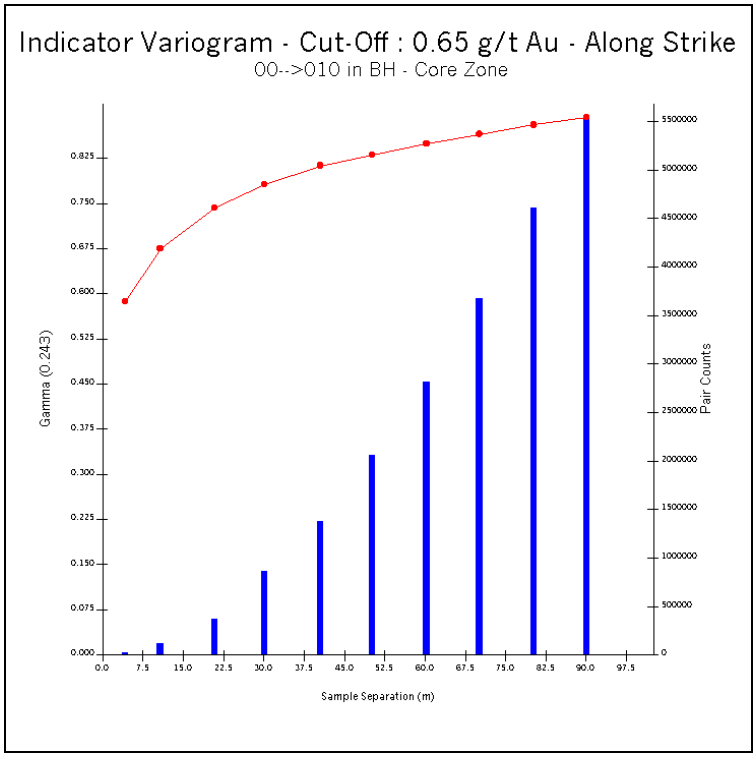

Figure C.54 Indicator Variogram – CORE Zone Cut-Off at 0.65 g/t Au – Along Strike

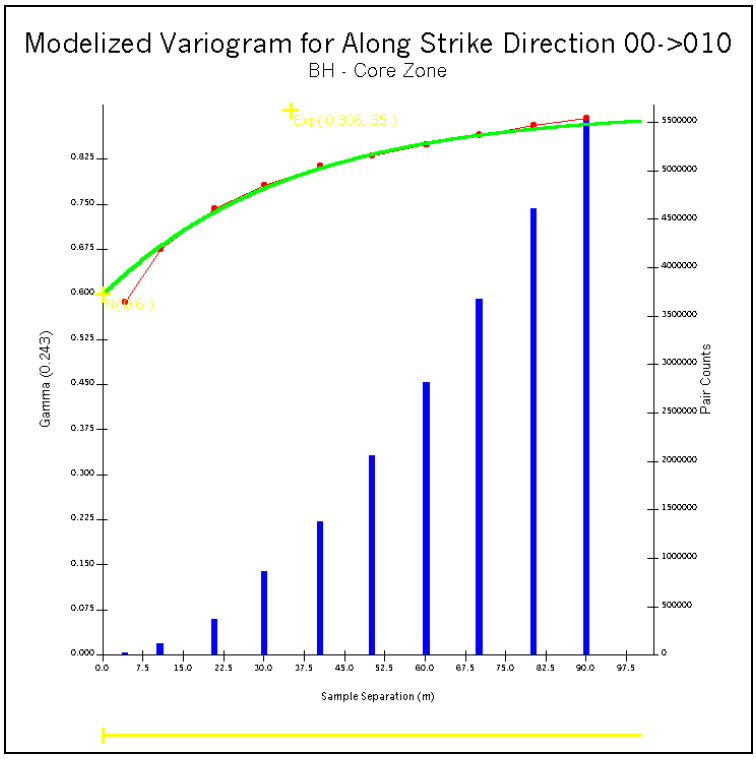

Figure C.55 Modelized Indicator Variogram – CORE Zone Cut-Off at 0.65 g/t Au – Along Strike

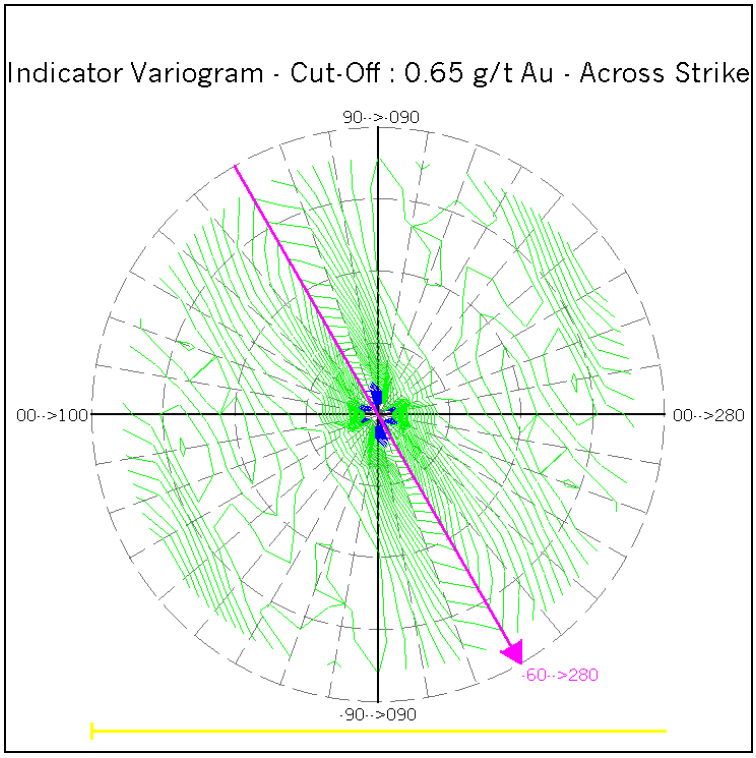

Figure C.56 Fan of Indicator Variograms – CORE Zone Cut-Off at 0.65 g/t Au – Across Strike

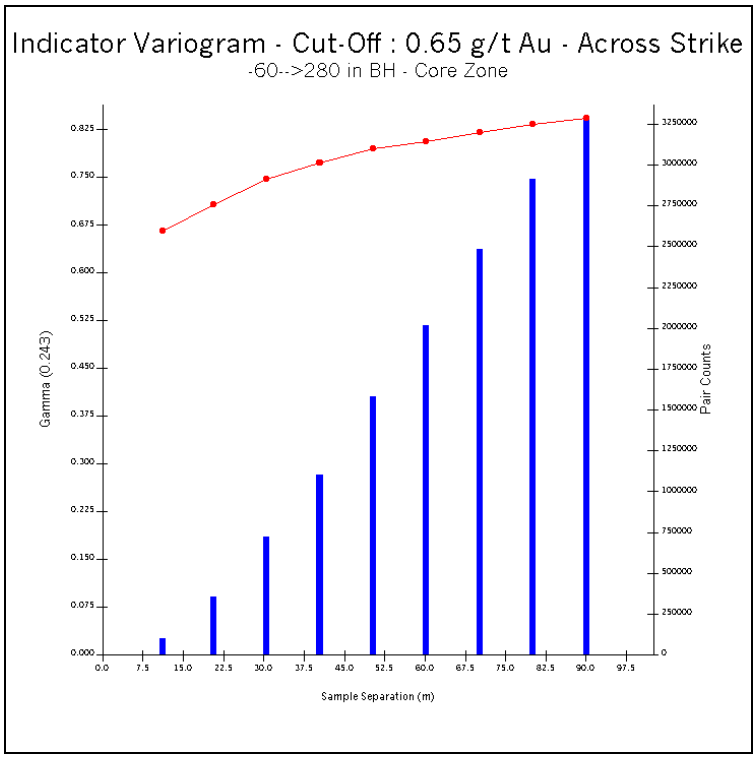

Figure C.57 Indicator Variogram – CORE Zone Cut-Off at 0.65 g/t Au – Across Strike

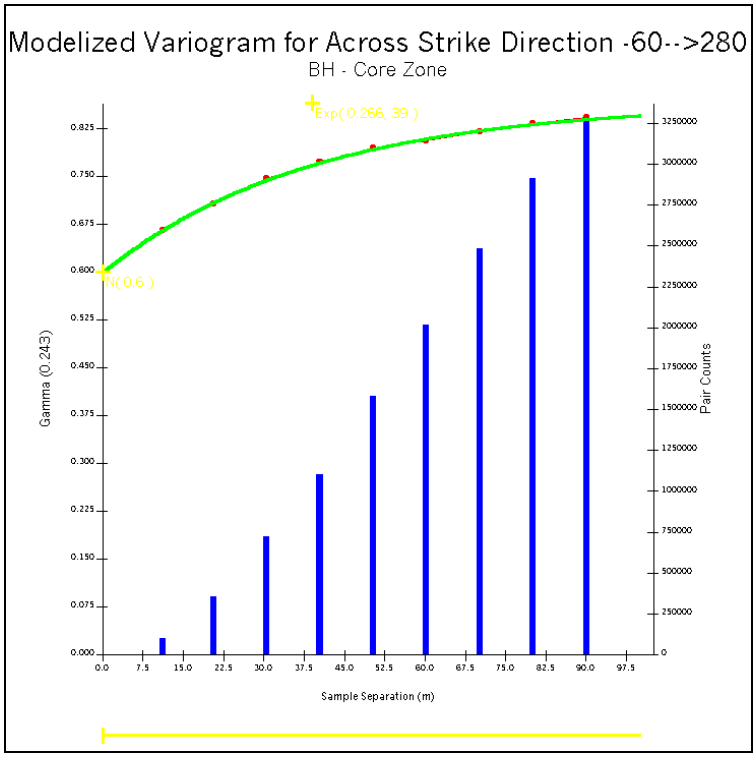

Figure C.58 Modelized Indicator Variogram – CORE Zone Cut-Off at 0.65 g/t Au – Across Strike

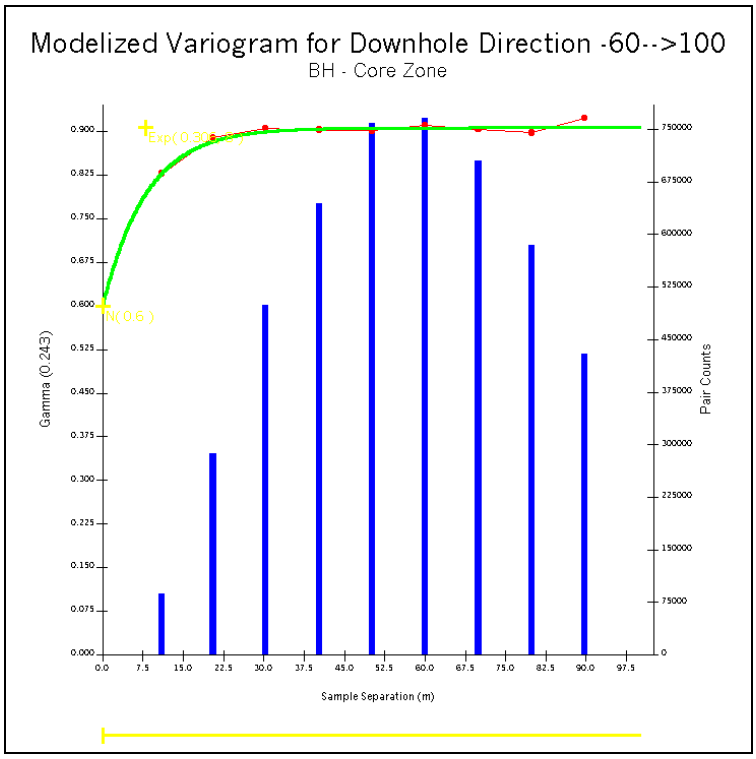

Figure C.59 Modelized Indicator Variogram – CORE Zone Cut-Off at 0.65 g/t Au – Downhole

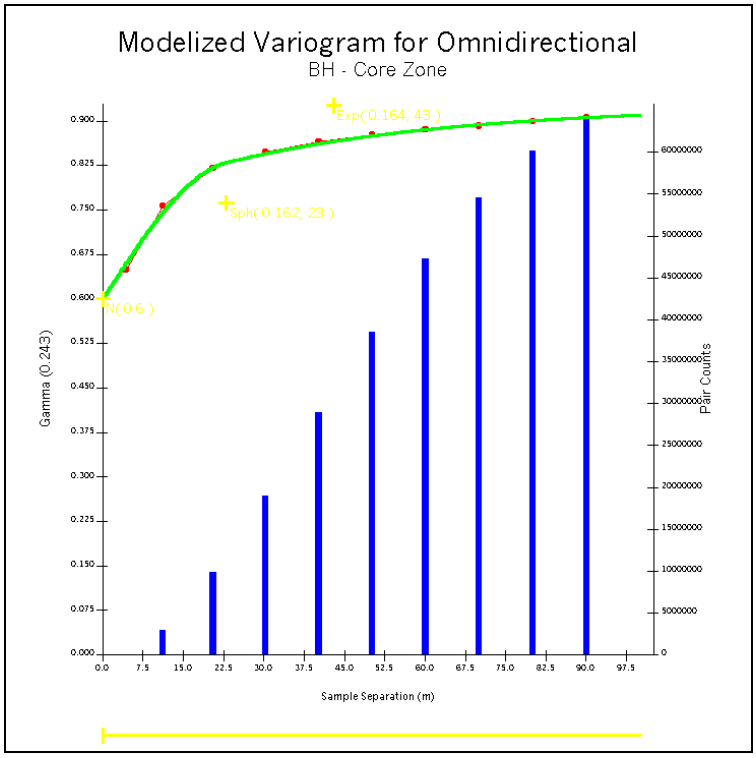

Figure C.60 Modelized Indicator Variogram – CORE Zone Cut-Off at 0.65 g/t Au – Omnidirectional

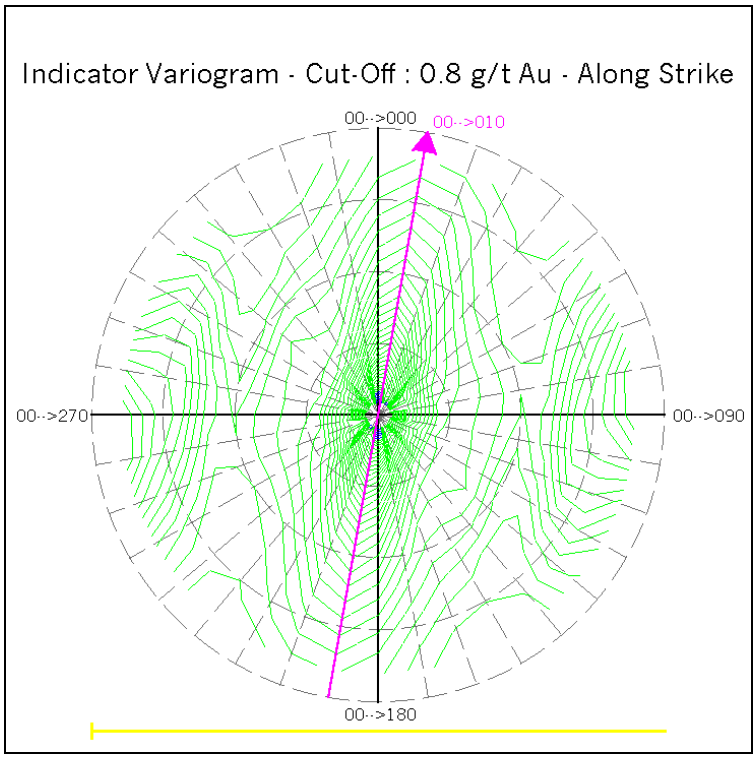

Figure C.61 Fan of Indicator Variograms – CORE Zone Cut-Off at 0.8 g/t Au – Along Strike

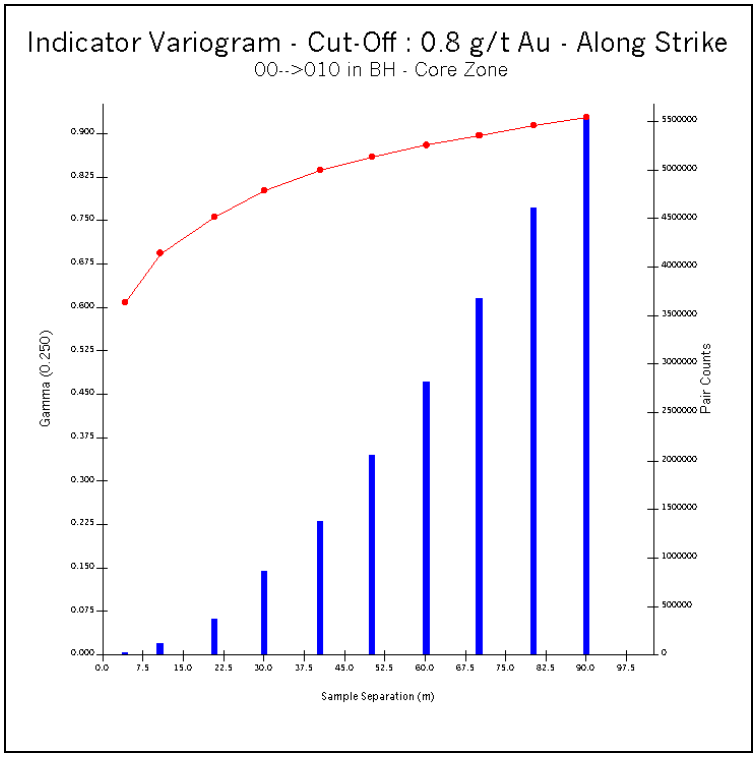

Figure C.62 Indicator Variogram – CORE Zone Cut-Off at 0.8 g/t Au – Along Strike

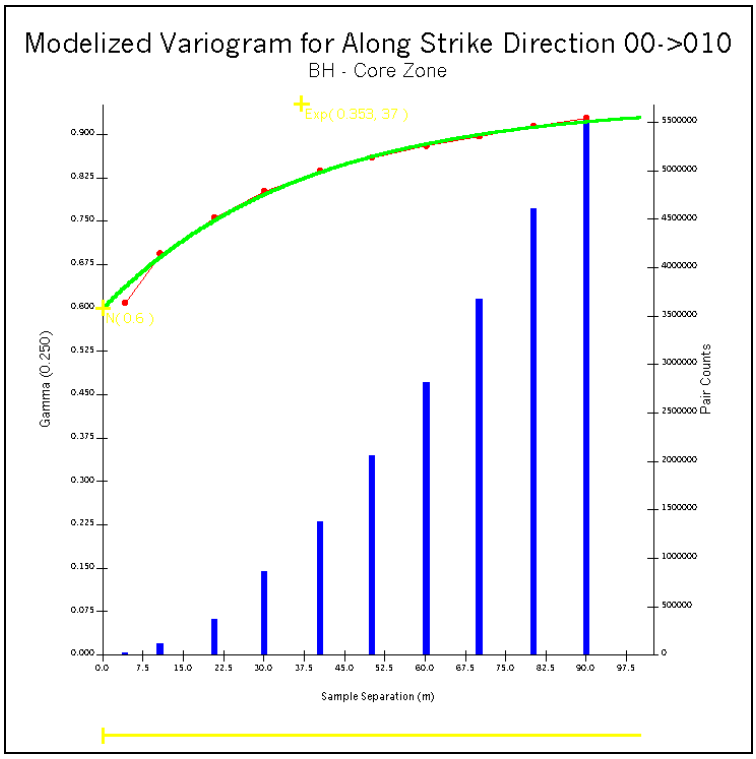

Figure C.63 Modelized Indicator Variogram – CORE Zone Cut-Off at 0.8 g/t Au – Along Strike

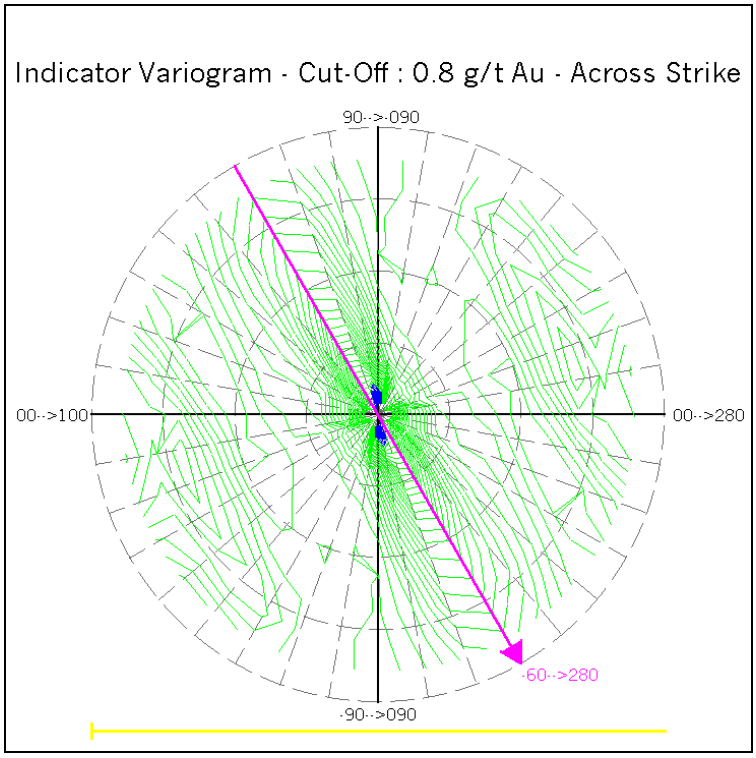

Figure C.64 Fan of Indicator Variograms – CORE Zone Cut-Off at 0.8 g/t Au – Across Strike

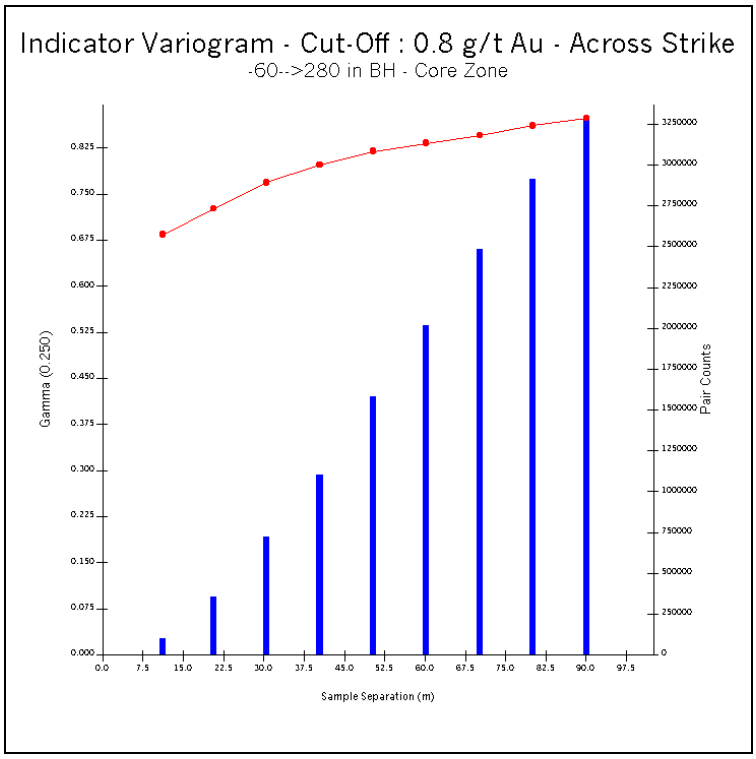

Figure C.65 Indicator Variogram – CORE Zone Cut-Off at 0.8 g/t Au – Across Strike

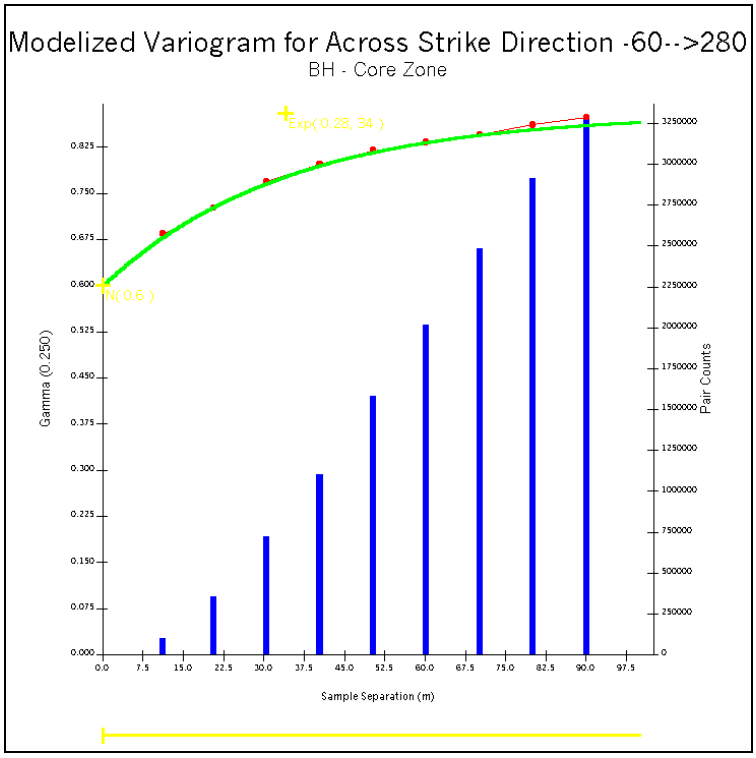

Figure C.66 Modelized Indicator Variogram – CORE Zone Cut-Off at 0.8 g/t Au – Across Strike

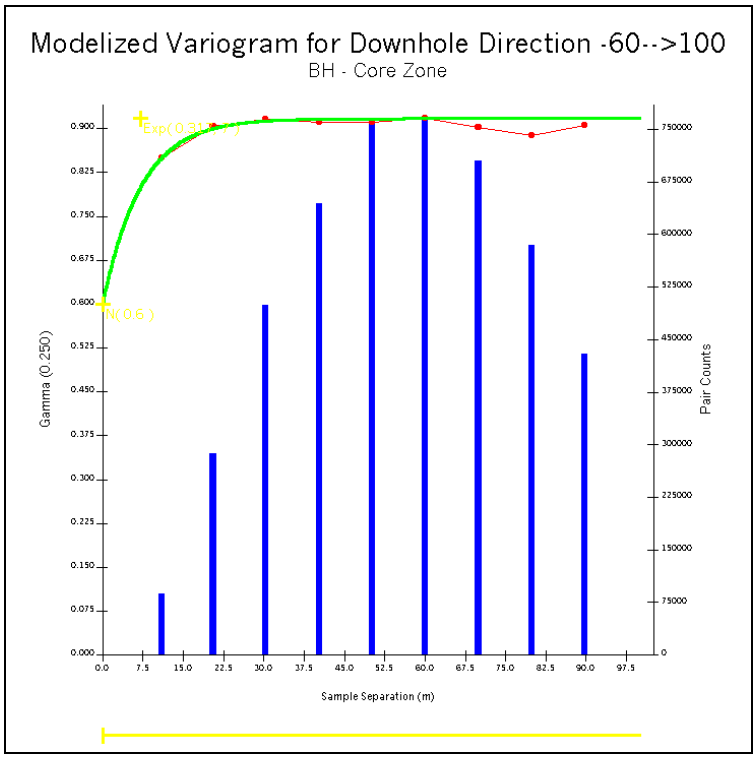

Figure C.67 Modelized Indicator Variogram – CORE Zone Cut-Off at 0.8 g/t Au – Downhole

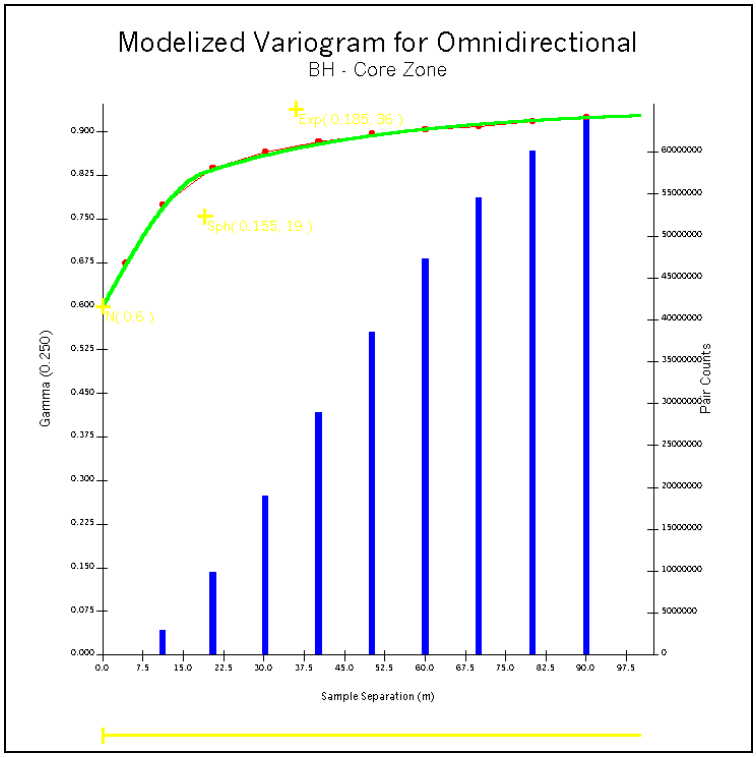

Figure C.68 Modelized Indicator Variogram – CORE Zone Cut-Off at 0.8 g/t Au – Omnidirectional

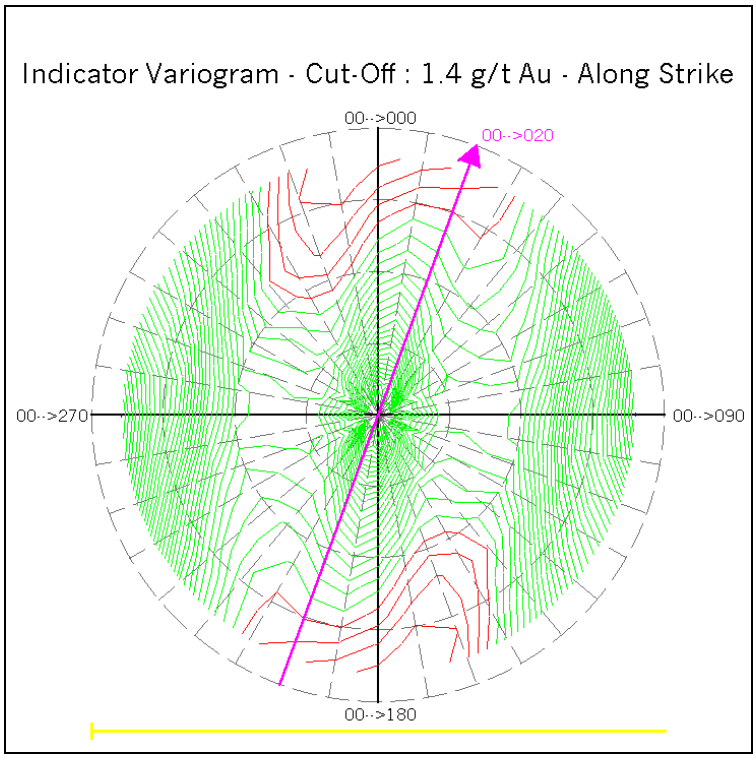

Figure C.69 Fan of Indicator Variograms – CORE Zone Cut-Off at 1.4 g/t Au – Along Strike

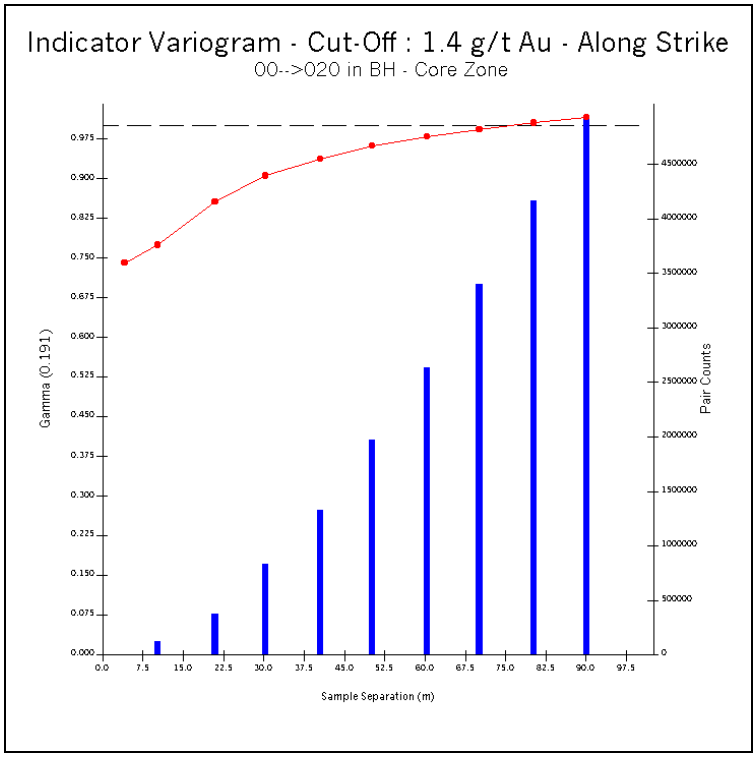

Figure C.70 Indicator Variogram – CORE Zone Cut-Off at 1.4 g/t Au – Along Strike

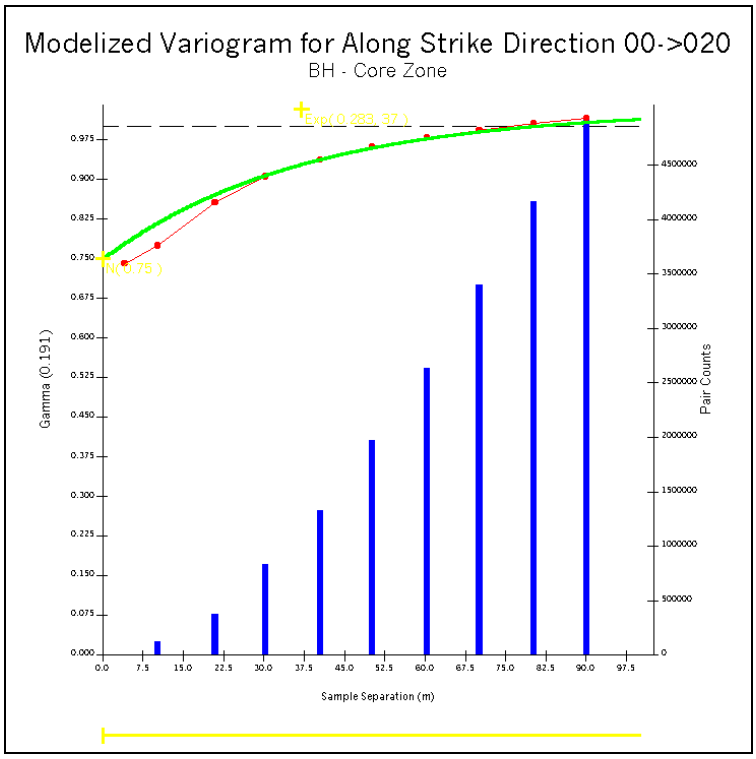

Figure C.71 Modelized Indicator Variogram – CORE Zone Cut-Off at 1.4 g/t Au – Along Strike

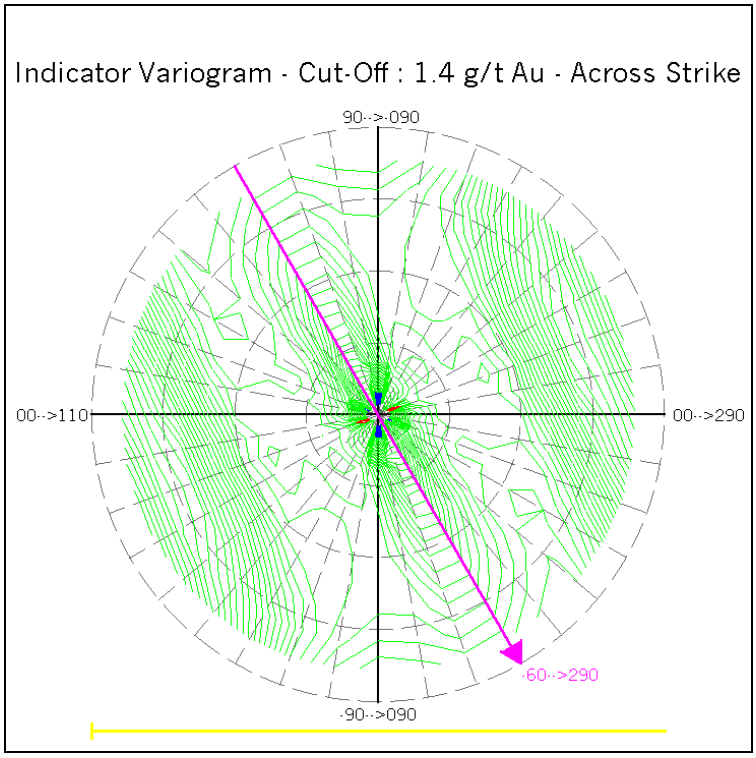

Figure C.72 Fan of Indicator Variograms – CORE Zone Cut-Off at 1.4 g/t Au – Across Strike

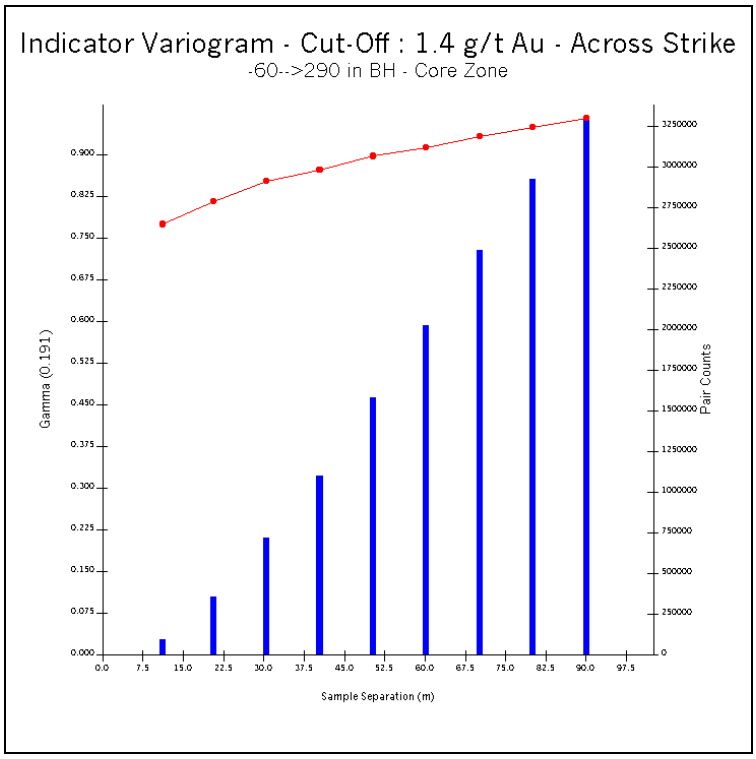

Figure C.73 Indicator Variogram – CORE Zone Cut-Off at 1.4 g/t Au – Across Strike

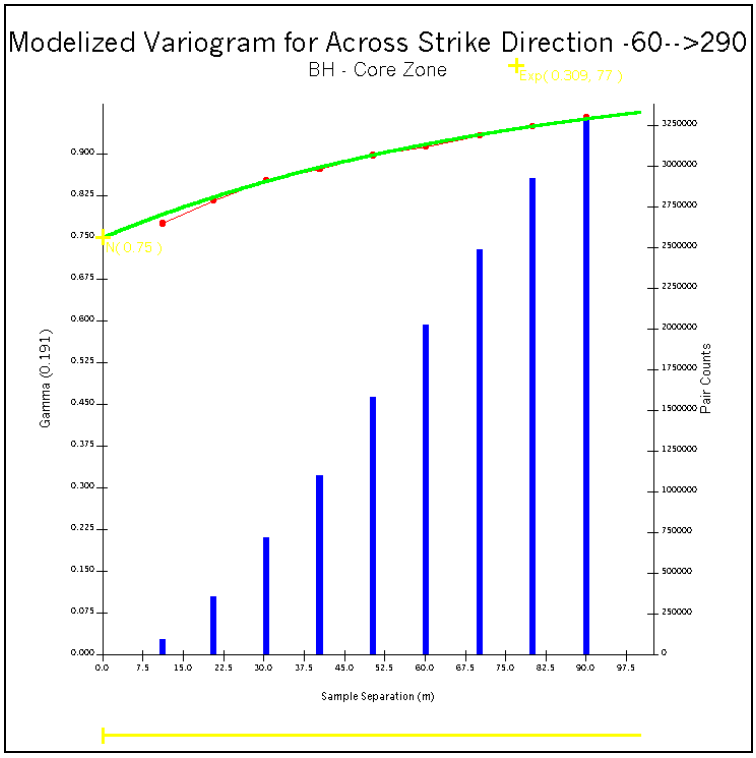

Figure C.74 Modelized Indicator Variogram – CORE Zone Cut-Off at 1.4 g/t Au – Across Strike

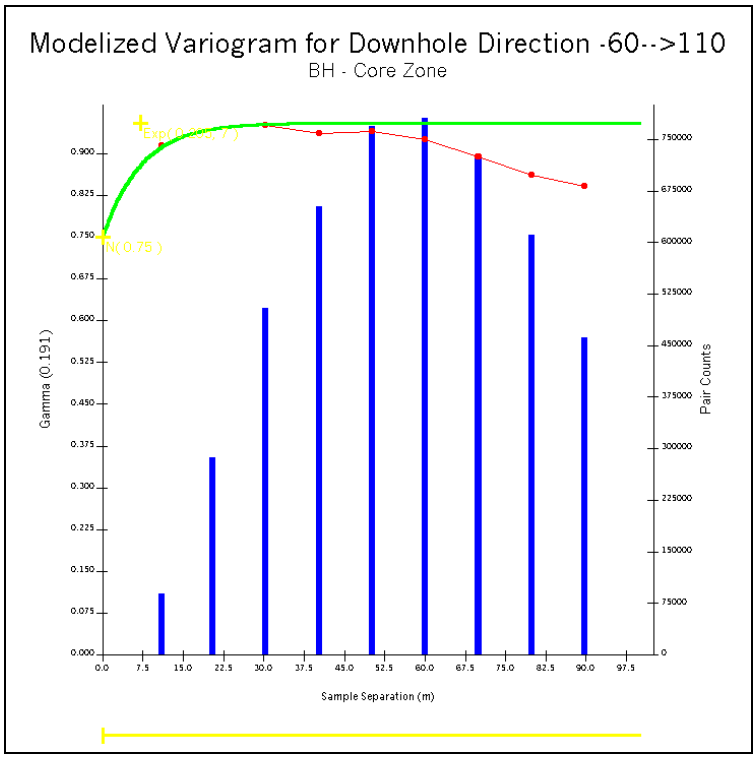

Figure C.75 Modelized Indicator Variogram – CORE Zone Cut-Off at 1.4 g/t Au – Downhole

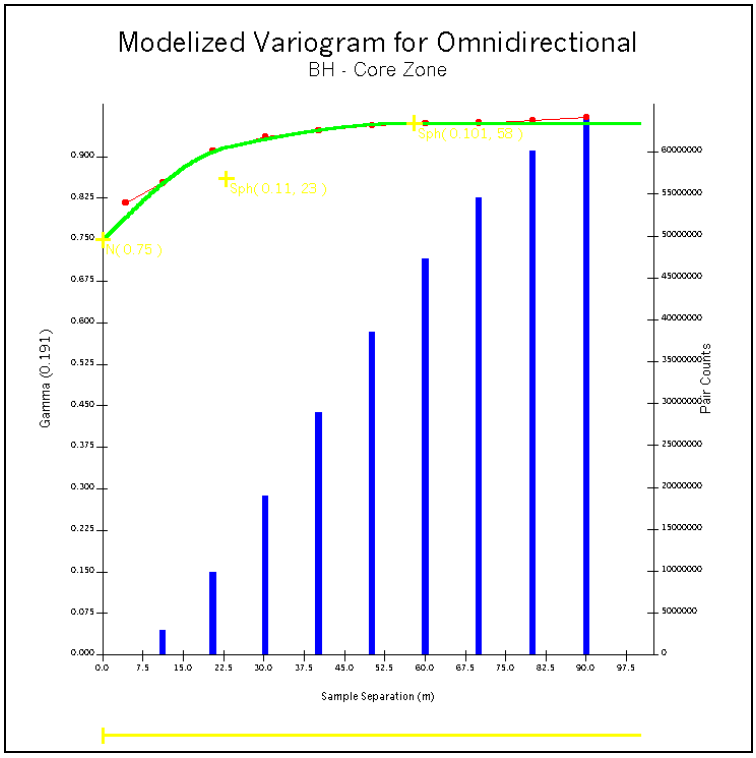

Figure C.76 Modelized Indicator Variogram – CORE Zone Cut-Off at 1.4 g/t Au – Omnidirectional

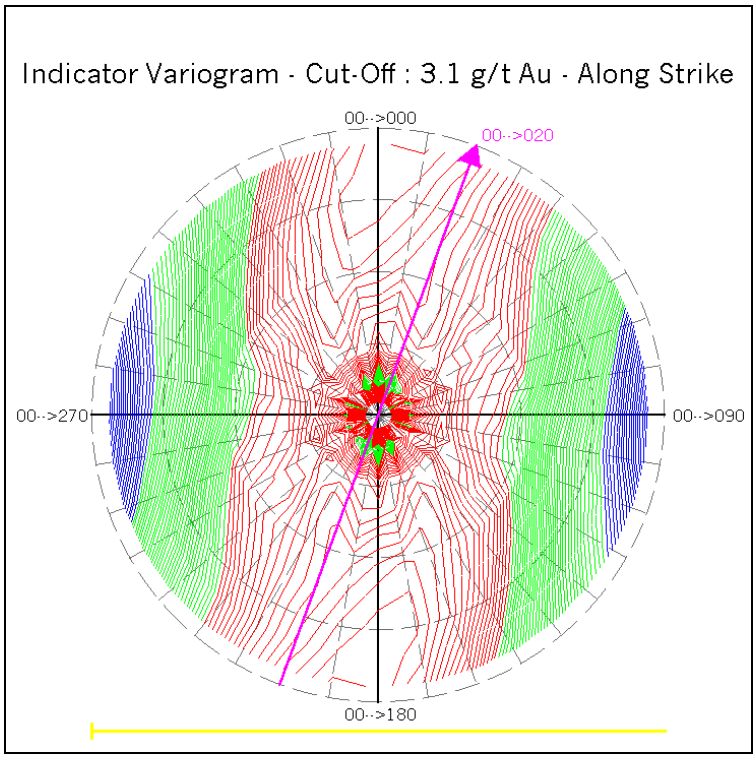

Figure C.77 Fan of Indicator Variograms – CORE Zone Cut-Off at 3.1 g/t Au – Along Strike

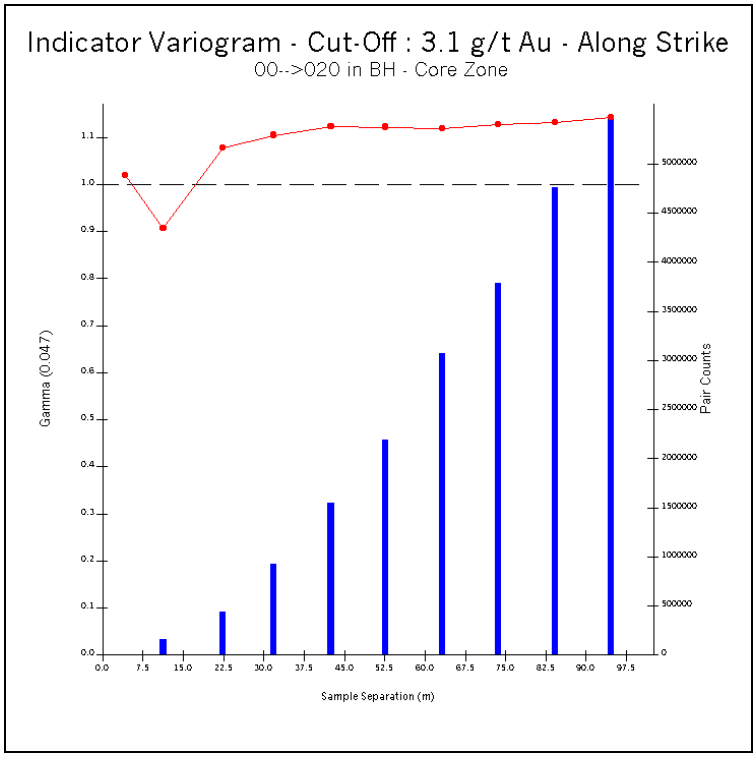

Figure C.78 Indicator Variogram – CORE Zone Cut-Off at 3.1 g/t Au – Along Strike

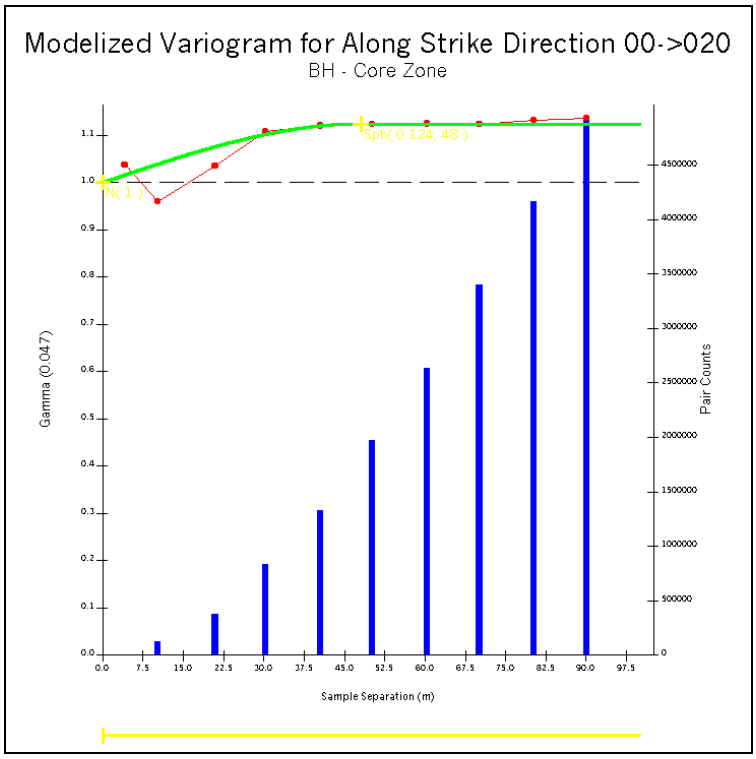

Figure C.79 Modelized Indicator Variogram – CORE Zone Cut-Off at 3.1 g/t Au – Along Strike

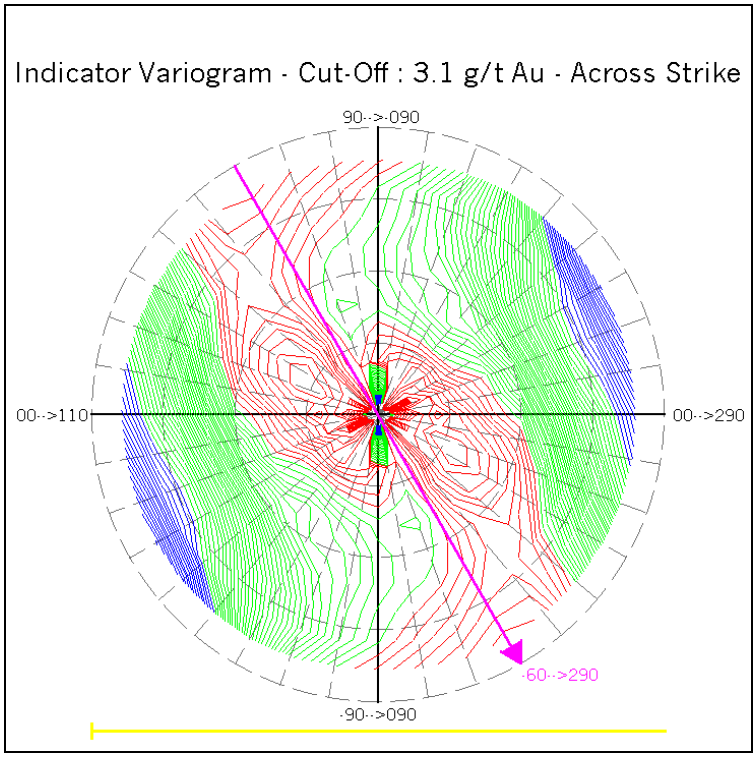

Figure C.80 Fan of Indicator Variograms – CORE Zone Cut-Off at 3.1 g/t Au – Across Strike

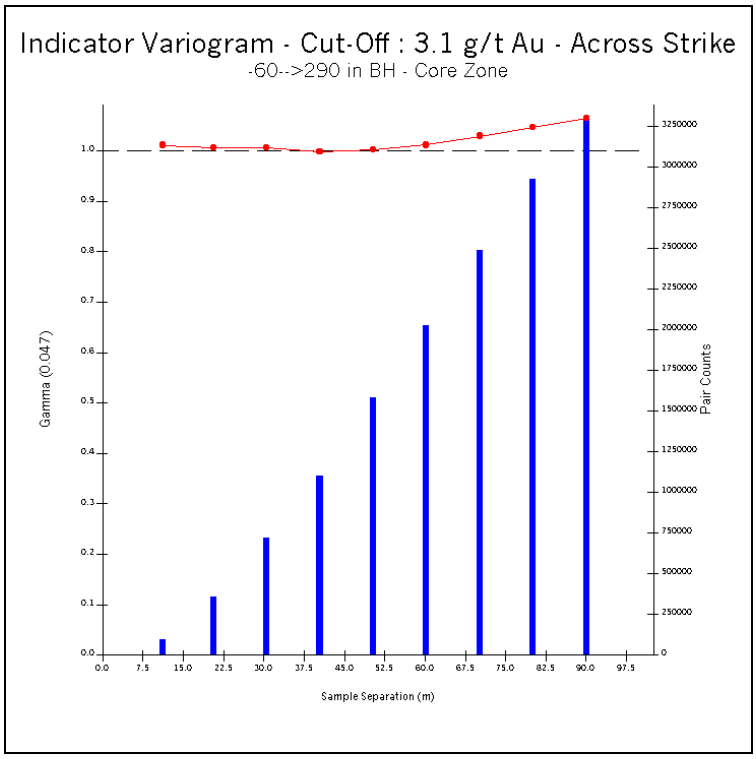

Figure C.81 Indicator Variogram – CORE Zone Cut-Off at 3.1 g/t Au – Across Strike

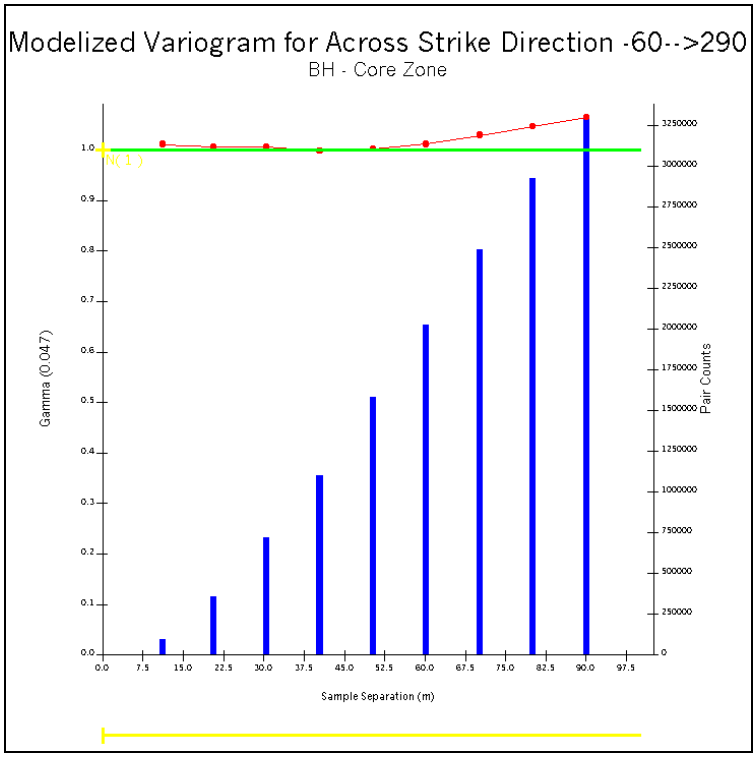

Figure C.82 Modelized Indicator Variogram – CORE Zone Cut-Off at 3.1 g/t Au – Across Strike

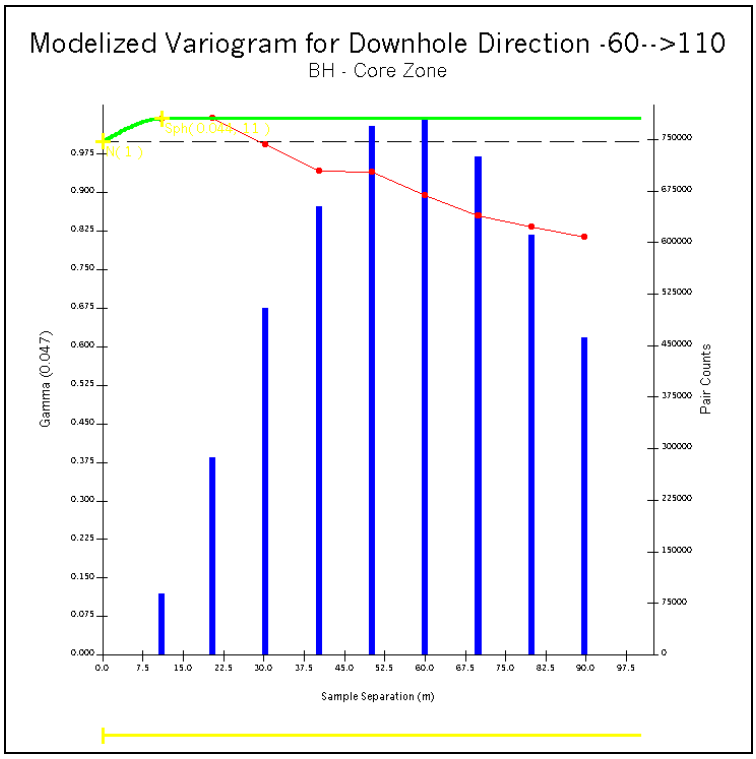

Figure C.83 Modelized Indicator Variogram – CORE Zone Cut-Off at 3.1 g/t Au – Downhole

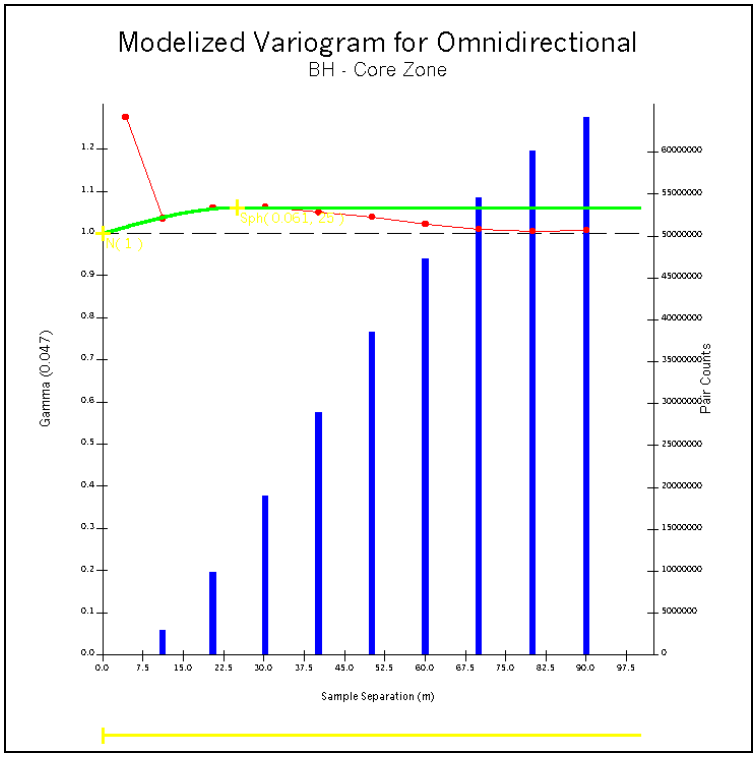

Figure C.84 Modelized Indicator Variogram – CORE Zone Cut-Off at 3.1 g/t Au – Omnidirectional

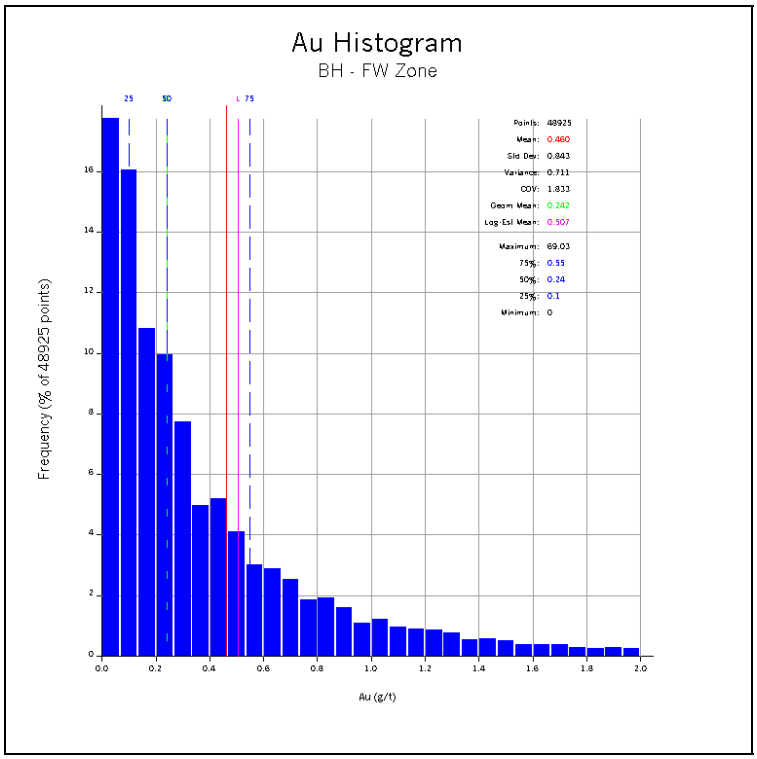

Figure C.85 Au Normal Histogram – FW Zone

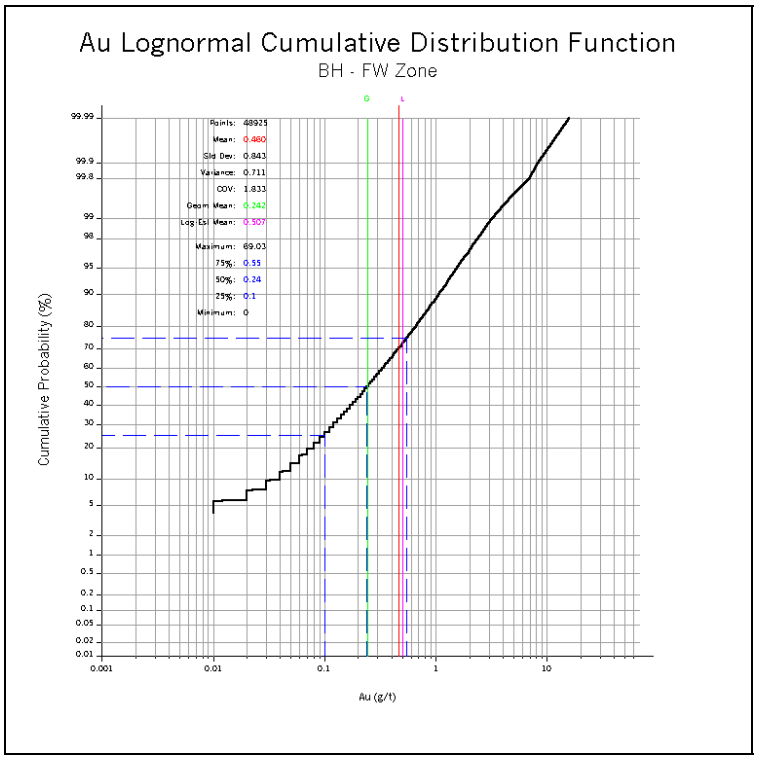

Figure C.86 Au Lognormal Cumulative Distribution Function – FW Zone

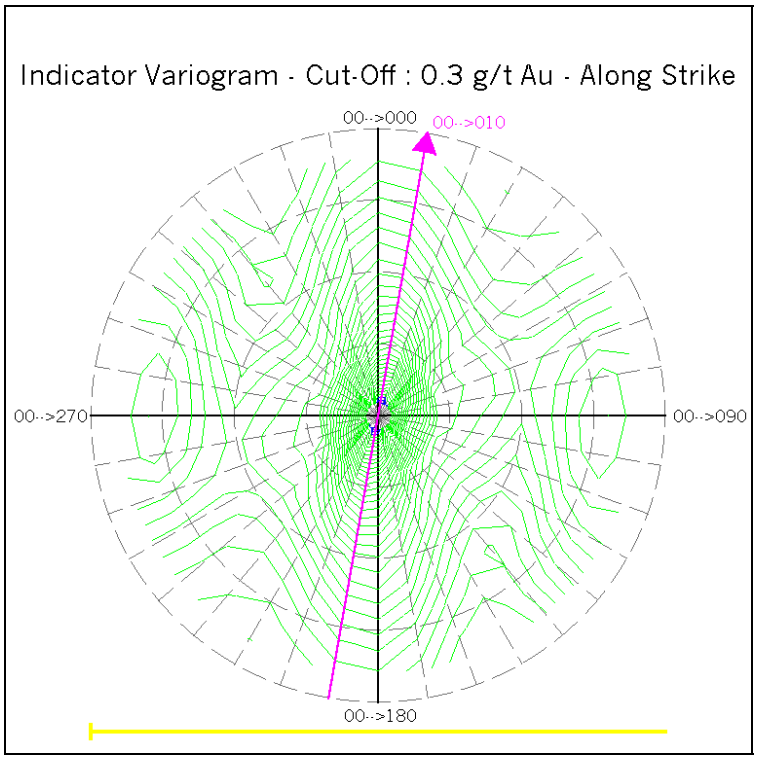

Figure C.87 Fan of Indicator Variograms – FW Zone Cut-Off at 0.3 g/t Au – Along Strike

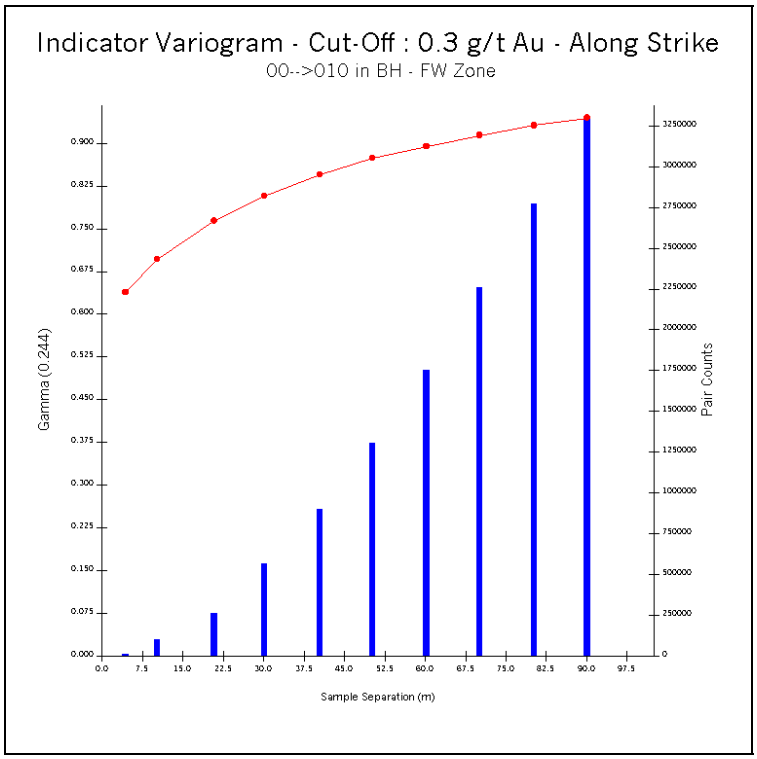

Figure C.88 Indicator Variogram – FW Zone Cut-Off at 0.3 g/t Au – Along Strike

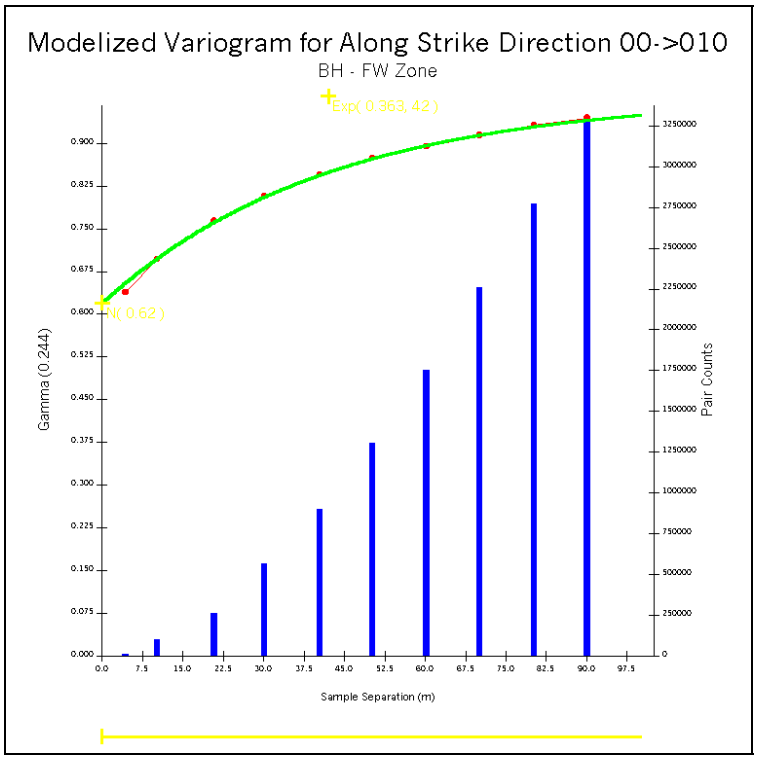

Figure C.89 Modelized Indicator Variogram – FW Zone Cut-Off at 0.3 g/t Au – Along Strike

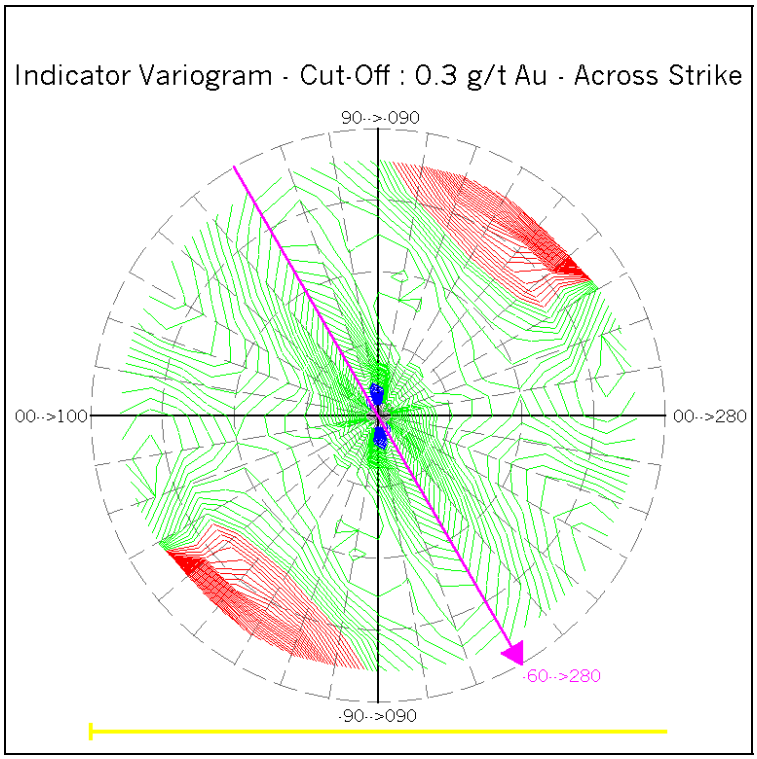

Figure C.90 Fan of Indicator Variograms – FW Zone Cut-Off at 0.3 g/t Au – Across Strike

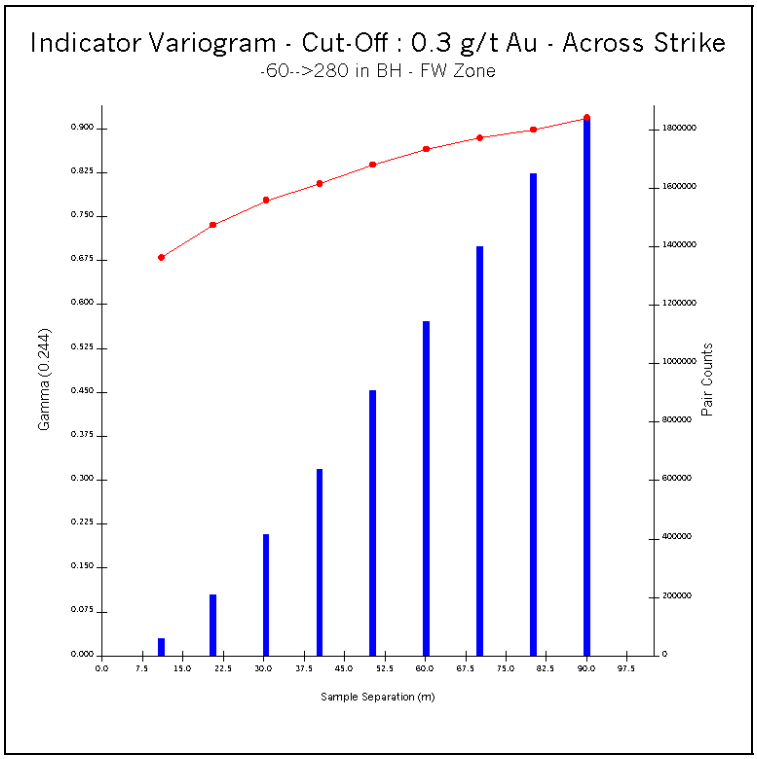

Figure C.91 Indicator Variogram – FW Zone Cut-Off at 0.3 g/t Au – Across Strike

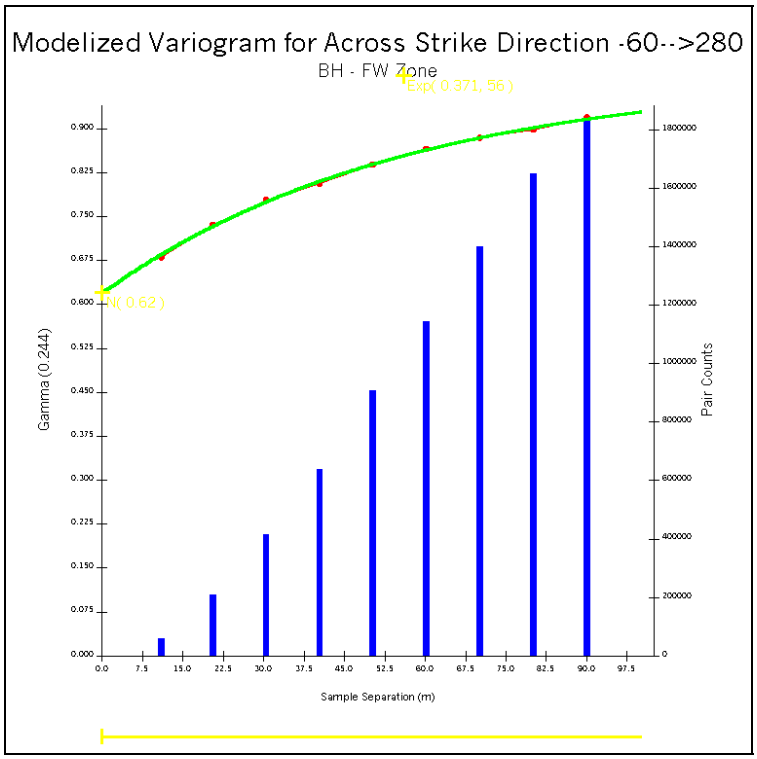

Figure C.92 Modelized Indicator Variogram – FW Zone Cut-Off at 0.3 g/t Au – Across Strike

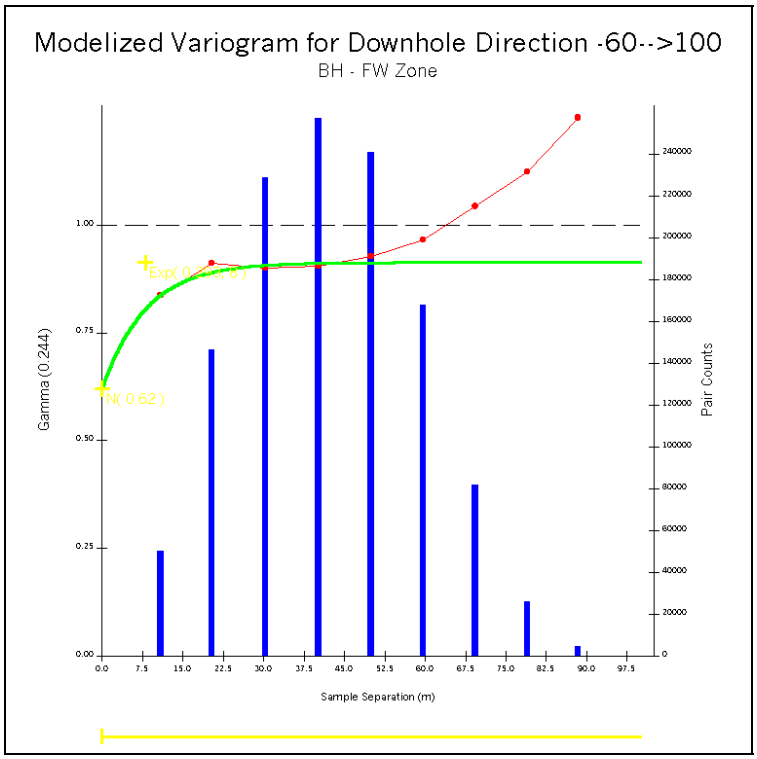

Figure C.93 Modelized Indicator Variogram – FW Zone Cut-Off at 0.3 g/t Au – Downhole

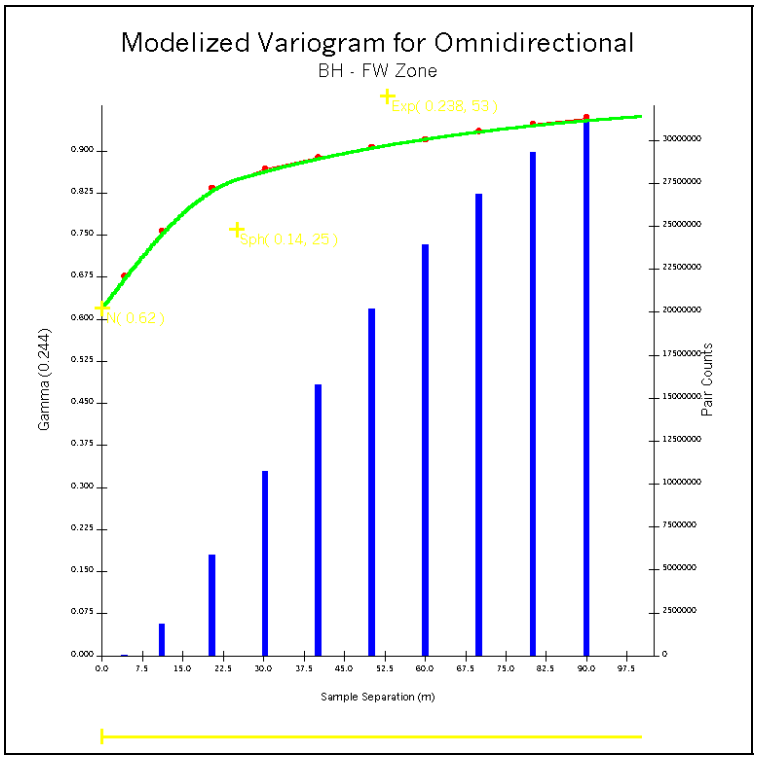

Figure C.94 Modelized Indicator Variogram – FW Zone Cut-Off at 0.3 g/t Au – Omnidirectional

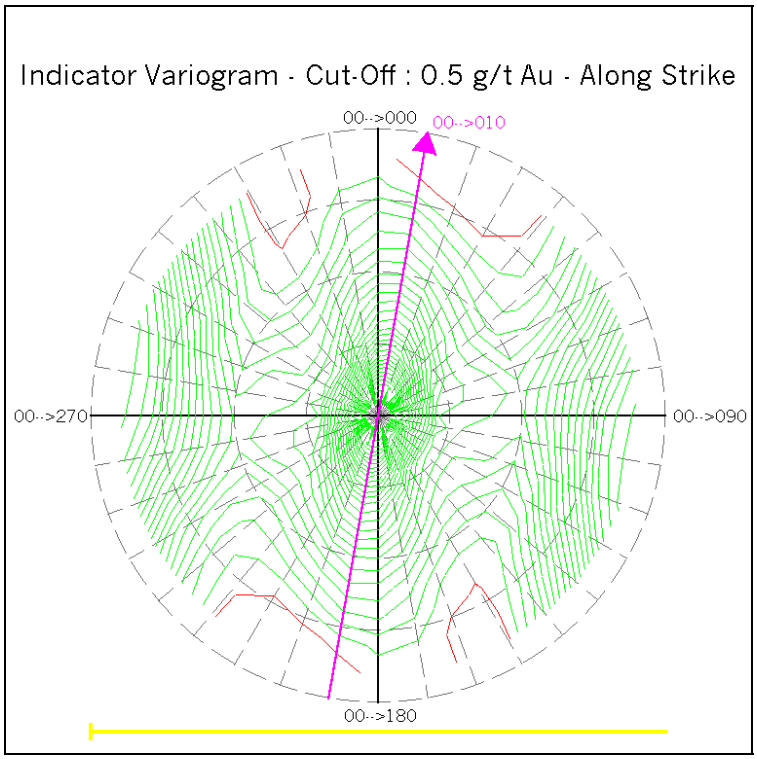

Figure C.95 Fan of Indicator Variograms – FW Zone Cut-Off at 0.5 g/t Au – Along Strike

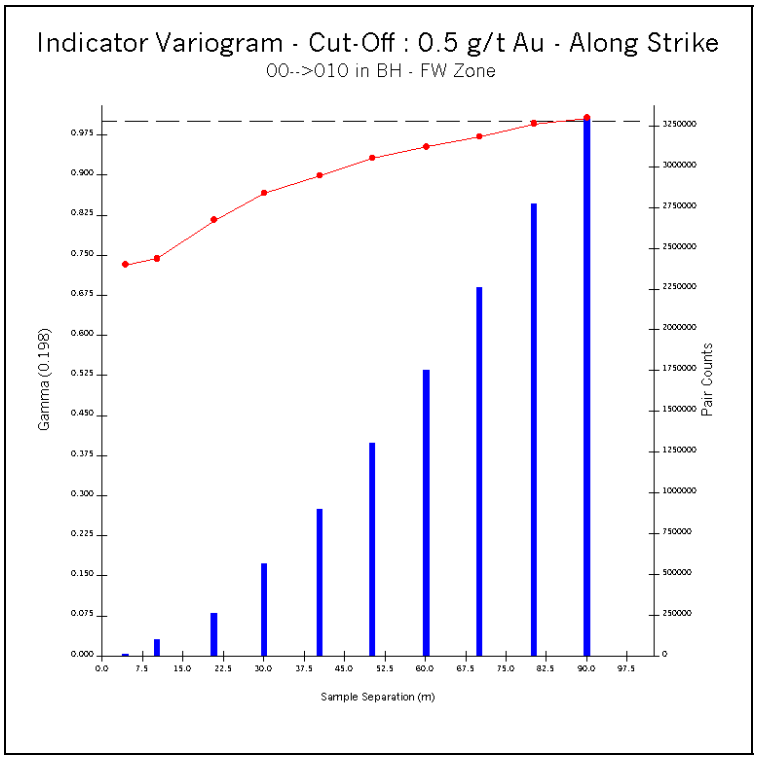

Figure C.96 Indicator Variogram – FW Zone Cut-Off at 0.5 g/t Au – Along Strike

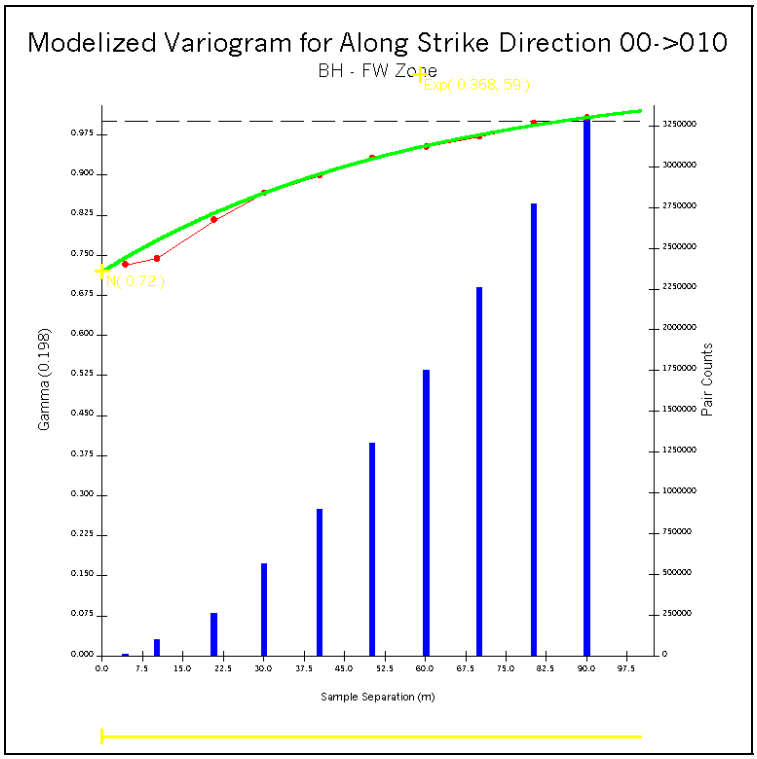

Figure C.97 Modelized Indicator Variogram – FW Zone Cut-Off at 0.5 g/t Au – Along Strike

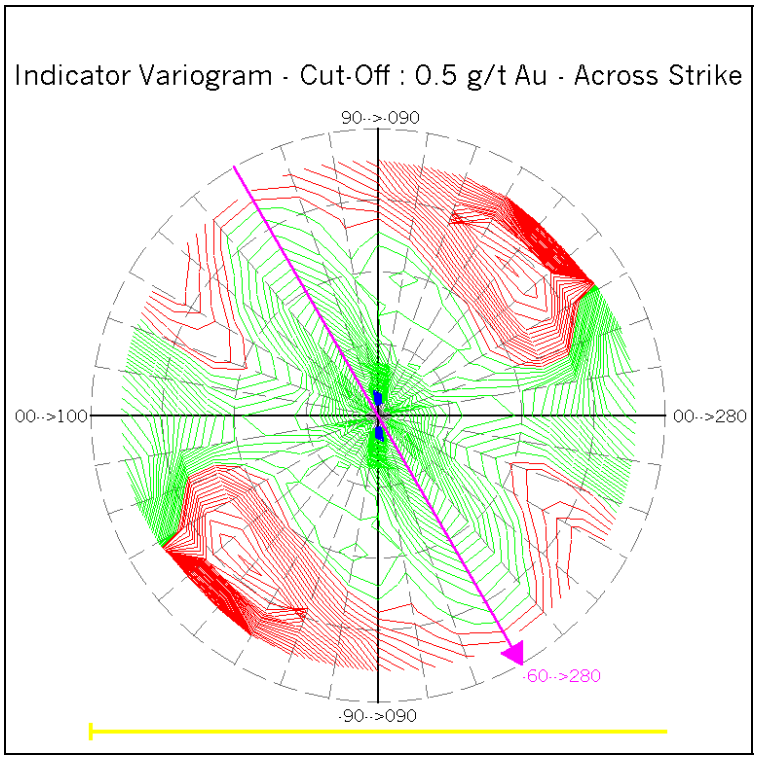

Figure C.98 Fan of Indicator Variograms – FW Zone Cut-Off at 0.5 g/t Au – Across Strike

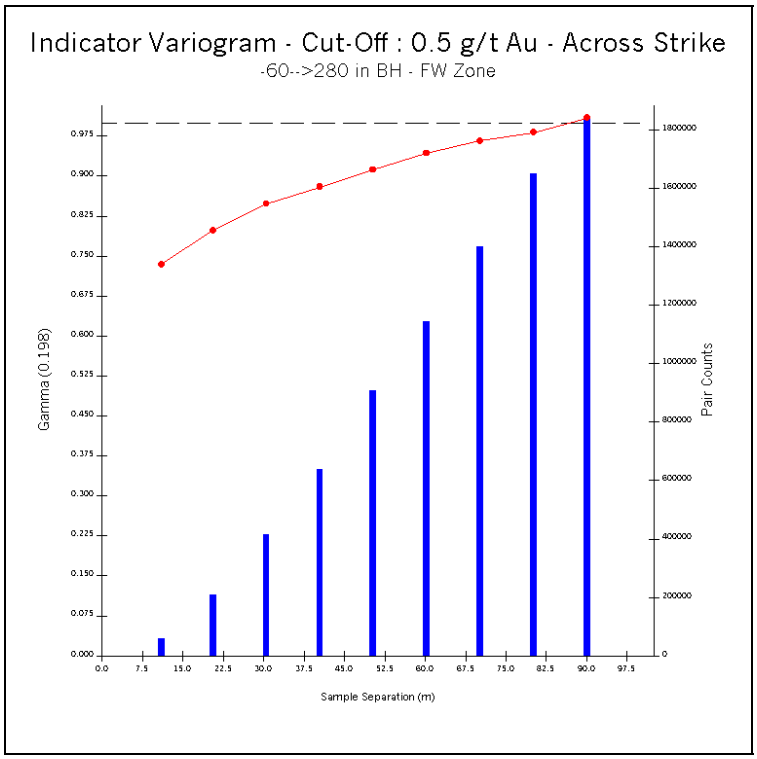

Figure C.99 Indicator Variogram – FW Zone Cut-Off at 0.5 g/t Au – Across Strike

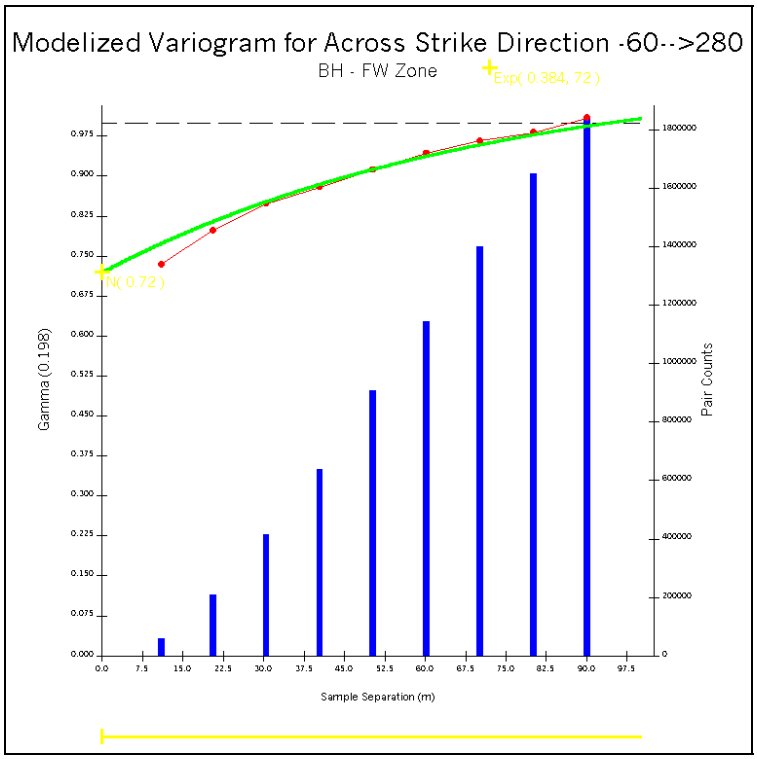

Figure C.100 Modelized Indicator Variogram – FW Zone Cut-Off at 0.5 g/t Au – Across Strike

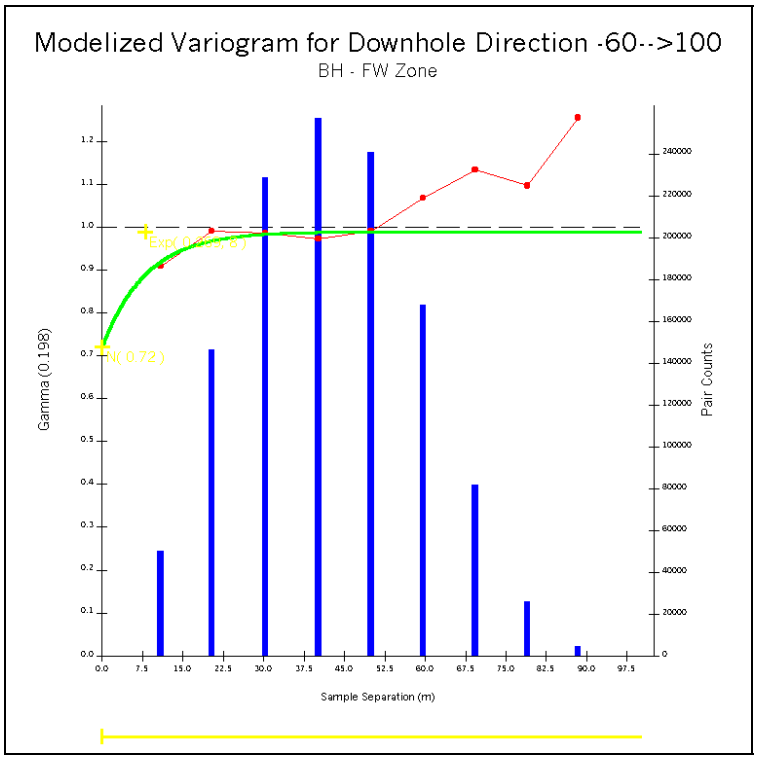

Figure C.101 Modelized Indicator Variogram – FW Zone Cut-Off at 0.5 g/t Au – Downhole

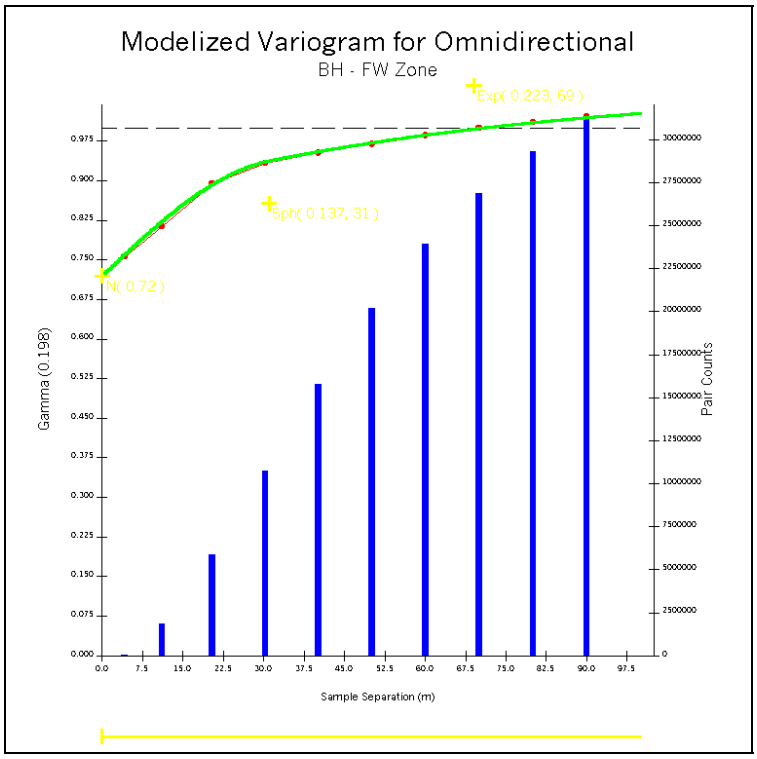

Figure C.102 Modelized Indicator Variogram – FW Zone Cut-Off at 0.5 g/t Au – Omnidirectional

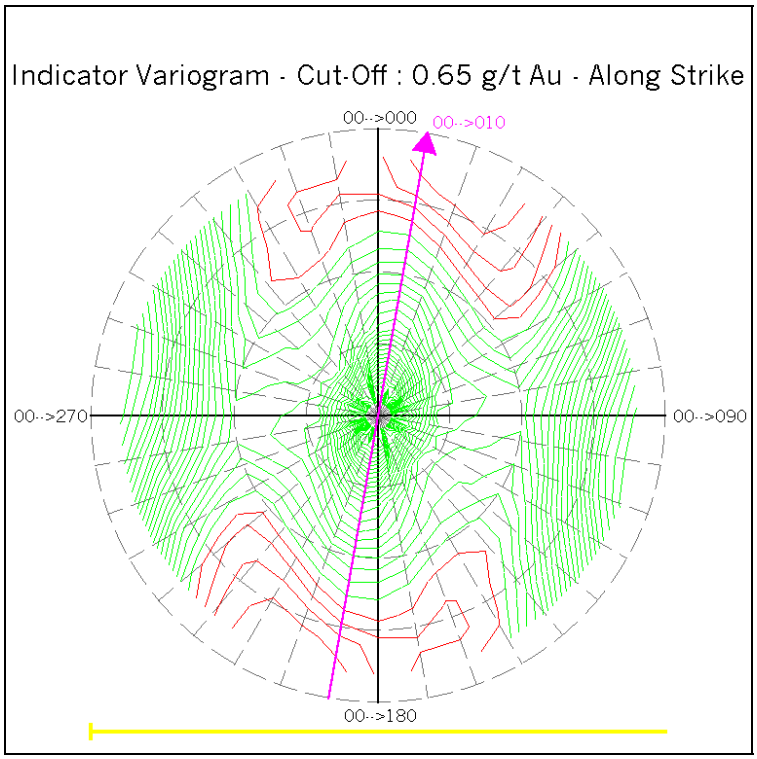

Figure C.103 Fan of Indicator Variograms – FW Zone Cut-Off at 0.65 g/t Au – Along Strike

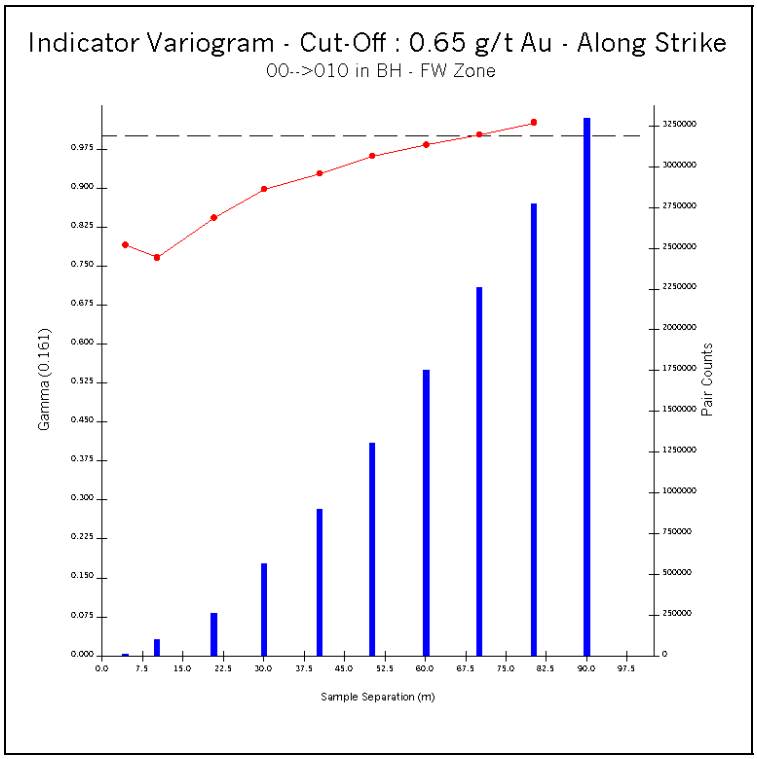

Figure C.104 Indicator Variogram – FW Zone Cut-Off at 0.65 g/t Au – Along Strike

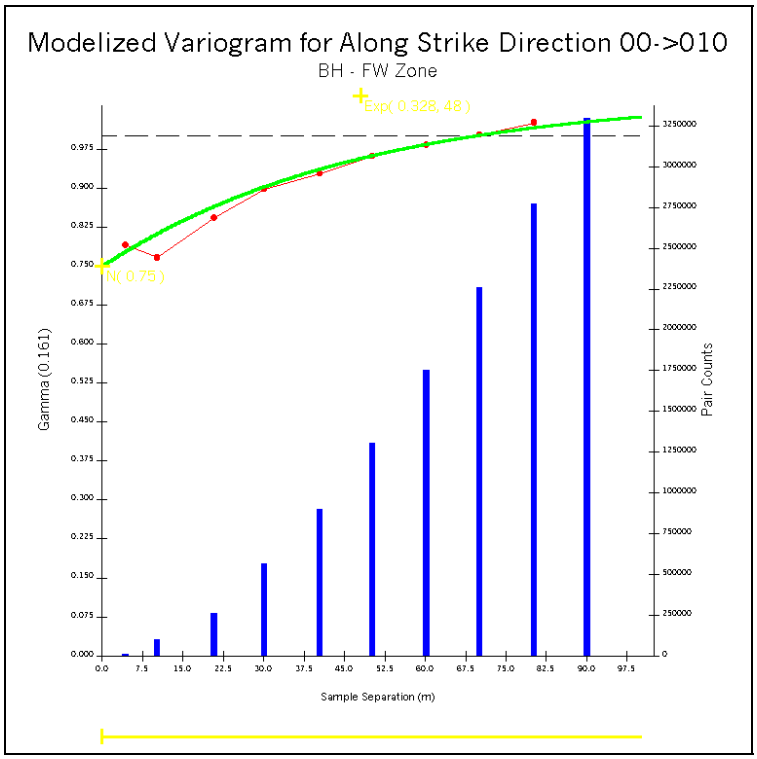

Figure C.105 Modelized Indicator Variogram – FW Zone Cut-Off at 0.65 g/t Au – Along Strike

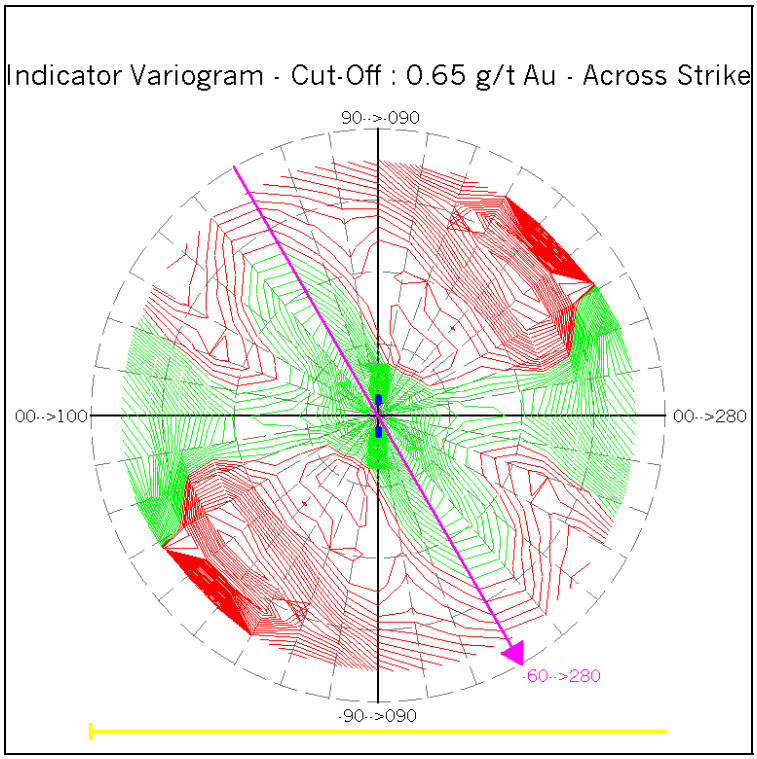

Figure C.106 Fan of Indicator Variograms – FW Zone Cut-Off at 0.65 g/t Au – Across Strike

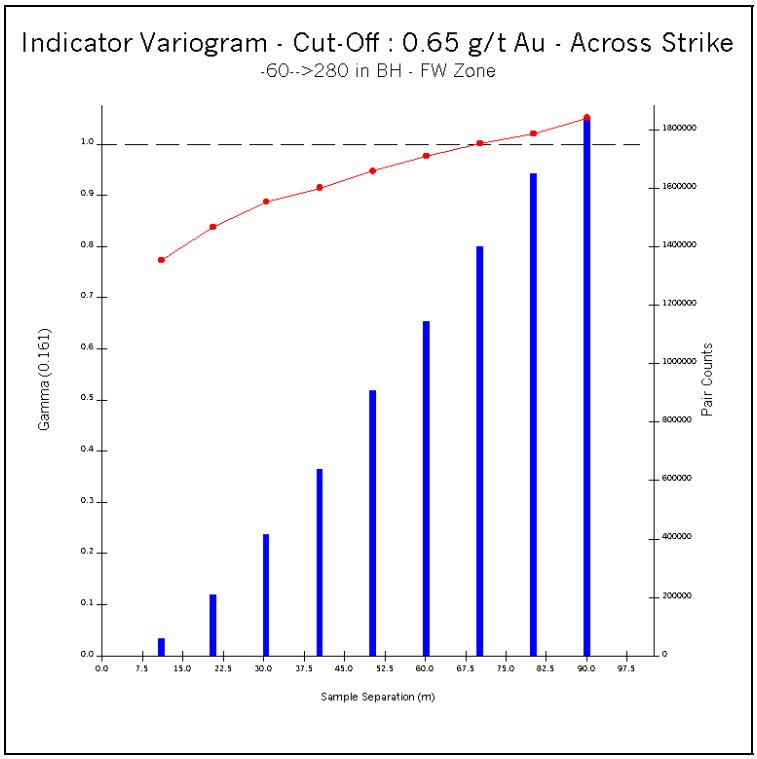

Figure C.107 Indicator Variogram – FW Zone Cut-Off at 0.65 g/t Au – Across Strike

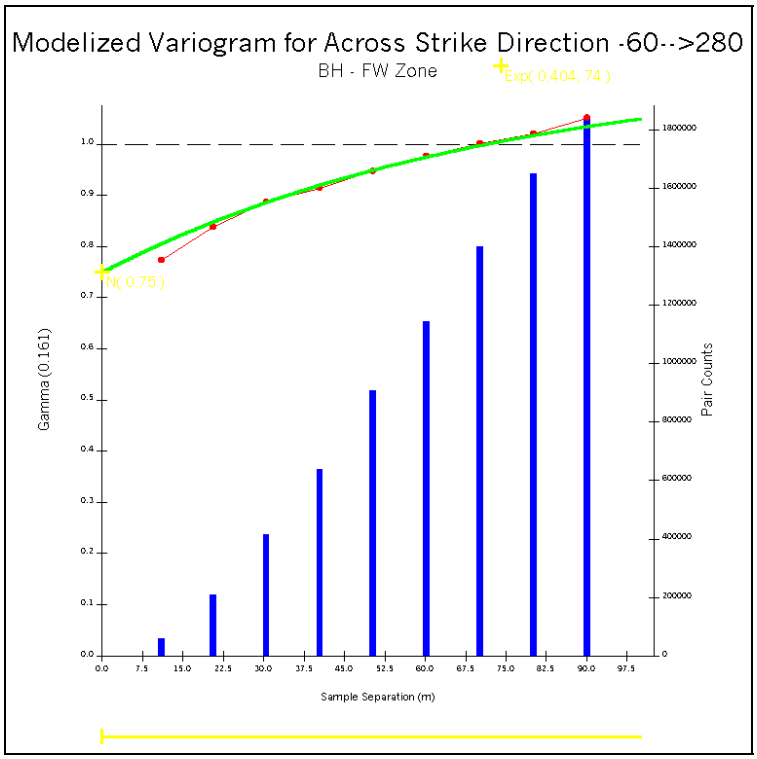

Figure C.108 Modelized Indicator Variogram – FW Zone Cut-Off at 0.65 g/t Au – Across Strike

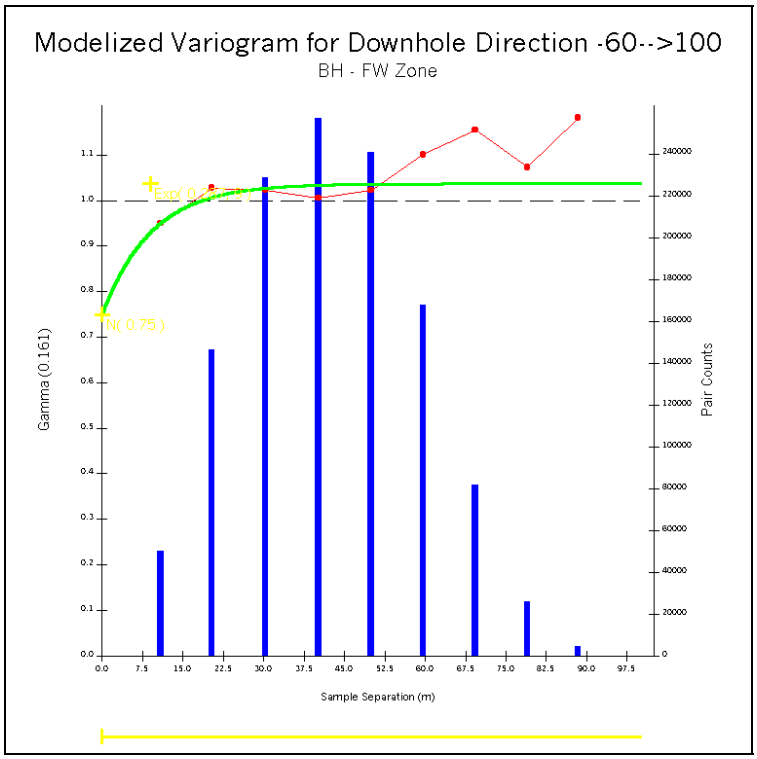

Figure C.109 Modelized Indicator Variogram – FW Zone Cut-Off at 0.65 g/t Au – Downhole

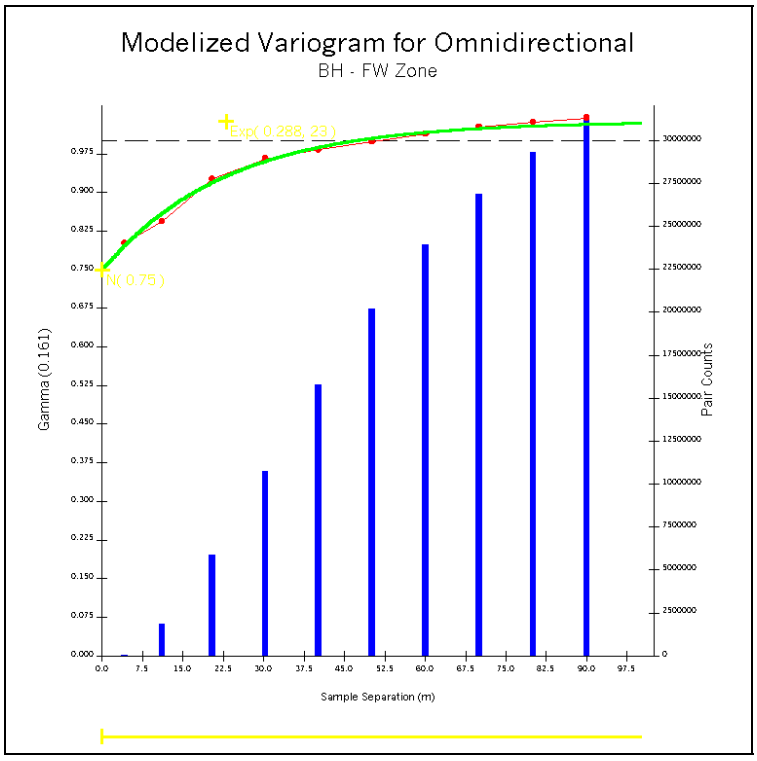

Figure C.110 Modelized Indicator Variogram – FW Zone Cut-Off at 0.65 g/t Au – Omnidirectional

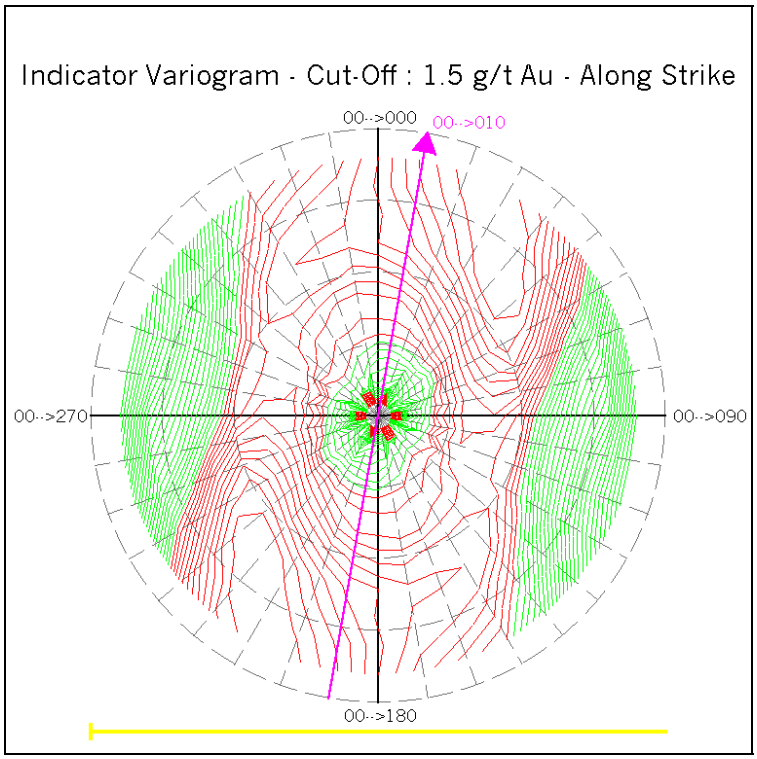

Figure C.111 Fan of Indicator Variograms – FW Zone Cut-Off at 1.5 g/t Au – Along Strike

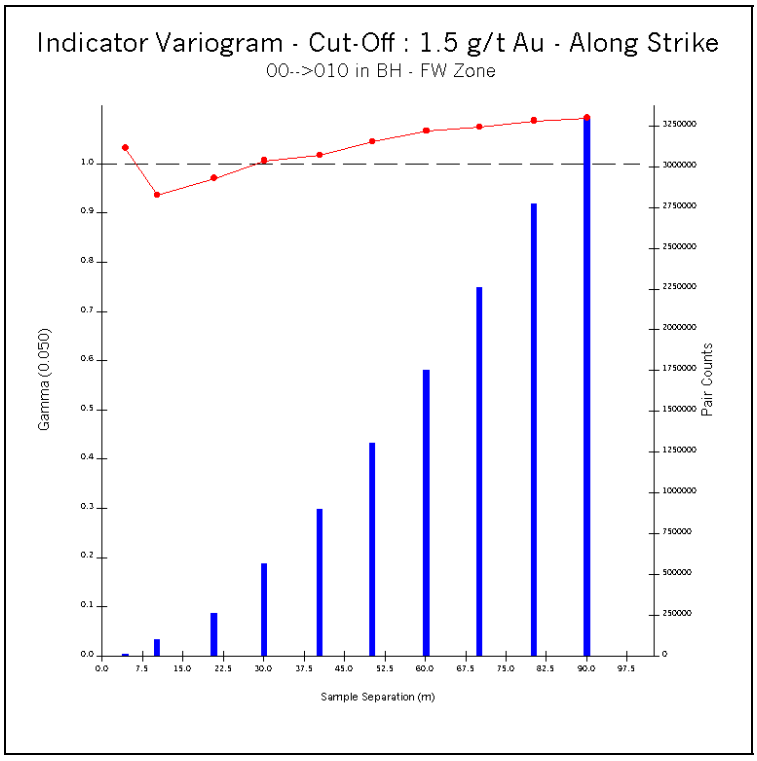

Figure C.112 Indicator Variogram – FW Zone Cut-Off at 1.5 g/t Au – Along Strike

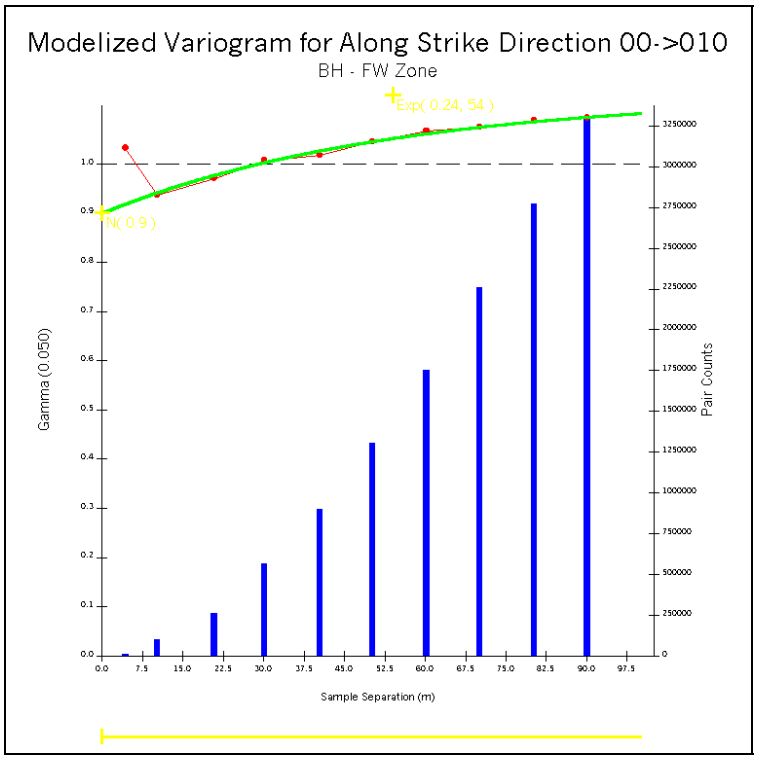

Figure C.113 Modelized Indicator Variogram – FW Zone Cut-Off at 1.5 g/t Au – Along Strike

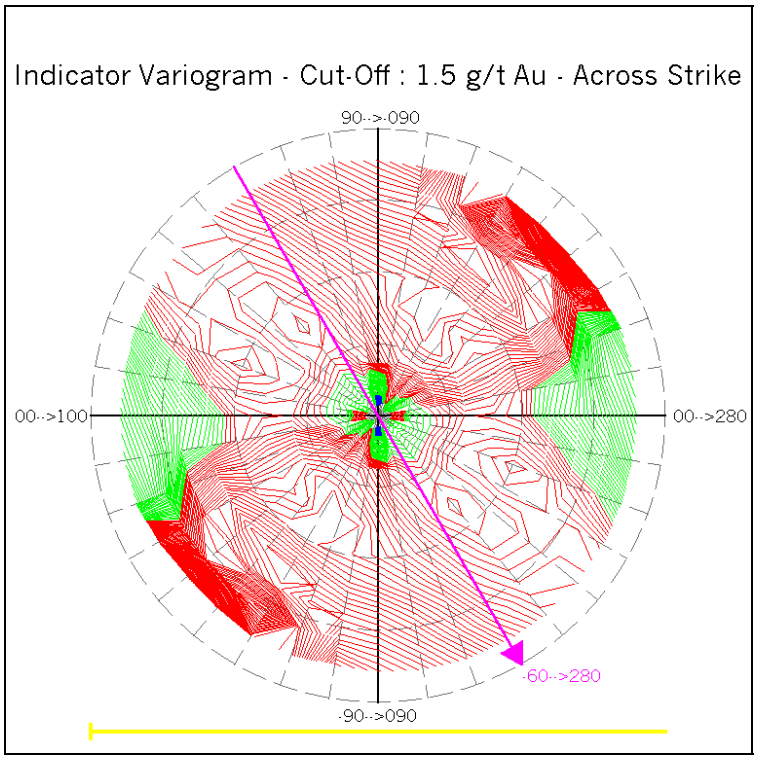

Figure C.114 Fan of Indicator Variograms – FW Zone Cut-Off at 1.5 g/t Au – Across Strike

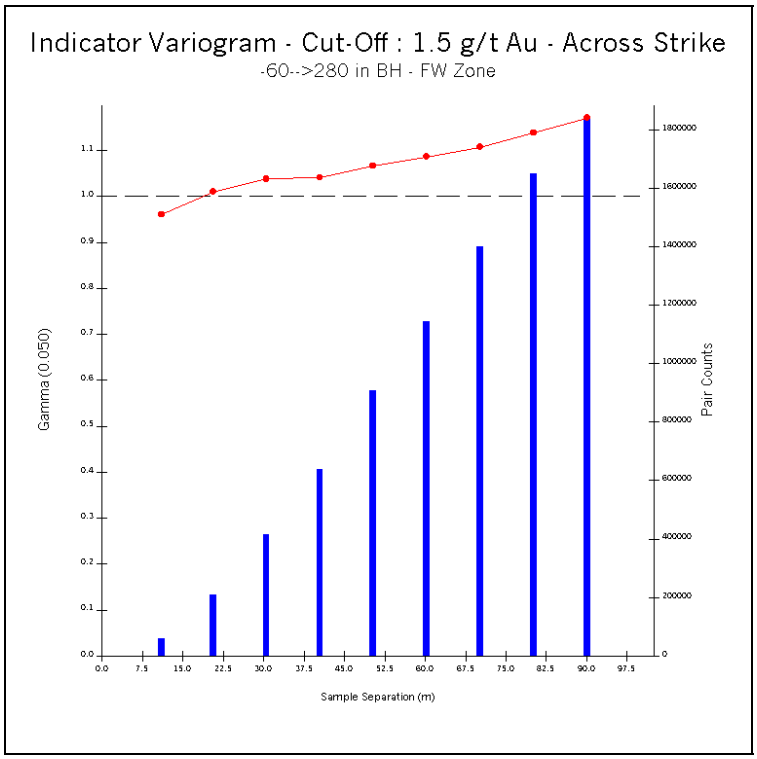

Figure C.115 Indicator Variogram – FW Zone Cut-Off at 1.5 g/t Au – Across Strike

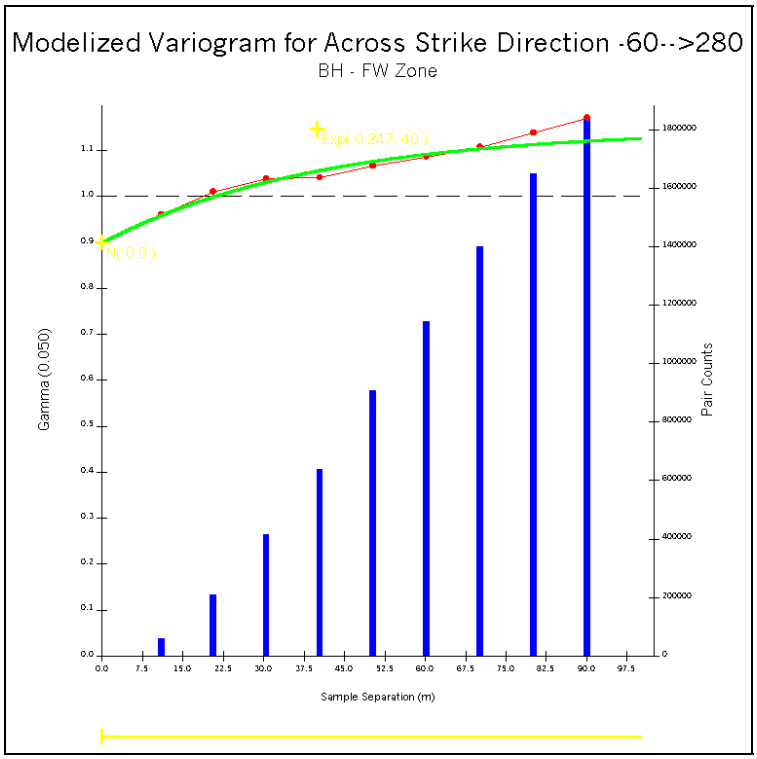

Figure C.116 Modelized Indicator Variogram – FW Zone Cut-Off at 1.5 g/t Au – Across Strike

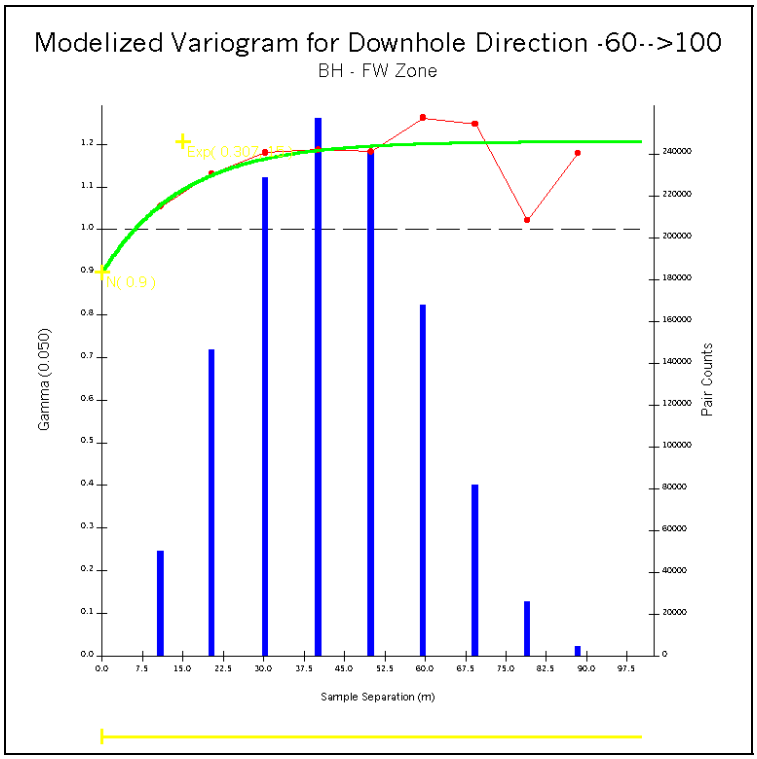

Figure C.117 Modelized Indicator Variogram – FW Zone Cut-Off at 1.5 g/t Au – Downhole

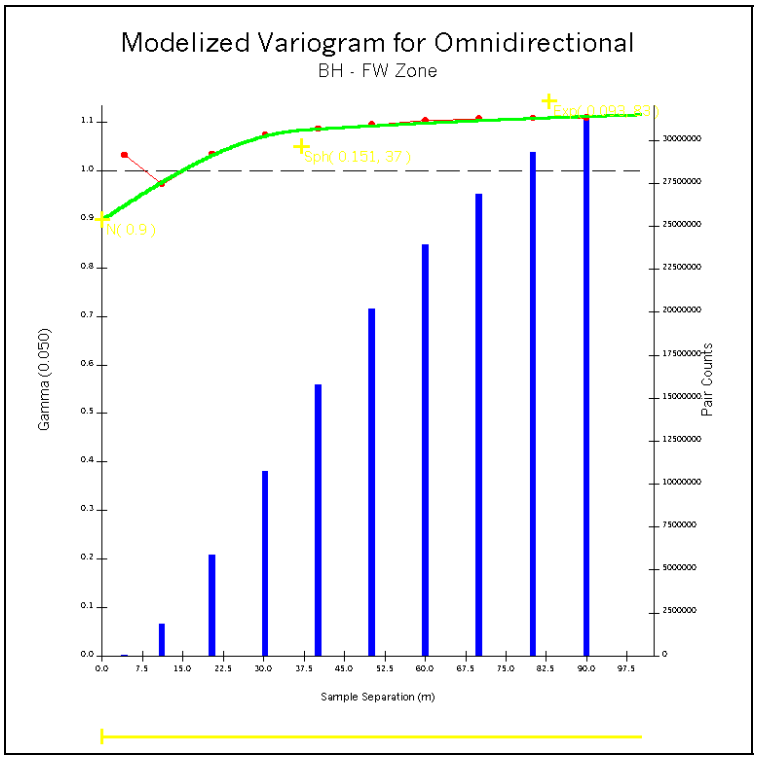

Figure C.118 Modelized Indicator Variogram – FW Zone Cut-Off at 1.5 g/t Au – Omnidirectional

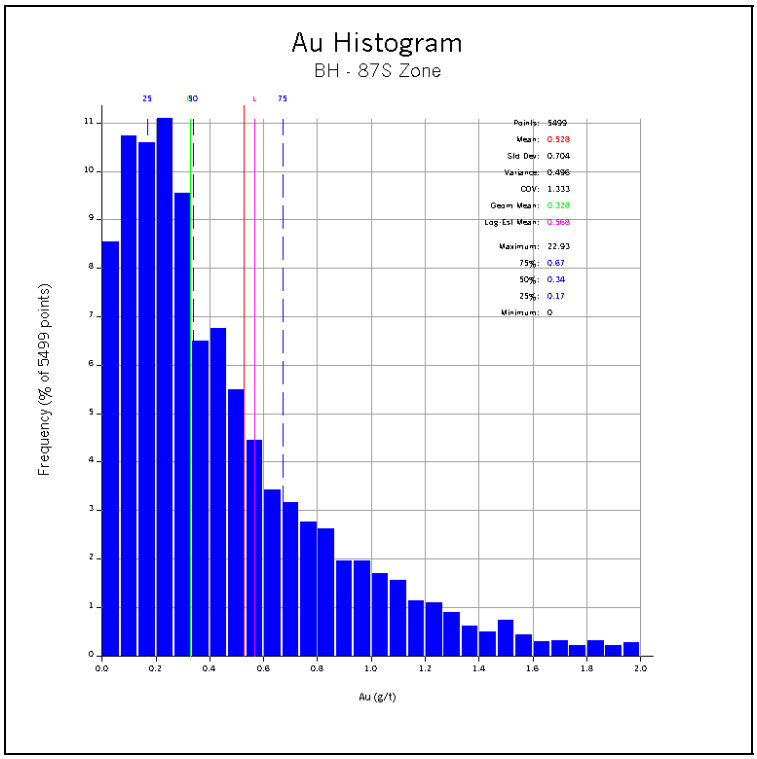

Figure C.119 Au Normal Histogram – 87S Zone

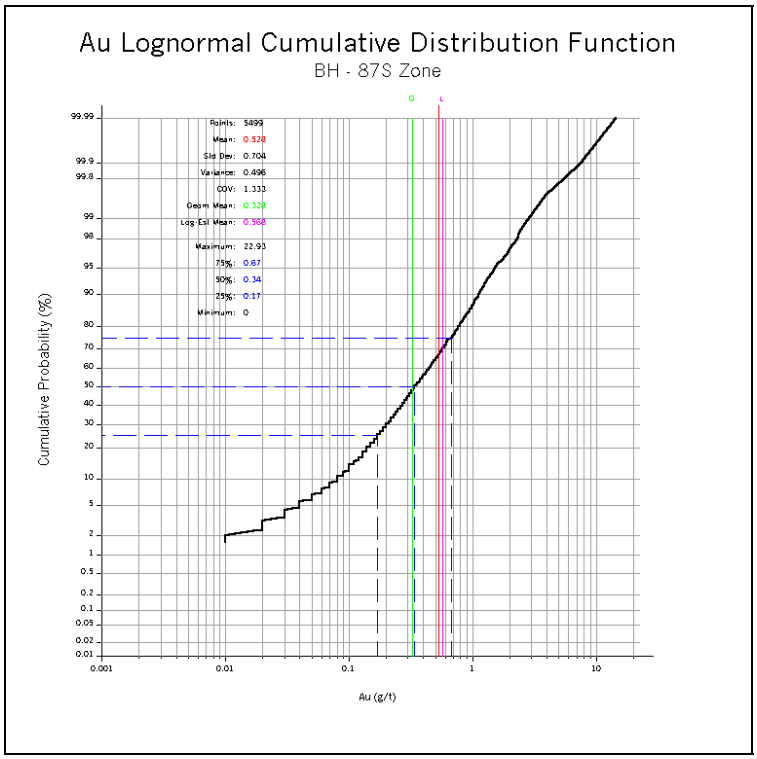

Figure C.120 Au Lognormal Cumulative Distribution Function – 87S Zone

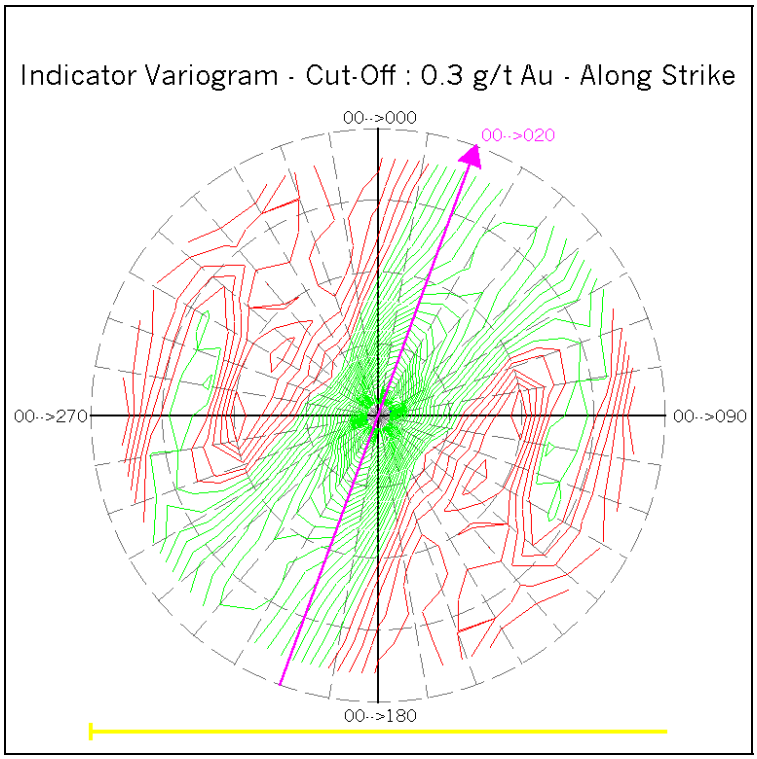

Figure C.121 Fan of Indicator Variograms – 87S Zone Cut-Off at 0.3 g/t Au – Along Strike

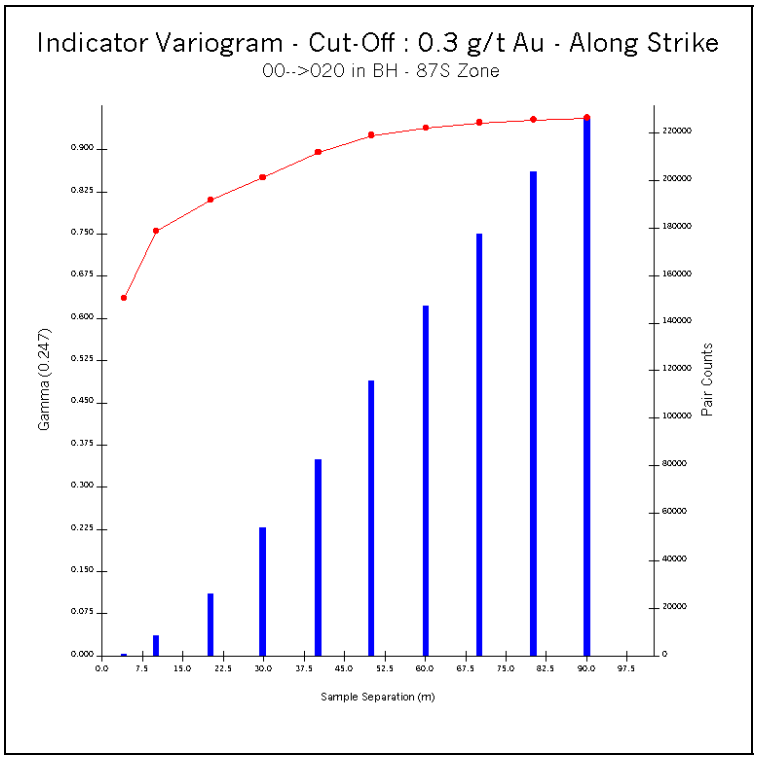

Figure C.122 Indicator Variogram – 87S Zone Cut-Off at 0.3 g/t Au – Along Strike

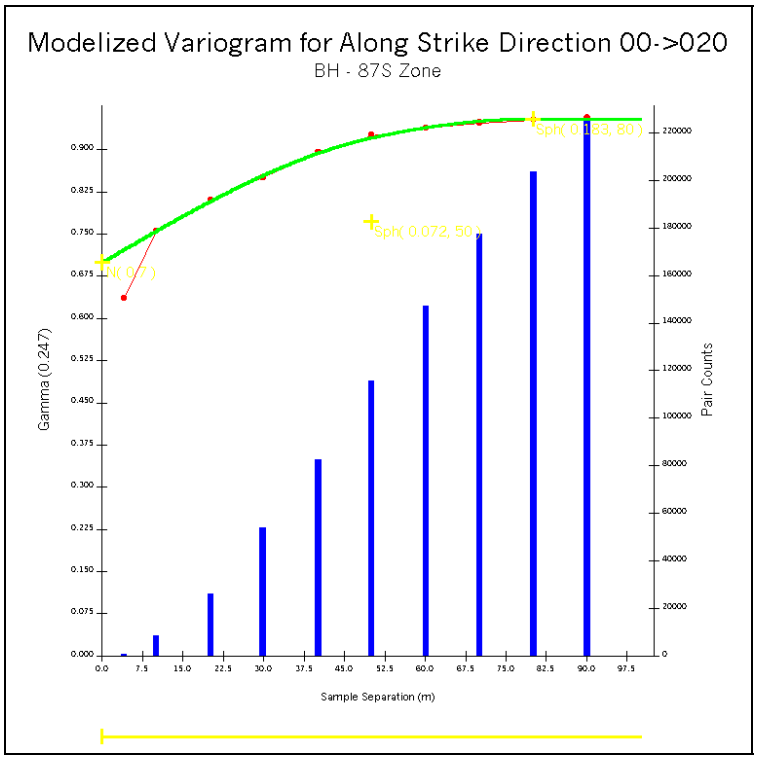

Figure C.123 Modelized Indicator Variogram – 87S Zone Cut-Off at 0.3 g/t Au – Along Strike

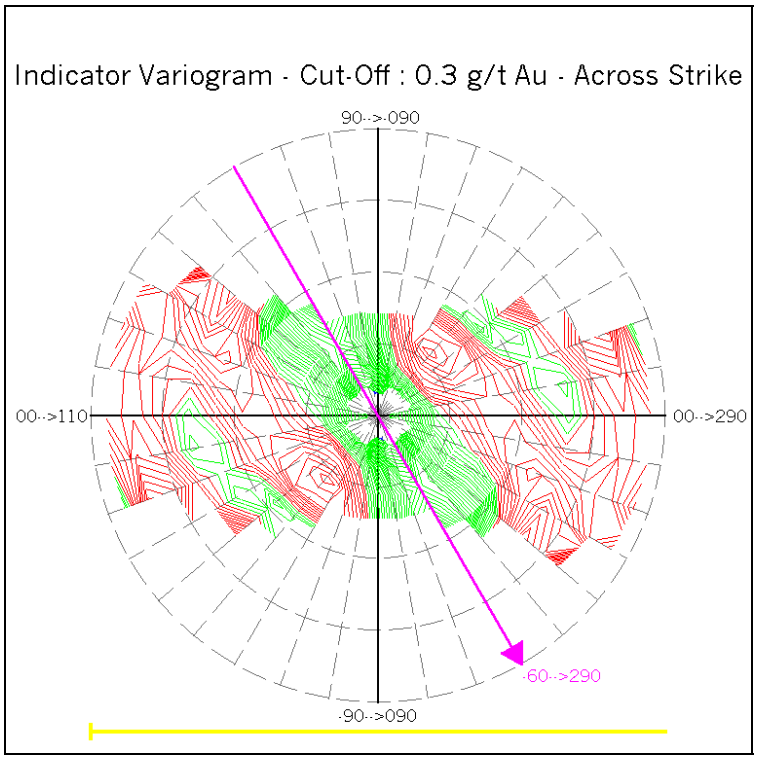

Figure C.124 Fan of Indicator Variograms – 87S Zone Cut-Off at 0.3 g/t Au – Across Strike

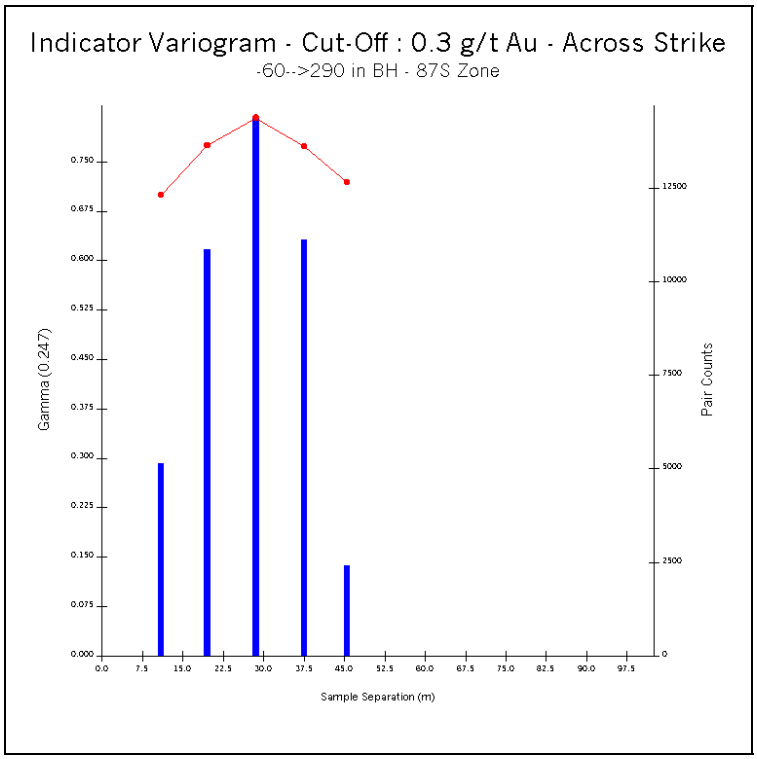

Figure C.125 Indicator Variogram – 87S Zone Cut-Off at 0.3 g/t Au – Across Strike

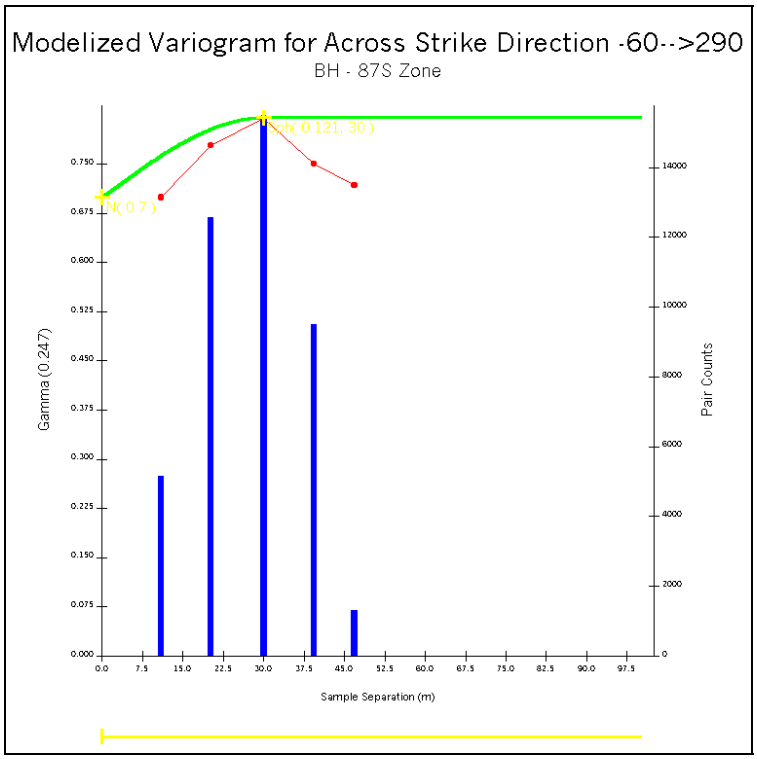

Figure C.126 Modelized Indicator Variogram – 87S Zone Cut-Off at 0.3 g/t Au – Across Strike

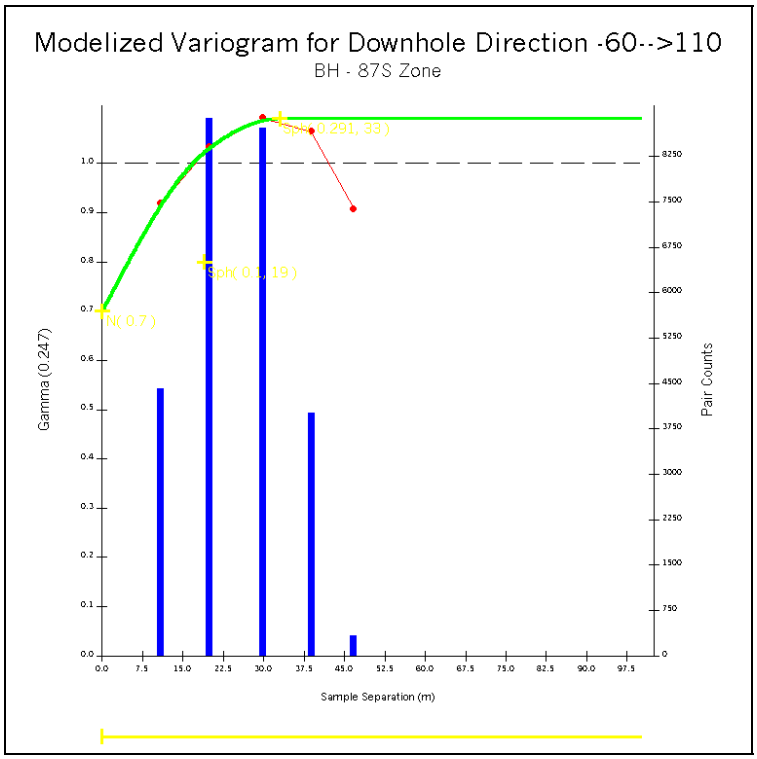

Figure C.127 Modelized Indicator Variogram – 87S Zone Cut-Off at 0.3 g/t Au – Downhole

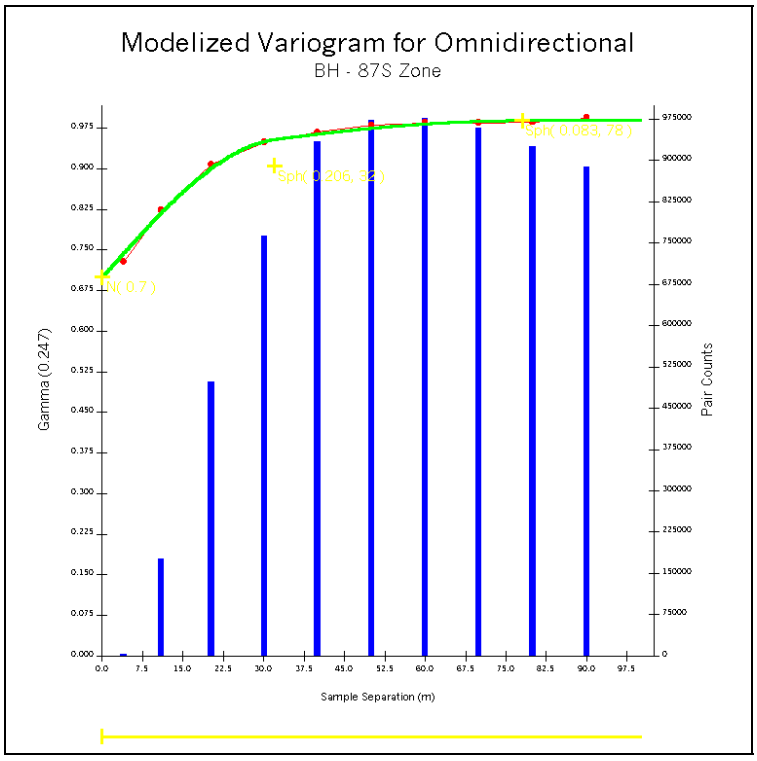

Figure C.128 Modelized Indicator Variogram – 87S Zone Cut-Off at 0.3 g/t Au – Omnidirectional

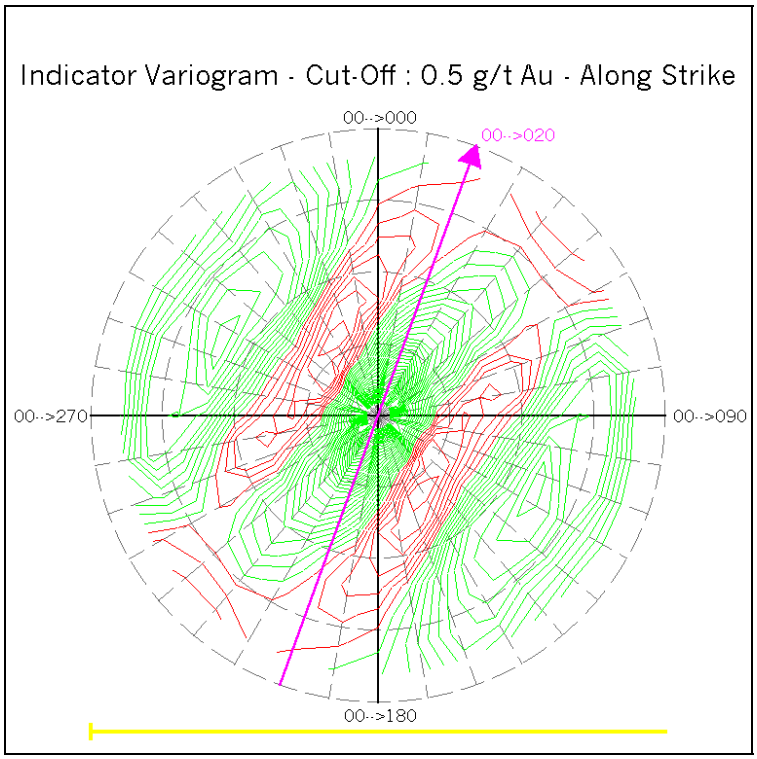

Figure C.129 Fan of Indicator Variograms – 87S Zone Cut-Off at 0.5 g/t Au – Along Strike

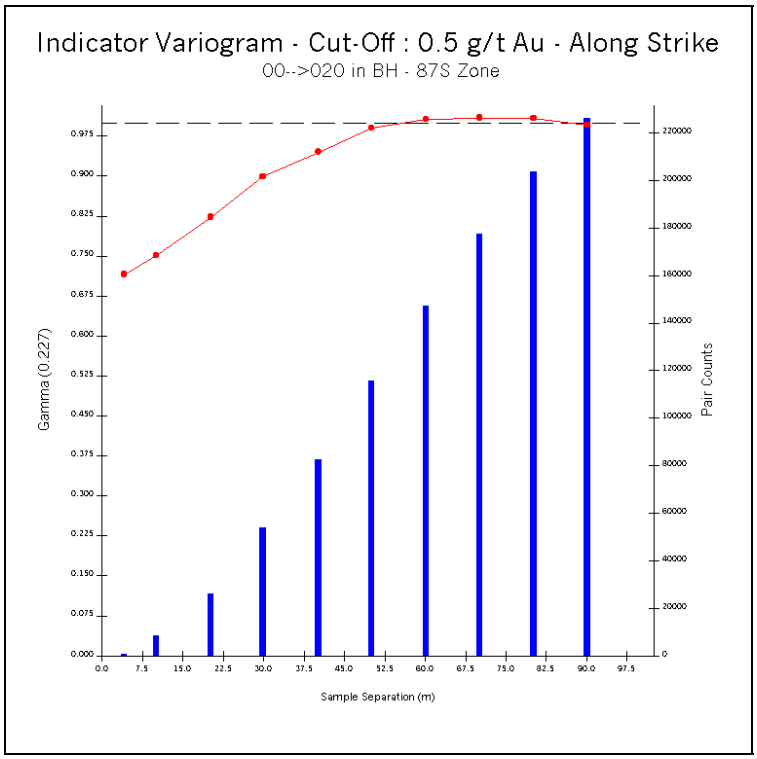

Figure C.130 Indicator Variogram – 87S Zone Cut-Off at 0.5 g/t Au – Along Strike

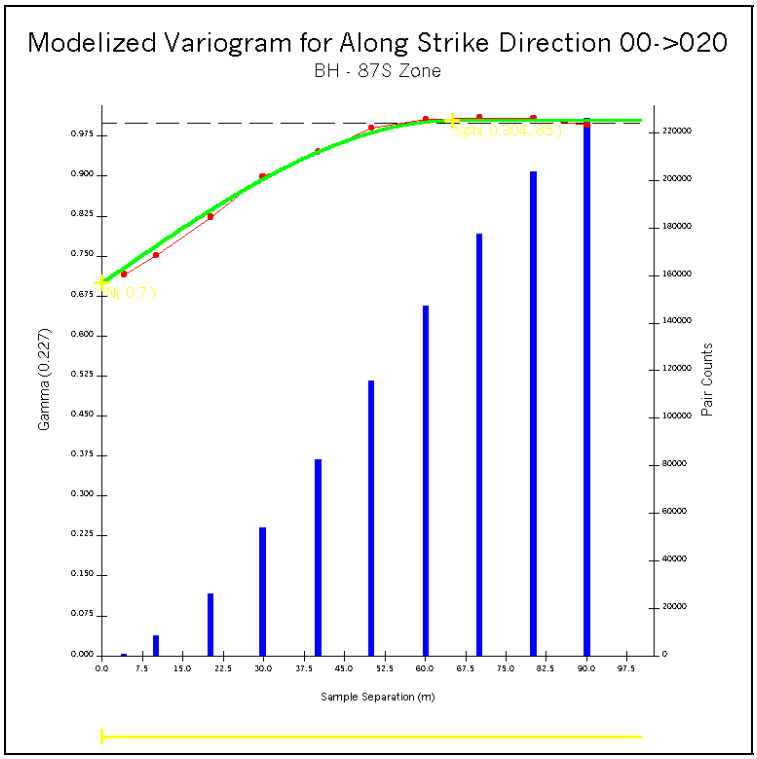

Figure C.131 Modelized Indicator Variogram – 87S Zone Cut-Off at 0.5 g/t Au – Along Strike

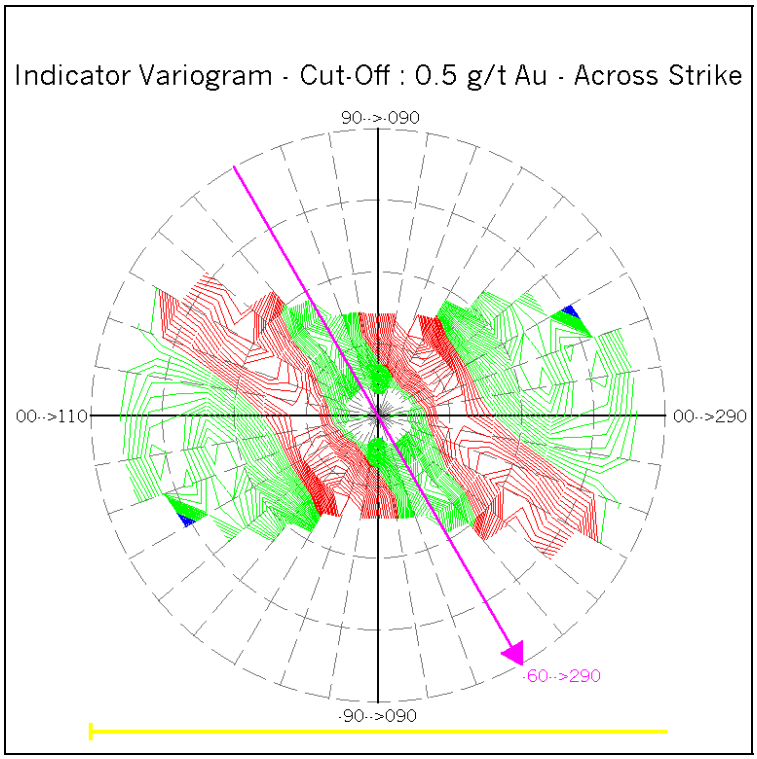

Figure C.132 Fan of Indicator Variograms – 87S Zone Cut-Off at 0.5 g/t Au – Across Strike

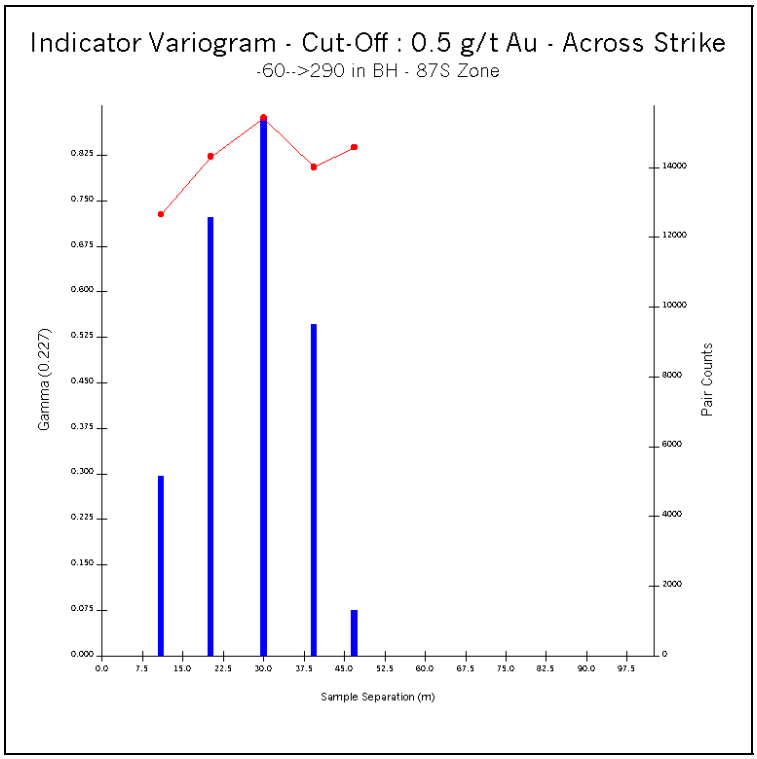

Figure C.133 Indicator Variogram – 87S Zone Cut-Off at 0.5 g/t Au – Across Strike

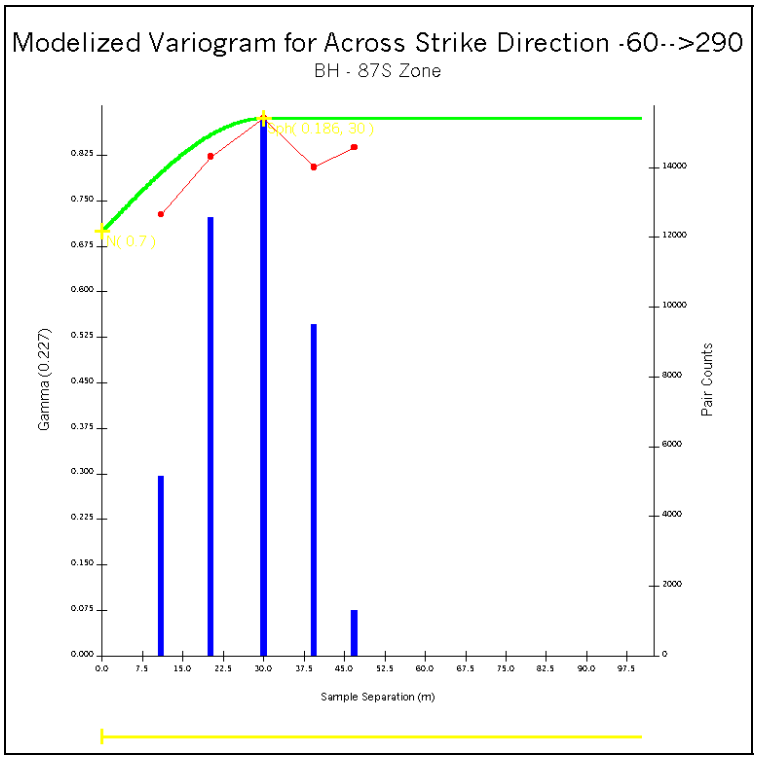

Figure C.134 Modelized Indicator Variogram – 87S Zone Cut-Off at 0.5 g/t Au – Across Strike

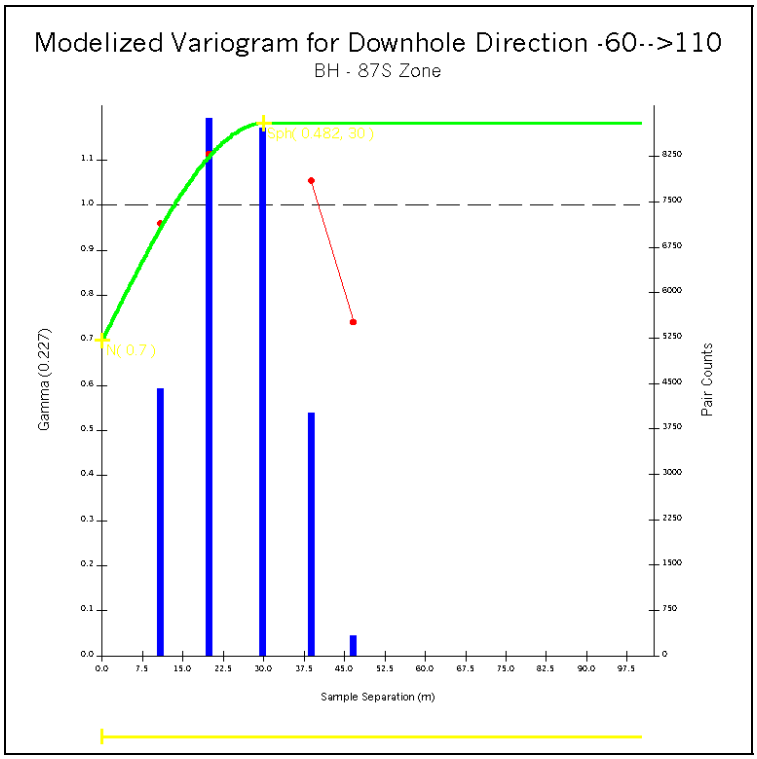

Figure C.135 Modelized Indicator Variogram – 87S Zone Cut-Off at 0.5 g/t Au – Downhole

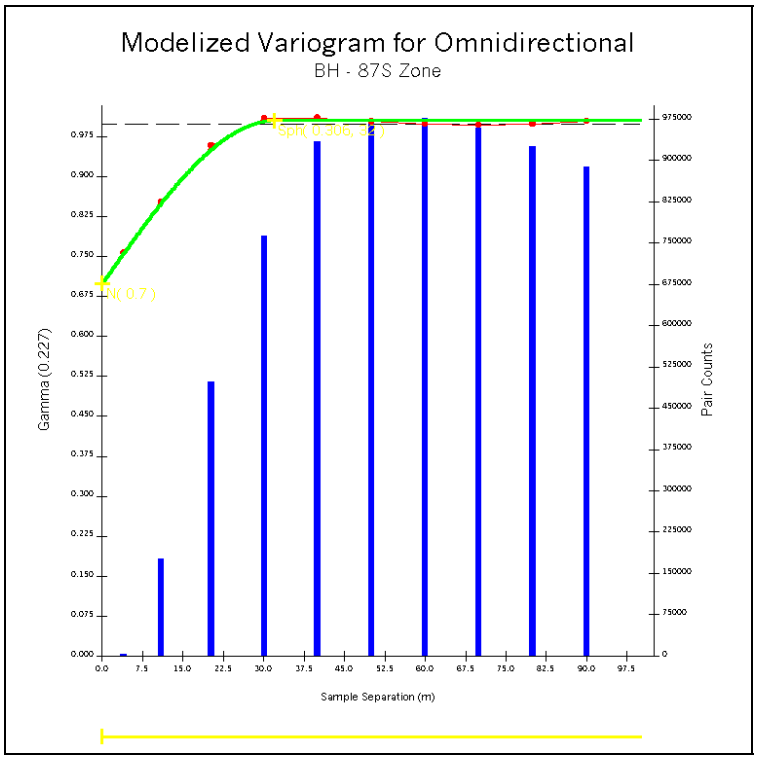

Figure C.136 Modelized Indicator Variogram – 87S Zone Cut-Off at 0.5 g/t Au – Omnidirectional

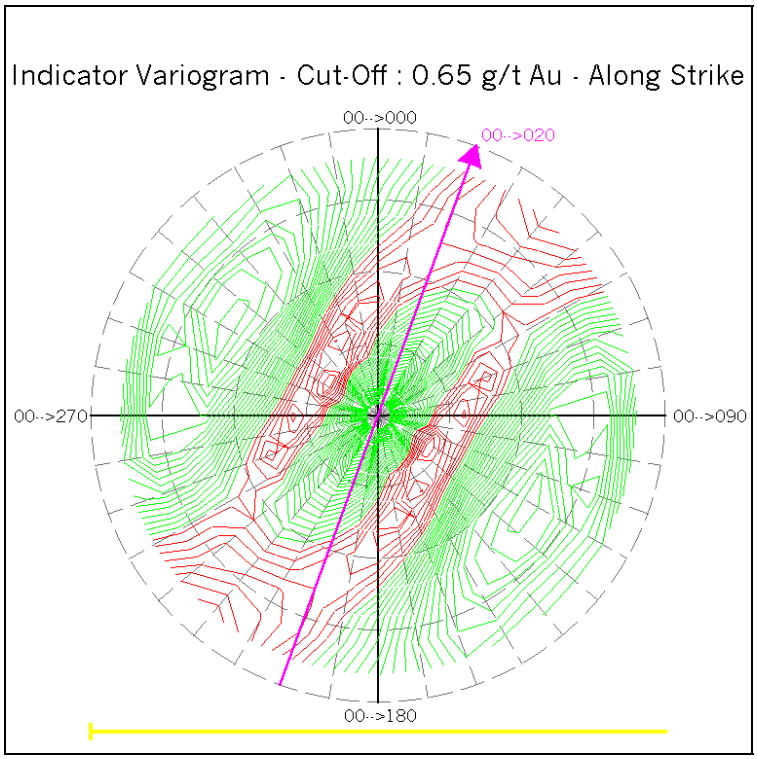

Figure C.137 Fan of Indicator Variograms – 87S Zone Cut-Off at 0.65 g/t Au – Along Strike

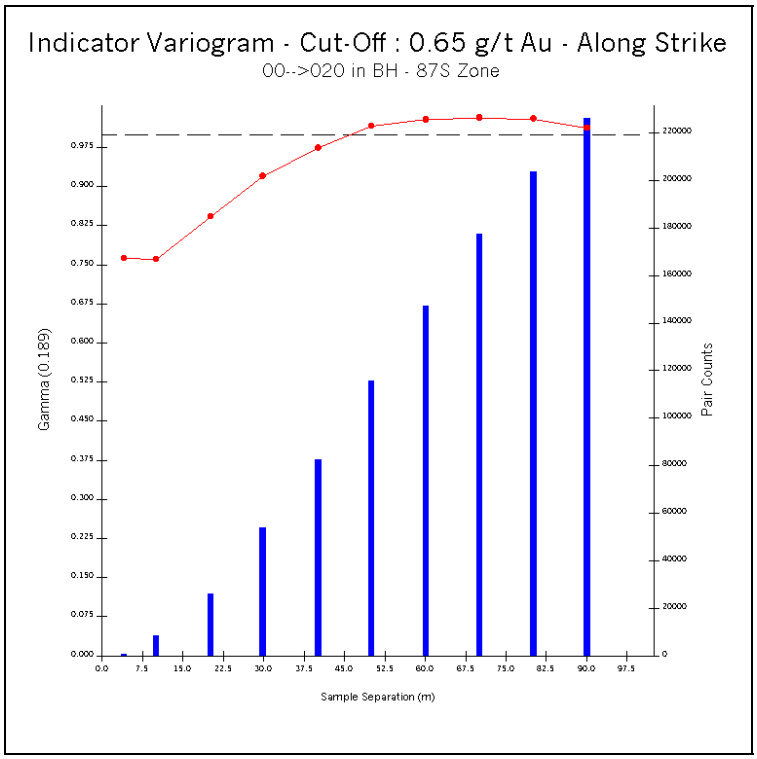

Figure C.138 Indicator Variogram – 87S Zone Cut-Off at 0.65 g/t Au – Along Strike

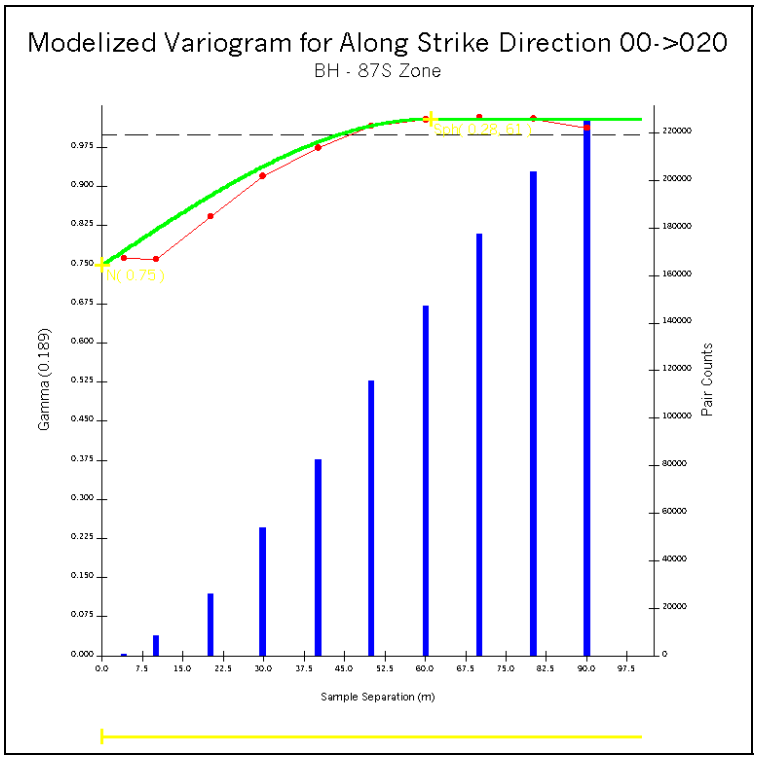

Figure C.139 Modelized Indicator Variogram – 87S Zone Cut-Off at 0.65 g/t Au – Along Strike

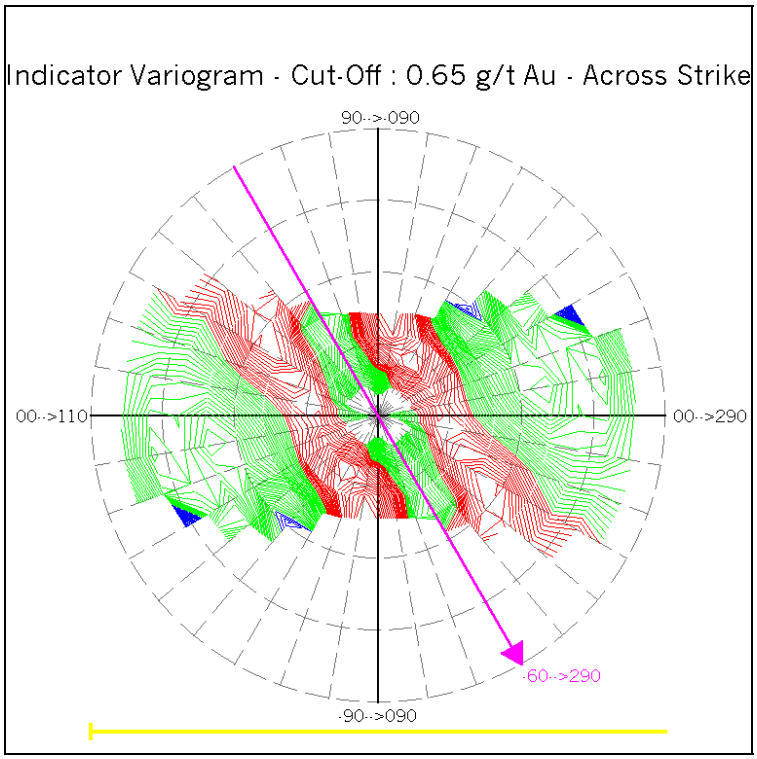

Figure C.140 Fan of Indicator Variograms – 87S Zone Cut-Off at 0.65 g/t Au – Across Strike

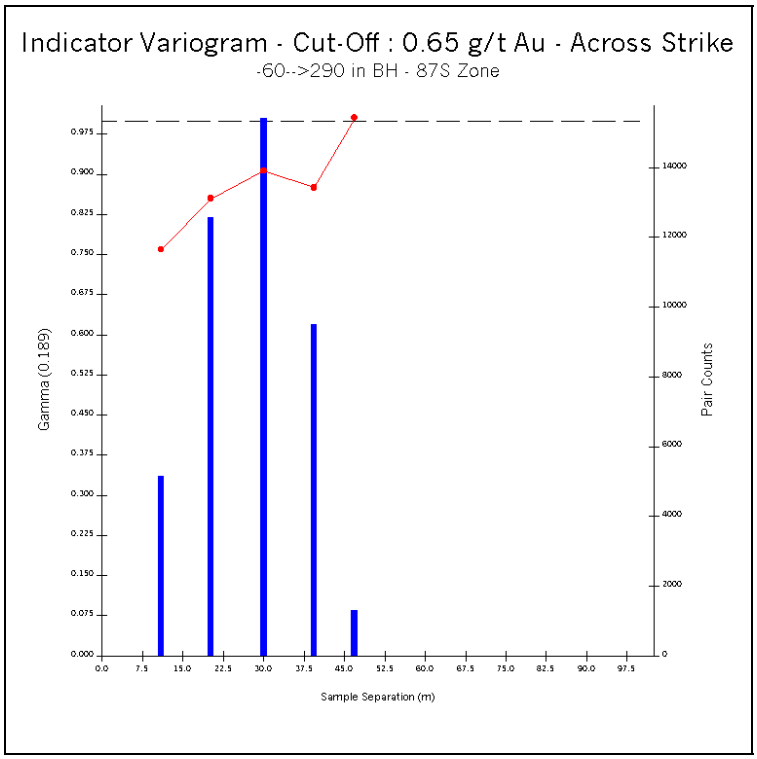

Figure C.141 Indicator Variogram – 87S Zone Cut-Off at 0.65 g/t Au – Across Strike

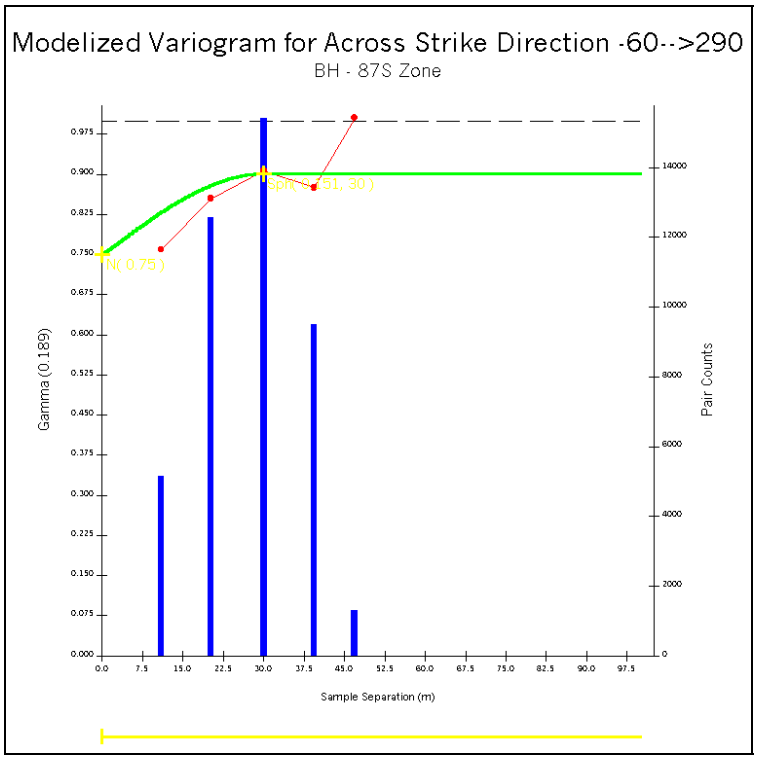

Figure C.142 Modelized Indicator Variogram – 87S Zone Cut-Off at 0.65 g/t Au – Across Strike

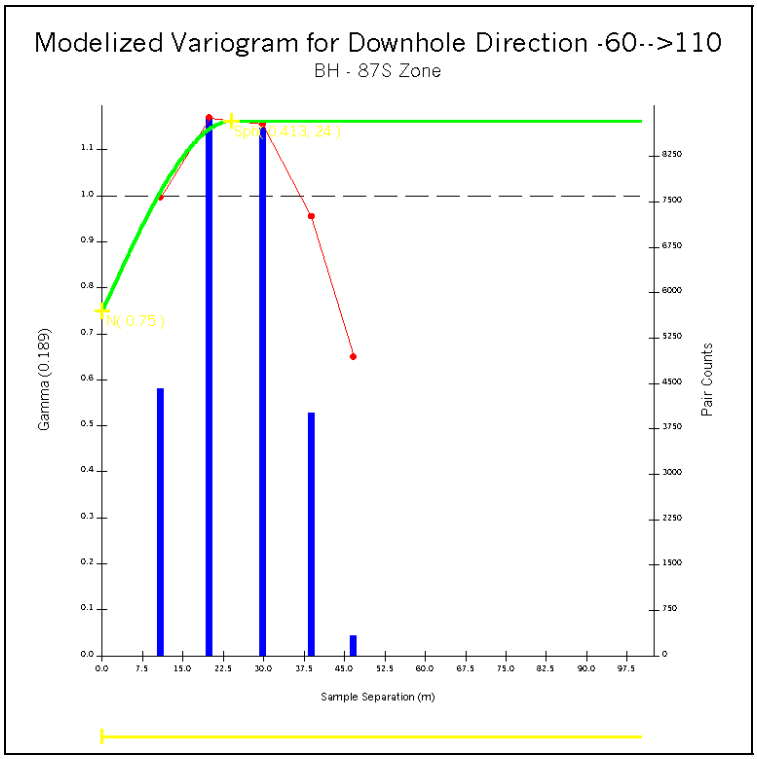

Figure C.143 Modelized Indicator Variogram – 87S Zone Cut-Off at 0.65 g/t Au – Downhole

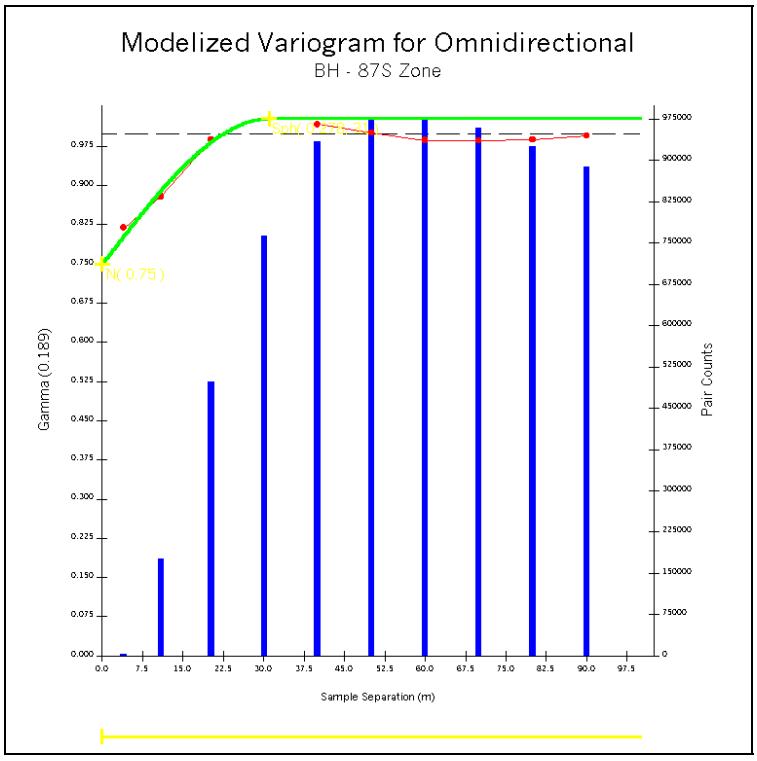

Figure C.144 Modelized Indicator Variogram – 87S Zone Cut-Off at 0.65 g/t Au – Omnidirectional

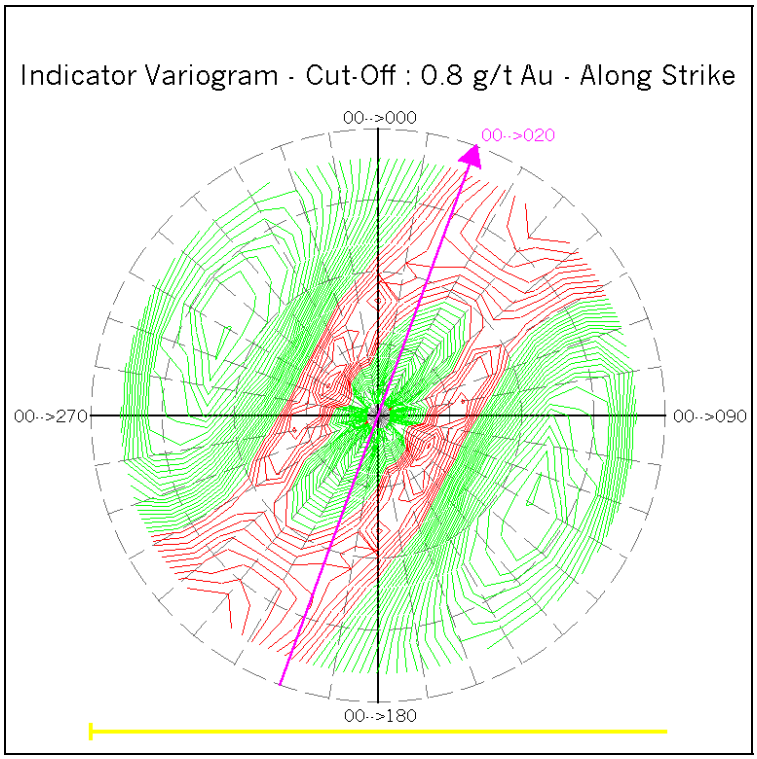

Figure C.145 Fan of Indicator Variograms – 87S Zone Cut-Off at 0.8 g/t Au – Along Strike

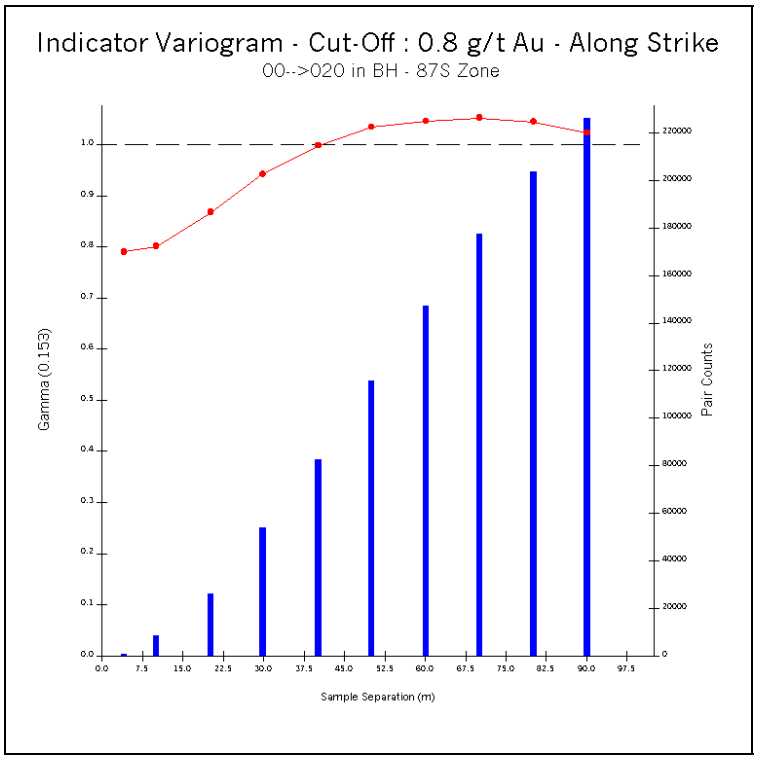

Figure C.146 Indicator Variogram – 87S Zone Cut-Off at 0.8 g/t Au – Along Strike

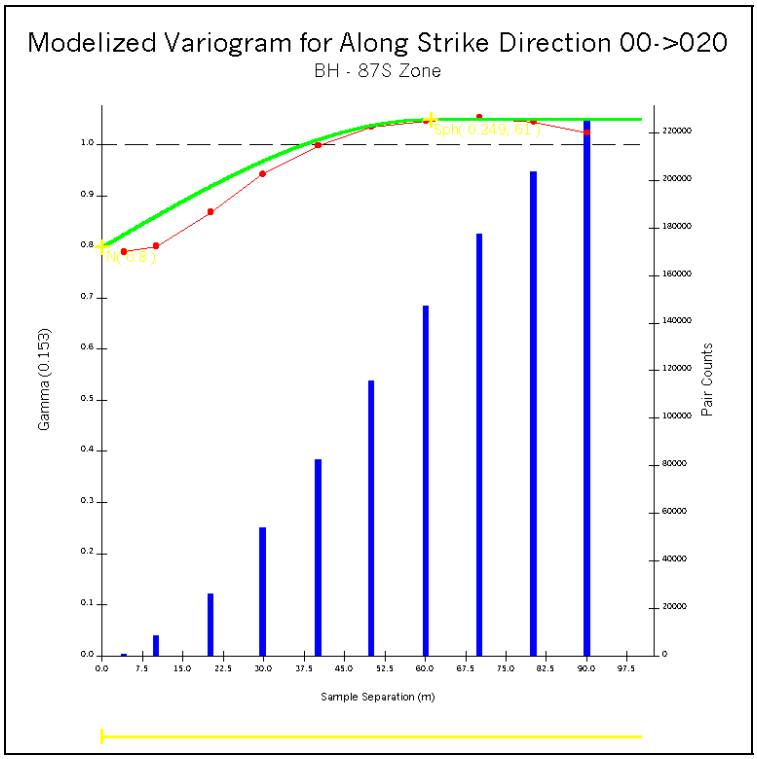

Figure C.147 Modelized Indicator Variogram – 87S Zone Cut-Off at 0.8 g/t Au – Along Strike

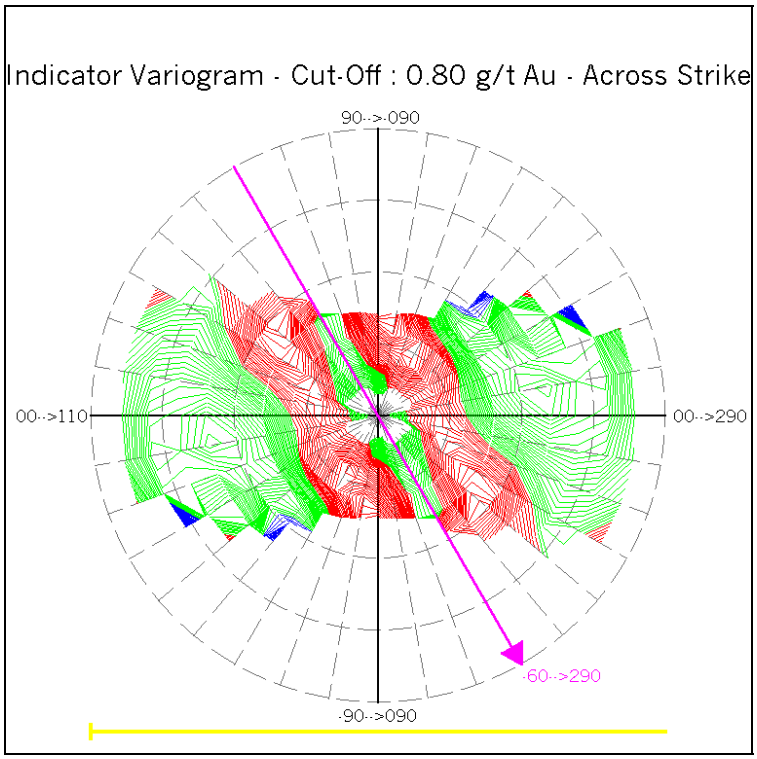

Figure C.148 Fan of Indicator Variograms – 87S Zone Cut-Off at 0.8 g/t Au – Across Strike

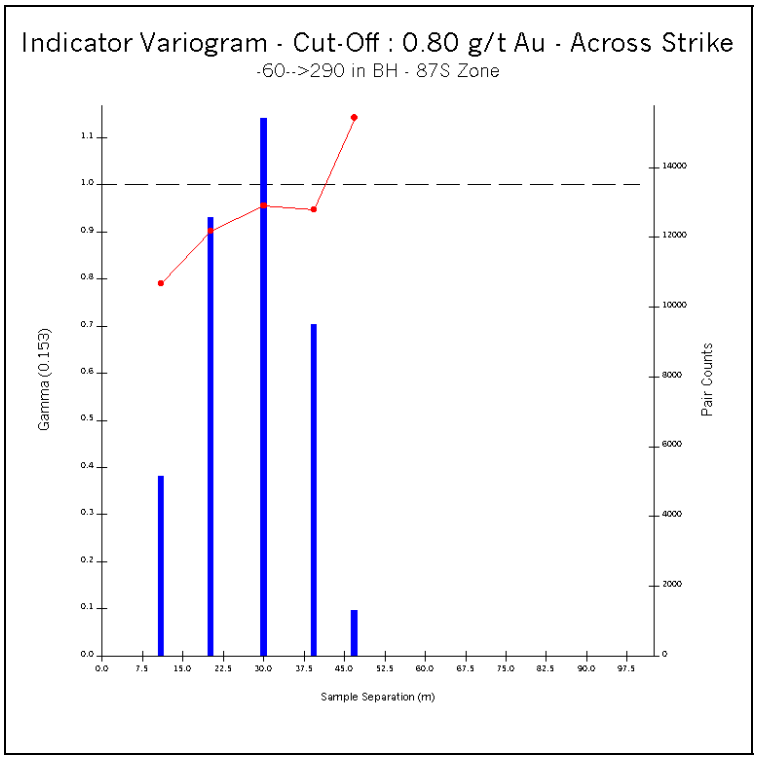

Figure C.149 Indicator Variogram – 87S Zone Cut-Off at 0.8 g/t Au – Across Strike

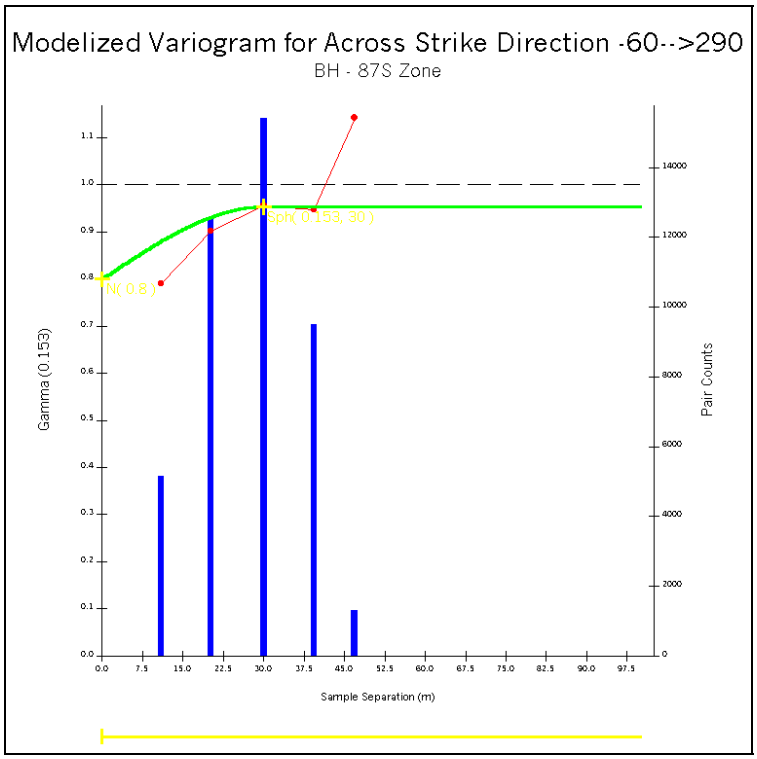

Figure C.150 Modelized Indicator Variogram – 87S Zone Cut-Off at 0.8 g/t Au – Across Strike

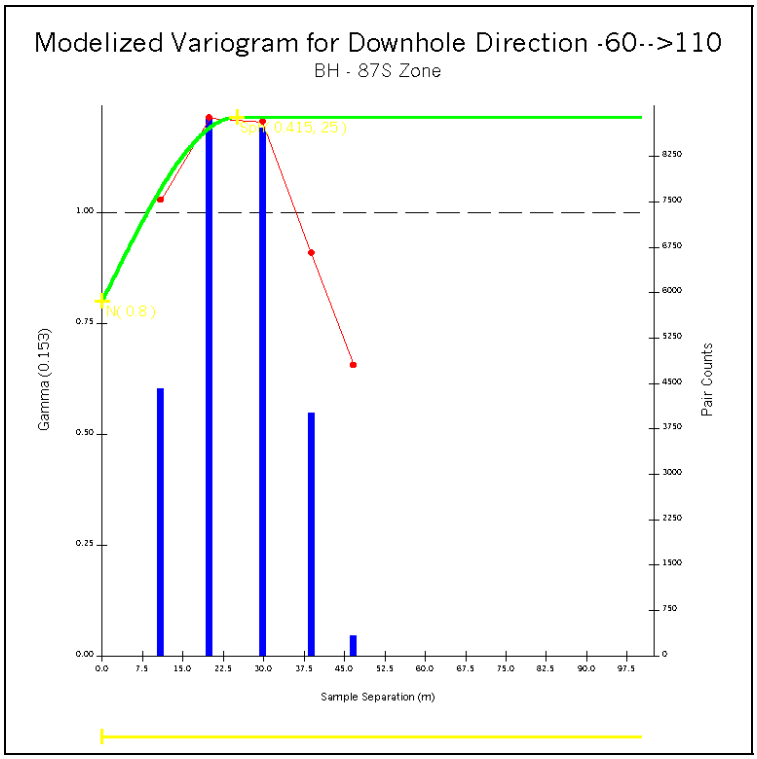

Figure C.151 Modelized Indicator Variogram – 87S Zone Cut-Off at 0.8 g/t Au – Downhole

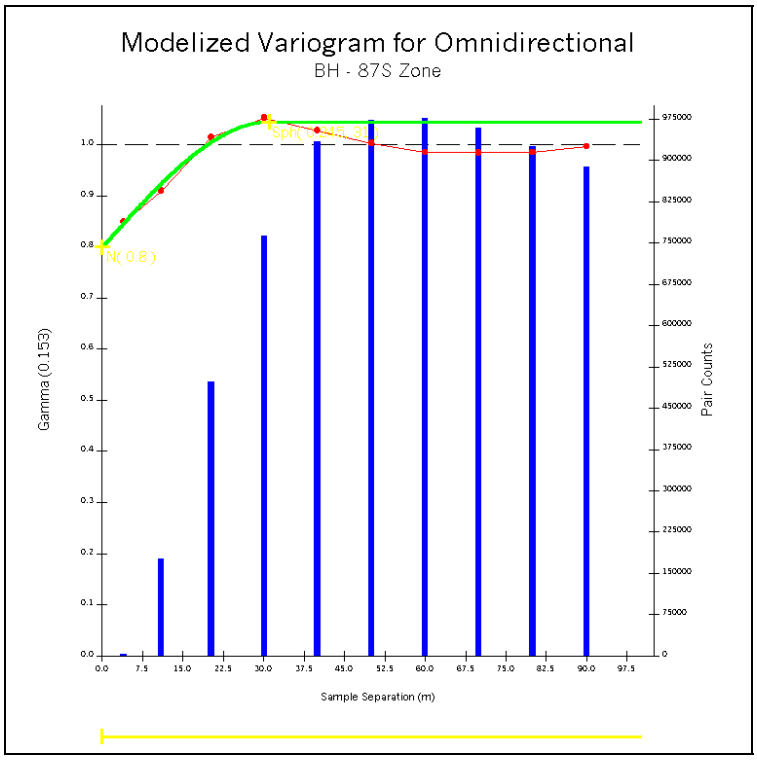

Figure C.152 Modelized Indicator Variogram – 87S Zone Cut-Off at 0.8 g/t Au – Omnidirectional

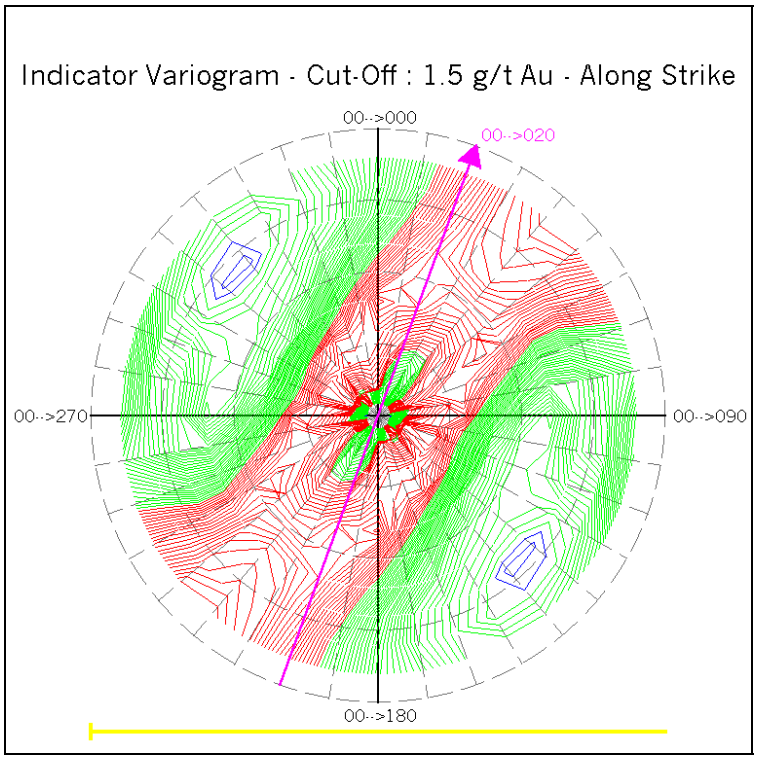

Figure C.153 Fan of Indicator Variograms – 87S Zone Cut-Off at 1.5 g/t Au – Along Strike

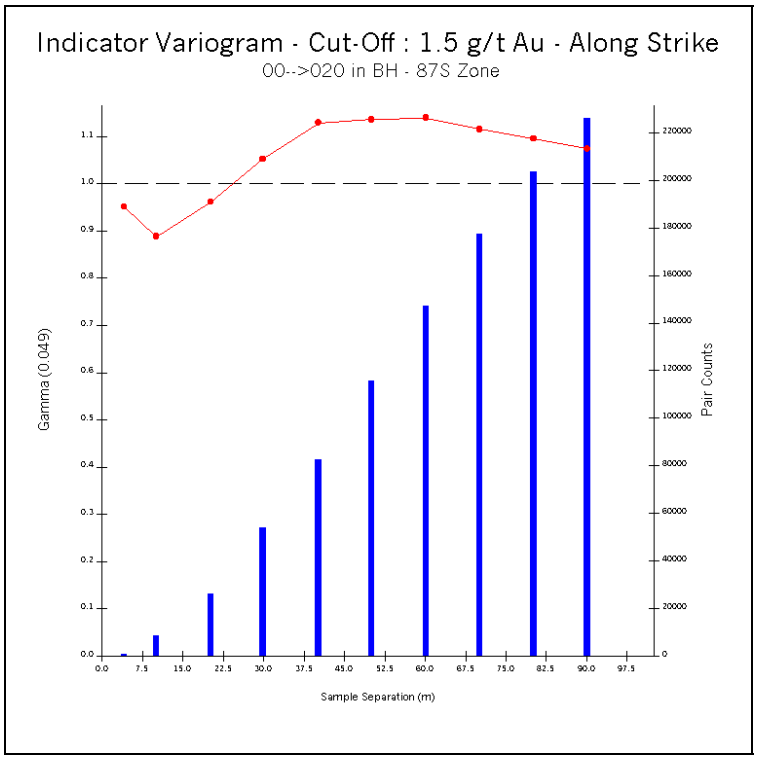

Figure C.154 Indicator Variogram – 87S Zone Cut-Off at 1.5 g/t Au – Along Strike

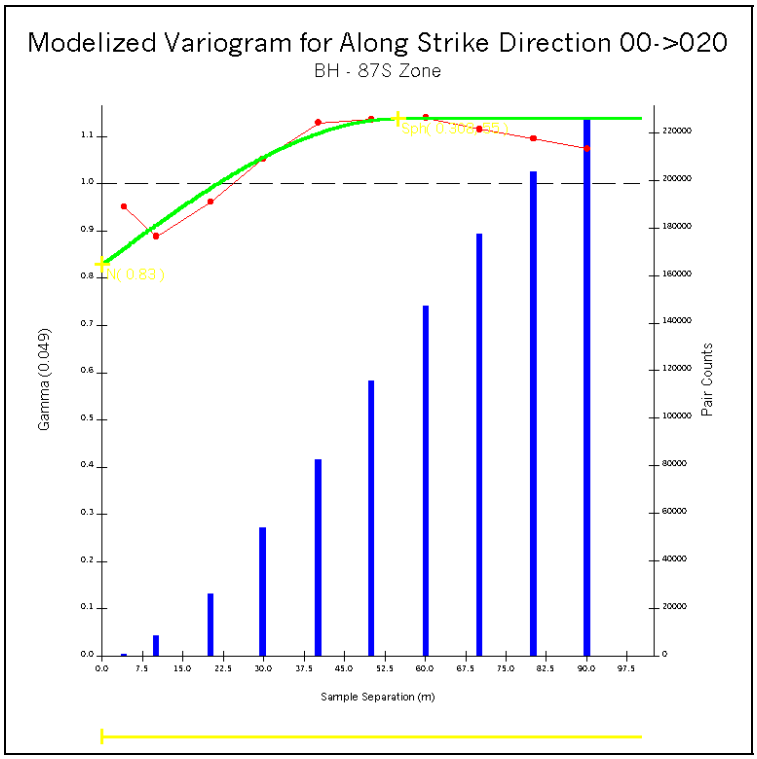

Figure C.155 Modelized Indicator Variogram – 87S Zone Cut-Off at 1.5 g/t Au – Along Strike

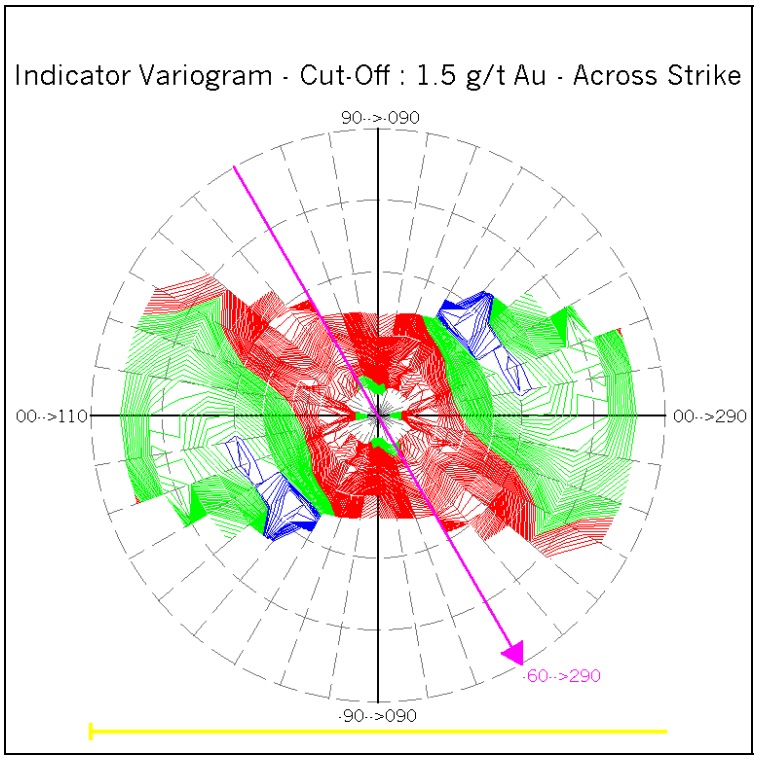

Figure C.156 Fan of Indicator Variograms – 87S Zone Cut-Off at 1.5 g/t Au – Across Strike

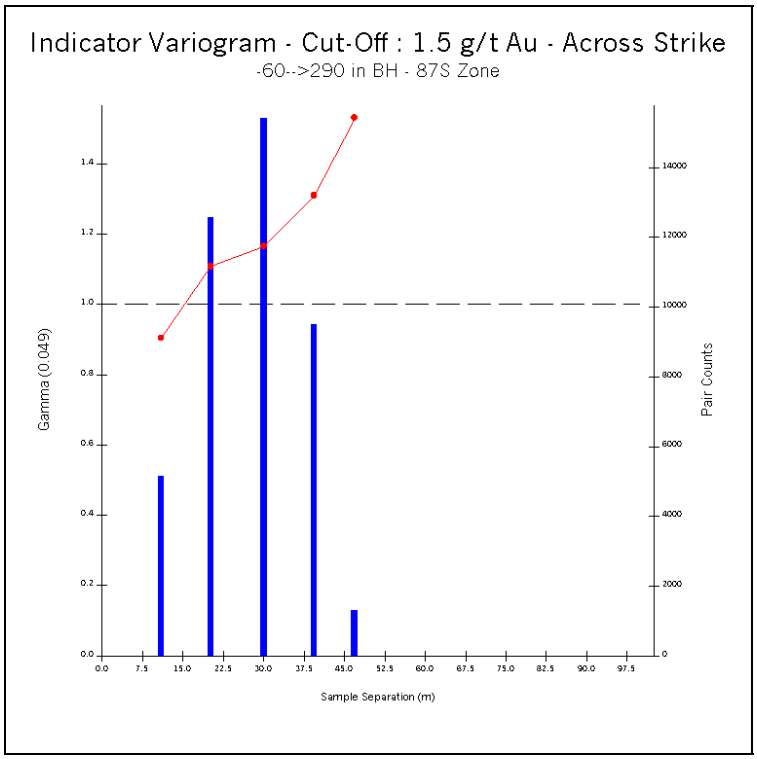

Figure C.157 Indicator Variogram – 87S Zone Cut-Off at 1.5 g/t Au – Across Strike

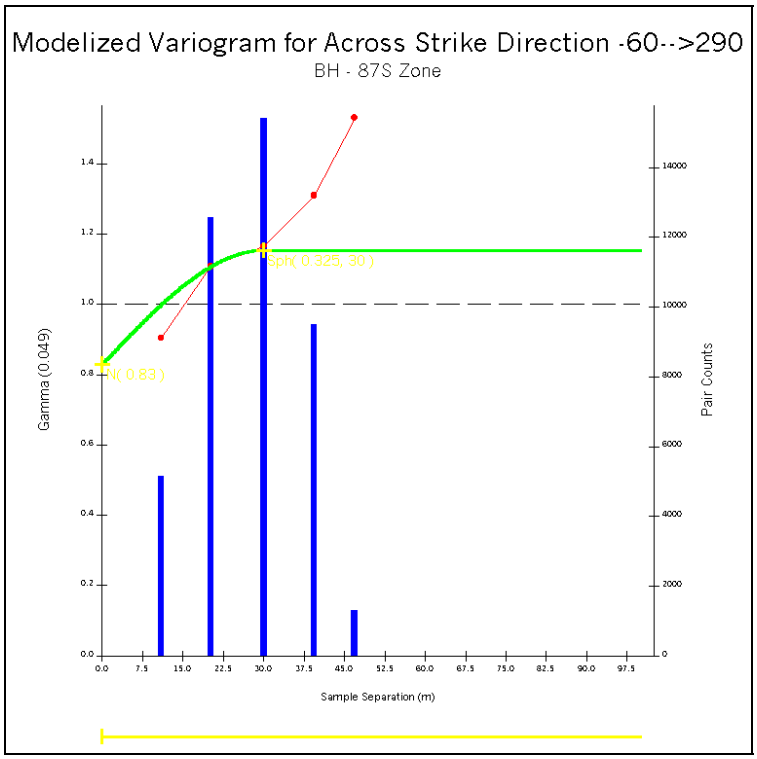

Figure C.158 Modelized Indicator Variogram – 87S Zone Cut-Off at 1.5 g/t Au – Across Strike

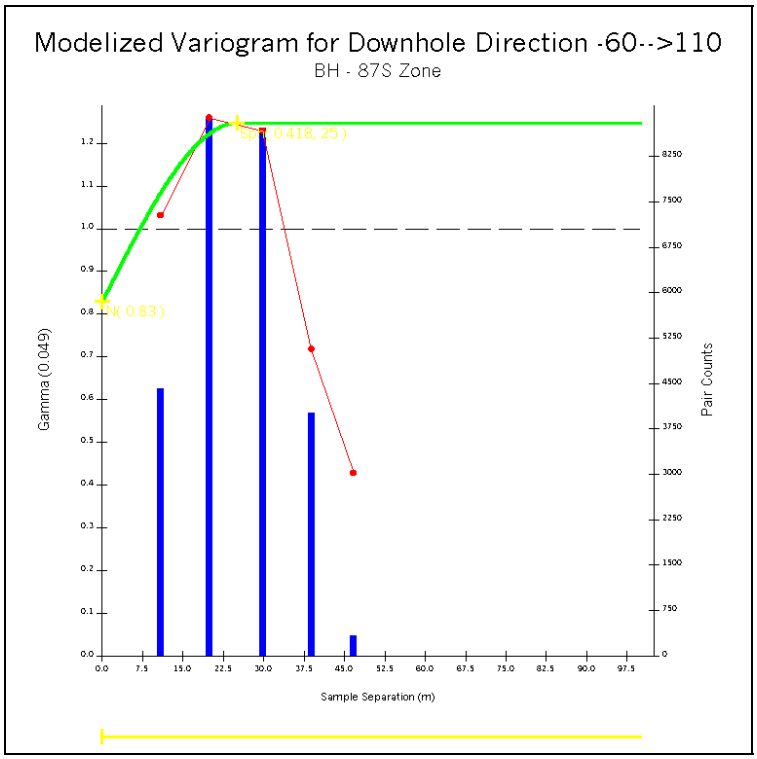

Figure C.159 Modelized Indicator Variogram – 87S Zone Cut-Off at 1.5 g/t Au – Downhole

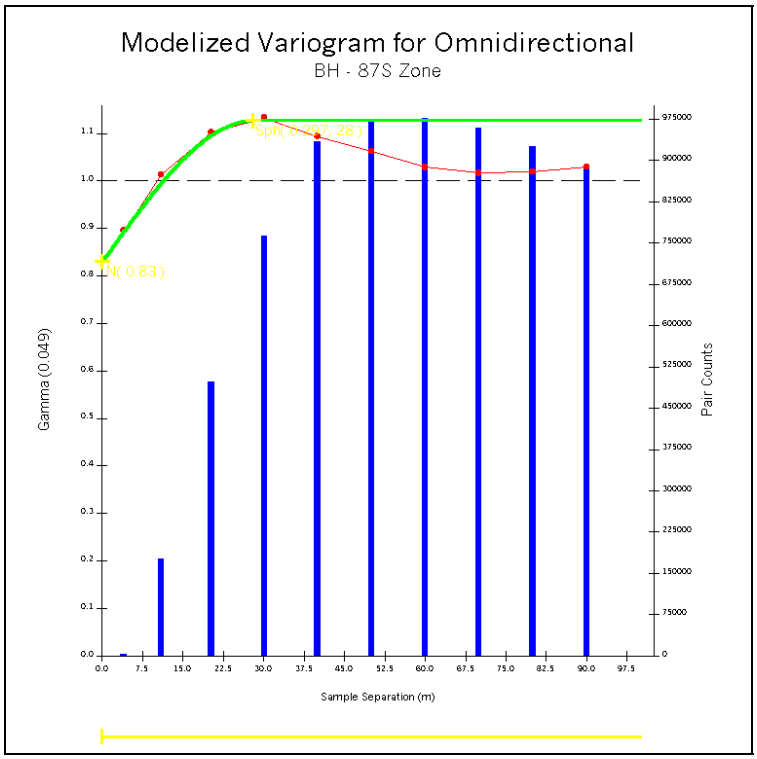

Figure C.160 Modelized Indicator Variogram – 87S Zone Cut-Off at 1.5 g/t Au – Omnidirectional